THE PHYSICAL REVIEW

A journal of experimental and theoretical physics established by E. L. Nichols in 1893

Published by the American Institute of Physics
for the
AMERICAN PHYSICAL SOCIETY

Officers

President

F. W. Loomis
University of Illinois
Urbana, Illinois

Vice-President

I. I. Rabi
Columbia University
New York, New York

Secretary

K. K. Darrow
Bell Telephone Laboratories
Office:
Columbia University
New York 27, New York

Treasurer

G. B. Pegram
Columbia University
New York 27, New York

Local Secretary
for the Pacific Coast

J. Kaplan
University of California at Los Angeles
Los Angeles, California

Managing Editor

John T. Tate
University of Minnesota
Minneapolis, Minnesota

BOARD OF EDITORS

Editor

J. T. Tate — S. A. Goudsmit — E. M. Purcell — V. F. Weisskopf

Associate Editors

S. A. Goudsmit — W. E. [illegible]
E. M. Purcell — R. G. [illegible]
V. F. Weisskopf — J. Ramsey

Manuscript for publication should be submitted to John T. Tate, University of Minnesota, Minneapolis, Minnesota. The authors' institutions are asked to pay a publication charge of $4 per page which, if assessed, will entitle the author to 100 free reprints. Instructions will be sent with galley proofs.

Inquiries and all correspondence concerning papers in the process of publication should be addressed to the Publication Manager, American Institute of Physics, 57 East 55 Street, New York 22, New York.

Subscription Price

United States and Canada $25.00
Foreign $27.00

Back Numbers[1]

Single back number rate when complete year is available:
Prior to 1949: $20.00
Thereafter: $27.00
Single issues: $2.50 each, prior to July, 1929;
$1.00 each, July, 1929–December, 1941;
$2.00 each, January, 1942–December, 1946;
$1.50 each, January, 1947–December, 1948.
Current issues: $2.50 each.
Supplement, 1893–1930: $4.00.

Orders and claims for back numbers should be addressed to the Business Office, Lancaster, Pennsylvania, or to the American Institute of Physics, 57 East 55 Street, New York 22, New York.

Subscription orders in the case of members of the American Physical Society should be addressed to the Treasurer; in the case of other subscribers, to the Business Manager, American Institute of Physics.

[1] Bound volumes of Physical Review, Cornell University Library, Ithaca, New York.

The Physical Review is published monthly by the American Institute of Physics at Prince and Lemon Streets, Lancaster, Pennsylvania.

Entered as second-class matter March [illegible] at the Post Office at Lancaster, Pennsylvania, under the Act of March 3, 1879.

Acceptance for mailing at special rate of postage provided for in paragraph 4, section 538, P. L. & R., authorized January 27, [illegible].

THE
PHYSICAL REVIEW

A journal of experimental and theoretical physics established by E. L. Nichols in 1893

SECOND SERIES, VOL. 76, NO. 12 DECEMBER 15, 1949

Are Mesons Elementary Particles?

E. FERMI AND C. N. YANG*
Institute for Nuclear Studies, University of Chicago, Chicago, Illinois
(Received August 24, 1949)

The hypothesis that π-mesons may be composite particles formed by the association of a nucleon with an anti-nucleon is discussed. From an extremely crude discussion of the model it appears that such a meson would have in most respects properties similar to those of the meson of the Yukawa theory.

I. INTRODUCTION

IN recent years several new particles have been discovered which are currently assumed to be "elementary," that is, essentially, structureless. The probability that all such particles should be really elementary becomes less and less as their number increases.

It is by no means certain that nucleons, mesons, electrons, neutrinos are all elementary particles and it could be that at least some of the failures of the present theories may be due to disregarding the possibility that some of them may have a complex structure. Unfortunately, we have no clue to decide whether this is true, much less to find out what particles are simple and what particles are complex. In what follows we will try to work out in some detail a special example more as an illustration of a possible program of the theory of particles, than in the hope that what we suggest may actually correspond to reality.

We propose to discuss the hypothesis that the π-meson may not be elementary, but may be a composite particle formed by the association of a nucleon and an anti-nucleon. The first assumption will be, therefore, that both an anti-proton and an anti-neutron exist, having the same relationship to the proton and the neutron, as the electron to the positron. Although this is an assumption that goes beyond what is known experimentally, we do not view it as a very revolutionary one. We must assume, further, that between a nucleon and an anti-nucleon strong attractive forces exist, capable of binding the two particles together. We assume that the π-meson is a pair of nucleon and anti-nucleon bound in this way. Since the mass of the π-meson is much smaller than twice the mass of a nucleon, it is necessary to assume that the binding energy is so great that its mass equivalent is equal to the difference between twice the mass of the nucleon and the mass of the meson.

According to this view the positive meson would be the association of a proton and an anti-neutron and the negative meson would be the association of an anti-proton and a neutron. As a model of a neutral meson one could take either a pair of a neutron and an anti-neutron, or of a proton and an anti-proton.

It would be difficult to set up a not too complicated scheme of forces between a nucleon and an anti-nucleon, without about equally strong forces between two ordinary nucleons. These last forces, however, would be quite different from the ordinary nuclear forces, because they would have much greater energy and much shorter range. The reason why no experimental indication of them has been observed for ordinary nucleons may be explained by the assumption that the forces could be attractive between a nucleon and an anti-nucleon and repulsive between two ordinary nucleons. If this is the case, no bound system of two ordinary nucleons would result out of this particular type of interaction. Because of the short range very little would be noticed of such forces even in scattering phenomena.

Ordinary nuclear forces from the point of view of this theory will be discussed below.

Unfortunately we have not succeeded in working out a satisfactory relativistically invariant theory of nucleons among which such attractive forces act. For this reason all the conclusion that will be presented will be

* Now at the Institute for Advanced Study, Princeton, New Jersey.

extremely tentative. It would be undesirable to assume that the attraction is due to a special field of force since in this case the quanta of this new field would be themselves new elementary particles which is just what we hope to be able to avoid. Therefore, only forces of zero range appear compatible with relativistic invariance. In Section II the attempt will be discussed to represent the interaction by a term of the fourth degree in the amplitudes of the nucleon fields. We do not know whether this attempt can be made mathematically self-consistent and we have not succeeded in finding a way to treat it, except by the most crude approximation. The main difficulty is that no stationary state exists with one pair of nucleons only, but only mixed states with one pair, two pairs and many pairs. In our simplified discussion we have neglected this important factor, and treated the problem of a nucleon and an anti-nucleon alone. Assuming hopefully that these mathematical difficulties can be overcome, we have investigated the symmetry properties of the quantum states of the system of a nucleon and an anti-nucleon, in particular for the states of total angular momentum zero, $^1S_0$ and $^3P_0$. The former of these two states corresponds to a pseudoscalar meson and the latter to a scalar meson. If the ground state of the two-nucleon system had a resultant angular momentum 1, one could get in a similar way a model of the vector meson.

A peculiarity of the wave functions of the meson is that they decrease extremely rapidly with the distance between the two nucleons, so that the dimensions of the meson appear to be of the order of magnitude of the Compton wave-length of the nucleon, which is roughly 1/10 of the classical electron radius. This feature may make the experimental detection of the complex nature of the meson extremely difficult.

In the Yukawa theory of nuclear forces it is postulated that virtual mesons are continuously created and re-absorbed in the vicinity of a nucleon. When two nucleons are close to each other, the process of absorption by one nucleon of the virtual meson originated by the other is responsible for the nuclear forces. According to the present view, the main features of this theory can be kept even when the assumption that the meson is an elementary particle is dropped.

One finds that in the vicinity of an isolated nucleon there is a tendency to pair formation of nucleons and anti-nucleons, which will be predominantly formed in the bound state, that is as π-mesons, because such bound states are energetically much lower. From this point on, the Yukawa theory can be taken over almost unchanged as a description of the mechanism of nuclear forces (see Section III).

If the program that has been outlined could be carried out in a mathematically satisfactory way, one might hope to be able eventually to establish a relationship between the strength of the ordinary nuclear forces and the meson mass. Indeed, the difference between the mass of two nucleons and the mass of the meson is the binding energy of the nucleon and the anti-nucleon system. In a consistent theory, therefore, the strength of the coupling term between a nucleon and an anti-nucleon should be adjusted to give the correct value for this binding energy. On the other hand, it is this same coupling which is responsible for the creation of virtual mesons near a nucleon and determines, therefore, the strength of the ordinary nuclear forces. In Section III an estimate of the nuclear forces, calculated as far as is possible according to this program, is given. Considering the extremely primitive mathematical means used, the agreement is not worse than what might be expected.

II. MESONS AS BOUND STATES OF A NUCLEON AND AN ANTI-NUCLEON

We proceed now to discuss the mathematical formalism needed in order to carry out the outlined program.

For this it is necessary to introduce attractive forces between a nucleon and an anti-nucleon capable of binding the two particles together into what we assume to be a meson.

As long as no requirements of relativistic invariance are introduced, this could be done merely by postulating an interaction potential of suitable depth and range. It is useful for what follows to formulate this in the language of the field theory as follows: Two types of particles, for example, protons and anti-neutrons, are described neglecting spin and relativity by two fields, P and A. It is convenient to use here these letters rather than the more usual ψ_P and ψ_A. The following Hamiltonian can be assumed in order to include the attractive potential:

$$\frac{\hbar^2}{2M}\int \nabla P^*\nabla P d^3\mathbf{r}+\frac{\hbar^2}{2M}\int \nabla A^*\nabla A d^3\mathbf{r} - \int\int P^{*\prime}P^{\prime}A^{*\prime\prime}A^{\prime\prime}V(|\mathbf{r}^{\prime}-\mathbf{r}^{\prime\prime}|)d^3\mathbf{r}^{\prime}d^3\mathbf{r}^{\prime\prime}. \quad (1)$$

The first two terms are the kinetic energy of protons and anti-neutrons and the last term introduces the interaction. In this non-relativistic case, states with one proton and one anti-neutron do not mix with any other states. One can therefore confine one's attention to such states only and it is well known that the Hamiltonian (1) is then completely equivalent to that of a two-particle problem with an interaction $V(|\mathbf{r}^{\prime}-\mathbf{r}^{\prime\prime}|)$.

Unfortunately no such simple situation obtains for relativistic particles in the hole theory. There are two reasons for this. One is that two-particle states mix with states in which additional pairs of particles form. The second is that only zero range forces can be used relativistically without adding an essentially new force field. For zero range forces no bound two-particle solution exists.

Since neutrons and anti-neutrons are symmetrical

particles, it is immaterial whether we call the anti-neutrons "holes" in a negative neutron sea or vice versa. Since we are interested primarily in an interaction between protons and anti-neutrons, the second alternative is preferable.

The simplest relativistically invariant interactions between these two fields are the usual[1] five types:[2]

$$\int A^*\beta A P^*\beta P d^3\mathbf{r} \qquad \text{(Scalar)}$$

$$\int \{A^*AP^*P - A^*\boldsymbol{\alpha}A\cdot P^*\boldsymbol{\alpha}P\}d^3\mathbf{r} \qquad \text{(Vector)}$$

$$\int \{A^*\beta\boldsymbol{\sigma}A\cdot P^*\beta\boldsymbol{\sigma}P + A^*\beta\boldsymbol{\alpha}A\cdot P^*\beta\boldsymbol{\alpha}P\}d^3\mathbf{r} \qquad \text{(Tensor)} \qquad (2)$$

$$\int \{A^*\boldsymbol{\sigma}A\cdot P^*\boldsymbol{\sigma}P - A^*\gamma_5 A P^*\gamma_5 P\}d^3\mathbf{r} \qquad \text{(Pseudovector)}$$

$$\int A^*\beta\gamma_5 A P^*\beta\gamma_5 P d^3\mathbf{r}. \qquad \text{(Pseudoscalar).}$$

The vector interaction in (2), like the Coulomb forces, has opposite signs for the interaction between a proton and a neutron and between a proton and an anti-neutron. It turns out that the tensor interaction also has this property while the scalar, pseudovector and pseudoscalar interactions have the same sign for a proton-neutron pair and a proton-anti-neutron pair.

As explained in the introduction, one needs an interaction that is attractive for a proton-anti-neutron pair and repulsive for a proton-neutron pair. Thus the vector and tensor interactions in (2) are the possible choices. For definiteness we shall take in what follows the vector interaction and write:

$$H^{\text{int}} = G\int \{A^*AP^*P - A^*\boldsymbol{\alpha}AP^*\boldsymbol{\alpha}P\}d^3\mathbf{r}. \qquad (3)$$

This Hamiltonian represents a δ-function interaction between a proton and an anti-neutron. Indeed, (3) may be written:

$$H^{\text{int}} = G\int\int A^{*\prime}P^{*\prime\prime} \times[\delta(\mathbf{r}'-\mathbf{r}'')(1-\boldsymbol{\alpha}_A\boldsymbol{\alpha}_P)]A'P''d^3\mathbf{r}'d^3\mathbf{r}''. \qquad (4)$$

[1] These are very similar to the interactions used in β-decay theory. See, e.g., H. A. Bethe, Rev. Mod. Phys. 8, 82 (1936). We use the same notation as Bethe's for the $\boldsymbol{\alpha}$-, β-, and γ-matrices.

[2] In the hole theory to make the vacuum expectation value of these interactions zero one needs actually to subtract from (2) certain terms. For example the correct scalar interaction to take is:

$$\int [N^*\beta N - \langle N^*\beta N\rangle_{\text{vac}}][P^*\beta P - \langle P^*\beta P\rangle_{\text{vac}}]d^3r,$$

where $\langle\ \rangle_{\text{vac}}$ means vacuum expectation value.

It has proved impossible to solve exactly the interaction problem of a proton and an anti-neutron to yield the "meson" bound state. We had to limit ourselves to the extremely crude description in terms of two-particle states only, disregarding thereby the complications due to multiple pair creation.

The following qualitative argument leads us to believe that this approximate description may be fairly good when the two particles are relatively far from each other and may break down when they are close. For a proton-anti-neutron state the unperturbed energy is larger than the actual energy by a little bit less than $2\ \text{Mc}^2$. For a state with an additional pair (two-pairs state), the energy difference[3] is $4\ \text{Mc}^2$, for an N-pairs state, $2N\ \text{Mc}^2$. One might expect that an N-pair state will last a time of the order of $\hbar/(2N\ \text{Mc}^2)$ during which the particles can move away about $\hbar/(2N\ \text{Mc})$. We expect, therefore, nucleons to be found away from the center up to about this distance. As N increases such configurations will become smaller and smaller. As a confirmation of this qualitative argument we find that actually for the two-nucleon state the wave function depends on the distance approximately as $\exp(-\text{Mc}r/\hbar)$.

We have attempted therefore to regard the effect of multiple pairs as perturbing the near parts of the single pair wave function as if the δ-function interaction were smeared over a region of dimensions about $\hbar/\text{Mc}$. This procedure is not relativistically invariant and should be substituted by a correct multiple-pairs theory. In lack of this we propose to follow up the two-particle theory assuming instead of the contact interaction one of range $\hbar/\text{Mc}$. The interaction will be modified accordingly by introducing instead of $G\delta(\mathbf{r}'-\mathbf{r}'')$ a finite range attractive potential $-V(|\mathbf{r}'-\mathbf{r}''|)$. With this the interaction term becomes

$$H^{\text{int}} = -\int\int A^{*\prime}P^{*\prime\prime}V(\mathbf{r})(1-\boldsymbol{\alpha}_A\cdot\boldsymbol{\alpha}_P)A'P''d^3\mathbf{r}'d^3\mathbf{r}''. \qquad (5)$$

For simplicity we will take for V a step function

$$\begin{aligned} V(\mathbf{r}) &= 0 && \text{for } r > \hbar/\text{Mc} \\ V(\mathbf{r}) &= V_0 = \text{constant} && \text{for } r < \hbar/\text{Mc}, \end{aligned} \qquad (6)$$

where

$$r = |\mathbf{r}'-\mathbf{r}''|, \quad \mathbf{r} = \mathbf{r}''-\mathbf{r}'.$$

We now adopt the two-particle approximation whereby the Schrödinger function will be a function of the spin and positional coordinates of the proton and the anti-neutron. The two spin indices running from 1 to 4 each yield a 16-component wave function. For states of zero total momentum each of the 16 components will depend only on the relative position $\mathbf{r}$.

The Schrödinger equation is:

$$\{-chi(\boldsymbol{\alpha}_P-\boldsymbol{\alpha}_A)\cdot\Delta + \text{Mc}^2\beta_A + \text{Mc}^2\beta_P - V(r)(1-\boldsymbol{\alpha}_A\cdot\boldsymbol{\alpha}_P)\}\psi = E\psi.$$

[3] See, however, Section III, especially footnote 5.

It is convenient to arrange the 16 components of ψ into a 4×4 matrix with the proton spin index vertical and the anti-neutron index horizontal.

For a $^1S_0$ state the rotational invariance specifies the dependence of the 16 components on the angular variables as follows:

$$\psi(^1S_0)=\begin{vmatrix} 0 & -if_1 & \frac{f_2}{r}(-x+iy) & \frac{f_2}{r}z \\ if_1 & 0 & \frac{f_2}{r}z & \frac{f_2}{r}(x+iy) \\ \frac{f_3}{r}(-x+iy) & \frac{f_3}{r}z & 0 & -if_4 \\ \frac{f_3}{r}z & \frac{f_3}{r}(x+iy) & if_4 & 0 \end{vmatrix}, \tag{7}$$

where f_1, f_2, f_3 and f_4 are functions of the distance r only. The other state of total angular momentum 0, namely, $^3P_0$, has a wave function similar *in form* to (7) in which, however, the first and second rows are interchanged with the third and fourth rows. The $^1S_0$ state yields a particle that behaves as a pseudoscalar meson, whereas the $^3P_0$ state behaves as a scalar meson. This fact surprised us because we had thought that the opposite would be the case. The reason is connected with the different transformation properties under space reflection of the large and small components of the wave functions of a Dirac particle. No such unexpected behavior would have been found if the neutron had been treated in the sense of the hole theory as the particle and the anti-neutron as the anti-particle.

Substituting in (6) one finds for f_1, f_2, f_3, f_4 the equations:

$$2\left[r\frac{d}{dr}\left(\frac{f_2}{r}\right)+3\frac{f_2}{r}\right]=\frac{-2\,\mathrm{Mc}^2+E+V}{c\hbar}f_1+\frac{3V}{c\hbar}f_4$$

$$=\frac{2\,\mathrm{Mc}^2+E+V}{c\hbar}f_4+\frac{3V}{c\hbar}f_1, \tag{8}$$

$$\frac{d}{dr}(f_1+f_4)=-\frac{E}{c\hbar}f_2,$$

$$f_2=f_3.$$

The lowest eigenvalue must be $E=\mu c^2$, the rest energy of the meson. This condition determines[4] the depth V_0 of the potential (6). Assuming the ratio 6.46 between the proton and meson masses one finds:[4]

$$V_0=26.4\ \mathrm{Mc}^2=24.6\ \mathrm{Bev}. \tag{9}$$

The corresponding normalized solution in a large volume Ω is:

$$r>r_0=\frac{\hbar}{\mathrm{Mc}}\begin{cases} f_1=-\dfrac{0.236}{(r_0^3\Omega)^{\frac{1}{2}}}\dfrac{1}{u}e^{-u} \\ f_2=f_3=-\dfrac{0.218}{(r_0^3\Omega)^{\frac{1}{2}}}e^{-u}\left[\dfrac{1}{u}+\dfrac{1}{u^2}\right] \\ f_4=\dfrac{0.202}{(r_0^3\Omega)^{\frac{1}{2}}}\dfrac{1}{u}e^{-u}, \end{cases} \tag{10}$$

$$r<r_0\begin{cases} f_1=-\dfrac{0.0136}{(r_0^3\Omega)^{\frac{1}{2}}}\dfrac{\sin v}{v} \\ f_2=f_3=\dfrac{0.370}{(r_0^3\Omega)^{\frac{1}{2}}}\left[\dfrac{\cos v}{v}-\dfrac{\sin v}{v^2}\right] \\ f_4=-\dfrac{0.0147}{(r_0^3\Omega)^{\frac{1}{2}}}\dfrac{\sin v}{v}, \end{cases} \tag{11}$$

where

$$u=rc/\hbar[M^2-(\mu^2/4)]^{\frac{1}{2}},\quad v=2.03(r/r_0).$$

Notice that the wave function at large distances decreases like $\exp[-cr/\hbar(M^2-\mu^2/4)^{\frac{1}{2}}]$; thus the geometrical size of the meson is of the order of $\hbar/\mathrm{Mc}$ which is the Compton wave-length of the nucleon.

The inconsistencies of this representation should be emphasized. In particular we have given arguments to prove that the two-particle description breaks down at distances $\hbar/\mathrm{Mc}$ and this very distance turns out to be the size of the meson. One could, therefore, state that the wave function becomes reliable only where it vanishes. Our only excuse in adopting it is that we have been unable to do better.

III. RELATIONSHIPS WITH THE YUKAWA THEORY

In spite of the differences between the Yukawa elementary particle model of the meson and the present model, most features of the Yukawa theory can be

[4] There are some undesirable solutions of (8) with energy values E that go to zero when $V_0\to 0$. These solutions are discarded because they do not adiabatically approach the state of two free particles when $V_0\to 0$. Also they would not appear at all if we had taken the neutron and the proton to be of different masses.

taken over even when the meson is pictured as a proton-anti-neutron bound pair denoted briefly as $(P+A)$.

The fundamental process of Yukawa's theory

$$P\rightarrow N+\pi^{+} \tag{12}$$

now becomes

$$P\rightarrow N+(P+A). \tag{13}$$

This last process essentially is the addition to a proton P of a neutron-anti-neutron pair: N, A. Such pair formation will be induced by the postulated interaction (5). Since the energy of the bound $(P+A)$-system is much lower than that of the free particles the state (13) will be formed rather than a three free-particles state.[5] The matrix element is obtained from (5) by substituting for P the wave function of the proton that disappears, for A the wave function of the anti-neutron that disappears (neutron that appears), for $A'^{*}P''^{*}$ the complex conjugate of the wave function (7) of the bound proton-anti-neutron that appears. In order to express the wave function of the disappearing anti-neutron in terms of that of the neutron that is created, one uses the charge conjugation transformation

$$A=\gamma_2\tilde{N}^{*},$$

where $\sim$ means transposed and * transposed and complex conjugate.

We calculate the matrix element for a transition from a slow proton to a slow neutron and a meson at rest. The calculation is straightforward and gives the following result:

$$\int\int V(r)N^{*\prime}Q(\mathbf{r})P''d^{3}\mathbf{r}'d^{3}\mathbf{r}'', \tag{14}$$

where Q is the matrix

$$Q=2i(f_1+f_4)\gamma_1\gamma_2\gamma_3+i(f_1-f_2)\gamma_1\gamma_2\gamma_3\gamma_4. \tag{15}$$

If the wave-length of the proton is long compared to $\hbar/\mathrm{Mc}$ (14) can be approximated by

$$\int N^{*}RPd^{3}\mathbf{r}, \tag{16}$$

where

$$R=\int V(r)Q(\mathbf{r})d^{3}\mathbf{r}. \tag{17}$$

[5] The contribution to the forces of the virtual creation of free-particle pairs has been discussed in Section II. It was interpreted there as modifying the interaction only at extremely short distances (Order $\hbar/\mathrm{Mc}$). Creation of bound pairs yields inter-nucleon forces of range $\hbar/\mu c$.

Using (10), (11), and (15), and carrying out the integration one finds:

$$R=i\left(\frac{2\pi\hbar^{3}c^{3}}{\Omega\mu c^{2}}\right)^{\frac{1}{2}}(5.3\gamma_1\gamma_2\gamma_3+0.11\gamma_1\gamma_2\gamma_3\gamma_4). \tag{18}$$

This expression can be compared with the conventional interaction of a pseudoscalar meson with nucleons in the Yukawa theory.[6] There are two essentially independent coupling constants: f, the so-called pseudoscalar interaction, and g, the pseudovector interaction. The nucleon-meson interaction Hamiltonian is:

$$i\int N^{*}\left\{f\gamma_1\gamma_2\gamma_3\phi+\sum_{\nu}\frac{\hbar}{\mu c}g\gamma_1\gamma_2\gamma_3\gamma_{\nu}\frac{\partial\varphi}{\partial x_{\nu}}\right\}Pd^{3}\mathbf{r} \tag{19}$$

where ϕ is the pseudoscalar meson field.

The corresponding matrix element for the production of a meson at rest is

$$i\frac{\hbar c}{(2\Omega\mu c^{2})^{\frac{1}{2}}}\int N^{*}(f\gamma_1\gamma_2\gamma_3+g\gamma_1\gamma_2\gamma_3\gamma_4)Pd^{3}\mathbf{r}.$$

Comparison with (18) gives

$$f=(4\pi\hbar c)^{\frac{1}{2}}\times 5.3,\quad g=(4\pi\hbar c)^{\frac{1}{2}}\times 0.11. \tag{20}$$

It has been proved by Case[7] that the terms f and g produce up to the second approximation nuclear forces of the same type. Indeed, their joint contribution is the same as would be obtained by putting $f=0$ and substituting g by

$$g'=g+f(\mu/2M). \tag{21}$$

We find, therefore,

$$g'=(4\pi\hbar c)^{\frac{1}{2}}\times 0.52$$

yielding for $g'^{2}/4\pi\hbar c$, that is for the analog of the fine structure constant, the value 0.27, which appears quite reasonable.

Naturally the similarity between the present point of view and the Yukawa theory can be carried on only up to a limited extent. The similarity breaks down on the one hand because of the finite size of the meson which introduces naturally a cut-off at short distances. On the other hand it breaks down for phenomena in which sufficiently high energies are involved to break up the meson.

[6] See for example: G. Wentzel, Rev. Mod. Phys. **19**, 1 (1947).
[7] K. M. Case, Phys. Rev. **76**, 14 (1949).

A Precise Determination of the Slow Neutron Cross Section of the Free Proton

EDWARD MELKONIAN
Columbia University, New York, New York
(Received August 19, 1949)

The total neutron cross sections of H_2, *n*-butane, and water have been measured with the Columbia slow neutron velocity spectrometer in the energy range 0.8 to 15 ev. Analysis of these data gives a value of 20.36±0.10 barns for the free proton cross section. In this energy interval the measurements confirm Placzek's theoretical prediction of the variation of the H_2 cross section. The technique of making absolute transmission measurements and the corrections for multiple scattering are discussed. Measurements on H_2 for neutron energies above 15 ev show a constant cross section to several thousand ev. Measurements on fused quartz in the energy interval 0.003 ev to 10 ev show interference effects.

INTRODUCTION

THE slow neutron cross section of the free proton is one of the important constants of nuclear physics inasmuch as the neutron-proton interaction involves elementary particles and hence lends itself to theoretical investigation. In particular, the free proton cross section used in conjunction with the results of the experiments on the scattering of neutrons by parahydrogen enables one to calculate the range of nuclear forces for the triplet interaction between neutron and proton.[1]

Because of the importance of the value of the free proton cross section, it has been measured by many investigators. An examination of these experiments indicated that a better determination was desirable. It is the purpose of this report to describe a precise determination of this quantity using measurements on H_2, *n*-butane, and H_2O. Comparison with previous results will be presented.

EXPERIMENTAL PROCEDURE

The Slow Neutron Velocity Spectrometer

This apparatus has been previously described in detail.[2] There has been one major change. The fundamental timing is now provided by a one-megacycle oscillator instead of a 100-kilocycle oscillator.[3] Much better resolution is thus made available. The following brief description emphasizes other improvements and adaptations and has been kept sufficiently general to serve for the following paper.[4]

The neutron spectrometer system uses the method of cyclotron arc modulation which confines neutron production to intervals of four to 1024 microseconds duration out of a 1024- to 32,768-microsecond cycle. Neutrons slowed down in a paraffin "source" slab are detected by BF_3 proportional counters at a distance of 6.0 meters (unless otherwise stated) from the paraffin source. A special selector system counts selectively those neutrons detected during adjustable time intervals after the neutron production. Knowledge of time of flight and distance enables calculation of neutron energy within the resolution limits.

Two paraffin source slabs have been in use. The "thin source" is effectively one inch thick and is used for timings less than 2048 microseconds to keep source delay time corrections to a minimum. For longer timings a "thick source" effectively three inches thick has been used to give greater intensities of low energy thermal neutrons. Appropriate delay time corrections are made.

The collimating system is similar to that used previously, but provision is made for handling the one-meter long gas sample holders. The mean position of the samples (gas or liquid) is 1.1 meters from the BF_3 counter. The slow neutron flux is collimated to 6.3-cm diameter. The detector subtends less than 3×10^{-4} of the 4π-solid angle viewed from the sample position; therefore no "geometry" corrections have been made in general except in the case of the determination of the free proton cross section where a high degree of refinement was sought. Even here the correction was less than 0.5 percent.

Absolute Measurement of Cross Section—The Standard Filter Technique

In the past, attempts at various times to repeat measurements on a given sample had frequently yielded sets of results each internally consistent, but differing among themselves by a few percent, which was considerably greater than the statistical uncertainty. This situation was climaxed by the occurrence of discrepancies in the measurements made with the two separate channels. Both counters were replaced with new ones with the hope of correcting this situation. Measurements using the new counters gave cross-section values systematically higher than any of the previous results. Exploratory tests seemed to indicate that these discrepancies arose because of a slight dependence of detection efficiency upon the counting rate. (The background rate was negligibly small in all cases.) The re-

[1] Wu, Rainwater, Havens, and Dunning, Phys. Rev. **69**, 236 (1946); M. Hamermesh and J. Schwinger, Phys. Rev. **71**, 678 (1947).
[2] Rainwater, Havens, Wu, and Dunning, Phys. Rev. **71**, 65 (1947).
[3] Havens, Rainwater, Wu, and Dunning, Phys. Rev. **74**, 1216A (1948).
[4] E. Melkonian, Phys. Rev. **76**, 1750 (1949).

sults could be explained if the counting efficiency were smaller for higher counting rates ("sample out" count) than for lower counting rates ("sample in" count). It was not known whether this dependence upon counting rate was caused by the counters or by the associated circuits, although subsequent tests seemed to indicate that the latter were at fault. This difficulty could be eliminated by making the counting rates approximately the same in the "in" and the "out" positions. This can be accomplished, for example, by using in the "out" position a sample of appropriate transmission whose cross section is known from other considerations to the required accuracy. Since the transmission of no such substance was known, a B_4C aperture system was constructed whose transmission is known absolutely from geometrical considerations. This device is denoted by the term "standard filter." The use of the standard filter has given results which are consistent within statistical uncertainty. The new results are systematically higher in cross section by a few percent (3 percent or less) in agreement with the assumptions given above.

A standard filter (for one channel) consists of two parts: (1) a "stator" which always remains in the beam in a fixed position and (2) a "rotor" which is used only when the sample is not in the beam.

The standard filter to give transmission equal to $\frac{1}{3}$ will be described. Standard filters to give other transmission values have been made in a similar way.

The stator consists of a disk of B_4C paraffin mixture one inch thick and five inches in diameter in which three equal wedge-shaped openings are cut out leaving three spokes each $\frac{1}{4}$ inch wide (Fig. 1). The cut-out portions extend radically out far enough (1.5 inches) so that the opening in the collimating system is more than fully exposed in the open sections of the stator.

The rotor consists of a similar disk but with only one wedge-shaped opening going to the exact center of the disk, the central angle of the opening being the same as in the case of the stator. When placed properly over the stator, the rotor covers two openings completely, leaving the third opening completely exposed. The stator spokes are wide enough so that the rotor edge is sufficiently far back that it cannot be "seen" by the neutron beam, and so that neutrons coming through the covered openings at the steepest angle possible cannot get through. *Thus each opening acts independently of the others, so that the number of neutrons going through a given opening is the same whether the other openings are covered or not.* When this device is accurately made, and the neutron beam is completely uniform across the three openings, then the number of neutrons reaching the detector when the rotor is used would be exactly $\frac{1}{3}$ the number without the rotor. Thus, for a sample having transmission approximately $\frac{1}{3}$, one alternates sample and rotor in the beam and gets a direct comparison of the sample transmission with that of the standard, at the same time getting approximately the same counting rates in both "in" and "out" positions and so avoiding errors resulting from the rate dependence of the detection efficiency.

For the neutron beam actually used the intensity is not the same for the three openings (as much as 30 percent variation from the average having been observed). Although the openings do not separately give exactly $\frac{1}{3}$ of the total intensity, the desired effect is obtained by exposing the three openings in sequence, each for $\frac{1}{3}$ of the time allotted to the "out" count. A residual effect still remains, as the counting rate (and hence detection efficiency) for the various openings is still not exactly the same as that for the "in" count. However, the variation of counting rate is now much less than without the standard filter. Also, there is a strong tendency to cancel out the error arising from this variation as long as the average counting rate with the standard filter matches that with the sample. A simple calculation shows that the error arising from this non-uniformity of the beam is negligible.

A solid one-inch thick piece of B_4C paraffin mixture is periodically placed in the rotor position to determine what counts would get through the solid portions of the standard filter system. Only data are used for which this background count is negligible. In general, the standard filter described here cannot be used for energies above 15 ev since the filter is not sufficiently opaque at these higher energies.

In the discussion so far it has been tacitly assumed that the efficiency of detection for this spectrometer system depends solely upon the instantaneous counting rate. This appears to be at least partially true. There is, however, some evidence to indicate that the detection efficiency at any instant depends somewhat upon the intensity in previous portions of the timing cycle. In the extreme limit, the detection efficiency might depend upon the intensity averaged over the entire cycle. For measurements between 0.5 and 15 ev, the repeat time used is 1024 microseconds, and cadmium is used to prevent overlapping with subsequent cycles. For the samples studied, as in the case of the determination of the free proton cross section, the transmission of the sample varies very little (~10 percent) over this interval. The ratio of "sample in" to "sample out"

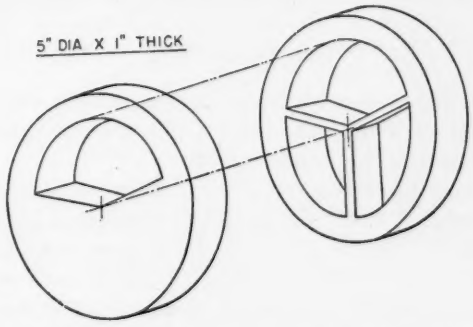

FIG. 1. Diagram showing standard filter to give a transmission of $\frac{1}{3}$. It is made of a B_4C paraffin mixture.

intensity is thus approximately the same whether instantaneous or averaged transmission values are considered, and there is no difficulty in choosing the appropriate standard filter. When longer repeat times are to be used where the sample transmission varies considerably, the choice of the proper standard filter transmission value is somewhat more difficult since it is not known whether the sample transmission of the portion of the cycle being studied should be matched, or whether the sample transmission averaged over the entire cycle should be matched. This problem arose in the case of H_2

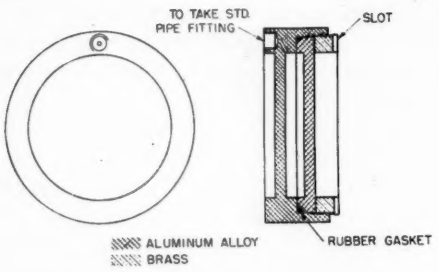

FIG. 2. Holder for liquid scatterer.

and methane when measurements with standard filter were made to timings of 4096 microseconds out of a repeat time of 8192 microseconds. In such cases compromise values were adopted between the possible extremes.

It should be stressed that the discrepancies corrected by the standard filter technique are at most 3 percent (under otherwise good conditions) and are usually less with new counters. Hence, uncertainties in the absolute values of previous measurements made with the spectrometer are only of this order. Most of the previous work was concerned primarily with the shape of the transmission curve (e.g., in the neighborhood of a resonance) and this is only slightly affected by the variation of detection efficiency with counting rate. Only when a precise determination of an absolute value for the cross section is desired is the use of the standard filter technique essential (with the present equipment).

An unsuccessful attempt to use fused quartz as a secondary standard filter in place of the less convenient primary standard filter is described in the Appendix.

Sample Holders

The holders used for liquid and gas samples were constructed of aluminum alloy to minimize attenuation of the neutron beam in the ends.

Several liquid sample holders of different design have been used. A particularly versatile design is shown in Fig. 2. A variety of sample thicknesses may be obtained by using interchangeable plates hollowed to different depths. Use of the valve allows filling with liquids having vapor pressure above atmospheric pressure (e.g., liquid *n*-butane). A "blank" having the same thickness of the same aluminum alloy was used in the sample "out" position.

The gas sample holder, shown in Fig. 3, can be used safely with gas pressures to 1000 p.s.i. These pressures are necessary when the gas being investigated has a low cross section. The brass to aluminum seals of the inlet, used in both gas and liquid sample holders, are gastight at the highest pressure used in testing (about 3000 p.s.i.). The seal itself is made in the seat below the threads. An identical evacuated sample holder was used in the "sample out" position.

Preparation and Purity of Samples, and Determination of Sample Thickness

The scatterers used in this investigation are included in those reported on in the following paper[4] to which reference is made for details on the preparation and purity of the samples and the determination of the number of grams per cm² in the path of the beam.

RESULTS

Neutron Energies between 0.5 and 15 ev

For the final measurements under the best experimental conditions, several different materials were in-

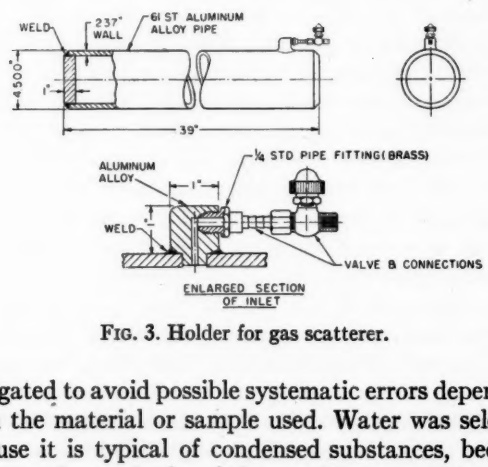

FIG. 3. Holder for gas scatterer.

vestigated to avoid possible systematic errors depending upon the material or sample used. Water was selected because it is typical of condensed substances, because there can be no doubt of the sample composition, and because several other investigators have used it. H_2 was used because it is the simplest hydrogen-containing substance and because it is a gas. (This latter point is important in connection with the multiple scattering correction which will be discussed later.) In addition, theoretical calculations of the expected σ *vs.* E dependence are most readily made for H_2. Gaseous *n*-butane was selected as a third scatterer somewhat different from the other two.

Measurements at sufficiently high energies to make the molecular binding effects completely negligible are not feasible as the poorer intensity accompanying the good resolution required makes it difficult to get the desired statistical accuracy. Also, the standard filter becomes partially transparent above 15 ev and hence

cannot be used. If measurements are made at energies at which binding effects are not negligible, suitable corrections must be made. Placzek has developed a theory[5] which shows that, at neutron energies large compared with the energy of spacing of the molecular vibrational levels, the cross section is linear in the reciprocal of the neutron energy, i.e.:

$$\sigma = \sigma_0 + \beta/E.$$

Thus, a plot of the cross-section data against the reciprocal of the neutron energy should give a straight line whose intercept is the free proton cross section. For the case of H_2, Placzek has given a calculated value for β which depends upon well-known constants of the H_2 molecule not related to neutron measurements. Only approximate calculations have been made in the case of water and *n*-butane.

The energy range chosen for measurement was approximately 0.5 to 15 ev. A repeat cycle of 1024 microseconds with cadmium filtering was used. Cyclotron on time and detection intervals of 32 and 64 microseconds were used, although most of the measurements were done with the latter for the sake of higher counting rates.

The experimental results are shown in Figs. 4–6, cross section being plotted against $1/E$. These data represent the average of several runs in each case. Correction has been made for capture of neutrons by protons assuming a $1/v$ variation of cross section, with the capture cross section taken as 0.3 barn at 0.025 ev. This correction is quite small, being only 0.05 barn at 1 ev. The statistical accuracy is indicated by vertical bars. Points above 15 ev have not been included because the standard filter becomes partially transparent.

The straight lines shown in these graphs have been obtained by means of least-square solutions using only the data above 0.8 ev. In this energy region, the straight line fit is seen to be good in accordance with Placzek's theory. Points below 0.8 ev have been included for H_2 and *n*-butane to show how deviation from the $1/E$ behavior begins.

The values of σ_0 and β (with their statistical standard deviations) for the best straight lines are listed in Table I. Placzek's theoretical values are also included for comparison. The agreement between observed and calculated values of β in the case of H_2 is considered satisfactory. The calculations in the case of H_2O are much more difficult and have been done roughly, so that only approximate agreement is expected.

The main contribution to the value of β arises from the existence of the "zero point energy" of an oscillator. In most phenomena, only energy differences contribute, so that the zero point energy is generally undetectable. It is interesting to note that we have here an experimentally observed phenomenon which depends almost entirely upon the presence of this quantum-mechanical effect.

The measured values of the cross section must be corrected for the effect of neutrons reaching the detector after one or more collisions in the scatterer. In spite of the very good geometry used, this effect of "in scattering" is not negligible although it is quite small. This effect has sometimes been corrected for by other investigators on the assumption that only the effect of single scattering is important so that the true transmission (i.e., for perfect geometry) is increased by an amount proportional to $(1-T)$, where T is the sample transmission. This is approximately true for T almost equal to unity. However, this treatment is sometimes applied when T is quite different from unity. Actually, this estimate would probably serve as a good upper limit to the correction for any magnitude of the transmission where it not for the fact that the detector used has a $1/v$ detection efficiency. Neutrons reaching the

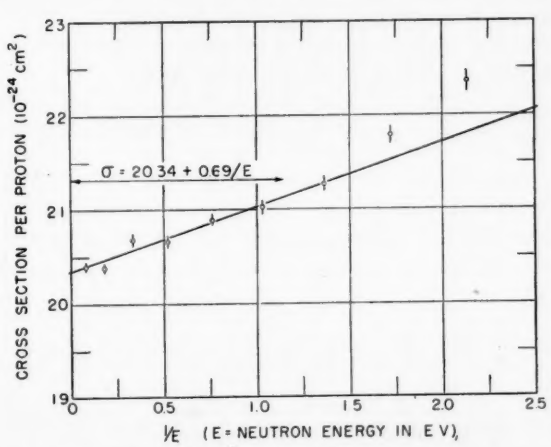

FIG. 4. The slow neutron cross section of H_2 gas in the energy region 0.5 to 15 ev. The average of measurements on samples of 0.0825 and 0.1417 g/cm² is shown. Correction for capture has been made.

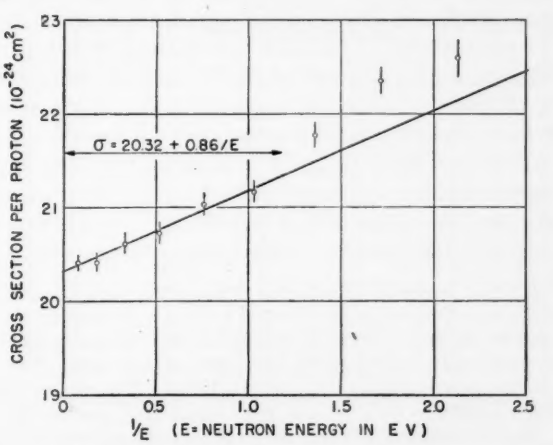

FIG. 5. The slow neutron cross section of H in gaseous *n*-butane in the energy region 0.5 to 15 e.v. The sample used contained 0.4351 g/cm². The carbon cross section was taken as 4.70 barns. Correction for capture has been made.

[5] The author is indebted to Dr. G. Placzek for communication of his results prior to publication.

TABLE I. Results of measurements and calculations.

Scatterer	σ_s in barns: As measured	Corrected for "In" scattering	β: Observed	Calculated (Placzek)
H_2	20.34±0.05	20.37	0.69±0.09	0.65
n-butane	20.32±0.08	20.35	0.86±0.14	
H_2O	20.27±0.06	20.37	1.36±0.11	1.0

detector after only one collision in the scatterer have essentially unchanged energy. However, neutrons reaching the detector after two or more collisions may have

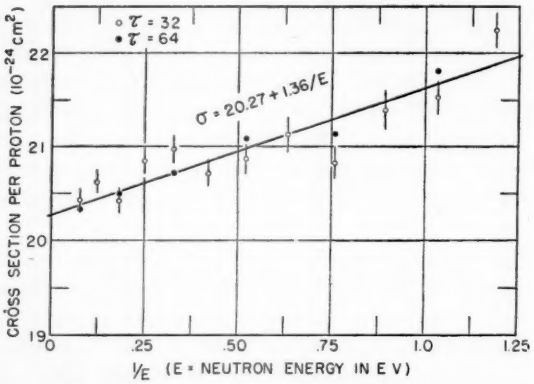

FIG. 6. The slow neutron cross section of H in H_2O in the energy region 1 to 15 ev. A 0.9407-g/cm² sample was used. The oxygen cross section was taken as 3.73 barns. Correction for capture has been made.

considerably reduced energy and, being detected more efficiently, contribute a large amount to the inscattering effect. Because of this, single and double scattering have been considered separately in the present investigation in order to arrive at the corrections to be applied to the measured values of the cross section.

The correction for single scattering considers only those neutrons which reach the detector after one collision in the scatterer. This amounts to an increase in the cross section of 0.025 for the water sample and 0.03 for the gas samples. (The latter correction is slightly larger because the "geometry" of the 94-cm long gas scatterer is effectively poorer than that of the water sample even though the mean positions are the same.)

The correction for double scattering considers only those neutrons which reach the detector after two collisions in the scatterer. In carrying out the calculations, the following facts have been taken into account:

(a) The detection efficiency for neutrons is proportional to $1/v$.

(b) Since the total time of flight for a slowed-down neutron must be the same as that for a neutron reaching the detector with no collision in the scatterer, the former neutron must have had greater energy initially than the latter. On a time of flight basis, a given spread is reflected in a larger spread after slowing down.

(c) The detected intensity has been taken as uniform on a time of flight basis. Actually there is a small decrease in detected intensity with increasing time of flight in the energy region used. This would tend to make the corrections slightly larger than calculated.

For the case of the gas scatterer the double-scattering correction is less than 1/20 of the single-scattering correction and hence may be neglected. However, for the water scatterer, this double-scattering correction turns out to be about as large as that for single scattering. Calculation of corrections for higher orders of scattering becomes increasingly complicated and has not been carried out. However, there is no reason to expect that these will be negligible. As an estimate of the total correction for water, the measured cross section has been increased by 0.10 which is twice the combined correction for single and double scattering. This correction is still only ½ percent of the measured cross section.

The reason for the difference in magnitude of the double-scattering correction for gas and liquid scatterers may be seen on the basis of simple considerations. Both liquid and gas samples have been so chosen that the sample thickness is approximately equal to the neutron mean free path in each case. For the gases, this is 94 cm; whereas for water (as well as for other condensed substances such as cetane, paraffin, etc., which have been used in the past) it is about 0.7 cm. The diameter of both water and gas samples is about 6.5 cm. Thus, for a gas scatterer, a neutron being deflected by a large angle after the first collision has a good chance of leaving the sample before making a second collision. For water, on the other hand, such a neutron has many mean free paths equivalent of material to pass through before leaving the sample, and thus has a good chance to make a second collision.

The corrected results are included in Table I. The agreement of the three determinations is excellent, but not as much confidence should be placed on the results on H_2O because of the uncertainty in the inscattering correction. It does serve to indicate, though, that no serious systematic errors are present. The results on H_2 should be weighted most heavily because the most data were taken on it and because the measured and theoretical values of the $1/E$ slope agree.

The free proton cross section is taken as 20.36 from these measurements. Statistical errors arising from

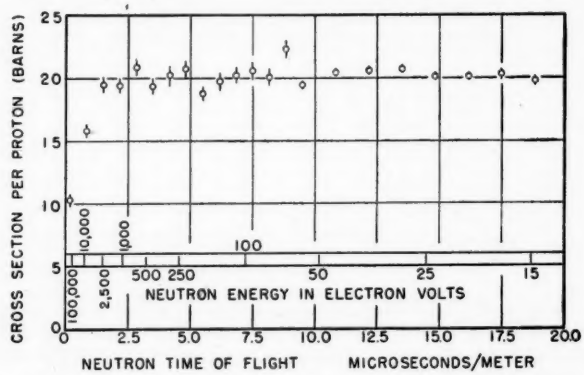

FIG. 7. The slow neutron cross section of H_2 for neutron energy greater than 15 ev. The sample used contained 0.1417 g/cm² of H_2.

counting and errors from determination of sample thickness indicate that a probable error of 0.10 should be placed on the stated figure.

An abstract of this work has been published.[6] Results reported still earlier[7] were made without the use of the standard filter and did not take into account the variation of the proton cross section above 1 ev.

The best previous determination of the free proton cross section has been made by Jones[8] who, using a similar set-up, obtained good statistical accuracy and corrected for molecular binding effects using Placzek's theory. His measurements on water and cyclohexane gave 20.0±0.3 and 20.1±0.3, respectively. His geometry was somewhat poorer than that used for the present measurements, and his final results include an additive correction of 0.25 for the effect of inscattering which he has evaluated on the assumption that the transmission is increased by an amount proportional to $(1-T)$. It is interesting to note that Jones' result is increased to ~20.3 (in good agreement with the results of the present measurements) if the inscattering correction method of this paper is used. The small difference between the results of this paper and those of Jones is thus probably due mainly to his use of too small a correction factor.

A previous determination with the Columbia slow neutron velocity spectrometer has been made by Rainwater, Havens, Dunning, and Wu[9] who reported a value of 20.6±1 from measurements on a paraffin scatterer.

Still earlier determinations have been summarized in reference 9. These measurements are characterized by: (1) use of liquid or solid scatterer, (2) relatively poor statistical accuracy in most cases, (3) poorer geometry than that for the determinations already discussed, and (4) no corrections for the effect of molecular binding where present.

Neutron Energies above 15 ev

In this energy region molecular binding effects are negligible. The neutron-proton cross section should decrease with increasing neutron energy as shown theoretically and checked by measurements to 6 Mev.[10]

Figure 7 shows measurements on H_2 using 4- and 8-microsecond cyclotron and detection on-times (without the standard filter technique). The cross section is seen to be constant until 2500 ev. Above this the results behave approximately as expected, but a detailed comparison with expectation is meaningless because of the relatively poor resolution used at the higher energies.

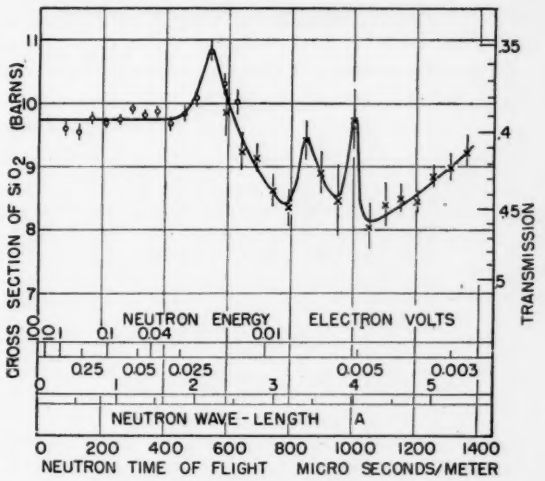

FIG. 8. The slow neutron cross section of fused quartz. The sample contained 9.583 g/cm². O—Source detector distance = 6.0 meters. ×—Source detector distance = 5.0 meters.

APPENDIX

Measurements on Fused Quartz

The standard filter technique is somewhat inconvenient to use and leads to almost a factor of two loss of detected intensity so that a calibrated secondary standard would be useful. Fused quartz (SiO_2) has elements with negligible capture in the slow neutron region and was expected not to show microcrystalline interference effects because of its supposed lack of long range crystalline structure. Thus it was expected to show a transmission nearly independent of neutron energy and hence to be suitable for use as a secondary standard. Figure 8 shows measurements on fused quartz made against a standard filter. Fairly large interference effects are evident which make this particular sample useless as a secondary standard. The shape of the curve is somewhat similar to that which would be expected for a liquid and is included here because of its interest in connection with the structure of vitreous materials.

ACKNOWLEDGMENTS

The author wishes to express appreciation to Professor J. R. Dunning who suggested this problem, and to Professors L. J. Rainwater and W. W. Havens, Jr. who took an active interest in the experiments and made numerous invaluable suggestions. Thanks are also due Professor T. I. Taylor for the mass spectrographic analyses of some of the gas samples; Drs. G. Placzek, H. A. Bethe, and O. Halpern for interesting discussions on several points; and Miss Miriam Levin and members of the cyclotron staff for assistance in making some of the measurements. The author also wishes to thank the AEC whose support made these researches possible.

[6] Melkonian, Rainwater, and Havens, Phys. Rev. **75**, 1295A (1949).
[7] E. Melkonian, Phys. Rev. **73**, 1265A (1948).
[8] W. B. Jones, Jr., Phys. Rev. **74**, 364 (1948).
[9] Rainwater, Havens, Dunning, and Wu, Phys. Rev. **73**, 733 (1948).
[10] D. Bohm and C. Richman, Phys. Rev. **71**, 567 (1947).

Slow Neutron Velocity Spectrometer Studies of O_2, N_2, A, H_2, H_2O, and Seven Hydrocarbons

EDWARD MELKONIAN
Columbia University, New York, New York
(Received August 19, 1949)

The slow neutron cross sections of free atoms of O, N, and A have been determined to be; O: 3.73, N: 9.96, A: 0.68 barn. Between 1 and 15 ev the N_2 curve shows an $E^{-\frac{1}{2}}$ slope of 0.34 barn$\times$(ev)$^{\frac{1}{2}}$ per atom. Measurements on these elements have been extended to over 10,000 ev with no resonances observed. Dependence of cross section upon neutron energy from 1 ev to 0.003 ev is presented for O_2, N_2, H_2, H_2O, methane, ethane, propane, *n*-butane, cetane, ethylene, 1,3-butadiene, and liquid *n*-butane. At the lowest energies, the large observed H_2 cross section is attributed largely to thermal translational motion of the molecule. The measurements on the hydrocarbons show the effect of the binding of H in various molecules. Comparison with the theories of Bethe and Arley is made. No difference has been detected in cross-section measurements on gaseous and liquid *n*-butane.

INTRODUCTION

THE Columbia University slow neutron velocity spectrometer has been used in numerous studies of the interaction of neutrons with matter.[1,2] The results obtained are in the form of cross section (or transmission) as a function of neutron energy. The previous reports have dealt with the study of materials in the solid or liquid state. The results of application of neutron spectroscopy to samples in the gas phase are presented here. Measurements on two liquid samples have been included for comparison.

For the elements studied the only purely nuclear phenomenon observed at low energies (<100 ev), aside from nuclear scattering, is the $1/v$ slope which is observed in the case of N and A and is attributed to neutron capture. This is indicative of resonances outside of the energy interval investigated. Capture of neutrons by O is known to be unobservably small for transmission measurements in this energy region. The capture cross section of H is small (being about 0.3 barn at 0.025 ev) and the expected $1/v$ slope is easily masked by other effects.

The non-nuclear effects observed below 1 ev are of molecular origin. One of these is chemical binding, the most important case of which is the fourfold increase of the H cross section when bound to a very heavy molecule. In addition, interference effects, inelastic scattering, and effects arising from the molecular thermal motion are observed. Cross-section measurements at low neutron energies (to 0.003 ev) for numerous materials are presented and demonstrate these phenomena, although it is rarely possible to make an experimental separation of the contributions of the various effects. In addition to these the O_2 cross section should have a contribution arising from the paramagnetic scattering of neutrons.

EXPERIMENTAL PROCEDURE

The slow neutron velocity spectrometer, the standard filter technique for making absolute transmission measurements, and the sample holders for liquid and gaseous scatterers have been described in detail in the preceding paper.[3] Where the standard filter has been used, it will be specifically stated. Otherwise, the effect of using the standard filter has been estimated and corrections made accordingly. In no case has the cross section been increased by more than 3 percent for this correction.

Transmission Measurements in the Low Energy Region

Some difficulty has been experienced in making measurements at neutron energies below 0.005 ev. These difficulties usually lead to too high a measured value for the transmission. Since all of the materials under investigation here show decreasing transmission with decreasing neutron energy, and since the intensity at low energies is very small compared with that at the thermal peak ($\sim$0.025 ev) the faster thermal neutrons might somehow influence the low energy results. Specifically, one or more of the following effects may give rise to erroneous results:

(1) Thermal neutrons inside the cyclotron enclosure may be scattered into the beam by air molecules and arrive at the detector at the same time as the slower neutrons under consideration. The possibility of this occurring has been minimized by replacing the 3.5-meter air path of the neutron beam inside the enclosure by a cadmium-shielded argon path, accomplished by the use of argon-filled, cadmium-lined, aluminum ducts. Argon is used because of its very low scattering cross section compared with air and other gases. This gives the additional benefit of diminishing the attenuation of

[1] L. J. Rainwater and W. W. Havens, Phys. Rev. **70**, 136 (1946). W. W. Havens and L. J. Rainwater, Phys. Rev. **70**, 154 (1946). Rainwater, Havens, Wu, and Dunning, Phys. Rev. **71**, 65 (1947). Havens, Wu, Rainwater, and Meaker, Phys. Rev. **71**, 165 (1947). Wu, Rainwater, and Havens, Phys. Rev. **71**, 174 (1947). Havens, Rainwater, Wu, and Dunning, Phys. Rev. **73**, 963 (1948).

[2] Rainwater, Havens, Dunning, and Wu, Phys. Rev. **73**, 733 (1948).

[3] E. Melkonian, Phys. Rev. **76**, 1744 (1949).

the neutron beam in the air path, the gain in intensity being about a factor of two at 0.003 ev.

(2) For condensed samples like H_2O it is possible for thermal neutrons to be slowed down by inelastic collisions in the scatterer and reach the detector at times corresponding to the slower neutrons. Some simple tests to establish the presence of such an effect have indicated that it is not important, but it could not be ruled out conclusively. However, Jones has given some evidence for the presence of such an effect in his measurements on water.[4]

(3) Sutton *et al*,[5] state that there is a continuous production of neutrons even during those portions of the cycle when the arc is not on. This effect was detected in connection with the present work by measuring the intensity distribution at very long timing by using a repeat time of 32,768 microseconds. The normal intensity should decrease very rapidly with increasing time of flight approximately as (time of flight)$^{-4}$. The observed curve showed this expected decrease to about 16,000 microseconds. Beyond this, the intensity was independent of timing and was attributed to the background production of neutrons. Measurement of the transmission of boron for these background neutrons showed that the mean energy is approximately kT. The intensity of this background varies somewhat with operating conditions but is usually sufficiently intense to distort measurements for neutron energies less than 0.005 ev.

All of these effects are aggravated by the adverse intensity ratio of the main part of the thermal distribution to the lower energy neutrons. All of them can be minimized by the use of Be and BeO filters which discriminate strongly against neutrons of energy greater than 0.01 ev but which become almost completely transparent at lower energies. The use of these filters should reduce the effects discussed above to a negligible amount. All of the results presented here for times of flight greater than 665 microseconds/meter were taken with 13 g/cm^2 of sintered Be in the beam. In a few cases, which will be specifically pointed out, 5.7 g/cm^2 of sintered BeO were used in addition to the Be. This addition of BeO may or may not give better results depending upon the relative amount of background. In any case, the improvement arising from the use of BeO is generally relatively small for measurements to 0.003 ev.

Preparation and Purity of Samples

The samples were obtained from various sources, and the purification required depended upon the amount and nature of the impurities.

O_2: This was obtained from the Matheson Company who stated that there was present as impurity 0.5 percent A and a small amount of N_2. These will not affect the measurements appreciably. To get rid of possible traces of H_2 and H_2O which would have a large effect, the O_2 was dried roughly with $CaCl_2$, passed over platinized asbestos at 300°C, dried with P_2O_5 and passed through a trap immersed in dry ice slush for final drying.

N_2: This was prepurified N_2 from Airco who claimed a purity of 99.999 percent. Mass-spectrographic analyses by the Columbia University Analytical Laboratory and by the Bureau of Standards indicated the presence of 0.2 percent A and 0.1 percent CO_2. In either case the gas was sufficiently pure and was used after passing through a dry ice trap to minimize the water vapor content.

H_2: This was electrolytic H_2 from Airco, who claimed an O_2 impurity less than $\frac{1}{2}$ percent (on a molar basis). Since the "sample thickness" determination is made by weighing (as will be discussed later) this amounts to a large error because of the large ratio of molecular weights. The purification process (to get rid of O_2 here) was essentially the same as that for the purification of O_2. A determination of the molecular weight of the purified sample was made as a check on the presence of heavier gases. The results showed a negligible amount of such impurities. In addition, mass-spectrographic analysis indicated no impurities. The sensitivity for detection of O_2 was such as to show 0.005 percent.

A: This was from Airco who listed the presence of 0.2 percent N_2. However, mass-spectrographic analysis indicated the presence of less than 0.05 percent of impurity (probably N_2). Because of the very large cross section of N_2 compared with that of A, the presence of even a small amount of N_2 is exaggerated. However, removal of the N_2 is very difficult for the amount of sample required ($\sim$500 liters at S.T.P.) and therefore the gas was used as furnished.

Methane, ethane, propane, *n*-butane, ethylene, and 1,3-butadiene: These were research grade gases obtained from Phillips Petroleum Company. The stated purities are (see Table I):

Water: Distilled water was used.

Cetane: ($C_{16}H_{34}$) This was obtained from du Pont with a claim of 95 percent purity, the impurities presumably being saturated hydrocarbons having a slightly different number of C atoms (e.g., $C_{15}H_{32}$, $C_{17}H_{36}$, etc.). Attempts at distillation using a packed column appeared to give no improvement in purity as determined by measuring the freezing point. Analysis of the hydrogen atom to carbon atom ratio gave 2.131 compared with 2.125 calculated from the formula.

TABLE I.

Gas	Mol. percent	Probable impurities
Methane (CH_4)	99.59	N_2, ethane, CO_2
Ethane (C_2H_6)	99.69±0.00	Propylene, propane
Propane (C_3H_8)	99.99+	None detected
n-butane (C_4H_{10})	99.78±0.08	Iso-butane
Ethylene (C_2H_4)	99.77±0.01	Propane, CO_2
1, 3-butadiene (C_4H_6)	99.72±0.06	Butene-1, butene-2

[4] W. B. Jones, Jr., Phys. Rev. 74, 364 (1948).
[5] Sutton, Hall, Anderson, Bridge, DeWire, Lavatelli, Long, Snyder, and Williams, Phys. Rev. 72, 1147 (1947).

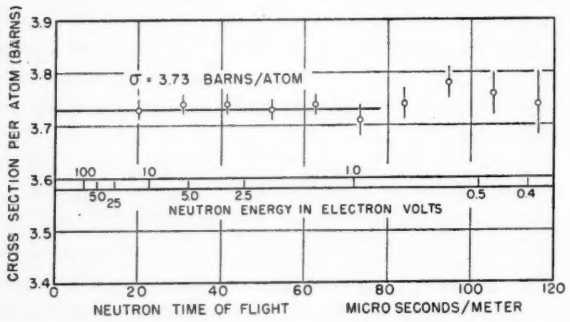
CROSS SECTION PER ATOM (BARNS)
σ = 3.73 BARNS/ATOM
NEUTRON ENERGY IN ELECTRON VOLTS
NEUTRON TIME OF FLIGHT
MICRO SECONDS/METER

FIG. 1. The slow neutron cross section of O_2 gas in the energy interval 0.4 to 15 ev. The sample contained 6.853 g/cm². A standard filter was used.

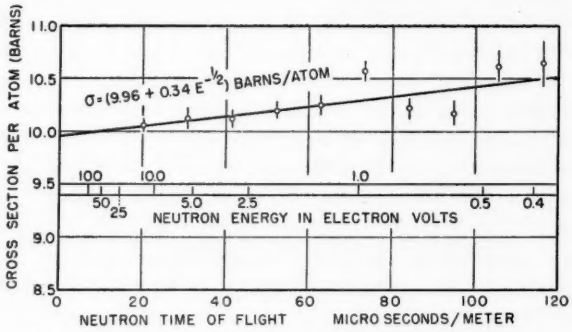
CROSS SECTION PER ATOM (BARNS)
σ = (9.96 + 0.34 E^-1/2) BARNS/ATOM
NEUTRON ENERGY IN ELECTRON VOLTS
NEUTRON TIME OF FLIGHT
MICRO SECONDS/METER

FIG. 2. The slow neutron cross section of N_2 gas in the energy interval 0.4 to 15 ev. The sample contained 2.312 g/cm². A standard filter was used.

Determination of "Sample Thickness"

The important quantity for cross-section calculation characteristic of the samples used is the number of molecules per cm² of area normal to the beam. Since this is most directly associated with the number of g/cm², weighing techniques were preferred over measurement of pressure, thus doing away with the necessity of knowing the exact gas laws. Also, pressure measurements are difficult to make accurately.

For the gas samples containing total weight of sample greater than 100 g (as for O_2, N_2, A), the weight of gas was determined directly by weighing the holder, before and after filling, on a large balance capable of handling 10 kg. Since the cross-sectional area of the holder varied somewhat along the length, the effective area was determined from the volume, measured by weighing water, and the known inside length.

When the total amount of gas sample was appreciably less than 100 g, as was the case for all of the gases containing hydrogen, the above determination was not sufficiently sensitive, and an alternative scheme was used. A small aluminum tank, of known volume and having dimensions and weight suitable for weighing on an ordinary analytical balance, was connected with the gas sample holder and filled with the sample gas at the same time. This allows determination of the density of the gas sample from which g/cm² can be computed using the known inside length of the sample holder.

SLOW NEUTRON CROSS SECTION OF FREE O AND N ATOMS

For the measurements above 0.4 ev neutron energy the cyclotron and detector on times were 64 microseconds. The standard filter technique was used since absolute cross-section values were sought. The results are shown in Figs. 1 and 2.

The molecular effects, which gave rise to the observed $1/E$ slope in the case of H_2, vary inversely as the atomic weight and are undetectable, unless great precision is attained, in the case of O_2 and N_2 as the change in cross section is only a few tenths of a percent. Hence, the usual time of flight abscissa is used on the graphs.

O_2 shows no other effect in this energy region so that the cross section is independent of energy. Using the data above 1 ev, the free oxygen cross section is found to be 3.73 ± 0.04 barns per atom. This supercedes the previously reported value of 3.68.[6,7]

N_2 exhibits neutron capture in the form of a $1/v$ slope. The reactions possible are $N_7^{14}(n, p)C_6^{14}$ and $N_7^{14}(n, \gamma)N_7^{15}$. Nitrogen is one of the very few elements which decay by heavy particle emission following slow neutron capture. For neutron energy above 1 ev the nitrogen cross section is best fitted by:

$$\sigma_N = (9.96\pm0.10+0.34E^{-\frac{1}{2}}) \text{ barns/atom.}$$

The free nitrogen cross section is thus 9.96 barns/atom (replacing the previously reported value of 9.74). The energy-dependent term should be a good measure of the capture cross section as no other significant effects are present in this energy region.

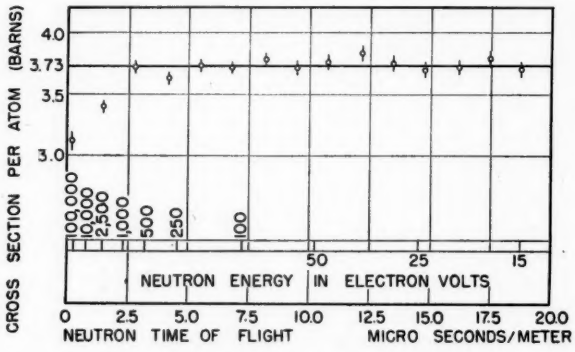

FIG. 3. The slow neutron cross section of O_2 gas above 15 ev using an 8.595-g/cm² sample.

CROSS SECTION OF O, N, AND A FOR NEUTRON ENERGIES GREATER THAN 15 EV

Above 15-ev molecular effects are negligible, and only the nuclear cross sections of the elements present are important. Figures 3–5 show measurements on the elements O, N, and A, respectively, using cyclotron and detector on times of 4 and 8 microseconds. Standard

[6] E. Melkonian, Phys. Rev. 73, 1265A (1948).
[7] Melkonian, Rainwater, Havens, and Dunning, Phys. Rev. 73, 1399 (1948).

filters are not available for this energy region, and the measured cross section values have been increased by 1 to 2 percent to account for the dependence of detector efficiency upon counting rate. In the case of O and N, the constant portions of the curves were adjusted to the free atom values determined previously. Since the free A cross section has not been determined with the aid of standard filters, we may obtain a fairly good value for it from the constant portion of Fig. 5 and get 0.68 barn/atom.

The measured values for the free atom cross sections of O, N, and A are listed in Table II. Expected potential scattering cross-section values calculated from $\sigma=4\pi R^2$ with $R=1.5\times10^{-13}$ A[1] are included for comparison.

Comparing with expected values, the nitrogen value is abnormally high, the argon value abnormally low, while the oxygen value is relatively in better agreement. Interpreting according to the theory of Feshbach, Peaslee, and Weisskopf[8] one would expect that nearby (relative to a very wide level spacing) energy levels are present. For nitrogen the energy level would be at a lower energy and hence would be virtual (i.e., at negative energy). Figure 4 shows that at higher neutron energies, the nitrogen cross section is dropping rapidly to a more normal value. For oxygen, the energy level is again virtual, and Fig. 3 shows a decrease in the cross section at higher energies. The continuation of these trends at still higher energies is shown in the graphs in the review article by Goldsmith, Ibser, and Feld.[9] The nitrogen cross section decreases continuously with increasing neutron energy, and reaches the expected potential scattering value of the cross section at about 1 Mev. The oxygen cross section decreases with increasing neutron energy to about 250 kev, but the potential scattering value of the cross section appears not to be reached. Instead, there are resonances at approximately 450, 900, and 4000 kev. (See, however, the more recent work of Adair *et al.*[10] where the oxygen cross section is found to be approximately constant at 3.8 barns between 20 and 350 kev.) For argon, the energy level must be at higher neutron energies, and Fig. 5 shows a rapid increase in cross section with increasing neutron energy.

TABLE II. Comparison of observed potential scattering values of the free atom cross sections.

Element	σ_{free}	$4\pi R^2$
N	9.96	1.64
O	3.73	1.80
A	0.68	3.31

CROSS SECTION RESULTS TO 0.003 EV NEUTRON ENERGY

Below 1 ev neutron energy, molecular effects are prominent. The following phenomena influence the cross section when a gaseous sample is used:

(1) *Thermal motion:* The thermal motion of the gas molecules gives rise to an increase in cross section with decreasing neutron energy. In the limiting case of low neutron velocity, this effect may be thought of as arising from a preponderance of cases in which neutrons are knocked out of the beam by molecules striking them from behind and from the sides over those cases where a neutron collides with a molecule directly in its path. In this limit of low neutron velocity, the cross section in the laboratory system varies inversely as the neutron velocity.

The above comments apply if the cross section is approximately constant in the relative coordinate system. They do not apply to a $1/v$ type of dependence which is unaffected by translational motion of the gas molecules.

(2) *Inelastic collisions:* When energetically possible, the neutron can be scattered while giving energy up to the molecule in the form of increased vibrational or rotational energy. Molecules in excited vibrational and

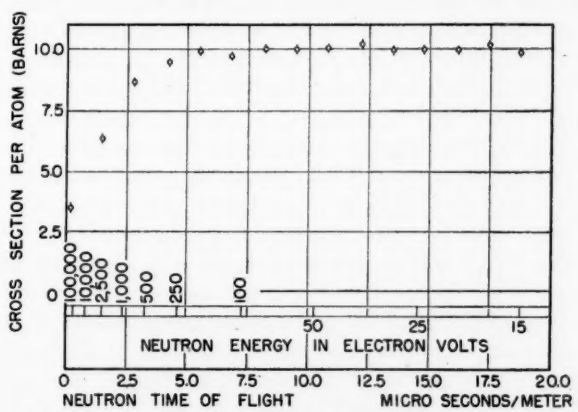

FIG. 4. The slow neutron cross section of N_2 gas above 15 ev using a 3.168-g/cm² sample.

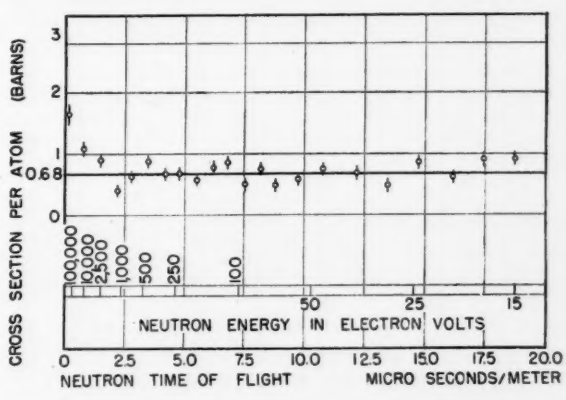

FIG. 5. The slow neutron cross section of A gas above 15 ev using an 11.71-g/cm² sample.

[8] Feshbach, Peaslee, and Weisskopf, Phys. Rev. **71**, 145 (1947).
[9] Goldsmith, Ibser, and Feld, Rev. Mod. Phys. **19**, 259 (1947).
[10] Adair, Barschall, Bockelman, and Sala, Phys. Rev. **75**, 1124 (1949).

rotational states can also scatter neutrons by giving up energy at the expense of excitation energy (so-called hyperelastic collisions). Both of these give contributions to the cross section in addition to the elastic cross section.

(3) *Interference effects:* For neutron wave-length small compared with atomic spacing in the molecule, the total cross section of the molecule is simply the sum of the individual atomic cross sections. However, when the neutron wave-length becomes comparable with the interatomic distances, interference effects between the waves scattered from the various atoms become important. For a diatomic molecule consisting of identical atoms of zero spin, this interference is constructive and at very long wave-lengths leads to a cross section which is just twice the cross section of the molecule at very short wave-lengths. When nuclear spins are not zero and the scattering amplitudes for the various spin orientations are different, or when different atoms are present, the interference effects may increase or reduce the cross section, depending upon the degree of difference (and in particular a difference in sign) of the

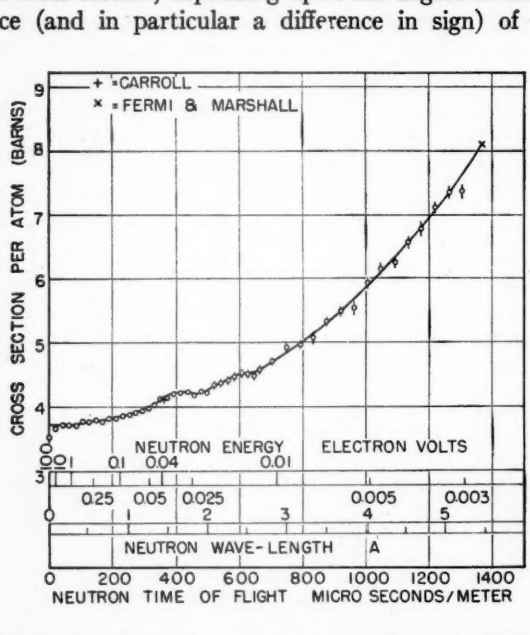
+ = CARROLL
× = FERMI & MARSHALL
CROSS SECTION PER ATOM (BARNS)
NEUTRON ENERGY ELECTRON VOLTS
0.1 0.04 0.01
0.25 0.05 0.025 0.005 0.003
NEUTRON WAVE-LENGTH A
0 200 400 600 800 1000 1200 1400
NEUTRON TIME OF FLIGHT MICRO SECONDS/METER

FIG. 6. The slow neutron cross section of O_2 gas to 0.003 ev. The average of several runs is shown, the samples varying from 6.7 to 8.6 g/cm². For timings greater than 665-microseconds/meter BeO filtering was used in addition to the usual Be filtering.

scattering amplitudes. In the limit of very slow neutrons (and molecules at rest and in the ground state) the cross section of a polyatomic molecule is given by:

$$\sigma = 4\pi\left(\sum_n \frac{m}{m_n} a_n\right)^2,$$

where a_n = scattering amplitude of nth atom (free), m = reduced mass of neutron and entire molecule, m_n = reduced mass of neutron and nth atom. This expression takes into account interference effects and the effect of chemical binding of atoms in the molecule (reduced mass effect). Elastic collisions only are possible in this limiting case as long as the temperature is low enough so that a negligible number of molecules are in excited states.

We now consider the results for the various materials investigated.

O_2: The results are shown in Fig. 6.

Oxygen has negligible capture in this energy region so that almost all of the increase in cross section below 1 ev is due to molecular effects. The oxygen nucleus has no spin and oxygen is predominantly of one isotope so that the interference effect tends to double the cross section at very low energies. The binding effect increases the cross section by six percent.

An additional contribution to the O_2 cross section is believed to be due to the paramagnetism of O_2 which gives rise to an interaction between the magnetic moment of the O_2 molecule and that of the neutron. At sufficiently low energies when the form factor for this effect approaches unity, calculations based on a formula given by Halpern and Johnson show that this interaction should contribute about five barns to the molecular cross section.[11,12]

N_2: The results are presented in Fig. 7.

The cross section for neutron capture contributes an appreciable amount to the total nitrogen cross section in this energy interval. Using the $E^{-\frac{1}{2}}$ slope based on measurements above 1 ev, the capture cross sections per atom are 2.15 and 6.2 barns at 0.025 and 0.003 ev, respectively. The slope below 1 ev is not a good measure of the capture cross section because of the incidence of molecular effects.

The interference effects are influenced by the nuclear spin of one. The binding effect tends to increase the low energy cross section by seven percent.

A: Results for neutron energy less than 1 ev have been published previously.[7] No new measurements have been made. The previous cross section results should be increased uniformly by about 1.5 percent since the standard filter was not used at that time.

H_2: Figure 8 shows the results of measurements.

The rapid increase in cross section at low energies is due primarily to the effect of thermal motion which exhibits its maximum influence in the case of H_2 since it is the lightest molecule. If the H_2 cross section were independent of energy in the absence of thermal translational motion, the cross section would be increased by a factor of 2.4 at 0.003 ev because of it. Actually this assumption is not quite true, and an approximate elimination of the effect of thermal translational motion was made on the assumption that the resulting dependence would be of the form of a constant plus a $1/v$ term. This "corrected" curve is included in Fig. 8 and is seen to be approximately of the form assumed. This curve is expected to be a good approximation to the

[11] O. Halpern and M. H. Johnson, Phys. Rev. **55**, 898 (1939).
[12] O. Halpern, Phys. Rev. **72**, 746 (1947).

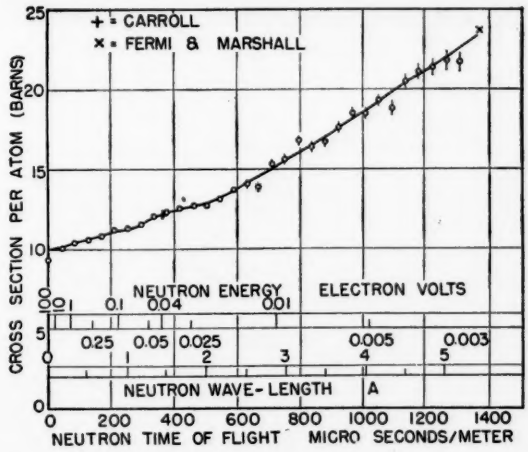
+ = CARROLL
× = FERMI & MARSHALL
CROSS SECTION PER ATOM (BARNS)
NEUTRON ENERGY ELECTRON VOLTS
0.1 0.04 0.01
0.25 0.05 0.025 0.005 0.003
NEUTRON WAVE-LENGTH A
NEUTRON TIME OF FLIGHT MICRO SECONDS/METER

FIG. 7. The slow neutron cross section of N_2 gas to 0.003 ev. For timings less than 665 microseconds/meter a 3.168-g/cm² sample was used; while for greater timings the sample contained 1.840 g/cm².

cross section as a function of relative velocity for neutron velocity equal to or greater than the mean molecular velocity. For lower neutron velocities, however, it should become progressively poorer because it can be shown that at these energies the observed cross section is more a measure of the cross section at neutron velocity equal to mean molecular velocity than of the cross section at the actual neutron velocity.

The reduced mass effect increases the cross section by $(\frac{2}{3}/\frac{1}{2})^2=1.78$. The scattering amplitudes are of different sign for triplet and singlet interaction so that the interference is sometimes constructive and sometimes destructive.

Methane, ethane, propane, n-butane, cetane, ethylene, and 1,3-butadiene: These results, shown in Figs. 9–15, give information concerning the effect of binding of protons in hydrocarbon molecules of varying size and, in some cases, having double bonds. The carbon cross section has been taken as 4.70 barns. For convenient comparison, these curves together with that for H_2 gas are shown together in Fig. 16. Here, approximate elimination of the effect of thermal translational motion has been performed in the way described above in the case of H_2 gas.

In the energy region above 0.1 ev all of the hydrocarbon curves are about the same, indicating that it is the influence of the C—H bond which dominates. At about the energy spacing of vibrational energy levels (0.5 ev) there is a sudden, rapid increase in cross section with decreasing neutron energy. This is probably to be interpreted as the setting-in of the effect of the binding. In the region 0.01 to 0.1 ev the cross sections for a given neutron energy increase in the order of increasing molecular weight. The differences between successively heavier molecules appear to decrease, as expected, although there is some irregularity probably due, in part, to the inaccuracy of the corrections which had to be made since the standard filter was not used for most of these measurements. In particular, the difference between *n*-butane and cetane is small considering the difference in molecular size.

Below 0.01 ev the hydrocarbon curves continue to increase and appear to converge somewhat. Values of cross section approximately four times the free cross section are readily reached, confirming Fermi's prediction of the effect of binding of H in heavy molecules.[13] Bethe has made quantitative calculations concerning the manner in which this binding takes place for neutron energies well below the energies of vibration of the C—H bond.[14] As a model, he considered the proton bound in an anisotropic potential well. His results are shown on the graph for cetane (Fig. 13) and indicate good agreement with the cross section of H in cetaine between 0.01 and 0.1 ev. (Here Bethe's own choice of the values of the vibration wave numbers, 3200 cm^{-1} parallel to the C—H bond and 800 cm^{-1} perpendicular to it, has been used.) Below 0.01 ev the agreement becomes increasingly poorer since Bethe's curve approaches $4\times20.36=81.4$ asymptotically while the experimental curve shows no such tendency.

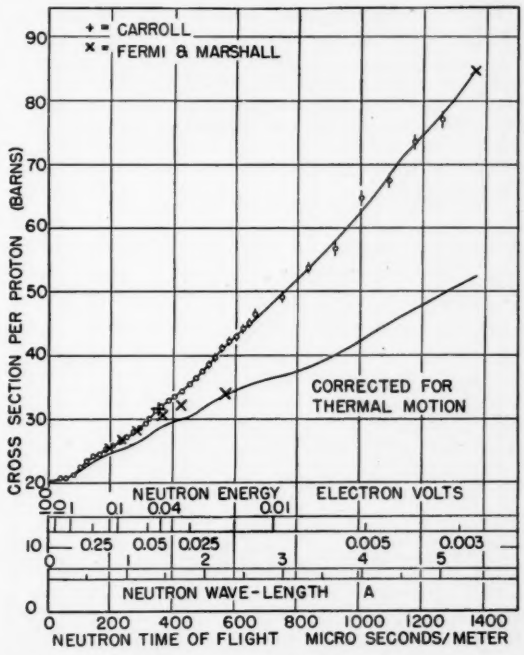
+ = CARROLL
× = FERMI & MARSHALL
CROSS SECTION PER PROTON (BARNS)
CORRECTED FOR THERMAL MOTION
NEUTRON ENERGY ELECTRON VOLTS
0.1 0.04 0.01
0.25 0.05 0.025 0.005 0.003
NEUTRON WAVE-LENGTH A
NEUTRON TIME OF FLIGHT MICRO SECONDS/METER

FIG. 8. The slow neutron cross section of H_2 gas to 0.003 ev. For timings less than 324 microseconds/meter the average of measurements on 0.1417- and 0.0825-g/cm² samples is shown. Between 324 and 665 microseconds/meter a 0.0825-g/cm² sample was used. Beyond 665 microseconds/meter the sample contained 0.0371 g/cm². For timings less than 665 microseconds/meter standard filters were used. For timings greater than 665 microseconds/meter BeO filtering was used in addition to Be filtering.

The major cause of this discrepancy is that the binding of the proton is not to an infinite mass but to a carbon atom which can vibrate with respect to neigh-

[13] E. Fermi, Ricerca Scient. VII–II, 13 (1936).
[14] H. A. Bethe, Rev. Mod. Phys. 9, 69, 117 (1937).

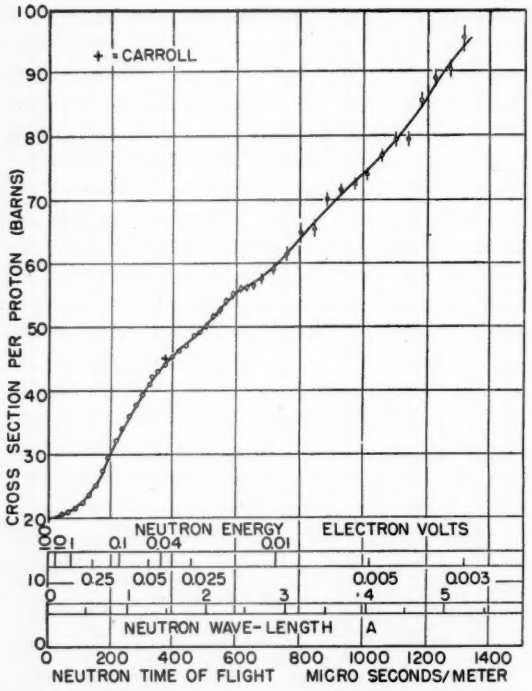
+ = CARROLL
CROSS SECTION PER PROTON (BARNS)
NEUTRON ENERGY ELECTRON VOLTS
NEUTRON WAVE-LENGTH A
NEUTRON TIME OF FLIGHT MICRO SECONDS/METER

FIG. 9. The slow neutron cross section of H in methane gas to 0.003 ev. For timings shorter than 665 microseconds/meter measurements were made on a 0.2462-g/cm² sample using the standard filter technique. The rest of the curve was taken with a 0.2258 g/cm² sample.

boring carbon atoms. In itself, the small weight of the carbon atom tends to make the cross section level off at 3.41 instead of at 4 times the free value. However, for the heavier molecules, many low energy C−C vibra-

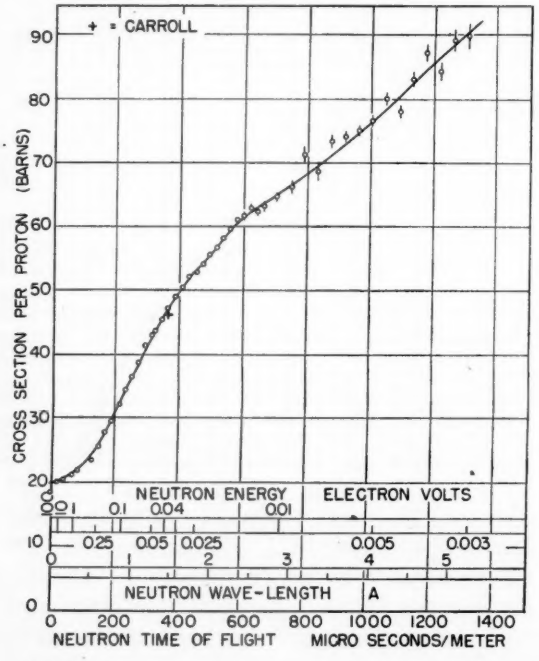
+ = CARROLL
CROSS SECTION PER PROTON (BARNS)
NEUTRON ENERGY ELECTRON VOLTS
NEUTRON WAVE-LENGTH A
NEUTRON TIME OF FLIGHT MICRO SECONDS/METER

FIG. 10. The slow neutron cross section of H in ethane gas to 0.003 ev. A 0.3055-g/cm² sample was used throughout.

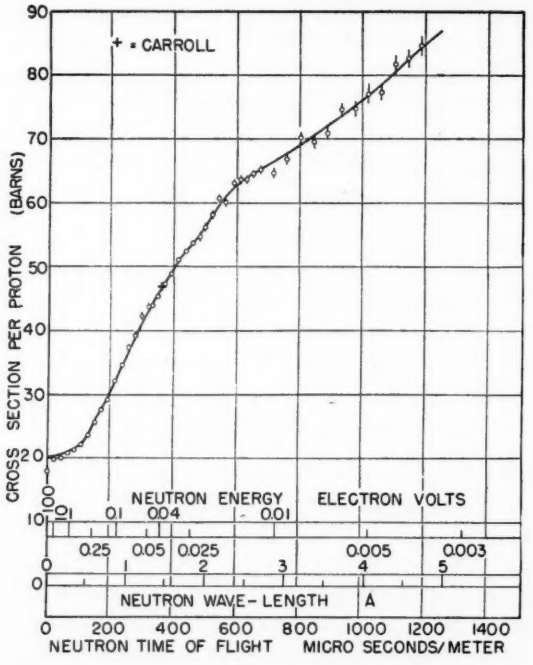
+ = CARROLL
CROSS SECTION PER PROTON (BARNS)
NEUTRON ENERGY ELECTRON VOLTS
NEUTRON WAVE-LENGTH A
NEUTRON TIME OF FLIGHT MICRO SECONDS/METER

FIG. 11. The slow neutron cross section of H in propane gas to 0.003 ev. For timings less than 324 microseconds/meter a 0.7694-g/cm² sample was used, while the remaining data were taken on a 0.2103-g/cm² sample.

tions are possible which give rise to elastic and inelastic scattering and account for the insufficiency of Bethe's

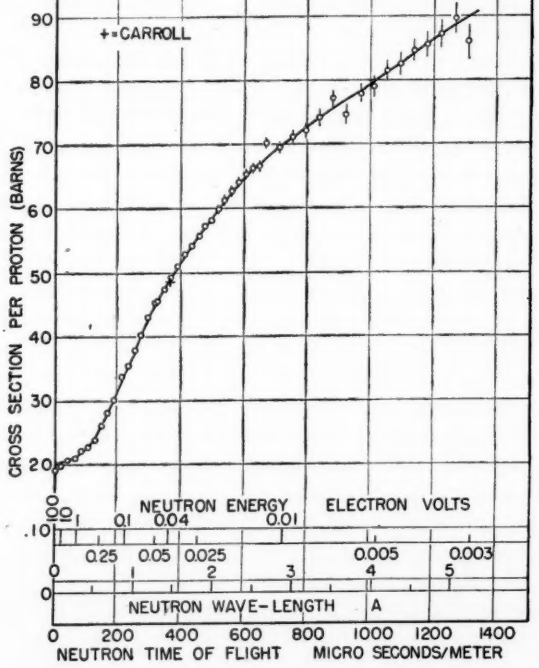
+ = CARROLL
CROSS SECTION PER PROTON (BARNS)
NEUTRON ENERGY ELECTRON VOLTS
NEUTRON WAVE-LENGTH A
NEUTRON TIME OF FLIGHT MICRO SECONDS/METER

FIG. 12. The slow neutron cross section of H in *n*-butane gas to 0.003 ev. A 0.2789-g/cm² sample was used for timings less than 665 microseconds/meter; while beyond this a 0.0808-g/cm² sample was used.

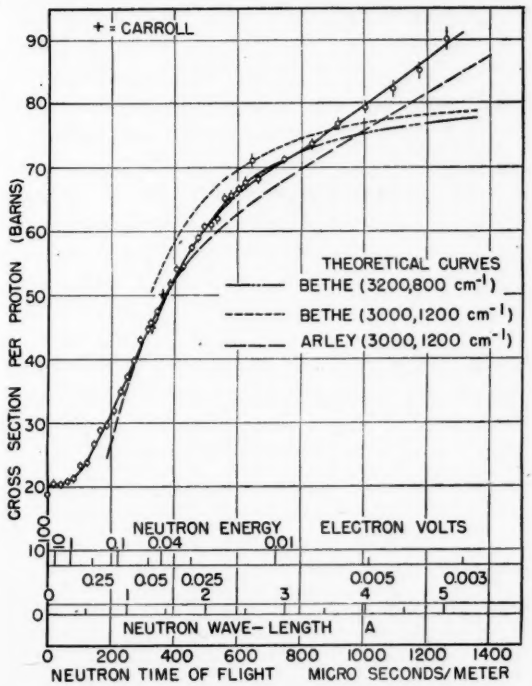

FIG. 13. The slow neutron cross section of H in liquid cetane to 0.003 ev. A 0.2439-g/cm² sample was used. Theoretical curves by Bethe (two choices of vibration frequencies) and by Arley (his own choice of vibration frequencies) are included.

treatment. N. Arley[15] has attempted to take these effects into consideration by using for calculation a model which makes the following assumptions:

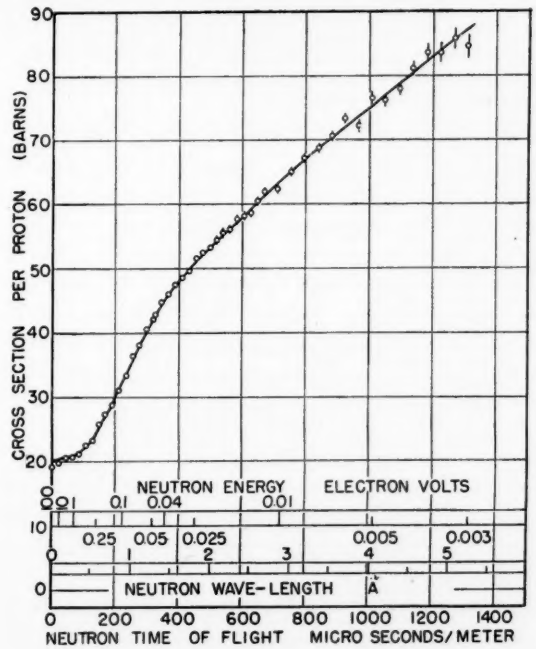
CROSS SECTION PER PROTON (BARNS)
NEUTRON ENERGY ELECTRON VOLTS
NEUTRON WAVE-LENGTH Å
NEUTRON TIME OF FLIGHT MICRO SECONDS/METER

FIG. 14. The slow neutron cross section of H in ethylene gas to 0.003 ev. A 0.3879-g/cm² sample was used.

[15] N. Arley, Kgl. Danske Vid. Sels. Math.-fys. Medd. **16**, 1 (1938).

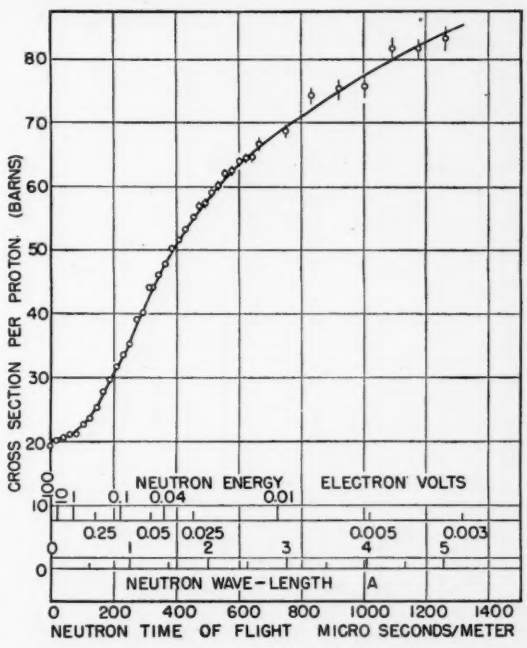
CROSS SECTION PER PROTON (BARNS)
NEUTRON ENERGY ELECTRON VOLTS
NEUTRON WAVE-LENGTH Å
NEUTRON TIME OF FLIGHT MICRO SECONDS/METER

FIG. 15. The slow neutron cross section of H in 1, 3-butadiene gas to 0.003 ev. A 0.4571 g/cm³ sample was used for timings less than 665 microseconds/meter, and for larger timings a 0.3347-g/cm² sample was used.

(1) Each proton is assumed to oscillate independently in an anisotropic harmonic potential. The vibration frequency in the direction along the C—H bond is taken as 3000 cm⁻¹ (0.37 ev)

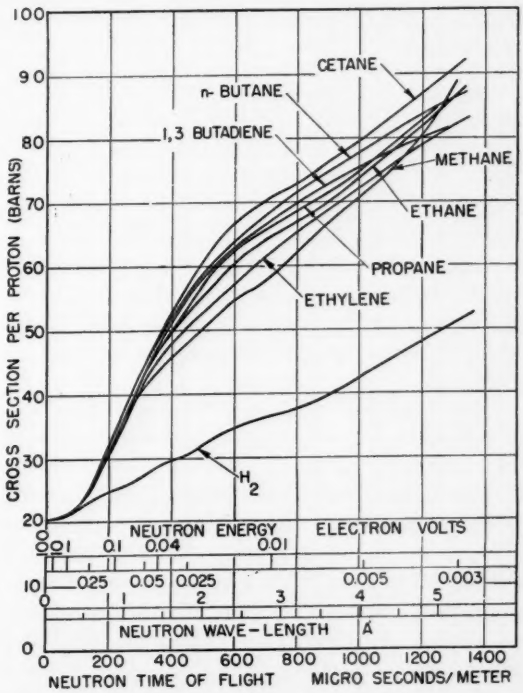

FIG. 16. A composite graph showing the slow neutron cross section of H in the hydrocarbons studied and in H_2 gas. Approximate corrections for the effect of thermal the translational motion have been made for the gas scatterers as described in the text.

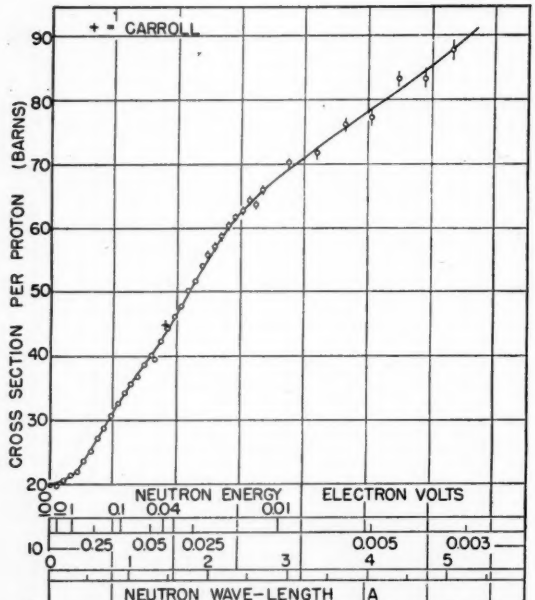

FIG. 17. The slow neutron cross section of H in water to 0.003 ev. A 0.3142-g/cm² sample was used throughout. BeO filtering was used in addition to the usual Be filtering for timings longer than 665 microseconds/meter.

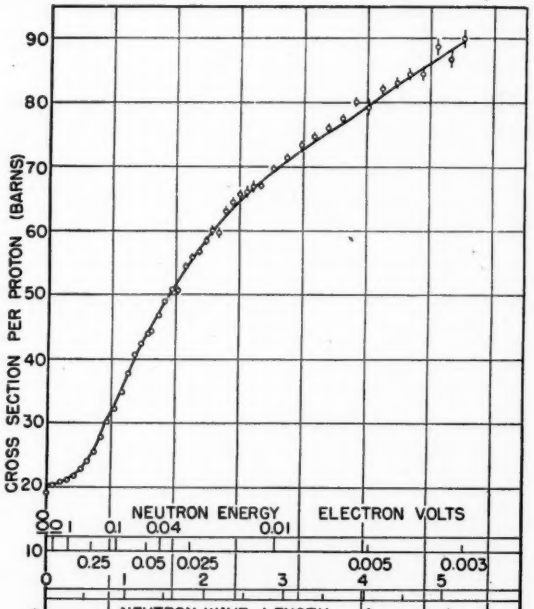

FIG. 18. The slow neutron cross section of H in liquid *n*-butane to 0.003 ev. A 0.272 g/cm² sample was used. The solid curve is that for gaseous *n*-butane.

while 1200 cm^{-1} (0.148 ev) is used for vibrations perpendicular to the C—H bond.

(2) The lower frequencies are taken into account by ascribing an effective mass, chosen as 14 times the neutron mass, to the system consisting of proton plus potential, and assuming that these "molecules" move freely like gas molecules with a Maxwellian distribution.

The results of calculation on the basis of this model are included in Fig. 13. It is seen that the cross section is no longer limited to four times the free cross section as before, but can now follow roughly the experimental curves. Arley's choice of vibration frequencies, somewhat different from that of Bethe, is in better agreement with recently measured values of these frequencies. Figure 13 includes a curve based on Bethe's theory but using Arley's figures. This does not agree as well with the cetane curve, but quantitative agreement is not to be expected.

There are other small effects which have not yet been taken into account. The binding of the carbon atom should contribute about 0.4 barn. Coherent scattering from the spinless carbon atoms should become increasingly important with increasing neutron wavelength and with increase in the number of carbon atoms in the molecule. Interference of the scattered neutrons from protons should add only a little to the cross section since singlet and triplet scattering amplitudes have opposite sign.

H_2O: The results, given in Fig. 17, look similar to those for the heavier hydrocarbons. The oxygen cross section has been taken as 3.73 barns.

Liquid n-butane: The direct determination of g/cm² was difficult and proved to be unreliable. The measured value was increased by 3.5 percent to make the cross-section curve give the correct value of the free proton cross section above 1 ev. The results are shown in Fig. 18. The solid curve of this graph has been taken from Fig. 12 and indicates that there is no significant difference between liquid and gaseous *n*-butane so far as neutron cross-section measurements are concerned.

Comparison with Previous Measurements

Numerous transmission measurements have been made using the neutrons absorbed by cadmium (*C* neutrons). Previous experience[2] indicates that the effective energy is not $kT=0.025$ ev as was supposed, but that when 0.04 ev is assumed agreement with spectrometer data is usually good. Carroll[16] made measurements of this kind on numerous gas, liquid, and solid scatterers. His observed cross-section values are plotted at 0.04 ev neutron energy on the corresponding graphs. Agreement is very good in general. Numerous measurements with *C* neutrons have been made on paraffin.[16,17] Carroll's[16] value of 49.8 ± 0.2 is typical of the best measurements. The only comparable measurement of the present investigation is that for cetane which gives 48.8 at 0.04 ev.

Two comparable sets of measurements have been made using neutron velocity spectrometers of the cyclo-

[16] Henry Carroll, Phys. Rev. **60**, 702 (1941).

[17] Dunning, Pegram, Fink, and Mitchell, Phys. Rev. **48**, 265 (1935). Goldhaber and Briggs, Proc. Roy. Soc. **A162**, 127 (1937). G. A. Fink, Phys. Rev. **50**, 738 (1936). Powers, Goldsmith, Beyer and Dunning, Phys. Rev. **53**, 947 (1938).

tron arc modulated type. Jones has reported measurements on water over the same energy range covered here.[4] His cross-section results are consistently lower than those of Fig. 17. For neutron energies greater than 0.005 ev this discrepancy amounts to only a few percent and may be attributed to difficulties of making absolute measurements. At lower energies, however, this difference becomes worse and reaches 10 percent at 0.003 ev. The larger cross-section results are probably more reliable because all known difficulties of measurement tend to give too low a value for the observed cross section. Rainwater, Havens, Dunning, and Wu have published spectrometer measurements on paraffin.[2] Between 0.05 and 0.005 ev their results are in agreement with Bethe's curve (with his own choice of vibration frequencies) which is shown in Fig. 13.

Using a crystal spectrometer Fermi and Marshall[18] have investigated H_2 gas at room temperature and at 83°K from 0.75 to 2.5A neutron wave-length. Their results for the gas at room temperature are included in Fig. 8 and indicate good agreement with the present measurements for wave-lengths shorter than 1.2A. At longer wave-lengths, however, there is a marked discrepancy. Again the larger values for the cross section are likely to be more reliable.

Fermi and Marshall[18] have also measured the cross section of O_2, N_2, and H_2 gases for neutrons filtered through BeO. They initially reported the effective wave-length of these neutrons as 5.1A, and their measured cross-section values were about 10 percent larger than the present results as the stated wave-length.[7] In a subsequent report,[19] however, they gave 5.43A as the effective wave-length. This value has been used in plotting their results on Figs. 6–8. The agreement is now much better.

ACKNOWLEDGMENTS

The author wishes to express appreciation to Professor J. R. Dunning who suggested this problem, and to Professors L. J. Rainwater and W. W. Havens, Jr., who took an active interest in the experiments and made numerous invaluable suggestions. Thanks are also also due to Professor T. I. Taylor for the mass-spectrographic analyses of some of the gas samples; Drs. G. Placzek, H. A. Bethe, and O. Halpern for interesting discussions on several points; and Miss Miriam Levin and members of the cyclotron staff for assistance in making some of the measurements. The author also wishes to thank the AEC whose support made these researches possible.

[18] E. Fermi and L. Marshall, Phys. Rev. **71**, 666 (1947).

[19] E. Fermi and L. Marshall, Phys. Rev. **75**, 578 (1949).

PHYSICAL REVIEW VOLUME 76, NUMBER 12 DECEMBER 15, 1949

The Stopping Power for Protons in Several Metals*

S. D. WARSHAW**
Institute for Nuclear Studies, University of Chicago, Chicago, Illinois
(Received August 15, 1949)

The rate of energy loss of low velocity (i.e., from 50 to 400 kev) protons has been measured in five different stopping materials: Be, Al, Cu, Ag, and Au. Agreement with previous measurements at higher velocities (greater than 400 kev) is good where such measurements have been published. The stopping measurements were made on foils prepared by an evaporation technique and are believed to be more accurate than measurements made on the usual (hammered or rolled) foils; the results give a value for stopping about 15 percent higher (in Au) and about 7 percent lower (in Al) than those published by Wilcox. A comparison to existing theory at very low and at high velocities (the critical velocity being defined as $e^2/\hbar$) was made with good agreement shown at the low end. The high end theory is of doubtful validity and gives a stopping power about 10 percent higher than observed. It is argued that this discrepancy cannot be accounted for by a proton charge less than unity due to the electron capture-loss process.

I. INTRODUCTION

SEVERAL recent discussions[1] of the stopping power for charged particles in the low velocity region make an experimental determination interesting from a theoretical point of view. An adequate theory of stopping power, in the region where ionic velocity becomes comparable with the orbital electronic velocity, does not really exist. The measurements that will be reported on in this paper are, therefore, compared to qualitative extensions of a familiar theory that is valid at very high proton energies, but rather less accurate for energy about 500 kev—and quite invalid below this point. A recent argument that should be valid in the region of "adiabatic" collisions, i.e., below about 15 kev, will also be discussed. The particular metals on which

* This work was supported by the Joint Program of the ONR and the AEC.

** Present address: Department of Physics, University of Southern California, Los Angeles, California.

[1] E. Fermi and E. Teller, Phys. Rev. **72**, 399 (1947); N. Bohr, Kgl. Danske Vid. Sels. Math.-fys. Medd. **18**, 8 (1948) (this work will be referred to as (N.B.) in the following); see also J. Knipp and E. Teller, Phys. Rev. **59**, 659 (1941).

stopping measurements have been made have been selected to cover a wide range in nuclear charge so that the resulting stopping curves should be of use to workers in the field of nuclear reactions involving thick targets.

Wilcox[2] has previously utilized the advantages of the Allen-type electron multiplier tube to determine the rate of energy loss for several light nuclei in gold and aluminum. However, one of Wilcox's results was a slight mass dependence in the stopping power, and while the failure to verify this result has been discussed elsewhere,[3] it was thought worthwhile to obtain again the stopping curves for protons in both of these metals.

The cross sections for proton energy loss in beryllium, copper, and silver have also been determined here, for energies less than 400 kev.

II. TECHNIQUES

The method for obtaining particles and obtaining data is essentially the same as described by Wilcox,[2] but the type of foils used is different.

A. Procedure

The source of energetic protons was the "kevatron" (400 kev Cockcroft-Walton circuit accelerator) which is described elsewhere.[4] After magnetic analysis, the beam of protons was allowed to strike a beryllium target button onto which was evaporated a very thin coat of gold. The protons which scattered from the gold then had an energy $E_0=196/198\ E_B$, where E_B is the accelerator voltage, with a negligible smearing due to the degradation in the thin layer. After 90° scattering and collimation, the protons (*a*) passed through an energy analyzer equipped with an Allen-tube detector, giving the initial energy, E_0, or (*b*) first passed through the thin metal foil mechanically interposed between the collimating slit and the entrance to the analyzer, giving the final energy E_f. The loss of energy in the foil is then E_0-E_f.

One technical difficulty, mentioned by Wilcox, was the progressive carbonization of target and foil by diffusion pump oil. This has been completely eliminated by the installation of a new pumping system, which pulls only through a large liquid-air trap provided with an extensive amount of baffling. It should be remarked here that, generally simultaneously with the appearance of oil on the target, the stopping power of the foils increased considerably; moreover, the carbonization did not necessarily take place at a constant or even a slow rate (an assumption made by Wilcox in correcting for this).

B. The Foils and Their Use

After many non-reproducible measurements using commercial (hammered and rolled) gold and aluminum foils, it was decided that the main difficulty was non-uniformity of the foils. For example, although such foils may sometimes be quite uniform, I am informed[5] that a non-uniformity of ±10 percent, or worse, of the average thickness over several square centimeters may be generally expected in hammered gold foil; rolled aluminum is much worse. It is believed that this was the principal reason for the mass dependence determined by Wilcox.

Therefore the foils used in these determinations were prepared by an evaporation technique described in detail elsewhere.[6] (Briefly, this amounts to evaporating the metal in vacuum onto a plate coated with an organic plastic, stripping the metal with its plastic backing from the glass, and dissolving the plastic.) The measurement of thickness was done interferometrically, i.e., the actual thickness of the foil in centimeters was obtained first, and converted to surface density by use of the bulk density of the metal. A possible objection to this is that the bulk density, because of porosity in the evaporated metal, is not appropriate. However, it is unlikely that the values are off by more than 4 percent and they are conceivably much better. To check this, for present purposes, four rolled and two evaporated foils were used to determine the stopping power in aluminum. The surface densities of the commercial foils were determined by accurately weighing known areas (about 50 cm^2). The resulting curves from the commercial foils deviated as much as 30 percent from the average curve. On the other hand, data from both of the evaporated foils fell on the same curve (within the standard deviation of all points) and furthermore within 8 percent of the average of the curves obtained from the commercial foils.

The two beryllium foils used[7] were prepared by an evaporation somewhat different from the one described above, and a spectro-chemical determination of the mass of beryllium corresponding to an accurately known area of foil was used for the thickness measurement. This procedure was necessary because the foils were small, irregularly shaped, very fragile, curled up pieces. The area measurement consisted of dropping a piece on the surface of still water, which immediately flattened it out, and bringing a clean glass plate up from underneath the floating foil; the metal adhered closely and smoothly to the glass surface. The outline of the piece of foil was then carefully traced several times on a sheet of heavy translucent paper, and a "gravimetric integration" performed. (The internal probable error of such area measurements was about 1.5 percent.) Then

[2] H. Wilcox, Phys. Rev. **74**, 1747 (1948).
[3] T. A. Hall and S. D. Warshaw, Phys. Rev. **75**, 891 (1949).
[4] L. del Rosario, Phys. Rev. **74**, 304 (1948).

[5] By H. C. Anderson of Hastings and Company, Inc., manufacturers of the gold leaf used.
[6] S. D. Warshaw, Rev. Sci. Inst. **20**, 623 (1949).
[7] I am indebted to H. Bradner at Berkeley for sending several batches of these, and to N. Nachtrieb of the Institute for the Study of Metals for performing the chemical determination. The only reason for the change in technique in the case of beryllium was that the foils were available and measured before the other technique was developed. See Fred, Nachtrieb, and Tomkins, J. Opt. Soc. Am. **37**, 279 (1947) for the chemical method.

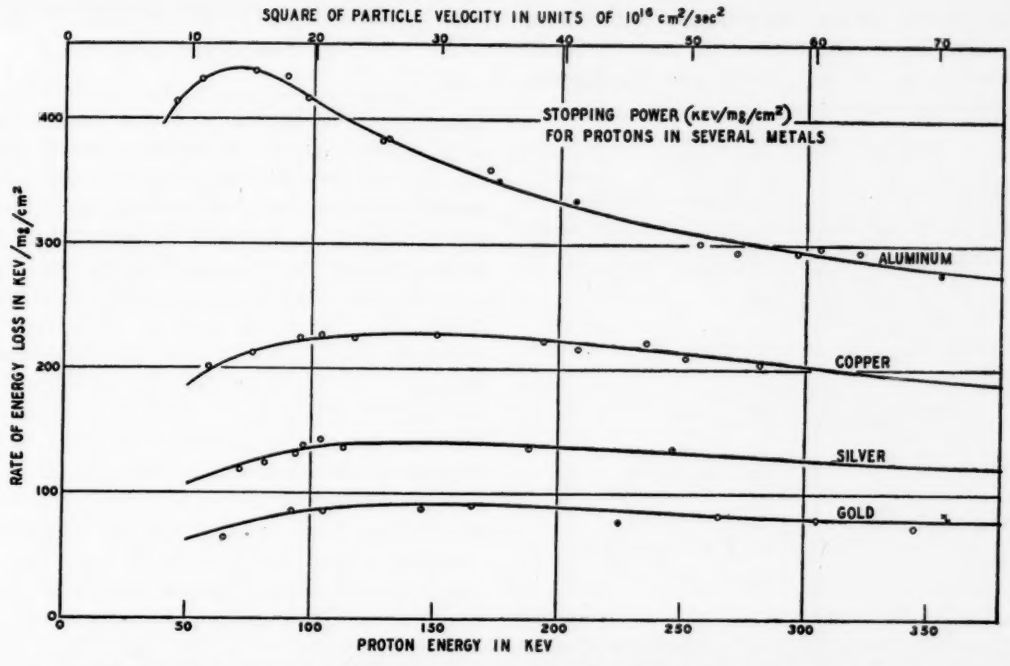

FIG. 1. The stopping power (unit thickness equals 1 mg/cm²) for gold, silver, copper, and aluminum. The few black dots on the gold and aluminum curves are points taken on hammered or rolled foils and normalized to the data from the evaporated foils. The crosses on the gold curve are points measured by Huus and Madsen.

the metal was dissolved off the plate by acid immersion and chemically analyzed. It was assumed here (and also for the interferometer technique) that the pieces of foil used for thickness determination had the same thickness as the piece used for stopping measurements, since they were prepared in the same evaporation.

C. Errors

The quantities measured in this determination, with their probable errors, are:

1. The initial energy E_0 (± 1.0 percent) kev,
2. The final energy E_f (± 1.0 percent) kev,
3. The foil surface density τ(± 2.5 percent) mg/cm².

The errors in the energy measurements, as stated, are actually slightly pessimistic. There is, first, a possible (but certainly small) uncertainty in the analyzer constant k,[8] and a possible uncertainty in the "peak height position" due to the finite window curve of the analyzer. The window width is $0.025E$ and the error in obtaining the peak height position is better than 10 percent of the window, so that this uncertainty is better than $0.0025E$. The analyzer voltage was measured by obtaining the current drain through a 50 meg$\pm$0.1 percent resistor stack in parallel with the analyzer plates; the drain was measured with a Weston d.c. milliammeter with a rated accuracy of one-half percent at full scale. Then the maximum uncertainty in the energy measurement is obtained by adding the independent errors without regard to sign; thus, $0.0025+0.001+0.005+0.005=0.013$. The probable error is, of course, 0.2 percent and we take the energy uncertainty as 1 percent for a safe figure. The uncertainty in the foil thickness is discussed above. If porosity is present, the thickness error should more properly be 1.5 percent, -4 percent, but the figure 2.5 percent was chosen because of the internal consistency mentioned in B above. (Actually, each of the two sets of data taken on the two evaporated Al foils differed from the average fitted curve including both sets by a standard deviation of better than 2 percent.)

The average energy loss is then taken as

$$\frac{E_0(1\pm 0.01)-E_f(1\pm 0.01)}{\tau(1\pm 0.025)}=\frac{\Delta E}{\tau}\pm 4.5 \text{ percent.}$$

(However, the standard deviation of points on all the curves from the graphically fitted curves was better than 2.5 percent. Hence, although the absolute heights may be in, say, 4 percent error, the shapes are quite accurate.) This average rate can be properly identified with the true, or instantaneous rate of loss, dE/dx, at the arithmetic average energy $\bar{E}=1/2(E_0+E_f)$, only if ΔE is very small. For some portions of the curve, the loss is of the order of one-third to one-half of the initial energy, however, and here a correction is required. This correction will turn out to be actually smaller than the errors inherent in the measurements; however, it is still significant since it can change the qualitative appearance of the curve.

[8] Defined by the expression $E=kV$, where V is the voltage (in kilovolts) necessary to produce maximum counting at the detector end of the instrument, and E (in kev) is the proton energy. For the analyzer used, $k=19.5$.

For the correction we may use a simple, linear extrapolation to zero foil thickness. Assume that in a small enough interval, the stopping curve can be approximated by a straight line,

$$-dE/dx=\lambda(E-E_0)-L_0, \tag{1}$$

where $-dE/dx$ is the true rate of loss, λ a constant and $-L_0$ the initial rate of loss; at energy E_0, $x=0$; at E_f, $x=\tau$. On rearrangement, (1) becomes

$$dE=L_0e^{-\lambda x}dx,$$

and integrating this over the foil gives, on rearrangement,

$$L_0=\Delta E/\tau(\lambda\tau/e^{\lambda\tau}-1). \tag{2}$$

The loss at $E=\bar{E}$, combined with (2), gives

$$\left.\frac{dE}{dx}\right|_{\bar{E}}=\frac{\Delta E}{\tau}\frac{\lambda\tau}{2}\coth\frac{\lambda\tau}{2}\approx\frac{\Delta E}{\tau}\left(1+\frac{(\lambda\tau)^2}{12}\right) \tag{3}$$

for small $\lambda\tau$. For the correction to be as much as, say, 2 percent, we must have $\lambda\tau\gtrsim 1/2$. Since the effect is, therefore, small ($\lambda\tau\ll 1$ in every case) the procedure was to plot the curve $\Delta E/\tau$ *versus* $\bar{E}$, determine λ from this curve in the neighborhood of each observed point, and correct the ordinates of each point by the factor in (3) to obtain dE/dx. The largest correction that was applied was one-half percent at the low energy end of the silver curve where $\lambda\tau=0.25$ (for $\tau=0.270$ mg/cm^2).

III. RESULTS AND CONCLUSIONS

A. Description of Results

The measured stopping curves for aluminum, copper, silver, and gold are given in Fig. 1, and for beryllium—in a separate graph for convenience in plotting—in Fig. 2; these give the loss in kilovolts per milligram per square centimeter *versus* the proton energy in kilovolts, and a velocity square scale is included at the top of each figure for convenience. The few black dots in the aluminum and gold data represent points from the data taken on commercial foils of essentially arbitrary thickness, and normalized to the data taken on the evaporated foils; the points used for normalization are not shown. There is no distinction made in Fig. 1 between the two evaporated foils used (0.146, 0.193 mg/cm^2) in the aluminum determination.

It should be pointed out that the gold curve (Fig. 1) is somewhat higher than either the "deuteron" or the "proton" curve published by Wilcox.[2] The aluminum curve, well-verified on several foils, is about 8 percent lower, at 300 kev, than the equivalent curve given by Wilcox.

Figure 3 gives the proton stopping power in electron volts per atom per square centimeter, extrapolated to 600 kev; those are constructed from the smooth curves of Figs. 1 and 2, with the aid of some of the conversion factors listed in Table I.

The extrapolation was carefully done by extending each of the curves in Fig. 3 (except that for gold) to a

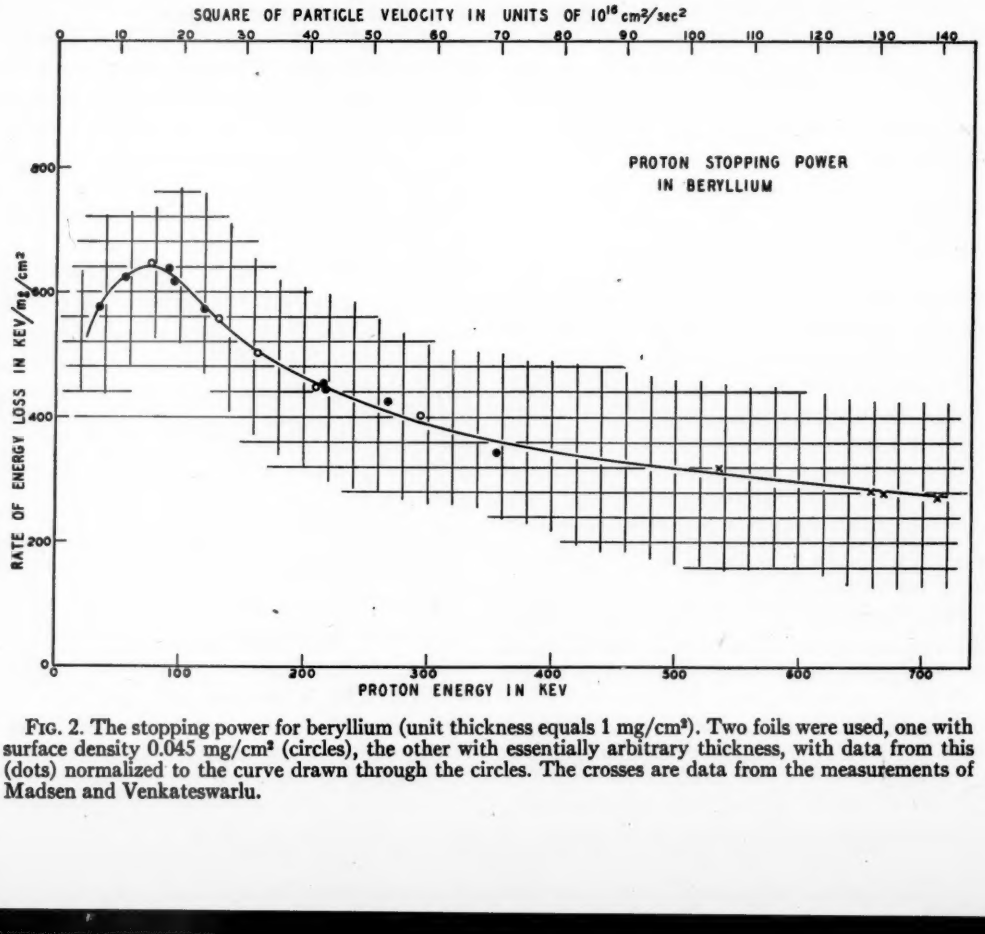

FIG. 2. The stopping power for beryllium (unit thickness equals 1 mg/cm^2). Two foils were used, one with surface density 0.045 mg/cm^2 (circles), the other with essentially arbitrary thickness, with data from this (dots) normalized to the curve drawn through the circles. The crosses are data from the measurements of Madsen and Venkateswarlu.

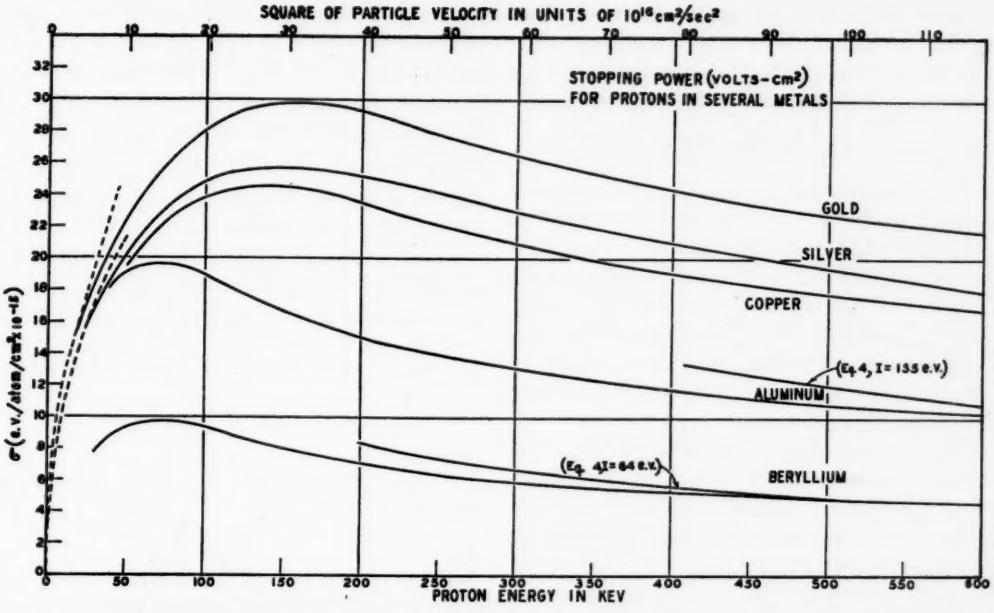

FIG. 3. The stopping power (unit thickness equals 1 atom/cm²) constructed from the smooth curves in Figs. 1 and 2. (Experimental points are not shown.) For comparison with existing theory, Eq. (4) is plotted for aluminum and beryllium using appropriate values for I, and the Fermi-Teller equation (Eq. (5)) is shown dotted for gold and silver.

high enough energy so that the familiar theoretical formula[9]

$$\sigma=\frac{4\pi e^4 Z}{mv^2}\left(\log\frac{2mv^2}{I}-\frac{C_K}{Z}\right)(\text{erg/atom/cm}^2), \qquad (4)$$

TABLE I. Conversion factors for stopping power.

Given \ Result	kev/mg/cm²	ev/atom/cm²	erg/cm
kev/mg/cm²	Au 1	0.327×10^{-15}	3.09×10^{-5}
	Ag 1	0.178	1.69
	Cu 1	0.105	1.43
	Al 1	0.045	0.44
	Be 1	0.015	0.30
ev/atom/cm²	3.06×10^{15}	Au 1	9.48×10^{10}
	5.35	Ag 1	9.48
	9.58	Cu 1	13.53
	22.32	Al 1	9.67
	66.76	Be 1	19.79
erg/cm	3.24×10^{4}	1.06×10^{-11}	Au 1
	6.30	1.06	Ag 1
	7.01	0.74	Cu 1
	23.10	1.03	Al 1
	33.74	0.51	Be 1

TABLE II. Excitation potentials for the elements used.

Metal	*Be	Al	Cu	Ag	Au
I(kev)	0.064	0.155	0.320	0.490	0.780

*I_{Be} is taken from Madsen's data.

[9] M. S. Livingston and H. A. Bethe, Rev. Mod. Phys. 9, 264 (1937). C_K is a correction for strong binding in the K-shell and given graphically by these authors. Z is the atomic number of the stopping material, v the proton velocity, m the electron mass, and e the charge on the electron.

would be valid, and smoothly joining the extrapolated experimental curves to Eq. (4) calculated using values of the average excitation potential I given in Table II.[10]

Pieces of beryllium foils from two different evaporations were used; the result of the chemical determination gave for one foil (circles in Fig. 2) a surface density of 0.045 ± 3.5 percent mg/cm², with the error obtained from measurement of three separate pieces, and four chemical runs on each piece. Unfortunately, only a few very small pieces were available for determining the thickness of the other foil used, and the deviation from average of the two pieces used was about 15 percent; since the average itself (0.054 mg/cm²) was about 20 percent too low to fit either the curve of the other foil, or previous measurements at higher energies, the data from this foil were normalized to the other (these points shown as black dots in Fig. 2). The resulting curve can be seen to fit the higher energy data of Madsen and Venkateswarlu[11] (crosses) quite well, thus verifying their measurement of the mean excitation potential and corroborating a theoretical[12] estimate ($I_{\text{theory}}=60$ ev) which was supposed to account for lattice effects.

Since the theoretical curve (4) can be expected to be valid only well above its position of maximum loss, given by 1250 I kev, the extrapolation for gold means an extension from 400 kev to several million volts! Fortunately, however, data taken by other workers[13]

[10] M. G. Mano, Comptes rendus 197, 319 (1933).
[11] C. Madsen and P. Venkateswarlu, Phys. Rev. 74, 648 (1948).
[12] A. Bohr, Kgl. Danske Vid. Sels. Math.-fys. Medd. 24, 14 (1948).
[13] T. Huus and C. B. Madsen, Phys. Rev. 76, 323 (1949).

has recently been published for gold (crosses in the gold curve of Fig. 1) which, in view of the good agreement (within 2 percent) with these measurements, establishes the stopping power for gold very well.

B. Comparison with the Theory

As pointed out in the introduction, there exists no adequate theory that can account for all the features of the curves in Fig. 3. The best that can be done would be to compare the high, and low, energy region extrapolations of these curves with existing theory. This procedure is useful, first to verify a previously unverified low energy equation for stopping, second to verify a rough treatment of stopping valid in this high (i.e., 300 to 600 kev) energy region but only for the heavy elements, and third, to provide a convenient check on the experimental consistency since Eq. (4), with the values of I in Table II, represents a survey of all previous high energy experimental data. The third point has already been commented on in part A above.

A simple argument based on the Thomas-Fermi model has been given by Fermi and Teller[1] which should account for the electronic stopping at proton velocities much less than the electron orbital velocity, i.e., from zero energy to about 20 kev. Their expression, in slightly different form than originally given, is

$$-\frac{dE}{dx}=\frac{4}{3\pi}\frac{E}{vt_0}\log\frac{137v_m}{c}(\text{erg/cm}), \tag{5}$$

where t_0 is a collection of constants (including the proton mass; $t_0=44.16\times10^{-15}$ sec.), v_m is the Fermi velocity, and c the velocity of light. Notice that the entire effect of the character of the stopping material is in the logarithmic factor (and in the density factor from Table I to convert to volt-square centimeters).

Superimposed on the electronic stopping is a nuclear stopping term. For the elements involved, and in this region of energy, direct calculation of an expression for this effect given by Bohr (N.B. Eqs. (2), (3), (9)) shows it to be negligibly small.

The result of calculating (5) is shown dotted in Fig. 3. (For clarity of the figure, copper is not shown.) The experimental data have been extrapolated downward and can be seen to join smoothly onto the dotted curve at about the energy that represents the approximate limit of validity of Eq. (5). While the agreement with the theory therefore happens to be quite good, it should be emphasized that a small change in the fit of the experimental curves for energy in the neighborhood of 70 kev can change this agreement so that it is only fair.

At higher energies we might expect that Eq. (4) would be valid, at least for aluminum and beryllium. Indeed, it is argued (N.B. Chapter 3) that (4) should be quite accurate whenever the parameter,

$$\kappa=\frac{2v_0}{v},\quad v_0\equiv e^2/\hbar,$$

is much smaller than unity, while the argument of the logarithmic factor in (4) remains large. For 500 kev protons, $\kappa=0.46$, while in aluminum $2mv^2/I=7$. On the other hand, (4) fits the data quite well at 500 kev in the case of beryllium, where $2mv^2/I=17$. The second criterion would thus seem to be stronger.

However, a possible discrepancy between the calculated and observed curves in this region might be due to an effective proton charge less than unity, due to an equilibrium between electron capture and loss by the moving proton. This effect can be estimated simply as follows. Let σ_c, σ_l be the cross sections for capture and subsequent loss, respectively, of an electron by the proton. Then, if σ_0 is the stopping power for neutral hydrogen and σ_1, for a unit-charged proton, the net stopping power is

$$\sigma_{\text{net}}=\frac{y}{1+y}\sigma_0+\frac{1}{1+y}\sigma_1,$$

where $y=\sigma_c/\sigma_l$.

Now, in the derivation[14] of Eq. (4) the final expression prior to (4) itself (ignoring C_K) is

$$\sigma=Z\frac{4\pi e^4}{mv^2}\int_{K_{\min}}^{K_{\max}}\frac{dK}{K}, \tag{4'}$$

where K is the difference between the initial and final wave-number vectors of the incident particle, $K_{\min}=\Delta E_{0n}/\hbar v$, $K_{\max}=2mv/\hbar$, and $\Delta E_{0n}=E_0-E_n$ is the difference in binding energies of the electron in the stopping material, excited by the moving incident particle from the ground level to the nth level. Equation (4') should, of course, be properly summed over all n, and all electrons; to a reasonable approximation, this is equivalent to replacing ΔE_{0n} by I. The significant point in (4') is that the integrand contains, implicitly, an excitation cross section, and therefore the square of the matrix element between initial and final states; in (4') the potential used was a Coulomb interaction between the proton and stopping electron. For the case of neutral hydrogen, the potential is of the form

$$V(R)=(1/R)e^{-2\alpha R}\cdot(1+\alpha R),$$

which is the average potential at a field point R measured from the proton at the origin with an electron in a $(1s)$-state moving at the Bohr radius $a_0=1/\alpha$. If this potential is used in place of the Coulomb potential, then the only change in the result (4') will be the introduction of a factor

$$\left(\frac{K^2}{4\alpha^2+K^2}+\frac{2\alpha^2K^2}{(4\alpha^2+K^2)^2}\right)^2$$

in the integrand. The integration is straightforward but tedious and the result is that in beryllium, the ratio σ_0/σ_1 is very nearly constant in the range 250 to 700 kev, and equal to 0.46. This means, that, very nearly,

$$\sigma_{\text{net}}=\frac{0.46y+1}{y+1}\sigma_1$$

with σ_1 given by Eq. (4).

The discrepancy at 350 kev, between the calculated and observed curves for beryllium, is about 10 percent; in order to account for this by the capture-loss process, we must have $y\doteq0.2$. But reasonable estimates by Bohr for σ_c and σ_l give[15]

$$y=\frac{Z}{Z^2+Z}(v_0/v)^4=(v_0/2v)^4.$$

Direct calculation of σ_{net} with this expression shows that the

[14] H. A. Bethe, Ann. d. Physik 5, 325 (1930).

[15] N.B. Eqs. (4.2.4), (4.3.5). σ_c is really valid only for heavier elements than beryllium, but the estimate of σ_l is good. The exponent is probably smaller than four but greater than three. In the case of aluminum, Bohr estimates a more rapid variation: $y=(4/Z^{\frac{1}{3}})(v_0/v)^5=(v_0/0.9v)^5$, somewhat more accurately than the corresponding result for beryllium.

change of charge effect can account for only a small part (i.e., less than one percent) of the stopping discrepancy. However, work now in progress on measurements of σ_c and σ_l, to be published by T. A. Hall, may modify this argument.

In the heavier elements Bohr (N.B. Chapter 3) attempts qualitative explanation for the somewhat different velocity dependence apparent in the region above the maximum (Fig. 3). The argument is based on the statistical model, i.e., it accounts for the stopping power due to electrons which actually are moving slower than the incident particle by introducing an appropriate electron density function into an expression like (4). However, since (4) itself cannot be very accurate in this energy region, even for the slowest electrons, this procedure should give only qualitative agreement, at best, with experiment. Using the statistical model for the number of electrons in the stopping atom with velocities less than u_s, Bohr puts

$$n(u_s)=Z^{\frac{1}{2}}(u_s/v_0).$$

For $u_s=v$, this means that roughly 20 percent of the electrons in gold, 30 percent in silver, and 45 percent in copper are moving more slowly than the incident proton at about 350 kev. The very firmly bound inner electrons will not contribute much to the stopping but there will still be a large group of intermediate electrons which probably have excitation cross sections that are significant compared to the cross sections for the loosely bound electrons, and may, therefore, be effective in stopping the moving proton. If, however, all these are ignored, and $n(u_s)$ is introduced into (4) with $I=\frac{1}{2}mu_s^2$, and the result integrated over u_s, then the stopping power becomes (N.B. Eq. (3.5.7))

$$\sigma=\text{const. } Z^{\frac{1}{2}}/v. \qquad (6)$$

It might be expected that if the inner electrons do contribute significantly, then (6) would be least accurate in gold, except, of course, that the statistical model itself is least accurate, for these three elements, in copper. However, both the physical argument and the very crude application of the statistical model are of a nature that there can be no insistence on other than qualitative agreement. Therefore, to verify Eq. (6), a tabulation was made of the quantity $b=\sigma v/Z^{\frac{1}{2}}$, which, according to (6), should be constant. The result is given in Table III, with b (in arbitrary units) shown for four energies.

TABLE III. Verification of Eq. (6).

	σ_{obs}(ev-cm^2 $\times 10^{-15}$) Energy (kev)					$b=\sigma v/Z^{\frac{1}{2}}$ Energy (kev)				
Z	350	400	450	550	$\frac{\Delta\sigma}{\sigma}$	350	400	450	550	$\frac{\Delta b}{b}$
29	19.9	19.2	18.3	17.3	13%	100	104	103	107	7%
47	21.9	21.0	20.7	18.7	15%	100	101	105	106	7%
79	25.4	24.4	23.2	22.0	15%	98	100	100	104	7%

For all three elements, b is significantly more constant than the observed stopping power, as indicated in the fractional change columns. However, the power of v is probably smaller than given in Eq. (6). (In fact a plot of $\log\sigma$ *versus* $\log v$ is not a very straight line, so that a power function is a poor approximation.) The power of Z is probably rather accurate since the fractional change in σ at a constant velocity is 25 percent compared to a corresponding change in b of only 3 percent. The indication is that a more careful application of the statistical model as outlined by Bohr might be fruitful.

ACKNOWLEDGMENTS

I would like to thank E. Fermi for an illuminating conversation, and S. K. Allison both for suggesting these measurements and for many valuable suggestions and discussions during their progress. Thanks are due also to T. A. Hall for his continued collaboration, without which this work could not have been completed.

Note added in proof: Approximate preliminary results, privately communicated by T. Hall, disagree only slightly with Bohr's estimates; Hall finds, e.g., a somewhat less marked dependence of y on the Z of the stopping material, but his results are still in substantial agreement with the rough theory.

Magnetic Analysis of the $Li^6(d,p)Li^7$ and $Li^7(d,p)Li^8$ Reactions

E. N. STRAIT AND W. W. BUECHNER
Laboratory for Nuclear Science and Engineering, Massachusetts Institute of Technology, Cambridge, Massachusetts
(Received July 29, 1949)

The energy release of the $Li^6(d,p)Li^7$ reaction has been measured as 5.006±0.014 Mev, using a semicircular magnetic analysis. The hitherto unobserved protons from the $Li^7(d,p)Li^8$ reaction have been found and their energy measured. The Q for this reaction has been determined as −0.193±0.008 Mev.

I. INTRODUCTION

THE various nuclear reactions of the lithium isotopes have been studied in considerable detail, the most comprehensive investigation being that of Rumbaugh, Roberts, and Hafstad.[1] These studies have shown that the reactions $Li^6(d,p)Li^7$ and $Li^7(d,p)Li^8$ occur. The first of these reactions was detected from the protons emitted. The protons from the second reaction were not found, and the reaction was inferred from the observed production of radioactive Li^8.

Two proton groups result from the $Li^6(d,p)Li^7$ reaction, and the difference in energy of these groups has been measured[2] to obtain the energy of the well-known, low lying level in Li^7. In the present experiment, the energy release of this reaction has been determined using a semicircular magnetic analyzer. This apparatus has also been used to search for the protons that result from the $Li^7(d,p)Li^8$ disintegration and to measure the Q for the reaction.[3]

II. APPARATUS AND EXPERIMENTAL PROCEDURE

The essential details of the experimental arrangement have been described previously.[4] The thin targets used were prepared by the evaporation of Li_2SO_4 onto platinum sheets. This compound was chosen since it can be obtained from the Atomic Energy Commission enriched in Li^6. The natural compound was used for the studies with Li^7, and the enriched targets were used for the Li^6 reaction. The oxygen in the target was not a complication in the present experiment, inasmuch as the proton groups that result from the deuteron bombardment of oxygen have energies that are considerably different from those of the protons that were being investigated.

As in our previous work,[2] the studies of the energies of the protons from the $Li^6(d,p)Li^7$ were simplified by the fact that, at the bombarding energy used, these protons have a $H\rho$ in the magnetic field which is close to that of polonium alpha-particles. This makes it possible to compare their energies directly. The energy of the incident deuteron beam was determined from measurements on the deflection of the deuterons elastically scattered from a thin film of platinum evaporated onto copper.

Protons from the $Li^7(d,p)Li^8$ reaction have an energy that is considerably less than the energy of the deuterons which are elastically scattered from the platinum support of the lithium target. While it is possible to count the proton tracks on the photographic plates even in the presence of the heavy deuteron background, most of the plates were taken with a thin aluminum foil placed directly in front of the emulsion surface. The foil was of such a thickness as to stop completely the scattered deuterons.

III. RESULTS

A large number of observations have been made on the two proton groups from $Li^6(d,p)Li^7$. No evidence has been found for any structure in either of the groups. From these measurements, we have obtained 5.006 ±0.014 Mev for the Q-value of the reaction leading to the formation of Li^7 in the ground state. Of the factors entering into the uncertainty in this value, 11 kev are due to uncertainties in the constants used in the conversion of observed $H\rho$ into particle energy, and 9 kev are due to experimental errors, most of which arise from an uncertainty in the angle of observation. The origin of these corrections has been discussed in an earlier paper.[5] Using the value 5.006±0.014 the mass difference between Li^7 and Li^6 is calculated to be 1.001213 ±0.000016, in good agreement with the mass-spectrograph values reported by Bainbridge.[6]

A low energy proton group was found when Li^7 was bombarded by deuterons, and the measurement on the variation of the energy of this group with changes in the incident energy has shown that it arises from the $Li^7(d,p)Li^8$ reaction. The Q-value for the reaction has been determined to be −0.193±0.008 Mev. This is in remarkably good agreement with the value obtained by Rumbaugh, Roberts, and Hafstad who calculated the Q-value to be −0.200 Mev on the basis of a comparison of the observed yield function for radioactive Li^8 with the predictions of the Breit formula. From this value, the Li^8-Li^7 mass difference is calculated to be 1.006797 ±0.000010.

[1] Rumbaugh, Roberts, and Hafstad, Phys. Rev. **54**, 657 (1938).
[2] Buechner, Strait, Stergiopoulos, and Sperduto, Phys. Rev. **74**, 1569 (1948).
[3] A preliminary account of this portion of the work was presented at the June, 1948, meeting of the American Physical Society, Phys. Rev. **74**, 1257 (1948).
[4] Buechner, Strait, Sperduto, and Malm, Phys. Rev. **76**, 1543 (1949).
[5] W. W. Buechner and E. N. Strait, Phys. Rev. **76**, 1547 (1949).
[6] K. T. Bainbridge, Preliminary Report No. 1, Nuclear Science Series, National Research Council (1948).

IV. ACKNOWLEDGMENTS

We wish to acknowledge the assistance of various members of the High Voltage Laboratory, particularly Mr. A. Sperduto and Dr. C. G. Stergis, now at Temple University. We are indebted to Mrs. H. Andrews, Miss C. O'Brien, and Mr. W. Tripp for reading the photographic plates.

This work was supported by the joint program of the Office of Naval Research and the Atomic Energy Commission.

PHYSICAL REVIEW VOLUME 76, NUMBER 12 DECEMBER 15, 1949

Investigations of the Capture of Protons and Deuterons by Deuterons

W. A. FOWLER, C. C. LAURITSEN, AND A. V. TOLLESTRUP
Kellogg Radiation Laboratory, California Institute of Technology, Pasadena, California

(Received August 26, 1949)

The capture of protons and deuterons by deuterons has been studied up to energies of 1.5 Mev. An upper limit of $\sim 10^{-31}$ cm^2 has been found for the $D(d\gamma)$ reaction near 1 Mev. The gamma-radiation from $D(p\gamma)$ has been found to have an angular distribution obeying a $\sin^2\theta$ law. The cross section of the reaction is given empirically from 0.5 to 1.5 Mev by $\sigma = 0.74E^{0.72} \times 10^{-29}$ cm^2 for E in Mev.

THE discovery at Los Alamos[1] of 20 Mev gamma-radiation with an angular asymmetry in yield from the capture of protons by tritons led us to investigate the possibility of the emission of similar radiation in the capture of deuterons by deuterons. The excitation of the He^4 nucleus produced in this capture was expected to be 24 Mev, slightly higher than that expected and observed in the capture of protons by tritons. Because of the large number of neutrons produced in the bombardment of deuterons by deuterons a triple coincidence counter arrangement was employed. Thick targets of heavy ice were bombarded by deuterons from the electrostatic generator at an energy of 1.24 Mev. Observations were made at angles from 0° to 135° with the incident beam.

Copious radiation was observed which produced electron secondaries having ranges in aluminum as measured by the coincidence method corresponding to energies up to 8 Mev. This radiation was considerably enhanced by the introduction of paraffin and various materials such as cadmium between target and counter and could be accounted for completely as radiation caused by the capture of neutrons in materials near the experimental set-up. Above 8 Mev it was possible to set an upper limit of 2×10^{-11} quanta per proton for the yield. On the assumption that the effective target width is about 0.5 Mev, the average cross section of the $D(d\gamma)$He^4 reaction near 1 Mev is calculated to be $< 10^{-31}$ cm^2. This upper limit is considerably less than that observed[2] in the $T(p\gamma)$He^4 reaction which has a cross section of $\sim 3 \times 10^{-28}$ cm^2 at 1.24 Mev rising to $\sim 10^{-27}$ cm^2 at 2.6 Mev. An explanation of the low yield in the $D(d\gamma)$ reaction has been given by Professor R. F. Christy in terms of arguments based on the identity of the incident and target deuterons. The odd ^1P state in He^4 apparently responsible for the radiation in the $T(p\gamma)$ reaction cannot be produced by any combination of deuterons and deuterons.

In the course of the above investigation it was decided to investigate also the bombardment of deuterons by protons. Preliminary measurements with the triple coincidence arrangement indicated gamma-ray emission and since no neutrons were observed measurements were continued with the standard double coincidence

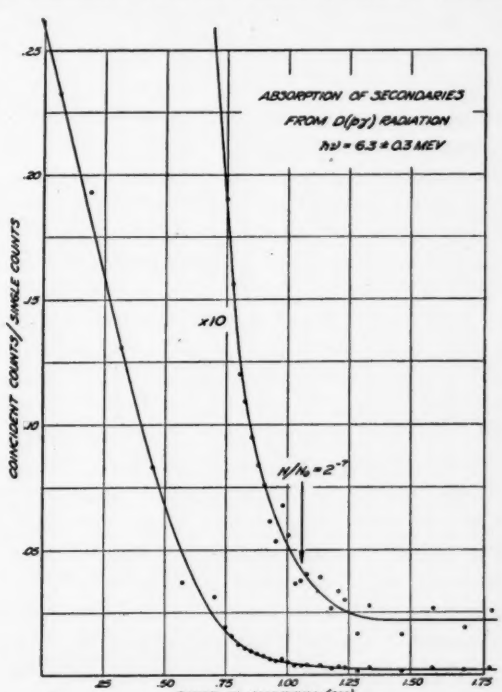

FIG. 1. Coincident counter measurements of the absorption of the secondaries produced in aluminum by the radiation from $D(p\gamma)$. The coincidence counts drop to 2^{-7} at 1.06 ± 0.05 cm of aluminum indicating a gamma-ray energy of 6.3 ± 0.3 Mev.

[1] Argo, Gittings, Hemmendinger, Jarvis, Mayers, and Taschek, Phys. Rev. **76**, 182 (1949). We are grateful to these authors for communicating to us the details of their investigations.

[2] R. F. Taschek, Phys. Rev. **76**, 584 (1949).

arrangement previously used.[3] The results of coincidence range measurements in aluminum made at a bombarding energy of 1.42 Mev with a thick target and at an angle of 90° with the incident beam are shown in Fig. 1. The number of coincidences decreases

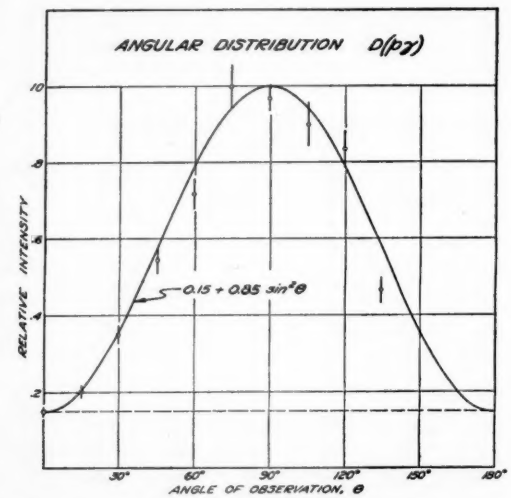

FIG. 2. Angular distribution of the $D(p\gamma)$ radiation as measured by a coincident counter arrangement subtending full angles of 30° and 45° at the target. A value of 0.04±0.02 for the point at 0° was found using an arrangement subtending 18°×30°.

by a factor of 2^7 at 1.06±0.05 cm of aluminum corresponding to a gamma-ray energy[3] of 6.3±0.3 Mev. The energy computed from the masses involved in the reaction $D(p\gamma)He^3$ is 6.17 at 1.0 Mev and 6.45 Mev at 1.42 Mev bombarding energy at 90° and we have thus attributed the radiation to the capture of protons by deuterons. Ordinary ice targets gave no radiation above background thus eliminating oxygen under proton bombardment as the source of the gamma-rays.

The angular distribution of the radiation from zero to 135° at a bombarding energy of 1.42 Mev is shown in Fig. 2. The curve shown in the figure is of the form $a+b\sin^2\theta$ with $a=0.15$ and $b=0.85$. This data was obtained with a coincidence counter aperture subtending full angles of 30° vertically by 45° horizontally. With this fairly poor angular resolution it was not possible to exclude the possibility that the angular distribution actually fitted a pure $\sin^2\theta$ law. For this reason the coincidence counter arrangement was moved back from the target until the full aperture angles were 18° vertically by 30° horizontally. A careful study was made of the ratio of intensities at 0° and 90° with this arrangement with the result that $I(0°)/I(90°)=0.04\pm0.02$. Even with the improved resolution the ratio was expected to be 0.03 on the basis of the $\sin^2\theta$ law and hence we conclude that the angular distribution does fit a $\sin^2\theta$ law within a few percent. This would indicate that the radiation emanates from an electric

[3] Fowler, Lauritsen, and Lauritsen, Rev. Mod. Phys. **20**, 236 (1948).

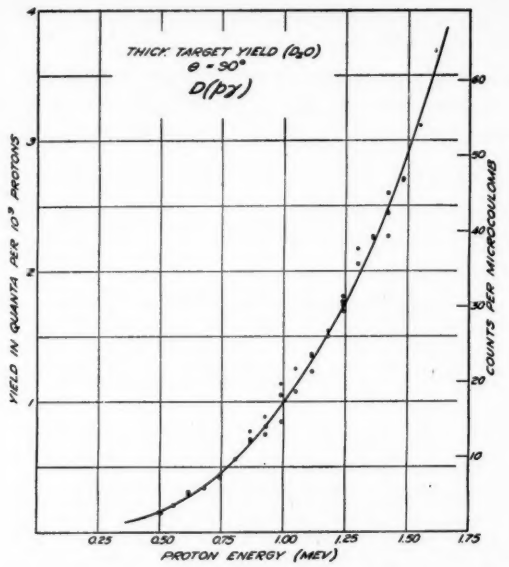

FIG. 3. The thick target yield curve at 90° for the radiation from $D(p\gamma)$. The yield is in quanta per 4π steradians per 10^9 protons.

dipole aligned with the direction of the incident proton beam. As the measurements were made with a thick target it can be concluded that the radiation at 0° is weak at all energies.

The thick target yield curve obtained at 90° as a function of bombarding energy is shown in Fig. 3. Because the single counts were comparable to background at low energies, coincidence counts have been employed in plotting the curve but the right ordinate has been normalized to the number of single counts produced at 1.42 Mev, where the background was small, in an aluminum lined counter 1.8 cm in diameter by 7.6 long at a distance of 3 cm from the target. The thick target yield at 90° in quanta per 4π steradians per 10^9 protons is given as the left ordinate. A logarithmic plot of the data indicates that $Y(90°)=E^{2.59}\times10^{-9}\gamma/p$ for E in Mev. The counting efficiency was assumed to be 4.5 percent independent of bombarding energy.[3] The total cross section obtained by differentiation of the yield curve and summing over all angles is found to be $\sigma=0.74E^{0.72}\times10^{-29}$ cm². In this calculation the variation in the stopping power of water has been taken into account and a small correction has been made for the variation of quantum energy with bombarding energy. Because of the low intensity of this radiation the coefficient in the expression has a probable error of the order of 50 percent near 1 Mev. The exponent indicating the relative variation with energy has a probable error of not more than 15 percent. A more careful determination of the absolute cross section is now underway.

In conclusion we wish to express our appreciation to Professors R. F. Christy and Aage Bohr for enlightening discussions of this problem. This work was assisted by the joint program of the AEC and the ONR.

Particle Groups from the Alpha-Particle Bombardment of Boron*

ROBERT J. CREAGAN**
*Sloane Physics Laboratory, Yale University,*** *New Haven, Connecticut*
(Received July 11, 1949)

Targets of natural boron and targets of 96 percent boron 10 have been bombarded by 7.45 Mev and 6.64 Mev cyclotron alphas. Seven charged particle groups have been observed. The Q-values calculated from the energy of the various groups have been assigned as follows: $Q_1=4.07$ Mev to the $B^{10}(a,p)C^{13}$ reaction; $Q_2=0.85$ Mev to the $B^{11}(a,p)C^{14}$ reaction; $Q_3=0.31$ Mev to the first excited state of carbon 13 at 3.76 Mev. Other values are: $Q_4=0.07$ Mev; $Q_5=-0.31$ Mev; $Q_6=-1.57$ Mev; $Q_7=-1.76$ Mev with assignments discussed. The assignments were checked with boron 10 targets and proton-gamma-coincidence technique. Gammas were detected by coincident counts from two photo-multiplier tubes observing the same naphthalene crystal. Excited states of carbon 13 were searched for, but not observed, at 0.8 Mev and 3.12 Mev.

INTRODUCTION

THE particles emitted from boron, bombarded by alphas, are the first in which the group structure of nuclear fragments was recognized. The reaction has been studied extensively by use of natural alpha-sources which require poor geometry to give appreciable yields. This led to considerable disagreement as to the energy released in the various possible reactions.[1] The energy released in these reactions is important because it determines the following: (a) the mass difference between boron 10 and carbon 13;[2] (b) the mass difference between boron 11 and carbon 14;[3] (c) the energy level of the first excited state of carbon 13;[1,4] (d) the possibility of the reaction $B^{10}(a,d)C^{12}$.[5,6] For the four reasons listed above it was considered desirable to repeat the experiments with the well-collimated cyclotron beam and consequent possibilities for better geometry and results.

It was considered that the best method for identifying the particle groups due to the $B^{11}(a,p)C^{14}$ reaction was to bombard targets of 96 percent boron 10 and compare results with those obtained by bombarding targets of natural boron.

To verify the existence of an excited state in carbon

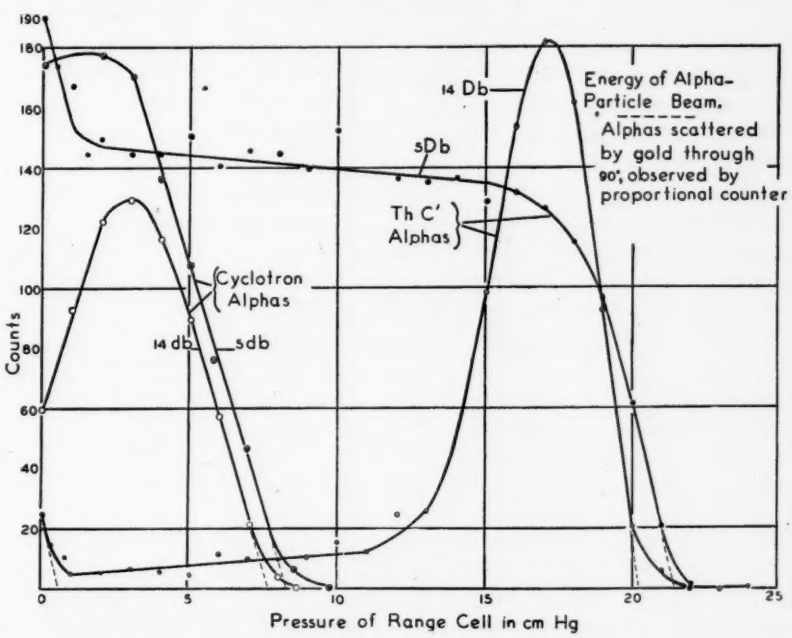

FIG. 1. The number of alpha-particles detected in a proportional counter as a function of the air pressure in a range-cell. Two curves were obtained by scattering cyclotron alphas through 90° by gold foil. The other two curves show the relative range of Th C and Th C′ alphas used for calibration. The 14 db curves count only the highest pulses while the 5 db curves count all pulses.

* Part of a dissertation presented to the faculty of the Graduate School of Yale University in partial fulfillment of the requirements for the degree of doctor of philosophy.
** Now at the Westinghouse Electric Corporation, Atomic Power Division, Pittsburgh, Pennsylvania.
*** Assisted by the Joint Program of the ONR and the AEC.
[1] W. Bothe and H. Maier-Leibnitz, Zeits. f. Physik **107**, 513 (1937).
[2] O. Merhaut, Physik. Zeits. **41**, 528 (1948).
[3] E. C. Pollard, Phys. Rev. **56**, 1168 (1939).
[4] Heydenburg, Inglis, Whitehead, and Hafner, Phys. Rev. **75**, 1147 (1949).
[5] E. C. Pollard and W. W. Eaton, Phys. Rev. **45**, 528 (1934).
[6] F. Joliot and I. Zlotowski, J. de phys. et rad. **9**, 393 (1938).

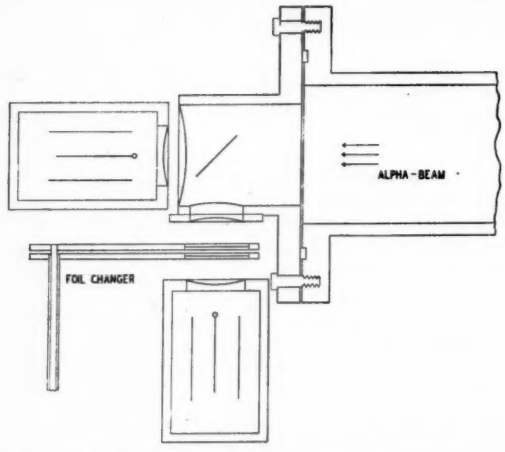

FIG. 2. A typical experimental set-up with the alpha-beam from the cyclotron impinging on the boron target and the emitted protons detected at 0° and 90° by proportional counters. The foil changer allowed range measurements to be made.

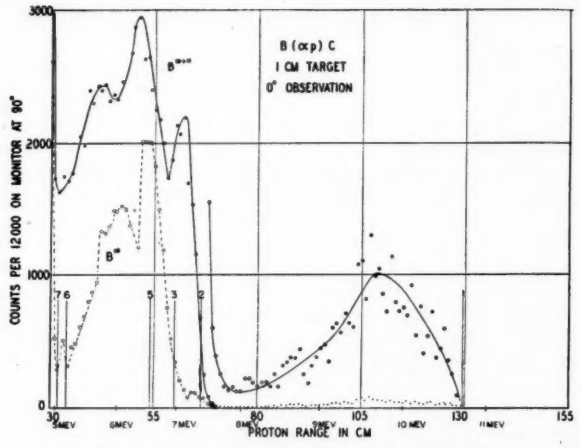

FIG. 3. Proton yield from alpha-particle bombardment of boron targets of separated and unseparated isotopes. Only the largest pulses were counted.

13, observation of proton-gamma-coincidences was considered the best evidence available, on the assumption that the excited state decayed by gamma-emission to the ground state of the residual nucleus. Coincidence technique would also be a check on the $B^{11}(a,p)C^{14}$ reaction end group because no proton-gamma-coincidences should be observed. Similarly the existence of recoil protons from the target could be identified.

PROCEDURE

The energy of the cyclotron alphas was determined in four different experiments: 1. The alpha-beam was passed through a range-cell, picked up by a probe in an evacuated volume, and observed by means of a galvanometer. The range, and hence energy, of the alphas was obtained by varying the air pressure in the range-cell (a pipe through which the alphas pass). 2. The alpha-beam was passed through a range-cell and was observed by a proportional counter at 0°. Calibration of counter depth and basic absorption (minimum amount of absorption in the path of the particles due to vacuum seal foil and foil on counter) was obtained by use of Th C and Th C′ alphas. 3. The alpha-beam was scattered by gold through 90°, passed through a range cell, and observed by a proportional counter. 4. The alpha-beam impinged on an aluminum foil covered with a thin film of vacuum grease and the recoil protons so produced were passed through a range-cell and observed at 0° by a proportional counter.

The various alpha-beam energy measurements gave an extrapolated value of 7.45 Mev with a mean deviation of 0.02 Mev, although the procedure does not warrant error limits smaller than 0.05 Mev. The beam spread at half-height is 0.3 Mev. All values were taken as the extrapolated value of the steepest part of the counts *vs.* range curve. Curves were taken counting all particles (integral curve), and only those particles near the end of their range (differential curve). The result of experimental method 3 above is given in Fig. 1 as an example of the results. The 14 db and 5 db refer to the attenuation introduced between the proportional counter pre-amp and the video amplifier.

Boron targets were made by evaporating boron onto gold foils. The gold foils were used to stop the alphas behind the target and thus prevent other nuclear reactions by the alphas. The boron was heated on a tungsten filament in a vacuum (~1 micron) and water-cooled gold (~8-cm air equivalent) was clamped above the filament so as to intercept the evaporating boron. This gave a smooth thin target. Most of the work was done with targets between 0.4 cm and 1-cm air equivalent, assuming that 1.25 mg/cm² of boron is equivalent to 1 cm of air. Target preparation was the same for natural boron and the 96 percent boron 10, since they were both in the form of 200 mesh amorphous powder.

The target was bombarded about a meter outside the cyclotron can and the charged particles emitted were observed by proportional counters at 90° and 0° as shown in Fig. 2. A typical run would consist in observing the number of proton counts at 0° as a function of range for a standard number of counts on the counter at 90°.

The absorption was varied by placing different thickness aluminum foils in the path of the protons. The energy of the particles was then determined from the 1937 Cornell range-energy diagrams.

The proportional counters were so biased that only those particles near the end of their range would record. This is possible because of the increased ionization per cm of path near the end of the particle range (Bragg curve) which produces a larger pulse in the proportional counter.

The results of the 0° and 90° observations are given in Fig. 3 and Fig. 4 respectively. The results obtained by putting a 1.13 cm aluminum foil in the incident alpha-beam to lower the energy of the beam is given in Fig. 5.

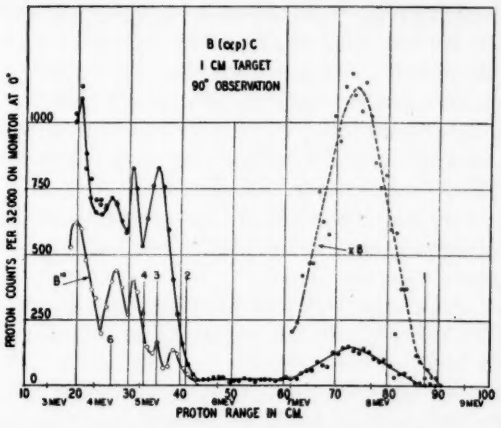

FIG. 4. Proton yield from alpha-particle bombardment of boron targets of separated and unseparated isotopes. Only the largest pulses were counted.

By extrapolation, the ranges of the various groups are determined and by using the standard Q-value equation, the energy released in the nuclear reaction is determined.

The bombardments were performed with boron 10 and natural boron targets.

To observe gammas emitted in coincidence with protons, protons are detected at 0° and gammas are detected at 90° as shown in Fig. 6. The iron shield around the photo-multiplier was necessary because of the stray magnetic field of the cyclotron deflector magnet. Both photo-multipliers observed the same crystal and only coincident counts from both were taken as gamma-counts. This served to lower the background noise counts from each photo-multiplier by the factor $2Tn_1n_2=A$; where A is the number of accidental counts observed when n_1 and n_2 random counts are fed into the respective inputs of the coincidence circuit. The resolving time T of the coincidence circuit[7,8] used in this experiment was 2.5 10^{-7} seconds. The video amplifiers[9,10] used have a 4-megacycle band width. Typical background in the cyclotron room for 1×1×2.5 cm naphthalene crystal with no cyclotron beam is 28 coincident counts per minute. For the weak alpha-particle beam used, typical counting rates were 5000–10,000 coincident counts per minute. Naphthalene crystals were used after earlier attempts with calcium fluoride and polystyrene had proven unsatisfactory. 931A photo-multiplier tubes were used, with approximately 150 volts for the first stage and 75 volts for subsequent stages. It was hoped that this arrangement might allow noise pulses introduced in later stages to be biased out. No great difference was observed. Dry-ice cooling was used more as a temperature stabilizer than as a low temperature device, and satisfactory results were obtained with no cooling. The output of the photo-multiplier tube was fed to a 6AK5 cathode follower, then to a 6J6 cathode follower (Fig. 7), which was matched to the 75-ohm cable leading from the cyclotron to the control room where the video amplifier with a 75-ohm resistor input was located. The two cathode followers in cascade gave a better amplification and impedance match between the photo-multiplier tube and the 75-ohm amplifier input than could be obtained with one tube.

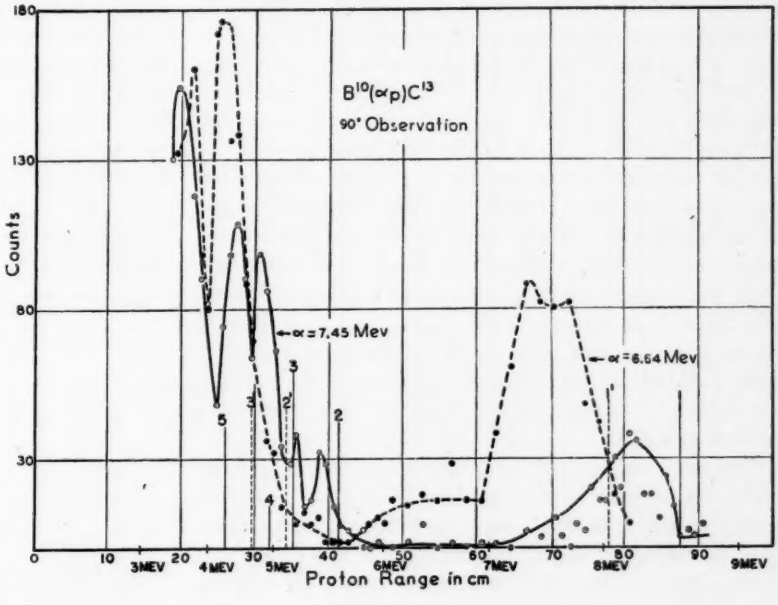

FIG. 5. Proton yield from alpha-particle bombardment of boron targets of 96 percent boron 10 at two different energies of the incident alphas.

[7] H. L. Schultz and E. C. Pollard, Rev. Sci. Inst. 19, 617 (1948).
[8] B. B. Benson, Phys. Rev. 73, 7 (1948).
[9] H. L. Schultz, Phys. Rev. 69, 689 (1946).
[10] B. B. Benson, Rev. Sci. Inst. 17, 533 (1946).

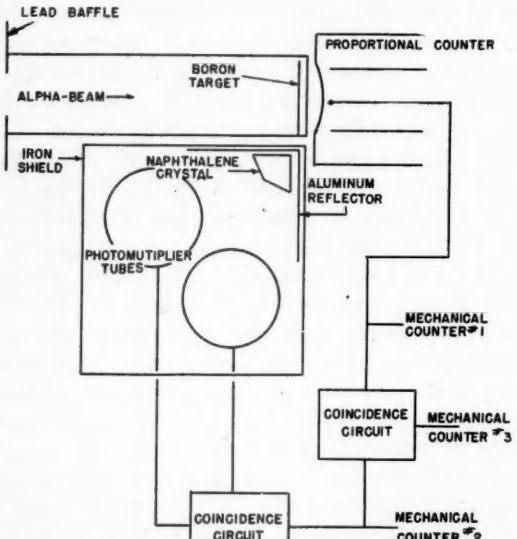

FIG. 6. Experimental arrangement for observing proton-gamma-coincidences emitted from a boron target bombarded by alpha-particles. The protons are detected in a proportional counter and the gammas are detected in a naphthalene crystal which is observed by two 931A tubes in coincidence.

RESULTS

The results of the study of group structure are illustrated in Figs. 3–5. The observed group structure corresponds to the following Q-values:

The longest proton group observed, designated group 1, gives a Q-value of 4.07 Mev with a mean deviation of 0.14 Mev for six determinations. This is a rough measure of the accuracy of the experimental values, although errors could exist to 0.2 Mev because of equipment and technique. The Q_1 value agrees well with the $Q=4.03$ Mev calculated from Mattauch's table of mass spectrographic data.[11] There seems to be a noticeable asymmetry in the yield of the end group at 90° and 0° with a ratio of 5 in favor of the 90° observation, if the yield is normalized in each direction with respect to the other groups. The predicted half-width of the end group was 1.07 Mev on the basis of energy-spread of incident alphas and the target thickness, while the experimentally determined half-width was 0.95 Mev. This agreement of the half-width of the end group, plus the fact that no dip occurred in the peak (except statistical fluctuations), are reasons for doubting the existence of an excited level in the carbon 13 nucleus at 0.8 Mev.[1]

The next longest proton group gives $Q_2=0.85$ Mev which has been assigned to the $B^{11}(a,p)C^{14}$ reaction[2] giving a mass difference between boron 11 and carbon 14 of 2.9940 mass units. The identity of the group was verified by bombarding 96 percent boron 10 targets. The group has a ratio of 13 between yield with natural boron and boron 10 targets (see Fig. 3).

[11] J. Mattauch and S. Flugge, *Nuclear Physics Tables* (Interscience Publishers, Inc., New York, 1946).

The next group: $Q_3=0.31$ Mev has been assigned to the first excited state of carbon 13 because it appears with separated and unseparated isotope targets. This indicates the first excited state of carbon 13 is 3.76 Mev above the ground state, in contrast to results published by other experimenters[1,4] who have given 0.8 Mev and 3.12 Mev, respectively, as the first excited state. Because of this disagreement, the proton spectrum in the pertinent ranges was studied intensively; however, the groups were not found.

The next group: $Q_4=0.07$ Mev has been assigned to the next excited state of carbon 13 at 4 Mev above ground level.

The next group gives a Q-value of -0.31 Mev if protons are assumed. If the group is assumed to consist of deuterons from the reaction $B^{10}(a,d)C^{12}$ the Q-value equals 1.55 Mev; a number in good agreement with the $Q=1.45$ Mev predicted by mass differences.[11] Deuteron emission in this reaction has been suggested,[5] and deuterons have been observed in cloud chamber work.[6] Data obtained by W. Bothe[12] at various angles and energies and ascribed to protons, gives the same mean deviation for Q-values when deuterons are assumed.

Group six: $Q_6=-1.57$ Mev is very weak and was observed only at 0° because of the basic absorption at 90°. If assigned to carbon 13 it implies an excited state at 5.64 Mev.

Group seven: $Q_7=-1.76$ Mev is apparently due to recoil protons observed at 0°. This assumption would specify an incident alpha-beam of 7.72 Mev, but it is considered that faulty extrapolation occurred due to basic absorption which masked all but the tail end of the recoil protons. This assumption, if true, would exclude the 5.9 Mev excited state of carbon 13.

For further verification of group assignments, proton-gamma-coincidence observations were made. The results are given in Table I. The lack of coincidences at 120 cm absorption indicates: (a) that the circuits are operating so that spurious coincidences are minimized, since only 2 coincidences were observed in two hours of cyclotron running time despite the high electrical noise background commonly found in cyclotron operation; (b) that this group has no associated gammas and hence implies a residual carbon 13 nucleus in a ground state;

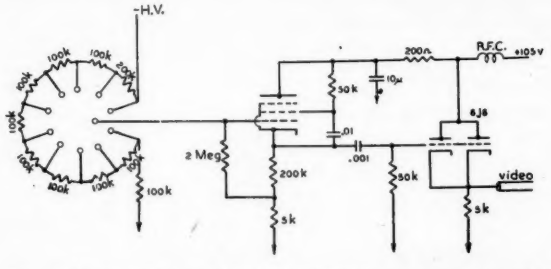

FIG. 7. A pre-amp for a 931A scintillation counter. The cathode resistor for the 6J6 cathode follower is a 75-ohm resistor in the input of the video amplifier.

[12] W. Bothe, Zeits. f. Physik 63, 381 (1930).

(c) that the 0.8 Mev excited state is improbable, because it would have contributed coincidences at 120 cm absorption. The naphthalene would be more efficient for a 0.8 Mev gamma than it would be for higher energy gammas which it later detects as coincidences.

The low coincidence rate at 62 cm absorption confirms Q_2 as belonging to a ground state transition and hence to $B^{11}(a,p)C^{14}$. The few coincidences observed can be accounted for by overlapping of the adjacent group as apparent from Fig. 3.

The 7.2 coincidences observed per 10^4 protons at 51 cm further substantiate the assignment of group 3 to an excited state of carbon 13 at 3.76 Mev and because of lack of coincidences at greater ranges it seems highly probable that this is the first excited state, since the naphthalene detector would be more efficient (Klein-Nishina formula) for lower energy gammas associated with a lower energy level.

The large coincidence rate at 41 cm and 44 cm absorption does not confirm the assumption that group five consists of deuterons, but rather implies that most of the particles are protons belonging to an excited state of carbon 13. The overlapping of groups in this region makes definite assignment of coincidences difficult.

The lack of coincidences at 30 cm absorption strengthens the assumption that group seven is due to recoil protons.

The data is given in Table I with two different counter settings because, while it was necessary to accept most pulses (semipeaked proportional counter) to get reasonable statistics for the end group, it also seemed desirable to bias the counter to accept only the largest pulses (peaked proportional counter) so as to separate the proton groups for better assignment of coincidences.

Because of the possible existence of a proton group due to an excited level of carbon 13 at the same range as the protons from the $B^{11}(a,p)C^{14}$ end group, proton-gamma-coincidences were observed with a boron 10 target. The results were similar to those given in Table I, and indicate no excited state at the range in question. The data was taken with protons observed at 90° and gammas observed at 30°. The solid angle of the counters was different at the different angles and no attempt was made to look for angular correlation of the proton gamma-coincidences.

TABLE I. Results of the proton-gamma-coincidence observation of the alpha-particle bombardment of boron.

Absorption	Number of runs	Number of protons	Approximate total time	Total number of coin.	Expected change coin.	Genuine coin.	Genuine coin. per 10^4 protons
Semipeaked proportional counter							
30 cm	7	69,600	34 min.	23	8.4	14.6	2.10
34	5	51,200	24	26	5.4	20.6	4.02
41	7	70,400	36	39	8.7	30.3	4.27
44	9	109,200	49	80	13.8	66.2	6.08
51	7	83,100	35	55	9.6	45.4	5.45
62	6	70,400	48	18	9.0	9.0	1.28
120	19	17,700	117	2	0.9	1.1	0.65
Peaked proportional counter							
30 cm	1	6,400	347 sec.	1	0.18	0.82	1.28
34	1	6,400	293	2	0.31	1.70	2.66
41	1	6,400	307	3	0.26	2.74	4.29
44	1	6,400	235	3	0.35	2.65	4.15
51	1	6,400	186	5	0.40	4.60	7.20
62	1	6,400	257	1	0.37	0.63	0.98

All results quoted in this paper have been repeated at least three times on different days and with equipment dismantled in between runs.

The over-all experimental efficiency of the naphthalene detector was about 1 percent, calculated on the assumption that one gamma is associated with each proton associated with a residual nucleus in an excited state. This is in qualitative agreement with a 4 percent efficiency calculated on the basis of the Klein-Nishina formula and consideration of crystal volume.

ACKNOWLEDGMENTS

It is a pleasure to acknowledge the advice and encouragement of Professor Ernest C. Pollard who suggested this topic. The author is also indebted to Professors Howard Schultz and Richard Humphreys for many informative discussions.

The Atomic Energy Commission isotope division is to be thanked for the use of boron 10.

Neutron Polarization*

J. FLEEMAN, D. B. NICODEMUS, AND H. H. STAUB**
Stanford University, Stanford, California
(Received September 1, 1949)

Experiments for the determination of the polarization cross section p of iron with monochromatic and non-monochromatic neutrons are described. The absolute value of p as well as its dependence on the neutron velocity is found to be in good agreement with the recent calculations of Steinberger and Wick and also with other experiments. For a complex neutron spectrum originating from a paraffin moderator $\bar{p}$ is found to be $(2.35\pm0.1)\times10^{-24}$ cm² in agreement with previous investigations. It is shown that the larger value of 3.15×10^{-24} cm² found by Hughes, Wallace, and Holtzman must be due to spectral differences. The approach of the magnetization of iron towards saturation is also investigated.

I. INTRODUCTION

THERMAL neutrons which pass through a slab of magnetized ferromagnetic material will undergo partial polarization because the scattering cross section depends, by way of the magnetic interaction of the iron atom and the neutron, on the relative orientation of the neutron spin and the magnetic moment of the iron atom. Bloch[1] first showed that the scattering cross section per nucleus of a magnetically saturated material can be written as

$$\sigma=\sigma_0\pm p, \tag{1}$$

where σ_0 represents the cross section for complete demagnetization (including a quadratic term due to magnetic interaction) and p the polarization cross section. The $\pm$ sign refers to the two possible magnetic quantum numbers $m_s=\pm\frac{1}{2}$ of the incident neutron. Although the magnetic contribution to σ_0 might be different for complete magnetization and complete demagnetization, the difference is so small that usually it can safely be neglected. As a consequence of the difference in the scattering cross section for the two states, $m_s=\pm\frac{1}{2}$, the intensity I of a beam of neutrons passing through a slab of iron will undergo an increase ΔI upon complete magnetization which is given by

$$\eta_\infty=\Delta I/I=\cosh npd-1 \tag{2}$$

$$\approx\tfrac{1}{2}n^2p^2d^2 \quad \text{for} \quad npd\ll1. \tag{2'}$$

d represents the thickness of the iron slab and n the number of iron atoms per unit volume.

If the iron is partially magnetized, not only will the neutrons passing through the material undergo polarization, but also the inhomogeneities of the magnetic field will induce transitions between the two states and thereby will again partly depolarize the beam. Halpern and Holstein[2] have made a detailed theoretical study of this effect and have shown that for partly magnetized iron Eq. (2′) has to be replaced by

$$\left.\begin{aligned}&\eta=\tfrac{1}{2}n^2p^2d^2f(\lambda/\epsilon d),\\ &f(x)=2x^2[e^{-1/x}+(1/x)-1]\end{aligned}\right\}, \tag{3}$$

where

The depolarization factor $f(\lambda/\epsilon d)$ depends on the lack of magnetic saturation,

$$\epsilon=\frac{M_\infty-M}{M_\infty}, \tag{4}$$

where M represents the actual magnetization, M_∞ its saturation value, and λ a parameter related to the size of the microcrystals in the iron. The microcrystals are supposed to be magnetically saturated but their deviation from perfect alignment is responsible for the incomplete magnetic saturation and the depolarization of the neutrons. The quantity λ depends not only on the average linear dimension δ of the microcrystals but in general also on a characteristic length $2\pi l$, the distance over which a neutron travels in the material during one full Larmor precession about the internal field B.

$$l=v/B\gamma, \tag{5}$$

where v is the velocity of the neutron and γ its gyromagnetic ratio (1.83×10^4 e.m.u.). For $v=2200$ m/sec. and $B=20{,}000$ gauss, l is about 6×10^{-4} cm. For the two extreme cases of large and small crystalline dimensions λ is given by

$$\left.\begin{aligned}&\lambda\approx\delta/2 \quad \text{for} \quad \delta\gg l\\ \text{and}\quad &\lambda\approx l^2/\delta \quad \text{for} \quad \delta\ll l\end{aligned}\right\}. \tag{6}$$

The polarization cross section p depends strongly on the velocity of the neutrons. In the first place, this dependence is caused by the form factor of the $3d$ electrons in the iron atom, which describes the magnetic moment density within the scattering atom. In the second place, since p represents an interference term between nuclear and magnetic scattering, it will exhibit a similar dependence on the neutron velocity as does the scattering cross section itself. In a crystalline material the scattered intensity is largely concentrated in the well-known Debye-Scherrer rings, whose number decreases rapidly with increasing de Broglie wave-length of the neutrons. Whenever the neutron wave-length becomes too large to satisfy the Bragg condition for a particular set of lattice planes

* Assisted by the Joint Programs of the ONR and the AEC.
** Now at the University of Zurich, Switzerland.
[1] F. Bloch, Phys. Rev. 50, 259 (1936); 51, 994 (1937).
[2] O. Halpern and T. Holstein, Phys. Rev. 59, 960 (1941).

there will be a discontinuous drop in the scattering intensity. These wave-lengths are given by

$$\lambda_c=\frac{2a}{(h_1^2+h_2^2+h_3^2)^{\frac{1}{2}}},$$

where a is the lattice constant of iron and h_1, h_2, h_3, the Miller indices of the lattice plane. For neutrons with wave-length larger than 4.04A no coherent crystalline scattering can take place and likewise one would expect the polarization effect to be absent. In addition to the coherent scattering, however, a small amount of diffuse incoherent scattering is present. It is caused by

(a) Scattering processes in which the neutron spin changes its orientation. Their effect is, however, negligible in the case of iron, since both predominant isotopes (Fe^{54} and Fe^{56}) have presumably zero spin.

(b) Lattice irregularities due to the presence of isotopes.

(c) Inelastic scattering due to temperature motion of the crystal lattice (Debye-Waller factor) and lattice imperfections.

Halpern[3] has shown that the incoherent scattering processes under (c) are the only ones which will contribute to the polarization cross section p.

Values of p have previously been calculated by Halpern, Hamermesh, and Johnson[4] and by Hamermesh.[5] Their results were very much smaller than the observed values.[6–9] More recently Steinberger and Wick[10] recalculated p for the velocities of the neutrons between 1000 and 2800 m/sec. They found values which were indeed considerably larger than those of Halpern, Hamermesh and Johnson, and Hamermesh. The increase is caused by the following factors: (1) The nuclear scattering cross section as redetermined, for instance, by Fermi and Marshall.[11] (2) The contribution of the diffuse temperature scattering. (3) A revised form factor of the $3d$ electrons in iron. The results of Steinberger and Wick† are shown as the solid curve in Fig. 4.

On the experimental side Powers[12] showed that polarization of the neutrons could be obtained only if the iron was almost completely magnetized, as one would expect from expression (3). For a thickness d of 1 cm, for instance, and $\lambda=\delta/2\sim10^{-3}$ cm, the function f(x), defined in (3) has the value 1/2 for $\epsilon=2.5\times10^{-3}$. In a detailed study Bloch, Hamermesh and Staub[6] and Bloch, Condit and Staub[8] investigated the dependence of the polarization effect η on the thickness d‡ and the degree of saturation ϵ. They showed that the polarization effect for complete saturation increases quadratically with the thickness. By direct magnetic measurements of ϵ at magnetizing fields up to 5000 gauss they found that the polarization effects could be represented by the expression (3) given by Halpern and Holstein. They also determined the value of $\bar{p}$ for an average thermal neutron velocity as about 2.1×10^{-24} cm². Subsequently Fryer measured the value of p with monochromatic neutrons at several different velocities. While the relative increase of p with decreasing velocity was in reasonable agreement with the predictions of Halpern, Hamermesh and Johnson, the absolute magnitude of p was much larger than the calaulated value.

More recently Hughes, Wallace, and Holtzman[9] (referred to hereafter as H.W.H.) made a detailed study of the neutron polarization effect. Instead of measuring ϵ directly, they determined the two parameters λ/ϵ and p from measurements of η at a number of values of d for a constant magnetization close to saturation. Utilizing the thermal neutrons from the graphite column of a pile, they determined an average value $\bar{p}$ of 3.15×10^{-24} cm² which is considerably larger than the value found in the previous work. H.W.H. also measured p for different neutron velocities, particularly in the region between the last two Bragg discontinuities. At low velocities they found p to be considerably larger than one value given by Fryer at $v=1310$ m/sec., while at higher velocities their results agree well with those of Fryer. A direct metallographic determination, as well as the fact that H.W.H. found $f(x)$ to be independent of the velocity of the neutrons, showed clearly that for the material used in their investigation the crystalline dimensions were large compared to the critical length l.

Since the measurements of p at low velocities of H.W.H. are in very good agreement with the theoretical predictions of Steinberger and Wick, it was felt that more accurate measurements should be made at higher velocities. The values of the atomic form factor F at low velocities are quite certain, since for $v=0$, F approaches unity. At higher velocities, however, the form factor depends very critically on the particular choice of the electron distribution and it is therefore of interest to verify the calculations of Steinberger and Wick in this region. In addition, the present investigation was made in order to determine the reason for the considerable discrepancy in the average value $\bar{p}$ as found at Stanford and by the Argonne Laboratory. H.W.H. suggested that the discrepancy was caused by an overestimate of the quantity ϵ by the Stanford workers. While $1/\epsilon$ is proportional to H^2, the square of the magnetizing field, in a region of moderate fields

[3] O. Halpern, Phys. Rev. **72**, 260 (1947).
[4] Halpern, Hamermesh, and Johnson, Phys. Rev. **59**, 981 (1941).
[5] M. Hamermesh, Phys. Rev. **61**, 17 (1942).
[6] Bloch, Hamermesh, and Staub, Phys. Rev. **64**, 47 (1943).
[7] E. M. Fryer, Phys. Rev. **70**, 235 (1946).
[8] Bloch, Condit, and Staub, Phys. Rev. **70**, 972 (1946).
[9] Hughes, Wallace, and Holtzman, Phys. Rev. **73**, 1277 (1948).
[10] J. Steinberger and G. C. Wick, Phys. Rev. **74**, 1207 (1948).
[11] E. Fermi and L. W. Marshall, Phys. Rev. **71**, 666 (1947).
† We are greatly indebted to Professor Wick for kindly sending us a copy of his curve prior to publication.
[12] P. Powers, Phys. Rev. **54**, 827 (1938).
‡ It should be noted that, contrary to the statement of Hughes, Wallace and Holtzman (see reference 9), both previous measurements (see references 6 and 8), at this laboratory were carried out with two different thicknesses of iron. It was indeed just the particular form of $f(x)$ predicting a linear increase of η at low magnetizing fields and a quadratic dependence near saturation which prompted the use of different thicknesses.

(1000 to 5000 gauss), it is to be expected that $1/\epsilon$ increases less rapidly at higher fields. The value of ϵ had been obtained by the Stanford group by direct magnetic measurement and the proportionality of $1/\epsilon$ with H^2 had been well established in the region of low H. The values of ϵ at higher fields were simply obtained by extrapolation of the quadratic law and could therefore indeed be overestimated and thereby cause an underestimate of $\bar{p}$. On the other hand, this explanation fails to account for the rather close agreement of the measurements with monochromatic neutrons and the fact that the saturation values of η were very closely proportional to d^2. It must, therefore, be discarded as a satisfactory explanation of the above-mentioned discrepancy; such an explanation can be found, however, as a consequence of differences in the distribution of the neutron velocities (see Section IV), particularly at low values.

II. EXPERIMENTAL ARRANGEMENT

a. Apparatus

The measurements of $\bar{p}$ were performed essentially with the same arrangement as used by Bloch, Condit, and Staub.[8] A beam of collimated slow neutrons from Be bombarded with 2.7-Mev deuterons and moderated in a block of paraffin surrounding the target of the cyclotron, passes through cadmium channels 6 in. long and with an opening of $1\frac{1}{2}$ in.$\times$2 in. attached to both sides of the iron sample. The samples $1\frac{1}{2}$ in.$\times$2 in. fit snugly into the gap of the magnet. The direction of the

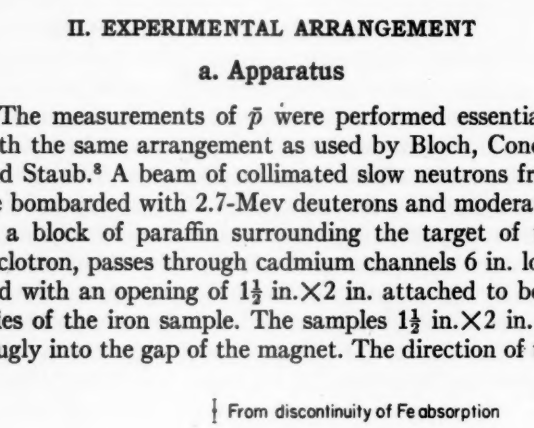

FIG. 1. Delay time Δt as a function of the neutron velocity v.

magnetization is at right angles to the neutron beam. For the present measurements two identical magnets were available and for larger thicknesses of the sample we distributed the iron equally between the two magnets which were operated so that they gave the same magnetizing field. Both fields always pointed in the same direction, and between the magnets there was no region where the field dropped to less than 100 gauss. Careful measurements showed that a piece of 1 in. thickness in one magnet and a $\frac{1}{2}$-in. piece in each magnet gave identical results. By using two magnets we were able to extend our measurements to thicknesses up to 2 in. with a certainty that the pieces were homogeneously magnetized. After passing through the iron blocks the neutrons entered the detector through a circular cadmium channel 30 in. in length and $2\frac{1}{4}$ in. in diameter. In this measurement the filling of the counter of 10-in. effective length consisted of B^{10} enriched boron trifluoride. Except for a $1\frac{1}{2}$ in.$\times$2 in. opening at the front, the chamber was shielded by cadmium, boron carbide, and a thick shield of hydrogenous material. The sensitivity of the detector for fast neutrons is considerably greater than that of the counter used by Bloch, Condit, and Staub. Consequently the present results cannot be compared immediately to the previous ones. The increased sensitivity of the enriched filling for fast neutrons will decrease throughout the polarization effects measured with non-monochromatic neutrons. The counter was placed at various distances, 2.74 m, 4 m, and 5 m, from the neutron source. The measurement of the magnetizing field H was done in the usual manner by placing a small rectangular search coil of $\frac{1}{16}$ in. thickness against the surface of the steel sample. The coil was calibrated against a proton nuclear induction signal. The plates of hot rolled steel were cut from the same material used in the previous investigations.[6-8]

For the measurements with monochromatic neutrons a modulation equipment of the usual design was built. A repetition frequency of 150, 250, or 300 cycles per sec. was derived from an audio frequency oscillator. Its sinusoidal output operated a pulse former which activated one univibrator, to provide the square-wave signal of variable duration τ_A (50 to 100 μsec.) for modulating the ion source of the cyclotron. Simultaneously the pulse former started a second univibrator, whose square pulse determined the variable interval t' (200 to 5000 μsec.) between production of neutrons and their detection. The trailing edge of the latter square pulse in turn operated a third univibrator providing the square pulse of duration τ_B for the activation of the detecting instrument. This latter process was performed by a conventional diode coincidence circuit receiving on one side the amplified pulses from the detector and on its other side the activating square pulse. The various pulses were displayed on a synchronized cathode-ray tube in order to determine their relative positions and duration. Time marks at 333 μsec. intervals served to calibrate the horizontal axis of the oscilloscope. A special circuit was incorporated which permitted the reading of the interval τ_B of the amplifier pulse, by means of a meter, to a high degree of accuracy. This was found necessary, since the system of monitoring the neutron intensity would not account for variations of the quantity τ_B.

The measurements of the polarization effect with non-monochromatic neutrons were monitored by an integrating boron trifluoride chamber receiving neutrons from the same region of the moderator at which

the main beam originated. For the measurements of the spectral distribution, intervals of equal total number of incident neutrons were determined by recording the total number of counts of the detector through an unmodulated channel. For the measurements of absorption and polarization with monoenergetic neutrons, an additional boron trifluoride counter for monitoring was placed in the vicinity of the main counter.

b. Calibration of Neutron Spectrometer

It is well known that the time interval t', elapsing between the time of the burst of ions in the source of the cyclotron and the time at which the detector becomes active does not give directly the actual flight time t of the neutrons. In fact, t' is always larger than t by an amount Δt,

$$t'=t+\Delta t,$$

The delay Δt is caused by the time required for accelerating the deuterons ($\sim$3 μsec.), slowing down of the neutrons to thermal energies ($\sim$5 μsec.), the effective lifetime of the neutrons in the paraffin (up to 200 μsec.) and delays in the detecting system ($\sim$5 μsec.). The main contribution caused by the finite lifetime of the neutrons in the moderator, due to its exponential character, does not represent simply a time delay but rather a spread with an average delay. Moreover, the average delay will depend on the particular velocity of the neutrons under consideration. In the present experiments we determined the total average delay Δt for the various velocities by three independent measurements. For high velocities (>3000 m/sec.) we measured the actual velocity by the transmission of the neutrons through Pyrex glass plates of various thicknesses. The boron content of the plates was determined at one velocity by comparison with the transmission through a plate of fused boron trioxide. Assuming the composition of Pyrex to be boron trioxide and silicon dioxide[13]) it was found that the boron trioxide content was 13.3±0.4 percent. The velocity of the neutrons was determined from the value of the absorption cross section of boron (743×10^{-24} cm^2 at $v=2200$ m/sec.,[13]) assuming the $1/v$ law and taking into account the attenuation due to silicon and oxygen. Since this additional attenuation is not very large and is due mainly to scattering, a constant cross section was assumed for O and Si. At intermediate velocities from 3000 m/sec. to 1500 m/sec. the delay was determined by comparing similar points in the neutron spectrum measured at two different distances L_1 and L_2. For instance, let t_1' and t_2' be the time interval at which one observes the intensity of the spectrum to have dropped to half its maximum value, measured at distances L_1 and L_2, respectively, between source and detector. Since the actual velocities are the same for both distances, one obtains Δt through the relation

$$v=\frac{L_1}{t_1'-\Delta t}=\frac{L_2}{t_2'-\Delta t}.$$

In this manner Δt was determined from the measurements of the spectrum at distances of 2.74 m and 5 m. For the lowest value of the velocity $v=983$ m/sec. we determined the delay by observing the spectral distribution of the neutron beam after passage through a plate of iron. Since, at a de Broglie wave-length $\lambda=4.04$A, corresponding to a velocity of 983 m/sec., the scattering cross section drops from a value of about 17×10^{-24} cm^2 discontinuously to almost zero, the transmitted spectrum exhibits a sudden increase in intensity at this point. This discontinuity can be very accurately located. Unfortunately, the other discontinuities occurring at velocities of 1390, 1700, 1960, etc., m/sec. are not nearly so pronounced and their location is not so easily determined. From the compound evidence of the various measurements which partially overlapped we were able to construct a plausible curve, shown in Fig. 1, describing the dependence of Δt on the velocity of the neutrons. For velocities at which the neutrons are in a pseudothermal equilibrium with the molecules of the moderator, the delay is of the order of 200 μsec., as should be expected, since this represents the average lifetime of a thermal neutron in paraffin. At higher velocities where many neutrons escape from the moderator without having undergone a large number of collisions, the delay time becomes gradually smaller. For velocities at which a thermal equilibrium distribution would contain hardly any neutrons the delay has dropped to about 20 μsec.

III. MEASUREMENTS

a. Experiments with Non-Monochromatic Neutrons

In a first series of experiments we measured the average polarization effect as a function of the thickness d of the sample with considerable accuracy for thicknesses from 0.635 to 5.08 cm in steps of 0.635 cm at a constant magnetizing field of $H=11{,}200$ gauss. The greater accuracy obtained in the present experiments is mainly due to the increased sensitivity of the detector. For every measurement counts were recorded alternately with the field on and off during short intervals monitored by the integrating boron trifluoride chamber. For every group of measurements the cadmium background ranging from 10 to 40 percent, according to the thickness of iron, was determined and subtracted from the results. No polarization effect could be observed for neutrons passing through cadmium. The net polarization effect η' is given by

$$\eta'=(N'-N)/(N-N_c),$$

where N', N and N_c are the total number of counts for an equal number of monitor intervals with the iron

[13] J. Rainwater and W. W. Havens, Jr., Phys. Rev. **70**, 136 (1946).

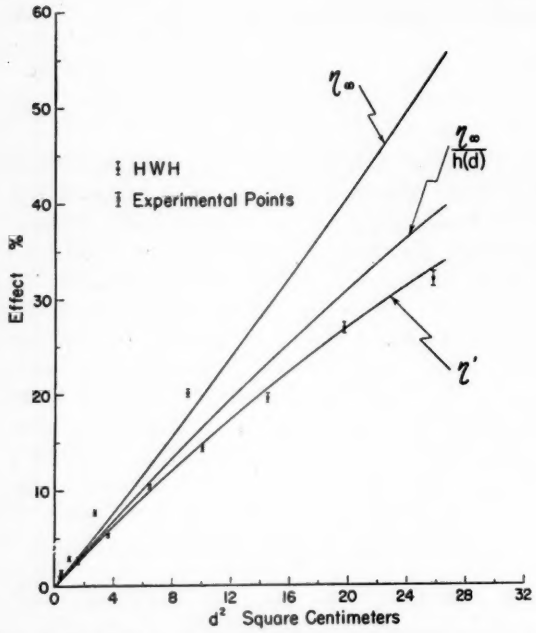

FIG. 2. Transmission effect *versus* d^2. Uppermost curve: $\eta_\infty = (\cosh npd - 1)$ calculated with $p = 2.35 \times 10^{-24}$ cm². Middle curve: η_∞/h calculated with the values of h as given in Figure 6. Lowest curve represents η' taking lack of saturation into account using $\lambda/\epsilon = 10$ cm.

magnetized, unmagnetized, and with a cadmium shield, respectively. The results of these measurements with their usual standard deviations are represented in Fig. 2. For comparison we have included in the figure the values given by H.W.H., measured at a field of 12,000 gauss, close to that at which our data were taken.

As the neutrons pass through increasing thicknesses of iron a non-monochromatic beam will change its spectral composition, and one can only determine values of p and λ/ϵ if proper corrections are applied for this change. If for every neutron velocity $npd \ll 1$ and assuming that the depolarization function $f(\lambda/\epsilon d)$ does not depend on the velocity, the observed transmission effect η' is given by

$$\eta' = \tfrac{1}{2} n^2 d^2 \frac{\int_0^\infty p^2(t) F(t) e^{-n\sigma(t)d} dt}{\int_0^\infty F(t) e^{-n\sigma(t)d} dt} f\left(\frac{\lambda}{\epsilon d}\right), \qquad (7)$$

where $F(t)$ represents the spectral distribution of the unattenuated neutron beam in terms of its time of flight t, and $p(t)$ the polarization cross section. If $\eta = h\eta'$ represents the transmission effect at the same thickness without spectral modification, the "hardening factor" h is given by

$$h(d) = \frac{\int p^2 F dt \int F e^{-n\sigma d} dt}{\int F dt \int p^2 F e^{-n\sigma d} dt}. \qquad (8)$$

The values of the hardening factor were computed on the basis of the measurements described below. In order to have a rough check on the calculation we measured the transmission effect $\eta''(d)$ for a thickness $d = 1''$ with a continuously unmagnetized piece of iron of thickness $d = 1''$ placed in the path of the beam. From Eqs. (7) and (8) it follows with the above-mentioned assumption that

$$[\eta'(d)]/[\eta''(d)] = [h(2d)]/[h(d)]. \qquad (9)$$

Relations Eqs. (7) and (9) hold, of course, only as long as $npd \ll 1$ for every value of v. For large thicknesses the relations become quite involved, particularly since

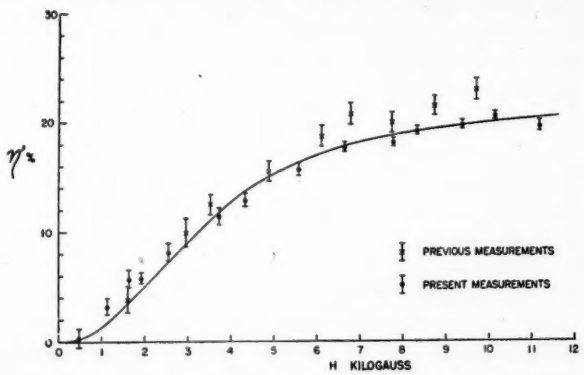

FIG. 3. Dependence of η' on magnetizing field H. Curve calculated with $p = 2.35 \times 10^{-24}$ cm² and using data from Fig. 6. ($d = 3.81$ cm.)

lack of saturation can no longer be described by the simple expression Eq. (3). For $d = 1''$, however, the approximation is still justifiable. The result of the measurement of η'' for $d = 2.54$ cm and with prefiltering by 2.54 cm of iron gave a ratio

$$[h(5.08)]/[h(2.54)] = 1.14 \pm .07.$$

Since, as mentioned before, the results of the previous investigation[8] were obtained with a detector of different spectral sensitivity, a direct comparison with the present results is not possible. It can be seen that for a thickness of $1\frac{1}{2}$ in. in the previous work η' was about 23 percent, as compared to 21 percent in the present investigation. It was therefore necessary to repeat the measurements of the dependence of η on the magnitude of the magnetizing field H. This was done for a thickness $d = 3.81$ cm in one of the magnets in the same manner as in the other measurements. The measured uncorrected values of η' are presented in Fig. 3, together with the values found by Bloch, Condit, and Staub.[8] The effect of the different spectral sensitivity is quite apparent. Values of the former work are somewhat higher than the present ones. This is to be expected, as the more shallow chamber used in the earlier work favors slower neutrons showing a higher polarization.

b. Experiments with Monochromatic Neutrons

As indicated in Section I, detailed measurements of the transmission effect with monochromatic neutrons

were made in the velocity region between 1400 m/sec. and 2800 m/sec. Data were taken at distances between source and detector of 2.74 m and 4 m with iron having a thickness of 2.54 cm and distributed equally between the two magnets and magnetized to 11,200 gauss. At a distance of 2.74 m the resolution was not very good, and even though the two time intervals τ_A and τ_B were reduced to 100 μsec. each, the exponential decay of the neutrons in the moderator reduces the resolution considerably. This is particularly true if the intensity of the neutrons decreases rapidly with increasing flight time. The data at 4 m are therefore much more reliable. As a check we also measured the transmission effect at a low velocity $v=1120$ m/sec. The observed values η of the transmission effect were divided by a constant value $f(x)=0.89$ as given in Section IV. The polarization cross section p follows then from Eq. (3) or the corresponding exact expression of Halpern and Holstein. The values of p determined in this manner are shown in Fig. 4. The horizontal bars represent the resolution due to the finite magnitude of τ_A and τ_B without taking into account the exponential decay of the neutron intensity.

For the determination of the hardening factor h, it is also necessary to know the spectral distribution quite accurately. As mentioned before, it was measured at two distances, 2.74 m and 5.0 m. The intensity at each value of t', measured for equal interval width τ_B, is

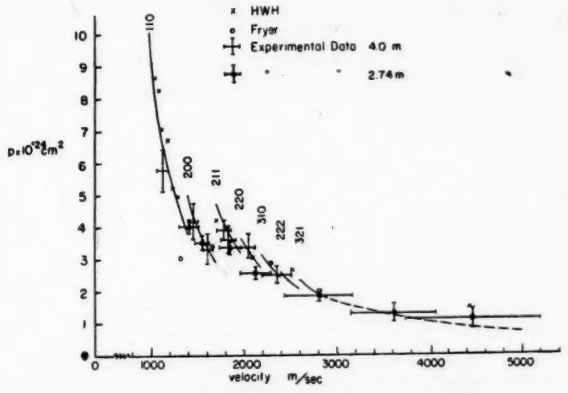

FIG. 4. Dependence of p on neutron velocity v. Curve according to Steinberger and Wick. Horizontal bars indicate resolution. Data of Fryer and H.W.H. are also included.

subject to various corrections. In the first place a small number (≈ 1 percent) of background counts has to be subtracted. In addition, at high neutron velocities there are always a number of low velocity neutrons present from the previous modulation cycle. Their number can be determined directly from the spectral distribution itself. Applying these two corrections one obtains the distribution $F'(t')$ per unit interval of time t'. Finally, since one wants to know the intensity in units of the inverse velocity, $t_0=t/L$, the variation of the delay Δt with flight time has to be considered. Since $F'(t')dt'$ $=F'(t+\Delta t)[1+(d\Delta t/dt)]dt$, one has $F(t_0)=$const. $\times F'(t_0L+\Delta t)[1+(d\Delta t/dt_0)/L]$. The values obtained in this manner for both distances are presented in Fig. 5. For comparison the figure also shows the distribution which one would expect if the neutrons were in equilibrium with the moderator. This function is a Maxwell distribution, multiplied with the velocity v to represent the flux and with the sensitivity function $[1-e^{-n_0\sigma(v)}]$ of the detector. n_0 represents the number of boron atoms per unit area of the detector, and $\sigma(v)$ $=a/v$ the cross section of boron. In terms of t_0 the function is therefore

$$F_M(t_0)=\frac{\text{const.}}{t_0^5}\exp\left(-\frac{m}{2kTt_0^2}\right)[1-e^{-n_0 a t_0}].$$

This function was matched to the experimental points for equal maximum value. Figure 5 shows that the positions of the maxima of the actual distribution and the Maxwellian are very close. For large values of t_0 there is a marked deficiency and for high velocities a rather large surplus of neutrons as compared to the Maxwellian; this is to be expected since the neutrons will not reach perfect thermal equilibrium in the moderator.

Finally, the determination of h also requires the knowledge of the total transmission cross section σ of iron as a function of the neutron velocity. Since H.W.H. made a very detailed investigation of this quantity, we determined σ as a check at three velocities, 1770, 3390, and 4750 m/sec. The values of σ were found to be 13.0 ± 0.1, 12.6± 0.1, and 12.5$\pm 0.1\times 10^{-24}$ cm^2, respectively, in good agreement with H.W.H.

In all our calculations we have assumed that, contrary to our previous belief, the size of the microcrystals in iron is large compared to the critical length l, as it was found by H.W.H. In order to ascertain this fact, the grain size in the iron samples was investigated

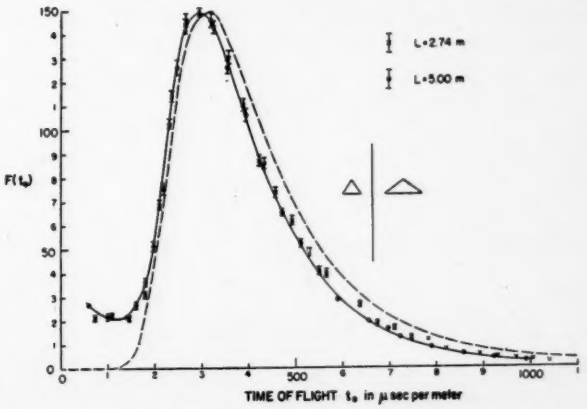

FIG. 5. Spectral distribution of neutrons per unit flight time interval. Dotted curve calculated for Maxwellian distribution at room temperature. The points on the right and on the left side of the vertical line were taken with different time intervals; the detection sensitivity in the two cases is indicated respectively by the two triangles.

metallographically.†† It was found that in two planes, oriented differently relative to the rolling direction of the steel, the average grain size was identical and equal to 35×10^{-4} cm. This is very much larger than the critical length and consequently the first alternative of Eq. (6) is well justified.

IV. RESULTS AND DISCUSSION

Figure 4 shows that the present experimental data are in good agreement with the recent calculations of Steinberger and Wick. Actually, these authors have computed p for the two alternatives, assuming the electronic wave function of the iron atom to have either zero slope or zero value at the atomic radius. The values of p computed for zero slope are somewhat smaller throughout and seem to fit the present data and those of H.W.H. somewhat better. These latter values were computed from the observed transmission effects η as given by these authors, using a constant value of $f(x)=0.81$. Four values of Fryer[7] were also recalculated on the basis of a constant $f(x)=0.71$. Our present data show rather clearly that the magnitude of the discontinuities of p at $v=1390$ and 1700 m/sec. are in good agreement with the calculations of Steinberger and Wick. There arises, of course, the question whether this agreement is not somewhat fortuitous. While the inelastic scattering due to thermal motion has been taken into account in the calculations, other sources of incoherent scattering have been disregarded. The only additional type of incoherent scattering which can contribute to the polarization are lattice imperfections, while spin-dependent scattering and isotopic-disorder scattering should not contribute to p. A preliminary study in this laboratory by Mr. M. Nielsen of the transmission of monochromatic neutrons through a single crystal of iron as suggested by Halpern[3] seems to indicate that the scattering cross section of a single crystal is considerably larger than one would expect from inelastic lattice scattering alone. However, the observed polarization effects in the single crystal seem to be very small, indicating, as is to be expected, that only the inelastic lattice scattering contributes to the polarization effect.

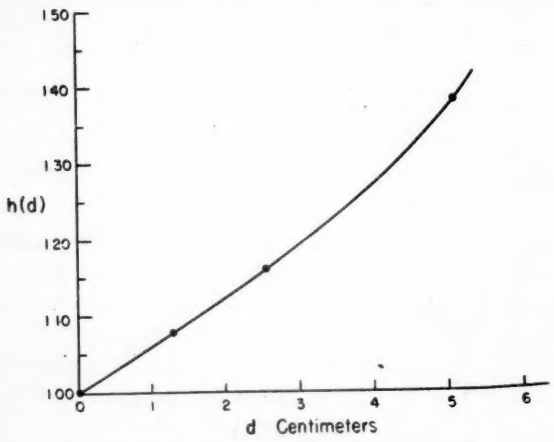

FIG. 6. Hardening factor h *versus* thickness d.

From the polarization cross section, the total transmission cross section and the spectral distribution, the values of the hardening factor h were calculated by numerical integration for three thicknesses of $d=1.27$, 2.54, and 5.08 cm, according to Eq. (8). The values of h for other thicknesses were obtained by interpolation according to the curve shown in Fig. 6. Since the theoretical values of p seem to be consistently somewhat higher than our observed values, we have lowered the theoretical values by 5 percent for our calculations. At velocities larger than 2800 m/sec. we have extrapolated Steinberger and Wick's curve, using the form factor given by Hamermesh.[5] The values of the transmission cross section σ were obtained from a curve fitted to the observed values of H.W.H. in such a manner that the ratio of the discontinuities agreed with that of the curve computed by Halpern, Hamermesh, and Johnson.[4] The results of the calculations of h for 2.54 and 5.08 cm are 1.163 and 1.39, respectively, giving a ratio of 1.19 as compared to the measured ratio 1.14 ± 0.07. Similarly, one can obtain a crude check of the calculations from the data of Bloch, Condit, and Staub. The difference in the observed values of $\bar{p}$ at $d=1.90$ and 3.8 cm indicates a ratio of the hardening factors of 1.15 ± 0.05 as compared to the calculated values of $1.256/1.116=1.12$. After correcting the values of η' with the calculated hardening factors, the average value $\bar{p}$ and the parameter λ/ϵ can be found by fitting the η-values to a law of the form,

$$\eta=(\cosh n\bar{p}d-1)f(\lambda/\epsilon d).$$

This law is not correct, of course, for $npd\approx1$, but should at least be a better approximation than a simple proportionality with d^2. The best fit is obtained with $\bar{p}=2.35\pm.1\times10^{-24}$ cm^2 and λ/ϵ lying between 5 and 35 cm with a most probable value of 10 cm. The reason for this large uncertainty is obvious. Since all $f(x)$ values deviate only little from unity, they are very insensitive to large variations in x, or in other words, the iron samples are indeed quite well saturated magnetically. The resultant value of $\bar{p}$ is in excellent agreement with the value given by Bloch, Condit, and Staub. If one applies the same corrections for hardening of the beam to their result (2.1 and 2.2×10^{-24} cm^2, respectively) one obtains the same value for both thicknesses of about 2.45×10^{-24} cm^2. The slightly larger value of $\bar{p}$ is of course caused by the use of a detector of different sensitivity. The value of 2.35×10^{-24} cm^2 is again very much lower than 3.15×10^{-24} cm^2 as given by H.W.H., but the reason for the difference seems clearly to lie in the different spectral composition of the neutrons and possibly a different sensitivity of the detector. The values of η' at different thicknesses d

†† We are greatly indebted to Professor O. C. Shepard of the Department of Metallurgical Engineering at Stanford for carrying out this investigation.

were measured by us at a field strength very close to that of H.W.H. Assuming that the degree of magnetic saturation is roughly the same, it appears from the fact that the values of H.W.H. at small d's are about 1.7 times larger than ours. The effective cross section should be $(1.7)^{\frac{1}{2}}$ times larger than in our case, or about 3.05×10^{-24} cm². Actually, the drop in the ratio of the values of η' of H.W.H. and the present measurements at larger thicknesses indicates that the degree of magnetic saturation in our case is slightly higher. In Fig. 2 the curve $\eta'=\eta_\infty f(x)/h$ is computed with the values of $\bar{p}$ and λ/ϵ as given above. We have also calculated by numerical integration over the measured spectrum the polarization cross section $\bar{p}$ which one would expect for non-monochromatic neutrons, again using the values of $p(v)$ of Steinberger and Wick, lowered by 5 percent. The calculations give $\bar{p}=2.42$, 2.45, 2.61×10^{-24} cm² for $d=1.27$, 2.54, and 5.08 cm, respectively, as compared to the measured value of 2.35×10^{-24} cm². For the purpose of evaluating $\bar{p}$ from the measured values of η we assumed a relation of the form: $\eta=[\cosh npd-1]f(x)$ to hold. While for $npd\ll1$ this is correct even for the case of a complex neutron spectrum, the relation certainly does not hold for $npd\sim1$ and $f(x)\neq1$ even for monochromatic neutrons. The exact law for monochromatic neutrons given by Halpern and Holstein is quite involved and for a complex neutron spectrum it would predict a rather complicated dependence of η on d. While the simple relation $\eta=\frac{1}{2}n^2\bar{p}^2d^2f(x)$ for large values of npd leads to an underestimate of η, a relation of the form $\eta=(\cosh npd-1)f(x)$ results for values of $f(x)$ close to unity in a slight overestimate of η. The agreement between the values of $\bar{p}$ calculated from the observed values of η and from the spectral distribution is satisfactory for thicknesses $d=1.27$ and 2.54 cm. For $d=5.08$ cm the difference of 12 percent between the value of $\bar{p}$ inferred from the observed values of η and that calculated from the spectral distribution is therefore not surprising in view of the fact that in this case, for certain values of the velocity, npd becomes as large as 4. For a true Maxwellian distribution and a thick detector, the calculation for $d=2.54$ cm gives a value of $\bar{p}=2.75\times10^{-24}$ cm², showing clearly the rather sensitive dependence of the transmission effect on the spectral distribution.

The evidence that the difference in the observed values of $\bar{p}$ is not caused by an overestimate of $1/\epsilon$ by Bloch, Condit, and Staub, as suggested by H.W.H., is further corroborated by the evaluation of the measurements of the dependence of η on H. With the value $\bar{p}=2.35\times10^{-24}$ cm² the quantity x is determined for each value of the field H, as represented in Fig. 7. In order to find the proportionality constant λ/d we used the direct magnetic measurements of Bloch, Hamermesh, and Staub in the region between 1600 gauss and

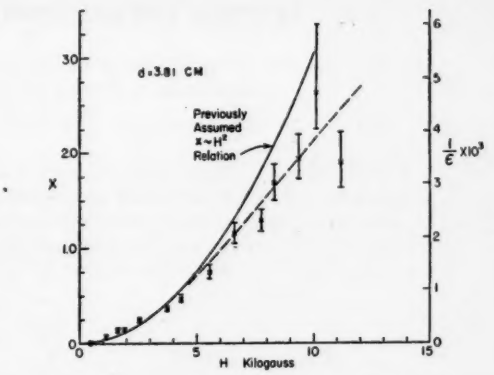

FIG. 7. Dependence of $1/\epsilon$ the degree of magnetic saturation on the magnetizing field H. Solid curve according to the previously assumed quadratic law.

4500 gauss. The observed values of x indeed fit the law $1/\epsilon=bH^2$ quite well in this region and the parameter λ is found to be $\lambda=(21.5\pm2)\times10^{-4}$ cm, and therefore the size of the microcrystals: $\delta=2\lambda=(43\pm4)\times10^{-4}$ cm. in close agreement with the metallurgical determination. Actually, not too much significance should be attributed to this agreement. The microcrystalline size δ as determined by neutron depolarization is certainly only to the order of magnitude equal to that of the average microscopic determination.

Finally, Fig. 7 shows, at the right-hand ordinate, how $1/\epsilon$ depends on H. It can indeed be seen that $1/\epsilon$ does not increase as rapidly with H as the quadratic law predicts for fields in excess of 5000 gauss. It is difficult to establish the exact form of the law since again the measured quantity $f(x)$ becomes increasingly less sensitive to changes in x. Assuming, for instance, a linear dependence as indicated in Fig. 7 by the dotted line, one can, with the reduced values of x and $f(x)$ replot the data of Bloch, Condit, and Staub. With the values $\bar{p}=2.45\times10^{-24}$ cm² and $\lambda=21.5\times10^{-4}$ cm their data fit the calculated curve exceedingly well. The value of $\bar{p}$ thus determined is slightly higher than either of the two reported previously. It is to be remembered, however, that the previous figures were not corrected for hardening. Although the present lower values of $1/\epsilon$ shift the points at the highest magnetic fields towards appreciably lower values of the abscissa, this does not noticeably affect the resultant value of $\bar{p}$ since η values at these points are close to the saturation value η_∞ as shown by their almost complete independence of $1/\epsilon$.

V. ACKNOWLEDGMENT

The authors wish to thank Professors F. Bloch and G. C. Wick for many helpful discussions and Mr. Melvin Nielsen for assistance in the construction of some of the equipment and the taking of data.

Multiple Diffuse Small Angle Scattering of X-Rays*

DAVID L. DEXTER AND W. W. BEEMAN
Department of Physics, University of Wisconsin, Madison, Wisconsin
(Received August 15, 1949)

The problem of multiple x-ray scattering from spherical particles of radius much larger than the wave-length is treated using the Guinier approximate scattering function. The total scattered intensity is found to be a sum of Gaussians in the polar angle with coefficients dependent on the sample thickness. A method is discussed for determining particle sizes from the variation of the width of the scattering curve with sample thickness. Experimental results are given for two carbon blacks.

INTRODUCTION

MUCH theoretical and experimental work has been done on the subject of small angle x-ray scattering, generally for the purpose of obtaining particle sizes, shapes, and size distributions.[1] Previous work has been based on the assumption that there is negligible multiple scattering so that the angular distribution of the scattered radiation is independent of the sample thickness.[2] In this paper we obtain an expression for the intensity of coherently scattered x-radiation as a function both of angular deviation from the incident beam direction and of sample thickness, especially for thicknesses great enough so that considerable multiple scattering occurs.

THEORETICAL

It is assumed that the incident beam is composed of parallel monochromatic x-rays of wave-length λ, that the Z axis (beam direction) is an axis of cylindrical symmetry, and that the radiation intensity is constant over the cross section of the incident beam. It is also assumed that the scattering material consists of randomly arranged identical spherical particles of radius $a \sim 10^2$ or $10^3\lambda$. No account is taken of refraction within the particles or of interparticle interference.

The calculations are based on Guinier's approximate single scattering function for a sphere,[3] which states

$$I(\theta)=N^2J\frac{r_0^2}{r^2}\exp\left(-\frac{1}{5}\left(\frac{2\pi a}{\lambda}\right)^2\theta^2\right), \qquad (1)$$

where $I(\theta)$ is the scattered intensity at a distance r from the particle and at an angle θ with the incident beam, N is the number of electrons in a particle, J the incident beam intensity, and r_0 the classical electron radius.

To simplify the calculation it is assumed that the x-radiation scattered from a particle P_i and intercepted by another particle P_j is a plane wave of intensity constant throughout P_j but proportional to r_{ij}^{-2}, where r_{ij} is the center-to-center distance of the ith and jth particles.

With this assumption the intensity of radiation scattered from P_j which was previously scattered from P_i is

$$I_{ij}=\left\{JN^2\frac{r_0^2}{r_{ij}^2}\exp\left(-\frac{2}{9}\left(\frac{2\pi a}{\lambda}\right)^2\theta_{ij}^2\right)\right\}\frac{N^2r_0^2}{R_j^2}\times\exp\left(-\frac{2}{9}\left(\frac{2\pi a}{\lambda}\right)^2\delta_{ij}^2\right). \qquad (2)$$

The coefficient 1/5 has been changed to 2/9 in order to have the area under the Gaussian agree with that under the curve of the exact scattering function. In this expression (see Fig. 1) θ_{ij} is the angle between the polar axis and the line connecting P_i and P_j, R_j is the distance from P_j to the observer, and δ_{ij} is the angle between "the line P_iP_j" and the direction of observation. Now expressing δ_{ij} in terms of θ_{ij}, θ_j (the angle between the direction of observation and the polar axis) and $\varphi_{ij}-\varphi_j$ (the difference between the azimuthal angle of "the line P_iP_j" and that of the direction of observation), one obtains

$$\delta_{ij}^2=\theta_{ij}^2+\theta_j^2+2\theta_{ij}\theta_j\cos(\varphi_{ij}-\varphi_j), \qquad (3)$$

where the angles θ_{ij}, θ_j, and δ_{ij} are assumed small. The twice-scattered radiation intensity from P_j is given by the summation of (2) over all particles P_i. Replacing the summation by an integration,

$$I_2(\theta_j)=K_2\int_0^{\pi}\int_{\varphi_j}^{2\pi+\varphi_j}\exp\left(-\frac{2}{9}\left(\frac{2\pi a}{\lambda}\right)^2\theta_{ij}^2\right)\times\exp\left(-\frac{2}{9}\left(\frac{2\pi a}{\lambda}\right)^2[\theta_{ij}^2+\theta_j^2+2\theta_{ij}\theta_j\cos(\varphi_{ij}-\varphi_j)]\right)\theta_{ij}d\theta_{ij}d\varphi_{ij}$$

$$=\frac{9\lambda^2}{16\pi a^2}K_2\exp\left(-\frac{1}{9}\left(\frac{2\pi a}{\lambda}\right)^2\theta_j^2\right), \qquad (4)$$

* This work was supported by ONR and the Wisconsin Alumni Research Foundation.

[1] A. Guinier, Ann. de physique 12, 161 (1939); R. Hosemann, Zeits. f. Elektrochemie 46, 535 (1940); B. E. Warren, J. App. Phys. 20, 96 (1949); Kratky and Porod, Acta Physica Austriaca II, 133 (1948). For further references see Shull and Roess, J. App. Phys. 18, 295 (1947).

[2] A multiple refraction treatment has been carried out by R. von Nardroff, Phys. Rev. 28, 240 (1926).

[3] A. Guinier, see reference 1.

where K_2 is independent of θ_j. In the evaluation of this integral use has been made of $2\pi a/\lambda \gg 1$. This relation, which ensures that the entire scattering process is concentrated in a very small angle about the forward direction, also enables us to neglect the integration with respect to r_{ij}, as has been done in (4), as long as we are interested only in the angular distribution and not in the intensity of the doubly scattered radiation. Stated in another way, the very small angular deviations in the scattered beam permit us to ignore any limitations on the directions from which P_j can receive once-scattered radiation even for P_j near the edge of the sample. Since all P_j scatter identically the total twice-scattered beam will have the angular distribution (4). An iteration procedure shows that the angular dependence of the kth scattered component is given by

$$I_k(\theta)=K_k \exp\left(-\frac{2}{9k}\left(\frac{2\pi a}{\lambda}\right)^2\theta^2\right). \tag{5}$$

The relative intensities of the various scattered components as a function of sample thickness can be found from a consideration of their growth and decay within the sample. Neglecting edge effects, let I_k now be the integrated (over angle) intensity of the kth scattered component. The unscattered component I_0 decays at a rate determined by absorption and by first scattering; I_1 grows at a rate proportional to the amount of unscattered radiation present and to the mass scattering coefficient, and decays at a rate proportional to I_1 times the sum of the mass absorption and the mass scattering coefficients. Both coefficients are independent of the previous history of the photon. Thus, let μ_a denote the mass absorption coefficient, μ_s the mass scattering coefficient, $\mu=\mu_a+\mu_s$ the total mass coefficient for decay of a given scattered component, and m the number of grams per cm² of the sample through which the beam has passed. Then

$$\begin{aligned} dI_0&=-\mu I_0 dm,\\ dI_1&=\mu_s I_0 dm-\mu I_1 dm,\\ &\cdots\\ dI_k&=\mu_s I_{k-1} dm-\mu I_k dm.\\ &\cdots \end{aligned} \tag{6}$$

These equations have the solution

$$\begin{aligned} I_k&=Je^{-\mu m}\mu_s{}^k m^k/k!,\\ \sum_{k=0}^{\infty} I_k&=Je^{-\mu_a m} \end{aligned} \tag{7}$$

and, as must be the case, summing over all I_k shows that the total intensity of the radiation in the sample decays at a rate determined only by true absorption.

By integrating the Guinier function over 4π solid angle μ_s can easily be shown to be $9nN^2r_0^2\lambda^2/8\pi a^2$, where n is the number of particles per gram. Let x be defined by

$$x\equiv\mu_s m=9nN^2r_0^2\lambda^2 m/8\pi a^2. \tag{8}$$

Since I_k in (7) is proportional to the total intensity over all angles in the kth scattered component the proper coefficients for the previously derived angular distributions can now be obtained easily.

$$2\pi C_k\int_0^{\pi}\exp\left(-\frac{2}{9k}\left(\frac{2\pi a}{\lambda}\right)^2\theta^2\right)\theta d\theta=Je^{-\mu m}x^k/k!,$$

$$C_k=\frac{8\pi a^2}{9\lambda^2}Je^{-\mu m}\frac{x^k}{kk!}, \tag{9}$$

for $k\neq 0$, and so the total scattered intensity is proportional to

$$I(\theta,m)=Je^{-\mu m}\frac{8\pi a^2}{9\lambda^2}\sum_1^{\infty}\frac{x^k}{kk!}\exp\left(-\frac{2}{9k}\left(\frac{2\pi a}{\lambda}\right)^2\theta^2\right). \tag{10}$$

For $x\ll 1$ only a small fraction of the incident radiation is scattered at all, and the scattering *versus* angle curve will be complicated at the center by the presence of the unscattered radiation, but as x becomes much larger than 1 the amount of unscattered radiation becomes neligible. For $x\gg 1$ it is clear that $x^k/kk!$ considered as a function of k has a maximum for k of the same order as x. If x is large enough, the important terms in the sum have an index k so large that Stirling's formula is applicable. The most important term, that is, the term with the largest coefficient, can now be obtained by maximizing $x^k/kk!$. It is the term for which $k=x$. The angular width of the kth scattered component at a height $1/e$ of the central maximum is

$$W=3\lambda(k/2)^{\frac{1}{2}}/\pi a. \tag{11}$$

On the assumption that for sufficiently thick scatterers the scattering curve will be very similar to that of the most intense scattered component we may calculate using $k=x$ and Eq. (8)

$$\alpha\equiv\frac{dW}{d(m)^{\frac{1}{2}}}=\frac{3\lambda}{\pi a\sqrt{2}}\mu_s{}^{\frac{1}{2}}=\frac{9\lambda^2 N r_0 (n)^{\frac{1}{2}}}{4\pi^{\frac{1}{2}}a^2} \tag{12}$$

and for particles of low atomic number, where the atomic weights of the constituent atoms are twice their

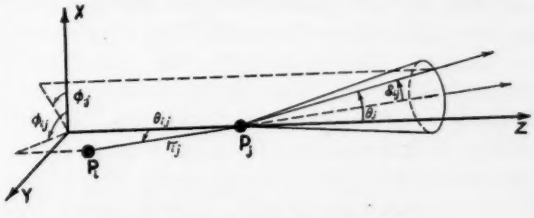

FIG. 1. Geometry of double scattering.

atomic numbers

$$\alpha=\frac{3\lambda^2}{4\pi}r_0L(3\rho/a)^{\frac{1}{2}}, \tag{13}$$

where L is Avogadro's number and ρ is the density within a particle. Thus

$$a=\frac{27}{16\pi^2}\lambda^4\frac{r_0^2L^2}{\alpha^2}\rho, \tag{14}$$

giving the particle radius from the slope of the width *versus* square root of the mass per unit area curve.

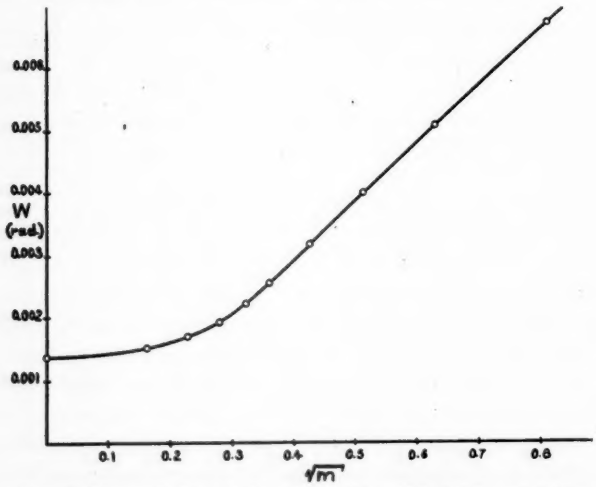

FIG. 2. Theoretical variation of the $1/e$ width of the total scattering curve as a function of the square root of m (in g/cm²) for $\lambda=1.54$A, $a=750$A, and $\rho=2$ g/cm³.

It should be noted that this method of determining particle sizes is not restricted to cylindrically symmetric geometry. With slit system or double-crystal spectrometer geometry the most important term is still that for which $k=x$, and the particle radius is given by the above.

Figure 2 shows the variation with $m^{\frac{1}{2}}$ of the theoretical scattering curve width for $\lambda=1.54$A, $\rho=2$ g/cm³, and $a=750$A. The circles were computed numerically from (10) at values of $x=0$, 1, 2, 3, 4, 5, 7, 10, 15, and 25. It is found that the slope in the vicinity of $x=10$ or $m^{\frac{1}{2}}=0.51$ ($\alpha=9.7\times10^{-3}$) is larger than the slope for x large as computed by means of Stirling's formula ($\alpha=8.6\times10^{-3}$). Thus the w *versus* $m^{\frac{1}{2}}$ curve has an inflection point, becomes slightly concave down and approaches a constant slope for x large. This is a result of the fact that for small x the most important term is that for which $k=x-2$, so that the total scattering curve has a width appreciably less than that of a Gaussian with $k=x$. For x large, however, the total scattering function width is closely equal to that of Gaussian with $k=x$. Thus for small x the index of the most important term increases more rapidly than x and the width consequently increases more rapidly than the square root of m, giving a larger slope at small x than the limiting value. By $x=25$ the slope has decreased to about $\alpha=9.1\times10^{-3}$.

EXPERIMENTAL

Multiple scattering is easily obtained experimentally if the mass absorption coefficient is not so great that absorption has reduced the intensity to an inconveniently low value before appreciable multiple scattering has occurred. Since

$$\mu_s=9nN^2r_0^2\lambda^2/8\pi a^2=1.08\lambda^2a\rho\times10^{22} \tag{15}$$

multiple scattering is feasible experimentally if

$$a_{\mathrm{A}}\gtrsim\mu_a/0.0108\lambda_{\mathrm{A}}{}^2\rho,$$

where the subscript A denotes that the quantity is expressed in angstrom units. For carbon particles with $a=750$A, $\rho=2$ g/cm³, and $\lambda=1.54$A μ_s is about 8 times greater than μ_a.

Figure 3 shows experimental results obtained with a three-crystal spectrometer[4] for two carbon blacks, Godfrey L. Cabot P-33 and Sterling L, using Fe radiation at 25–32 kv. Comparisons of theory and experiment are complicated by the wide distributions of particle sizes usually encountered in colloidal materials. In particular the measured single scattering width of P-33 is much too small as may be seen from a comparison of Figs. 2 and 3. Since the total scattering coefficient per electron of a particle goes up as the radius of the particle, and the scattered energy is concentrated in an angle inversely proportional to the radius, a few large particles may invalidate any measurement of the single scattering width. In addition the average particle size in our samples is greater than one generally attempts to measure with single scattering techniques and thus the problem of correctly subtracting the unscattered radiation is greatly aggravated.

We have attempted the customary plot of log of scattered intensity *versus* the square of the scattering angle of our single scattering data for P-33. Particle sizes differing by two orders of magnitude could be obtained from different parts of the curve. Most of this difficulty also can be attributed to interference of the unscattered radiation.

Much less equivocal and more reasonable estimates of particle size can be obtained by applying (14) to the linear parts of the curves of Fig. 3. Particle radii were found to be 770 and 480A for P-33 and Sterling L, respectively. The P-33 particle size obtained in this way is larger than that found by earlier workers, who find mean radii of from 370 to 670A. It agrees much better with a weighted average size, $\Sigma f(a)a^3/\Sigma f(a)a^2$ which is obtained naturally from adsorption data, where $f(a)$ is the distribution function of the radii. Values between 715 and 780A have been obtained for this quantity from electron microscope and nitrogen adsorption data.[5]

[4] To be described soon in J. App. Phys.

[5] For a comparison of work on P-33, see R. B. Anderson and P. H. Emmet, J. App. Phys. 19, 367 (1948).

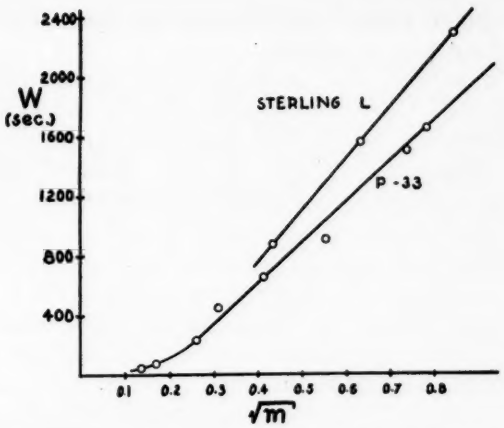

FIG. 3. Experimental curves for carbon blacks with $\lambda=1.93$A showing the variation of the curve width with $m^{\frac{1}{2}}$ (m in g/cm^2).

Electron micrographs were taken of Sterling L by Dr. Paul Kaesberg of the University of Wisconsin. There was a great deal of clustering into large agglomerates but most of the individual particles were of radii 150 to 500A.

For sufficiently thick samples a linear relation between the width of the scattering curve and the square root of the mass per unit area would be expected even for a distribution of particle sizes. To calculate what weighted average is thus obtained seems a formidable problem which we have not attempted. However, our agreement with the careful nitrogen adsorption work of Anderson and Emmet[5] is evidence that the method will be useful for particles too large to be treated by standard single-scattering methods and yet so small that refraction is not appreciable.

For much larger particles ($a\gtrsim 10$ microns) correct particle sizes are expected from von Nardroff's multiple refraction treatment, based on geometric optics,[2] in which is considered only the term corresponding to the most probable number of x-ray-particle interactions. The fact that he obtains a Gaussian for his final multiple refraction formula is a result of statistical analysis, and not of the single-process function, which is the cause of the series of Gaussians obtained here.

According to both multiple process theories α varies directly with $\lambda^2(\rho/a)^{\frac{1}{2}}$ with different proportionality constants in the two cases. Thus varying the experimental parameters does not distinguish between the theories.

Experimental intensity *versus* angle curves were obtained using Godfrey L. Cabot Spheron Grade 6 carbon black with the three-crystal spectrometer and Fe radiation. Six samples were tested with m ranging from 0.0210 to 0.5918 g/cm^2. The thicker specimens show a definite narrow pip at the center, corresponding to the unscattered radiation. This was also observed with the thinner P-33 samples. The thinner specimens of Spheron Grade 6 with $x\lesssim 1$ cannot be unambiguously separated into scattered and unscattered curves as for the thicker samples, but the ratio of unscattered central ordinate to scattered ordinate is in at least good qualitative agreement with the multiple scattering formulas assuming infinite slit geometry. A curve for a sample of intermediate thickness, $m=0.1625$ g/cm^2 is reproduced in Fig. 4. The narrow peak of unscattered radiation merges abruptly into the scattered intensity curve, showing a ratio of peak height to scattered radiation height of between 10 and 14. This is to be compared with the ratio 10.7 as predicted from the multiple scattering equations assuming $a=150$A. For the two thickest samples x is equal to 4.18 and 7.12, and more unscattered central intensity is present than the theory predicts by a factor of about 3 and 8, respectively. This is due to the presence of second order radiation, which, because of its lower total mass coefficient, becomes important for thick samples.

A radius of about 150A for Spheron Grade 6 was obtained by Anderson and Emmet.[5] Our measurements from Eq. (14) give a somewhat larger result (roughly 180A). The reliability of our measurement is doubtful as we were not able to reach high scattering multiplicities with these smaller particles.

The importance of the observation of the pip is, of course, that it is further strong experimental evidence that we are dealing with a low order multiple process where the undeviated incident radiation has still a reasonable probability of getting through. If the cause of the broadening were refraction one would expect a smooth angular distribution (a Gaussian without a pip). This follows from the fact that the cross section for refraction is the geometrical cross section. Even with our thinnest samples a traversing ray must penetrate many particles. Thus if refraction were a correct physical model for particles in this size range it would have to be a highly multiple refraction. According to

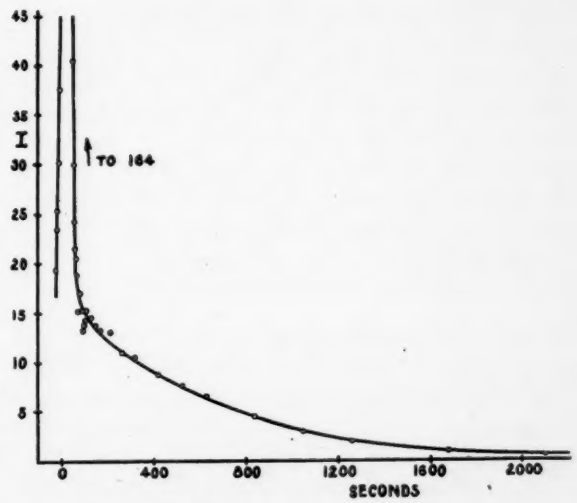

FIG. 4. Scattered intensity from Godfrey L. Cabot Spheron Grade 6 carbon black as a function of angle with $\lambda=1.93$A, $\rho=2$ g/cm^3, $m=0.1625$ g/cm^2, and $a\sim 150$A.

the multiple refraction theory the width of the single Gaussian would be 4530 seconds for the curve shown in Fig. 4.

The theory developed in this paper should be applicable, without serious modification, to the passage of slow neutrons through colloidal materials. Indeed, because of the relatively lesser importance of neutron absorption, higher scattering multiplicities would be experimentally obtainable.

The authors wish to express their appreciation to Godfrey L. Cabot, Incorporated, for the carbon black samples used, to Dr. Paul Kaesberg for the electron micrographs of Sterling L and to Mr. Michael Shurman who assisted with the numerical calculations.

PHYSICAL REVIEW VOLUME 76, NUMBER 12 DECEMBER 15, 1949

The Density Effect for Cosmic-Ray Mesons*

W. L. WHITTEMORE AND J. C. STREET
Lyman Laboratory of Physics, Harvard University, Cambridge, Massachusetts

(Received September 9, 1949)

This paper deals with a detailed study of individual pulses produced by fast cosmic-ray mesons in a specimen of silver chloride. A discussion is given of the pulse distributions obtained from the experiment, which was designed to show the increase with energy of the rate of ionization in the relativistic region and the correction to this increase due to the density effect. The measured values are compared with theoretical distributions which take fluctuation and density effect into account. It is concluded that the results agree well with the fluctuation theory developed by Symon and the density effect corrections as given by Halpern and Hall.

1. INTRODUCTION

IN 1945 van Heerden[1] reported the technique of using a crystal of silver chloride as an ionization detector. Such a detector is sufficiently sensitive to measure the ionization produced by a singly charged particle ionizing at the minimum rate. Hofstadter[2] has reported the observation of pulses produced in silver chloride and certain other substances by gamma-rays.

The theoretical treatment of the average ionization produced by fast particles has been given by Bethe and by Bloch. Their results have been summarized by Heitler.[3a] Curves are available in an article by Rossi and Greisen.[3b]

The Bethe-Bloch theory pertains to the case of disperse media. For a condensed medium an additional effect, called the density effect, reduces the rate of ionization for charged particles. The mechanism for the density effect is the polarization of the atoms of the medium with the resulting reduction of the distant electromagnetic interactions. This effect, first suggested by Swann and discussed briefly by Fermi,[4] has been treated in detail by Wick,[5] and Halpern and Hall.[6] The theory of average ionization for an energetic particle ionizing near the minimum rate has been tested experimentally by Corson and Brode[7] and Hazen,[8] who partially verified the rise in the rate of ionization in the relativistic region predicted by the theory. Further tests were performed by Hayward[9] and Hereford[10] to search for the existence of the density effect. Both of these workers report results which agree with the Bethe-Bloch theory of ionization as corrected for the density effect by Halpern and Hall. In each case, however, the experiment is indirect and the results sketchy.

The theory of ionization, including polarization effects, seems to be sound, but has not been tested thoroughly at high energy. In the crystal counter we have an instrument suited for such a study. We cannot directly compare the rate of ionization deduced from the crystal pulse with the *average* rate of ionization given in the above-mentioned theory because the pulses produced in the crystal by monoenergetic particles suffer a large fluctuation due to the fluctuation in energy loss. Landau[11] has investigated this fluctuation in energy lost by a particle in traversing a *thin* thickness of absorber. Similar calculations, carried out in detail by Symon[12] for all thickness of absorber, make it possible to predict the fluctuation in energy loss for mesons. Believing the crystal ionization detector to be ideally suited for the study of ionization at high energy, we have attacked the problem in the following manner.

* Assisted by the ONR and AEC.

[1] P. J. van Heerden, "The crystal counter," dissertation, Utrecht (1945).

[2] R. Hofstadter, Phys. Rev. **72**, 977 (1947); Phys. Rev. **72**, 1120 (1947).

[3a] W. Heitler, *The Quantum Theory of Radiation* (Oxford University Press, London, 1936), p. 218.

[3b] B. Rossi and K. Greisen, Rev. Mod. Phys. **13**, 240 (1941).

[4] W. F. G. Swann, J. Franklin Inst. **226**, 598 (1938); E. Fermi, Phys. Rev. **57**, 485 (1940).

[5] G. C. Wick, Nuovo Cimento **21**, 7 (1943).

[6] O. Halpern and H. Hall, Phys. Rev. **73**, 477 (1948).

[7] D. Corson and R. B. Brode, Phys. Rev. **53**, 773 (1938).

[8] W. E. Hazen, Phys. Rev. **67**, 269 (1945).

[9] E. Hayward, Phys. Rev. **72**, 937 (1948).

[10] F. L. Hereford, Phys. Rev. **74**, 574 (1948).

[11] L. Landau, J. Phys. U.S.S.R. **8**, 201 (1944).

[12] K. R. Symon, "Fluctuations in energy loss by charged particles," dissertation, Harvard University (1948).

2. PROCEDURE AND EQUIPMENT

The ionization curve for any charged particle, and in particular for mesons, plotted as a function of range, momentum, or energy, exhibits a unique point which is useful as a reference value in carrying out the experiment. This reference point is a minimum in the ionization or rate of energy-loss curve which, for mesons, occurs at about 250 Mev. Mesons having higher, or lower, energies than this ionize at a greater rate, and on the average, produce greater pulses in the crystal than those ionizing at the minimum rate. From the total energy spectrum of cosmic-ray mesons at sea level, those mesons were selected which ionized at the minimum rate. Another group was selected which ionized at a predictably greater rate. The crystal was arranged so as to examine the pulses of first one group and then the other. Because of a statistical fluctuation in the rate of ionization, the pulse heights due to mesons in each group were spread out into a distribution. The plan was to compare the shape of the experimental distributions of pulses in these two groups with the predicted pulse-height distributions and to compare the separation of the maxima of the two experimental distributions with that of the predicted distributions. The shapes of the distributions, especially for the minimum ionization group, constitute a check on the uniformity of response of the crystal specimen. The comparison of the measured separation of the maxima of the two experimental distributions with the predicted separation provides a test of the theory of the density effect.

It is well known that at sea level about eighty percent of the cosmic-ray events recorded by a vertical Geiger counter telescope are due to single mesons passing through the system. The remainder of the events is mainly due to electrons which, if of low energy, can be absorbed or, if of high energy, can be made to form an electron shower with high probability. A shower detector can be used to make the equipment relatively insensitive to multiple rays. The apparatus which permitted the study of only those events involving a single high energy meson is shown in Fig. 1. Above the crystal was placed a 1.8-cm slab of lead. Immediately below the crystal was a piece of lead 8.9 cm thick, large enough to cover completely the solid angle (0.1 steradian) defined by the Geiger counters C_1 and C_2. Between the counters C_2 and AC_2 were 23 cm of lead and between the counters AC_2 and C_3 there were 76 cm of lead and 2 cm of iron.

In addition to the desired events, a few, in which high energy mesons did not penetrate the crystal, were selected by the geometrical arrangement shown in Fig. 1. The solid angle was defined by the Geiger counter C_1 and the three counters at C_2. To select only those mesons penetrating the crystal, it would have been necessary to use only one counter in tray C_2. With three counters in tray C_2, the addition to the counting rate due to the particles penetrating the crystal was much

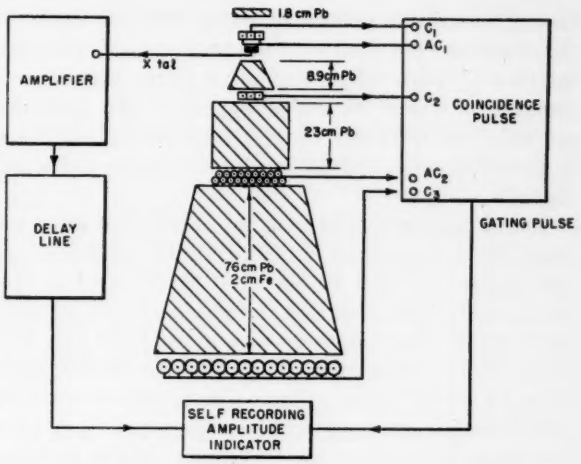

FIG. 1. Arrangement of counters and lead and block diagram of circuits.

larger than the addition due to those missing it. The counting rate was very small; therefore, the few events not involving the crystal were accepted in order to increase by nearly a factor of three the desired number. It seemed unwise to use an arrangement which required too long an observation period because of the uncertainty of maintaining constant operation of the crystal.

As suggested above, it was possible to eliminate a large number of electrons by using a shower detector in anticoincidence. The counters used to detect showers were those designated by AC_1 in Fig. 1. These two counters were connected in parallel and attached to the anticoincidence channel of the coincidence circuit. Thus, whenever a pulse appeared at C_1 simultaneously with one at AC_1, the event was very likely a shower and was automatically not recorded. To cause the largest number of electrons possible to produce showers, the optimum thickness of lead for producing showers was placed above the apparatus.

This entire equipment was placed in a room underground. Over the room there was a six-inch concrete roof covered with two feet of cinders, ashes, and dirt. Above this there was only sky for the entire solid angle subtended by the equipment. It was not essential for this experiment to place the equipment under a thin roof because energetic mesons observed at sea level do not interact strongly with matter. Hence, the absorber above the equipment did not alter appreciably the nature of the meson-component of the radiation used in the experiment.

The Geiger counters in tray AC_2 were 10-inch cylindrical glass counters with copper foil cathodes $\frac{7}{8}$ inch in diameter with an anode of 15-mil tungsten wire (in general the symbol C stands for coincidence, AC for anticoincidence, and the subscript denotes the tray). The counters in tray C_3 were 20-inch glass cylinders with copper cathodes 2 inches in diameter. The counters in the trays marked C_1, AC_1, and C_2 were each constructed from copper in units of three, each individual counter

having a sensitive volume of about $1\times1\times1\frac{1}{2}$ inch. All the counters were filled with the standard alcohol-argon mixture (1 part ethyl alcohol, 9 parts argon) to a pressure of about 10 cm of mercury. The operating potential was 990 volts, the plateau of each counter was at least 150 volts, and the mean overvoltage was about 75 volts.

The circuits employed were not unusual for an experiment of this type. The electronic circuit for the Geiger counters was similar to one used by Valley,[13] in that each counter tray like that designated by AC_2 and C_2 was divided into subgroups of 4 counters or less, each group being connected to its own 6AK5 pentode operating at normal plate voltage. The several type 6AK5 pentodes shared a common plate resistor so that all of the Geiger counters in the tray functioned as one tube because of the signal addition property of the common plate resistor. The coincidence circuit, which employed the familiar Rossi-type coincidence elements, produced a long gating pulse of 5000 μsec. duration following the desired chain of events at the Geiger counters.

The polycrystalline specimen of rolled silver chloride was supplied by the Harshaw Chemical Company. The preparation (mainly careful heat treatment and electrode surfacing) and detailed investigation of the crystal will be given in a forthcoming paper. For the purposes of this report it will suffice to say that the crystal was used as an ionization chamber. Full voltage saturation could not be obtained for the maximum voltage used. The degree of saturation (75 percent) obtained with the maximum field available (5240 volt/cm) did not vary during the experiment, which lasted four weeks. The capacity with respect to ground at the input of the amplifier was 72 ± 3 $\mu\mu$f. Most of this was due to the crystal.

The pulse produced in the crystal by a meson was amplified with a Los Alamos Model 100 preamplifier and amplifier with a pulse rise time of about 0.5 μsec. and a voltage gain of about 300,000. The crystal pulse, after amplification, was delayed before being fed into the self-recording amplitude indicator. The design of the indicator was based on a pulse lengthener due to Elmore modified so as to provide a means for blanking out all pulses from the crystal except those accompanied by the gating pulse from the coincidence circuit. The apparatus worked as follows. Depending on whether tray AC_2 or C_3 was used, the meson selected by the counters C_1 and C_2 stopped in the 23-cm block of lead or penetrated all of the lead. The pulse of ionization produced in the crystal by the meson was amplified and fed to the amplitude indicator which made a permanent record. A contribution to each of the two groups of events was made each day. This would eliminate any long term variation of the equipment. It was recognized that a better procedure would have given a simultaneous record of both groups requiring, however, more elaborate recording equipment.

[13] G. E. Valley, Phys. Rev. 72, 772 (1947).

3. EXPERIMENTAL RESULTS

With the apparatus shown in Fig. 1, the counting rates for the mesons stopping in the 23 cm of lead and for those penetrating 112 cm of lead as well as the counting rate for all mesons penetrating at least 8.9 cm of lead are shown in Table I. In this table we have quoted the standard error determined from the number of counts. The accidental counting rate is, in every case, far smaller and will be neglected.

The present experiment was made uncertain to some extent by scattering. Since scattering is more important for mesons of lower energy, the data most affected are those obtained for mesons stopping in the 23-cm block of lead. A computation has shown that, since the scattering falls off inversely with the energy, the majority of the mesons scattering out of the beam did not have an energy greatly in excess of 10^9 electron volts, and thus would not be expected to ionize at a substantially greater rate than did those which stopped in the lead. Therefore, we feel that the contribution of these pulses to the minimum ionization distribution could not have altered its shape or the position of its maximum by more than the uncertainty already inherent in the distribution.

In Fig. 2, we have exhibited the experimentally obtained differential distributions of mesons possessing the required ranges in lead. The data accumulated during the experiment were analyzed with allowance made for the slight non-linearity of the amplifier. The distributions will be discussed in terms of the voltage input to the main amplifier; but this voltage divided by 82 ± 8, the gain of the preamplifier, will give the voltage pulse at the crystal. The two histograms have essentially the same shape. The main difference is that the histogram obtained for mesons penetrating 112 cm of lead is displaced toward the region of larger pulses by a small amount, as it should be if the rate of ionization increases for high energy mesons.

The separation between the two curves is not large, however. That the separation is real and not due to statistical variation is seen from the fact that, when the two histograms are compared at and near their peaks, the relation of each rectangle of the histogram for mesons penetrating 112 cm of lead bears the relation to the other histogram it should if this histogram is indeed displaced to the region of larger pulses. In particular, the four rectangles to the left of the peak of the histogram for penetrating mesons are less high than the corresponding ones of the histogram for stopped mesons, whereas the rectangle at the peak and the next four are larger than the corresponding ones for the stopped mesons. A definite correlation exists for these nine rectangles. This relationship between the rectangles for the two histograms could occur by chance only once in $(2)^9=512$ times. The small probability that the separation between the histograms occurred by chance is taken as proof of the reality of the separation of the two distributions.

The values of the average and most probable pulses for the histograms will be useful later for the discussion of the results. For reasons to be discussed later, we cut off each histogram at a certain fraction of its peak, both below and above the peak, using the remaining part to calculate the average. For the histogram due to mesons stopping in 23 cm of lead, we used the portion of the data for the pulse heights between 1.60×10^{-2} volt and 3.40×10^{-2} volt. For the other histogram, we used the data for the pulse heights between 1.70 and 3.60×10^{-2} volt. The averages of the pulse heights computed for the case of mesons stopping in 23 cm of lead and those penetrating 112 cm of lead are 2.09 and 2.13×10^{-2} volt respectively. The most probable values for the pulse heights read from the histograms are $1.81(\pm5)\times10^{-2}$ volt and $1.88(\pm5)\times10^{-2}$ volt respectively.

4. DISCUSSION OF RESULTS

We would now like to derive as well as possible the distribution of pulses that one should expect from the experiment and to compare these with those obtained experimentally to see whether there is agreement with theory. We first assume that the crystal is a perfect ionization detector; later we take account, to a certain extent, of imperfections in the crystal, indicating experimental evidence of the divergence of the observations from those expected with an ideal instrument. The starting point for the calculation of the pulse height distributions are two sets of data, the first (theoretical) giving the average rate of ionization of mesons in iron as a function of their remaining range in air, and the second (experimental) giving the differential distribution of mesons as a function of their range in air. The collision loss was taken for iron rather than for silver chloride because calculations of the collision loss for silver chloride were not available and the ones for iron are not very different. This caused a small error in the predicted pulse heights which is of no consequence since the curve to be derived for the distribution as a function of average ionization will be used only illustratively. Actually two curves were considered for the collision loss, one taken from the usual formulas, and a second including the density effect, use being made of the results given by Halpern and Hall.[6] The curve giving the differential distribution of mesons at sea level as a function of the range in air represents the sum of the best experimental measurements to date.[14] From these combined data one can eliminate the range and compute in a standard but tedious manner curves giving the differential distribution of mesons at sea level as a function of the average rate of ionization in the crystal. There will be two such curves, depending upon whether or not the density effect is taken into account. The two curves are exhibited in Fig. 3, where the distribution is plotted on an arbitrary scale as a function of the average rate of ionization. The sharp, narrow peak, which is the same whether the density effect is included or not, gives the distribution for those mesons which penetrate 9 cm of lead and then stop in an additional 23 cm of lead. The other two solid portions of the curve are the distributions of those mesons which penetrate at least 112 cm of lead.

TABLE I. Counting rates of mesons of various penetrating powers.

	Mesons with range >8.9 cm of Pb	Mesons with 8.9 <range <32 cm Pb	Mesons with range >112 cm Pb
Counting rate	18.5±0.4/hr.	4.0±0.2/hr.	7.5±0.4/hr.
Percentage of mesons	100 percent	22±1 percent	41±2 percent

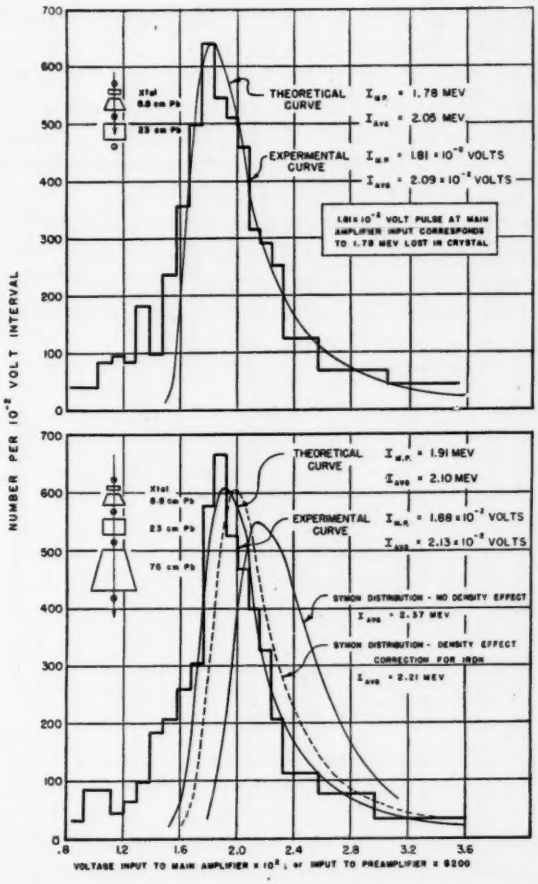
NUMBER PER 10^{-2} VOLT INTERVAL
THEORETICAL CURVE
EXPERIMENTAL CURVE
SYMON DISTRIBUTION - NO DENSITY EFFECT
SYMON DISTRIBUTION - DENSITY EFFECT CORRECTION FOR IRON
VOLTAGE INPUT TO MAIN AMPLIFIER

FIG. 2. Pulse height distributions due to cosmic-ray mesons selected as indicated. Histograms are experimental data.

Assuming no fluctuation in ionization, the curve in Fig. 3, taking the density effect into account, would represent the expected distribution in pulse sizes, since the crystal is relatively thin for high energy mesons, and the energy of the particle would change but little in passing through it.

There is, however, a substantial fluctuation in the rate of ionization of a high energy meson in penetrating a thin absorber. This fluctuation in ionization is contributed to a large degree by the higher energy transfers involved in the collision process. The very complete tables given in K. Symon's thesis[13] make it a simple

[14] B. Rossi, Rev. Mod. Phys. **20**, 545 (1948).

matter to calculate the effect of fluctuation on the distribution of pulse heights given in Fig. 3. The calculations give directly the expected distributions of energy losses in the 0.3-cm specimen of silver chloride used in the experiment. These presumably correspond to the expected pulse height distributions modified by a suitable proportionality constant.

In the calculation of the fluctuation, it is sufficient to consider directly the effect of the fluctuation spread on the single peak due to mesons that stopped in 23 cm of lead. However, the distribution of mesons penetrating

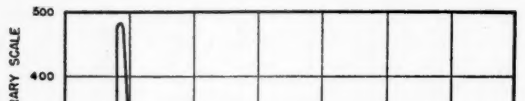

FIG. 3. Calculated distribution of mesons at sea level as a function of the average rate of ionization.

112 cm of lead must be treated as consisting of at least five separate bands, each modified by fluctuations. The reason for this is that the unmodified distribution in this case is about as broad as the spread due to fluctuation. The sum of the modified bands must be taken as the expected distribution. These calculations were made using the Symon results which do not take the density effect into account and the resulting curves are shown in Fig. 4.

It was not possible to calculate the exact distribution when the density effect is taken into account because, as yet, no numerical data for this effect in silver chloride are available. The nearest that one can come, *a priori*, to the proper correction is to apply the density-effect correction for iron. This, at best, is only an approximation to the proper correction. The correction, which depends on the energy of the incident particle, was determined from the curve for iron in Fig. 5, taken from the work of Halpern and Hall.[6] The curve for mesons stopping in 23 cm of lead was not altered because the density-effect correction for iron for mesons of this energy amounted to 0.5 percent at most. The correction for the other distribution was considerable. Each of the five bands, into which the distribution of average rate of ionization for mesons penetrating 112 cm of lead was split, corresponds to a different high energy. For each of these energies, the density-effect correction was determined from Fig. 5 for the case of iron. Considering the distributions in Fig. 4, we see that the effect of fluctuations in energy loss and the density effect are both very important in modifying the distribution in average ionization shown in Fig. 3.

Several additional effects might cause a broadening of the observed distributions. These are the fluctuation in identical pulses caused by imperfections in recorder, amplifier noise, and the difference in pulse sizes due to the variation in path lengths in the crystal. Careful analysis of each source reveals that the additional broadening due to these effects is small compared to the large fluctuation predicted by Symon.

To make comparison with the experimental results, we have added to Fig. 2 the various theoretical curves. Because the density effect is small for the mesons which stopped in 23 cm of lead, we have neglected this correction for these mesons and fitted the theoretical distribution of stopped mesons to the experimental histogram so that both distributions have the same average abscissa between the values of 1.60 and 3.40×10^{-2} volt (upper graph). The fitting process called essentially for a determination of the correlation between the energy lost in the crystal and the resulting voltage peak. The result of the fitting is that an average energy loss of 2.05 Mev corresponded to an average pulse of 2.09×10^{-2} volt at the input of the main amplifier. The theoretical most probable energy loss, 1.78 Mev, corresponded to a pulse height of $1.81\ (\pm5)\times10^{-2}$ volt at the input.** The histogram for stopped mesons has the same shape as the Symon distribution except in its initial part which exhibits an excess number of small pulses. The fluctuation theory predicts that 5 percent of the pulses should saturate the amplifier; indeed, 5 percent of the pulses did. The widths at half-value of the theoretical and experimental curves agree very well. There is a slight difference between the peaks of the two distributions, but not more than would be expected statistically.

The essential dissimilarity between the distributions appears for small pulses. The histogram has a tail for small pulses, constituting about 16 percent of the total area, whereas the theoretical curve falls abruptly to a very small fraction of its maximum value on this part of the curve. The excess number of small pulses observed in the experiment is most likely due to poor regions in the

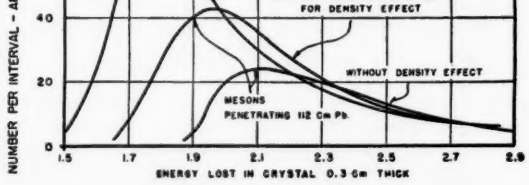

FIG. 4. Expected pulse distributions modified by allowance for fluctuation in energy loss.

** Using these values and the fact that 75 percent voltage saturation was obtained, we calculate that, on the average, 6.6 ± 0.7 electron volts were required to release one conduction electron in the crystal.

crystal. It is not clear whether the failure of the crystal was due to spotty variations throughout the volume, or to poor regions near the edges. Attempts to obtain larger crystals of good quality have not been successful. Detailed area tests of a crystal using cosmic rays are too slow to be practical. Since the histogram agrees well with the theoretical distribution over most of the range of pulses, we conclude that the major portion of the crystal behaved as an efficient detector of ionization.

In Fig. 2 (lower graph), we have plotted the theoretical distribution curves for mesons penetrating 112 cm of lead. In fitting these curves to the amplitude scale, use was made of the result cited above that 1.81×10^{-2} volt corresponds to 1.78 Mev lost in the crystal. The distribution with no correction for the density effect is obviously a poor approximation to the experimental results. The width at half-value of the theoretical curve is somewhat large and the average of this curve is far too great. The theoretical distribution, corrected for the density effect by an amount appropriate for iron as described above, is shown in the same figure. This curve is a fair approximation to the experimental distribution, but the agreement is still not good because the average energy loss is 2.21 Mev, whereas the average of the experimental curve is 2.10 Mev, when the tail due to small pulses is neglected.

Lacking a theoretical density-effect correction derived especially for silver chloride, we have evaluated the correction needed to get good agreement between the experimental and theoretical distributions. It is possible to make a reasonable guess at the correction because the shape of the curve (as a function of p/μ) for the correction is known from the work of Halpern and Hall.[6] All that remains is to determine one parameter. Over a considerable range, the correction is represented by a straight line when plotted as a function of p/μ on semilog paper (see Fig. 5). The dashed curve of Fig. 5 gives the correction, which, when applied to the theoretical distribution, best describes the results of the experiment. The resulting calculated pulse distribution fits the experimental data well. The widths at half-value agree very well. The theory predicts that about 9 percent of the pulses should saturate the amplifier, whereas actually 6.5 percent did. For this distribution, as for the one due to mesons stopping in 23 cm of lead, a relatively large number of pulses were smaller than the theory predicts. The explanation here, as before, is probably that these pulses are due to regions of low sensitivity.

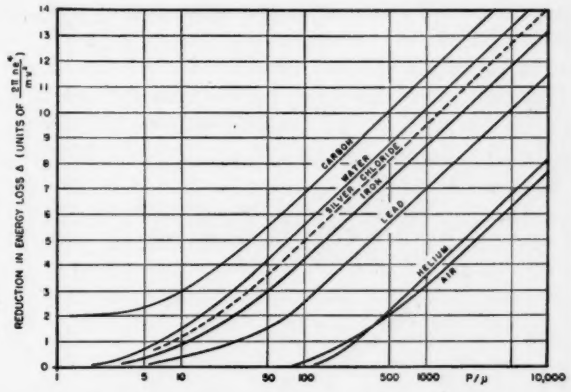

FIG. 5. Reduction in ionization loss due to density effect for various materials (after Halpern and Hall). $2\pi ne^4/mc^2$ for silver chloride is 0.0685 Mev/(g/cm²).

In the light of the material presented in this section, we draw the following conclusions. In the first place, the fluctuation theory of Symon seems to be well verified experimentally for the two groups of high energy mesons selected for this experiment. In the second place, the density effect for high energy mesons provides a satisfactory explanation of the fact that we obtained a smaller increase in the rate of ionization than the theory of Bethe and Bloch predicts.

We wish to express our indebtedness to Dr. M. L. Sands for many helpful suggestions on circuit design, to Dr. H. G. Voorhies who aided in taking some of the data, and to Mr. Carl Johnson and Mr. Stanley Gardner who were responsible for the mechanical construction of the crystal holder and certain other parts of the equipment.

On the Nuclear Evaporation in Cosmic Rays and the Absorption of the Nucleonic Component. I*

G. BERNARDINI, G. CORTINI, AND A. MANFREDINI
Instituto di Fisica dell'Universita, Centro di Fisica Nucleare, Roma, Italy

(Received August 8, 1949)

The absorption of the star-producing radiation was studied with the sensitive emulsion method. The results are connected with the behavior of the nucleonic component, as it is indicated, on the basis of some recent experimental data.

I

BY the sensitive emulsion method the production and behavior of nuclear evaporations or stars was studied to some extent. We were mainly interested in the comparison of the absorption of the star-producing radiation** in several materials and in the analysis of the energy and distribution of prongs. Some preliminary results were already given in previous issues.[1]

The experiments were performed partly at the Laboratorio della Testa Grigia*** (3500 meters above sea level****), partly with balloons. The L.T.G. results so far available are those concerning the absorption of the s.p.r. in Pb and in Al, while the balloon results were used to study the absorption of the s.p.r. in air.

Other authors[2] have recently performed similar experiments, and their data will also be considered here.

The plates used were Ilford C2, 100 micron thick, whose processing was either the conventional one, or a two-bath method similar to the one described by Blau and De Felice.[3]

Scanning was usually made with a magnification of about 300x, but now and then some plates were scanned with a high magnification oil-immersion objective as a test. The differences observed between the results obtained by the two scanning procedures were always negligible, whether concerning the stars or the mesons. Furthermore, the results of the scanning of every plate were systematically reproduced on a map. In this way the random distribution of events was continuously checked.

In order to obtain an estimate of star-fading we exposed some plates of different thicknesses and different makes for 80 days at L.T.G., and developed part of them soon afterwards, while the remainder were kept for about 70 days in Rome under more than 50 cm of lead before being developed. Comparing the numbers of stars, we found that star-fading is not at all negligible (about 10 percent per month) and is variable for different samples of the same type of emulsion.

This first part of our work concerns the absorption of the s.p.r. and its connection with the absorption processes of the nucleonic component.

TABLE I. Absorption of the s.p.r. in lead.

Absorber thickness (in g/cm²)	0	23	68	111	152	375
N_S	100	109±4.3	80±4.5	72±5	71±7.5	28±3.2

II

Our absorption experiments in Pb and in Al were made in a very trivial way, using rather large boxes of the absorbing material and placing small packages of plates under different thicknesses.

The boxes were so wide that for every azimuth the angle covered round the vertical direction was not less than 45°. We shall discuss the point of geometrical conditions later. The boxes were placed in the plate-room of the L.T.G., which was particularly safe against moisture and temperature changes. Its walls are of wood and have an average thickness of 1.2 g/cm². During exposure time the average temperature was 12°C.

To avoid confusion with scattering processes we consider only the stars with at least 3 prongs. The stars arising from radioactive contamination were excluded following the usual criterion.

The results of the absorption measurements in Pb and Al are summarized in Tables I and II, where N_S indicates the star population, i.e., the number per cm³ per day of stars having 3 or more prongs (in the tables for convenience the number N_S for the unshielded

TABLE II. Absorption of the s.p.r. in aluminum.

Absorber thickness (in g/cm²)	0	13.7	61	103
N_S	100	93±8	76±6.8	64±5.9

* A short account of this paper was given at the Bristol Symposium on Cosmic Radiation (September 1948).

** In the following, indicated by the initial letters "s.p.r."

[1] Bernardini, Cortini, and Manfredini, Phys. Rev. 74, 845 (1948); 74, 1878 (1948); Cortini, Manfredini, and Persano, Nuovo Cimento 5, 292 (1948); G. Cortini and A. Manfredini, Nature 165, 992 (1949).

*** In the following, indicated by the initial letters "L.T.G."

**** In the following, indicated by the initial letters "m.s.l."

[2] E. P. George, Nature 162, 333 (1948). E. P. George and A. C. Jason, Proc. Phys. Soc. 62, 243 (1949). Harding, Lattimore, Li, and Perkins, Nature 163, 319 (1949). Lord, Schein, and Vidale, Phys. Rev. 76, 171 (1949). H. Yagoda, N. Kaplan, and C. H. Conner, Bull. Am. Phys. Soc. 24, 16 (1949).

[3] M. Blau and J. A. De Felice, Phys. Rev. 74, 1198 (1948).

plates was normalized to 100). The N_S are corrected by the number of stars generated at sea level, before exposure.

The measurements in Pb demonstrate a small transition effect. Such a feature is not apparent in Al, but errors are very large in this case. The values of N_S in Al and in Pb (when the equilibrium condition is reached) *versus* thicknesses, roughly follows an exponential law. If we consider the total star population as a measure of the intensity of the s.p.r., we can deduce the following absorption thicknesses of the s.p.r. in Pb and in Al from the data collected in Tables I and II:

$$L_{\mathrm{Pb}}=300\pm20 \quad L_{\mathrm{Al}}\simeq200 \text{ g/cm}^2.$$

Similar data were taken for air. In this case the intensity of the star population at several altitudes was obtained by sending some plates up with balloons. During the flights the temperature held between 7 and 18°C. The plates were placed in the upper part of the gondolas, and were wrapped in light materials like board, Bakelite, etc. The storage batteries of the radio equipment were placed beside the plates, about 10 cm apart.

To estimate the absorption thickness of the s.p.r. in air, an exponential absorption law was assumed (see later). Consequently, knowing the values of pressure transmitted during the flight, that is, the behavior of pressure *versus* time, we are able to evaluate the absorption thickness of the s.p.r. in air. We have obtained:

$$L_{\mathrm{air}}=135\pm4 \text{ g/cm}^2.$$

III

It has been pointed out many times[1] that the indicated values of L_{air}, L_{Pb}, and L_{Al}, which are in good agreement with those derived by other authors,[2,3] allows us to exclude the possibility that any appreciable fraction of the star population might be due either to the electron-photon component or to the μ-meson component. Hence it appears almost certain that nucleons and π-mesons play the principal role in the creation of the stars.

Let us briefly examine the contribution of the π-mesons.

The fast π-mesons, i.e., the π-mesons having a kinetic energy larger than 50 Mev cannot strongly contribute to the production of the star-population, because in such a case we should observe a large transition effect between air and condensed materials. On the contrary the values collected in Tables I and II appear to demonstrate only a small transition effect in Pb, which is probably due to slow nucleons and slow mesons.

The slow negative π-mesons (the so-called sigma-mesons in Bristol's phenomenological nomenclature) do not contribute to a great extent to the star population. On the average we found that only about 5 percent of the observed stars were produced by an observable negative π-meson. Concerning this value of the ratio between sigma-mesons and stars, many factors must be taken into account; particularly the fading effect, which can reduce this ratio, and the thickness of the condensed material placed upon the plates during the exposure time. About the fading we have no definite information, but from the figures obtained with different exposure times (ranging between 40 days and 3 months) we can conclude that fading does not change the order of magnitude of the ratio between sigma-mesons and stars.

About the second point, we must observe that because of the shortness of the mean life of the π-meson, the observed sigma-mesons are, of course, locally produced with both unshielded and shielded plates. Most of them certainly originate with the stars themselves in some processes like those of "double stars". But at the same time we may take it for granted that in the condensed materials, like Al and Pb, part of the observed mesons arise from the locally generated hard showers. As a matter of fact, Piccioni[4] showed in a very recent work that the local hard showers are mainly composed of π-mesons of both signs. Now, in a condensed material the negative (fast) π-mesons slow down in a very short time and most of them are captured by the nuclei and do not disintegrate. Consequently, the ratio between sigma-mesons and stars ought to increase from air to condensed materials.

Our statistics on sigma-mesons are rather poor (about 300 cases) but are sufficient to indicate clearly the existence of such an effect, and just of the expected order of magnitude (see Section II). We found, however, that the ratio of the numbers of sigma-mesons to stars never exceeds 10 percent and we believe this is the upper limit of the contribution given by the slow π-mesons to the star population.[5]

Having thus examined every type of known cosmic-ray component, except the nucleonic one, *we are compelled to consider this component as the almost unique intensive radiation able to produce the nuclear evaporations.*

IV

There is a different type of event which appears to be essentially connected with the nucleonic component. This is the so-called local hard shower discovered by Janossy. In the cosmic-ray field they are considered high energy processes. A rough estimate of their energies is possible from the well-known experiments by Janossy and others.[6] One finds that the number of mesons in a hard shower is, on the average, of the order of 10 and

[4] Communicated in an invited paper at the meeting of the American Physical Society, New York, January, 1949; see O. Piccioni, Phys. Rev., to be published.

[5] This result appears to be in agreement with some preliminary results by I. F. Quercia and B. Rispoli in an experiment with a fast ionization chamber working in coincidence with a set of delayed counters.

[6] See, for instance, D. Broadbent and L. Janossy, Proc. Roy. Soc. **A190** (1947).

that the energy of these mesons is some hundreds of Mev. This picture agrees with the brilliant results recently obtained by the Bristol and Bruxelles groups with the NT4 Kodak plates.[7] It agrees also on the lines of the theory of the multiple production of mesons given by Heisenberg,[8] Oppenheimer *et al.*,[9] and further discussed by Wataghin[10] and Heisenberg.[11] Thus the energy involved in such types of processes is of the order of some Bev.

On the contrary, a nuclear evaporation is usually a low energy process. However, some recent results on the absorption of the hard shower producing radiation demonstrate, with increasing evidence, a quite close correlation between these two phenomena. We would indicate how it appears possible to establish this correlation by merely drawing a comparison between the aforementioned experiments on hard showers and the ones previously described on the s.p.r.

After the recent measurements performed by several authors[12] in aircraft up to about 10,000 m it is possible to deduce that the hard shower producing radiation is absorbed in the atmosphere following an exponential law and that the corresponding absorption thickness appears to be

$$95 \leq \lambda_{air} \leq 135 \text{ g/cm}^2.$$

The rather large differences between the results of different experiments arise probably from differences existing in the devices employed by the researchers. These devices actually appear to be able more or less to enhance some features of the showers themselves, as for instance their multiplicity, penetration in lead, etc. Thus, in most of them it is believed that the penetrating particles are a mixture of mesons and secondary protons. This is very clearly indicated in the pictures by Lovati, Mura, Salvini, and Tagliaferri[13] and by Fretter[14] obtained with a tray of lead screens in cloud chamber. Because those secondary nucleons very often create some subsequent showers or other nuclear processes, it is clear that the instruments which are more or less able to detect those secondary processes apparently give an absorption thickness larger than the true absorption thickness of the primary radiation (see Wataghin[12]).

These "cascade processes" in nuclear collisions may be called on to explain the discrepancies observed in the measurements of λ. This conclusion may be stressed by the observation that the lower air limit for λ_{air} was found by George and Jason[12] by comparing the hard shower intensity between 3500 m and sea level with an experimental device highly selective for hard showers composed by particles of very high energy.

One intermediate value of λ_{air}, that is, $\lambda_{air}=120$ g/cm^2 is supplied by the results of very careful measurements performed by Tinlot.[12] In Tinlot's experiments two penetrating particles are sufficient to trigger a coincidence, and, consequently, Tinlot's device does not discriminate as much in favor of processes involving such high energies. The upper limit for λ_{air} was obtained by Cocconi[15] with measurements at Echo Lake (3260 m.s.l.) but it is believed that Cocconi's device was sensitive to rather low energy processes, because with that apparatus only one particle was required to penetrate about 20 cm of Pb. For the other particles, ranges of about one inch could be sufficient to bring about a coincidence.

In conclusion *we consider it reasonable to assume as average absorption thickness in air for the hard shower-producing radiation the intermediate value* $\lambda_{air}=120$ g/cm^2.

TABLE III. Comparison of the absorption thicknesses of the s.p.r. and the hard shower-producing radiation found by various authors in various materials.

	Hard showers of middle energy		Stars				
	Cocconi (s.l.)	Tinlot and Gregory	George Jason	Rome Group	Perkins *et al.*	Schein *et al.*	Yagoda *et al.*
Air	133±7	120	150±7	135±4		148	143±3
Lead	310±30	310	310±20	300±20			
Al				220			
C	140±20						
Ice					200		
Fe		200					

V

In addition to the mentioned experiments, the absorption of the hard shower-producing radiation in several materials was recently studied by Cocconi[15] and, independently, by Tinlot and Gregory.[16] Concerning Cocconi's experiment we wish to consider for the moment only the results of Ithaca, that is, near sea level. The values found by Cocconi for the absorption thicknesses in Pb, Fe, and C are reported in the first column of Table III. In the second column of Table III there are reported the values obtained by Tinlot and Gregory on the top of Mount Evans (4250 m.s.l.). We

[7] Kindly communicated to us by Professor C. F. Powell and Dr. G. P. S. Occhialini.

[8] W. Heisenberg, Zeits. f. Physik **101**, 533 (1936); **113**, 61 (1939); *Cosmic Radiation* (Dover Publications, New York, 1946), p. 124.

[9] Lewis, Oppenheimer, and Wouthuysen, Phys. Rev. **73**, 127 (1948).

[10] G. Wataghin, Phys. Rev. **75**, 693 (1949).

[11] Kindly communicated by the author.

[12] G. Wataghin, Phys. Rev. **71**, 453 (1947); Maze, Freon, Daudin, and Auger, Rev. Mod. Phys. **21**, 14 (1949); J. Tinlot, Phys. Rev. **73**, 1476 (1948); E. P. George and A. P. Jason, Nature **161**, 248 (1948).

[13] Lovati, Mura, Salvini, and Tagliaferri, Nuovo Cimento, VI (1949). The authors gave one estimate of the cross section for the production of stars apparently in very good agreement with our result. But in this estimate they consider without discrimination every type of penetrating particles crossing the lead plates of the cloud chamber. Consequently the value found for the cross section would be an upper limit and it corresponds to the generation process only (the absorption process being, of course, a different matter).

[14] W. B. Fretter, work communicated at the Meeting of the American Physical Society, Pasadena, November 1948. We are grateful to the author for having kindly sent us the manuscript and the photographs.

[15] G. Cocconi, Phys. Rev. **75**, 1074 (1949).

[16] J. Tinlot and B. Gregory, Phys. Rev. **75**, 519 (1949); **75**, 520 (1949).

believe that the experimental arrangement employed by Tinlot and Gregory is better protected than Cocconi's against the spurious showers produced by particles coming in sideways. To compare with the behavior of the s.p.r., the values of absorption thickness L found for this radiation by Perkins *et al.*[2], George and Jason,[2] and by us, are collected in the third to fifth columns of Table III. Correlation between these data and the data of the first and second columns seems to be rather close, and in spite of the fact that the values of L referred to Al and H_2O are larger than those relative to the shower-producing radiation, it appears rather improbable that this correlation is due to pure chance.

Consequently, one would be driven to conceive a common origin for the two processes in spite of the differences in the energies involved.

Usually, because of the energies and the exponential behavior of the intensity of shower-producing radiation, one thinks that the nucleons which originate the hard showers mainly constitute the effective residual of the primary nucleons. This conclusion is very questionable in some experiments which are able to detect showers composed of particles of rather low energy, but it is perhaps reasonable, for instance, in the experiments performed by Janossy *et al.*[6] and by George and Jason,[12] who employed such a set of counters in coincidence that the energy of the showers detected in their apparatus was actually at least of the order of some Bev.

Thus we can assume that the number of nucleons able to produce hard showers is of the same order as the residual of the primary nucleons, and we can see now if it might be possible to attribute also a large fraction of the stars to the residual of the primary nucleonic component. A brief evaluation demonstrates that this is not the case.

VI

If the number of stars/cm³/sec. at a distance h in g/cm² from the top of the atmosphere is N_S, the number I' of nucleons arriving at this altitude and able to produce stars with a cross-section σ' must be:

$$I'=N_S/\sigma'\mathfrak{N}, \tag{1}$$

where $\mathfrak{N}$ is the number of atoms/cm³ from which the stars can be originated.

Taking into account the composition of the Ilford C2 emulsion, we estimate that $\mathfrak{N}$ is 4.72×10^{22}/cm³. The value of N_S at 3500 m.s.l. ($h=685$ g/cm²) is given by our results on the star population. They agree very well with the results recently obtained by George and Jason,[2,17] Yagoda, Kaplan, and Conner.[2] Neglecting the fading effect, we find $N_S=14.2\pm0.5$ stars/cm³/day in plates without any superimposed absorber. The number of stars/cm³/sec. is therefore 1.65×10^{-4}, and consequently we can write

$$\sigma'I'=3.5\times10^{-27}\ \text{sec.}^{-1}. \tag{2}$$

The true value is certainly higher because of the fading effect. After our measurements on this phenomenon the above stated figures can be enlarged by about 20 percent.

Now, considering the absorption of the hard shower-producing radiation in the atmosphere, the intensity of the residual nucleonic component can be evaluated from the intensity of the primary component at the top of the atmosphere.[18]

Using the well-known Gross transformation, the integral intensity observed at any atmospheric depth h is expressed by

$$I=2\pi I_0\left[e^{-h/\lambda_{air}}+\frac{h}{\lambda_{air}}E_i\left(-\frac{h}{\lambda_{air}}\right)\right]. \tag{3}$$

This formula is deduced by assuming a directional exponential absorption with an absorption thickness λ_{air}. Putting $\lambda_{air}=135$ g/cm², and $I_0=0.1$ cm^{-2} sec.$^{-1}$ sterad.$^{-1}$ (that is probably a rather high value; see Rossi[19]) we find

$$I=5.9\times10^{-4}\ \text{cm}^{-2}\ \text{sec.}^{-1}. \tag{4}$$

Thus, if we attribute the production of the stars to this residual of primary component, comparing (2) with (4) we find

$$\sigma'=5.9\times10^{-24}\ \text{cm}^2.$$

Now this value is about 7 times larger than the average geometrical cross-section σ of the nuclei in the emulsion.

If we take for λ_{air} the more reasonable value indicated before, that is, $\lambda_{air}=120$ g/cm², the same evaluation gives

$$I=2.8\times10^{-4}\ \text{cm}^{-2}\ \text{sec.}^{-1}.$$

and, consequently, a cross section 15 times the geometrical cross section. We can conclude that *the number of nucleons from which the stars arise is at least 10 times larger than the number of residual primary particles.*

VII

In order to understand this conclusion it appears necessary to conceive of the fast nucleonic component as being accompanied by a retinue of nucleons which belong to an intermediate energy range, that is, composed by nucleons having energies of some hundreds of Mev. Before discussing this point it is convenient to set forth some experimental facts which can, in this way, find a reasonable interpretation.

We would examine these facts separately. They are: (a) The proton group observed with a cloud-chamber

[17] In a previous work (see reference 2) these authors gave a rather low value for N_S, that is, 8.5, while in a later communication they give $N_S=14.65$ stars/cm³/d, in very good agreement with our figure.

[18] J. A. Van Allen and H. E. Tatel, Phys. Rev. **73**, 245 (1948); Gangnes, Jenkins, and Van Allen, Phys. Rev. **75**, 57 (1949).

[19] B. Rossi, Rev. Mod. Phys. **20**, 574 (1948).

device at 9000 m by Anderson *et al.*[20] This proton group constitutes a peaked maximum in the spectrum of the positive particles given by these authors.

Among the ionizing particles detected by the apparatus of the Pasadena group, the electrons are mainly excluded. Moreover, these particles are practically coming in from the vertical direction, because the cloud chamber is countercontrolled. Consequently, the number of these particles may be considered as a relative measurement of the intensity of the non-electronic component in the vertical direction.

Anderson *et al.* found that 30 percent of all the particles having a momentum p between 0.4 and 1.6×10^6 gauss-cm are certainly identifiable as protons. For $1.6<p<10\times10^6$ the positive particles, which constitute the peaked maximum mentioned above, appear to be about 30 percent of the particles in bulk, included within the same momentum ranges. It is reasonable to consider the larger part of these particles as protons, too. The absolute intensity of the non-electronic component having a momentum in the ranges indicated before appears to be, after the estimates given by Rossi[19]:

$$0.8\times10^{-1}\ \text{cm}^{-2}\ \text{sec.}^{-1}\ \text{sterad.}^{-1}.$$

Thus the number of these slow protons should be about 2.4×10^{-2} cm^{-2} sec.$^{-1}$ sterad.$^{-1}$. This is just the order of magnitude to be expected from the star population, which, taking into account the above indicated increase with the altitude, would give for the *integrated* intensity of the s.p.r. about 0.1 cm^{-2} sec.$^{-1}$.

A more accurate comparison would require some information about the angular spread of the secondary nucleons round the direction of the primary ones. However, it is easy to observe that a larger fraction of the nucleons which create the stars are neutrons. In fact, if the number of slow protons having an energy under 1 Bev and coming in near the vertical direction is about 2×10^{-2} cm^{-2} sec.$^{-1}$ sterad.$^{-1}$, the number of nucleons having energies larger than 1 Bev and coming in in the same direction can be estimated (and that is a lower limit) directly, considering these nucleons as the residual of the primary component. Near the vertical direction, at 9000 m.s.l., this residual would be about

$$0.1\times e^{-305/120}=0.8\times10^{-2}.$$

Consequently it would appear that the number of slow protons is only about 3 times the fast nucleons, in disagreement with the number of nucleons evaluated as starting from the star population. This clearly means that for energies under 1 Bev, neutrons contribute strongly to the production of stars. More exactly, if we assume that the ratio between slow and fast nucleons is about 10, the number of neutrons in the s.p.r. must be at least twice the number of protons.

(b) One draws a quite similar result from the experiments performed by Alikhanian *et al.*[21] at 3250 mi. above sea level with a completely different technique. The results of these experiments indicate the presence of a group of ionizing particles (named "third component" by the authors), having moments between 0.7 and 2.0×10^6 gauss-cm. The interpretation of this group given by the authors is perhaps rather questionable. From some range measurements it appears to them to be composed of particles having masses of the order of 1000 m_e.

We like to consider this group as a slow proton group having the same origin as the group detected at 9000 m by the researchers of Pasedena. This opinion is supported by the following arguments.

Its intensity is 10 percent of the total mesonic component. After Rossi's figures it is easy to conclude that its absolute intensity is about 1.7×10^{-3} cm^{-2} sec.$^{-1}$ sterad.$^{-1}$. Consequently, the ratio between the proton group observed at 9000 m and this one at 3250 m is about 12.

If we consider an exponential decrease with an absorption thickness of 140 g/cm^{-2} (see Table III) between 9000 m (315 g/cm^{-2}) and 3250 m (700 g/cm^{-2}), we find an attenuation factor of about 15 in fairly good agreement with the preceding estimate.

We would also remark that, evaluating the integral intensity of the s.p.r. at 3500 m as was indicated in Section VI, one finds that the *total flux* of s.p.r. is about 4.10^{-3} cm^{-2} sec.$^{-1}$; that is, about 25 percent of the total mesonic flux. The comparison with the relative intensity of the proton group found by Alikhanian *et al.* give us again the indication that a large fraction (about $\frac{2}{3}$) of the s.p.r. is composed of neutrons.

A similar conclusion was reached by George and Jason[2] but we believe that they overestimate the fraction of neutrons. Actually, these authors start their evaluation from the particles identified as protons in the well-known Blackett spectrum at sea level where the slow protons are probably underestimated on account of the countercontrol device. This device selects protons coming in close to the vertical, while, on the contrary, the star-producing neutrons and protons are very probably distributed rather isotropically. Moreover, they consider, as a cross section for the production of stars, the one deduced from the absorption thickness of the s.p.r. in the emulsion (that is, 200 g/cm^{-2}): Now we believe that this is not correct, because absorption thickness is essentially determined by the fast nucleons which support the prevailing part of the s.p.r., i.e., the nucleons having energies around 200 Mev and in equilibrium with the fast ones. (*Note added in proof.*—See Part II of this work.) On the contrary, we assumed in the preceding estimates, as a cross section for the production of the stars by these

[20] Adams, Anderson, Lloyd, Rau, and Saxena, Rev. Mod. Phys. **20**, 334 (1939).

[21] Alikhanian, Alikhanov, and Weissenberg, J. Phys. U.S.S.R. **9**, 97 (1947).

slow nucleons, the geometrical one (nuclear radius $R=1.5\times10^{-13}\ A^{1/3}$).[22]

(c) The intensity of bursts and their behavior in the atmosphere is in very good agreement with the similar features concerning the star population. Indeed the corresponding absorption thickness in air found by several authors[23] is $L_{air}=138$ g/cm^2.

An accurate comparison of the absolute intensities is not possible because of the production of stars in the walls of the ionization chamber and owing to the cut-off acting on the pulse size. But the absolute intensity of the observed bursts is of the right order of magnitude with regard to the star population detected in our plates.

It was already pointed out by Rossi[19] that in the burst curve there is some evidence for a transition effect near the top of the atmosphere. This indicates that the intensity of the star-producing radiation decreases in the first layers of the atmosphere much less than the assumed intensity of the residual primary component.

In other words, as was stated by Rossi,[19] the absorption curve of the burst in the atmosphere diverges markedly from that which can be evaluated with the Gross transformation, assuming an absorption thickness of 135 g/cm^2. The intensity of bursts at 3500 m.s.l. is just about 10 times that which could be expected if its generating radiation were submitted to a directional exponential absorption with the absorption thickness now indicated. Of course, this fact becomes clearly understandable if one assumes that after some absorption lengths an equilibrium condition is reached between the primary nucleons and the secondary ones able to produce bursts, the multiplicity of secondary creation being about 10 as we have evaluated before.

(d) A clear transition effect of the same type was indeed very recently observed by Schein *et al.* in plates screened with different thicknesses of lead and exposed at about 30,000 m.s.l.[24]

(e) Qualitative, but strong evidence of the production of secondary nucleons in penetrating showers is given by several pictures by the authors quoted in footnotes 13 and 14.

(f) Some direct evidence of stars connected by a fast prong identifiable with a proton was recently obtained by G. Occhialini *et al.*,[25] and by us, in NT4 Kodak plates.

VIII

The arguments stated above substantiate the idea that in crossing the atmosphere the nucleonic component undergoes a cascade process through which a *primary proton gives rise on the average to more than 10 secondary nucleons having energies of the order of magnitude of some hundreds of Mev.*

It is easy to conceive the origins of this cascade process. They are the production of fast secondary nucleons both in inelastic and quasi-elastic collisions in nuclear matter.[26] Actually it is easy to see that even in the case of a totally inelastic collision, a primary nucleon having an energy of some Bev may be able to produce two secondary nucleons of several hundreds of Mev.

At the same time it is possible to argue that a fast nucleon crossing the nuclear matter has a probability of some percent to transfer a rather high momentum to one secondary nucleon in a quasi-elastic collision. In this way inelastic and fast knock-on nucleons greatly (and rapidly) increase the percentage of ~100 Mev nucleons and are very efficient in the production of stars. The nuclear cascade might supply a reasonable interpretation of some puzzling questions, as the nuclear size dependence on the absorption thickness for hard shower-producing radiation and for s.p.r. and the rather large values of the corresponding absorption thicknesses in comparison to the geometrical ones.

All these questions will be examined in the second part of this work and in a paper by B. Ferretti, after a deeper and more quantitative discussion about star structure and the corresponding energies.

We are very glad to express our acknowledgments to Professor B. Ferretti who informed us in several useful discussions of the results obtained developing quantitatively some arguments expressed in this paper. We thank Professor W. Heisenberg and Professor E. Amaldi for some interesting discussions and advice.

[22] We do not know to what extent this assumption can be considered correct. For instance, the cross section measured by Gardner for the stars in photographic emulsion initiated by α particles appears to be smaller than the geometrical one by a factor larger than two.

If these figures could be extended to the nucleons of about 200 Mev, we should find that the s.p.r. would be composed of about 80 percent neutrons. The numerical evaluation deduced in Section VI by Anderson's measurements and by our data concerning the star population should be modified in the same direction. Particularly the evaluated multiplicities of secondary nucleons from which the stars arise would be increased by about a factor 2.

[23] See B. Rossi, reference 19, p. 552.

[24] Kindly communicated by author. A similar effect was found by Freier, Ney, and Oppenheimer, Phys. Rev. 75, 1451 (1949).

[25] Kindly communicated by author.

[26] We are much indebted to Dr. S. A. Wouthuysen for a very interesting discussion about this point.

The Division of Nuclear Charge in Fission

D. C. BRUNTON
Chalk River Laboratory, National Research Council of Canada, Chalk River, Ontario, Canada
(Received August 19, 1949)

Recent measurements of fission fragment energies emphasize the difficulty of reconciling the variations in kinetic energy with current hypotheses of charge distribution. The assumption of a close relationship between charge and kinetic energy is used here to derive a new distribution. The energy associated with each possible charge division between a pair of fragments of given masses is computed and compared with the measured energy as a function of frequency for the same mass pair. In this way a charge-frequency curve is derived on the assumption that most of the variation in fragment kinetic energy is associated with variation in the division of primary charge. The marked disagreement between the charge distribution arrived at here and previous hypotheses is discussed, and the relation between charge distribution and stable nucleon shells is considered.

I. INTRODUCTION

LITTLE experimental evidence exists on the distribution of nuclear charges of primary fission fragments. A direct physical measurement of the nuclear charge and frequency of occurrence has not been undertaken owing to the fact that the fragments are not completely stripped of electrons.[1] Many nuclear charges and yields in the decay chains have been measured through chemical properties and radiations, but these yields are measured some time after the fission event and, in general, after an unknown number of β-disintegrations. In a few cases, where the nuclide concerned is shielded by stable isobars, the primary yield is measured, which is the frequency of occurrence of a given nuclear charge for a given nuclear mass. Such measurements have been used to derive a charge distribution based on the hypothesis of equal chain-lengths (see Section III).

In the present paper new measurements[2] of the kinetic energies of paired fission fragments will be used in an attempt to explain the observed large variations ($\sim$40 Mev) in kinetic energy. These variations can arise from two causes: (1) variations in the number of neutrons emitted per fission and (2) variations in the charges of the primary fragments. The former has been discussed by Way and Wigner[3] and will be examined later, while the latter is the subject of the present paper. A frequency *vs.* kinetic energy curve for a given mass pair is obtained from the measurements reported previously.[2] The relation between energy and charge is computed from a semi-empirical mass formula. Association of the energies in the two cases leads to a curve of charge distribution.

II. CHARGE DISTRIBUTION SUGGESTED BY THE VARIATION IN KINETIC ENERGY OF FISSION FRAGMENTS

A typical example of the curves of frequency *vs.* kinetic energy, obtained from the contour diagrams,[2] is shown in Fig. 1 for the case $A_L=95$, $A_H=141$ (where A_L and A_H are the mass numbers of the light and heavy fragments, respectively). To get a value for the total variation in kinetic energy the linear portions of this curve were extrapolated to zero frequency. The resulting value is 41 Mev for the case shown, and it is evident from the figure that this value is a conservative estimate for the extreme range.

The kinetic energy, and its variation, are related to the other energies emitted promptly or delayed, as follows:

$$E_t=E_k+E_r+E_d,$$

where E_t = total energy release in fission, = mass difference between the initial nuclei (e.g., $U^{235}+n$) and the final products (e.g., $_{42}Mo^{95}$ and $_{59}Pr^{141}$), E_k = total kinetic energy of the two fragments, E_r = kinetic energy of prompt neutrons and γ-ray energy, and E_d = energy released in β-, γ-, and neutrino radiation as the primary fragments decay to stable neuclei. If Δ is used to denote the maximum variation,

$$\Delta E_t=\Delta E_k+\Delta E_r+\Delta E_d\approx 40 \text{ Mev}+\Delta E_r+\Delta E_d.$$

E_r is the sum of contributions from two fragments, and the average contribution per fragment is some fraction (say one-half) of the difference between consecutive binding energies of neutrons. Therefore, on the average, $E_r\approx 5$ Mev and $\Delta E_r\approx 10$ Mev, and these vary slowly with the number of neutrons emitted. (In view of the experimental accuracy and the nature of this estimate it is probably not significant that this value E_r(average) does not agree with the experimental value used below.) Thus the major part of ΔE_k may arise from (1) fluctuations in the number of neutrons per fission and hence from ΔE_t, or from (2) variations in nuclear charge of the primary fragments with consequent variation in E_d.

Using the equal chain-length hypothesis of Glendenin, Coryell, and Edwards,[4] Way and Wigner[3] found that about three-quarters of ΔE_k had to be assigned to fluctuations in neutron emission and about one-quarter to variations in charge splitting. A neutron evaporation reduces E_t by the binding energy of the neutron in one

[1] N. O. Lassen, Phys. Rev. **68**, 142 (1945).
[2] D. C. Brunton and G. C. Hanna, Phys. Rev. **75**, 990 (1949).
[3] K. Way and E. P. Wigner, Phys. Rev. **73**, 1318 (1948).
[4] Glendenin, Coryell, and Edwards, CL-LEG-1 (1946); Coryell, Glendenin, and Edwards, Phys. Rev. **75**, 337 (1949).

of the final products (i.e., by about 8 Mev), and brings the fragment closer to stability, so that E_d is also reduced by 2–3 Mev. The net effect on E_k is therefore 5–6 Mev. Consequently, to account for the observed ΔE_k by this process a range from zero to 6–8 neutrons per fission is required. This range of neutron emission and the known average number of neutrons per fission make it difficult to account for the shape of the frequency *vs.* kinetic energy curve (e.g., Fig. 1). As pointed out by Way and Wigner,[3] an asymmetrical distribution having a sharp cut-off on the high energy side would be expected from the hypothesis of equal chain-lengths.

In order to see what the consequences are, the other alternative (No. 2 above) is assumed, namely, that ΔE_k arises mainly from the variations in charge division of the primary fragments. (Probably the correct answer lies somewhere between the two extremes.)

Considering only fission into a given mass pair and with a fixed number of prompt neutrons, say one per fragment (i.e., $\Delta E_t=0$), ΔE_d is calculated from the variation in prompt energy, E_p, associated with all possible pairs of primary charges. E_p is defined by

$$E_p=E_k+E_x,$$

where $E_x=E_r$ plus the binding energies of the prompt neutrons and is therefore the excitation energy of the primary fragments. Consequently,

$$\Delta E_p=\Delta E_d.$$

For fission in U^{235}, then,

$$E_k+E_r=M(235,92)+n -[M(A_L-1,Z_L)+M(A_H-1,Z_H)+2n],$$

where $M(A,Z)$ is the mass of a nucleus of mass number A and charge Z, and n is the mass of a neutron.

The binding energy of a neutron in the nucleus A,Z is given by

$$\text{B.E.}=M(A-1,Z)+n-M(A,Z).$$

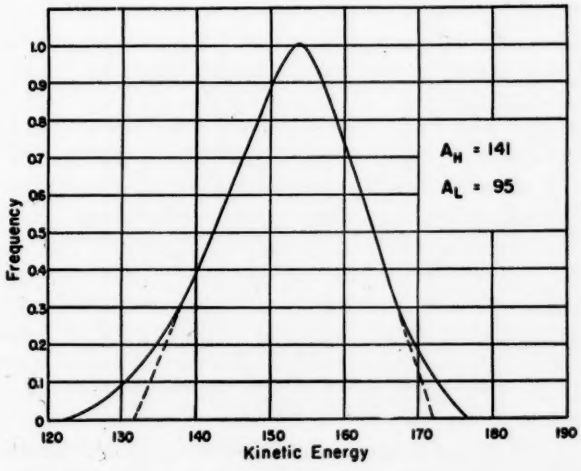

FIG. 1. Frequency curve for the total kinetic energy E_k of fission fragment pairs with masses 95 and 141 units.

Therefore

$$E_k+E_r=M(235,92)+n -[M(A_L,Z_L)+M(A_H,Z_H)+\text{2B.E.}]$$

or

$$E_p=E_k+E_x=M(235,92)+n -[M(A_L,Z_L)+M(A_H,Z_H)].$$

The mean value of $E_x\approx 20$ Mev is made up as follows:

Mean value of the neutron kinetic energy per fission $\approx$ 5 Mev[5]
Mean value of the prompt γ-energy per fission $\approx$ 5 Mev[5]
Mean value of the neutron binding energy per fission $\approx$ 10 Mev[6]
Total 20 Mev.

The range of values of E_p may be calculated for any mass pair if the ranges of values of Z_L and Z_H are known. The upper limits of Z_L and Z_H cannot be set precisely; but from the negative result obtained by Glendenin[7] in a search for positron emitters among the fission fragments, from stability considerations, and from the observation of significant primary yields in certain shielded nuclides such as Br^{82}, Rb^{86}, and Cs^{136}, it seems reasonable to take the upper limits of Z_L and Z_H as the stable charge values for the mass numbers A_L and A_H. The lower limits are then established by the condition that the fragments occur in pairs with $Z_L+Z_H=92$.

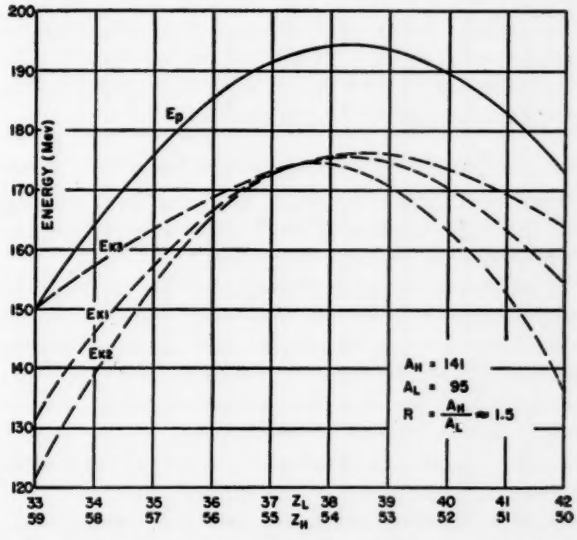

FIG. 2. Prompt fission energy, $E_p=E_k+E_x$, as a function of charge, computed using the semi-empirical formula of Feenberg. (See reference 6.) E_{k1} is the kinetic energy curve assuming E_x = a constant, while E_{k2}, and E_{k3} are the limiting curves when E_x is not assumed constant.

[5] M. Deutsch, *The Science and Engineering of Nuclear Power* (Addison-Wesley Press, Inc., Cambridge, Mass., 1947), Vol. I, Chapter 2.

[6] This was calculated from Feenberg's semi-empirical formula, Rev. Mod. Phys. **19**, 239 (1947).

[7] L. E. Glendenin, Plutonium Project Report **9B**, 7.3.1 (1946).

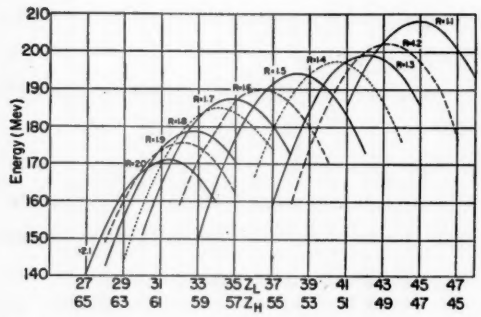

FIG. 3. Family of E_p curves for a sequence of values of $R=A_H/A_L$.

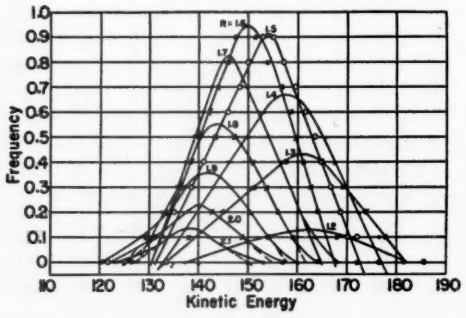

FIG. 4. Family of E_k curves (from contour diagrams previously published, see reference 2) for a sequence of values of R.

The relation between E_p and Z for the case $R=A_H/A_L=1.5$ (i.e., $A_L=95$, $A_H=141$) is shown by the solid line in Fig. 2. The upper limits are given by $Z_L=42$, $Z_H=59$ from the stability of nuclides Mo^{95} and Pr^{141}. The complete range of Z values is thus given by the charge pairs $Z_L/Z_H=33/59$, $34/58$, $\cdots 42/50$. The calculations of E_p were made, using Feenberg's modification of the semi-empirical formula:[6]

$$M(A,Z)=M(A,Z_A)+\alpha[(Z-Z_A)^2/A],$$

where the constants α and Z_A are given by Feenberg[6] and the stable masses $M(A,Z_A)$ are derived from the packing fraction curve of Dempster.[8]

Since the constants in formulas of this type are determined by fitting to the measured values of atomic masses (or packing fractions) and since sufficiently accurate mass-spectrometer measurements have not been reported for the very heavy elements, the accuracy of the formula is questionable in this region. However, recent computations by Stern[9] of the masses of heavy elements, using the energy relations of the natural radioactive series, are in fair agreement with the values derived from the formula above. The mass of U^{235} estimated by Stern is $\sim$1.5 Mev lower than the value used in the present calculation. Thus, although the absolute values of E_p cannot be relied on with certainty, there is evidence that they are not far in error. The relative values of E_p and consequently, ΔE_p, depend on the accuracy of the Z_A values and on the reliability of the parabolic energy surface a long way from the stable valley. Feenberg's Z_A values are the mean Z's for stable nuclei, but unfortunately there is no experimental test of the formula in the region where it is applied in these computations.

Comparison of Figs. 1 and 2 shows that the measured maximum variation in E_k is about 41 Mev, and the calculated maximum variation in E_p is about 44 Mev. Such close agreement is not maintained over the whole range of R values, but nowhere does a large discrepancy exist between these quantities. A family of E_p curves is shown in Fig. 3, and the corresponding family of E_k curves in Fig. 4. (Figure 3 is computed for the nearest A-odd nuclei to R values of 1.1, 1.2, $\cdots$ to avoid the irregularities associated with energies of A-even nuclei.) A comparison of the energy ranges ($E_{\max}\rightarrow E_{\min}$) for E_p and E_k as a function of A is shown in Fig. 5. It may be noted that the displacement of the two areas of Fig. 5 is approximately 22 Mev, which may be compared with the mean value, 20 Mev, of the excitation energy. The agreement is an indication that the absolute values of the E_p are not much in error.

The close agreement between ΔE_p and ΔE_k in general is here considered an indication that the variation in kinetic energy arises from variation in the charge of the primary fragments. If, therefore, we assume that E_x is roughly constant, independent of the charge pair, the E_k *vs.* charge curve is obtained by shifting the E_p curve parallel to the energy axis by an amount E_x(mean)$=20$ Mev (curve E_{k1} of Fig. 2). The effect of variations in E_x is illustrated by curves E_{k2} and E_{k3} of Fig. 2. Variations in E_x are restricted by the conditions that the resultant curve must have the same mean displacement from the E_p curve as E_{k1} and the measured value for ΔE_k. Actually curves E_{k2} and E_{k3} are limiting cases, assuming that the distribution involves the full range of charge values.

A curve of frequency *vs.* nuclear charge can be obtained from Figs. 1 and 2 by reading off frequencies and nuclear charges for a set of E_k values. Before this was

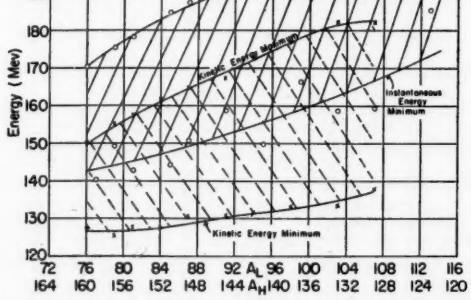

FIG. 5. E_p and E_k areas as a function of mass pair. Maximum and minimum values are plotted in each case. The wide scatter in E_p minimum is due to the variation in the stable charge with mass number.

[8] A. J. Dempster, Phys. Rev. 53, 869 (1938).
[9] M. O. Stern, Rev. Mod. Phys. 21, 316 (1949).

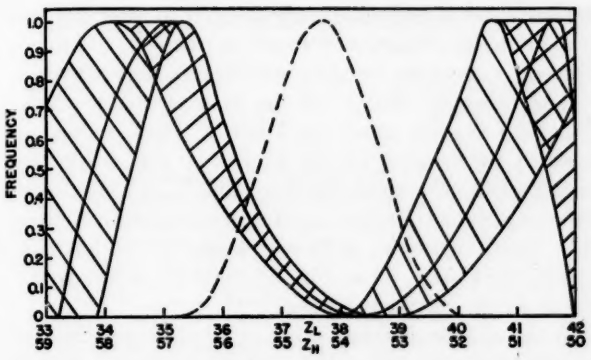

FIG. 6. Charge distribution from Equal Chain-length Hypothesis obtained from Glendenin *et al.* (see reference 4) (dashed curve). The broad band gives the charge division derived from energy measurements. $A_H=141$, $A_L=95$.

done, however, the values of E_k in Fig. 2 were reduced by 2 Mev to bring the maximum into agreement with that measured (Fig. 1). This shift of energy happens to be approximately equivalent to changing to Stern's value[9] for the mass of U^{235}. The charge distributions obtained from Fig. 1 and E_{k1}, E_{k2}, and E_{k3} (thus modified) in Fig. 2 are shown in Fig. 6. The double-humped broad band for charge distribution must be regarded only as a possible one. If some unknown condition, such as nuclear structure, operates to favor a high or low ratio of Z_H to Z_L, one of the humps will be depressed or eliminated. The variations in the lengths of the slopes of the E_p *vs.* Z curves of Fig. 3 give some indication that for $R\approx 2$, high ratios of Z_H to Z_L prevail and conversely for R values close to unity.

III. CURRENT HYPOTHESES OF CHARGE DISTRIBUTION IN FISSION

Well-known hypotheses on charge distribution are (1) the postulate of "unchanged charge distribution;" (2) the postulate of "minimum decay energy" of Wigner and Way,[3] and (3) the postulate of "equal chain-length" of Glendenin, Coryell, and Edwards.[4]

The first postulate assumes that the most probable division of charge is that which gives the same ratio of most probable charge, Z_p, to mass A in the fission fragments as the ratio Z to A in the fissile nucleus. This postulate has been modified by Present[10] to include an asymmetry in the initial charge distribution of the fissile nucleus arising from Coulomb forces. The second postulate assumes that the most probable charge division in fission is that in which the total decay energy of the two chains is a minimum. The third postulate asserts that fission occurs in such a manner that the most probable charge division gives equal values for the lengths of decay chains of the light and heavy fragments. For this purpose the chain-length is defined as Z_p-Z_A where Z_A is the most stable charge of a nucleus of mass number A.

The three postulates have been examined against the experimental evidence[3,4,10] with the result that the postulate of Glendenin *et al.* is considered to be in closest accord with the facts available.

The postulate of equal chain-lengths has been assumed to cover all modes of fission and all materials fissile by slow neutrons. The main support of the postulate has come from measured primary yields for four nuclides (Xe^{135}, Cs^{136}, Br^{82}, and Rb^{86}) in uranium fission, and Cs^{136} in plutonium fission. These yields, when plotted against $Z-Z_p$, lie on a single smooth curve. Four of these five examples are, however, shielded nuclides, and since a stable configuration may be a determinative factor in charge distribution, it is doubtful if these cases are representative samples of the primary nuclides. Other evidence on primary fission yields is frequently at variance with this hypothesis but the experimental results are of doubtful validity as pointed out by Glendenin *et al.*[4]

IV. THE "EQUAL CHAIN-LENGTH" HYPOTHESIS AND KINETIC ENERGY MEASUREMENTS

That the hypothesis of "equal chain-lengths" is in disagreement with the charge distribution derived here is seen from Fig. 6. Similarly, the most probable charge from the "unchanged charge distribution" postulate and from "minimum decay energy" postulate fall in the valley between the two humps of Fig. 6.

An alternative approach is to assume the validity of one of these hypotheses, for example: equal chain-lengths, and examine the excitation energy necessary to reconcile the hypothesis to the kinetic energy measurements. The curve marked E_k in Fig. 7 shows the approximate kinetic energy *vs.* charge curve derived from the energy distribution of Fig. 1, and the charge distribution of Glendenin *et al.*[4] The mean excitation

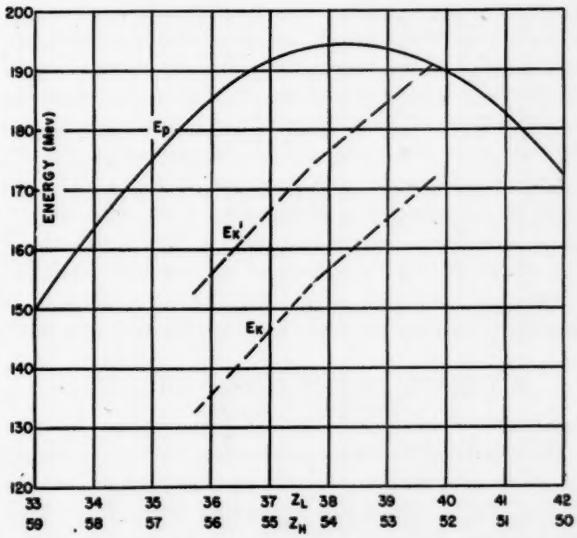

FIG. 7. E_p is the prompt energy curve shown in Fig. 2. E_k is the kinetic energy as a function of charge derived from the energy distribution of Fig. 1 and the charge distribution of Glendenin *et al.* (see reference 4). E_k' shows E_k displaced so as to give the correct value to E_π(mean).

[10] R. D. Present, Phys. Rev. **72**, 7 (1947).

TABLE I. Range of values for the most probable charge pairs and neutron pairs.

R	A_L	A_H	Z_{pL}	Z_{pH}	N_{pL}	N_{pH}
2.1	77	159	28–29 33	64–63 59	49–48 44	95–96 100
2.0	79	157	29–30 34	63–62 58	50–49 45	94–95 99
1.9	81	155	29–30 33–34	63–62 59–58	52–51 48–47	92–93 96–97
1.8	85	151	30–31 35–36	62–61 57–56	55–54 50–49	89–90 94–95
1.7	87	149	31–32 36–37	61–60 56–55	56–55 51–50	88–89 93–94
1.6	91	145	33–34 38–40	59–58 54–52	58–57 53–51	86–87 91–93
1.5	95	141	34–36 40–42	58–56 52–50	61–59 55–53	83–85 89–91
1.4	99	137	37–38 42–43	55–54 50–49	62–61 57–56	82–83 87–88
1.3	103	133	38–39 43	54–53 49	65–64 60	79–80 84
1.2	107	129	39–40 45–46	53–52 47–46	68–67 62–61	76–77 82–83

energy obtained from Fig. 7 is ~35 Mev, which is much greater than the known value of ~20 Mev. A value of 35 Mev corresponds roughly to an emission of four neutrons per fission—a number outside the limits (1–3 neutrons per fission) quoted for this constant in the Smyth report.[11] This value of 35 Mev for the excitation energy depends on the absolute values for E_p. The agreement between the calculated E_p values and the measured E_k values indicated an absolute error of only ~2 Mev. However, this does not constitute proof of the absolute accuracy and to the extent that these values are in doubt the E_p (or E_k) curve may be translated parallel to the energy axis. The E_k^1 curve of Fig. 7 represents a translation of the E_k curve such that the mean value of $E_z = 20$ Mev. The consequence of this translation is that the E_k^1 curve intersects the E_p curve, and the three charge pairs 40/52, 41/51, and 42/50 are energetically impossible. This therefore requires a charge distribution with a sharp cut-off for low values of Z_H/Z_L, which is inconsistent with the distribution assumed and with the measurement of primary yields for the shielded nuclides Br^{82} and Rb^{86}.

V. CHARGE DISTRIBUTION AND STABLE NEUTRON SHELLS

The charge distribution derived in Section II tempts one to remark on the structure of heavy nuclei and the role of the stable shells associated with the "magic numbers" of Mayer.[12] Although the charge distribution derived here is not sufficiently defined to offer any real test of the appearance of these numbers in the fission process, some very tenuous speculation may be made.

The range of values for the most probable charge pair (Z_{pL},Z_{pH}) is shown in Table I. These values are selected by drawing curves similar to Fig. 6 for each of the mass pairs tabulated. N_{pL} and N_{pH} are the corresponding values for the most probable neutron pairs. The upper figures in each row apply to the left-hand charge peak (e.g., as in Fig. 6) while the lower figures apply to the right-hand peak.

If the charge distribution is at all similar to the one suggested here and if the "magic numbers" play a determinative part in the fragment structure, it is possible by examination of Table I to propose how these stability conditions affect the fragment nuclides.

(a) For fission into a high mass ratio (about 1.8) the light fragment may be associated with the stable neutron shell N (the number of neutrons) = 50. This conclusion requires a long chain for the light fragment and a short chain for the heavy fragment, which is the converse of Present's[10] prediction for asymmetrical fission.

(b) For fission in a low mass ratio (about 1.4) the heavy fragment may be associated with the stable neutron shell of $N = 82$, or the proton shell $Z = 50$.

(c) For intermediate mass ratio (about 1.6) no "magic number" appears in the N or Z columns; however, an interpretation is possible in terms of a nuclear core with $N = Z$. This core is considered indestructable and aside from this core the nucleus divides with the same charge to mass ratio in the fragments as in the residue of the compound nucleus. If this core goes with the light fragment, the charge pair appears in the right hand peak of Fig. 6, and conversely. A simple calculation of the charge shifts of these two peaks gives a mass $A = 35 \rightarrow 50$ for this core, which may be associated with the highly stable nucleon configuration of Ca^{40} ($N = 20$, $Z = 20$).

VI. CONCLUSION

The charge distribution suggested here is inconsistent with previous hypotheses, but it is not in conflict with primary yield measurements and would readily explain abnormally high primary yields for nuclides close to stability or low yields well off the stable curve as may occur in the case of delayed neutron emitters. It is not possible, however, from the data available to derive a precise charge distribution for any particular mass value, and hence no direct comparison with primary yields can be made. The association with nuclear shell structure is very uncertain and, indeed, just within the bounds of possibility.

VII. ACKNOWLEDGMENT

The author is indebted to Dr. B. W. Sargent and Mr. W. B. Thompson for much helpful advice and criticism.

[11] H. D. Smyth, *Atomic Energy for Military Purposes* (Princeton University Press, Princeton, 1945).
[12] M. G. Mayer, Phys. Rev. 74, 235 (1948).

The Effect of Nuclear Motion on Atomic Magnetic Moments

M. PHILLIPS
Department of Physics, Brooklyn College, Brooklyn, New York
(Received August 18, 1949)

The effect of the finite mass of the nucleus on the Zeeman pattern of multi-electron atoms is investigated. This effect consists of two parts, one due to the motion of the core and nucleus about the center of mass, the other an exchange phenomenon between the electrons themselves. Both are of order m/M, where M is the mass of the nucleus.

THE effect of the finite mass of the nucleus on the Zeeman pattern of multi-electron atoms is small, but with the increasingly high precision attainable in the measurement of magnetic moments[1] it may become quantitatively significant. While the apparent anomalies of the g ratios in atoms consisting of one electron outside closed shells are qualitatively understood in terms of the "intrinsic" moment of the electron, there remain small discrepancies between theory and experiment. The present consideration does little or nothing to resolve these discrepancies, but it seems desirable to investigate all relevant factors which might effect the interpretation of the experimental results.

To take account of the motion of all the charged particles composing an atom let $\mathbf{r}$ and $\mathbf{r}_i$ be the position vectors of the nucleus and electrons with respect to a fixed point. The total kinetic energy is then

$$T_0=(1/2M)\mathbf{p}^2+(1/2m)\textstyle\sum_i \mathbf{p}_i^2$$

where $\mathbf{p}$ and $\mathbf{p}_i$ are the momenta conjugate to $\mathbf{r}$ and $\mathbf{r}_i$. It is in this system of coordinates that a constant field $\mathbf{H}$ is represented by the vector potential $\mathbf{A}=\frac{1}{2}\mathbf{H}\times\mathbf{r}$, and can be introduced into the Hamiltonian by the well-known substitution $\mathbf{p}\rightarrow\mathbf{p}-Ze\mathbf{A}/c$ and $p_i\rightarrow\mathbf{p}_i+e\mathbf{A}_i/c$. To first order in H,

$$T=T_0+T_H=(1/2M)(\mathbf{p}^2-(2Ze/c)\mathbf{p}\cdot\mathbf{A}) +(1/2m)\textstyle\sum_i[\mathbf{p}_i^2+(2e/c)\mathbf{p}_i\cdot\mathbf{A}_i]$$

and

$$T_H=-(Ze/2Mc)\mathbf{H}\cdot\mathbf{r}\times\mathbf{p}+(e/2mc)\textstyle\sum_i \mathbf{H}\cdot\mathbf{r}_i\times\mathbf{p}_i.$$

Transforming to the Hamiltonian operator in the usual way, $\mathbf{p}\rightarrow(\hbar/i)\text{grad}$, and assuming that the magnetic field is directed along the z axis,

$$T_H=(eH/2c)(\hbar/i)\{(-Z/M)(\mathbf{r}\times\nabla_r)_z +(1/m)\textstyle\sum_i(\mathbf{r}_i\times\nabla_{ri})_z\}.$$

If we now introduce the coordinate vector $\mathbf{R}$ of the center of mass, and the relative coordinates $\mathbf{s}_i$ of the electrons with respect to the nucleus,

$$\mathbf{s}_i=\mathbf{r}_i-\mathbf{r},\quad (m+Mm)\mathbf{R}=M\mathbf{r}+m\textstyle\sum\mathbf{r}_i,$$

that portion of the Hamiltonian operator which varies as the first power of H becomes:

$$T_H=\frac{eH}{2c}\frac{\hbar}{i}\Big\{-\frac{Z}{M}\Big[\Big(\mathbf{R}-\frac{m}{M+Nm}\sum_i\mathbf{s}_i\Big) \times\Big(\frac{M}{M+Nm}\nabla_R-\sum_i\nabla_{s_i}\Big)\Big]_z +\frac{1}{m}\sum_i\Big[\Big(\mathbf{R}+\frac{M+(N-1)m}{M+Nm}\mathbf{s}_i-\frac{m}{M+Nm}\sum_{j\neq i}\mathbf{s}_j\Big) \times\Big(\frac{m}{M+Nm}\nabla_R+\nabla_{s_i}\Big)\Big]_z\Big\}.$$

It is legitimate to neglect the motion of the center of mass, so that $\mathbf{R}$ and the momentum conjugate to $\mathbf{R}$ may be set equal to zero. The terms of interest are therefore:

$$T_H=\frac{eH}{2c}\frac{\hbar}{i}\Big\{\Big(-\frac{Z}{M}\frac{m}{M+Nm}+\frac{M+(N-1)m}{M+Nm}\Big) \times\sum_i(\mathbf{s}_i\times\nabla_{s_i})_z-\frac{1}{M+Nm}\Big(\frac{Zm}{M}+1\Big) \times\sum_{j\neq i}[(\mathbf{s}_j+\nabla_{s_i})_z+(\mathbf{s}_i\times\nabla_{s_j})_z]\Big\}.$$

For a neutral atom, in which N, the number of electrons, is equal to Z, the nuclear charge number, this simplifies to the expression:

$$T_H=\frac{eH}{2mc}\frac{\hbar}{i}\Big\{\Big(1-\frac{m}{M}\Big)\sum_i(\mathbf{s}_i\times\nabla_{s_i})_z -\frac{m}{M}\sum_{j\neq i}[(\mathbf{s}_j\times\nabla_{s_i})_z+(\mathbf{s}_i\times\nabla_{s_j})_z]\Big\} =T_{H0}+T_{H1}.$$

The first term, T_{H0}, gives rise to the well-known eigenvalue l_z for each electron, although it is to be noticed that the factor $(1-m/M)$ enters. The second term, T_{H1}, is analogous to the "specific isotope effect"

[1] P. Kusch and H. M. Foley, Phys. Rev. 74, 250 (1948).

in atomic spectra,[2] and has already been mentioned in connection with atomic g values.[3]

The matrix elements of $(s_i \times \nabla s_j)_z$ may be readily evaluated in terms of radial integrals if all quantities are expressed in polar coordinates and determinantal electronic wave functions are used. Only exchange integrals will contribute for any given configuration, and these always enter with a negative sign because of the antisymmetry of the atomic wave functions. Those pairs of electrons will interact which have the same spin, opposite individual parity, and m_l values differing by ± 1. This means, for example, that a p valence electron in an atom such as gallium or indium will interact with one s electron in each closed s shell, and two d electrons in each closed d shell. (The sum of all such interactions between electrons within closed shells is zero, just as T_{H0} is zero in that case.)

For the normal configuration of an atom like gallium or indium, consisting of an n_0p valence electron outside closed s and d shells, the total contribution due to interaction with these shells is

$$T_{H1}=\frac{eHh}{2mc}\frac{m}{M}\frac{2}{3}\Big\{\sum_{n\geq 1}\int_0^\infty R(ns)rR(n_0p)r^2dr \times\int_0^\infty R(n_0p)\frac{\partial R(ns)}{\partial r}r^2dr -\sum_{n\geq 3}\int_0^\infty R(nd)rR(n_0p)r^2dr\Big[\int R(n_0p)\frac{\partial R(nd)}{\partial n}r^2dr +3\int_0^\infty R(n_0p)\frac{1}{r}R(nd)r^2dr\Big]\Big\}.$$

Here r refers to the polar coordinates, r, θ, ϕ, relative to the nucleus, and R is the appropriate single electron radial wave function. The summation, of course, extends only over closed shells.

The radial integrals in the expression above are elementary in terms of hydrogenic wave functions, but the results of such computations can serve only as a very rough guide, since the penetrating p orbit and all the core orbits involved are distorted by the charge distribution of the core itself. The matrix elements of r are relatively well known, because of their relation to the intensities of radiation from the ionized atom. The integrals involving $1/r$ and the derivatives of the wave functions, however, are difficult to estimate. The main contribution to these integrals comes from inside the core, where the distribution of nodes is very critical. The use of hydrogenic wave functions and the same screening constant for the n_0s and n_0p electrons causes the interaction with the closed n_0s shell to be exactly zero, although the interaction with the inner s shells does not vanish. Also, in the case of the normal $4p$ state of gallium, the first term of the interaction with the $3d$ shell vanishes, since the derivative of $R(3d)$ is a constant times $R(3p)$. The net result, using hydrogenic wave functions for gallium, is that T_{H1} is somewhat less than, although of the same order as, the correction for the motion of the core as a whole, i.e., the sum of the radial integrals in the bracket above is slightly less than unity. There is no obvious reason why improved wave functions should not give an answer several times as great as this, although not of a higher order. A very similar result is obtained for indium: again the contribution of the overlapping s shell is zero, although there is a non-vanishing interaction with deeper s shells and both d shells.

It would be routine, although tedious, to evaluate T_{H1} using numerically integrated wave functions with something like a self-consistent field. At present the experimental precision does not seem to warrant such a calculation, especially since the relativistic correction is presumably somewhat more important.

APPENDIX

To write the matrix elements in polar coordinates:

$$(s_i\times\nabla s_j)_z=\Big(x_i\frac{\partial}{\partial y_j}-y_i\frac{\partial}{\partial x_j}\Big)=\frac{i}{2}(\eta_i\bar{\zeta}_j-\bar{\eta}_i\zeta_j)=G(i,j),$$

where

$$\eta_i=x_i+iy_j=r_i\sin\theta_i e^{i\phi_i}$$

and

$$\zeta_i=\frac{\partial}{\partial x_i}+i\frac{\partial}{\partial y_i}=\sin\theta_j e^{i\phi_j}\Big(\frac{\partial}{\partial r_j}+\frac{\cos\theta_j}{r_j\sin\theta_j}\frac{\partial}{\partial\theta_j}+\frac{i}{r_j\sin^2\theta_j}\frac{\partial}{\partial\varphi_j}\Big).$$

The integrals to be evaluated are then:

$$-\int d\tau_1\int d\tau_2\{v(1)u_p(2)Gu_p(1)v(2)+v(2)u_p(1)Gu_p(2)v(1)\}.$$

Here u_p is the wave function of the valence electron, and v is the single particle function for the interacting core electron. When these wave functions are introduced the angular integrals are elementary, and the matrix element of $(s_i\times\nabla s_j)_z+(s_j\times\nabla s_i)_z$ involving any s shell is

$$-\frac{i}{3}\int_0^\infty R(ns)rR(n_0p)r^2dr\Big[\int_0^\infty R(ns)\frac{\partial R}{\partial r}(n_0p)r^2dr -\int_0^\infty R(n_0p)\frac{\partial R(ns)}{dr}r^2dr+2\int_0^\infty R(ns)\frac{1}{r}R(n_0p)r^2dr\Big] =+\frac{2i}{3}\int_0^\infty R(ns)rR(n_0p)r^2dr\int_0^\infty R(n_0p)\frac{\partial R(ns)}{\partial r}r^2dr.$$

The analogous result for the interacting d electron with azimuthal quantum number equal to zero is

$$\frac{2i}{15}\int_0^\infty R(n_0p)rR(nd)r^2dr\Big[\int_0^\infty R(n_0p)\frac{\partial R(nd)}{dr}r^2dr +3\int_0^\infty R(n_0p)\frac{1}{r}R(nd)r^2dr\Big].$$

The interaction with the d electron having azimuthal quantum number 2 gives

$$-\frac{4i}{5}\int_0^\infty R(n_0p)rR(nd)r^2dr\Big[\int R(n_0p)\frac{\partial R(nd)}{\partial r}r^2dr +3\int_0^\infty R(n_0p)\frac{1}{r}R(nd)r^2dr\Big].$$

The final expression for T_{H1} in the main body of the paper is just the sum of all such matrix elements, multiplied by the constants in the Hamiltonian.

[2] D. S. Hughes and C. Eckart, Phys. Rev. **36**, 694 (1930).
[3] M. Phillips, Phys. Rev. **60**, 100 (1941).

Experimental Investigations of Magneto-Hydrodynamic Waves

S. LUNDQUIST
The Royal Institute of Technology, Stockholm, Sweden
(Received August 29, 1949)

The importance of magneto-hydrodynamic phenomena to different parts of cosmic physics is becoming more and more evident. This fact and the extreme mathematical difficulties involved in an exact treatment of many problems make it necessary to consider the possibility for experimental investigations. In this paper the fundamental equations are solved for cylindrically limited waves, a case which seems to be best adapted for experiments. It is shown that an "ideal" magneto-hydrodynamic wave in a liquid with finite conductivity can exist only in a certain frequency interval. The upper limit is set by the conductivity and the magnetic field strength. Above this value the waves degenerate into skin-waves. The lowest frequency is determined by the geometrical dimensions and by the conductivity. Waves in different liquids are compared, and liquid sodium is found to be the best medium for an experiment. A brief account is given for a preliminary experiment and other investigations are proposed.

I. INTRODUCTION

THE mutual interaction between electromagnetic and hydrodynamic forces in an electrically conducting fluid which is subject to a magnetic field gives rise to a certain type of waves, called magneto-hydrodynamic waves, which travel in the direction of the outer magnetic field carrying with them an induced magnetic field as well as a velocity field.

This phenomenon was discovered in 1942 by Alfvén.[1] In the following year Alfvén outlined a theory of sunspots.[2] According to this theory, the spots are generated by a disturbance in the central part of the sun and then transported to the surface by means of magneto-hydrodynamic waves.

Walén has made a detailed theoretical study of the waves.[3] He considers especially traveling magneto-hydrodynamic whirl-rings. Such a ring may give rise to a bipolar spot pair when intersecting the surface.

In three papers Alfvén has developed his theory of sunspots further and also made comparisons with observations.[4,5] He has also given a theory for the granulation and the heating of the solar corona, based on magneto-hydrodynamic waves.[6]

Recently, some theories on the origin of the cosmic radiation have been proposed, in which magneto-hydrodynamic phenomena play an important role.[7–9]

From the above it is seen that these waves are very important in cosmic physics. Many problems connected with the waves are difficult to treat mathematically, even with the computing machines now existing, so it will be necessary to consider the possibility for an experimental investigation. This is done in the following paragraphs. A brief account of a preliminary experiment is also given.

[1] H. Alfvén, Nature **150**, 405 (1942); Arkiv. f. Mat. Astr. o. Fys. **Bd 29 B**, No. 2 (1942).
[2] H. Alfvén, Arkiv. f. Mat. Astr. o. Fys. **Bd 29 A**, No. 12, (1943).
[3] C. Walén, Arkiv. f. Mat. Astr. o. Fys. **Bd 30 A**, No. 15 and **Bd 31 B**, No. 3 (1944).
[4] H. Alfvén, M.N.R.A.S. **105**, 1, 390 (1945).
[5] H. Alfvén, Arkiv. f. Mat. Astr. o. Fys. **Bd 34 A**, No. 23 (1948).
[6] H. Alfvén, M.N.R.A.S. **107**, 211 (1947).
[7] R. D. Richtmyer and E. Teller, Phys. Rev. **75**, 1729 (1949).
[8] E. Fermi, Phys. Rev. **75**, 1169 (1949).
[9] H. Alfvén, Phys. Rev. **75**, 1732 (1949).

II. THE FUNDAMENTAL EQUATIONS

The motion of an incompressible fluid with the density ρ, the electrical conductivity σ, and the permeability μ, placed in a magnetic field H_0 is described by Maxwell's equations

$$\text{curl}\mathbf{H}=4\pi/c\cdot\mathbf{i} \tag{1}$$

$$\text{curl}\mathbf{E}=-\frac{\mu}{c}(\partial\mathbf{H}/\partial t) \tag{2}$$

$$\text{div}\mu\cdot\mathbf{H}=0 \tag{3}$$

$$\mathbf{i}=\sigma\left(\mathbf{E}+\frac{\mu}{c}\mathbf{v}\times\mathbf{H}\right) \tag{4}$$

and the hydrodynamical equations

$$\frac{d\mathbf{v}}{dt}=\frac{\mu}{\rho c}\mathbf{i}\times\mathbf{H}-\frac{1}{\rho}\text{grad}p, \tag{5}$$

$$div\mathbf{v}=0. \tag{6}$$

Here $\mathbf{v}$ denotes the material velocity, $\mathbf{H}$ and $\mathbf{E}$ the magnetic and the electric field strength, respectively, $\mathbf{i}$ the current density, and p the pressure. In (1) the displacement current has been neglected. As Walén has shown, this system of equations may be reduced in the following way. Eliminating $\mathbf{i}$ and $\mathbf{E}$, we have

$$\frac{1}{c}\frac{\partial\mathbf{H}}{\partial t}=\frac{c}{4\pi\mu\sigma}\text{curl curl}\mathbf{H}-\frac{1}{c}\text{curl}\mathbf{v}\times\mathbf{H} \tag{7}$$

$$\frac{d\mathbf{v}}{dt}=\frac{\mu}{4\pi}\text{curl}\mathbf{H}\times\mathbf{H}-\frac{1}{\rho}\text{grad}p. \tag{8}$$

Putting $\mathbf{H}=\mathbf{H}_0+\mathbf{h}$, where $\mathbf{h}$ is the induced magnetic field, and $a^2=c^2/4\pi\mu\sigma$, we get after some transforma-

tions:

$$\frac{\partial \mathbf{h}}{\partial t}-a^2\Delta\mathbf{h}-(\mathbf{H}_0\nabla)\mathbf{v}+(\mathbf{v}\nabla)\mathbf{H}_0=\operatorname{curl}\mathbf{v}\times\mathbf{h} \tag{9}$$

$$\frac{\partial \mathbf{v}}{\partial t}-\frac{\mu}{4\pi\rho}[(\mathbf{H}_0\nabla)\mathbf{h}-(\mathbf{h}\nabla)\mathbf{H}_0]+\frac{1}{\rho}\operatorname{grad}\left(p+\frac{\rho v^2}{2}+\frac{\mu}{4\pi}\mathbf{H}_0\cdot\mathbf{h}\right)=\mathbf{v}\times\operatorname{curl}\mathbf{v}-\frac{\mu}{4\pi}\mathbf{h}\times\operatorname{curl}\mathbf{h}. \tag{10}$$

These equations determine **h** and **v**. They are not linear. Walén, however, has shown that if the conductivity σ is infinite, the equations reduce to a linear system, the right members of (9) and (10) exactly canceling in this case. With some approximation the same is true for a finite but still very good conductivity. In an experiment where the amplitudes are small, we can simply neglect the second-degree terms. For this case and with a homogeneous outer magnetic field, we get:

$$[(\partial/\partial t)-a^2\Delta]\mathbf{h}=(\mathbf{H}_0\nabla)\mathbf{v} \tag{11}$$

$$\frac{\partial \mathbf{v}}{\partial t}=\frac{\mu}{4\pi\rho}(\mathbf{H}_0\nabla)\mathbf{h}-\frac{1}{\rho}\operatorname{grad}\left(p+\frac{\rho v^2}{2}+\frac{\mu}{4\pi}\mathbf{H}_0\cdot\mathbf{h}\right). \tag{12}$$

III. A SPECIAL SOLUTION OF THE EQUATIONS

Equation (3) requires the motion to be closed. The simplest way of satisfying this condition in an experiment is to choose a motion in which the liquid rotates about a fixed axis. This case seems to be of general interest for experimental investigations and therefore we deduce the corresponding solution. We assume the rotation to take place in a plane perpendicular to the vertical magnetic field B_0 and around the z axis of a cylindrical reference system (r, φ, z). The components of **v** and **h** are:

$$v_r=0,\quad v_\varphi=v,\quad v_z=0$$
$$h_r=0,\quad h_\varphi=h,\quad h_z=0.$$

That **v** and **h** are parallel is seen by considering the induced currents. Equations (11) and (12) may be written

$$\frac{\partial h}{\partial t}=a^2\left(\frac{\partial^2 h}{\partial r^2}+\frac{1}{r}\frac{\partial h}{\partial r}-\frac{h}{r^2}+\frac{\partial^2 h}{\partial z^2}\right)+H_0\frac{\partial v}{\partial z} \tag{13}$$

$$\frac{\partial v}{\partial t}=\frac{\mu H_0}{4\pi\rho}\frac{\partial h}{\partial z}. \tag{14}$$

Eliminating v, we get

$$\frac{\partial^2 h}{\partial t^2}=a^2\frac{\partial}{\partial t}\left[\frac{\partial^2 h}{\partial r^2}+\frac{1}{r}\frac{\partial h}{\partial r}-\frac{h}{r^2}+\frac{\partial^2 h}{\partial z^2}\right]+V^2\frac{\partial^2 h}{\partial z^2}, \tag{15}$$

where

$$V^2=(\mu H_0^2)/(4\pi\rho). \tag{16}$$

We want to find a wave with the angular frequency ω, which travels along the z axis, i.e., all quantities are to vary as $\exp(j\omega t+\alpha z)$. Accordingly, we put $\partial/\partial t=j\omega$ and $\partial/\partial z=\alpha$.

Then (15) may be written

$$\frac{\partial^2 h}{\partial r^2}+\frac{1}{r}\frac{\partial h}{\partial r}+\left(k^2-\frac{1}{r^2}\right)h=0, \tag{17}$$

where $k^2=\alpha^2+(\omega^2+\alpha^2V^2)/j\omega a^2$. A solution of (17), which is zero for $r=0$, is

$$h=A\cdot J_1(kr)\cdot\exp(j\omega t+\alpha z) \tag{18}$$

with

$$\alpha^2=(j\omega k^2a^2-\omega^2)/(j\omega a^2+V^2), \tag{19}$$

where J_1 is the Bessel function of the first order.

By means of the original equations the other variables are found:

$$v=\frac{\mu\alpha H_0}{j4\pi\omega}\cdot h \tag{20}$$

$$i_r=-\alpha c/4\pi\cdot h \tag{21}$$

$$i_z=\frac{kc}{4\pi}\frac{J_0(kr)}{J_1(kr)}\cdot h \tag{22}$$

$$E_r=-\frac{\mu\alpha}{j\omega c}(V^2+j\omega a^2)\cdot h \tag{23}$$

$$E_z=\frac{\mu a^2 k}{c}\cdot\frac{J_0(kr)}{J_1(kr)}\cdot h. \tag{24}$$

Suppose that we want to study the waves under the following simple experimental conditions: (a) The liquid is contained in a cylinder with the radius R and the height L; (b) at the bottom, $z=0$, a motion $v(r,t)=v_0\cdot r/R\cdot e^{j\omega t}$ is excited.

The following boundary conditions determine the solution:

(1) $r=R$ $\quad i_r=0$ $\quad\because h=0$
(2) $z=0$ $\quad v=v_0\cdot r/R\cdot e^{j\omega t}$
(3) $z=L$ $\quad i_z=0$ $\quad\because h=0$.

The first condition gives the proper values k_ν of k as solutions of the equation $J_1(k_\nu R)=0$. The corresponding α_ν are then given by (19).

Conditions (2) and (3) may be satisfied in this way. We consider the repeated reflections of the waves. A wave traveling up to the surface is reflected without phase difference in v but h is in opposite phase in the upward wave and the downward wave. At the bottom the conditions for h and v are reversed. In a point z we add all the waves traveling up and down.

$$v(z)=v(0)(e^{\alpha z}+e^{\alpha(2L-z)}-e^{\alpha(2L+z)}-e^{\alpha(4L-z)}+\cdots)$$

or

$$v(z)=v_0\cdot\frac{\cosh\alpha(L-z)}{\cosh\alpha L}. \tag{25}$$

The solution is

$$v(r,z,t)=\sum_{\nu=1}^{\infty} A_\nu J_1(k_\nu r)\cdot\frac{\cosh\alpha_\nu(L-z)}{\cosh\alpha_\nu}\cdot e^{j\omega t}. \quad (26)$$

For $z=0$ and $r<R$ we have

$$v_0\cdot\frac{r}{R}=\sum_{\nu=1}^{\infty} A_\nu J_1(k_\nu\cdot r), \quad (27)$$

from which the A_ν may be determined. Finally, we give the expression for the velocity in a point (r,z), valid for $0\leq r<R$ and $0\leq z\leq L$

$$\frac{v(r,z)}{v(r,0)}=\sum_{\nu=1}^{\infty}\frac{2}{k_\nu\cdot rJ_2(k_\nu R)}\cdot J_1(k_\nu r)\frac{\cosh\alpha_\nu(L-z)}{\cosh\alpha_\nu L}. \quad (28)$$

IV. IDEAL WAVES AND DEGENERATED WAVES

Introducing $U=j\omega/\alpha$ we see that the field strength of the waves varies as $\exp[j\omega(t-z/U)]$, where U is the phase velocity. A complex value of U means damping of the waves. Equation (19) may be written

$$\frac{1}{U^2}=\frac{1}{V^2}\frac{1-j(k^2a^2/\omega)}{1+j(\omega a^2/V^2)}. \quad (29)$$

The propagation of the waves depends upon both the frequency, ω, and the wave number, k; i.e., upon the spectrum of the wave in time and space. If the conductivity is infinite ($a=0$), we get $U=\pm V$. In this case all waves travel without damping with the same constant velocity $V=H_0\mu^{\frac{1}{2}}(4\pi\rho)^{-\frac{1}{2}}$, parallel or antiparallel to the magnetic field H_0. Every velocity-state is moving with this speed without any deformation. Equation (20) gives $v/V=h/H_0$, and accordingly, we have $\rho v^2/2=\mu h^2/8\pi$, which means the ideal case in which kinetic and magnetic energy are equal.

In reality we always have $a\neq 0$ but in the cosmical applications k and ω are so small that the waves may be considered as ideal.

At high frequencies (or if $V\to 0$ and $k\to 0$) we get $U\simeq a\omega^{\frac{1}{2}}e^{j\pi/4}$ and $v\simeq 0$ which means a damped pure electromagnetic wave, independent of H_0 and ρ. The waves have degenerated into skin-effect waves.

If the frequency is very low we get $U\simeq\pm V\cdot\omega^{\frac{1}{2}}(ka)^{-1}\cdot e^{j\pi/4}$, which is another type of degenerated waves, where the degeneration is due to the finite value of k. If $k=0$, i.e., $R=\infty$ (or plane waves), we get ideal waves for all frequencies $\omega\ll V^2/a^2$.

V. CONDITIONS FOR AN EXPERIMENT

From (29) we infer that the conditions for getting "ideal" magneto-hydrodynamic waves are

$$k^2a^2/\omega\ll 1 \quad (30)$$

$$\omega a^2/V^2\ll 1 \quad (31)$$

or together

$$k^2a^2\ll\omega\ll V^2/a^2. \quad (32)$$

In order that this shall be possible we must have $V^2\gg k^2a^4$ or

$$H_0R\gg 3.83(4\pi)^{-\frac{1}{2}}c^2\sigma^{-1}\rho^{\frac{1}{2}}\mu^{-\frac{1}{2}}, \quad (33)$$

where k has been replaced by $3.83/R$, corresponding to the lowest wave number, which is possible in a cylinder of the radius R.

In an experiment it is desirable to get a small required magnetic field H_0 and small dimensions. Equation (33) tells us that the required value of $H_0\cdot R$ is small if $\sigma\mu^{\frac{1}{2}}\rho^{-\frac{1}{2}}$ is large. The permeability, μ, being always ≈ 1, we may take $\sigma\rho^{-\frac{1}{2}}$ as a measure of the property of a medium for magneto-hydrodynamic experiments.

The relative values of $\sigma\rho^{-\frac{1}{2}}$ for some possible media are as follows: liquid sodium, 35; liquid lithium, 11; liquid sodium-potassium alloy, 10; mercury, 1; arc discharge in air at 100 mm Hg, 0.1.

Mercury is perhaps most simple to handle, but an experiment with liquid sodium would certainly give much more information.

In Figs. 1 and 2 the phase-velocity and the damping of a magneto-hydrodynamic wave in liquid sodium, corresponding to the lowest possible wave number, k_1,

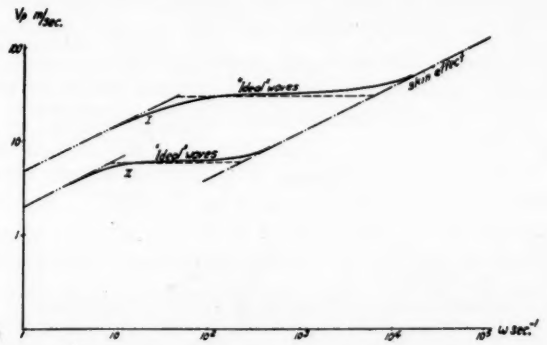

FIG. 1. Phase velocity of magneto-hydrodynamic waves in liquid sodium: —— phase velocity V_p, - - - - ideal wave velocity V_0, —·— degeneration at high frequencies (skin-effect), —··— degeneration at low frequencies. I—Cylinder radius $R=12$ cm. Magnetic field strength $H_0=10{,}000$ gauss. II—Cylinder radius $R=25$ cm. Magnetic field strength $H_0=2000$ gauss.

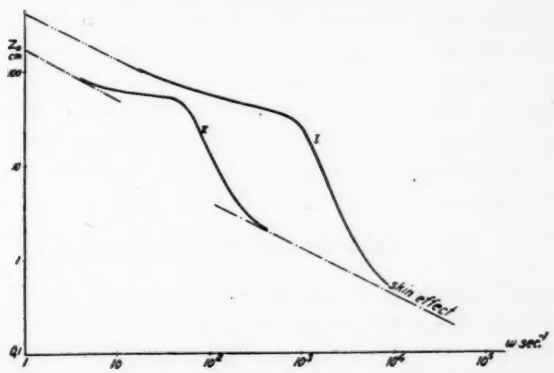

FIG. 2. Damping of magneto-hydrodynamic waves in liquid sodium: —— Z_0 = distance for damping of the wave to e^{-1}, —·— damping at high frequencies (skin-effect), —··— damping at low frequencies. I, II—See text to Fig. 1.

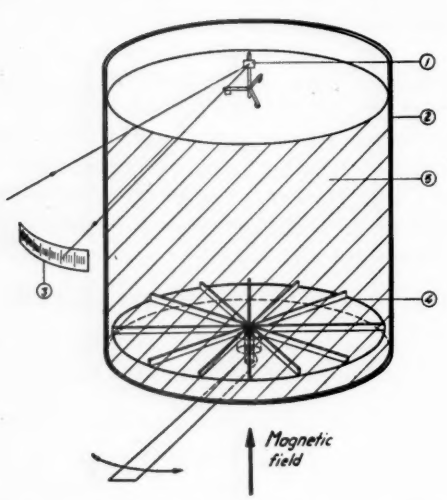

FIG. 3. Arrangement of the experiment on magneto-hydrodynamic waves in mercury: (1) floating mirror, (2) stainless steel cylinder, (3) scale, (4) vibrating disk, (5) mercury.

are given as a function of the frequency for two different cylinder radii.

VI. INFLUENCE OF THE VISCOSITY

In a viscous fluid we get, instead of Eqs. (13) and (14),

$$\frac{\partial h}{\partial t}=a^2\Delta h+H_0\frac{\partial v}{\partial z} \tag{34}$$

$$\frac{\partial v}{\partial t}=\frac{\mu H_0}{4\pi\rho}\frac{\partial h}{\partial z}+\nu\Delta v, \tag{35}$$

where ν denotes the kinematic viscosity.

If $\nu=0$, Eq. (20) gives $v=(\alpha\mu H_0/j4\pi\rho\omega)\cdot h$. We put this value into the last term of (35) and eliminate v between (34) and (35). With $\partial/\partial t=j\omega$ and $\partial/\partial z=\alpha$ we get

$$-\omega^2 h=\Delta h\left(j\omega a^2+\frac{\nu V^2\alpha^2}{j\omega}\right)+\alpha^2V^2h. \tag{36}$$

If $\nu\ll(\omega^2a^2/\alpha^2V^2)=(U^2/V^2)\cdot a^2$, the viscosity may be neglected. If it may not be neglected the influence of the viscosity is to increase the damping of the waves. For an "ideal" wave a^2 should be replaced by $a^2+\nu$, and then we see that the viscosity is unimportant if $\nu\ll a^2$. For liquid sodium ν/a^2 is about 10^{-5} and so the viscosity certainly may be neglected.

VII. A PRELIMINARY EXPERIMENT

An experiment on magneto-hydrodynamic waves in mercury has been carried out at this laboratory. The mercury was contained in a stainless steel cylinder with the diameter 15 cm and the height 15 cm (see Fig. 3). The waves were excited at the bottom by means of a disk with radial strips and the measurements were made by means of a mirror floating on the surface.

The apparatus was placed in a vertical magnetic field with a maximal value of 13,000 gauss. The disk was mechanically driven to perform torsional vibrations with a small amplitude. The damping and the phase difference between surface and bottom were measured directly by means of a stopwatch. The frequency was varied between 0.1 and 1 cm/sec. for different values of the magnetic field. In Fig. 4 the results are compared with the theoretical values.* The discrepancy between theory and experiment may be due to the experimental difficulties to keep the surface of the mercury clean. A layer rapidly formed on the surface, making further measurements impossible. We hope to find the reason for the discrepancy and intend also to repeat the experiment in liquid sodium, if technically possible.

VIII. SOME PROBLEMS SUITED FOR EXPERIMENTAL INVESTIGATIONS

In cosmical physics the conductivity may often be considered as infinite and the waves are correctly described by Eqs. (9) and (10), the right members being equal to zero. These equations are formally linear, but do not permit the adding of solutions to get a new solution. Suppose, in particular, that we have two waves traveling into each other. In each wave alone we have a perfect balance between magnetic forces and centrifugal forces. By adding the waves it may happen that we get a wave which is not balanced, e.g., if the induced fields are antiparallel but the material velocities parallel. A detailed discussion is given in the paper by Walén. This problem is very difficult to treat mathematically. An experimental investigation may be able to give at least a qualitative picture of the situation if sufficiently large amplitudes may be excited that the second-degree terms are important. The condition for this is $h\approx H_0$, or for an ideal wave $v\approx V$.

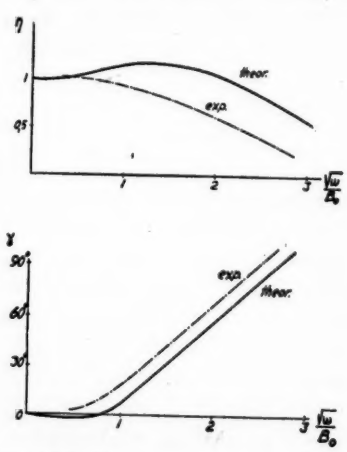

FIG. 4. Measurements on magneto-hydrodynamic waves in mercury. η=amplitude at surface/amplitude at bottom. γ=phase difference between bottom and surface.

* These values have been calculated in the same way as in Section III, only with the exception that the excited velocity at the bottom has been assumed to be $v_0\cdot r/R$ when $0\leq r\leq R_1$, and $v_0\cdot R_1/R\cdot(R-r)/(R-R_1)$ when $R_1\leq r\leq R(R_1/R=0.96)$, which ought to be closer to the real velocity distribution. The difference between these values and Eq. (28) does not exceed 10 percent.

One interesting experiment would be to study the reflection of a magneto-hydrodynamic whirl-ring at a non-conducting surface. Especially important for the theory of sunspots is the behavior of rings parallel to the magnetic field.

The generation of the whirl-rings by convection also ought to be studied.

The experiments with waves in mercury have given the impression that all magneto-hydrodynamic phenomena have a quite different character than the corresponding purely hydrodynamic phenomena. Perhaps many theories on hydrodynamic problems in cosmical physics have to be reconsidered.

ACKNOWLEDGMENTS

I want to express my gratitude to Professor H. Alfvén, who has suggested this work.

PHYSICAL REVIEW VOLUME 76, NUMBER 12 DECEMBER 15, 1949

The Decay Scheme of Hf^{181}

ARNE LUNDBY
Institute for Atomic Energy Studies and Norwegian Defense Research Establishment, Oslo, Norway
(Received July 11, 1949)

The radiations of Hf^{181} have been studied with delayed coincidence and absorption techniques. No γ-rays are found to precede the formation of the 20-microsecond metastable state in Ta^{181}, thus confirming the decay scheme of Chu and Wiedenbeck. From the values of the internal conversion coefficients together with delayed coincidence absorption measurements it is concluded that the previously reported 0.134-Mev γ-ray is most probably emitted from another metastable state of about one-second duration in Ta^{181}. A theoretical discussion of the multipole order of the different radiations lead to assignments of probable spin and relative parity values to the excited states of Ta^{181}. Beginning with the ground state, the deduced spin and parity values are: $7/2(\pm)$, $1/2(\pm)$, $5/2(\pm)$, and $1/2(\mp)$.

SOME uncertainty exists as to the succession of the γ-transitions in Ta^{181}, following the β^--decay of Hf^{181}. The metastable state in Ta^{181} of 20-μsec. duration was first observed by DeBenedetti and McGowan,[1] and later studied by Bunyan *et al.*[2] The β-rays, γ-rays, and conversion electrons have been subject to investigations by several authors,[3] some of which claim to have observed a γ-transition preceding the formation of the metastable state.

With the delayed coincidence recorder in Fig. 1 we have remeasured the half-life of the metastable state in Ta^{181} [4] with both the differential and integral procedures, the results being in agreement with earlier determinations. Inserting a 1-mm lead absorber between the source and the Geiger counter in the B channel and then in the A channel, we find a genuine delayed coincidence rate of 1.5 min.$^{-1}$ (corresponding to infinitely long resolving time) and less than 10^{-2} min.$^{-1}$, respectively. With the same Pb absorbers in front of both Geiger counters, we could detect neither delayed nor instantaneous coincidences exceeding the random coincidences and in the latter case the background coincidence rate due to cosmic rays and other instantaneous coincidence sources. We therefore conclude that γ-rays with an energy larger than 0.25 Mev can scarcely precede the isomeric transition nor can two or more such γ-rays follow each other in cascade. The modified decay scheme of Chu and Wiedenbeck[3] given in Fig. 2 therefore appears to be the most satisfactory at present.

Taking into account window absorption in the Geiger counters, the delayed coincidence absorption measurements[2] are in excellent agreement with the result from the β-spectrograph[3] as to the value of the integrated internal conversion coefficients for the different electron energy groups.

A theoretical interpretation of the decay scheme meets with certain difficulties owing to a lack of exact numerical calculations of the internal conversion coefficients in the relativistic region. However, some numerical calculations have been carried out for the natural radioactive elements ($Z=83$).[5] In the approximate calculations, the ratio of the number of conversion electrons to the number of gamma-rays, the branching ratio N_e/N_γ, is proportional to Z^3,[6] thus making the internal conversion in Ta about 35 percent less than in RaC. We have applied this correction factor to the numerical calculations referred to above in the following comparison of experiment with theory.

[1] S. DeBenedetti and F. K. McGowan, Phys. Rev. **70**, 569 (1946).

[2] Bunyan, Lundby, Ward, and Walker, Proc. Phys. Soc. **61**, 300 (1948).

[3] Cork, Shreffler, and Fowler, Phys. Rev. **72**, 1209 (1947); Beneš, Ghosh, Hedgran and Hole, Nature **162**, 261 (1948); K. Y. Chu and M. L. Wiedenbeck, Phys. Rev. **75**, 226 (1949).

[4] The sources were irradiated in the big pile at the Atomic Research Establishment, Harwell, England.

[5] H. R. Hulme, Proc. Roy. Soc. **A138**, 643 (1932); H. M. Taylor and N. F. Mott, Proc. Roy. Soc. **A138**, 665 (1932).

[6] This is because of the volume concentration factor, the radius of the K-orbit being proportional to $1/Z$.

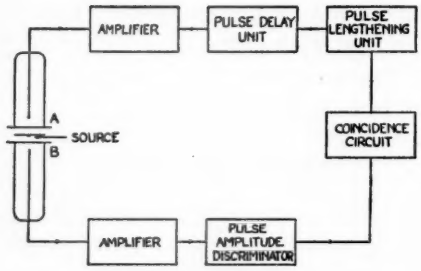

FIG. 1. Schematic diagram of delayed coincidence recorder.

Chu and Wiedenbeck[3] have determined the ratio of the number of conversion electrons emitted in the different transitions to the total number of β-rays preceding the isomeric transition (Table I in their paper). Correcting for the branching between the γ_2- and γ_3-transitions according to Fig. 2, the value of N_e/N_γ is found to be 0.031 for the K-shell in the case of the 0.471-Mev transition. Theoretical calculations[5] give for the same ratio 0.0065 for an electric dipole, 0.018 for an electric quadrupole, and 0.065 for a magnetic dipole transition. The 0.471-Mev γ-radiation is therefore most probably of a mixed electric quadrupole and magnetic dipole character.

For the 0.337-Mev transition the corrected experimental value for the branching ratio in the K-shell is 0.067, while the theoretical calculations give: electric dipole 0.015, electric quadrupole 0.047, and magnetic dipole 0.13. This transition is thus apparently also of a mixed electric quadrupole and magnetic dipole character.

The ratio between internal conversion in the K- and L-shells is for the 0.471-Mev transition 3.0 and for the 0.337-Mev transition 3.6. This is about half the values predicted by theory for an electric quadrupole transition.[7] Numerical calculations have not been carried out for conversion of magnetic multipole radiations in the L-shell. The relative magnitudes of the two K to L ratios are in general agreement with the fact that this ratio should be inversely proportional to the γ-ray energy when other conditions are equal.

As will appear later, the 0.471-Mev and 0.337-Mev transitions are most probably emitted from the same excited state of Ta^{181}. According to the liquid drop model of the nucleus[8] the energy dependence of the transition probability for a multipole γ-radiation should be as E^{2l}, where E is the γ-ray energy and l is the multipole order. For the two radiations in question the ratio of the transition probabilities should be $(0.471/0.337)^4 = 3.8$ according to this theory, while experiments yield a value between 2 and 3. The agreement is reasonable, considering the very rough assumptions made in the liquid drop theory of the nucleus.

The branching ratios for the 0.130-Mev and 0.134-Mev transitions in the K-shell are about 1.3 and 2.8, respectively. Unfortunately, numerical calculations of N_e/N_γ have not been carried out for such low energies. From a rough extrapolation of the data given by Fisk and Taylor[9] it is apparent that electric dipole and quadrupole transitions are ruled out. The extrapolated theoretical value of the branching ratio for magnetic dipole transitions is also rather low, taking into account the fact that the internal conversion in the K-shell decreases in favor of conversion in the L-shell when the energy of the γ-ray approaches the binding energy of the K-electrons. On the other hand, no numerical calculations have been performed for electric octopole transitions. However, comparing the variation of N_e/N_γ with l in the non-relativistic theory[10] and in the exact theory, one can make a rough estimate of the branching ratio which is to be expected for electric octopole radiation in the latter case. The result is about 1.5–2, which is somewhat larger than the experimental value for the 0.130 transition. We can therefore conclude that this γ-radiation is probably of an electric octopole or magnetic quadrupole character or a mixture of both.

A further check on the value for the spin change in this transition can be obtained from the rough energy-lifetime relation which has been deduced from the liquid drop model of the nucleus. This relation being valid for a pure γ-transition, the observed value for the half-life (2.10^{-5} sec.) must be corrected for the probability of ejection of conversion electrons. The corrected half-life comes out as 2.10^{-4} sec. Theoretical calculations give, on the other hand, the following values for τ_γ:

l	2	3	4
τ_γ(sec.)	10^{-10}	10^{-4}	218

For $l=3$ the experimental and theoretical results differ by a factor of 2, which must be considered as a satisfactory agreement. Both the internal conversion coefficient and the energy-lifetime relation therefore lead to the same conclusion, *viz.*, that the 0.130-Mev radiation is electric octopole and/or magnetic quadrupole radiation.

The 0.134-Mev transition is, however, more exceptional. The branching ratio being in this case even larger than for the 0.130-Mev transition, the radiation is probably of multipole order 3 or possibly 4.[11] We have recorded the delayed coincidence rate for different time delays with three different absorbers (2-, 20-, and 40-mg/cm^2 aluminum foils) between the source and the Geiger counter in the A channel. The results agreed to within the statistical error in the measurements, which was about 3 percent. The lower metastable state can therefore scarcely have a half-life which lies in the interval from one to some hundred microseconds. If,

[7] J. B. Fisk, Proc. Roy. Soc. **A143**, 674 (1934).
[8] See, e.g., I. S. Lowen, Phys. Rev. **59**, 834 (1941).
[9] J. B. Fisk and H. M. Taylor, Proc. Roy. Soc. **A146**, 178 (1934).
[10] M. H. Hebb and E. Nelson, Phys. Rev. **58**, 486 (1940).
[11] A $0\rightarrow 0$ transition is of course ruled out owing to the fact that the ground state of Ta^{181} has half-integer spin.

however, the lifetime of this state exceeds 10^{-2} sec. and is less than the lifetime of Hf^{181}, it would be very difficult to detect. This would certainly be the case if the transition gives rise to a magnetic 2^3-pole or electric 2^4-pole radiation. Correcting the theoretical half-life for $l=4$ for the probability of internal conversion, the result comes out as a few seconds. A probable working hypothesis is therefore to assume that the 0.134-Mev transition is of magnetic 2^3-pole and/or electric 2^4-pole character.

Finally the β-transition from the ground state of Hf^{181} to the higher metastable state in Ta^{181} will be considered. From the values of the disintegration constant and the maximum energy of the β-particles, we find that the position of the point in the Sargent diagram for the β-emitters in the heavier elements[12] corresponds to a once-forbidden transition.

Collecting the results of the above discussion as to the nature of the different transitions, we arrive at the most probable spin and parity assignments to the different nuclear states as indicated in Fig. 2. We have tried a number of alternative models for the decay scheme, but all of them seem to be in disagreement with experiments. It should be remarked that the transition between the two metastable states is very rare owing to the special selection rule operating when the centers of mass and charge of a system coincide. If this transition had not been forbidden it had been necessary to assign a spin 13/2 or larger to the first excited state of Ta^{181}.

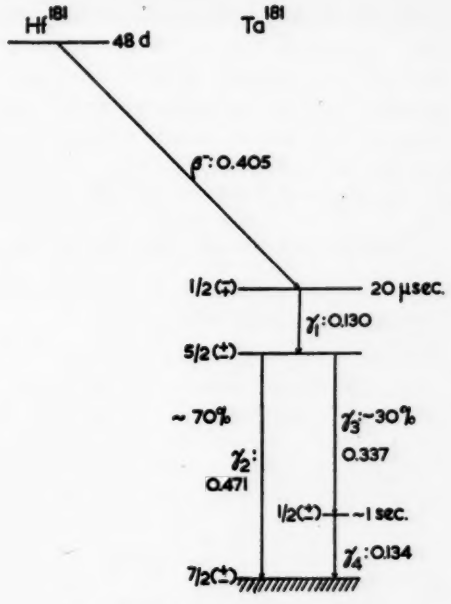

FIG. 2. The decay scheme of Hf^{181}.

Note added in proof: Comparison with recent discussions of nuclear shell structures (e.g., M. G. Mayer, Phys. Rev. **75**, 1969 (1949)) shows that the energy-levels of Ta^{181} all appear within the same shell. The states in order of increasing excitation energy are then supposed to be formed by the odd proton moving in $g_{7/2}$, $s_{1/2}$, $d_{3/2}$ or $d_{5/2}$ and $h_{11/2}$ orbits. The problem still arises as to why the direct transition from metastable to ground state does not occur. Special selection rules must apparently operate in this case.

[12] N. Feather and E. Bretscher, Proc. Roy. Soc. **A165**, 545 (1938). N. Feather, Nature **161**, 451 (1948).

PHYSICAL REVIEW VOLUME 76, NUMBER 12 DECEMBER 15, 1949

Multiple Scattering of Neutrons. II. Diffusion in a Plate of Finite Thickness

OTTO HALPERN AND R. K. LUNEBURG
University of Southern California, Los Angeles, California
(Received February 24, 1949)

The diffusion of neutrons in an infinite plate of finite thickness is studied. Analytic expressions are derived for the density and current of the returning and transmitted neutrons at the boundaries. Density and current distribution inside the material at sufficiently large distances from the boundaries are also calculated.

INTRODUCTION

IN I we succeeded[1] in obtaining a rigorous analytical solution for the density and current distributions of neutrons which have been impinging with an arbitrary velocity distribution upon a plate of infinite thickness; the neutrons were assumed to undergo elastic isotropic scattering processes and capture inside the material.

We here extend the treatment under the same physical assumptions to the case of a plate of finite thickness; in the limit of very large thickness the results, of course, will have to agree with those of I. The solutions given here will be *asymptotically* valid if the thickness of the plate is large compared with the mean free path of the neutrons inside the material. They will, therefore, become rigorous for the limiting case of infinitely large thickness.

The treatment is here extended considerably farther than in the first paper. We obtain information not only

[1] This second paper (see Halpern, Luneburg, and Clark, Phys. Rev. **53**, 173 (1938), referred to as I) appears belatedly due to reasons beyond the control of the authors; much of its content has been presented orally at an earlier opportunity (Phys. Rev. **56**, 1068 (1939)).

about the distribution functions at both boundaries but also about significant regions in the interior of the plate. It was, furthermore, possible to put the new transcendental function which represents the main part of the solution into a form which permits easy use in the evaluation of individual problems. Tables for the solution and auxiliary functions are given.

1. FORMULATION OF THE PROBLEM

The distribution function $w(x, \xi)$ satisfies the well-known transport equation (see I)

$$\xi(\partial w/\partial x)+Aw=B\bar{w}(x), \quad \bar{w}=\int_{-1}^{+1} w d\xi. \tag{1}$$

If the plate is located between $x=0$ and $x=l$, then we want to find a solution of (1) with the boundary conditions

$$w(0, \xi)=(f\xi), \quad \xi>0, \tag{1.1}$$

$$w(l, \xi)=0, \quad \xi<0. \tag{1.2}$$

Here, $f(\xi)$ is a known function.

It has been found useful in I to introduce a Laplace transformation of $w(x, \xi)$ or $\bar{w}(x)$. We here generalize the transformation by writing

$$u(z)=-B/z\int_0^l \bar{w}(x)e^{Ax/z}dx, \tag{1.3}$$

the upper limit being given by the actual thickness of the plate. Since we are in particular interested in the boundary values $w(0, \xi)$ and $w(l, \xi)$, it is important to notice that they are already determined by $u(z)$ and that we need to invert the Laplace transformation only if we are interested in values of w in the interior of the plate. This statement can be proven as follows: We first notice that (1) is solved by the integral equation

$$w(x, \xi)=e^{-(Ax/\xi)}\left[w(0, \xi)+B/\xi\int_0^x \bar{w}(x)e^{Ax/\xi}dx\right], \tag{1.4}$$

which gives, in particular,

$$w(l, \xi)=e^{-\lambda/\xi}\left[w(0, \xi)+B/\xi\int_0^l \bar{w}(x)e^{Ax/\xi}dx\right] \tag{1.41}$$

with the abbreviation $\lambda=Al$.

Introducing (1.3) into (1.41) one obtains

$$w(l, \xi)=e^{-(\lambda/\xi)}[w(0, \xi)-u(\xi)], \tag{1.5}$$

and specializing (1.5) for $\xi>0$ and $\xi<0$,

$$w(0, \xi)=u(\xi), \quad \xi<0 \tag{1.61}$$

$$w(l, \xi)=e^{-\lambda/\xi}[f(\xi)-u(\xi)], \quad \xi>0. \tag{1.62}$$

The relations (1.61) and (1.62) prove the statement made.

It may be noted that $u(z)$ is regular in the whole complex plane with the exception of the origin, which constitutes an essential singularity.

2. AN INTEGRAL EQUATION FOR $u(z)$

Introducing the function $v(\xi, z)$ by the relation

$$v(\xi, z)=-B/z\int_0^l w(x, \xi)e^{Ax/\xi}dx \tag{2.1}$$

so that

$$u(z)=\int_{-1}^{+1} v(\xi, z)d\xi, \tag{2.11}$$

one obtains from (2.1) and (1)

$$v(\xi, z)+\sigma\frac{z}{\xi-z}u(z)=-\frac{\sigma\xi}{\xi-z}[w(l, \xi)e^{\lambda/z}-w(0, \xi)] \tag{2.2}$$

with the abbreviation $\sigma=B/A$.

If we now put

$$\rho(z)=1+\sigma z\int_{-1}^{+1}\frac{d\xi}{\xi-z}=1+\sigma z\log\frac{z-1}{z+1}, \tag{2.3}$$

one obtains by integrating (2.2) over ξ the relation

$$\rho(z)u(z)=-\sigma\int_{-1}^{+1}\frac{\xi}{\xi-z}[w(l, \xi)e^{\lambda/z}-w(0, \xi)]d\xi. \tag{2.4}$$

If we now replace $w(l)$ and $w(0)$ in (2.4) by the expressions given for them in (1.61) and (1.62), one obtains an integral equation for $u(z)$,

$$\rho(z)u(z)=\sigma\int_0^1\frac{\xi b(\xi)}{\xi-z}(1-e^{\lambda/z-\lambda/\xi})d\xi+\sigma\int_{-1}^0\frac{\xi u(\xi)}{\xi-z}d\xi$$
$$+\sigma e^{\lambda/z}\int_0^1\frac{\xi u(\xi)e^{-\lambda/\xi}}{\xi-z}d\xi. \tag{2.5}$$

We assume without restriction of generality that $f(\xi)=\delta(\xi-z_0)$ and write (2.4) in the form

$$\rho(z)u(z)=\sigma\int_{-1}^0\frac{\xi w(0, \xi)}{\xi-z}d\xi-\sigma e^{\lambda/z}\int_0^1\frac{\xi w(l, \xi)}{\xi-z}d\xi$$
$$+\sigma\int_0^1\frac{\xi f(\xi)}{\xi-z}d\xi$$
$$=\sigma\int_{-1}^0\frac{\xi w(0, \xi)}{\xi-z}d\xi-\frac{\sigma z_0}{z-z_0}$$
$$-\sigma e^{\lambda/z}\int_0^1\frac{\xi w(l, \xi)}{\xi-z}d\xi\cdots. \tag{2.6}$$

If we define a pair of new functions $U(z)$ and $V(z)$ by

the equations

$$U(z)=1+\frac{z_0-z}{z_0}\int_{-1}^{0}\frac{\xi w(0,\xi)}{\xi-z}d\xi, \tag{2.61}$$

$$V(z)=\frac{z_0-z}{z_0}\int_{0}^{1}\frac{\xi w(l,\xi)}{\xi-z}d\xi, \tag{2.62}$$

we can write (2.6) in the form

$$\rho(z)u(z)=\frac{\sigma z_0}{z_0-z}[U(z)-e^{\lambda/z}V(z)]. \tag{2.7}$$

The functions U and V can also be expressed directly as integrals containing $u(z)$ by introducing (1.61) and (1.62) into (2.61) and (2.62)

$$U(z)=1+\frac{z_0-z}{z_0}\int_{-1}^{0}\frac{\xi u(\xi)}{\xi-z}d\xi, \tag{2.71}$$

$$V(z)=e^{-\lambda/z_0}-\frac{z_0-z}{z_0}\int_{0}^{1}\frac{\xi u(\xi)e^{-\lambda/\xi}}{\xi-z}d\xi. \tag{2.72}$$

Inspection of (2.71) and (2.72) proves that the function U and V are regular, respectively, in the right and left half of the complex plane.

Letting $z=0$, we obtain in (2.61) and (2.62)

$$U(0)=1+\int_{-1}^{0}w(0,\xi)d\xi, \tag{2.81}$$

$$V(0)=\int_{0}^{1}w(l,\xi)d\xi. \tag{2.82}$$

Equations (2.81) and (2.82) show that the neutron density at the near and far boundaries are determined, respectively, by $U(0)$ and $V(0)$.

Similarly, by letting $z\to\infty$, one obtains the relations

$$z_0[U(\infty)-1]=\int_{-1}^{0}\xi w(0,\xi)d\xi, \tag{2.83}$$

$$z_0V(\infty)=\int_{0}^{1}\xi w(l,\xi)d\xi. \tag{2.84}$$

Equations (2.83) and (2.84) express the returning and transmitted current in terms of $U(\infty)$ and $V(\infty)$.

3. REGULARITY CONDITIONS FOR U AND V

In analogy with the treatment of I we shall here show that the functions U and V are uniquely determined by the regularity conditions. For this purpose we rewrite (2.7) as follows:

$$\frac{1}{\rho(z)}[U(z)e^{-(\lambda/2z)}-V(z)e^{\lambda/2z}]=\frac{z_0-z}{\sigma z_0}U(z)e^{-(\lambda/2z)}\equiv K(z). \tag{3.1}$$

The right side of (3.1) is everywhere regular except at the origin; it follows that

$$\frac{1}{\rho(z)}[U(z)e^{-(\lambda/2z)}-V(z)e^{\lambda/2z}]$$

can *only be singular at the origin*; since, furthermore, $K(z_0)=0$, it follows with the aid of (2.71) and (2.72),

$$U(z_0)e^{\lambda/2z_0}=V(z_0)e^{\lambda/2z_0}, \tag{3.11}$$

$$U(z_0)=1, \tag{3.12}$$

$$V(z_0)=e^{-(\lambda/z_0)}. \tag{3.13}$$

Since $K(z)$ is everywhere regular except possibly at the origin, the same will hold true for its even and odd parts. Now, from (3.1) we have

$$K(z)+K(-z)=\frac{1}{\rho}[\{U(z)-V(-z)\}e^{-(\lambda/2z)}+\{U(-z)-V(z)\}e^{\lambda/2z}], \tag{3.21}$$

$$K(z)-K(-z)=\frac{1}{\rho}[\{U(z)+V(-z)\}e^{-(\lambda/2z)}-\{U(-z)+V(z)\}e^{\lambda/2z}]. \tag{3.22}$$

We introduce a pair of auxiliary functions which are both regular in the right hand of the complex plane $F(z)$ and $G(z)$,

$$F(z)=U(z)-V(-z), \tag{3.31}$$

$$G(z)=U(z)+V(-z) \tag{3.32}$$

and can, therefore, write (3.21), (3.22) as

$$K(z)+K(-z)=\frac{1}{\rho}[F(z)e^{-(\lambda/2z)}+F(-z)e^{\lambda/2z}], \tag{3.41}$$

$$K(z)-K(-z)=\frac{1}{\rho}[G(z)e^{-(\lambda/2z)}-G(-z)e^{\lambda/2z}]. \tag{3.42}$$

We thus obtain the following conditions for F and G:

(1) F and G are both regular in the right-half plane.

(2) The expressions given by the right sides of (3.41) and (3.42) are regular everywhere except possibly at the origin.

(3)
$$\tfrac{1}{2}[F(z_0)+G(z_0)]=1, \tag{3.43}$$

$$\tfrac{1}{2}[G(-z_0)-F(-z_0)]=e^{-(\lambda/2z_0)}. \tag{3.44}$$

The conditions (3.43) and (3.44) are a consequence of (3.12), (3.13) and (3.31), (3.32).

The regularity conditions will turn out to be sufficient to determine uniquely F and G. Before proceeding to establish this result, we want to obtain a relation between F and G. Multiplying (3.41) by $Ge^{-(\lambda/2z)}$ and (3.42) by $Fe^{-(\lambda/2z)}$ and subtracting, one obtains the result that

$$1/\rho[G(z)F(-z)+F(z)G(-z)]$$

is regular in the right-half plane. Since it is an even function of z, it must, therefore, be regular in the whole z plane and thus equal to a constant C

$$G(z)F(-z)+F(z)G(-z)=C\rho(z). \tag{3.5}$$

4. INTEGRAL EQUATIONS FOR F AND G

We shall first find two functions F and G which satisfy the first two regularity conditions but not (3.43), (3.44). In place of (3.43), (3.44) we require that

$$\frac{F(\infty)}{[\rho(\infty)]^{\frac{1}{2}}}=\frac{G(\infty)}{[\rho(\infty)]^{\frac{1}{2}}}=1. \tag{4.1}$$

Let us denote these special functions by φ and ψ.

If we now split (as in I) ρ into factors,

$$\rho(z)=P(z)P(-z), \tag{4.2}$$

$P(z)$ being a regular function in the right-half plane, then we obtain by multiplying (3.41), (3.42) with $P(z)$ the result that the expressions

$$\frac{\varphi(z)}{P(-z)}e^{-(\lambda/z)}+\frac{\varphi(-z)}{P(-z)}-1, \tag{4.21}$$

$$\frac{\psi(z)}{P(-z)}e^{-(\lambda/z)}-\frac{\psi(-z)}{P(-z)}+1, \tag{4.22}$$

are regular in the right-half plane. The function

$$\rho(z)=1+\sigma z\log(z+1)/(z-1) \tag{4.23}$$

vanishes at the two points $z=\pm\alpha$. If $\sigma<\frac{1}{2}$ then α is real; if $\sigma>\frac{1}{2}$ then α is purely imaginary.

We now consider a closed path of integration L in the z plane which shall enclose the real axis between 0 and 1 as well as the point $+\alpha$. Replacing z in (4.21), (4.22) by s and multiplying by $[1/(2\pi i)][1/(s+z)]$, we integrate along the closed path L in the s-plane. It shall be assumed that the point $s=-z$ lies outside the closed path of integration. Then the integral is zero and we obtain the relations

$$\frac{\varphi(z)}{P(z)}=1-\frac{1}{2\pi i}\int_L\frac{\varphi(s)e^{-(\lambda/s)}}{P(-s)}\frac{ds}{s+z}, \tag{4.31}$$

$$\frac{\psi(z)}{P(z)}=1+\frac{1}{2\pi i}\int_L\frac{\psi(s)e^{-(\lambda/s)}}{P(-s)}\frac{ds}{s+z}. \tag{4.32}$$

By making

$$\varphi(z)=a(z)P(z), \tag{4.41}$$

$$\psi(z)=b(z)P(z), \tag{4.42}$$

we obtain

$$a(z)=1-\frac{1}{2\pi i}\int_L\frac{P(s)}{P(-s)}e^{-(\lambda/s)}\frac{a(s)}{s+z}ds, \tag{4.51}$$

$$b(z)=1+\frac{1}{2\pi i}\int_L\frac{P(s)}{P(-s)}e^{-(\lambda/s)}\frac{b(s)}{s+z}ds. \tag{4.52}$$

We now contract the path of integration to a small loop around the section $(0, 1)$ of the real axis, leaving α outside. This gives us

$$a(z)=1+\frac{P^2(\alpha)}{\rho'(\alpha)}e^{-(\lambda/\alpha)}\frac{a(\alpha)}{\alpha+z}-\int_0^1\frac{\tau(s)e^{-(\lambda/s)}a(s)}{s+z}ds, \tag{4.61}$$

$$b(z)=1-\frac{P^2(\alpha)}{\rho'(\alpha)}e^{-(\lambda/\alpha)}\frac{b(\alpha)}{\alpha+z}+\int_0^1\frac{\tau(s)e^{-(\lambda/s)}b(s)}{s+z}ds \tag{4.62}$$

in which $\tau(s)$ stands for the discontinuity of $P(s)/P(-s)$ on the real axis.

The functions a and b thus satisfy two regular integral equations; we know from general theorems that there exists *only one* solution if the associated homogenous equations do not happen to have any other but the trivial solutions $a=b=0$.

We can now construct with the aid of

$$\varphi(z)=P(z)a(z),\quad \psi(z)=P(z)b(z),$$

the pair of functions F and G satisfying (3.43), (3.44) as follows: The first two regularity conditions are satisfied by

$$F(z)=C_1P(z)a(z), \tag{4.71}$$

$$G(z)=C_2P(z)b(z), \tag{4.72}$$

with arbitrary constants C_1 and C_2. These two constants can now be used to satisfy (3.43) and (3.44) also. For this purpose we insert (3.31) and (3.32) into (3.12) and (3.13) and obtain, after adding and subtracting,

$$C_1\varphi(z_0)+C_2\psi(z_0)=2, \tag{4.73}$$

$$-C_1\varphi(-z_0)+C_2\psi(-z_0)=2e^{\lambda/z_0}. \tag{4.74}$$

These equations give for C_1 and C_2 the expressions

$$C_1=\frac{1}{\rho(z_0)}[\psi(-z_0)-\psi(z_0)e^{-(\lambda/z_0)}], \tag{4.75}$$

$$C_2=\frac{1}{\rho(z_0)}[\varphi(-z_0)+\varphi(z_0)e^{-(\lambda/z_0)}]. \tag{4.76}$$

In (4.75) and (4.76) use has been made of (3.5) which now reads

$$\psi(z)\varphi(-z)+\varphi(z)\psi(-z)=2\rho(z). \tag{4.77}$$

The explicit expressions for F and G can now be written down:

$$F(z)=\frac{P(z)a(z)}{\rho(z_0)}[P(-z_0)b(-z_0)-P(z_0)b(z_0)e^{-(\lambda/z_0)}], \tag{4.81}$$

$$G(z)=\frac{P(z)b(z)}{\rho(z_0)}[P(-z_0)a(-z_0)+P(z_0)a(z_0)e^{-(\lambda/z_0)}], \tag{4.82}$$

$$\frac{2U(z)}{P(z)}=a(z)\left[\frac{b(-z_0)}{P(z_0)}-\frac{b(z_0)e^{-(\lambda/z_0)}}{P(-z_0)}\right]+b(z)\left[\frac{a(-z_0)}{P(z_0)}+\frac{a(z_0)e^{-(\lambda/z_0)}}{P(-z_0)}\right], \quad (4.83)$$

$$\frac{2V(z)}{P(-z)}=-a(-z)\left[\frac{b(-z_0)}{P(z_0)}-\frac{b(z_0)e^{-(\lambda/z_0)}}{P(-z_0)}\right]+b(-z)\left[\frac{a(-z_0)}{P(z_0)}+\frac{a(z_0)e^{-(\lambda/z_0)}}{P(-z_0)}\right]. \quad (4.84)$$

The formulas (4.83) and (4.84) together with (2.7) express $u(z)$ as function of $a(z)$ and $b(z)$; a simple substitution would lead to an explicit though somewhat lengthy equation for $u(z)$. Later applications make it appear advisable to express $u(z)$ with the aid of two auxiliary functions $f(z)$ and $g(z)$ which in turn are defined with the aid of $a(z)$ and $b(z)$. We write:

$$f(z)=\frac{a(-z)}{P(z)}e^{\lambda/2z}+\frac{a(z)}{P(-z)}e^{-(\lambda/2z)}, \quad (4.85)$$

$$g(z)=\frac{b(-z)}{P(z)}e^{\lambda/2z}-\frac{b(z)}{P(-z)}e^{-(\lambda/2z)}. \quad (4.86)$$

The combination of Eqs. (4.83) to (4.86) and (2.7) leads directly to the wanted expression for $u(z)$:

$$u(z)=\frac{\sigma z_0}{2(z_0-z)}e^{\lambda/2z-\lambda/2z_0}[f(z)g(z_0)-f(z_0)g(z)]. \quad (4.9)$$

5. ASYMPTOTIC EXPRESSIONS

Equations (4.61) and (4.62) can immediately be solved for a plate of infinite thickness; in that case, the integral disappears on account of $e^{-\lambda/z}\to 0$. We can also derive an asymptotic solution of (4.61) and (4.62) valid for all cases in which

$$e^{-\lambda}\ll e^{-(\lambda/\alpha)}. \quad (5.1)$$

In this latter case, the integral becomes small and we obtain asymptotically

$$a(z)=1+\frac{2\alpha S(\alpha)e^{-(\lambda/\alpha)}}{\alpha+z}a(\alpha), \quad (5.11)$$

$$b(z)=1-\frac{2\alpha S(\alpha)e^{-(\lambda/\alpha)}}{\alpha+z}b(\alpha) \quad (5.12)$$

with the abbreviation

$$S(\alpha)=\frac{1}{2\alpha}\frac{P^2(\alpha)}{\rho'(\alpha)}. \quad (5.13)$$

$a(\alpha)$ and $b(\alpha)$ are in this approximation given by

$$a(\alpha)=1/[1-S(\alpha)e^{-(\lambda/\alpha)}], \quad (5.14)$$

$$b(\alpha)=1/[1+S(\alpha)e^{\lambda/\alpha}], \quad (5.15)$$

so that we finally can write

$$a(z)=1+\frac{2\alpha S(\alpha)e^{-(\lambda/\alpha)}}{1-S(\alpha)e^{-(\lambda/\alpha)}}\frac{1}{\alpha+z}, \quad (5.21)$$

$$b(z)=1-\frac{2\alpha S(\alpha)e^{-(\lambda/\alpha)}}{1+S(\alpha)e^{-(\lambda/\alpha)}}\frac{1}{\alpha+z}. \quad (5.22)$$

We are primarily interested in $w(0,\xi)$ and $w(l,\xi)$, which are given by $u(\xi)$ and $u(\xi)e^{-(\lambda/\xi)}$, respectively, (cf. (1.61) and (1.62)) and, therefore, need to construct asymptotic expressions for

$u(z)$ in the case $-1<z<0$,
$u(z)e^{-(\lambda/z)}$ in the case $0<z<1$,

or, referring to (4.9),

$f(z)e^{\lambda/2z}$ and $g(z)e^{\lambda/2z}$ for $-1<z<0$,
$f(z)e^{-(\lambda/2z)}$ and $g(z)e^{-(\lambda/2z)}$ for $0<z<1$.

Combining (4.85), (4.86), (5.21), and (5.22) we obtain $-1<z<0$:

$$b(z)e^{\lambda/2z}\sim\frac{a(z)}{P(-z)}\sim\frac{1}{P(-z)}\left[1+\frac{2\alpha S(\alpha)e^{-(\lambda/\alpha)}}{1-S(\alpha)e^{-(\lambda/\alpha)}}\frac{1}{\alpha+z}\right], \quad (5.31)$$

$$g(z)e^{\lambda/2z}\sim-\frac{b(z)}{P(z)}\sim-\frac{1}{P(-z)}\left[1-\frac{2\alpha Se^{-(\lambda/\alpha)}}{1+Se^{-(\lambda/\alpha)}}\frac{1}{\alpha+z}\right]. \quad (5.32)$$

$0<z<1$:

$$b(z)e^{-(\lambda/2z)}\sim\frac{a(-z)}{P(z)}\sim\frac{1}{P(z)}\left[1+\frac{2\alpha Se^{-(\lambda/\alpha)}}{1-Se^{-(\lambda/\alpha)}}\frac{1}{\alpha-z}\right], \quad (5.41)$$

$$g(z)e^{-(\lambda/2z)}\sim\frac{b(-z)}{P(z)}\sim\frac{1}{P(z)}\left[1-\frac{2\alpha Se^{-(\lambda/\alpha)}}{1+Se^{-(\lambda/\alpha)}}\frac{1}{\alpha-z}\right]. \quad (5.42)$$

If we introduce these last asymptotic expressions into (4.9), we obtain the final expressions

$$w(0,z)=\frac{\sigma z_0}{(z_0-z)P(-z)P(z_0)}-\frac{2\sigma z_0\alpha S^2(\alpha)e^{-(2\lambda/\alpha)}}{1-S^2e^{-(2\lambda/\alpha)}}\times\frac{1}{(\alpha-z_0)(\alpha+z)}\frac{1}{P(z_0)}\frac{1}{P(-z)}, \quad (5.5)$$

$$w(l,z)=\frac{2\sigma z_0\alpha Se^{-(\lambda/\alpha)}}{1-S^2e^{-(2\lambda/\alpha)}}\frac{1}{(\alpha-z_0)\cdot(\alpha-z)}\frac{1}{P(z_0)}\frac{1}{P(z)}. \quad (5.6)$$

Equations (5.5) and (5.6) permit a simple interpretation. For $\lambda\to\infty$ the second term in (5.5), disappears and we obtain the result derived in I. Equation (5.6) gives an explicit expression for the transmitted density distribution.

6. LIMITING CASE OF VERY SMALL CAPTURE

In the case of $\sigma\to\frac{1}{2}$, as given by (cf. 4.23)

$$\sigma=\frac{1}{\alpha\log(\alpha+1)/(\alpha-1)}, \tag{6.1}$$

α becomes very large; we, therefore, shall look for an expansion in negative powers of α. We find for $S(\alpha)$ (cf. (5.13)), treating the denominator first:

$$\alpha^3\rho'(\alpha)=\frac{\alpha^2}{(\alpha/2)\log(\alpha+1)/(\alpha-1)}\times\left[\frac{1}{1-(1/\alpha^2)}-(\alpha/2)\log\frac{\alpha+1}{\alpha-1}\right], \tag{6.2}$$

or up to terms of order $1/\alpha^2$.

$$\alpha^3\rho'(\alpha)=\frac{2}{3}\left[1+\frac{13}{15a^2}\right]. \tag{6.21}$$

To expand $\alpha^2P^2(\alpha)$, we use the relation (cf. I, (37))

$$P(z)=(1-2\sigma)^{\frac{1}{2}}+\sigma\int_0^1\frac{s}{s+z}\frac{ds}{P(s)}. \tag{6.22}$$

If we add $P(-z)$ and put $z=\alpha$, then we obtain, because of $P(-\alpha)=0$, the relation

$$P(\alpha)=2(1-2\sigma)^{\frac{1}{2}}+2\sigma\int_0^1\frac{s^2}{s^2-\alpha^2}\frac{ds}{P(s)}. \tag{6.23}$$

Now (6.1) gives

$$2\alpha(1-2\sigma)^{\frac{1}{2}}\sim\frac{2}{\sqrt{3}}\left(1+\frac{2}{15\alpha^2}\right), \tag{6.24}$$

and it then follows from (6.23)

$$\alpha\left[\alpha P(\alpha)-\frac{2}{\sqrt{3}}\right]\sim-\int_0^1\frac{s^2ds}{P(s)} \tag{6.25}$$

in which the integral has to be taken for $\sigma=\frac{1}{2}$. We introduce a numerical constant m by the relation

$$m=\sqrt{3}\int_0^1\frac{s^2ds}{P(s)}=2\left[1-\frac{1}{\pi}\int_0^{\pi/2}\frac{\log3(1-t\,\mathrm{ctg}t)/\sin^2t}{\sin^2t}dt\right], \tag{6.26}$$

m can be found from I to be equal to 1.43. Thus we have

$$\alpha P(\alpha)=(2/\sqrt{3})[1-(m/2\alpha)], \tag{6.27}$$

and from (6.27), (6.21), and (5.13),

$$\int S(\alpha)=1-(m/\alpha). \tag{6.28}$$

Equations (5.5) and (5.6), therefore, take on the following form for $\sigma\to\frac{1}{2}$ and $\alpha\to\infty$,

$$w(0,z)=\frac{z_0}{2(z_0-z)}\frac{1}{P(-z)}\frac{1}{P(z_0)}-\frac{z_0}{2(m+\lambda)}\frac{1}{P(z_0)P(-z)}, \tag{6.3}$$

$$w(l,z)=\frac{z_0}{2(m+\lambda)}\frac{1}{P(z_0)P(z)}. \tag{6.4}$$

7. SOME EXPRESSIONS FOR $P_\sigma(z)$ FOR $\sigma\sim\frac{1}{2}$

The new transcendental function $P(z)$, which plays a fundamental role in our theory, has been studied in great detail by one of the authors (R.K.L.). We give here a few results of this mathematical investigation which may be useful for applications. We also add in form of tables certain numerical data which will be of assistance in the use of the theory.

The function $P_\sigma(z)$ can be represented for values of σ in the neighborhood of $\frac{1}{2}$ by the following expression:

$$1/[P_\sigma(z)]=[Q_\sigma(z)]/[P_0(z)]. \quad P_0(z)=P(z)\sigma=\tfrac{1}{2}. \tag{7.1}$$

Here, $Q_\sigma(z)$ is defined by

$$Q_\sigma(z)=\frac{1}{1+(q_1/P_0)(1-2\sigma)^{\frac{1}{2}}+(q_2/P_0)(1-2\sigma)+(q_3/P_0)(1-2\sigma)^{\frac{3}{2}}}. \tag{7.2}$$

The functions q_i can be determined as polynomials of z multiplied by P_0 and its first derivative. These expansions are valid for $z<1$. We present in Table I numerical values for $P_\sigma^{-1}(z)$, (q_i/P_0) for values of z between 0 and 1. Table II contains values of $P_\sigma^{-1}(z)$ as function of z in the range between 0 and 1 and of σ in the range between 0.5 and 0.4.

We also state the result that the straight line which approximates P_0 with the smallest quadratic deviation is given by

$$1/P_0=1.08+1.84z. \tag{7.3}$$

8. INVERSION OF THE LAPLACE TRANSFORMATION

While the distribution at the boundaries is, according to (1.61) and (1.62), given by $u(z)$, knowledge of the conditions inside the scatterer requires explicit determination of w. Since, according to (1.3),

$$u(z)=-\frac{B}{z}\int_0^l\bar{w}(x)e^{Az/z}dx, \tag{1.3}$$

TABLE I. Values of $P_0^{-1}(z)$ and of q_i/P_0.

$\backslash z$	0.0	0.1	0.2	0.3	0.4	0.5	0.6	0.7	0.8	0.9	1.0
$P_0^{-1}(z)$	1.000	1.241	1.446	1.640	1.827	2.011	2.193	2.373	2.552	2.730	2.907
q_1/P_0	0.000	0.173	0.346	0.520	0.693	0.866	1.039	1.212	1.386	1.559	1.732
q_2/P_0	0.000	0.113	0.162	0.189	0.214	0.236	0.252	0.260	0.270	0.278	0.286
q_3/P_0	0.000	−0.050	−0.082	−0.109	−0.129	−0.142	−0.154	0.169	−0.180	−0.190	−0.198

or with $A/z=-\gamma$,

$$\frac{1}{\sigma\gamma}u(-A/\gamma)=\int_0 \bar{w}(x)e^{-\gamma x}dx, \tag{8.1}$$

we see that $(1/\sigma\gamma)u(-A/\gamma)$ is the Laplace adjoint of $\bar{w}(x)$. The inversion gives $\bar{w}$ in the form

$$\bar{w}(x)=(1/2\pi i\sigma)\int_L u(-A/\gamma)e^{\gamma x}(d\gamma/\gamma). \tag{8.2}$$

Here L can be the imaginary axis or any line parallel to it; we can also deform the path of integration into any closed curve L_1 which stays in the *left*-half plane and intersects the real axis in the origin with an angle of 90°. This is permissible because $u(z)$ is regular in the left-half plane. If $\bar{w}$ is determined from the inversion theorem, we obtain an expression for w by introducing (8.2) into (1.4) and integrating over x,

$$w(x,\xi)=w(0,\xi)e^{-(Ax/\xi)}+\frac{1}{2\pi i}\int_{L_1}\frac{u(s)}{s-\xi}(e^{-(Ax/s)}-e^{-(Ax/\xi)})ds. \tag{8.3}$$

Since the curve L_1 can be chosen arbitrarily small, we may construct it so that the point ξ is excluded. Then the second term on the right side of (8.3) becomes simply

$$\frac{1}{2\pi i}\int_{L_1}\frac{u(s)}{s-\xi}e^{-(Ax/s)}ds. \tag{8.31}$$

If $\xi>0$ we obtain w directly from 8.31

$$w(x,\xi)=f(\xi)e^{-(Ax/\xi)}+\frac{1}{2\pi i}\int_{L_1}\frac{u(s)e^{-(Ax/s)}}{s-\xi}ds. \tag{8.41}$$

For $\xi<0$ we have $w(0,\xi)=u(\xi)$ and, therefore,

$$w(x,\xi)=u(\xi)e^{-(Ax/\xi)}+\frac{1}{2\pi i}\int_{L_1}\frac{u(s)e^{-(Ax/s)}}{s-\xi}ds \tag{8.42}$$

or

$$w(x,\xi)=\frac{1}{2\pi i}\int_{L_2}\frac{u(s)e^{-(Ax/s)}}{s-\xi}ds,$$

where L_2 *includes* the point $s=\xi$. In both cases the imaginary axis is equivalent to L_1 and L_2. This gives

$\xi<0$:

$$w(x,\xi)=\frac{1}{2\pi i}\int_{-i\infty}^{+i\infty}\frac{u(s)e^{-(Ax/s)}ds}{s-\xi}. \tag{8.5}$$

$\xi>0$:

$$w(x,\xi)=f(\xi)e^{-(Ax/\xi)}+\frac{1}{2\pi i}\int_{-i\infty}^{+i\infty}\frac{u(s)e^{-(Ax/s)}}{s-\xi}ds. \tag{8.6}$$

9. DISTRIBUTION INSIDE A PLATE OF INFINITE THICKNESS: ASYMPTOTIC FORMULAS

If the thickness of the plate becomes infinite, we find after some simple calculations

$$u(z)=\frac{\sigma z_0}{z_0-z}\frac{1}{P(z_0)}\frac{1}{P(-z)}. \tag{9.1}$$

$\xi>0$:

$$w(x,\xi)=\delta(\xi-z_0)e^{-(Ax/\xi)}-\frac{\sigma z_0}{P(z_0)}\frac{1}{2\pi i}\int_{-i\infty}^{+i\infty}\frac{e^{Ax/s}ds}{(s+\xi)(s+z_0)P(s)}. \tag{9.2}$$

$\xi<0$:

$$w(x,\xi)=-\frac{\sigma z_0}{P(z_0)}\frac{1}{2\pi i}\int_{-i\infty}^{+i\infty}\frac{e^{Ax/s}ds}{(s+\xi)(s+z_0)P(x)}; \tag{9.3}$$

and from (9.1) and (8.2),

$$\bar{w}(x)=-\frac{z_0}{P(z_0)}\frac{1}{2\pi i}\int_{-i\infty}^{+i\infty}\frac{e^{Ax/s}ds}{s(s+z_0)P(s)}. \tag{9.4}$$

Instead of integrating along the imaginary axis, we can also integrate along a closed curve L_1 which includes all singularities of $1/P$ in the left half of the complex plane; these are the point $s=-\alpha$ and the sector $-1\leqq s\leqq 0$. The curve L_1 can in turn be split into two separate closed curves L_0 and L' including the point $s=-\alpha$ and the section $(-1,0)$ separately. For *large* values of Ax, the main contribution comes from the curve L_0; the integral around it will, therefore, give us

TABLE II. Values of $P_\sigma^{-1}(z)$.

$\sigma\backslash z$	0.0	0.1	0.2	0.3	0.4	0.5	0.6	0.7	0.8	0.9	1.0
0.500	1.00	1.24	1.45	1.64	1.83	2.01	2.19	2.37	2.55	2.73	2.91
0.499	1.00	1.23	1.42	1.60	1.77	1.94	2.10	2.25	2.40	2.55	2.70
0.498	1.00	1.23	1.41	1.59	1.75	1.90	2.06	2.20	2.35	2.49	2.62
0.496	1.00	1.22	1.40	1.57	1.72	1.86	2.00	2.13	2.27	2.39	2.52
0.494	1.00	1.22	1.39	1.55	1.69	1.84	1.96	2.09	2.21	2.32	2.44
0.492	1.00	1.21	1.38	1.54	1.67	1.81	1.93	2.05	2.17	2.27	2.38
0.490	1.00	1.21	1.37	1.53	1.66	1.79	1.90	2.01	2.13	2.22	2.32
0.485	1.00	1.20	1.36	1.50	1.62	1.74	1.85	1.95	2.05	2.14	2.23
0.480	1.00	1.19	1.35	1.48	1.59	1.70	1.80	1.89	1.98	2.06	2.14
0.470	1.00	1.18	1.32	1.44	1.55	1.64	1.73	1.81	1.88	1.96	2.02
0.460	1.00	1.17	1.30	1.41	1.51	1.60	1.67	1.74	1.81	1.87	1.92
0.450	1.00	1.17	1.29	1.39	1.48	1.55	1.63	1.69	1.75	1.80	1.85
0.440	1.00	1.16	1.27	1.37	1.45	1.52	1.58	1.64	1.70	1.75	1.79
0.430	1.00	1.15	1.26	1.35	1.42	1.49	1.55	1.60	1.65	1.69	1.73
0.420	1.00	1.15	1.25	1.33	1.40	1.46	1.52	1.57	1.61	1.65	1.68
0.410	1.00	1.14	1.24	1.31	1.38	1.44	1.49	1.53	1.58	1.61	1.64
0.400	1.00	1.13	1.23	1.30	1.36	1.41	1.46	1.50	1.54	1.57	1.60

an asymptotic expression for w. Remembering that

$$\frac{1}{P'(\alpha)}=\frac{P(\alpha)}{\rho'(\alpha)},$$

we obtain easily

$$w(x,\xi)=\frac{\sigma z_0}{P(z_0)}\frac{P(\alpha)}{\rho'(\alpha)}\frac{e^{-(Ax/\alpha)}}{(\alpha-\xi)(\alpha-z_0)}, \tag{9.5}$$

$$\bar{w}(x)=\frac{z_0}{P(z_0)(\alpha-z_0)}\frac{P(\alpha)}{\alpha\rho'(\alpha)}e^{-(Ax/\alpha)}. \tag{9.6}$$

If we allow α to approach ∞ ($\sigma\to\frac{1}{2}$), we thus obtain

$$w(x,\xi)=\frac{\sqrt{3}}{2}\frac{z_0}{P(z_0)}, \tag{9.7}$$

$$\bar{w}(x)=\sqrt{3}\frac{z_0}{P(z_0)}. \tag{9.8}$$

10. THE DISTRIBUTION INSIDE A PLATE OF FINITE THICKNESS

$u(z)$ is in this general case given by (4.9). Introducing (4.9) into (8.41) and (8.42) and replacing x by xl, we obtain the following rigorous solution for $w(x,\xi)$

$$w(x,\xi)=\frac{\sigma z_0}{2}e^{-(\lambda/2z_0)}[g(z_0)I_1-f(z_0)I_2]+\begin{cases}f(\xi)e^{-(\lambda x/\xi)} & \xi>0\\ 0 & \xi<0.\end{cases} \tag{10.1}$$

In (10.1) the following notation has been used:

$$I_1(x,\xi)=\frac{1}{2\pi i}\int_{-i\infty}^{+i\infty}\frac{f(s)e^{(\lambda/2s)-(\lambda x/s)}ds}{(z_0-s)(s-\xi)}, \tag{10.21}$$

$$I_2(x,\xi)=\frac{1}{2\pi i}\int_{-i\infty}^{+i\infty}\frac{g(s)e^{(\lambda/2s)-(\lambda x/s)}ds}{(z_0-s)(s-\xi)}. \tag{10.22}$$

If we now use the expressions for f and g as given by (4.85) and (4.86), we have

$$2\pi iI_1(x,\xi)=\int_{-i\infty}^{+i\infty}ds\left[\frac{a(-s)e^{\lambda(1-x)/s}}{P(s)(z_0-s)(s-\xi)}+\frac{a(s)e^{\lambda x/s}}{P(-s)(z_0-s)(s-\xi)}\right], \tag{10.31}$$

$$2\pi iI_2(x,\xi)=\int_{-i\infty}^{+i\infty}ds\left[\frac{b(-s)e^{\lambda(1-x)/s}}{P(s)(z_0-s)(s-\xi)}-\frac{b(s)e^{-(\lambda x/s)}}{P(-s)(s-\xi)(z_0-s)}\right]. \tag{10.32}$$

The path of integration can now be replaced by new paths, namely the curves L_1 in the first term and L_2 in the second term of the right side. The curves $L_1(L_2)$ lies in the left- (right-) half plane only and consist of two parts enclosing the sector $-1, 0(0, 1)$ and the point $-\alpha(+\alpha)$. We now assume λ to be so large that

$$e^{-(\lambda x)/\alpha}\ll e^{-\lambda x}.$$

Then the contributions in $L_1(L_2)$ coming from the sections $-1, 0(0, 1)$ will be of the order of $e^{-\lambda x}(e^{-\lambda(1-x)})$ and can be neglected compared with the contributions from the integration around $-\alpha(+\alpha)$. Under these assumptions we have

$$I_1(x,\xi)=\frac{a(\alpha)P(\alpha)}{\rho'(\alpha)}\times\left[\frac{e^{-\lambda(1-x)/\alpha}}{(\alpha+z_0)(\alpha+\xi)}+\frac{e^{-(\lambda x/\alpha)}}{(\alpha-z_0)(\alpha-\xi)}\right], \tag{10.41}$$

$$I_2(x,\xi)=\frac{b(\alpha)P(\alpha)}{\rho'(\alpha)}\times\left[\frac{e^{-\lambda(1-x)/\alpha}}{(\alpha+z_0)(\alpha+\xi)}-\frac{e^{-(\lambda x/\alpha)}}{(\alpha-z_0)(\alpha-\xi)}\right]. \tag{10.42}$$

Since the term $\delta(z_0-\xi)e^{-(\lambda x)/\xi}$ can also be neglected, we find from (10.41), (10.42), and (10.1)

$$w(x,\xi)=\frac{\sigma z_0}{2}\frac{P(\alpha)}{\rho'(\alpha)}e^{-(\lambda/2z_0)}\times\left[\frac{g(z_0)a(\alpha)-f(z_0)b(\alpha)}{(\alpha+z_0)(\alpha+\xi)}e^{-\lambda(1-x)/\alpha}+\frac{g(z_0)a(\alpha)+f(z_0)b(\alpha)}{(\alpha-z_0)(\alpha-\xi)}e^{-(\lambda x/\alpha)}\right]. \tag{10.5}$$

In order to determine the expressions within the brackets, we use the previously derived asymptotic expressions for a, b, f, g. These formulas were obtained under the assumption that $e^{-\lambda}\ll e^{-\lambda/\alpha}$; terms of the order $e^{-\lambda/\alpha}$ are retained in them. This procedure is only consistent if $e^{-\lambda/\alpha}\gg e^{-\lambda x}$, since in (10.5) terms of the order of $e^{-\lambda x}$ have been neglected. We, therefore, have to require

$$\lambda/\alpha<\lambda x,\quad x>1/\alpha.$$

Similarly,

$$\lambda/\alpha<\lambda(1-x),\quad (1-x)>1/\alpha.$$

This leaves as conditions for the validity of the asymptotic approximations

$$1/\alpha<x<1-1/\alpha \tag{10.51}$$

or $\alpha>2$. The formulas will, therefore, be valid only sufficiently far *inside* the scatterer but not near the boundaries $x=0$ and $x=1$. For these cases we have already obtained expressions before.

Assuming (10.51) to be valid, we now collect the expressions:

$$a(\alpha)=1/(1-Se^{-\lambda/\alpha}),\quad b(\alpha)=1/(1+Se^{-\lambda/\alpha}),$$

$$f(z_0)e^{-(\lambda/2z_0)}=\frac{1}{P(z_0)}\left[1+\frac{2\alpha Se^{-(\lambda/\alpha)}}{(1-Se^{-(\lambda/\alpha)})(\alpha-z)}\right], \quad (10.52)$$

$$g(z_0)e^{-(\lambda/2z_0)}=\frac{1}{P(z_0)}\left[1-\frac{2\alpha Se^{-(\lambda/\alpha)}}{(1+Se^{-(\lambda/\alpha)})(\alpha-z)}\right]. \quad (10.53)$$

Introducing these expressions into (10.5), we have

$$e^{-(\lambda/2z_0)}[g(z_0)a(\alpha)-f(z_0)b(\alpha)]=\frac{-2Se^{-(\lambda/\alpha)}(\alpha+z_0)}{(1-S^2e^{-(2\lambda/\alpha)})(\alpha-z_0)}\frac{1}{P(z_0)}, \quad (10.54)$$

$$e^{-(\lambda/z_0)}[g(z_0)a(\alpha)+f(z_0)b(\alpha)]=\frac{2}{P(z_0)(1-S^2e^{-(2\lambda/\alpha)})}, \quad (10.55)$$

and thus finally for w

$$w(x,\xi)=\frac{z_0}{P(z_0)(\alpha-z_0)}\frac{2\sigma\alpha S}{P(\alpha)(1-S^2e^{-(2\lambda/\alpha)})}\times\left[\frac{e^{-(\lambda x/\alpha)}}{\alpha-\xi}-Se^{-\lambda/\alpha}\frac{e^{-\lambda(1-x)/\alpha}}{\alpha+\xi}\right] \quad (10.6)$$

or by integrating over ξ,

$$\bar{w}(x)=\frac{z_0}{P(z_0)(\alpha-z_0)}\frac{2S(\alpha)}{P(\alpha)(1-S^2e^{-2\lambda/\alpha})}\times[e^{-(\lambda x/\alpha)}-Se^{-\lambda/\alpha}e^{-\lambda(1-x)/\alpha}]. \quad (10.61)$$

In the special case of $x=\frac{1}{2}$, we have

$$\bar{w}(\tfrac{1}{2})=\frac{z_0}{(\alpha-z_0)P(z_0)}\frac{2Se^{-(\lambda/2\alpha)}}{P(\alpha)(1+Se^{-(\lambda/\alpha)})}. \quad (10.62)$$

Let us now compare this density, valid in the middle of a plate of thickness l, with the density at the far boundary of the plate of thickness $l/2$. This last quantity is given by (5.6) after integration over ξ:

$$\bar{w}(l/2)=\frac{z_0}{(\alpha-z_0)P(z_0)}\frac{2\alpha\sigma Se^{-(\lambda/2\alpha)}}{1-S^2e^{-(\lambda/\alpha)}}\times\int_0^1\frac{dz}{(\alpha-z)P(z)}. \quad (10.63)$$

To evaluate the definite integral in (10.63), we remember that

$$P(z)=(1-2\sigma)^{\frac{1}{2}}+\sigma\int_0^1\frac{sds}{(s+z)P(s)}=1-\sigma z\int_0^1\frac{ds}{(s+z)P(s)}, \quad (10.64)$$

or for $z=-\alpha$,

$$\int_0^1\frac{ds}{(\alpha-s)P(s)}=\frac{1}{\sigma\alpha}. \quad (10.65)$$

Thus,

$$\bar{w}(l/2)=\frac{z_0}{(\alpha-z_0)P(z_0)}\frac{2Se^{-(\lambda/2\alpha)}}{1-S^2e^{-\lambda/\alpha}}. \quad (10.66)$$

The ratio $\bar{w}(\frac{1}{2})/\bar{w}(l/2)$ is given by

$$\frac{\bar{w}(\frac{1}{2})}{\bar{w}(l/2)}=\frac{1-S^2e^{-\lambda/\alpha}}{P(\alpha)(1+Se^{-\lambda/\alpha})}. \quad (10.67)$$

For large α, but $e^{-\lambda/2\alpha}\ll 1$, we then obtain

$$\bar{w}(1/2)/\bar{w}(l/2)\sim(\alpha/2)\sqrt{3}. \quad (10.68)$$

11. APPLICATIONS OF THE THEORY

The theory here developed obviously lends itself to the evaluation of a large number of experiments dealing with diffusion of neutrons. So far as we know, no investigations are reported in the literature which have been made with sufficient care of the geometrical conditions so as to allow immediate evaluation. It is to be expected that the presently available intensities of neutron beams will soon permit a number of investigations of interest in this field.

One of the authors (O.H.) has extended the present theory to include the treatment of the diffusion of polarized neutrons under the influence of spin dependent forces.[2] More detailed calculations will be reported shortly in a following paper.

[2] Otto Halpern, Phys. Rev. **75**, 1633A (1949).

Hyperfine Structure in the Band Spectrum of the Mercury Hydride HgH

S. MROZOWSKI
Department of Physics, University of Buffalo, Buffalo, New York
(Received August 22, 1949)

The structure of the spectrum of the mercury hydride has been reinvestigated with a more powerful experimental arrangement. In 1931 a complex structure due to different isotopes of mercury was discovered (Part I) and a closer study with improved apparatus led in 1935 to the establishment of a new band spectroscopic effect of the so-called nuclear isotope shift (Part II), the correlation of which with the corresponding atomic effect was explained by Bohr. Certain differences in structure between lines belonging to different branches seemed to be detectable, and these differences were subjected in this paper (Part III) to a careful study. In the bands of the system $^2\Pi_i \rightarrow {}^2\Sigma$ a new (fifth) component was found on the short wave-length side for P and R band lines (Fig. 1). This component is gradually merging with the fourth for higher rotational energies. In the Q lines a corresponding component is overlapped with the fourth for lower rotational energies and causes for higher rotational energies a deviation of the measured position of the fourth component toward too small separations. Careful measurements of separation reveal that the fifth component in P and R lines should be correlated to the mercury isotope 199 (Fig. 2). Since the intensity of this component is equal only to 9 percent of the total intensity of the group of components, the fifth component does not represent the whole contribution of 16.45 percent of the isotope 199. It is concluded therefore that the lines emitted by the molecules containing the isotope 199 must be split at least into two components. Thus a first proof of the existence of a hyperfine structure in band spectra is obtained. The approximate structures of groups of components corresponding to the odd isotopes 199 and 201 are obtained by subtracting the intensities corresponding to even isotopes from the intensity curves found by measuring the intensity distribution for the whole group of components (Fig. 3, a, b and c). No satisfactory explanation of the structures obtained could be found. The results of the measurements of the separation of components corresponding to even isotopes deviate from the expected ones (normal rotational isotope effect) and the deviation (difference of 27 percent in slope) cannot be explained by any known cause. An additional strong anomaly of a different kind is found for higher rotational energies in the bands of the system $^2\Sigma' \rightarrow {}^2\Sigma$ (Fig. 4).

INTRODUCTION

A NUMBER of years ago the author[1] found a complex structure in the band spectrum of the mercury hydride molecule. Already in 1918 Nagaoka[2] and in 1921 Gehrcke and Glaser[3] performed experiments designed to detect a structure of band lines in the same spectrum, a structure which would be analogous to the long-known, but not yet explained at that time, complex structure of the atomic spectrum of mercury. Their failure to observe the complex structure was probably caused chiefly by the inadequacy of their light sources for this purpose (broad lines). The structures found by the author[1] seemed to deviate from the structures expected for a normal rotational and vibrational isotope effect of different isotopes of mercury. Subsequent investigations[4] carried out with a more adequate apparatus and an improved technique led to the establishment of a new effect in band spectra, the so-called nuclear isotope shift. Nuclear isotope shifts were found later by the author also in the spectra of HgD,[5] HgH^+ and HgD^+,[6] and finally in ZnH.[7] The correlation of this effect with the well-known isotope shift in the atomic spectrum of mercury was explained by Bohr.[4,5]

The study of such narrow structures requires the crossing of a high resolving interference apparatus with a large prism spectrograph. Only band spectra of hydrides and deuterides were investigated until now, since they have sufficiently wide spacings between band lines. Moreover the existence of the nuclear isotope shift could be proved only for molecules containing the even isotopes of the metals. The structure of all lines found in HgH and HgD differs from the structure expected for a simple overlapping of the normal isotope effect with the nuclear shift, showing an anomalous behavior of the lines emitted by molecules containing odd isotopes of mercury. A similar effect of an apparent absence of lines corresponding to the odd isotopes of cadmium has been observed by Svensson[8] in the cadmium hydride spectrum. A tentative explanation of this behavior put forward by the author[4,5] was based on the assumption of a presence of a hyperfine structure causing a splitting of the lines in question into several weaker components. This explanation found a certain support in the results of the work on the spectra of HgH^+ and HgD^+.[6] In this latter spectrum, which is of the type $^1\Sigma \rightarrow {}^1\Sigma$, no hyperfine structure splitting is expected. In agreement with this it was found that the lines corresponding to the odd isotopes seems not to reveal any anomalous behavior.

Since at the time no clear proof of the existence of a hyperfine structure in any band spectrum has been given,[9] the clarification of the origin of the deviations

[1] S. Mrozowski, Zeits. f. Physik **72**, 776 (1931). Subsequently will be designated as Part I.
[2] H. Nagaoka, Sci. Pap. Inst. Phys. and Chem. Research (Tokyo) **1**, 1 (1918).
[3] E. Gehrcke and L. C. Glaser, Ann. d. Physik **65**, 605 (1921).
[4] S. Mrozowski, Zeits. f. Physik **95**, 524 (1935). Part II.
[5] S. Mrozowski, Zeits. f. Physik **99**, 236 (1936).
[6] S. Mrozowski, Phys. Rev. **58**, 332 (1940).
[7] S. Mrozowski, Phys. Rev. **58**, 597 (1940).
[8] E. Svensson, Nature **131**, 28 (1933).
[9] A small but distinct broadening of the first few lines in branches was observed by Hulthén and Heimer (Nature **129**, 56 (1932)) for the $^1\Sigma \rightarrow {}^1\Pi$-bands of bismuth hydride BiH. This broadening was tentatively explained as an unresolved hyperfine structure splitting. The author made a few photographs of these bands and also of the AlH bands with the big Chicago grating, but was unable to find any structure in view of the considerable

of finer details in the complex structure of the spectra HgH and HgD seemed of considerable importance. Already in Part II certain peculiarities in the structure of lines and differences in intensity distribution between lines belonging to Q branches on one side, and to P and R branches on the other were noted. They are especially well visible in the (0, 0) band of the $^2\Pi_i \rightarrow {}^2\Sigma$-system ($\lambda$4017). The closer examination of these anomalies was the starting point of this investigation. This paper constitutes therefore the Part III of the author's work on the complex structure of the lines in the spectrum of HgH. The photographs of the spectrum were made in Poland in the summer of 1939 at the Institute of Theoretical Physics of the University of Warsaw, the microphotometer recordings were obtained a few years later at the Department of Physics of the University of Chicago. The results of this investigation gave the first convincing proof of the existence of hyperfine structure in band spectra. They were briefly reported at a meeting of the Am. Phys. Society several years ago.[10] More recently hyperfine structures due to electric quadrupole moments of the nuclei were found by others in pure rotational spectra of a number of molecules (microwave region). Since in this work a splitting of levels is found for the isotope Hg_{199} which has a nuclear spin $\frac{1}{2}$ (no quadrupole moment) the hyperfine structure here reported is undoubtedly due to the interaction of the electrons with the magnetic moments of the nuclei. In other words the effect here reported is an exact counterpart of the hyperfine structure in atomic spectra.

EXPERIMENTAL

The experimental arrangement was the following: an all water-cooled mercury arc of a special design (Part II) was run in an atmosphere of hydrogen at low current densities (0.7–0.9 amp. per cm^2). The discharge was observed in an end-on arrangement. As a high resolving instrument a heavily aluminized (Hochheim's alloy) Fabry-Perot etalon with different plate separations was used. The interference pattern was projected by an excellent achromatic lens on the slit of a 1.5 meter large interchangeable spectrograph of Hilger. This time a high speed glass optics was available for this spectrograph and the bands in the region λ3600–λ4400 could be obtained with a considerably higher dispersion than before, the dispersion being for instance for the band λ4017 around 5A/mm in comparison to 13 A/mm used in Part II. The improvement in comparison to Part II was however much greater than the ratio of these numbers would indicate, since a Fabry-Perot etalon is giving smaller separations between consecutuve orders than does a Lummer-Gehrcke plate and consequently considerably smaller widths of the spectrographic slit could be used. Thus many lines could be easily observed in regions which were inaccessible before on account of overlappings. Especially the investigation of the region of the band λ4017, which is reproduced in Fig. 1 and which constitutes the immediate long wave-length extension of the part reproduced in Fig. 2, Part II, was of great importance.

With such an arrangement the exposure time did not exceed 10 minutes. For such short exposures no special precautions to keep a constant pressure and temperature had to be observed. Photographs were made using also a hollow cathode discharge tube instead of the mercury arc. Construction details of the hollow cathode tube were given in a previous paper.[6] In view of the lower temperature of the gas in the discharge tube, sharper components are obtained. However, the branches are much less extended, therefore such plates were used only for measurements of separations in the immediate neighborhood of the band origins. The intensity of the band spectrum is much lower and considerably longer exposures had to be used (1 hour or more).

RESULTS

Separation of Components

A photograph obtained with the mercury arc and a Fabry-Perot etalon of 11.2 mm plate separation is reproduced in Fig. 1. Characteristic differences can be detected in the structure of different lines. Comparing for instance the two neighboring lines $Q_1 20$ and $R_2 12$, marked by dots on Fig. 1, we see that $Q_1 20$ has two strong central components, a weaker one on the side of shorter wave-lengths and a very weak one on the side of long wave-lengths. In $R_2 12$ we find two strongest and the weakest components, but the short wave-length component is split into two components both of them being weaker than the corresponding single component of $Q_1 20$, but both stronger than the weakest component of $R_2 12$ and $Q_1 20$. This difference is typical for the P and R lines on one hand and Q lines on the other, as it can be seen by inspection of Fig. 1. The separation of the short wave-length doublet in P and R decreases in the band toward the shorter wave-length's, so that beyond the mercury atomic line marked in Fig. 1, no splitting is observed any more. The two components merge into a single one and the structure of the R lines becomes similar to the Q lines. On the other hand, for very high rotational quantum numbers the distance of the short wave-length component from the central one increases less rapidly for the Q lines. The component becomes wide and loses its sharpness, especially on the side of the longer wave-lengths (toward the strong central doublet). Approximately the same relations are found in the (0, 1) band λ4219; since however the isotope effect separations are smaller the P and R lines even for high rotations still reveal a fifth component. The Q lines show only 4 components without any decrease in sharpness.

width of the lines. It appears that such a study should be carried out not with a common discharge tube, but with a hollow cathode tube at liquid air temperature.

[10] S. Mrozowski, Phys. Rev. 63, 63 (1943).

The state of affairs for the band λ4017 is best seen from Fig. 2, where the results of the measurements of separations of components for a great number of lines are given. The distances of components were measured on several plates for different Fabry-Perot plate separations with a traveling microscope and the separations determined by a non-linear interpolation (taking the variation of the distances of consecutive orders into consideration). For the two central components (Nos. 2 and 3) a very good straight line dependence is found; a little less consistent results are obtained for the weakest component (No. 1). For the short wave-length component (No. 4) the splitting for R and P lines into two components (Nos. 4 and 5) at longer wave-lengths and the deviation of No. 4 at higher frequencies toward smaller separations for the Q lines are well represented.

If the correlation to the different even isotopes of mercury given in Part II is true, the components Nos. 1–4 correspond to isotopes of mercury 204, 202, 200 and 198. It is then evident from Fig. 2 that the fifth component having an intermediate slope of the line in Fig. 2 (between 200 and 198) should belong to the isotope 199. However, the intensity of this component is slightly smaller than that of the fourth, and therefore does not represent the total contribution of the isotope 199 to the pattern (see below the results of measurements of intensities). Another component belonging to 199 should be present and is probably overlapped with the component No. 3. For the Q lines and for longer wave-lengths the component No. 5 is probably almost exactly overlapped with No. 4 producing a relatively higher apparent intensity of the component No. 4. The gradual separation of the two for higher frequencies produces the relative decrease of the measured separation of components Nos. 3 and 4, and the broadening of the component No. 4.

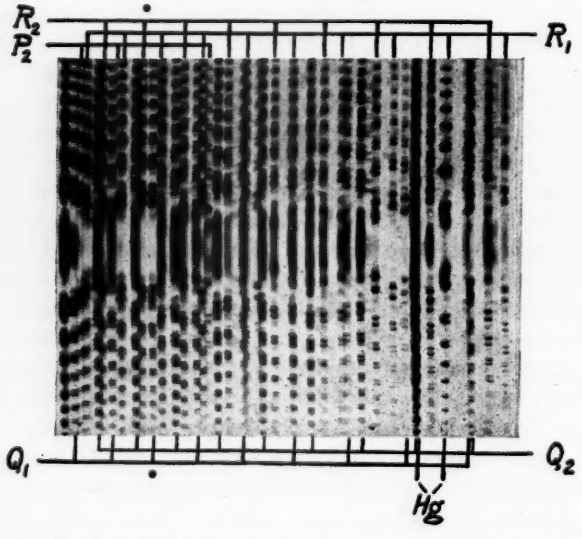

FIG. 1. Photograph of a part of the (0, 0) band at λ4017 of the mercury hydride system $^2\Pi_{\frac{1}{2}} \rightarrow {}^2\Sigma$ made with a Fabry-Perot etalon and a large glass spectrograph. Q lines reveal four, P and R lines five components.

The separation of components for the even isotopes of mercury at the position of the band origin (zero line) is given by the very small normal vibrational isotope effect of 0.008 cm^{-1} and the much greater nuclear isotope shift of about 0.062 cm^{-1}. The last value is obtained from the average of the distances 1–2, 2–3 and 3–4; it is a little smaller than the value reported in Part II (for the reason see below). The slope of the lines in Fig. 2 is given by the rotational isotope effect relative to the isotope 201 taken as the horizontal line of reference. For two mercury isotopes differing in mass by one unit $1-\rho$ is equal to $\delta=1.21\times10^{-5}$, the expected slopes of the lines No. 3 (and No. 2) and No. 4 (No. 1) are $2.\delta=2.42\times10^{-5}$ and $6.\delta=7.3\times10^{-5}$. Instead of this we find 3.1×10^{-5} and 9.3×10^{-5}, that is values greater by more than 27 percent. This deviation was already noticed in Part II and was explained by Bohr as an increase of the nuclear isotope shift caused by the increase of the separation of the proton from the nucleus of the mercury atom at higher rotations. However, the measurements were not as accurate as the present ones and it was believed at that time that the deviations occur only at higher rotational quantum numbers. Therefore the extrapolation to the zero band line was executed assuming only a normal rotational isotope effect in the neighborhood of the band origin, and the value for the nuclear isotope shift found 0.0665 cm^{-1} was higher than the value obtained in this paper. With the new measurements for HgH and the new way of determination of the separations at the band origin the difference in the linear dependence of the nuclear isotope shift from the oscillational energy found previously for the spectra HgH and HgD (see Fig. 4 of reference 5) turns out to be non-existent, both lines being given by the same equation $\Delta\nu_{\text{n.osc.sh.}}=0.0554+1.03\times10^{-5}\times\nu_{\text{osc.}}$

Stenvinkel[11] suggested a different explanation for the deviations from the normal rotational isotope effect. He pointed out that instead of the simplified formula for the rotational isotope effect used by the author, namely $\Delta\nu_{\text{rot}}=(1-\rho^2)\cdot\nu_{\text{rot}}$, the more general formula should be applied, namely

$$\Delta\nu_{\text{rot}}=(1-\rho^2)\cdot K-(1-\rho^3)\cdot L-(1-\rho^4)\cdot M$$

where

$$K=B_e'J'(J'+1)-B_e''J''(J''+1),$$
$$L=\alpha_e'(v'+\tfrac{1}{2})J'(J'+1)-\alpha_e''(v''+\tfrac{1}{2})J''(J''+1),$$

and

$$M=D'J'^2(J'+1)^2-D''J''^2(J''+1)^2.$$

A deviation from the simplified formula in the same direction as the observed one will be obtained. The deviation from the simplified formula can be easily calculated using the values of the constants for the HgH spectrum reported by Rydberg[12] and by Fujioka and

[11] G. Stenvinkel, "Das bandenspektrum des zinkhydrides," dissertation, Stockholm (1936).

[12] R. Rydberg, Zeits. f. Physik 73, 74 (1931).

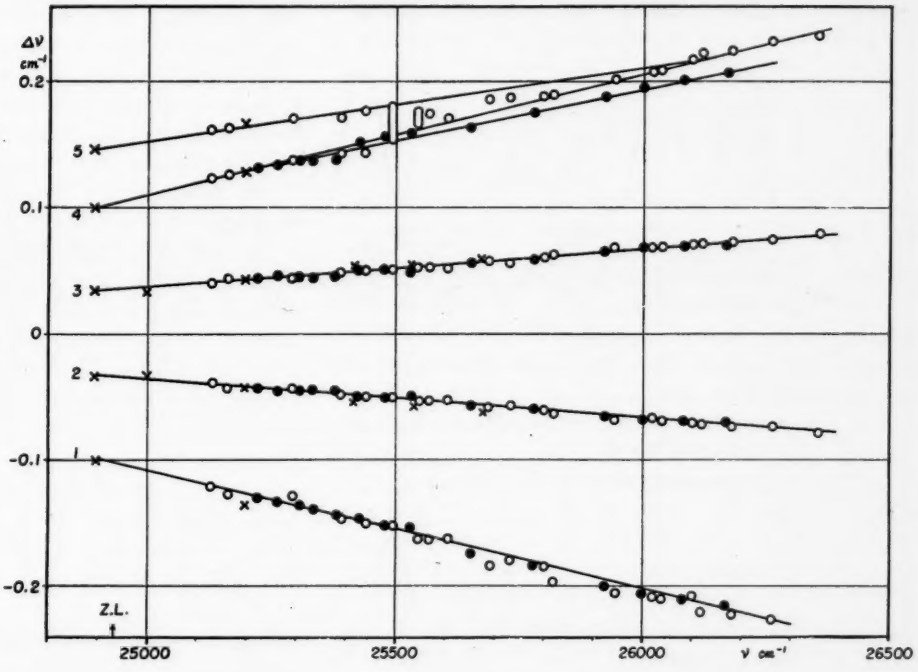

FIG. 2. Separations of components measured in the band λ4017. Open circles—lines belonging to R branches, filled in circles—Q branch lines, crosses —P branch lines.

Tanaka.[13] Since $\nu_{rot}=K-L-M$ and for small δ's $1-\rho^n=n\cdot\delta$, we get $\nu_{rot}=2\delta\cdot\nu_{rot}-\delta\cdot L-2\delta\cdot M=2\delta(\nu_{rot}-\frac{1}{2}L-M)$. Substituting $\alpha'=0.25$, $\alpha''=0.312$, $D'=2.9\times10^{-4}$, $D''=3.8\times10^{-4}$, we find for J' and J'' around 30 a formula $\Delta\nu_{rot}=2\delta(\nu_{rot}+100)$. The correction of 100 cm^{-1} can give only an explanation of a small part, in fact not more than one-fourth of the observed deviation for the Q and R band lines. The small extra deviation for the P lines (crosses around $\nu=25500$ cm^{-1}) toward higher separations can be explained very well by Stenvinkel's correction. However the linear dependence of the main deviation from the rotational frequency ν_{rot} and the absence of a greater deviation for P lines presents a difficulty for any kind of explanation including the one suggested by Bohr (Part II). It was thought at first that maybe too small separations are obtained toward the band edge due to an attraction of components for smaller separations, but this seems hardly probable, since the results were checked with Fabry-Perot etalons with several different plate separations.

It can also be seen from a comparison of the mercury hydride and mercury deuteride spectra, that the deviation cannot be caused by any correction terms from the formula for the normal rotational isotope effect. For a given ν_{rot} (high quantum numbers J) the deviation given by the member M in the formula should constitute the same percentage of the normal separation in both spectra, that is the deviation should be double for the mercury deuteride. For the member L the contribution of which is smaller than of the former one in these spectra, the deviation should be $\sqrt{2}$ times bigger than for the hydride spectrum. In the spectrum of the mercury deuteride[5] however the absolute deviation is smaller than in the hydride spectrum and constitutes only 10 percent of the total rotational separation. The linear dependence of the separation from ν_{rot} is easily noticeable on Fig. 2 of the paper on the mercury deuteride spectrum.[5]

[13] Y. Fujioka and Y. Tanaka, Sci. Pap. Inst. Phys. and Chem. Research (Tokyo) 34, 713 (1938).

Relative intensities

In order to obtain more information about the hyperfine structure in the spectrum of mercury hydride the intensity distribution in the complex structure for many lines in the band λ4017 was investigated. Alternately with the Fabry-Perot photographs of the mercury hydride spectrum direct photographs of a pure mercury arc spectrum from another source were made on the same plate. The slit of the spectrograph was illuminated by the light of this source avoiding the interference apparatus by inserting a prism in front of the slit. A sharp image of a platinum step filter was focused on the slit and by an appropriate lens arrangement a uniform illumination of the whole image was obtained. The densities of the interference patterns and of the comparison intensity marks were determined with a recording microphotometer (Moll-Type A). The transmission of the steps in the filter was measured for different wave-lengths using a monochromator and a photo-cell. The microphotometer recordings were evaluated and the intensity distribution in a group of components was determined applying a procedure described by the author in a paper on isotope shifts in the atomic spectrum of boron.[14] Corrections for the

[14] S. Mrozowski, Zeits. f. Physik 112, 223 (1939).

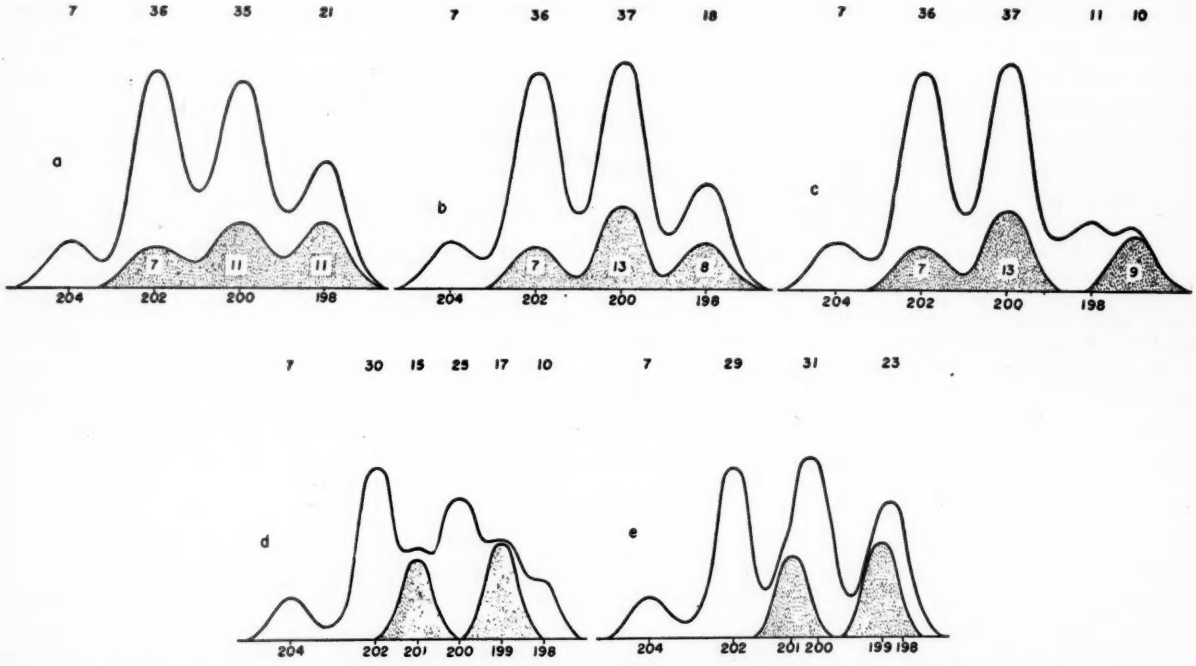

FIG. 3. Intensity distribution in a group of components for lines of the band λ4017: (a) Q_2 lines around 25500 cm^{-1}, (b) R_1 lines around 25800 cm^{-1}, (c) R_2 lines around 25300 cm^{-1}, (d) predicted structure in absence of hyperfine structure and for an even distribution of isotopes of mercury, for lines around 25700 cm^{-1}, (e) predicted structure in absence of hyperfine structure but for an assymetrical position of odd isotopes (like in the atomic spectrum of mercury), for lines around 25700 cm^{-1}.

scattered light were subtracted. The final curves obtained are far from being as accurate as in the case of the spectrum of boron. A less sensitive microphotometer was used this time and a wider slit in the microphotometer had to be applied in view of the small width of the spectrographic slit. A considerable amount of extra broadening of components was thus introduced in the pattern. Less importance therefore should be attached to the exact shape of the lines and the considerations should rather be limited to a discussion of the total intensity of a component (that is to the area enclosed by the curves).

The results obtained are presented in Fig. 3, graphs a, b, and c. Graph a gives a typical intensity distribution for a Q_2 branch line, the curve was obtained as an average from several Q_2 lines in the neighborhood of $\nu = 25500$ cm^{-1}. Graph b is for R_1 lines around $\nu = 25800$ cm^{-1}, where the fourth and fifth component are already merged together into one, and graph c is for R_2 lines around $\nu = 25300$ cm^{-1} (both are averages over several lines). As can be seen from these graphs, the difference noticed in Part II concerning a higher intensity of the component No. 3 (isotope 200) in R lines than in Q lines appears to be real. The curves were drawn assuming the same total intensity for the first component in all three cases. It was expected that this is the only component to be likely free from overlappings and its intensity should be proportional to the concentration of the isotope 204. For this end the curves were approximately decomposed into single curves corresponding to different components and their areas determined by use of a planimeter. The assumption turned out to be well supported by the experiment, since the area of the first component was found to be in all cases equal or a little bigger than 7 percent of the total area of the group (see Table I). To the total intensity of the remaining components (Nos. 2–5) all other mercury isotopes are therefore contributing. By subtracting the intensities of the even isotopes 202, 200 and 204 from the pattern the shaded areas were found, which approximately represent the distribution of intensities in the group of components emitted by the odd isotopes 201 and 199 of mercury. Since there are at least three components and only two emitting isotopes the existence of a hyperfine structure splitting in this band spectrum is thus definitely established. The shaded areas give only a very rough (smeared-out) picture of the structure of the spectrum corresponding to an overlapping of the pattern for two odd isotopes, since the presence of several closely spaced components overlapped with the strong lines of the even isotopes (202 and 200) could be only revealed by a very accurate study of the shape of the lines, which was made impossible in this case by the considerable width of the slit used in the microphotometer. The uncertainty in the intensities corresponding to the shaded components should not be bigger than ± 2. The internal consistency of the results for different band lines was much higher, but since there are so many factors affecting the final values, the author thinks it better to refrain from claiming any higher accuracy.

In Fig. 3, two graphs d and e are added in order to

compare the structures obtained with structures predicted for the case of an absence of hyperfine structure splitting. Graph d gives the expected structure of a group for the case of an even distribution of isotopes (like in the normal isotope effect) and graph e represents the expected structure for lines around $\nu=25700$ cm^{-1} and for an overlapping of the normal effect with a nuclear isotope shift, assuming the nuclear isotope shift to be proportional to the shifts observed in the atomic spectrum of mercury (centers of gravity for isotopes 201 and 199 very near to the positions of isotopes 200 and 198). For higher rotations the components corresponding to odd isotopes would move away from the even isotopes 200 and 198 (normal rotational effect) and a structure approaching Fig. 3d would be observed (around $\nu=26300$ cm^{-1} 6 components should be found). The numbers given on top of each graph are relative peak intensities. Although the last curve bears some similarity with curves a and b the difference in peak intensities is well outside of the limits of errors of the measurements.

As to the theoretical interpretation of the hyperfine structure patterns for the two odd isotopes it seems to present certain serious difficulties. Hulthén[9] pointed out that the coupling of the nuclear spin with the molecular axis should break down already at low rotational energies and for medium and high rotational quantum numbers J the nuclear spin should be coupled with the axis of rotation of the molecule. For the excited state $^2\Pi$ a very small hyperfine separation is expected since the electronic orbital momenta and the electronic spins are coupled with the molecular axis and the interaction should at least partly average out for all except the lowest rotational energy states. In the ground state $^2\Sigma$ both the electronic spin and nuclear spin are coupled with the axis of rotation and their interaction should cause an observable splitting, especially since the $p\sigma$-electron has an not negligible density of wave function in the neighborhood of the nucleus.[5] A total separation of the order 0.1 cm^{-1}, which is considerably smaller than the separations in the hyperfine structure of the atomic levels of mercury (for instance, 0.7 cm^{-1} for 6^3P_1) seems to be of the right order of magnitude. For all branches a similar hyperfine structure is expected, which should be a partially overlapped doublet ($I_{199}=\frac{1}{2}$) with an inverted quartet ($I_{201}=\frac{3}{2}$) with separations approximately independent from the rotational energy. However, this is not in agreement with observations. To explain the difference in separation and in relative intensities of hyperfine structure components for different branches the existence of a measurable separation in the $^2\Pi_{\frac{1}{2}}$-state and the emission of components corresponding to transitions involving a change of the direction of the nuclear spin relative to the rotational axis has to be assumed. But then the similarity of the structures for P and R lines becomes difficult to explain. In conclusion the author finds himself unable to suggest any satisfactory interpretation of the results.

TABLE I. Concentration of isotopes of mercury in percent.

Isotope	Concentration
204	6.85
202	29.3
201	13.7
200	23.8
199	16.45
198	9.9

The $^2\Sigma^I \rightarrow {}^2\Sigma$-Bands

In connection with this work the system $^2\Sigma^I \rightarrow {}^2\Sigma$ of short wave-length bands was reinvestigated using a Fabry-Perot etalon and the quartz optics for the spectrograph. Results of measurements of the separations for the two strongest components are given in Fig. 4. The presence of the anomaly reported in Part II for the 32700 cm^{-1} band is checked and a similar anomaly is found for the band 33900 cm^{-1}. Toward longer wavelengths (away from the band origin) the separations after reaching a minimum start increasing, instead of showing a steady decrease. Further the slope of the decrease in the neighborhood of the band origin is about 15 to 20 percent smaller than expected. The intensity distribution in the lines correspond to Fig. 3c with the

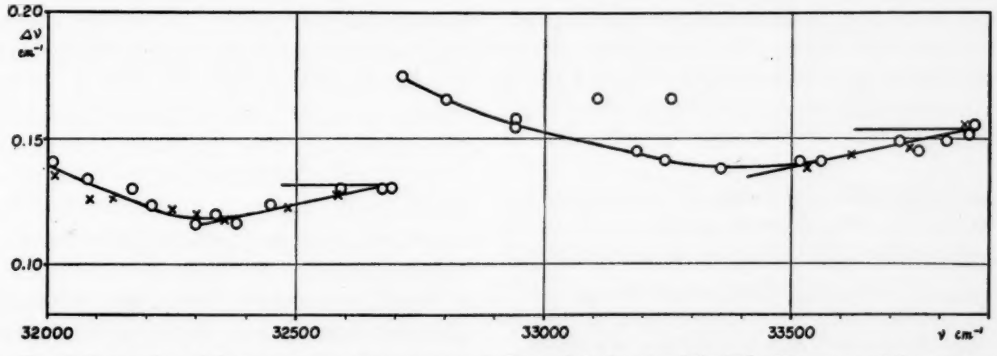

FIG. 4. Separation of the two strongest components in lines of the bands of the $^2\Sigma^I \rightarrow {}^2\Sigma$-system of the mercury hydride. The anomalous increase of the separation in the long wave-length parts of each band is so strong as to overbalance the linear decrease caused by the normal rotational isotope effect. Circles—new measurements, crosses—previous results reported in Part II.

only difference that the fifth component (9 percent of total intensity) is in a considerably greater distance from the fourth component, approximately equal to the distance of the third and fourth components (200–198). All P and R lines reveal a similar structure.

This work was undertaken in the hope to clarify certain minor features of the structure of the lines in the spectrum of the mercury hydride, and to bring about the first proof of the existence of hyperfine structure in band spectra. The author believes that the second aim was achieved in a satisfactory manner. However, the general relations have not been clarified by this investigation. Just on the contrary, attempts to find an explanation of the hyperfine structure and of the deviations from the normal rotational isotope effect are meeting serious difficulties. It seems that a clarification of the problems brought forward can be expected from a thorough theoretical study of hyperfine structure and nuclear isotope shift effects in diatomic molecules.

Note added in proof.—The availability of concentrated samples of the isotope Hg_{199} has been recently announced [C. P. Keim, Phys. Rev. **76**, 1270 (1949)]. A corresponding study of the hyperfine structure of its hydride spectrum is in preparation at this laboratory.

PHYSICAL REVIEW VOLUME 76, NUMBER 12 DECEMBER 15, 1949

Some Aspects of Paramagnetic Relaxation

ARIANNA WRIGHT
Radcliffe College, Cambridge, Massachusetts
(Received July 13, 1949)

This paper concerns the effect of interactions inside the spin system in giving a finite line width to the energy absorption lines in an oscillating magnetic field. The principal calculations are of absorption coefficients at low frequencies for copper salts. These absorption coefficients refer in most cases to the aperiodic line near zero frequency and not to the Larmor line. The first step is a discussion of the general procedure for reconstructing a shape function $f(\nu)$ from its moments. The special case in which the zeroth, second, and fourth moments are known arises in the absence of a constant magnetic field, and at the Larmor frequency in a constant magnetic field perpendicular to the oscillating field. These cases are discussed and compared with experiment in Section III; extensive calculations have already been made by Van Vleck in the second case. The magnitude of the exchange coupling is the decisive factor, as pointed out by Gorter and Van Vleck; and various methods of calculating this magnitude from experimental data are given. Low frequency absorption in a perpendicular field is discussed on the basis of a Gaussian approximation in Section IV, and the agreement with the experiments of Volger, Vrijer, and Gorter is good. In Section V it is shown that quantitative calculations only emphasize the discrepancy, pointed out by Broer, between theory and experiment for low frequency absorption in a parallel constant field. An explanation of the discrepancy is given in terms of the difficulty in resolving out the different lines in this case, due to the exchange broadening of the Larmor line, in contrast to the exchange narrowing of the Larmor line in a perpendicular field. In Section VI a calculation of the isolated susceptibility of a spin system is given for strong fields; it is found to be 0.80 of the thermodynamic or adiabatic susceptibility of Casimir and du Pré, even in the absence of exchange.

I. INTRODUCTION

THIS paper is a condensation of the doctoral thesis submitted by the author at Harvard University, June, 1949. Its purpose is to discuss quantitative calculations on energy absorption by a paramagnetic salt in a magnetic field; these calculations being restricted to absorption in which the line breadth is due to interactions inside the spin system. The calculations of this paper are similar to those of Van Vleck[1] on the Larmor line in a perpendicular field; in the following paragraphs line shapes will be calculated for other lines of interest.

There are three principal cases which concern us; those in which the energy levels of the salt between which the absorption takes place are those which exist

A. in the absence of a constant magnetic field ($H=0$),

B. in the presence of a field $H=H_D$ perpendicular to the relatively weak field $H_0\exp(2\pi i\nu t)$ from which energy is absorbed,

C. in the presence of a field $H=H_c$ parallel to the oscillating field $H_0\exp(2\pi i\nu t)$.

These three cases have been studied experimentally at relatively low frequencies by Gorter, Broer, and others at Leiden.[2,3] Cases A, B, and C are treated in Sections III, IV, and V, respectively. Remarks concerning the applicability of these methods to absorption at the Larmor frequency in a perpendicular field are made at the conclusion of Section III. Energy absorption at the Larmor frequency and at double the Larmor frequency in a parallel field is approached from the more familiar standpoint of the so-called isolated susceptibility of the spin system in Section VI. Absorption at high multiples of the Larmor frequency has not been investigated experimentally. Figure 1 summarizes the investigations made here and elsewhere on paramagnetic relaxation phenomena.

Broer[4] has shown that energy absorption due to spin-spin interaction is characterized completely by the

[1] J. H. Van Vleck, Phys. Rev. **74**, 1168 (1948).

[2] L. J. F. Broer and J. Kemperman, Physica **13**, 465 (1947).

[3] Volger, de Vrijer, and Gorter, Physica **13**, 62 (1947).

[4] L. J. F. Broer, thesis, Amsterdam, 1945.

shape function $f(\nu)$ defined by

$$f(\nu)\Delta\nu=\sum_{\nu-\Delta\nu/2}^{\nu+\Delta\nu/2}|M_{kl}|^2 \quad (1)$$

with M_{kl} being a matrix element of the total magnetic moment of the salt between two states k and l of the spin system. All matrix elements are included in the right-hand sum for which the frequency difference $\nu_{kl}=(E_k-E_l)/k$ of the two states k and l falls in the range $\nu-\Delta\nu/2\leq\nu_{k,l}<\nu+\Delta\nu/2$. The increment $\Delta\nu$ must be small from a macroscopic standpoint, yet large enough so that a good many pairs of discrete states k, l are included in the sum. Experimental results are expressed in terms of $f(\nu)$; the following sections deal with methods of approximating to this shape function.

The Hamiltonian of the spin system, whose wave functions are those between which the matrix elements $M_{k,l}$ in Eq. (1) are to be calculated, is taken to be

$$\mathcal{H}=-g\beta H\sum_i S_{zi}+\sum_{i>j}g^2\beta^2r_{ij}^{-3}[\mathbf{S}_i\cdot\mathbf{S}_j-3(\mathbf{S}_i\cdot(\mathbf{r}/r)_{ij})(\mathbf{S}_j\cdot(\mathbf{r}/r)_{ij})]+\sum_{i>j}g^2\beta^2r_{ij}^{-3}A_{ij}\mathbf{S}_i\cdot\mathbf{S}_j=\mathcal{H}_0+\mathcal{H}_1 \quad (2)$$

with $\mathcal{H}_0$ and $\mathcal{H}_1$ defined by

$$\mathcal{H}_0=-g\beta H\sum_i S_{zi}+\sum_{i>j}g^2\beta^2r_{ij}^{-3}[B_{ij}S_{zi}S_{zj}+C_{ij}\mathbf{S}_i\cdot\mathbf{S}_j]+\sum_{i>j}g^2\beta^2r_{ij}^{-3}A_{ij}\mathbf{S}_i\cdot\mathbf{S}_j, \quad (3)$$

$$\mathcal{H}_1=\sum_{i>j}g^2\beta^2r_{ij}^{-3}[D_{ij}S_{i+}S_{j+}+D_{ij}^*S_{i-}S_{j-}+E_{ij}(S_{i+}S_{zj}+S_{zi}S_{j+})+E_{ij}^*(S_{i-}S_{zj}+S_{zi}S_{j-})]. \quad (4)$$

The coefficients B_{ij}, C_{ij}, D_{ij}, and E_{ij} are defined by

$$B_{ij}=-3(\tfrac{3}{2}\gamma_{ij}^2-\tfrac{1}{2}); \quad C_{ij}=-\tfrac{1}{3}B_{ij};$$
$$D_{ij}=-\tfrac{3}{4}(\alpha_{ij}^2-\beta_{ij}^2-2i\alpha_{ij}\beta_{ij}); \quad E_{ij}=-\tfrac{3}{2}\gamma_{ij}(\alpha_{ij}-i\beta_{ij}), \quad (5)$$

where α_{ij}, β_{ij}, γ_{ij} are the direction cosines of $(\mathbf{r}/r)_{ij}$ with respect to the x, y, and z axes, respectively; these axes being chosen so that H, the constant magnetic field, is along the z axis. The first term in (2), $-g\beta H\sum_i S_{zi}$, is the Zeeman energy; the expression

$$\sum_{i>j}g^2\beta^2r_{ij}^{-3}[\mathbf{S}_i\cdot\mathbf{S}_j-3(\mathbf{S}_i\cdot(\mathbf{r}/r)_{ij})(\mathbf{S}_j\cdot(\mathbf{r}/r)_{ij})]$$

is the magnetic dipole interaction energy;

$$\sum_{i>j}K_{ij}\mathbf{S}_i\cdot\mathbf{S}_j=\sum_{i>j}A_{ij}g^2\beta^2r_{ij}^{-3}\mathbf{S}_i\cdot\mathbf{S}_j$$

is the exchange energy. It is supposed, in using (2), that

A. The orbital contribution to the magnetic moment of a paramagnetic atom is quenched completely out by the interaction of the surrounding crystalline electric fields. A first-order correction to this approximation is made by using, not $g=2$, but g as derived from static susceptibility measurements. (The spin only susceptibility is given theoretically by

$$\chi_0=C/T=(\tfrac{1}{3})Ng^2\beta^2S(S+1)/kT,$$

with β the Bohr magneton, k Boltzmann's constant, and N the number of paramagnetic atoms per cubic centimeter. The effective gyromagnetic ratio g as here defined is given by twice the square root of the ratio of the experimental to the theoretical susceptibility.

B. There is no crystalline potential term in the Hamiltonian. This is equivalent to assuming, as far as calculations of the line shape are concerned, that $S=\frac{1}{2}$, or else that for some reason the crystalline splitting is negligibly small. For $S=\frac{1}{2}$, according to Kramer's theorem,[5] the twofold degenerate level of an atom cannot be split by any electric field, no matter what its strength or asymmetry. Comparison with experiment will be limited in the following to copper salts for which S is indeed $\frac{1}{2}$. Calculations in Section VI are not concerned with line shape and hold for any S.

The unperturbed Hamiltonian is $\mathcal{H}_0$, the perturbing energy $\mathcal{H}_1$ enters in the calculations of Sections IV and V. The four terms in $\mathcal{H}_1$ as given in (4) will be called $\mathcal{H}_1^{(1)}$, $\mathcal{H}_1^{(2)}$, $\mathcal{H}_1^{(3)}$, and $\mathcal{H}_1^{(4)}$, respectively, and are conveniently separated by this breakup for use in the perturbation processes of Sections IV, V, and VI.

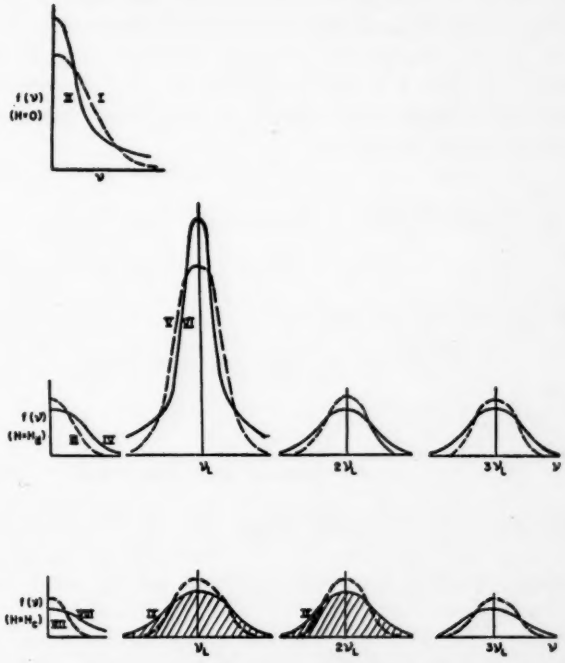

FIG. 1. The function $f(\nu)$ for no constant magnetic field ($H=0$); for a constant magnetic field perpendicular to the oscillating field ($H=H_D$), and for a constant magnetic field parallel to the oscillating field ($H=H_c$). The dotted lines are for negligible exchange; the solid lines show the effect of exchange. The various lines are discussed in the following places: Curve I; Broer, references 4, 7. Curve II; Section III of this paper. Curves III, IV; Section IV of this paper. Curves V, VI; Van Vleck, reference 1; see also end of Section II. Curves VII, VIII; Section V of this paper. Shaded Area IX; Section VI of this paper.

[5] H. A. Kramers, Proc. Phys. Soc., Amsterdam 33, 959 (1930).

In the so-called strong field limit, in which H is supposed very much larger than fields characterizing the dipolar and exchange energies, the unperturbed energy levels of $\mathcal{H}_0$ are just

$$E_{M'} = -g\beta HM' \tag{6}$$

with M' the z component of the magnetic moment and a true quantum number for this system. Here the absorption, according to the simple Larmor precession picture, is at the Larmor frequency in a perpendicular field (or at zero frequency in no field). The usefulness of the form (4) for the perturbing energy results from the fact that in the strong field limit non-vanishing matrix elements for a given term of (4) are obtained only between wave functions differing in their associated energy values by one specific multiple of $h\nu_L$, ν_L being the Larmor frequency $g\beta H/h$. Thus, in the strong field limit the perturbing energy introduces additional absorption only at other multiples of the Larmor frequency; absorption bands appear near frequencies 0, $2\nu_L$, $3\nu_L$, and in high order perturbation processes at still higher multiples of the Larmor frequency.

II. THE METHOD OF MOMENTS*

Because of the large number of energy levels of the spin system it is not feasible to compute wave functions, matrix elements M_{kl}, and thus $f(\nu)$ from (2), (3), and (4) in a straightforward way. The only method of procedure that has proved useful up to the present time is the method of moments in which the following quantities are calculated:

$$\begin{aligned}
&\int_0^\infty f(\nu)d\nu = \sum_{k\neq l} |M_{kl}|^2 = \mathrm{Spur}|M^2|,\\
&\int_0^\infty \nu^2 f(\nu)d\nu = \sum_{k,l} \nu_{kl}^2 |M_{kl}|^2\\
&\qquad = -h^{-2}\,\mathrm{Spur}\psi_1^2;\ \psi_1 = (M\bar{U}-\bar{U}M),\\
&\int_0^\infty \nu^4 f(\nu)d\nu = \sum_{k,l} \nu_{kl}^4 |M_{kl}|^2\\
&\qquad = h^{-4}\,\mathrm{Spur}\psi_2^2;\ \psi_2 = M\psi_1-\psi_1 M.
\end{aligned} \tag{7a}$$

The quantities on the left in Eqs. (7a) are the moments of $f(\nu)$, by definition. In the following paragraphs average symbols for these moments will be used, as given in Eqs. (7b):

$$\int_0^\infty f(\nu)d\nu = \langle\nu^0\rangle_{Av};\ \left(\int_0^\infty \nu^k f(\nu)d\nu\right)\Big/\langle\nu^0\rangle_{Av} = \langle\nu^k\rangle_{Av}. \tag{7b}$$

The equivalence of the moments in this case to the right-hand members of Eqs. (7a) has been shown by Waller[6] and Broer[7] according to the general laws of matrix multiplication. For a single absorption band the relevant matrix elements $M_{k,l}$ (where k and l are such that $(E_k-E_l)/h$ is approximately the energy difference corresponding to the particular band under consideration) may be either those of the operator $g\beta\sum_i S_{zi}$, or $g\beta\sum_i S_{xi}$, in a zeroth approximation, or those obtained from these operators by perturbation calculations with the perturbing energies (4). The energy $\bar{U}$ consists of all the Hamiltonian with eigenvalues small compared to the Larmor energy $h\nu_L$. If $H=0$, $\bar{U}$ consists of the complete Hamiltonian (2); if $H\neq 0$, $\bar{U}$ is just $\mathcal{H}_0$.

It is simpler to consider the problem of calculating $f(\nu)$ from its moments for a single absorption band, rather than for all such bands at once. Once these moments (7) are known, the function $f(\nu)$ can in principle be reconstructed in the following way. Suppose $f_2(\nu)$ is defined by

$$f_2(\nu) = \langle\nu^0\rangle_{Av}(2/\pi\langle\nu^2\rangle_{Av})^{\frac{1}{2}}\exp(-\nu^2(2\langle\nu^2\rangle_{Av}) \tag{8}$$

with $\langle\nu^0\rangle_{Av} = \int_0^\infty f(\nu)d\nu$. Then $f_2(\nu)$ fits the zeroth and second moments. Let $f_k(\nu)$ be a function fitting the moments $\langle\nu^0\rangle_{Av}$, $\langle\nu^2\rangle_{Av}$, $\cdots$, $\langle\nu^k\rangle_{Av}$. Then a function $f_{k+2}(\nu)$ fitting the moments $\langle\nu^0\rangle_{Av}$, $\cdots$, $\langle\nu^k\rangle_{Av}$ and also $\langle\nu^{k+2}\rangle_{Av}$ is

$$f_{k+2}(\nu) = f_k(\nu) + \left\{\left[\langle\nu^{k+2}\rangle_{Av} - \int_0^\infty \nu^{k+2} f_k(\nu)d\nu\right]\Big/(k+2)!\right\}(d/d\nu)^{k+2}f_2(\nu), \tag{9}$$

since if the second term of (9) is multiplied by any power of ν up to and including ν^k, and integrated from 0 to ∞, the result is zero; however, for ν^{k+2} the result is

$$\langle\nu^{k+2}\rangle_{Av} - \int_0^\infty \nu^{k+2} f_k(\nu)d\nu.$$

From this fact it follows that

$$\int_0^\infty \nu^j f_{k+2}(\nu)d\nu = \int_0^\infty \nu^j f_k(\nu)d\nu = \langle\nu^j\rangle_{Av},\ (j=0,\cdots,k)$$

and

$$\int_0^\infty \nu^{k+2} f_{k+2}(\nu)d\nu = \langle\nu^{k+2}\rangle_{Av}.$$

The properties of the second term can be seen by integrating by parts; j of the $k+2$ derivatives of (9) can be used to get rid of ν^j, one of the remaining derivatives can be used to integrate, and the result is proportional to $(d/d\nu)^{2m+1}f_2(\nu)$. But the operator $(d/d\nu)^{2m+1}$ just multiplies $f_2(\nu)$ by a polynomial of odd order, which vanishes at the origin, and $f_2(\nu)$ vanishes at ∞. If j is $k+2$, however, all $k+2$ of the derivatives must be used to act on ν^{k+2} and replace it simply by a factorial $(k+2)!$ This $(k+2)!$ just cancels the $(k+2)!$ in the denominator of (9); $\int_0^\infty f_2(\nu)d\nu$ remains, and this integral

* E. T. Whittaker and G. Robinson, *The Calculus of Observations* (Blackie & Son, Ltd., London, 1937), Chapter 8.

[6] I. Waller, Zeits. f. Physik **79**, 370 (1932).

[7] L. J. F. Broer, Physica **10**, 801 (1943).

is one. Thus, $f_{k+2}(\nu)$ fits all moments up to and including $\langle\nu^{k+2}\rangle_{Av}$. By means of the formula (9) a sequence of functions can thus be constructed, on the basis of known moments, converging to $f(\nu)$.

III. ABSORPTION WITH NO CONSTANT MAGNETIC FIELD PRESENT

The present section is concerned with calculating the moments (7), for $H=0$, substituting these moments into the appropriate formula (9), and comparing the approximate shape function thus obtained with the experimental results. There is only one absorption band to be considered here centered about zero frequency. The relevant magnetic moment is

$$M_z=g\beta\sum_i S_{zi}. \tag{10}$$

The relevant energy is the complete Hamiltonian (2); the operator expressions to be calculated and averaged are the right-hand sides of (7); $\mathrm{Spur}M_z^2$, $-h^{-2}\mathrm{Spur}(\mathfrak{IC}M_z-M_z\mathfrak{IC})^2$ etc.

The first two moments have been calculated by Broer.[4,7] His results are, in brief,

$$\int_0^\infty f(\nu)d\nu=\tfrac{1}{3}Ng^2\beta^2S(S+1)=kT\chi_0, \tag{11}$$

$$\int_0^\infty \nu^2 f(\nu)d\nu=-h^{-2}\,\mathrm{Spur}\psi_1^2=kT\chi_0\langle\nu^2\rangle_{Av}, \tag{12}$$

$$\psi_1=\left[U+V,g\beta\sum_i S_{zi}\right]=-3ig^3\beta^3\sum_{k\neq l}\times\{r_{kl}^{-3}(\mathbf{S}_k\times(\mathbf{r}/r)_{kl})_z(\mathbf{S}_l\cdot(\mathbf{r}/r)_{kl})\}, \tag{13}$$

$$\langle\nu^2\rangle_{Av}=\int_0^\infty \nu^2 f(\nu)d\nu\Big/\int_0^\infty f(\nu)d\nu=g^2\beta^2H_i^2/h^2, \tag{14}$$

$$H_i^2=2g^2\beta^2S(S+1)\sum_P r_{Pq}^{-6}. \tag{15}$$

The appropriate approximation (9) is $k+2=2$, $k=0$; (9) becomes

$$f_2(\nu)=(2/\pi\langle\nu^2\rangle_{Av})^{\frac{1}{2}}\langle\nu^0\rangle_{Av}\exp(-\nu^2/2\langle\nu^2\rangle_{Av}). \tag{16}$$

An important point to notice is that $\langle\nu^2\rangle_{Av}$ is independent of the exchange constant A. The mathematical reason for this is that the exchange energy $\sum_{i>j}K_{ij}\mathbf{S}_i\mathbf{S}_j$ commutes with $g\beta\sum_i S_{zi}$; thus the operator ψ_1 of (13) is independent of A. This point will be discussed more fully later, in Section IV.

The experimental results which we will discuss are usually limited because of technical difficulties to such low frequencies that only $f(0)$ can be determined; they are expressed in terms of a quantity $\rho'(0)$ defined by

$$\rho'(0)=\pi f(0)/2kT\chi_0. \tag{17}$$

According to (16) and (17) the theoretical formula for $\rho'(0)$ is

$$\rho'(0)=(\pi/2\langle\nu^2\rangle_{Av})^{\frac{1}{2}}=(\pi/2)^{\frac{1}{2}}(h/g\beta H_i). \tag{18}$$

Table I summarizes (18) *versus* experimental values for certain copper salts. The quantity $\bar{C}$, given in the last column of Table I, is the empirical correction factor to the theory based on the zeroth and second moments only. The following paragraphs attempt to estimate $\bar{C}$ as it differs from unity.

In order to take into account the effects of exchange which are responsible[8,1] for the discrepancies indicated in Table I, it is necessary at least to calculate the fourth moment, as this is the first moment to depend on A, the exchange constant. The appropriate formula is

$$\langle\nu^4\rangle_{Av}=\int_0^\infty \nu^4 f(\nu)d\nu\Big/\int_0^\infty f(\nu)d\nu \tag{19}$$

$$\int_0^\infty \nu^4 f(\nu)d\nu=h^{-2}\,\mathrm{Spur}\psi_2^2 \tag{20}$$

$$\psi_2=[U+V,\psi_1];\quad \psi_1 \text{ given in (13).} \tag{21}$$

Direct commutation results in

$$\psi_2=-9g^5\beta^5{\sum_{k,l}}'[A_{kl}{}^{(1)}+(1+A_{kl})A_{kl}{}^{(2)}]r_{kl}^{-6}-3g^5\beta^5{\sum_{k,l,l'}}'[(1+A_{kl})B_{kll'}+D_{kll'}]r_{kl}^{-3}r_{kl'}^{-3} \tag{22}$$

with

$$A_{kl}{}^{(1)}=(\mathbf{S}_i\cdot(\mathbf{r}/r)_{kl})^2[(\mathbf{r}/r)_{kl}\times((\mathbf{r}/r)_{kl}\times\mathbf{S}_k)]_z \tag{23}$$

$$2A_{kl}{}^{(2)}=\{[(\mathbf{S}_k\times(\mathbf{r}/r)_{kl})\times\mathbf{S}_l]_z,\ (\mathbf{S}_l\cdot(\mathbf{r}/r)_{kl})\}_+ +\{\mathbf{S}_l\cdot\mathbf{S}_k\times(\mathbf{r}/r)_{kl},\ (\mathbf{S}_k\times(\mathbf{r}/r)_{kl})_z\}_+ \tag{24}$$

$$B_{kll'}=[(\mathbf{S}_k\times\mathbf{S}_l)\times(\mathbf{r}/r)_{kl'}](\mathbf{S}_{l'}\cdot(\mathbf{r}/r)_{kl'})+(\mathbf{S}_k\times\mathbf{S}_l\cdot(\mathbf{r}/r)_{kl})(\mathbf{S}_{l'}\times(\mathbf{r}/r)_{kl'})_z \tag{25}$$

$$-\tfrac{1}{3}D_{kll'}=[(\mathbf{S}_k\times(\mathbf{r}/r)_{kl})\times(\mathbf{r}/r)_{kl'}]_z(\mathbf{S}_l\cdot(\mathbf{r}/r)_{kl})\times(\mathbf{S}_{l'}\cdot(\mathbf{r}/r)_{kl'}+(\mathbf{S}_k\times(\mathbf{r}/r)_{kl}\cdot r_{kl'})\times(\mathbf{S}_l\cdot(\mathbf{r}/r)_{kl})(\mathbf{S}_{l'}\cdot(\mathbf{r}/r)_{kl'})_z. \tag{26}$$

The symbol $\{A,B\}_+$ or $[A,B]_+$ is taken to mean $AB+BA$; and the symbol $\{A,B\}$ or $[A,B]$ means $AB-BA$.

For a spin of $\frac{1}{2}$ it is easy to show that

$$A_{kl}{}^{(2)}+A_{lk}{}^{(2)}=0, \tag{27}$$

and since the $A_{kl}{}^{(2)}$ terms occur symmetrically in (22), the relation (27) causes the A^2 terms to drop out of (22). Since the crystalline potential terms were omitted originally, this theory will be applied only to substances with a spin of $\frac{1}{2}$; therefore we shall, for the sake of simplicity, omit the $A_{kl}{}^{(2)}$ term from now on. This term will presumably be only a small correction for not too large S.

[8] C. J. Gorter and J. H. Van Vleck, Phys. Rev. **72**, 1128 (1947).

The next problem is to square the expression (22) with the $A_{kl}^{(2)}$ term omitted. Omission of terms whose average is zero results in

$$\psi_2^2 = K_1 + K_2 + K_3 \tag{28}$$

with

$$K_1 = 81 g^{10}\beta^{10} \sum_{k,l}{}' A_{kl}^{(1)} r_{kl}^{-12}, \tag{29}$$

$$K_2 = 81 g^{10}\beta^{10} \sum_{k,l,l'}{}' A_{kl}^{(1)} A_{kl'}^{(1)} r_{kl}^{-6} r_{kl'}^{-6} \tag{30}$$

$$K_3 = 9 g^{10}\beta^{10} \sum_{i=0}^{5} L_i \tag{31}$$

$$L_0 = \sum_{k,l,l'}{}' A_{kl} B_{kll'} r_{kl}^{-3} r_{kl'}^{-3} \times [P^6_{kll'} A_{kl} B_{kll'} r_{kl}^{-3} r_{kl'}^{-3}] \tag{32}$$

$$L_1 = 2 \sum_{kll'}{}' A_{kl} B_{kll'} r_{kl}^{-3} r_{kl'}^{-3} \times [P^6_{kll'} B_{kll'} r_{kl}^{-3} r_{kl'}^{-3}] \tag{33}$$

$$L_2 = 2 \sum_{kll'}{}' D_{kll'} r_{kl}^{-3} r_{kl'}^{-3} \times [P^6_{kll'} A_{kl} B_{kll'} r_{kl}^{-3} r_{kl'}^{-3}] \tag{34}$$

$$L_3 = \sum_{kll'}{}' B_{kll'} r_{kl}^{-3} r_{kl'}^{-3} [P^6_{kll'} B_{kll'} r_{kl}^{-3} r_{kl'}^{-3}] \tag{35}$$

$$L_4 = 2 \sum_{kll'}{}' D_{kll'} r_{kl}^{-3} r_{kl'}^{-3} [P^6_{kll'} B_{kll'} r_{kl}^{-3} r_{kl'}^{-3}] \tag{36}$$

$$L_5 = \sum_{kll'}{}' D_{kll'} r_{kl'}^{-3} r_{kl}^{-3} [P^6_{kll'} D_{kll'} r_{kl}^{-3} r_{kl'}^{-3}]. \tag{37}$$

The L_0 term will, when evaluated, be proportional to A^2; it is the only "pure" exchange term in ψ_2^2. The two terms L_1 and L_2 will be proportional to A; they are terms coupling dipole and exchange interactions. The terms L_3, L_4, and L_5 are pure dipole terms, along with K_1 and K_2. In evaluating numerically the various terms of (28), two assumptions will be made: first, that exchange acts only between nearest neighbors, and thus $A_{ij}=0$ unless i, j are nearest neighbors; and second, that the paramagnetic atoms are arranged on a simple cubic lattice, so that the number of nearest neighbors is $z=6$.

There are two factors affecting the relative difficulty of numerically evaluating the L_i's. One of these results from the fact that $D_{kll'}$ is a far more complicated expression than $B_{kll'}$. Thus in L_i terms in which $D_{kll'}$ enters, approximation methods will be used. Secondly it is far simpler to evaluate sums involving exchange interactions, since the pairs of atoms involved do not have to be summed over all possible pairs of neighbors. Involved algebraic manipulation and numerical calculation finally results in[9]

$$9 g^{10}\beta^{10}\,\mathrm{Spur} L_0 = 40.7 g^{10}\beta^{10} S^3 (S+1)^3 A^2 d^{-12}, \quad \text{(error small)}, \tag{38}$$

$$9 g^{10}\beta^{10}\,\mathrm{Spur} L_1 = 89 g^{10}\beta^{10} N A S^3 (S+1)^3 d^{-12}, \quad \text{(error small)}, \tag{39}$$

$$9 g^{10}\beta^{10}\,\mathrm{Spur} L_2 = -80 g^{10}\beta^{10} N A S^3 (S+1)^3 d^{-12}, \quad \text{(estimated error negative and less than } -12 \text{ percent)}, \tag{40}$$

$$9 g^{10}\beta^{10}\,\mathrm{Spur} L_3 = 75 g^{10}\beta^{10} N S^3 (S+1)^3 d^{-12}, \quad \text{(estimated error positive and less than 25 percent)}, \tag{41}$$

$$9 g^{10}\beta^{10}\,\mathrm{Spur} L_4 = -110 g^{10}\beta^{10} N S^3 (S+1)^3 d^{-12} \quad \text{(estimated error negative and less than 25 percent)}, \tag{42}$$

$$9 g^{10}\beta^{10}\,\mathrm{Spur} L_5 = 1.7 \cdot 10^2 g^{10}\beta^{10} N S^3 (S+1)^3 d^{-12}, \quad \text{(estimated error positive and less than 25 percent)}, \tag{43}$$

$$\mathrm{Spur} K_2 = 83 g^{10}\beta^{10} N S^3 (S+1)^3 d^{-12}, \quad \text{(error small)}, \tag{44}$$

$$\mathrm{Spur} K_3 = [22 - 7S^{-1}(S+1)^{-1}] g^{10}\beta^{10} N S^3 \times (S+1)^3 d^{-12}, \quad \text{(error small)}. \tag{45}$$

It is seen that L_1 and L_2 cancel, within the accuracy of the evaluation of the lattice sums. Omission of these two terms then yields for $h^{-4}\,\mathrm{Sp}\psi_2^2$:

$$h^{-4}\,\mathrm{Sp}\psi_2^2 = g^{10}\beta^{10} N d^{-12} h^{-4} S^3 (S+1)^3 [40.7 A^2 + 2.4 \cdot 10^2 - 7S^{-1}(S+1)^{-1}]. \tag{46}$$

Division by $\langle \nu^0 \rangle_{Av}$ from (11), and use of (14) then results in

$$\langle \nu^4 \rangle_{Av} = h^{-4}\,\mathrm{Sp}\psi_2^2 / \langle \nu^0 \rangle_{Av} = (\langle \nu^2 \rangle_{Av})^2 [0.43 A^2 + 2.6 - 0.1 S^{-1}(S+1)^{-1}] \tag{47}$$

for the fourth moment. Possibly a term proportional to A, of magnitude probably positive and less than $0.1A$, may be present. The coefficient 2.6 is accurate to around 25 percent. Thus the value $[2.6 - 0.1/S(S+1)]$ implies that, to within the accuracy of our calculations, if A is negligible, the mean fourth frequency is just what one would get by integrating the function (16) times ν^4 from zero to infinity. If there is no appreciable exchange, the function (16) is therefore a good approximation to the actual function describing the shape of the line. This fact has been demonstrated by Van Vleck[1] in connection with the Larmor line in a perpendicular field; Pake and Purcell[10] have tested this theoretical prediction for the substance CaF_2 and found it to be very well confirmed experimentally.

The formula for $f_4(\nu)$ is

$$f_4(\nu) = kT\chi_0 (2/\pi \langle \nu^2 \rangle_{Av})^{\frac{1}{2}} \{1 + ([\langle \nu^4 \rangle_{Av} - 3\langle \nu^2 \rangle_{Av}^2]/4!)(d/d\nu)^4\} \exp(-\nu^2/2\langle \nu^2 \rangle_{Av}). \tag{48}$$

TABLE I. Gaussian approximation to $f(\nu)$: theory *versus* experiment for $\rho'(0)$.

Substance	H_i	Form (18) for $\rho'(0)$	Exp. $\rho'(0)$	$\overline{C} = \left(\frac{\text{Exp. } \rho'(0)}{\text{Form (18)}}\right)$
$Cu(NH_4)_2(SO_4)_2 \cdot 6H_2O$	200	2.0	5.7	2.8
$CuSO_4 \cdot 5H_2O$	370	1.1	4.2	3.8
$Cu(BrO_3)_2 \cdot 6H_2O$	250	1.6	7.1	4.4
$CuCl_2 \cdot 2H_2O$	590	0.69	6.0	8.7

[9] A. Wright, thesis, Harvard, 1949.
[10] G. E. Pake and E. M. Purcell, Phys. Rev. **74**, 1184 (1948).

Formulas (48) and (17) result in

$$\rho'(0)=(\pi/2\langle\nu^2\rangle_{Av})^{\frac{1}{2}}[1+\tfrac{1}{8}(\langle\nu^4\rangle_{Av}/\langle\nu^2\rangle_{Av}^2-3)]. \quad (49)$$

A comparison of (18) and (49) shows that a theoretical calculation, say $\bar{C}'$, of the coefficient $\bar{C}$ of Table I, in this approximation, is just

$$\bar{C}'=\{1+\tfrac{1}{8}[\langle\nu^4\rangle_{Av}/\langle\nu^2\rangle_{Av}^2-3]\}=1+(\tfrac{1}{8})0.43A^2. \quad (50)$$

In a purely formal way, without considering whether or not the function (48) is a good enough approximation to the actual shape function, the A which is necessary according to the experimental values for $\bar{C}$, given in Table I, can be calculated from formula (50). These values of A are called A_1 and are listed in column 3 of Table II.

Now let us investigate the convergence of the sequence (9) near the origin $\nu=0$, as it depends on the magnitude of A. The next approximation, $f_6(\nu)$, will differ from $f_4(\nu)$ by

$$f_6(\nu)-f_4(\nu)=\left[\langle\nu^6\rangle_{Av}-\int_0^\infty \nu^6 f_4(\nu)d\nu\right]\Big/6!$$
$$\times(d/d\nu)^6\exp(-\nu^2/2\langle\nu^2\rangle_{Av}). \quad (51)$$

At the origin this becomes

$$-15[\langle\nu^6\rangle_{Av}-15\langle\nu^2\rangle_{Av}\langle\nu^4\rangle_{Av}+30(\langle\nu^2\rangle_{Av})^3]/[6!(\langle\nu^2\rangle)_{Av}^3]. \quad (52)$$

The condition that the expression (49) for $\rho'(0)$ be a good approximation is therefore that

$$|15[\langle\nu^6\rangle_{Av}-15\langle\nu^2\rangle_{Av}\langle\nu^4\rangle_{Av}+30(\langle\nu^2\rangle_{Av})^3]/[6!(\langle\nu^2\rangle_{Av})^3]|$$
$$\ll[\langle\nu^4\rangle_{Av}/(\langle\nu^2\rangle_{Av})^2-3]/8. \quad (53)$$

The moment $\langle\nu^6\rangle_{Av}$ is not known; however it is reasonable to expect that

$$\langle\nu^6\rangle_{Av}\cong[C_1A^4+C_2A^2+C_3](\langle\nu^2\rangle_{Av})^3 \quad (54)$$

with $C_1\cong 0.1$, $C_2\cong 3$, and $C_3\cong 15$.[9] The expression (53), written, using (54), in terms of A, becomes

$$|0.1A^4-3A^2|\ll 2.5A^2 \quad \text{or}$$
$$A\ll[(1/0.1)(2.5+3)]^{\frac{1}{2}}=7. \quad (55)$$

Thus, for $A\ll 7$ formula (49) will be an adequate approximation. When A is of the order of 7 or larger however, the convergence of the sequence (9) will be very slow and another approach is indicated. We will return briefly to this question after we have considered other methods of estimating A accurately.

There are two further methods of estimating A which we will consider. The first of these is based on the formula (56) below for the ratio of the specific heat constant b to Curie's constant C, in terms of A and H_i of (15):

$$(b/C)=(b_{\text{mag.}}+b_{\text{exch.}})/C=(H_i^2/2)[1+0.36A^2]. \quad (56)$$

This formula is due to Van Vleck;[11] the experimental determination of (b/C) has been made from spin-lattice relaxation data by Broer and Kemperman,[2] and by Volger, Vrijer, and Gorter,[3] for Cu salts. Column 4 of Table II gives (b/C) as derived from their data; column 5 gives A_2 as obtained from these values of (b/C) and formula (56).

The second method is based on formula (57), due to Opechowski,[12] for the temperature constant Θ occurring in the Curie-Weiss formula for the static susceptibility $\chi=C/(T-\Theta)$, in terms of b, the gas constant R, and the number of nearest neighbors $b-b_{\text{mag.}}$ of a paramagnetic atom:

$$(b-b_{\text{mag.}})/R=b_{\text{exch.}}/R=3\Theta^2/2z. \quad (57)$$

Formula (56) in turn relates b to A and H_i. The number of nearest neighbors z is usually 6; R is $8.315\cdot 10^7$. Column 6 of Table II gives values for several salts; column 7 gives values for A_3, as derived from formulas (57), with (56) and these values for Θ.

The first point to be noticed in Table II is that A_2 and A_3 agree well for all substances for which both methods are available. The agreement is well within experimental error. Thus we may regard A as known from A_2 and A_3.

For $CuNH_4(SO_4)_2\cdot 6H_2O$ the actual A is thus about 4.5. The inequality (55) is satisfied to a first order of magnitude, but not accurately. This is reflected in the fact that A_1 is 6; thus A_1 and A_2 certainly agree to order of magnitude, but not accurately. The disagreement is moreover in the proper direction. For $A=4.5$ the left-hand side of (53) is negative; therefore, as can be seen from (52), the next contribution to $\rho'(0)$ is positive. Thus the actual A should be, and is, smaller than A_1. Unfortunately, no data on $\rho'(0)$ are available for $CuK_2(SO_4)_2\cdot 6H_2O$; thus no A_1 can be calculated. The agreement would presumably be a little better for this substance.

The remaining substances do not have exchange coupling of such a magnitude, as indicated by A_2 and A_3, that the inequality (55) is satisfied. Thus the parentheses in the A_1 column indicate that (48) and (49) are not good approximations and agreement with A_2 and A_3 should not be expected. All the A_1 in parentheses are less than A_2 and A_3, as would be expected, since the next contribution (52) to $\rho'(0)$ is negative in these cases. Thus the values for A_2 and A_3 are at least adequate to account for the observed values of $\rho'(0)$.

Thus we may say that the above theory agrees with experiment as far as it goes. For the substances with very large values of the exchange constant, another mathematical method of approach to the problem other than that based on (8) and (9) is indicated. The same mathematical situation exists at the Larmor frequency in a perpendicular field; calculations on this

[11] J. H. Van Vleck, J. Chem. Phys. 5, 320 (1937).
[12] W. Opechowski, Physica 4, 181 (1937).

TABLE II. Magnitude of the exchange coupling by various methods.

Substance	H_i	A_1	$(b/C)\cdot 10^{-6}$	A_2	Θ	A_3
$Cu(NH_4)_2(SO_4)_2\cdot 6H_2O$	200	6	0.18	4.5	—	—
$CuK_2(SO_4)_2\cdot 6H_2O$	220	—	0.12	3.3	0.052	3.3
$CuSO_4\cdot 5H_2O$	370	(7)	10–20	25	−0.70	25
$Cu(C_5H_5N)(NO_3)_2$	140	—	0.25	8.3	—	—
$CuCl_2\cdot 2H_2O$	590	(12)	—	—	−5	120
$Cu(BrO_3)_2\cdot 6H_2O$	250	(8)	—	—	1.5	80

subject have been made by Van Vleck.[1] However, the available data for this case also applies to substances for which the exchange coupling is very large, such as $CuSO_4\cdot 5H_2O$ and $CuCl_2\cdot 2H_2O$. The approximation method (9) is not adequate for these cases either. It is uncertain as to what alternate procedure could be used.

Van Vleck[1] has indicated an interesting analogy between the relaxation theory of Bloembergen, Purcell, and Pound,[13] relating to phenomena in substances with molecular rotation, and the theory in terms of moments. He points out that this analogy would predict a value for the line breadth for very large exchange coupling of the order of magnitude $h\langle\Delta\nu^2\rangle_{Av}/\tilde{A}$. The quantity $\tilde{A}$ relates to Van Vleck's notation; changing over the notation to that in terms of A, and using the value which Van Vleck has obtained for the mean square frequency of the Larmor line, we have that the line width should be of the order of magnitude of $2(\langle\Delta\nu^2\rangle_{Av})^{\frac{1}{2}}/A$.

Half-widths of the Larmor line have been obtained for two Cu salts, $CuSO_4\cdot 5H_2O$ and $CuCl_2\cdot 2H_2O$. (Van Vleck has pointed out that, in an effort to reduce the broadening in cupric salts due to anisotropy in the g-factor,[14] it is advisable to use relatively small constant fields, inasmuch as this broadening is proportional to the applied field. Thus the half-breadths which we will use are those furnished by the measurements of Zavoisky,[15] at relatively low resonant frequencies.) We have obtained an A value for each of these two substances: 25 and 120, respectively. The half-widths according to the formula in the preceding paragraph would then be for the two substances, respectively, ~16 gauss and ~5.5 gauss. The observed values are 175 and 125 gauss. One would not expect the difference between observed and predicted values to be off by more than a factor of about two or three because of proportionality factors which could not be obtained through the analogy. However, the conclusive point is that the predicted *ratio* of the two line breadths, which should be independent of any proportionality factors, is ~3. The observed ratio is 1.4. Thus the approach of Bloembergen, Purcell, and Pound does not seem applicable in this case. It is uncertain as to just what the mathematical approach should be.

[13] Bloembergen, Purcell, and Pound, Phys. Rev. **73**, 679 (1948).
[14] M. H. L. Pryce, Nature **162**, 538 (1948).
[15] E. Zavoisky, J. Phys. U.S.S.R. **10**, 170, 197 (1945).

IV. ABSORPTION IN THE APERIODIC LINE IN A PERPENDICULAR MAGNETIC FIELD

In the presence of a perpendicular magnetic field the single absorption band centered about zero frequency shifts to an absorption band centered about the Larmor frequency $g\beta H/h=\nu_L$. In addition, because of the presence of the spin-spin interaction which spoils any selection rule, absorption bands of weaker intensity are present at frequencies of approximately 0, $2\nu_L$, and $3\nu_L$ (and in higher order perturbation processes at still higher multiples of the Larmor frequency). A direct calculation of $\sum_{k,l}'|M_{k,l}|^2$, $\sum_{k,l}\nu_{kl}^2|M_{kl}|^2$, $\cdots$ including all pairs of states k,l as was done in Section III in connection with absorption for no magnetic field present would be completely inappropriate. The sum $\sum_{k,l}'|M_{k,l}|^2$ would give the area under the function $f(\nu)$ including all the absorption lines: in the remaining moments the higher frequency bands would actually contribute more due to the weighting factors of ν_{kl}^2, ν_{kl}^4, $\cdots$. No information at all could be obtained in this way about the low frequency band.

It is necessary to limit the states k,l appearing in the various series in some way to states with energy differences which are $\ll g\beta H$. The problem is to construct, by means of perturbation formulas, an operator expression from $g\beta\sum_i S_{xi}$ which gives the correct matrix elements $(M_x)_{k,l}$ between levels with small energy differences (small compared to $g\beta H$) and no matrix elements for other pairs of states. If we designate this expression by $(M_x)_{l.f.}$, (l.f. meaning low frequency), then the moments to be calculated are

$$\mathrm{Sp}(M_x)_{l.f.}^2;\quad -h^{-2}\,\mathrm{Sp}[\mathcal{H}_0(M_x)_{l.f.}-(M_x)_{l.f.}\mathcal{H}_0]^2;\quad \cdots. \tag{58}$$

A first-order perturbation theory is sufficient to give non-vanishing matrix elements of $g\beta\sum_i S_{xi}$ between states for which $\nu_{kl}\ll\nu_L$. The perturbed low frequency elements for $g\beta\sum_i(S_{xi}-iS_{yi})$ and for $g\beta\sum_i(S_{xi}+iS_{yi})$ will first be calculated, and then an average taken to obtain the low frequency elements of $g\beta\sum_i S_{xi}$. This procedure will be simpler and less ambiguous because the selection rules $\Delta M=-1$ and $\Delta M=+1$ for $\sum_i(S_{xi}-iS_{yi})$ and $\sum_i(S_{xi}+iS_{yi})$, respectively, are sharper than the selection rule $\Delta M=\pm 1$ for $\sum_i S_{xi}$; thus the energy terms of (4) involved in the respective calculations will be more sharply separated from one another.

According to first-order perturbation theory the new wave functions are

$$\psi^{(1)M'P'}=\psi^{(0)M'P'}+\sum_{M'''=M'\pm 2,\pm 1}\times\psi^{0M'''P'''}(\mathcal{H}_1)^{M'''P''';M'P'}/(M'''-M')g\beta H, \tag{59}$$

the factor $(M'''-M')g\beta H$ in the denominator representing a difference of unperturbed energy levels according to (6). Use of the Hermitian properties of the perturbing energy and of the formula

$$F_{M'P';M''P''}=\int\psi^{*M'P'}F\psi^{M''P''}d\tau \tag{60}$$

for the matrix elements of an operator results in the following expression for the first-order perturbed wave functions of an operator F:

$$(F^{(1)})_{M'P';M''P''}=(F^{(0)})_{M'P',M''P''}+\sum_{M'''(\neq M'')P'''}(F^{0})_{M'P';M'''P'''}\times(\mathcal{H}_1)_{M'''P''';M''P''}/(M'''-M'')g\beta H+\sum_{M'''(\neq M')P'''}(\mathcal{H}_1)_{M'P';M'''P'''}\times(F^{0})_{M'''P''';M''P''}/(M'''-M')g\beta H. \quad (61)$$

Let the operator F now be $g\beta\sum_i(S_{xi}-iS_{yi})$. The zeroth-order elements $F^{(0)}{}_{M'P';M''P''}$ are then

$$(F^{(0)})_{M'P';M''P''}=\delta^{M'}{}_{M'-1}(F^{(0)})_{M'P';M'+1P''}. \quad (62)$$

Substitution of (62) into (61), together with $M'=M''$ in order to get low frequency elements, results in

$$F^{(1)}{}_{M'P';M'P''}=[F^{0}\mathcal{H}_1{}^{\Delta M=-1}-\mathcal{H}_1{}^{\Delta M=-1}F^{0}]_{M'P'M'P''}/g\beta H_D. \quad (63)$$

That part of $\mathcal{H}_1$ with matrix elements of the type

$$(\mathcal{H}_1)_{M'+1,P''';M'P''} \text{ or } (\mathcal{H}_1)_{M'P';M'-1,P'''} \text{ is } \mathcal{H}_1{}^{(3)}; \quad (64)$$

therefore (64) becomes

$$[g\beta\textstyle\sum_i(S_{xi}-iS_{yi})]_{l.t.}=(1/H_D)[\sum_i(S_{xi}-iS_{yi}),\mathcal{H}_1{}^{(3)}]. \quad (65)$$

A similar expression holds for the matrix elements

$$[g\beta\textstyle\sum_i(S_{xi}+iS_{yi})]_{l.t.}:$$

$$[g\beta\textstyle\sum_i(S_{xi}+iS_{yi})]_{l.t.}=(1/H_D)[\sum_i(S_{xi}+iS_{yi}),\mathcal{H}_1{}^{(4)}], \quad (66)$$

the appropriate part of $\mathcal{H}_1$ being $\mathcal{H}_1{}^{(4)}$. Direct commutation results in

$$[g\beta\textstyle\sum_i(S_{xi}+iS_{yi})]_{l.t.}=(g^2\beta^2/H_D)\sum_{i,j}{}' F_{ij}{}^{*}r_{ij}{}^{3}\times[2S_{zi}S_{xj}-S_{xi}S_{zj}-S_{yi}S_{yj}] \quad (67)$$

$$[g\beta\textstyle\sum_i(S_{xi}-iS_{yi})]_{l.t.}=-(g^2\beta^2/H_D)\sum_{i,j}{}' F_{ij}r_{ij}{}^{-3}\times[-2S_{zi}S_{zj}+S_{xi}S_{xj}+S_{yi}S_{yj}]. \quad (68).$$

An average of (67) and (68) then results in

$$[g\beta\textstyle\sum_i S_{xi}]_{l.t.}=(g^2\beta^2/H_D)\sum_{i,j}{}'(-\frac{3}{2}\gamma_{ij}\alpha_{ij})r_{ij}{}^{-3}\times[2S_{zi}S_{zj}-S_{xi}S_{xj}-S_{yi}S_{yj}]. \quad (69)$$

It must be remembered that the direction cosines in (69), and in the commutator of (69) with $\mathcal{H}_0$, refer to axes such that the magnetic field is along the z axis. In order to make use of the usual lattice sums in any equations the transformation formulas

$$\gamma_{ij}=\lambda_1\alpha_{ij}'+\lambda_2\beta_{ij}'+\lambda_3\gamma_{ij}';\ \alpha_{ij}=\nu_1\alpha_{ij}'+\nu_2\beta_{ij}'+\nu_3\gamma_{ij}' \quad (70)$$

must be used. The expression which will be obtained for the zeroth and second moments of $f(\nu)$ will be functions of the cosines λ_1, λ_2, λ_3 of the field H_0 with respect to the crystalline axes; and also of the direction cosines ν_1, ν_2, ν_3 of the oscillating field $H_0\exp(2\pi i\nu_2)$ with respect to these axes. These expressions will then be averaged over all directions of λ_1, λ_2, λ_3, ν_1, ν_2, ν_3. The two resultant moments will refer to a powder, and will be those of interest since the physical measurements have been made only on powders.

In order to calculate the zeroth moment of $f(\nu)$, (69) must be squared and averaged over the spin functions, then the transformation formulas (70) must be applied, and appropriate lattice sums substituted. For a calculation of the second moment, the commutator of (69) with $\mathcal{H}_0$ is the expression to be squared and evaluated. The results of these two calculations are

$$\langle\nu^0\rangle_{Av}=0.72g^4\beta^4NS^2(S+1)^2H_D{}^{-2}d^{-6}\times[1+6.8(\lambda_1{}^2\nu_1{}^2+\lambda_2{}^2\nu_2{}^2+\lambda_3{}^2\nu_3{}^2)] \quad (71)$$

$$\langle\nu^2\rangle_{Av}=g^4\beta^4\hbar^{-2}d^{-6}[1+6.8(\lambda_1{}^2\nu_1{}^2+\lambda_2{}^2\nu_2{}^2+\lambda_3{}^2\nu_3{}^2)]^{-1}\cdot\{S(S+1)[-50(\lambda_1{}^6\nu_1{}^2+\lambda_2{}^6\nu_2{}^2+\lambda_3{}^6\nu_3{}^2)+100(\lambda_1{}^2\lambda_2{}^2\nu_3{}^2+\lambda_1{}^2\lambda_3{}^2\nu_1{}^2+\lambda_2{}^2\lambda_3{}^2\nu_1{}^2)-100\lambda_1{}^2\lambda_2{}^2\lambda_3{}^2+(43+49A^2)(\lambda_1{}^2\nu_1{}^2+\lambda_2{}^2\nu_2{}^2+\lambda_3{}^2\nu_3{}^2)+32(\lambda_1{}^4+\lambda_2{}^4+\lambda_3{}^4)+(-26+3A^2)]-7A^2(\lambda_1{}^2\nu_1{}^2+\lambda_2{}^2\nu_2{}^2+\lambda_3{}^2\nu_3{}^2)\}. \quad (72)$$

In calculating $\langle\nu^2\rangle_{Av}$ the terms involving a single power of A have been calculated to be zero or have been estimated to be small. Thus in view of difficulties involved in calculating them they have been omitted. Because of an accidental cancellation it was possible to calculate the pure dipole terms in (72) accurately without too great difficulty, also the pure exchange terms are accurate. The expression for $\langle\nu^0\rangle_{Av}$, (71), is also accurate. The appropriate expressions for a powder have been calculated by averaging (71) and (72) over λ_1, λ_2, λ_3, ν_1, ν_2, ν_3 as

$$\langle\nu^0\rangle_{Av}=1.7g^4\beta^4NS^2(S+1)^2H_D{}^{-2}d^{-6}, \quad (73)$$

$$\langle\nu^2\rangle_{Av}=g^4\beta^4\hbar^{-2}d^{-6}[S(S+1)(5.0+5.0A^2)-0.6A^2]. \quad (74)$$

The approximation to $f(\nu)$ if two moments are known is just $f_2(\nu)$, a Gaussian shape function:

$$f_2(\nu)=(2/\pi\langle\nu^2\rangle_{Av})^{\frac{1}{2}}\exp(-\nu^2/2\langle\nu^2\rangle_{Av}), \quad (75)$$

$\langle\nu^0\rangle_{Av}$, and $\langle\nu^2\rangle_{Av}$ being given by (73) and (74), respectively. Such a Gaussian is presumably a good approximation to the shape function, since exchange enters into the mean square frequency (74) in contrast

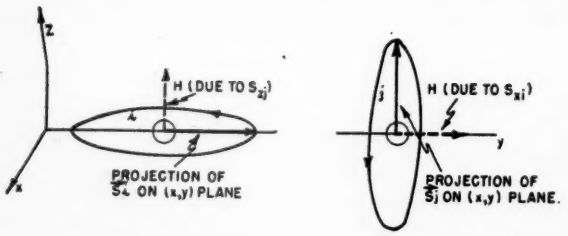

FIG. 2. Explanation of exchange broadening in terms of Larmor precessions; the quantity $S_{xi}+S_{xj}$ remain constant (zero) at all points of the cycle, thus no energy can be absorbed in the x direction.

to the situation for the line with no field present or for the Larmor line in a perpendicular field. Therefore, there is no such phenomenon as exchange narrowing present to any great degree in the case that we are discussing, but rather an exchange broadening. The situation here is not critically dependent upon the higher moments to any large extent, since (74) with (75) takes both dipole and exchange forces into account. The fourth moment calculated mathematically will be of the order A^4; also the fourth moment calculated from (75) is of order A^4. Similarly, all higher moments are given correctly as regards order of magnitude by integrating (75).

It is perhaps interesting to consider the difference between exchange narrowing and exchange broadening on the basis of a Larmor precession model. The first point to be noticed is that dipolar broadening is always present. One can in the usual way,[13] regard a dipolar term of the type $\sum_{i>j}g^2\beta^2r_{ij}^{-3}B_{ij}S_{zi}S_{zj}$ as analogous to a sort of Zeeman energy, with $\sum_j g\beta r_{ij}^{-3}B_{ij}S_{zj}$ representing a mean dipolar field due to atoms j acting on the magnetic moment $g\beta S_{zi}$ of atom i. This field will vary as atom i varies; thus the resonance frequency will shift slightly over the crystal and the absorption line will be spread out. A measure of the magnitude of the dipolar field is H_i; thus we expect, and always find, a term in the root-mean-square frequency proportional to H_i.

The question arises as to why the exchange interaction cannot always be treated in a similar way, and why there is not always a term in the root-mean-square frequency proportional to AH_i. Figure 2 illustrates an explanation in terms of Larmor precessions for the case of absorption in the absence of a magnetic field. The mathematical explanation is, of course, that $g\beta\sum_i S_{xi}$, the relevant component of the magnetic moment, commutes with the exchange energy, as pointed out in Section III. The exchange interaction, as far as just two atoms are concerned, is proportional to $S_{xi}S_{xi}+S_{yi}S_{yj}+S_{zi}S_{zj}$. Figure 2 interprets the term $S_{zi}S_{zj}$ as a field in the z direction, S_{zj}, due to atom j, acting on atom i; and the term $S_{yi}S_{yj}$ is similarly interpreted as a field in the y direction due to atom i acting on atom j. Figure 2 is drawn for an instant of time such that $S_{yi}>0$, $S_{zj}>0$. The moments S_{xi}, S_{xj} at this particular instant of time are zero, and the directions of precession, as shown in the figure, are such that the sum $S_{xi}+S_{xj}$ remains zero at all later points of the cycle. Thus any absorption due to the precessional motion of one of the atoms is canceled by an equal and opposite effect due to the other atom, and no net absorption at a frequency other than zero can occur as a result of the effects of exchange.

We thus see that there will be no exchange broadening in this case. Not only will the exchange precessions cause no spreading of the absorption however, but they will tend to disrupt the precessional effects of the dipole terms which do contribute to the broadening. Thus there will finally be a certain narrowing effect of the exchange interaction.

The cancellation shown in Fig. 2 depends on the equality of the magnitudes of the magnetic moments under consideration for the two atoms i and j. If the magnetic moments are to be calculated by means of a perturbation calculation, then the magnitude of this moment for an atom will vary over the crystal as the mean field acting on the atom varies. The magnitudes in Fig. 2 for atoms i and j will not be the same and cannot cancel at all instants of time. In this case the exchange effects can be pictured as fluctuating fields, and exchange broadening is present.

Experiments[3] have determined the variation of the absorption coefficient $\rho'(0)$ as a function of the magnetic field H_D. According to the definition (17), for a shape function (75), $\rho'(0)$ in large fields is given by

$$\rho'(0)=0.61[0.30(1+0.9A^2)]^{-\frac{1}{2}}(H_i^2/2H_D^2)\times[\pi^{\frac{1}{2}}h/(2^{\frac{1}{2}}g\beta H_i)]. \quad (76)$$

We know, moreover, what $\rho'(0)$ is for $H_D=0$; the expression (18) times $\bar{C}$, with $\bar{C}$ determined experimentally (see Table I). A reasonable method of combining $\rho'(0)$ for no field and (76) into one formula is on the basis of a Debye curve

$$\rho'(H_D,\nu=0)=\rho'(0,0)(H_i^2/2)/[(H_i^2/2)+pH_D^2] \quad (77)$$

with p as calculated on this basis given by

$$p=0.9\bar{C}[1+0.9A^2]^{\frac{1}{2}}. \quad (78)$$

The experiments of Volger, Vrijer, and Gorter determine $(\rho'(H_D)/\rho'(H_D=0))$ as a function of H_D for several Cu salts. Consequently, a direct comparison of (77), (78) with experiment is possible. Figure 3 shows this comparison for Cu salts, for which $\bar{C}$ has also been measured. Curve A in Fig. 3 shows (77) for $p=0.9\bar{C}[1+0.9A^2]^{\frac{1}{2}}$, as given in (78); curve B shows (77) for $p=0.9[1+0.9A^2]^{\frac{1}{2}}$. Both these cases are important for two reasons. In the first place, this correction in formula (78) is in a sense a phenomenological one. The value of $\bar{C}$ as it differs from unity is due to higher order corrections to the theory for an A of zero; these corrections are very difficult to evaluate. In the second place, there will be higher order corrections to the function (75), which could be taken into account by

introducing an analogous constant $\bar{K}$ into (75) and (76). Then (78) would be

$$p=0.9(\bar{C}/\bar{K})(1+0.9A^2)^{\frac{1}{2}}. \quad (79)$$

It is believed that these corrections will be of a lower order of magnitude than in the case with no field present, since the mean square frequency includes the first-order effect of exchange as well as of the dipole forces. Thus $\bar{K}$ will never exceed $\bar{C}$. However, for a substance such as $CuCl_2 \cdot 2H_2O$, in which A is very large, it is possible that these corrections might be appreciable. Thus, the experimental curve in large fields should lie somewhere between (77) with $p=0.9\bar{C}(1+0.9A^2)^{\frac{1}{2}}$ and with $p=0.9(1+0.9A^2)^{\frac{1}{2}}$. A glance at Fig. 3 shows that for $Cu(NH_4)_2(SO_4)_2 \cdot 6H_2O$, the substance for which we might expect the best agreement, the curves agree at large H_D pretty well with the experimental curves. It is gratifying that the curve with the observed value of $\bar{C}$ in p agrees a little better as far as numerical values go with the experimental curve. It is also to be noted that the curve with $\bar{C}=1$ in p lies above the experimental curve at large H_D, thus the correction to (75) is small and $\bar{K}$ is less than $\bar{C}$.

The increase near the origin over the theoretical curves, present in all the substances investigated, is due to the absorption from the Larmor line, which is not yet resolved out for these values of the magnetic field. The position of the Larmor line is $\nu_L \alpha H_D$, and a field strength roughly the breadth of the Larmor line in Gauss is necessary to resolve out this line. Due to the exchange narrowing of the Larmor line in a perpendicular field this is accomplished for relatively weak fields in a perpendicular field; however in a parallel field the Larmor line is exchange broadened, and the resolution is difficult to obtain. This point will be referred to later (see the end of Section V).

V. ABSORPTION AT LOW FREQUENCIES IN A PARALLEL MAGNETIC FIELD

The relevant component of the magnetic moment whose shape function $f(\nu)$ is to be investigated is in this case

$$M_z=g\beta\sum_i S_{zi}. \quad (80)$$

It has been pointed out by Broer[4,7] that low frequency matrix elements of this operator vanish, when these elements are calculated on the basis of a first-order perturbation treatment. Use of a second-order perturbation theory is necessary. As Broer observes, the moments of the shape function, $\langle\nu^0\rangle_{Av}$, $\langle\nu^2\rangle_{Av}$, $\cdots$ will be proportional to (H_i^4/H_c^4) in such a situation. Now, in describing the experimental results it is customary to

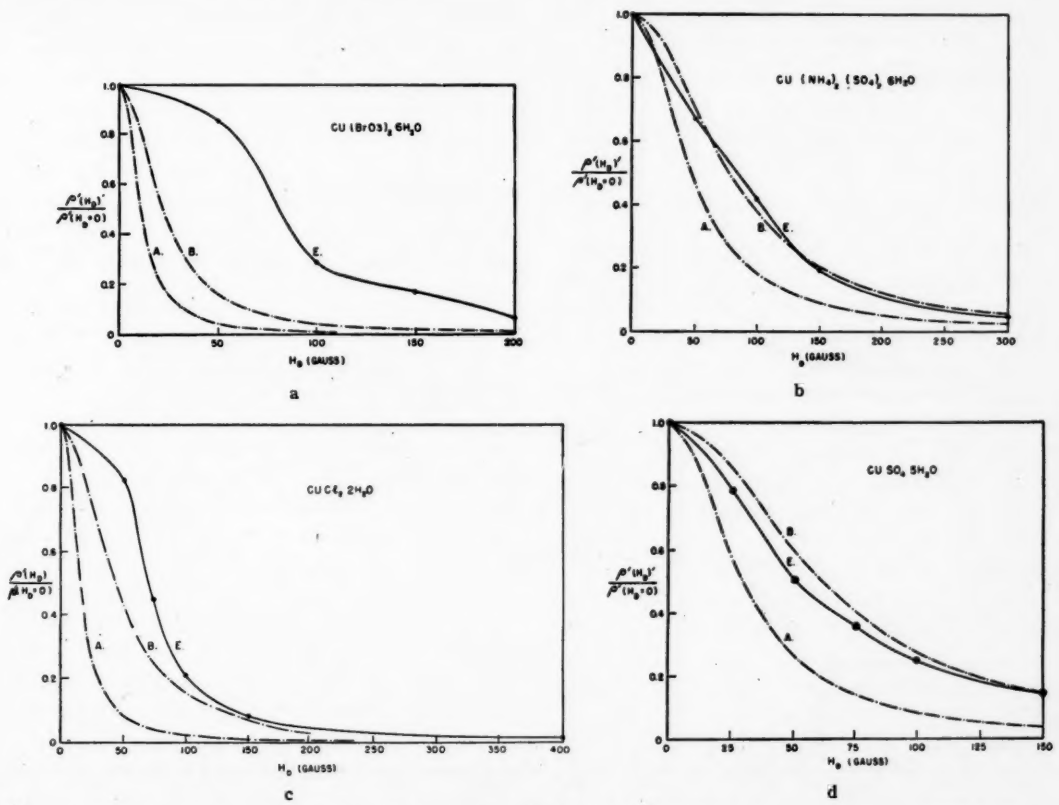

FIG. 3. The theoretical variation with field strength of the absorption coefficient at zero frequency, $\rho'(H_D)$. Curves E are the experimental curves. Curves A are theoretical curves of the type (77) with p given in (78); curves B are theoretical curves of the type (77) with p given by (78) without a $\bar{C}$. The reasons for these two theoretical curves are given in the text.

modify the definition (17) in the presence of a parallel magnetic field. The usual definition in the presence of a magnetic field H_c is

$$\rho'(0)=\pi[2kT\chi_{\text{adiabatic}}]^{-1}f(0);\qquad \chi_{\text{adiabatic}}=b\chi_0/(b+CH_c)^2. \quad (81)$$

Thus two powers of H_c are removed by the definition (81), therefore, according to the theory for the aperiodic line the quantity $\rho'(0)$ as defined by (81) should be proportional to H_i^2/H_c^2.

Experiments have been carried out for magnetic fields several times the mean dipolar field H_i for a good many substances; in no case has a significant decrease been observed. Figure 4 summarizes the observed situation: the first number in parenthesis gives the mean dipolar field for the salt.

It was uncertain as to whether or not this effect was compatible with the theory, since no quantitative calculations had been made. Therefore, we have calculated the zeroth and second moments of $f(\nu)$; and obtained an approximation to the absorption coefficient $\rho'(0)$ by fitting the known $\rho'(0)$ at zero field and the calculated value at large fields with a Debye curve. The zeroth and second moments have been calculated to be

$$\langle\nu^0\rangle_{Av}=3.0g^6\beta^6NS^2(S+1)^3H_c^{-4}d^{-12}=0.13\chi_0kT(H_i^2/2H_c^2)^2 \quad (82)$$

$$\langle\nu^2\rangle_{Av}=2.4(1+1.8A^2)g^4\beta^4h^{-2}d^{-6}=0.19(1+1.8A^2)g^2\beta^2H_i^2/h^2. \quad (83)$$

Both formulas are calculated for a specific direction of the field H_c, corresponding to $\lambda_1=\lambda_2=0$, $\lambda_3=1$. Also the expression (83), because of its complicated nature, has been calculated for a spin of $\frac{1}{2}$. The theoretical formula for $\rho'(0)$, according to (82) and (83), can be reasonably taken to be

$$\rho'(H_c,\nu=0)=\rho'(0,0)[(H_i^2/2)/(H_i^2/2+pH_c^2)], \quad (84)$$

with

$$p=\bar{C}[3.0(1+1.8A^2)^{\frac{1}{2}}(1+0.36A^2)], \quad (85)$$

just as in the perpendicular field case. Formula (85) shows that the predicted decrease of $\rho'(0)$, proportional to $1/H_c^2$, should take place in fields the order of $H_i/A^{\frac{1}{2}}$; thus quantitative calculations only emphasize the discrepancy between theory and experiment. For

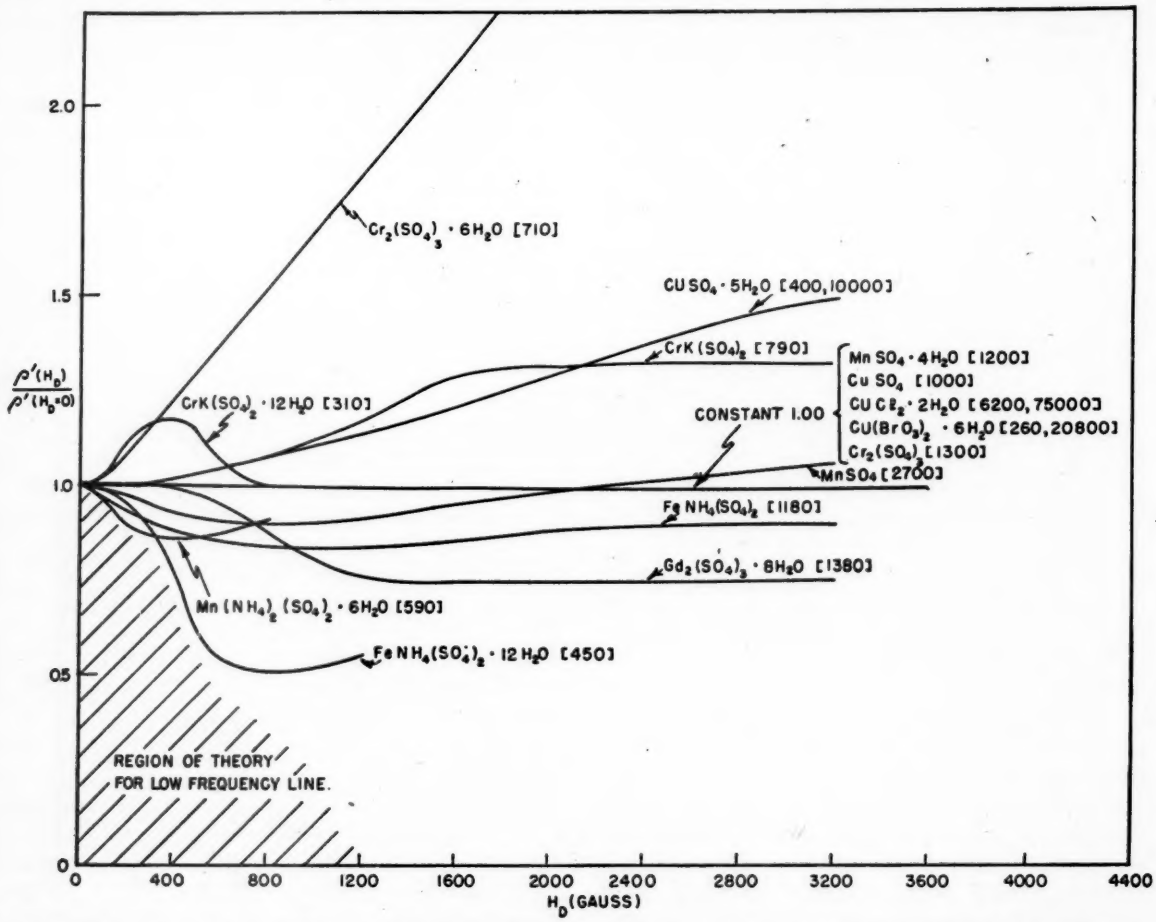

FIG. 4. Experimental variation of $\rho'(H_c)$ as a function of H_c, the parallel constant magnetic field, for various salts. The first term in brackets in H_i, the second term (given when known) is AH_i. (*Note:* The subscripts to H which appear in the figure should be C, not D.)

this reason a sketch of the calculation of (82), (83), (84), and (85) shall not be given.[9] Instead, a proposed explanation of this discrepancy will be presented.

It must be remembered, as was mentioned at the conclusion of Section IV, that a certain minimum field strength is necessary to resolve out the Larmor line and make measurements at low frequencies actually refer to the aperiodic line. Now, in a parallel field the Larmor line is exchange broadened; this means that the breadth of this line, which is of order of magnitude of the mean square frequency of the line, varies as

$$[1+\text{const.}\cdot A^2]g\beta H_i/h. \tag{86}$$

Also it is to be noticed that the field strength necessary to resolve out this line is roughly (86), its line breadth, measured in Gauss. Thus exchange broadening of the Larmor line in a parallel field implies that field larger by factors of 10 or 100 than the mean dipolar field are necessary to effect this resolution. Such fields have not yet been used experimentally, as the second term in parentheses in Fig. 4 shows. This term is AH_i, and is given for those (copper) salts for which A is known. Thus the experimental data actually refers to the unresolved Larmor line, for which $\rho'(0)$, as defined by (81), should be roughly constant for fields so far used.

A number of effects will influence the variation of $\rho'(0)$. First, the shift of position of the Larmor line must be taken into account; second, its shape about this mean position is important; and third, the low frequency line will have a small effect. A combination of these variations causes the observed behavior shown in Fig. 4 and makes this behavior somewhat difficult to predict. Also an arbitrary factor has been removed in the definition (81), which probably is not quantitatively correct. If too large a factor has been removed, $\rho'(0)$ increase with H_c, and vice versa. The important thing to notice is that the average behavior is around constancy.

VI. THE ADIABATIC AND ISOLATED SUSCEPTIBILITIES

The situation with regards to the Larmor line in a parallel constant field is slightly different from that for the absorption lines corresponding to the various conditions discussed in the preceeding sections. There are no measurements on the absorption line as regards its shape and intensity in this case; thus the mean square frequency is not of interest. However the sum of $\langle\nu^0\rangle_{Av}=\int_0^\infty f(\nu)d\nu$ for the Larmor line and for the line at double the Larmor frequency is just proportional to the isolated susceptibility for the spin system in large fields. This latter susceptibility is of a great deal of interest as far as its numerical agreement or disagreement with the adiabatic susceptibility of Casimir and du Pre[16] is concerned.

[16] H. B. G. Casimir and F. K. du Pre, Physica 5, 507 (1938).

The experimental situation is as follows: in studies of spin-lattice relaxation usually the susceptibility χ'_{lattice}[16] obeys a relation of the following sort within the accuracy of the experiments,

$$\chi'_{\text{lattice}}=\chi_\infty+(\chi_0-\chi_\infty)/(1+\rho^2\nu^2), \tag{87}$$

with ρ a constant with respect to ν. According to one point of view, χ_∞ is the contribution to the susceptibility $\chi=(\partial M/\partial H_c)_T$, obtained upon differentiation of $M=[\sum_i[-\partial W/\partial H_c]\exp(-W_i/kT)]/[\sum_i\exp(-W_i/kT)]$, keeping the factors $\exp(-W_i/kT)$ constant, and differentiating only $(-\partial W_i/\partial H_c)$ with respect to H_c. For sufficiently high frequency the spin system may be considered isolated; and since the distribution of systems in the various energy states, given by the factors $\exp(-W_i/kT)$, cannot change for an isolated substance, the quantity

$$\chi_{\text{iso}}=[\sum_i(-\partial^2W_i/\partial H_c^2)\exp(-W_i/kT)]/[\sum_i\exp(-W_i/kT)]$$

thus obtained is the isolated susceptibility of the system according to statistical mechanics. On the other hand, according to the thermodynamic theory of Casimir and du Pre,[16] χ_∞ is the adiabatic susceptibility

$$\chi_{\text{adiabatic}}=[b/(b+CH_c^2)]\chi_0. \tag{88}$$

It is not definite as to whether these quantities, the isolated and the adiabatic susceptibilities, are actually the same.**

The adiabatic susceptibility is in large fields inversely proportional to H_c^2:

$$\chi_{\text{adiabatic}}\sim(b/C)\chi_0/H_c^2;\ (b/C)=(1+0.36A^2)H_i^2/2. \tag{89}$$

Matrix elements of the magnetic moment $g\beta\sum_i S_{zi}$ which are, when squared and averaged, inversely proportional to H_c^2, can be obtained with the Hamiltonians (3) and (4) for the unperturbed and perturbing energies, by using a first-order perturbation theory. Division by kT will then result in the isolated susceptibility in large fields for a system with the Hamiltonian [(3)+(4)]. It is found that the appropriate matrix elements will be just the area under $f(\nu)$ for the Larmor line plus this area for the line at double the Larmor frequency.

A perturbation formula similar to (63) is necessary. The usual commutation relations then result in the following expression for the isolated susceptibility in

** Van Vleck (unpublished) has calculated an expression for the difference between the two susceptibilities. His results show that the difference between the two susceptibilities will vanish only if the energies W_i or the derivatives $\partial W_i/\partial H_c$ coincide for all states i of the spin system, or if the energy depends on the fields H_c as $W_i=W_i^{(0)}\varphi(H_c)+\psi(H_c)$ with φ, ψ the same for all i. The actual expression which he obtains for the difference $\chi_{\text{ad}}-\chi_{\text{iso}}$ is

$$(1/kT)[(\langle W^2\rangle_{Av}-\bar{W}^2)(\langle W'^2\rangle_{Av}-\langle W'\rangle_{Av}^2)-(\langle WW'\rangle_{Av}-\bar{W}\langle W'\rangle_{Av})^2]/[\langle W^2\rangle_{Av}-\bar{W}^2],$$

W' being $(\partial W/\partial H_c)$.

large fields:

$$\chi_{\text{iso}}=[kTH_c^2]^{-1}\left[\sum_{i=1}^{4}\langle|\mathcal{H}_1{}^i|^2\rangle_{\text{Av}}\right]. \quad (90)$$

The energy terms can be easily squared and averaged; when this is done the following result is obtained:

$$\chi_{\text{iso}}=\frac{4}{9}g^4\beta^6S^2(S+1)^2(kTH_c^2)^{-1}\sum_{i,j}{}'\,r_{ij}^{-6}[|F^{ij}|^2+|D^{ij}|^2]. \quad (91)$$

It is necessary to make substitutions similar to (70) in (91), and then average over all directions of λ_1, λ_2, λ_3. The following values then result for the lattice sums:

$$\sum_{i,j}{}'|F^{ij}|^2r_{ij}^{-6}=\sum_{i,j}{}'|D^{ij}|^2r_{ij}^{-6}=2.52. \quad (92)$$

Substitution into (91) then gives

$$\chi_{\text{iso}}=2.24g^4\beta^4S^2(S+1)^2/(kTH_c^2). \quad (93)$$

Use of $\chi_0=Ng^2\beta^2S(S+1)/3kT$ and (15) then results in

$$\chi_{\text{iso}}=0.80\chi_0H_i^2/2H_c^2. \quad (94)$$

L. J. F. Broer has made an independent calculation of the ratio of the adiabatic and isolated susceptibilities for spins in a large field without exchange (private communication). He arrived at the factor of 0.80. This factor is the same as that of (94).

VII. ACKNOWLEDGMENTS

In conclusion, the writer should like to take this opportunity of expressing her deep appreciation to Professor J. H. Van Vleck for suggesting this subject as a research topic. She would like to acknowledge his invaluable counsel and helpful criticism. Also she would like to express her appreciation for the Atomic Energy Commission Predoctoral Fellowship which made this research possible.

PHYSICAL REVIEW VOLUME 76, NUMBER 12 DECEMBER 15, 1949

Precision Wave-Length Measurements of the 1.1- and 1.3-Mev Lines of Co^{60} with the Two-Meter Focusing Curved-Crystal Spectrometer*

DAVID A. LIND, J. R. BROWN, AND JESSE W. M. DUMOND
California Institute of Technology, Pasadena, California

(Received August 15, 1949)

Recent improvements in the two-meter focusing curved-crystal gamma-ray spectrometer are described which have extended its quantum energy range well above 1 Mev and have also yielded much better luminosity and resolving power than were obtained initially. The improved components are (1) the crystal holder whose aperture and resolving power have been nearly doubled and (2) the collimator the new model of which can now discriminate between the reflected and transmitted beams when these differ in direction by only 8 minutes of arc, a threefold improvement over our first model. Our plans for further possible improvements and the factors governing these are also discussed. Wave-lengths of two gamma-rays emitted following β-decay of Co^{60} have been measured with this new equipment using a source of about 50 mc strength and found to have values of $(9.308\pm0.005)\times10^{-11}$ cm and $(10.580\pm0.005)\times10^{-11}$ cm corresponding to quantum energies of 1.3316 ± 0.0010 Mev and 1.1715 ± 0.0010 Mev, respectively. The lines appear to have equal intensities. The integrated reflection coefficient of the (310) planes of the curved-quartz crystal still appears to follow a λ^2-dependence on wave-length down to 9 x.u. the shortest so far observed.

EXTENSION OF THE WAVE-LENGTH RANGE OF THE TWO-METER FOCUSING CURVED-CRYSTAL GAMMA-RAY SPECTROMETER

THE two-meter focusing curved-crystal gamma-ray spectrometer[1–3] has up to the date of the work here described, been applied only to the measurement of nuclear gamma-ray lines of quantum energy equal to or less than 640 kev.[4–7] Many natural and artificial radioactive sources of great interest exist however which have lines in the quantum energy range from 1 to 2 Mev and even far beyond this. Our present experience in measuring these ultra-short wave-lengths by direct crystal diffraction has shown that the upper limit of quantum energy beyond which the precision of the method falls to a value comparable with the precision obtainable with the magnetic β-ray spectrometer is probably fixed by the characteristics of the crystal planes used for the diffraction. In the case of our present two-meter curved-crystal spectrometer utilizing the (310) planes of quartz this limiting precision for the measurement of wave-lengths seems to correspond to an uncertainty of about ±0.005 x.u. This uncertainty is essentially constant independent of the wave-length measured. Thus, at a wave-length of 5 x.u. or about 2.5 Mev, a precision of the order of one part in a thousand in wave-length measurement can still be obtained. It has, therefore, seemed well worth while to try to extend the range of applicatility of the instrument as far as possible above the 1 Mev value. Such an extension requires the following two improvements in the method.

* Assisted by the Joint Program of the AEC and the ONR.

[1] Jesse W. M. DuMond, Rev. Sci. Inst. **18**, 626 (1947).
[2] DuMond, Lind, and Cohen, Rev. Sci. Inst. **18**, 617 (1947).
[3] D. A. Lind, Rev. Sci. Inst. **20**, 233 (1949).
[4] DuMond, Lind, and Watson, Phys. Rev. **73**, 1392 (1948).
[5] Watson, West, Lind, and DuMond, Phys. Rev. **75**, 505 (1949).
[6] DuMond, Lind, and Watson, Phys. Rev. **75**, 1226 (1949).
[7] Lind, Brown, Klein, Muller, and DuMond, Phys. Rev. **75**, 1544 (1949).

(1) The collimator which arrests the transmitted beam but allows the selectively reflected beam to pass unhindered to the multicellular counter, must be improved as regards the minimum angular difference between the directions of these two beams for which it will satisfactorily give the above-mentioned discrimination with adequate contrast.[8] At 3 Mev, for example, and with the (310) planes of quartz, the angular difference between the reflected and transmitted beams is only 8 minutes of arc.

(2) Since the reflecting power of the crystal planes diminishes with dimishing wave-length λ about as λ^2 every means must be directed toward compensating for this rapid loss in intensity without doing so at the expense of increased background. The means at our disposal for this are about five in number as listed below.

(a) We may increase the thickness of the curved-crystal slab. The limit here for quartz with our two-meter radius is at about 2 mm thickness, if the crystal is to have any margin of safety against breakage. Such lamina are now in preparation but to date have not been tried. This will be a twofold gain over the present 1 mm thickness.†

(b) The cross section of the gamma-ray beam may be increased by increasing the window aperture in the curved-crystal clamping holder. Several limitations enter here. Large and perfect specimens of quartz are extremely difficult to obtain beyond a certain size. If the beam has too large an angular opening the resolving power diminishes because of what may be called cylindrical aberration[9] and also vertical divergence. In order to utilize a larger beam opening, the cross section of the multicellular counter or other intensity measuring device must be increased and unless this can be done without a correspondingly great increase in background counting rate, there will be no real gain in contrast to compensate for the loss of crystal reflecting power with decreasing wave-length. The counter background comes from cosmic rays, local radiation from radioactivity of the building and other surroundings, and internal radioactivity of the counter (chiefly alpha-activity in the lead partitions of the counter).

(c) Increased crystal reflection may be sought by using other Miller indices and other crystals. The choice is not wide here, however, because of several restrictions. First, one is limited to small grating constants of the order of one angstrom without which the angular difference between transmitted and reflected beams becomes so small that the construction of a collimator for discriminating between them is practically impossible. Second, the crystal must approach as closely as possible the ideally perfect type in order to give the requisite resolving power. Third, it must be obtainable in large samples free from twinning or distortion with extreme parallelism of the reflecting planes (to within a second or so of arc) over large samples. Fourth, it must be capable of being bent elastically without cleaving or yielding along slip planes. Fifth, it must permit taking high (optical) precision surface figuring and be sufficiently inert chemically to retain its figure and resist deterioration. Preparations are under way to try about five different planes in quartz and a few other crystals such as topaz and sheelite.

(d) Increased counter efficiency (without corresponding increase in background counting rate) may be sought. This can be obtained partly by adjusting the *thickness* of the partitions (from which electrons are ejected by the gamma-ray beam) to an optimum value for the hardness of radiation to be studied. Also, the *number* of partitions should be increased as far as possible. Developments of this sort are under way in the form of a series of multicellular counters of square cross section (to fit more closely the cross section of the beam) in which twice as many partitions per unit length of beam can be introduced as in our present multicellular counters. In the new counter the spacing between partitions is only 0.25 inch and the four-pronged anode spiders between partitions are omitted. Instead of these, four parallel 2-mil tungsten anode wires pass axially through four sets of $\frac{3}{8}$-inch holes in

FIG. 1. Comparison of new and old lead collimators for the two-meter focusing curved-crystal gamma-ray spectrometer. To indicate the scale, a horizontal one-foot rule can be seen at the back of the lead shielding on the new collimator. The cylindrical multicellular counter and the upper half of the lead shields that cover it have been removed. The semicircular cavity that can be seen in the end of the first circular lead shield is provided to accommodate the battery of anticoincidence counters which in operation are situated above the multicellular counter to protect it from cosmic rays. A meter stick stands vertically near the old collimator which is at the right. Both collimators are 30 inches long. The insert is an enlarged view of the exit end of the new collimator, the thicker ends of the tapering lead partitions being visible.

[8] The transmitted beam to be suppressed by the collimator may be from 500 to 2000 times as intense as the selectively reflected beam which it is the object of the instrument to measure.

† Since this manuscript was submitted, we have now had a 2-mm thick quartz lamina bent to a radius of two meters for two months without breakage.

[9] For a discussion of this geometrical aberration, see p. 629 and Fig. 3 of reference 1.

all of the partitions. These counters are, however, still under development and study, and have not been used in the presently described measurements on Co^{60}.

(e) Increased source strength may be sought. There is no gain however, if the source covers a wider arc of the focal circle (in the direction of dispersion of the instrument) than that defined by the resolving power of the crystal. With our present two-meter instrument, this calls for source widths of the order of 0.001 inch. Increased source strength therefore implies increased *specific* source activity and this is limited by the bombarding flux available for exciting the activation.

As we have indicated, four of the five means of increasing intensity listed above (namely, a, c, d and e) are still under development. In the work to be described in this article, the chief improvements effected were under headings (b) and (d), increased crystal window aperture and somewhat increased counter efficiency by the use of more partitions. The counters of square cross section however (with four longitudinal wires and no four pronged spiders) had not as yet been developed when the present work on Co^{60} was done. Specifically, the important improvements made for the present Co^{60} work were:

(1) A new crystal holder with much larger aperture than the first, 1.7×2 inches in dimensions, traversed by two thin horizontal ribs to give extra support to the crystal so as in insure accurate curvature throughout the active window surface. This holder has a focal length of 196 cm and by some improvements in mechanical stiffness of the equipment for the initial grinding of the cylindrical surface,[2] it has been possible to obtain a profile so accurate as to give us a resolution of 0.05 x.u. as regards the aberrations from perfect focusing. This new crystal holder represents a twofold gain over our first attempt both in respect to luminosity and resolving power.

(2) A new collimator with twenty-four (instead of seven) die-cast tapering lead alloy partitions thirty inches long whose thickness at the entry end is only 40 mils. To insure no loss in the fraction of radiation transmitted through such a collimator, these partitions must be rigorously straight and true, a very difficult requirement to meet. In our present new collimator, the transmission which was designed theoretically to be 50 percent turned out by measurement to be about 35 percent. The geometry of the new collimator is such that if we ignore scattering upon and penetration of the radiation into the lead plates the least angular difference between transmitted and reflected beams between which the collimator will discriminate is 8 minutes of arc. This corresponds to a calculated theo-

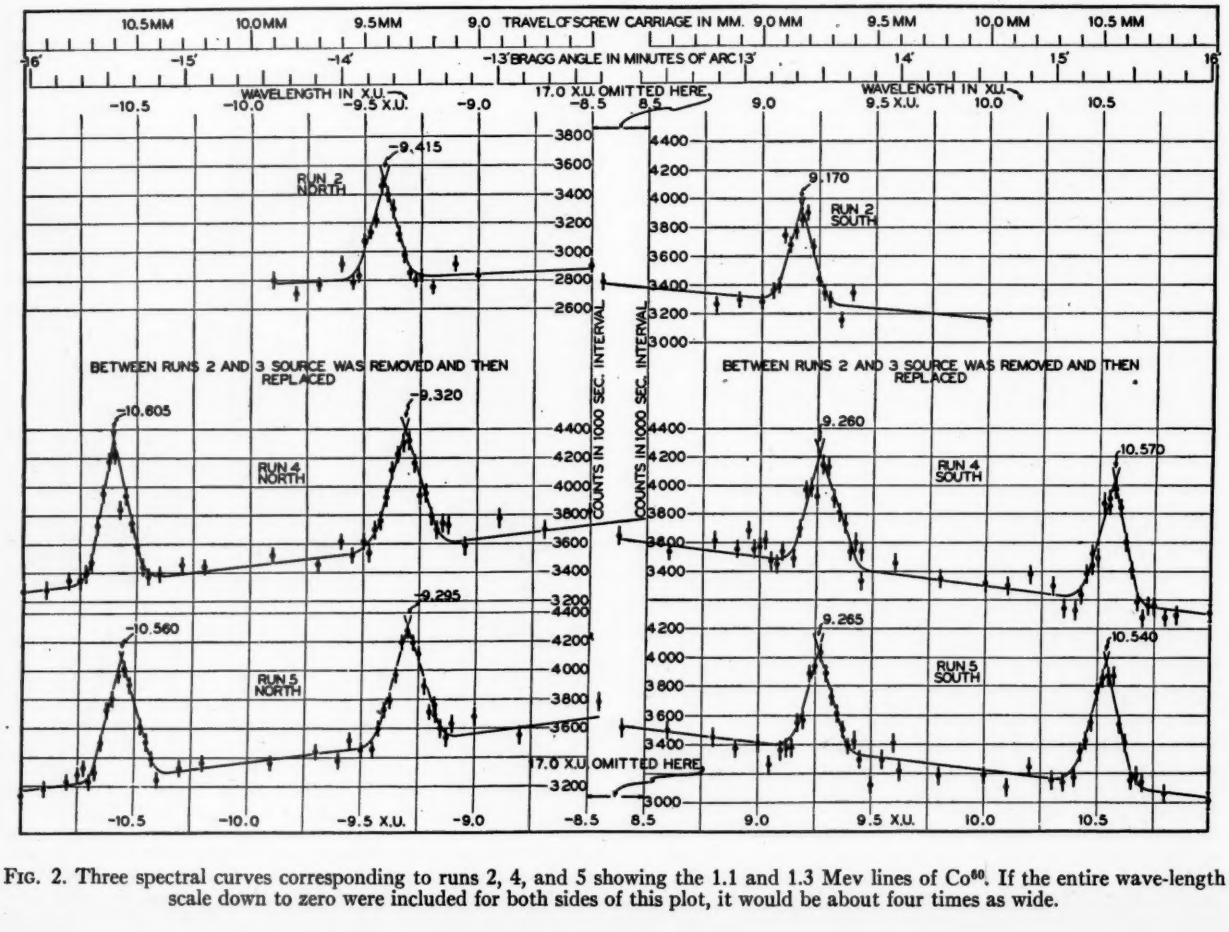

FIG. 2. Three spectral curves corresponding to runs 2, 4, and 5 showing the 1.1 and 1.3 Mev lines of Co^{60}. If the entire wave-length scale down to zero were included for both sides of this plot, it would be about four times as wide.

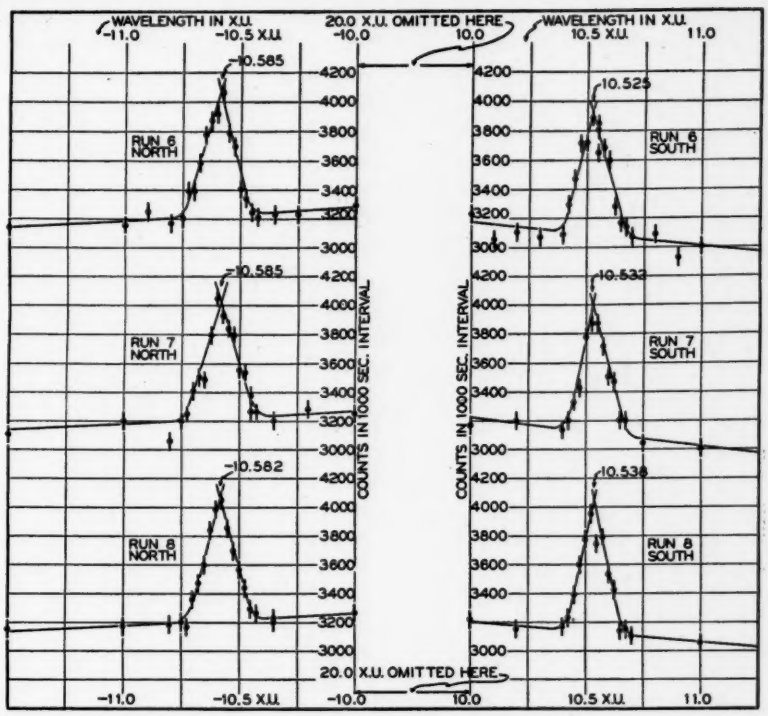

FIG. 3. Three spectral curves, runs 6, 7, and 8, on the 1.1-Mev line of Co^{60}. The scales of this figure are similar in all respects to those of Fig. 2.

retical upper working limit of quantum energy of 3 Mev if the (310) planes of quartz are used. This is a threefold improvement over our first collimator (as regards limiting quantum energy). Figure 1 is a photograph of the two-meter instrument looking from the detector end toward the source end in which the multicellular counter and some of its lead shielding have been removed. The exit end of the collimator is thus exposed to view and the thicker ends of the twenty-four tapering lead partitions are thus visible. The insert in this figure is an enlargement of this rear end of the new collimator in order to show the exit ends of the partitions more clearly. For comparison, the old collimator is also shown just to the right of the new one, the exit end in this case also being the one exposed.[10]

APPLICATION TO THE STUDY OF GAMMA-RAYS FROM Co^{60}

Figure 2 shows three of our spectral curves obtained by reflections from both sides of the crystal planes. Run 1 (not shown) was exploratory in nature to locate the 1.3-Mev line. Run 2 shows the 1.3-Mev line of Co^{60} while runs 4 and 5 show both the 1.1- and 1.3-Mev lines. In run 2, a single line profile of the 1.1-Mev line (not plotted in Fig. 2) was also run on the right-hand side only. The source was taken out of its holder after run 2 to permit temporary study of another much shorter lived source, Ta^{182}. The Co^{60} source was then replaced in the instrument and another exploratory run (No. 3, not shown) was made to relocate the lines. This removal and replacement of the source accounts for the slight shift in the line positions on the instrument scale, a shift corresponding to a displacement of the source in the source holder of about 0.07 mm. The *separation* however between the reflections from the two sides of the crystal planes (which is used as the measure of the wave-length) is very reproducible from run to run. The scales at the top of Fig. 2 show the Bragg angles of reflection in minutes of arc and also the displacement of the wave-length screw carriage in millimeters. The wave-length scale is also shown at both top and bottom in nominal x units.[11] To save space, some 17 x.u., or more than three times the total width of the figure, is omitted from the wave-length scale in the space at the center of Fig. 2 between the right- and left-hand orders. It will be noted also that the spectral lines do not occur at exactly the same nominal scale readings on the two sides. This is because

[10] Plans are under way for a still better collimator which we hope to construct with tungsten partitions. Because of the greater density of tungsten, it will be possible to design this for about 80 percent theoretical transmission. The partitions will not be tapered in thickness but will be retained in converging grooves in heavy steel guide plates at top and bottom. This collimator will have the same theoretical limiting angular discriminating power but in addition will have a truncated or trapezoidal transmission characteristic (because the partitions do not taper in thickness) so that there will be a finite small range of angles over which the maximum 80 percent transmission obtains. This places less rigid retuirements on the mechanical features of the instrument which must hold the direction of the reflected beam nearly invariable in the collimator slots.

[11] Nominal x units on the wave-length drum of the instrument are convertible into true x units (Siegbahn scale) by dividing the instrument reading by the factor 1.00024 which we have established with high precision by measurements on the x-ray lines of the *K*-spectrum of tungsten.[6] These wave-lengths in x units are then converted from the Siegbahn scale to milliangstroms by multiplying them by 1.00203.

TABLE I. Wave-length measurements of two gamma-ray lines from Co^{60}.

1.3-Mev line			1.1-Mev line	
	Screw reading (double)	Weight factor		Screw reading (double)
Run 1	18.570	0.5	Run 6	21.111
Run 2	18.595	1.0	Run 7	21.118
Run 3	18.578	0.5	Run 8	21.121
Run 4	18.585	1.0		
Run 5	18.573	1.0	Average	21.117
Average	18.582			
Corrected results	$(9.308\pm0.005)\times10^{-11}$ cm 1331.6 kev±1.0		Corrected results	$(10.578\pm0.005)\times10^{-11}$ cm 1171.8 kev±1.0
			Runs 2, 4, 5 Corrected results	$(10.583\pm0.005)\times10^{-11}$ cm 1171.3 kev±1.0
			Average	
			6, 7, 8 Weight 1 2, 4, 5 Weight 0.5	$(10.580\pm0.005)\times10^{-11}$ cm 1171.5 kev±1.0

of a slight decentering of the "β-point"[12] of the instrument relative to the "zero" of the instrument scale which can easily be shown to introduce entirely negligible error. The ordinate scales for the different runs are indicated by numbers giving the total number of counts observed at each setting for a standard counting interval which was uniformly 1000 sec. for all the runs plotted in Fig. 2.

Figure 3 shows three more runs taken on the 1.1-Mev line alone. This gives a good idea of the reproducibility of the measurements, when the instrument is working at its best. The scales on this figure are similar to those of Fig. 2 in all respects.

Table I shows the results of all these measurements on the two lines of Co^{60}. The columns marked "screw reading (double)" give the distance, in terms of the wave-length screw (nominal x units) between line peaks as reflected in the first order to the left and to the right of the (310) planes of the quartz lamina. These screw readings must be (1) halved to obtain nominal x units and (2) converted to milliangstroms by the procedure explained in footnote 11. This procedure gives the wave-lengths shown under "corrected results." The conversion to kev energy units has been effected by means of the conversion factor 12395×10^{-8}, the wave-length associated with one ev.[13] It will be noted in Table I that less weight has been assigned to the 1.3-Mev wave-lengths obtained from the exploratory runs 1 and 3. This is because these curves were taken with a shorter counting interval than the rest, their primary object being to locate the positions of the lines to sufficient accuracy to permit planning an economical schedule of settings for the more careful runs. Also, less weight was assigned to the 1.1-Mev wave-lengths obtained in runs 2, 4, and 5 than in the three later very satisfactory runs 6, 7, and 8. In run 2, the wave-length of the single 1.1-Mev line had to be determined by measuring its distance from the neighboring 1.3-Mev line. Also, the counting interval in this case was only 5 minutes. In run 4, there were counter troubles which were not extremely serious but sufficient to make repetitions of some of the readings desirable. Such repetitions required reversing the direction of travel of the screw carriage to reach a previous setting and then proceeding as before. We have found that such a procedure in the middle of a run may introduce minute but detectable hysteresis effects which may lead to small errors in the wave-lengths readings. There was a suspicion also in run 5 that the β-point of the instrument might have shifted ever so slightly in going from the reflections on one side to those on the other. Checks were therefore made on the 1.1-Mev wave-length in runs 4 and 5 by measuring the *separations* from the adjacent 1.3-Mev lines. In the case of run 5, it was found that a slight β-point shift had indeed occurred and therefore in this run the wave-length *differences* from the adjacent 1.3-Mev lines together with the average value of these latter were used (instead of the separation between right and left hand orders) and only half-weight was assigned to this individual value. All of these deviations are small and give no cause for alarm regarding the reliability of our final average results which are shown at the bottom of Table I.

INTEGRATED REFLECTION COEFFICIENT AT 9 X.U.

The 1.3-Mev line at 9 x.u. is the shortest wave-length we have so far studied and it was of interest to measure the integrated reflection coefficient of the (310) planes of our quartz crystal at this wave-length for comparison with the data at longer wave-lengths. The same method was followed as that used for previous nuclear gamma-ray lines. The total counting rate in the directly trans-

[12] The "β-point" is the point on the focal circle to which the reflecting planes of the quartz crystal would converge if produced. This is therefore the point on the focal circle which corresponds to the true zero of wave-length. The nominal scale of the instrument wave-length screw has a nominal zero point which never agrees exactly with the "β-point" because of slight variations in the way in which the source is adjusted in its holder and in other instrument adjustments. Such deviations are however quite unimportant.

[13] J. W. M. DuMond and E. R. Cohen, Rev. Mod. Phys. **20**, 82 (1948).

mitted beam was determined by setting the instrument at "zero wave-length" so that the primary beam was directly transmitted through the crystal and collimator to the counter. Because this direct beam was far too intense to be measured by the counter directly, absorbing sheets were introduced into the beam and the absorption curve (logarithm of counting rate against thickness of absorber) was extrapolated back to zero absorption thickness to determine the true counting rate. One-half of this direct beam counting rate we associate with each of the two lines since our spectra show that they are quite closely equal in intensity. On this basis, we find for the 1.1 Mev line 4.97 counts in the diffracted beam per 10,000 counts in the direct beam, and for the 1.3-Mev line 4.12 counts in the diffracted beam per 10,000 counts in the direct beam. This is *not* the integrated reflection coefficient but it gives a basis from which the latter can be calculated. Such a calculation[14] is too involved for the scope of the present paper, but it has been shown that the integrated reflection coefficient for wave-lengths from $\lambda=200$ x.u. down to $\lambda=30$ x.u. diminishes quite closely as λ^2. The present measurements at 9 x.u. agree substantially with this law. If anything, they lie slightly higher than the λ^2 line determined at longer wave-lengths but we cannot guarantee that this is a significant deviation.

[14] A paper by D. A. Lind on this question of the integrated reflection coefficient for the (310) planes of quartz as a function of wave-length over a very wide range of wave-lengths is now in preparation.

COMPARISON WITH PREVIOUS WORK

The shortest wave-lengths measured previously by direct crystal diffraction are, we believe, those observed with the photographic crystal spectrometer of Frilley.[15] The shortest of Frilley's lines was 16 x.u. or 770 kev quantum energy. From an examination of Frilley's photograph it seems doubtful whether a precision in this wave-length determination better than ± 2.0 percent could be claimed. We believe it safe, therefore, to say that the present measurements of the 1.1- and 1.3-Mev lines of Co^{60}, quite independent of their high precision, set a new record for the shortest wave-lengths ever measured directly. They surpass Frilley's hardest lines as to quantum energy by a factor of nearly two. The precision is, of course, from 50 to 100 times that of Frilley's spectra.

These results are far from representing the limit of the instrument even in its present state of development. We believe it quite possible with our present collimator and crystal holder to go to 2 Mev and perhaps somewhat beyond this. With the improved tungsten partition collimator and further improvements in the crystal and the detecting system such as we have outlined above, it is probable that the limit can be pushed still further upward very substantially.

[15] Frilley, thesis, Paris, 1928. For reproductions of Frilley's spectra, see Rutherford, Chadwick, and Ellis, *Radiations from Radioactive Substances* (Cambridge University Press, London, 1939), p. 380.

PHYSICAL REVIEW VOLUME 76, NUMBER 12 DECEMBER 15, 1949

Penetration and Diffusion of Hard X-Rays through Thick Barriers. III. Studies of Spectral Distributions*

P. R. Karr and J. C. Lamkin
National Bureau of Standards, Washington, D. C.

(Received August 15, 1949)

Two kinds of spectral distributions of gamma-rays are discussed. These are (1) spectra found in an infinite medium with an uniformly distributed monochromatic source, and (2) equilibrium spectra obtained in an artificial penetration problem. Curves are shown for various media and for various energies of the source photons. The relations of these spectra to the general problem of γ-ray penetration is discussed.

IN this note we report some results of a study of two rather simple problems in multiple γ-ray scattering.[1–4] These results may have some interest in themselves and also serve to illuminate certain features of the general problem of γ-ray penetration.

The first problem to be discussed is the following: a time-independent monochromatic source of gamma-rays is distributed uniformly in an infinitely extended, isotropic medium which is capable of absorbing gamma-rays by means of photoelectric effect and pair production, and of scattering them by Compton effect. The problem is to find the steady state spectrum in the medium, i.e., the average number of photons per cm^3 per unit energy range, as a function of the photon energy.

Solutions are to be found for various media and for various energies of the source photons. An experimental study of this problem has recently been described[5] by workers at the Naval Research Laboratory. For this reason we call this the "N.R.L." problem.

* Work supported by an ONR contract.

[1] Bethe, Fano, and Karr, Phys. Rev. **76**, 538 (1949). (Part I of the series "Penetration and diffusion of hard x-rays through thick barriers".)

[2] U. Fano, Phys. Rev. **76**, 739 (1949). (Part II of the series.)

[3] U. Fano, Nucleonics (to be published).

[4] L. V. Spencer and F. A. Jenkins, Phys. Rev. **76**, 1885 (1949).

[5] W. R. Faust and M. H. Johnson, Phys. Rev. **75**, 467 (1949).

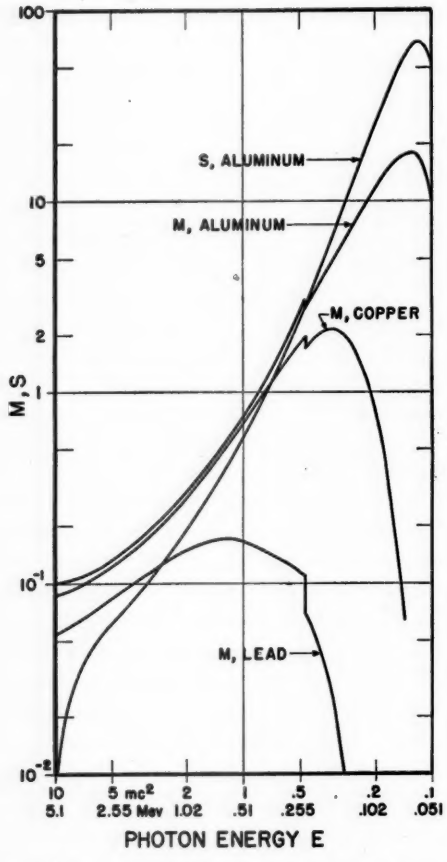

FIG. 1. "N.R.L." spectra M and "equilibrium" spectrum S for $E_0=10$ mc² (5.1 Mev). The ordinate M represents the number of photons per Mev per cm³ for a source density of 1 photon per cm³. S is plotted in arbitrary units.

The problem is governed by the following integral equation:

$$\mu(E)M(E)=k(E_0, E)+\int_E^{E_0} k(E', E)M(E')dE', \quad (1)$$

where μ is the total "narrow beam" absorption coefficient, E_0 is the energy of the source photons, E is the energy of the scattered photons, $k(E', E)dE$ is the probability per unit path length (which is proportional to the probability per unit time) that a photon of energy E' will be Compton-scattered to the interval between E and $E+dE$, and MdE is the density of photons in the energy range dE per unit density of the source photons.

In Eq. (1) the term $\mu(E)M(E)$ represents the rate of disappearance of photons of energy E. Under steady-state conditions this must be balanced by the rate of *creation* of photons of the same energy. The term $k(E_0, E)$ represents the rate of creation of photons by direct scattering from the source photons, and the integral represents the rate of creation by scattering from secondary photons.

The term $k(E_0, E)$ drops discontinuously to zero at an energy E such that $(mc^2/E)-(mc^2/E_0)=2$, since by virtue of the Compton relation, a primary photon cannot be degraded to a point below this energy. For this reason there is a discontinuity in M amounting to $k(E_0, E)/\mu(E)$ at $E=[1/E_0+2/mc^2]^{-1}$.

Solutions of Eq. (1) have been obtained by numerical integration. Figure 1 is a plot of M *vs.* E for various media, with the primary energy $E_0=10\ mc^2$. One notes that M rises with decreasing E until a certain point when a rather rapid decrease sets in. The rise is due, roughly speaking, to the fact that successive Compton scatterings of a photon decrease its energy, on the average, by decreasing amounts, thus tending to create a piling-up effect at lower energies. The rather sudden drop is due to the rapid increase of μ at low energies because of the photoelectric effect. The discontinuity discussed above is well in evidence.

Figure 2 illustrates the effect of different primary energies in the same medium. It has been found that when we plot M for the same medium with different primary energies, the curves all have the same shape except for those energies which are rather close to the primary energy, where a "transient" effect occurs. In fact when we plot, as in Fig. 2, the photon density per Mev per unit rate of creation of source photons, which is $M/[\mu(E_0)c]$, (c being the velocity of light), the curves very nearly coincide, except for the "transient." The remaining difference is considerable only when E_0 is in the region where pair production accounts for a sizable fraction of the total absorption coefficients.

In the above problem, the spectrum does not depend on the position in space. The problem, nevertheless,

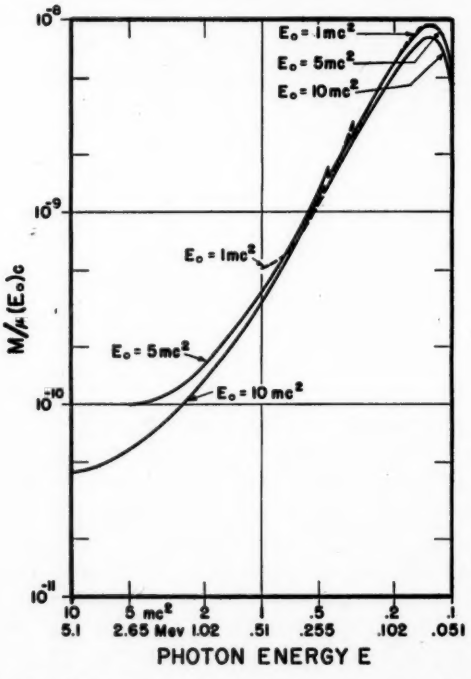

FIG. 2. "N.R.L." spectra for aluminum for several values of E_0. The ordinate $M/\mu(E_0)c$ represents the number of photons per Mev per cm³ for a rate of generation of 1 source photon per sec. per cm³.

has a relation to the more difficult problem of penetration through a medium of a monochromatic broad beam of γ-rays. In the latter problem the spectral density is a function of E and two additional variables, z the penetration distance, and θ the direction of the photons with respect to the z direction. If we average over-all values of z and θ we obtain $M(E)$, the solution of the N.R.L. problem. Now in the penetration problem, one is particularly interested in great depths of penetration, i.e., large z. The N.R.L. function $M(E)$ is a *biased* estimate of the spectral density for the penetration problem for large z and θ averaged out: the spectral density function for large z is steeper on the high energy side than $M(E)$ because those photons that penetrate large thicknesses tend to have been scattered many times with little energy degradation.

We turn now to a discussion of another spectrum which is biased in the *opposite* sense relative to the penetration problem. The problem in which this spectrum arises, which we call the "equilibrium" problem, is a modification of the penetration problem in the following sense: the photons are supposed to be Compton scattered and to lose energy according to the usual probability functions, but the angular deflections are disregarded and all photons are assumed to continue forward in the positive z direction. Furthermore the source is not monochromatic but is supposed to have a spectrum so chosen that the *same* spectrum obtains for all values of z with attenuation according to $\exp[-\mu(E_0)z]$ where E_0 is now the peak energy in the spectrum. The equation for this problem is:

$$[\mu(E)-\mu(E_0)]S(E)=\int_E^{E_0} k(E', E)S(E')dE', \quad (2)$$

where $S(E)$ represents the spectral distribution. Solutions of (2) have been obtained by a combination of methods. We find, just as in the N.R.L. case, that the curves for a given medium but with different values of E_0 all have the same shape except for an initial transient. The "equilibrium" spectra resemble qualitatively the N.R.L. spectra except for E near E_0. The portion of an "equilibrium" curve near E_0 is much steeper than for the N.R.L. curve for the same E_0 and medium. This portion of the curve starts as $(E_0-E)^{K_0-1}$ where K_0 is a parameter discussed in reference 1. In fact the entire rising portion of an equilibrium curve is steeper than the corresponding N.R.L. spectrum. (An equilibrium curve which illustrates this is given in Fig. 1, for $E_0=10\ mc^2$, in aluminum; it is to be compared with the corresponding N.R.L. curve in the figure.) Furthermore the equilibrium problem has been so formulated that its spectra are somewhat steeper than the corresponding spectra of the penetration problem for any finite value of z, with θ averaged out.

Thus the two problems treated above give some insight into the penetration problems since the spectra obtained bracket the penetration problem spectra. It may be noted in this connection that in a penetration problem with monochromatic source and no angular deflection, the Laplace transform $y(E, p)$ of the spectral distribution $Y(E, x)$ [2] satisfies an equation intermediate between (1) and (2), in that $\mu(E)-p$ appears on the left-hand side of the equation, rather than $\mu(E)$ as in (1) and $\mu(E)-\mu(E_0)$ as in (2). Here p is the transform variable and $\mu(E_0)>p>0$.

A more complete analysis of these problems will be published at a later date. We wish to thank Dr. U. Fano for much valuable advice and assistance.

PHYSICAL REVIEW VOLUME 76, NUMBER 12 DECEMBER 15, 1949

Pressure Dependence of Line Width in Infra-Red Spectra

FRANK MATOSSI
Naval Ordnance Laboratory, White Oak, Silver Spring, Maryland
(Received August 15, 1949)

The effect of coupling of molecular vibrations on line width in infra-red spectra is dealt with. Line widths due to this effect are proportional to the square root of pressure. Numerical discussion indicates that at least part of the line width in water-vapor spectra can be ascribed to this effect.

1. INTRODUCTION

RECENT discussions[1] of experiments on the dependence of absorption in infra-red band spectra on pressure have indicated that the usual assumption of proportionality of the line width to pressure, which is based on Lorentz' theory of damping by impacts, might not always be correct. A line width proportional to the square root of pressure would be in better agreement with the observations, at least for water vapor. Indeed, already in 1925, Holtsmark[2] pointed out that a coupling effect should yield such a law for the line width.

The interaction of the molecules, considered as coupling of oscillators with essentially the same eigenfrequency, gives rise to a splitting of the frequencies the amount of which depends on the distance and the

[1] F. Matossi and E. Rauscher, Zeits. f. Physik **125**, 418 (1949); W. M. Elsasser, Harvard Meteorological Studies Nr. 6 (1942), p. 46 f. (there also other references are to be found).

[2] J. Holtsmark, Zeits. f. Physik **34**, 722 (1925).

orientation of the oscillating dipoles, and this is equivalent to line broadening. The line width is obtained by averaging the distribution of the frequencies over the distances and orientations. This concept has been worked out in detail only for atoms with parallel orientation of the induced dipoles, but it is easy to extend Holtsmark's result, with the aid of general formulas developed earlier,[3] to the case of molecules.

In this paper, it is intended to give the theoretical expression for the dependence of line width on pressure in molecular spectra according to Holtsmark's procedure and to discuss its consequences. It can be shown that at least some part of the line width in water vapor spectra may be ascribed to the coupling effect. The numerical details depend mainly on the value of the "effective charge" of the oscillating molecular dipoles and the "effective diameter" of the molecules which are not known very exactly.

2. METHOD OF CALCULATION

Referring for all details of Holtsmark's method to his paper,[3] we give only an outline of the calculation. The system of dipole oscillators satisfies the equations

$$\ddot{q}_i+\omega_0^2 q_i+\sum_{k=1}^{n} a_{ik}q_k=0, \quad i\neq k, \quad i=1, 2, \cdots n, \quad (1)$$

for the normal coordinates q_i with

$$a_{ik}=\frac{\epsilon^2 e^2}{\mu r_{ik}^3}[\cos\vartheta_k-3\cos\vartheta_i(\cos\vartheta_i\cos\vartheta_k +\sin\vartheta_i\sin\vartheta_k\cos(\varphi_i-\varphi_k))]. \quad (2)$$

Here ω_0 is the undisturbed eigenfrequency of the oscillators; ϵe is the "effective" charge, defined as ratio of dipole moment and atomic distance; e, the normal elementary charge; μ is the reduced mass of the (diatomic) molecule; ϑ_i is the angle of the molecular dipole of molecule i with the direction of r_{ik}, the distance between two interacting molecules; ϑ_k is the angle between the dipoles i and k. $\varphi_i-\varphi_k$ is the angle between the plane containing the two dipoles and the plane containing r_{ik} and one of the dipoles. a_{ik} is essentially the coupling force of a dipole on the oscillating atom of another one, divided by the dipole moment. The dipole moment is always meant as the vibrating moment. A permanent moment does not change the results with respect to line width.

From (1), a secular equation for ω is obtained, in the usual manner, with roots ω_τ, for which the relation

$$\frac{1}{2}\sum_{\tau=1}^{n}(\omega_\tau^2-\omega_0^2)=\sum_{i,k} a_{ik}a_{ki}, \quad i<k, \quad (3)$$

can be derived. In (3), the sum on the right-hand side may be transformed into an integral in introducing the probability

$$W(a_{ik})da_{ik}=(1/4\pi V)r_{ik}^2 dr_{ik}\sin\vartheta_i d\vartheta_i \sin\vartheta_k d\vartheta_k d\varphi_i d\varphi_k \quad (4)$$

that the coordinates r, ϑ, φ have such values that (2) lies between a_{ik} and $a_{ik}+da_{ik}$ (V = volume). Integration and division by n yields $\langle(\omega_\tau^2-\omega_0^2)\rangle_{Av}$, from which $\langle(\omega_\tau-\omega_0)^2\rangle_{Av}$ can be obtained in approximating $\omega_\tau^2-\omega_0^2$ by $2\omega_0(\omega_\tau-\omega_0)$.

Assuming that the frequencies are distributed according to a Gaussian error function, b, the half-width at half-height is given by

$$b=1.18\langle(\omega_\tau-\omega_0)^2\rangle_{Av}, \quad (5)$$

and the final result is

$$b=\frac{1.18}{24\pi^{\frac{1}{3}}c^2}(8)^{\frac{1}{3}}\frac{\epsilon^2 e^2 N^{\frac{1}{3}}}{\mu r_0^{\frac{1}{3}}\omega_0}. \quad (6)$$

Here r_0 is the minimum distance of two molecules or the molecular diameter; N is the number of absorbing molecules per unit volume; b and ω_0 are given as wave numbers; c = velocity of light.

3. DISCUSSION

The introduction of ϵ and μ and the generalization of Eqs. (2) and (4) are the changes applied to Holtsmark's paper.

Before the numerical evaluation, we want to discuss some objections that have been raised against Holtsmark's paper and its translation into quantum mechanics.[4] These objections refer to (a) the use of a Gauss distribution;[5] (b) the neglecting of the change of the damping constant by the coupling;[5] (c) the use of a constant value r_0.[6]

(a) Only if a Gauss distribution is assumed will there be a definite relation between the mean square of the frequency deviation and the line width. For a dispersion distribution, $\langle(\omega_\tau-\omega_0)^2\rangle_{Av}$ becomes infinite despite a finite line width, and Holtsmark's method would have to be modified. But as far as a Gauss distribution is a fair approximation to the shape of a line, it can be used in connection with methods adapted to it.

(b) The damping constant, and with it the line width, is changed by the coupling. An estimate of the influence of this effect may be obtained from the results of a previous paper.[7] According to it, the ratio b/b_0 of the line widths with and without coupling influence on damping constant can be derived as

$$b/b_0=\left[1+\frac{\alpha^2}{2}\frac{\omega_0^2}{b_0^2}\right]^{\frac{1}{2}}-\frac{\alpha}{2c}\frac{\omega_0}{b_0},$$

[3] J. Holtsmark, Ann. d. Physik 58, 577 (1919).

[4] J. Frenkel, Zeits. f. Physik 59, 198 (1930).
[5] V. Weisskopf, Zeits. f. Physik 75, 287 (1932).
[6] L. Schuetz-Mensing, Zeits. f. Physik 61, 655 (1930).
[7] F. Matossi, Phys. Zeits. 40, 323 (1939).

in which α is the ratio k'^2/k^2; k and k' being defined by the potential energy $\frac{1}{2}k^2(q_1^2+q_2^2)+k'^2q_1q_2$ of two oscillators. For a particular crystal, α has been estimated to about 0.04. In this case, b/b_0 would indeed be much greater[8] than 1. But we can assume α to be much smaller in gases. For $\alpha<4b_0/\omega_0$, b/b_0 will be less than 1 with a minimum value of about 0.7 for $\alpha=2^{\frac{1}{2}}b_0/\omega_0$. Therefore, we seem justified to use Holtsmark's method in our case.

(c) More critical is the objection of Schuetz-Mensing. She points out that, instead of a constant r_0, the pressure dependent mean distance of the nearest neighbors should be used as the lower limit of the possible distances. For this mean distance, the expression $\rho=0.55N^{-\frac{1}{3}}$ is derived. Then b will become proportional to N instead of $N^{\frac{1}{2}}$, and the order of magnitude of b will be considerably changed too. We do not see any reason why possible distances smaller than the mean distance shall be excluded. The objection considered here would, in my opinion, be applicable only if the distribution of the molecules would be a static one but not if, in collisions, molecules actually may come closer together. It is to be admitted that a rigorous method should take into account the deviation of the interaction law from (2) at small distances and also the different time intervals the molecules stay in different distances. But as long as the distribution is determined by purely geometrical considerations, as it is done by both authors, there is no reason to abandon r_0 in favor of ρ. Even if the effects just mentioned would have been considered, their influence on the distribution would probably not be pressure dependent. However, to neglect them means that r_0 should be considered as an "effective" diameter only.

Weisskopf has included the coupling effect in those which are covered by the Lorentz-Lorenz formula and which give proportionality of b to p. But that can be done only with interactions that can be described by a polarization proportional to the exciting field. However, the existence of the zero-point energy of an oscillator gives a coupling cause independent of the external field. This same argument only justifies the identification of N with the total number of molecules and not the number of excited ones. Of course, the last considerations are applicable only to real oscillators and not to an oscillator model of electronic transitions. Therefore, Holtsmark's coupling broadening might be meaningless in electronic spectra,[9] where, however, the coupling effects of Weisskopf and Schuetz-Mensing become important.

Criticizing further: According to (6), b is required to vary with ω_0, for which there is no indication in the observations yet.

The foregoing remarks are not beyond doubt; but in view of the results of the numerical evaluation in the next section and the observations mentioned at the beginning, it seems that Holtsmark's method might still furnish a fair approach to the problem of line width in infra-red spectra, although an estimate of its rigorousness is not yet possible.

4. NUMERICAL EVALUATION

For a numerical evaluation, we choose data that approximately refer to absorption in saturated water vapor at normal conditions. We put $\omega_0=1500$ cm^{-1}, $r_0=2\times10^{-8}$ cm, $\mu=$reduced mass of an OH molecule, $N=0.5\times10^{-18}=$number of water molecules per cm^3. Then, from the measured value of the line width,[10] $b=0.12$ cm^{-1}, we obtain $\epsilon=0.41$. This is a reasonable value, although somewhat large compared with the estimates from dipole measurements and infra-red spectra.[11] Slight changes in r_0 or N do not invalidate this qualitative statement.

The numerical result seems to indicate that the coupling effect plays a decisive role in the broadening of infra-red lines. But the coupling effect alone is certainly not a sufficient cause of line broadening, because it cannot account for the influence of foreign molecules. Therefore, also collision broadening has to be considered.

Estimating the contribution of collisions from well-known formulas, the ratio of coupling width to impact width is about 1:1. Taking this into account,[12] the value of ϵ computed above would have to be changed to $\epsilon=0.29$ which is even more acceptable. An experimental test of the relative importance of collision and coupling effects may be provided by shifting the contributions of the two effects by changing the partial pressure of the absorbing gas, because collision broadening should essentially depend on total pressure while coupling broadening is a function of the number of absorbing molecules only. In view of the discussion in Section 3, final judgment as to the significance of coupling broadening in Holtsmark's sense is not yet advisable.

5. SUMMARY

Discussing Holtsmark's treatment of coupling broadening and its numerical evaluation, it is stated that at least part of the line width in infra-red spectra might be due to the coupling effect which would yield a $p^{\frac{1}{2}}$-law for the line width as it seems to be required by recent observations.

[8] This does not mean that lines in crystals are very broad, because the regular distribution of the ions tends to sharpen the lines.

[9] Neither is it applicable to pure rotation spectra without modifications. Therefore, microwave results (see W. Gordy, Rev. Mod. Phys. **20**, 668 (1948)) do not necessarily contradict our results.

[10] G. E. Becker and S. H. Antler, Phys. Rev. **70**, 300 (1946); A. Adel, Phys. Rev. **71**, 806 (1947).

[11] D. M. Dennison, Phil. Mag. **1**, 195 (1926).

[12] Assuming additivity of both widths which is not rigorously correct.

Carbon Dioxide in the Infra-Red Solar Spectrum

LEO GOLDBERG, ORREN C. MOHLER, ROBERT R. MCMATH, AND A. KEITH PIERCE
McMath-Hulbert Observatory, University of Michigan, Pontiac, Michigan
(Received August 29, 1949)

Wave-length measurements are given for lines in thirteen vibration-rotation bands of carbon dioxide observed between 1.5μ and 2.1μ in the infra-red solar spectrum and in the laboratory. The observations were made with the McGregor spectrometer and Cashman cell of the McMath-Hulbert Observatory. Among the thirteen bands, seven originate from the ground state and two from the first excited state of $C^{12}O_2^{16}$. The remaining four are identified with ground state transitions in the isotopic molecules $C^{13}O_2^{16}$ and $C^{12}O^{16}O^{18}$.

The rotational constants α_1, α_2, and α_3 have been determined from analysis of the rotational structures. The mean value found for B_{000} is 0.3906 cm^{-1} and for the equilibrium position $B_e = 0.3920$ cm^{-1}.

I. INTRODUCTION

CARBON dioxide is one of the principal absorbers in the earth's atmosphere of solar radiation in the infra-red spectral region from 1.5μ to 20μ. Between 1.5μ and 2.5μ, it is represented by numerous vibration-rotation bands which are grouped at approximately 1.6μ and 2.0μ. Langley[1] recorded two bands at 2.01μ and 2.05μ, which he designated as ω_1 and ω_2. Langley's bands are two of a group of three that result from transitions between the ground state and the triad of excited vibrational levels 04_01, 12_01, and 20_01. The third member of this group, ω_0, occurs at 1.95μ but is partially obscured by water-vapor absorption. Adel[2] later observed all three bands with a resolution higher than Langley's and succeeded in resolving them into their rotational structures.

In addition to the bands at 2μ, Barker and Wu[3] also recorded in the laboratory four weaker unresolved bands of CO_2 at 1.54μ, 1.57μ, 1.60μ and 1.65μ. The 1.6μ bands also arise from the ground state, and terminate in the excited levels 06_01, 14_01, 22_01, and 30_01. According to Adel and Lampland[4] this quartet of bands is represented by a single small absorption in the low resolution prismatic solar spectrum. The bands are plainly visible on Langley's and Abbot's early tracings.

The recent installation of a Cashman lead-sulfide cell and an all-reflecting spectrometer in the McGregor tower has made possible the mapping of the near infra-red solar spectrum with a resolution of about 50,000.[5] With this resolution the carbon dioxide bands at 1.6μ and 2.0μ are fully resolved and are well suited for detailed study. In addition to the afore-mentioned bands, several new band structures have been found and identified with the isotopes $C^{13}O_2^{16}$ and $C^{12}O^{16}O^{18}$, as well as with transitions from the first excited vibrational state of CO_2. This paper deals with the measurement and partial analysis of the various CO_2 bands in the solar spectrum between 1.5μ and 2.5μ.

TABLE I. Near infra-red bands of carbon dioxide in the solar spectrum.

Identification	ν_0(obs)	ν_0(calc)	Designation	Disp. (mm/A)	Sec Z
			$C^{12}O_2^{16}$		
2.06μ	4853.48	4852.8	$0\ 0_0\ 0-\begin{Bmatrix}0\ 4_0\ 1\\1\ 2_0\ 1\\2\ 0_0\ 1\end{Bmatrix}$	3.1	laboratory
2.01μ	4977.78	4981.4		3.1	laboratory
1.96μ	5099.64	5104.3		3.1	laboratory
1.65μ	6075.98	6071.0	$0\ 0_0\ 0-\begin{Bmatrix}0\ 6_0\ 1\\1\ 4_0\ 1\\2\ 2_0\ 1\\3\ 0_0\ 1\end{Bmatrix}$	2.7	7.0
1.60μ	6227.90	6235.5		4.7	1.1
1.57μ	6349.56	6358.4		4.7	1.2
1.54μ	6503.08	6515.4		2.7	17.4
2.08μ	4807.60	4805.6	$0\ 1_1\ 0-\begin{Bmatrix}0\ 5_1\ 1\\1\ 3_1\ 1\\2\ 1_1\ 1\end{Bmatrix}$	3.1	1.6
2.01μ	4965.36	4970.5		3.1	2.5
—	—	5131.6		—	—
			$C^{13}O_2^{16}$		
2.10μ	4748.06	4737.8	$0\ 0_0\ 0-\begin{Bmatrix}0\ 4_0\ 1\\1\ 2_0\ 1\\2\ 0_0\ 1\end{Bmatrix}$	6.2	26.3
2.05μ	4887.30	4892.1		3.1	2.4
—	—	5046.0		—	—
			$C^{12}O^{16}O^{18}$		
2.09μ	4791.22	4797.5	$0\ 0_0\ 0-\begin{Bmatrix}0\ 4_0\ 1\\1\ 2_0\ 1\\2\ 0_0\ 1\end{Bmatrix}$	6.2	20.4
2.04μ	4904.75	4909.4		3.1	2.4
—	—	—		—	—

II. OBSERVATIONAL

Table I lists the CO_2 bands that form the subject of the present study. Column one gives the approximate band centers in microns, for convenience of reference. Columns two and three give the observed and calculated frequencies of the band centers in cm^{-1}. Two of the isotopic and excited state bands are so overlaid by other stronger CO_2 bands that it was not possible to measure the band centers nor to assign rotational quantum numbers. Column four gives the quantum numbers involved in the various vibrational transitions. The excited levels enclosed in brackets are in resonance interaction and it is therefore not possible to assign quantum numbers unambiguously to any one level in either group. Column five gives the dispersion of each tracing in mm/A, and column six records the secant of the sun's zenith distance at the midpoint of each tracing.

Reproductions of the ω_0, ω_1, and ω_2 bands are shown in Fig. 1. Although the bands are quite well resolved,

[1] S. P. Langley and C. G. Abbot, Ann. Astrophys. Obs. Smithsonian Inst. I, 127 (1900).
[2] Arthur Adel, Astrophys. J. 97, 190 (1943).
[3] E. F. Barker and Ta-You Wu, Phys. Rev. 45, 1 (1934).
[4] Arthur Adel and C. O. Lampland, Astrophys. J. 87, 198 (1938).
[5] Robert R. McMath and O. C. Mohler, J. Opt. Soc. Am. (to be published).

accurate measurement of many of the components, particularly of ω_0 and ω_1, is hindered both by saturation of the strong lines and by blends with strong lines of water vapor. Although the number of unblended and unsaturated lines in each band appeared to be sufficient for an accurate evaluation of the rotational constants, it seemed desirable as a check to obtain laboratory tracings of the 2μ bands. The source employed for this purpose was a 2000-watt incandescent lamp placed just in front of the entrance slit of the monochromator. CO_2 vapor was generated from dry ice at the bottom of a cylindrical tube, six feet long, placed horizontally inside the spectrometer. The wave-length scale for the laboratory tracings was transferred from the solar tracing by simple superposition of unblended lines of CO_2.

The isotope bands at 2.04μ and 2.05μ, shown in Fig. 2, are the $C^{12}O^{16}O^{18}$ and $C^{13}O_2^{16}$ analogs of ω_1. The C^{13} isotope band corresponding to ω_0 falls in the middle of the ω_1 band and is therefore not observed. Portions of the O^{18} companion to ω_0 are visible on low sun tracings between ω_0 and ω_1, but the band is mostly obscured by water vapor. The isotope bands corresponding to ω_2 are not present on tracings made at high solar altitudes, which is to be expected in view of the relative weakness of ω_2. Both isotope bands do appear, however, on special low sun tracings obtained on September 26–27, 1948, as shown in Fig. 3. The region illustrated in Fig. 3 contains also a combination band of N_2O, centered at 2.13μ, as well as a portion of the 2.08μ excited-state band of CO_2. The latter band is also shown in Fig. 4.

The 1.57μ and 1.60μ bands appear well developed on noon-day tracings (see Fig. 5). The weaker bands at 1.54μ and 1.65μ, however, are ordinarily not present, and low sun tracings are required to bring them out. All four bands are well resolved and suitable for measurement, except for occasional blends, chiefly with solar lines of Fe I, Mg I, and Si I.

III. THE DETERMINATION OF WAVE-LENGTH

The second column of Table II lists the observed wave numbers of individual lines in the various CO_2 bands. An index of refraction for air equal to 1.000272 was adopted to convert all measured wave-lengths to wave number units. The following procedure[5] was employed to establish the wave-length scale. A series of standard lines was selected at intervals of approxi-

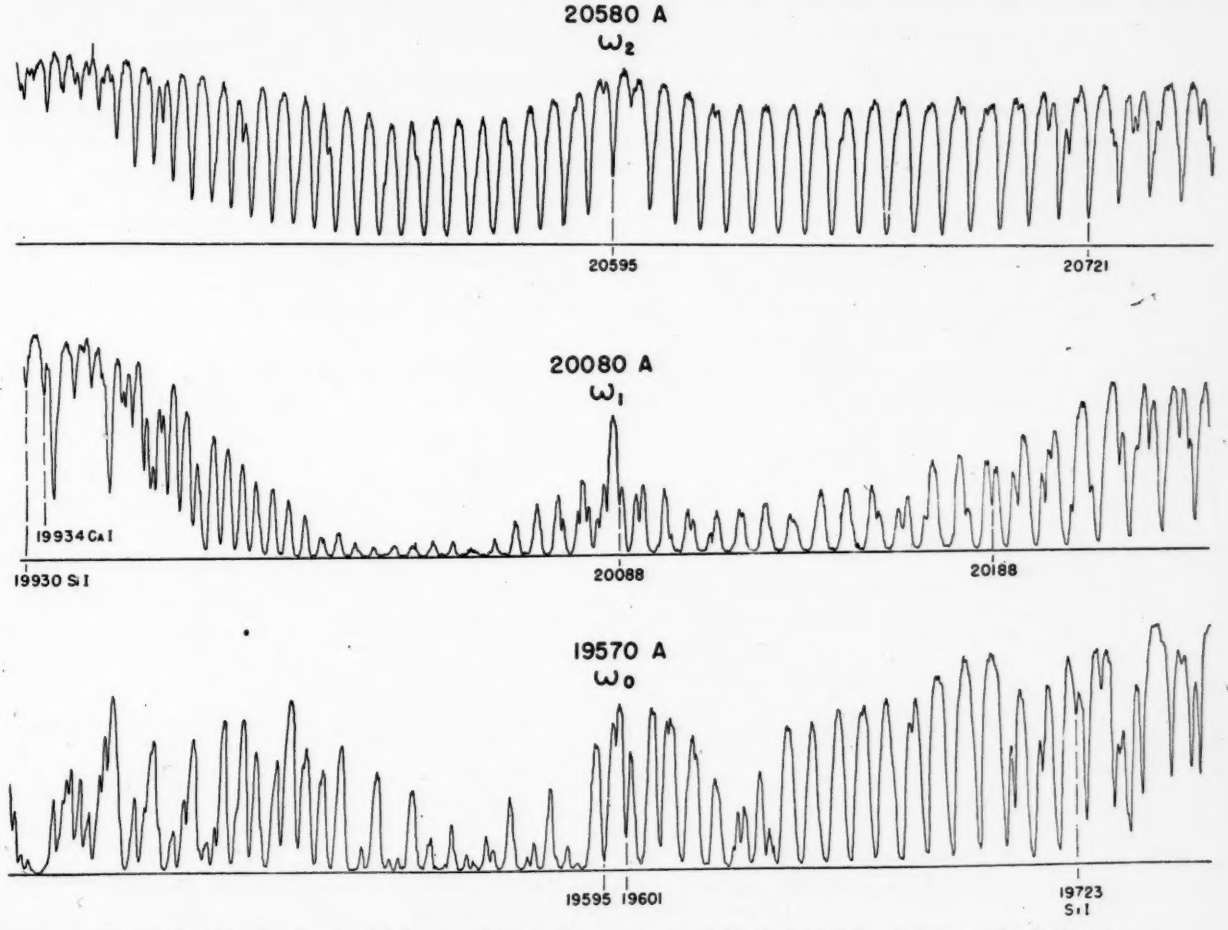

FIG. 1. Combination bands of CO_2 near 2μ in the solar spectrum. Solar lines of Si I and Ca I are also indicated. The horizontal line denotes zero intensity.

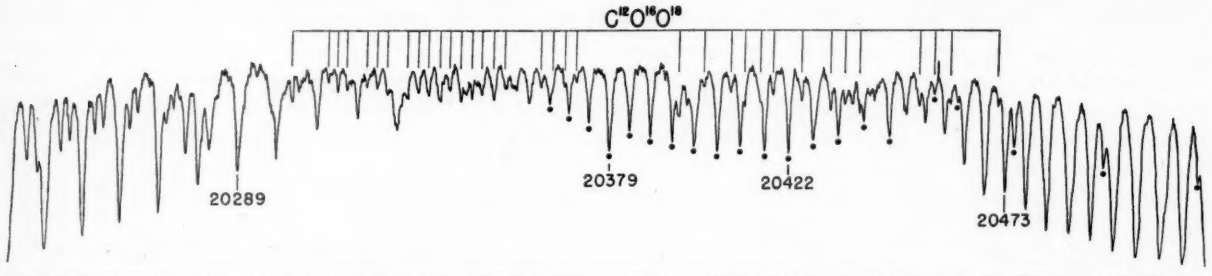

FIG. 2. Isotopic bands of CO_2 in the solar spectrum. The dots indicate lines due to $C^{12}O^{16}$, whereas the vertical lines denote a band of $C^{12}O^{16}O^{18}$. The horizontal lines denote zero intensity.

mately 50A and the wave-length of each line determined with reference to visible Fraunhofer lines in the third- and fourth-order grating spectra. Usually, about three independent determinations were made for each line, the estimated probable error of the mean wave-length being about 0.1A. The dispersion was then calculated from successive pairs of lines and plotted against the wave-length. According to the grating formula as applied to the McGregor spectrometer, the dispersion should increase slowly with wave-length, and in the infra-red the relation should be linear for a spectrum interval of about 2500A. Thus,

$$dx/d\lambda = a + b\lambda, \tag{1}$$

where a and b are constants, and x is the distance in mm from an arbitrary point, in the direction of the dispersion. Integration of Eq. (1) gives the relation between x and λ, *viz.*:

$$x = a\lambda + \tfrac{1}{2}b\lambda^2 + c. \tag{2}$$

For a given wave-length region, the constants a and b were determined from Eq. (1) by least squares and the constant c was adjusted to produce the best fit with the observed wave-lengths of the standard lines. The determination of the wave-length scale for the 1.6μ region is illustrated in Table III and Fig. 6. The measured wave-lengths of the standard lines are given in the first column of Table III and the measured dispersions in the second column. The latter are shown plotted against wave-length in Fig. 6. In general, dispersions were not calculated for line pairs closer than about 50A. The constants of the straight line drawn through the plotted points, determined by least squares, are $a=3.4829$ mm/A, and $b=0.00007869$ mm/A^2. The residuals in the third column of Table III are the differences between the observed wave-lengths of column two and those calculated from Eq. (2) with the foregoing constants. On the whole, the quadratic formula gives an excellent representation of the measured standard wave-lengths. The residuals larger than about ± 0.05A probably arise from non-uniform motion of the recording paper.

IV. IDENTIFICATIONS OF NEW BANDS

The band centers given in the third column of Table I were calculated from formulas derived by Adel and Dennison.[6] For each band the upper vibrational level is in so called Fermi resonance with two or more neighboring levels. The energies of n such resonating levels are given by the solution of an nth-order determinant. For the triad of levels $\begin{Bmatrix} 2 & 0_0 & 1 \\ 1 & 2_0 & 1 \\ 0 & 4_0 & 1 \end{Bmatrix}$, the deter-

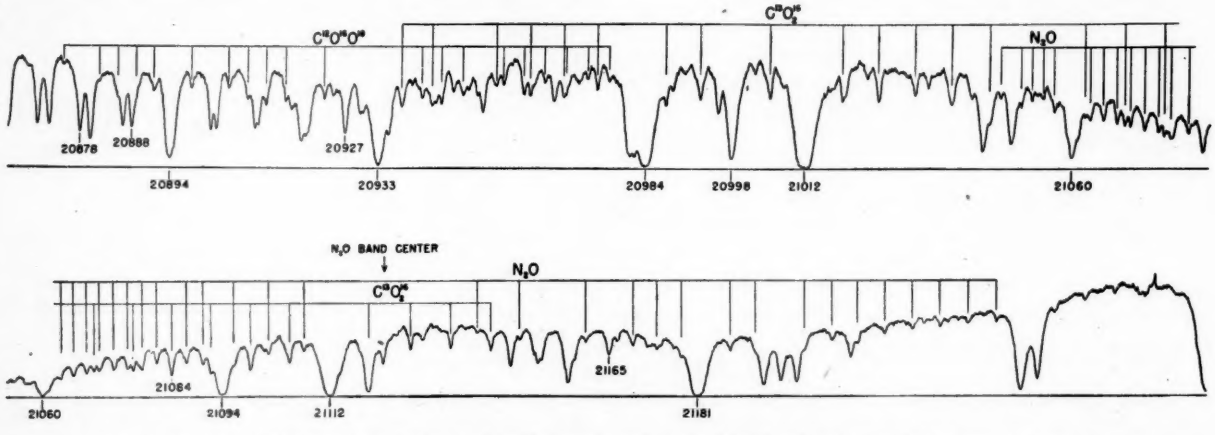

FIG. 3. Bands of $C^{12}O_2^{16}$ and $C^{12}O^{16}O^{18}$ in the solar spectrum. A combination band of N_2O also appears weakly. The horizontal line denotes zero intensity.

[6] See David M. Dennison, Rev. Mod. Phys. **12**, 175 (1940).

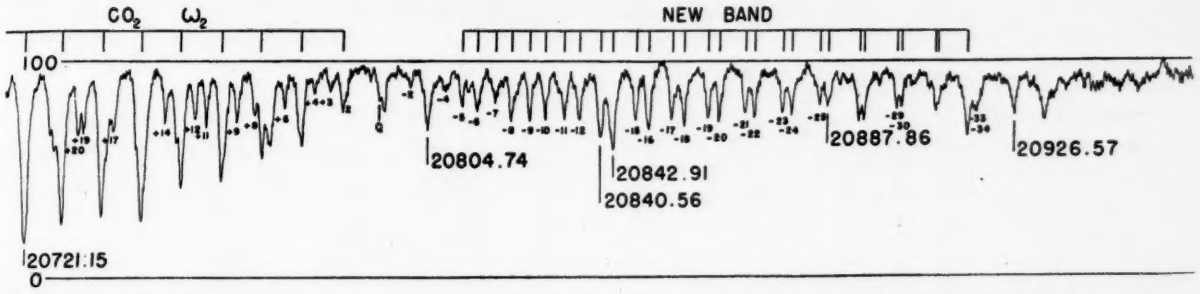

FIG. 4. The excited-state band of CO_2 at 2.08μ in the solar spectrum. The values of m are indicated below unblended lines. The horizontal line denotes zero intensity.

minant has the form

$$\begin{vmatrix} W_{041}-W & -\sqrt{2}b & 0 \\ -\sqrt{2}b & W_{121}-W & -b \\ 0 & -b & W_{201}-W \end{vmatrix}=0. \qquad (3)$$

In Eq. (3), W_{041}, W_{121} and W_{201} are the energies in cm^{-1} of the unperturbed levels, calculable in terms of the potential constants, and $b^2=5081$ cm^{-2}. The potential constants for CO_2 were determined by Adel and Dennison in 1933 from an analysis of all then-existing band centers. A re-analysis of the CO_2 spectrum based on the data of the present investigation undoubtedly would lead to some refinement of the potential constants. Nevertheless, the constants of Adel and Dennison are more than adequate for the calculations needed to establish the identity of isotope and difference bands of CO_2.

The Bands of $C^{13}O_2^{16}$ and $C^{12}O^{16}O^{18}$

The great strength of the ω_0, ω_1, and ω_2 bands of $C^{12}O_2^{16}$ in the solar spectrum suggests that faint bands arising from the same vibrational-rotational transitions in the molecules $C^{13}O_2^{16}$ and $C^{12}O^{16}O^{18}$ should also be present in the spectrum. Since the isotopes are heavier than the ordinary CO_2 molecules, their vibrational frequencies are somewhat lower, actually by 58 to 115 cm^{-1}, than those of $C^{12}O_2^{16}$. In theory, the calculation of band centers for the isotopes of CO_2 would require an entirely new set of potential constants appropriate to the isotopic molecules. As a satisfactory first approximation, however, D. M. Dennison[7] has suggested the following simple modification of the potential constants of CO_2. For the linear symmetrical molecule XY_2, in which the X atom is replaced by an isotope $X^{(i)}$, the following relation holds between the zero-order frequencies of XY_2 and $X^{(i)}Y_2$:[8]

$$\omega_1^{(i)}/\omega_1=1;$$

$$f^2=\left(\frac{\omega_2^{(i)}}{\omega_2}\right)^2=\left(\frac{\omega_3^{(i)}}{\omega_3}\right)^2=\frac{1+(2m_Y)/(m_X^{(i)})}{1+(2m_Y)/(m_X)} \qquad (4)$$

where ω_1, ω_2, and ω_3 are the zero-order frequencies,

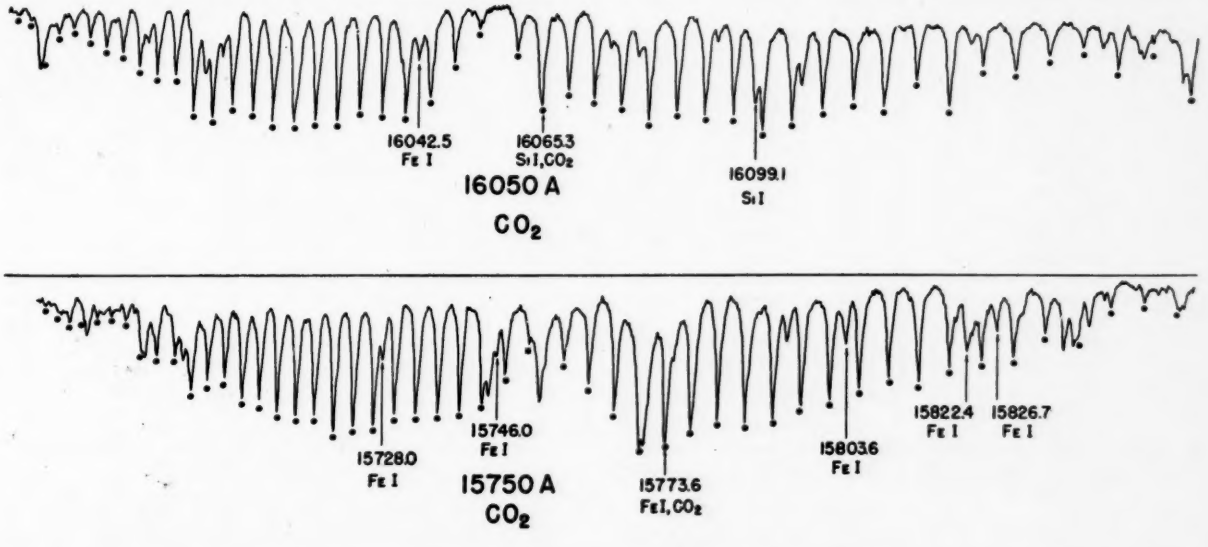

FIG. 5. Combination bands of CO_2 near 1.6μ. The CO_2 lines are indicated by dots and solar lines of Fe I and Si I are also shown. The horizontal line denotes zero intensity.

[7] D. M. Dennison, private communication.
[8] Gerhard Herzberg, *Infra-Red and Raman Spectra of Polyatomic Molecules* (D. Van Nostrand Company, Inc., New York, 1945), p. 230.

TABLE II. Measured wave numbers of rotational lines of CO_2.

m	ν(obs)	O−C
2.06μ band $C^{12}O_2^{16}$		
+1	4854.27	+0.01
3	4855.83	+0.03
5	4857.29	−0.04
7	4858.82	−0.02
9	4860.33	0.00
11	4861.78	−0.02
13	4863.23	−0.03
15	4864.69	−0.01
17	4866.13	+0.01
19	4867.53	0.00
21	4868.98	+0.06
23	4870.37	+0.08
25	4871.74	+0.09
27	4873.00	+0.01
29	4874.29	−0.02
31	4875.59	−0.02
35	4878.12	−0.05
37	4879.39	−0.03
39	4880.66	0.00
41	4881.86	−0.01
43	4883.05	−0.02
+45	4884.29	+0.03
−2	4851.92	0.00
4	4850.31	−0.03
6	4848.76	+0.03
8	4847.06	−0.06
10	4845.42	−0.06
12	4843.76	+0.03
14	4842.12	−0.05
16	4840.50	+0.01
18	4838.82	−0.01
20	4837.11	+0.04
22	4835.39	+0.05
26	4831.86	+0.04
28	4830.08	+0.04
30	4828.27	+0.03
32	4826.46	+0.03
34	4824.57	−0.02
36	4822.74	−0.01
38	4820.85	−0.03
40	4818.99	−0.02
−42	[4817.09	−0.02
2.01μ band $C^{12}O_2^{16}$		
+1	4978.52	−0.04
3	4980.12	+0.03
5	4981.58	−0.06
7	4983.07	+0.02
9	4984.50	+0.02
11	4985.88	−0.01
13	4987.27	+0.01
15	4988.61	0.00
17	4989.90	−0.02
19	4991.15	−0.06
21	4992.42	−0.05
25	4994.88	−0.01
29	4997.20	+0.01
31	4998.32	+0.03
33	4999.39	+0.02
35	5000.39	−0.02
37	5001.44	+0.01
39	5002.45	+0.04
41	5003.40	+0.03
43	5004.30	+0.01
45	5005.17	−0.01
47	5006.05	0.00
49	5006.89	+0.01
+51	5007.66	−0.02
−2	4976.25	+0.03
4	4974.58	−0.04
6	4972.94	−0.05
2.01μ band $C^{12}O_2^{16}$		
8	4971.33	0.00
10	4969.62	−0.02
12	4967.93	0.00
14	4966.18	0.00
16	4964.43	+0.03
18	4962.61	+0.01
20	4960.74	−0.02
22	4958.85	−0.05
24	4957.01	0.00
26	4955.11	+0.03
28	4953.11	−0.02
30	4951.17	+0.02
32	4949.16	+0.02
34	4947.12	+0.08
36	4945.00	−0.03
38	4942.93	−0.01
40	4940.82	+0.01
42	4938.69	+0.04
44	4936.50	+0.03
46	4934.28	+0.02
48	4932.06	+0.04
50	4929.71	−0.04
−52	4927.43	−0.02
1.96μ band $C^{12}O_2^{16}$		
+3	5101.94	−0.02
5	5103.51	+0.04
7	5104.97	0.00
9	5106.48	+0.04
11	5107.90	+0.01
13	5109.37	+0.05
15	5110.79	+0.06
17	5112.10	−0.01
19	5113.50	+0.02
21	5114.82	0.00
23	5116.13	+0.01
25	5117.39	+0.05
27	5118.69	−0.03
31	5121.14	−0.07
33	5122.45	+0.03
35	5123.55	−0.05
37	5124.76	−0.01
41	5127.03	−0.01
+43	5128.21	+0.07
−2	5098.01	−0.06
4	5096.45	−0.04
6	5094.84	−0.03
8	5093.22	−0.02
10	5091.58	−0.01
12	5089.94	+0.03
14	5088.26	+0.07
16	5086.58	+0.08
18	5084.79	+0.03
20	5082.99	−0.01
24	5079.35	−0.07
26	5077.55	−0.05
28	5075.74	−0.02
30	5073.93	+0.04
32	5072.02	+0.01
36	5068.13	−0.05
38	5066.20	−0.03
40	5064.29	+0.03
−42	5062.31	+0.04
1.65μ band $C^{12}O_2^{16}$		
+3	6078.26	−0.05
5	6079.81	−0.04
7	6081.37	0.00
9	6082.96	+0.07
11	6084.40	0.00
13	6085.88	−0.01
1.65μ band $C^{12}O_2^{16}$		
15	6087.40	+0.03
17	6088.92	+0.08
19	6090.33	+0.03
21	6091.74	0.00
23	6093.19	+0.02
25	6094.56	−0.03
29	6097.35	−0.05
31	6098.77	−0.01
33	6100.11	−0.04
35	6101.56	+0.05
+39	6104.24	+0.05
−2	6074.38	−0.03
4	6072.80	−0.03
6	6071.17	−0.07
8	6069.66	+0.02
10	6068.04	0.00
12	6066.38	−0.03
14	6064.80	+0.02
16	6063.18	+0.04
18	6061.53	+0.04
20	6059.88	+0.04
22	6058.11	−0.05
24	6056.57	+0.09
26	6054.77	−0.02
28	6053.13	+0.04
30	6051.33	−0.04
−32	6049.61	−0.04
1.60μ band $C^{12}O_2^{16}$		
+1	6228.72	+0.05
3	6230.19	0.00
5	6231.67	−0.02
7	6233.14	−0.01
9	6234.58	−0.01
11	6235.98	−0.02
13	6237.38	0.00
15	6238.78	+0.05
17	6240.07	+0.01
19	6241.36	+0.01
21	6242.64	+0.02
23	6243.89	+0.03
25	6245.06	0.00
27	6246.23	−0.01
29	6247.40	0.00
31	6248.49	−0.03
33	6249.59	−0.03
35	6250.68	0.00
37	6251.74	+0.03
39	6252.72	0.00
+41	6253.69	−0.01
−2	6226.35	+0.02
4	6224.72	−0.01
6	6223.06	−0.05
8	6221.43	−0.03
10	6219.77	0.00
12	6218.06	−0.01
14	6216.36	+0.03
16	6214.55	−0.01
18	6212.77	0.00
20	6210.92	−0.02
22	6209.10	+0.01
24	6207.21	0.00
26	6205.33	+0.03
28	6203.36	−0.01
30	6201.44	+0.04
32	6199.44	+0.03
34	6197.40	+0.03
36	6195.33	0.00
38	6193.26	+0.01
40	6191.15	+0.01
42	6188.96	−0.05
1.57μ band $C^{12}O_2^{16}$		
+1	6350.29	−0.04
3	6351.91	+0.05
5	6353.36	+0.01
7	6354.81	0.00
9	6356.23	−0.02
11	6357.64	−0.01
13	6359.02	−0.01
15	6360.39	+0.02
17	6361.69	0.00
19	6362.94	−0.02
21	6364.24	+0.01
23	6365.41	−0.04
25	6366.63	−0.02
27	6367.80	−0.01
29	6368.94	−0.01
31	6370.04	−0.02
33	6371.13	0.00
35	6372.19	+0.01
+37	6373.24	+0.05
−2	6348.08	+0.09
4	6346.47	+0.07
6	6344.78	+0.01
8	6343.08	−0.03
10	6341.40	−0.02
12	6339.71	0.00
14	6337.94	−0.03
16	6336.21	+0.02
18	6334.41	−0.02
20	6332.56	+0.01
22	6330.64	−0.05
24	6328.79	−0.05
26	6326.87	−0.01
28	6324.95	+0.03
30	6322.95	+0.01
32	6320.87	−0.06
34	6318.88	−0.02
36	6316.84	+0.01
38	6314.77	+0.04
40	6312.57	−0.03
42	6310.42	−0.02
44	6308.27	0.00
−46	6306.08	+0.04
1.54μ band $C^{12}O_2^{16}$		
+5	6506.95	+0.08
7	6508.43	+0.05
9	6509.92	+0.05
11	6511.36	+0.01
13	6512.80	0.00
15	6514.20	−0.02
17	6515.65	−0.02
19	6517.05	−0.02
21	6518.49	+0.03
23	6519.89	+0.06
25	6521.21	+0.02
27	6522.53	0.00
29	6523.81	−0.04
31	6525.09	−0.06
33	6526.36	−0.06
35	6527.68	−0.02
37	6528.92	−0.04
41	6531.44	+0.03
+43	6532.68	+0.07
−2	6501.45	−0.02
4	6499.89	+0.02
6	6498.28	+0.01
10	6494.99	−0.03
12	6493.38	+0.01
14	6491.66	−0.04
16	6490.01	0.00
18	6488.33	+0.02

TABLE II.—(*Continued*).

m	ν(obs)	O−C
1.54μ band $C^{12}O_2^{16}$		
20	6486.52	−0.07
22	6484.83	−0.02
24	6483.07	−0.03
28	6479.58	+0.05
30	6477.69	−0.03
34	6474.09	+0.03
36	6472.24	+0.01
38	6470.40	+0.04
−40	6468.51	+0.03
2.08μ band $C^{12}O_2^{16}$		
+3	4809.97	+0.03
4	4810.70	+0.04
6	4812.17	+0.03
8	4813.62	+0.01
9	4814.49	+0.01
11	4815.94	−0.03
12	4816.51	−0.01
13	4817.41	−0.03
14	4817.91	−0.03
16	4819.28	−0.05
17	4820.33	0.00
19	4821.77	+0.02
20	4822.05	−0.01
21	4823.18	+0.02
22	4823.38	−0.01
25	4825.97	+0.03
26	4825.97	−0.02
27	4827.30	0.00
+28	4827.30	+0.04
−2	4806.14	+0.09
4	4804.51	+0.04
5	4803.66	+0.04
6	4802.87	−0.01
7	4802.01	+0.01
8	4801.23	−0.04
9	4800.33	−0.03
10	4799.58	−0.06
11	4798.66	−0.04
12	4797.98	−0.02
15	4795.33	+0.01
16	4794.70	+0.02
17	4793.63	+0.03
18	4793.05	+0.05
19	4791.88	+0.02
20	4791.33	+0.03
21	4790.08	−0.02
22	4789.59	0.00
23	4788.29	−0.02
24	4787.84	−0.03
25	4786.48	−0.03
26	4786.09	−0.04
29	4782.85	+0.01
30	4782.58	−0.03
31	4780.96	−0.02
32	4780.82	−0.01
35	4777.22	+0.03
−36	4777.22	0.00

m	ν(obs)	O−C
2.01μ band $C^{12}O_2^{16}$		
+5	4969.14	−0.04
7	4970.66	0.00
9	4972.08	−0.03
11	4973.49	−0.04
12	4974.13	−0.03
13	4974.91	−0.01
14	4975.50	−0.02
16	4976.82	−0.03
17	4977.66	+0.03
18	4978.17	+0.02
19	4978.97	+0.05
20	4979.45	+0.03
+22	4980.65	0.00
−7	4959.72	0.00
9	4958.07	+0.02
11	4956.36	+0.02
14	4953.81	0.00
16	4952.04	−0.01
18	4950.32	+0.03
20	4948.48	+0.01
22	4946.70	+0.05
23	4945.52	0.00
25	4943.62	+0.01
27	4941.66	−0.03
29	4939.71	−0.02
30	4939.11	0.00
31	4937.74	0.00
32	4937.17	0.00
34	4935.22	+0.01
36	4933.22	−0.01
38	4931.20	−0.03
2.10μ band $C^{12}O_2^{16}$		
+3	4750.40	+0.01
5	4751.94	+0.01
7	4753.45	0.00
9	4754.96	0.00
11	4756.44	−0.02
15	4759.42	−0.02
19	4762.32	−0.02
21	4763.76	−0.02
25	4766.62	0.00
27	4768.01	0.00
29	4769.41	+0.01
31	4770.81	+0.04
35	4773.47	+0.02
+37	4774.76	−0.03
−2	4746.52	+0.02
4	4744.92	0.00
6	4743.33	0.00
8	4741.73	−0.01
10	4740.13	0.00
12	4738.51	0.00
14	4736.87	−0.01

m	ν(obs)	O−C
2.10μ band $C^{13}O_2^{16}$		
20	4731.90	−0.03
22	4730.25	−0.01
−24	4728.60	+0.02
2.05μ band $C^{13}O_2^{16}$		
+3	4889.65	+0.05
5	4891.11	+0.01
7	4892.57	−0.01
9	4894.01	−0.01
11	4895.44	0.00
13	4896.83	0.00
15	4898.20	+0.01
17	4899.52	0.00
19	4900.84	+0.01
21	4902.12	+0.01
23	4903.37	+0.03
25	4904.62	0.00
27	4905.77	−0.01
29	4906.95	0.00
31	4908.09	0.00
33	4909.19	−0.01
+35	4910.33	+0.04
−2	4885.73	−0.01
6	4882.51	−0.01
12	4877.48	0.00
18	4872.18	−0.02
24	4866.66	−0.02
28	4860.88	−0.03
−36	4854.90	+0.02
2.09μ band $C^{12}O^{16}O^{18}$		
+9	4797.65	+0.05
11	4798.95	−0.01
15	4801.65	+0.02
16	4802.25	−0.03
19	4804.26	+0.03
20	4804.84	−0.01
22	4806.08	−0.03
23	4806.69	−0.04
25	4807.93	−0.02
26	4808.56	+0.01
28	4809.76	+0.01
29	4810.33	−0.01
+30	4810.96	+0.04
−3	4788.96	−0.04
5	4787.48	−0.01
8	4785.21	0.00
10	4783.65	0.00
12	4782.09	+0.01
13	4781.30	+0.01
14	4780.51	+0.02

m	ν(obs)	O−C
2.09μ band $C^{12}O^{16}O^{18}$		
15	4779.70	+0.02
17	4778.06	0.00
21	4774.73	−0.02
22	4773.90	−0.02
23	4773.08	+0.01
24	4772.20	−0.02
25	4771.35	−0.02
26	4770.50	−0.01
27	4769.66	+0.02
28	4768.78	0.00
29	4767.91	+0.01
30	4767.02	0.00
−31	4766.15	+0.01
2.04μ band $C^{12}O^{16}O^{18}$		
+4	4907.65	+0.03
5	4908.28	−0.05
6	4909.02	0.00
7	4909.72	+0.01
9	4911.12	+0.05
10	4911.71	−0.03
11	4912.41	+0.01
12	4913.14	+0.08
13	4913.72	+0.01
14	4914.37	+0.01
15	4915.06	+0.09
16	4915.60	−0.03
17	4916.27	+0.01
18	4916.88	0.00
19	4917.49	0.00
21	4918.70	0.00
22	4919.26	−0.04
23	4919.87	−0.02
25	4921.01	−0.04
26	4921.58	−0.04
27	4922.12	−0.07
+31	4924.50	+0.10
−3	4902.53	0.00
4	4901.72	−0.05
6	4900.25	+0.01
8	4898.70	+0.01
9	4897.94	+0.04
10	4897.06	−0.05
11	4896.31	0.00
13	4894.67	−0.01
15	4893.02	−0.01
16	4892.18	0.00
17	4891.33	−0.02
20	4888.83	+0.05
21	4887.86	−0.05
22	4887.03	0.00
23	4886.18	+0.04
−26	4883.44	0.00

and m_X and m_Y are the masses of the atoms X and Y, respectively. The superscript (i) denotes the isotope atom, in this case C^{13}. For $m_X=12$, $m_Y=16$ and $m_X^{(i)}=13$, $f=0.97154$. The potential constants were then altered as follows:

$$\begin{array}{lll} \omega_1^{(i)}=\omega_1 & x_{11}^{(i)}=x_{11} & x_{12}^{(i)}=fx_{12} \\ \omega_2^{(i)}=f\omega_2 & x_{22}^{(i)}=f^2x_{22} & x_{13}^{(i)}=fx_{13} \\ \omega_3^{(i)}=f\omega_3 & x_{33}^{(i)}=f^2x_{33} & x_{23}^{(i)}=f^2x_{23}. \\ & b^{(i)}=f^{\frac{1}{2}}b & \end{array} \qquad (5)$$

Similarly, for the linear symmetrical molecule XY_2, in which one of the Y atoms is replaced by $Y^{(i)}$, we have

$$f_1=1-\frac{\Delta m_Y}{4(m_Y+\Delta m_Y)};$$

$$f_2=f_3=1-\frac{m_X}{2(m_X+2m_Y)}\times\frac{\Delta m_Y}{(m_Y+\Delta m_Y)}. \qquad (6)$$

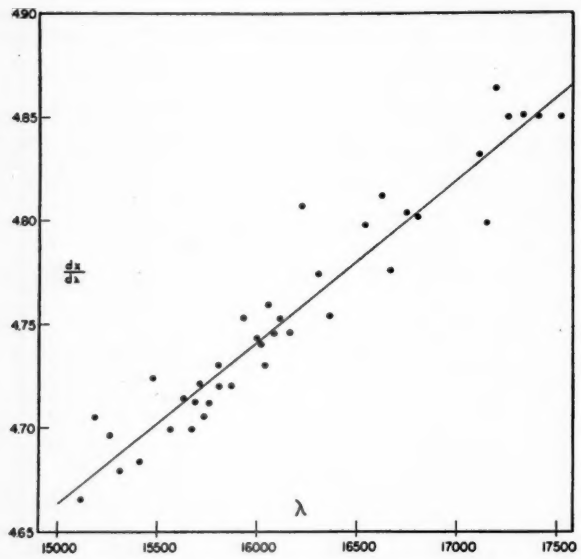

FIG. 6. Variation of dispersion with wave-length on solar tracings in the 1.6μ region. The dots represent individual measurements and the straight line has been determined by least squares.

Equations (6) are valid if the mass difference $\Delta m_Y = m_Y^{(i)} - m_Y$ is small compared with m_Y. For $C^{12}O^{16}O^{18}$ we obtain $f_1 = 0.97222$, and $f_2 = f_3 = 0.99242$. The modified potential constants were then obtained by multiplying ω_1, ω_2, and ω_3 by f_1, f_2, and f_3, respectively; x_{11}, x_{22}, and x_{33} by f_1^2, f_2^2, and f_3^2, respectively; x_{12}, x_{13}, and x_{23} by f_1f_2, f_1f_3 and f_2f_3, and b by $(f_1f_2f_3)^{\frac{1}{2}}$.

The solution of the determinant (3), carried out with the aid of the approximate potential constants for $C^{13}O_2^{16}$ and $C^{12}O^{16}O^{18}$, leads to the values of the band centers in column three of Table I. As a check on the method of calculation, the centers of the 2μ bands of $C^{12}O_2^{16}$ were also computed, the results agreeing exactly with those obtained originally by Adel and Dennison.

Since the ω_1 band is easily the most intense of the 2μ triad, its isotope companions have the highest probability of appearing in the solar spectrum. The calculated centers are, for $C^{13}O_2^{16}$, 4892.1 cm^{-1}, and for $C^{12}O^{16}O^{18}$, 4909.4. As shown in Fig. 2, weak bands are found at 4888.84 cm^{-1} and at 4904.75 cm^{-1}. The negative branch of the $C^{13}O_2^{16}$ band falls on the positive branch of the relatively strong ω_1 band, although several individual components of the former may be recognized. The negative branch of the $C^{12}O^{16}O^{18}$ band is also blended with the positive branch of the neighboring band of $C^{13}O_2^{16}$. It is interesting to note that the lines of the $C^{12}O^{16}O^{18}$ band have approximately one-half the spacing of those of ω_1, whereas the spacing of the $C^{13}O_2^{16}$ band is practically identical with that of ω_1. These facts are precisely in accordance with theory. Because of the identity of the oxygen atoms in ordinary CO_2, and also because the spin of the oxygen nucleus is zero, alternate rotational lines (those arising from antisymmetric levels) are absent. Conversely, since the $C^{12}O^{16}O^{18}$ molecule is not symmetrical, every rotational line appears.

The weakest isotope bands are those corresponding to ω_2, the calculated positions being 4737.8 cm^{-1} for $C^{13}O_2^{16}$ and 4797.5 cm^{-1} for $C^{12}O^{16}O^{18}$. The observed centers are 4748.06 cm^{-1} and 4791.22 cm^{-1}, respectively. Although the discrepancy between the observed and the calculated centers for the $C^{13}O_2^{16}$ band is 10 cm^{-1}, its intensity and spacing render the identification quite conclusive. The C^{13} isotope band corresponding to ω_0 falls in the middle of the positive branch of ω_1 and is not observed. Portions of the O^{18} companion to ω_0 are visible on low sun tracings in the region between ω_0

TABLE III. Determination of wave-length scale.

λ(obs)	dx/dλ	O−C	λ(obs)	dx/dλ	O−C
15073.39		+0.17	16126.12		−0.06
	4.665			4.746	
15151.56		+0.19	16195.34		+0.14
	4.705			4.807	
15207.50		−0.20	16241.79		−0.32
15230.50		+0.06	16284.87		−0.04
	4.696			4.774	
15283.37		−0.17	16316.33		−0.07
	4.679			4.754	
15335.45		−0.03	16404.76		+0.13
	4.691				
15376.97		+0.02	16435.22		+0.02
	4.683			4.778	
15438.62		+0.18	16505.12		+0.05
	4.724			4.798	
15501.30		−0.02	16561.85		−0.12
15531.89		+0.02	16589.75		+0.17
	4.699			4.812	
15591.61		+0.08	16645.96		−0.04
	4.714			4.776	
15661.97		−0.01	16681.05		+0.05
	4.699				
15677.57		−0.05	16719.18		+0.02
	4.712			4.804	
15695.80		0.00	16771.44		−0.17
	4.721			4.802	
15719.12		−0.04	16835.75		0.00
	4.705				
15736.08		+0.04	16890.24		+0.06
	4.712				
15769.42		0.00	17081.40		+0.08
	4.730			4.832	
15789.06		+0.03	17138.41		−0.01
	4.720			4.799	
15822.98		+0.04	17156.56		+0.14
				4.864	
15837.78		+0.04	17225.62		−0.06
	4.720			4.850	
15888.67		+0.18	17284.42		−0.18
	4.753				
15960.05		0.00	17302.23		+0.08
				4.851	
15980.88		0.00	17362.16		+0.01
	4.743			4.851	
16002.26		−0.07	17439.84		0.00
	4.741				
16024.45		−0.01	17470.48		−0.04
	4.730			4.850	
16046.48		−0.02	17564.09		0.00
	4.759				
16056.44		−0.03			
	4.746				
16100.98		−0.02			
	4.753				
16126.12		−0.06			

and ω_1, but at long atmospheric paths this region also becomes filled with lines of water vapor.

The Excited-State Bands

Evidence has already been given[9] for the identification of the 2.08μ band as one of the triad of bands originating from the excited vibrational level 01_10 and terminating in the three upper levels $\begin{Bmatrix} 2 & 1_1 & 1 \\ 1 & 3_1 & 1 \\ 0 & 5_1 & 1 \end{Bmatrix}$. The calculated center of the band is 4805.6 cm^{-1}, the observed value 4807.60 cm^{-1}. The calculated centers of the remaining two bands of the triad, at 4970.5 cm^{-1} and at 5131.6 cm^{-1}, fall within the strong bands ω_0 and ω_1. Numerous individual lines nevertheless appear to be present and to show the expected doublet pattern. Enough lines of the former band occur to permit a determination of the band center with the aid of the value of B_{010} derived from the 4807.60 cm^{-1} band. The resulting "observed" value is 4965.36 cm^{-1}, in good agreement with theory. It is interesting to note that as predicted by theory, all values of J, both even and odd, occur in the difference bands, in contrast to the ground state bands, where lines arising from levels of even J only are found.

V. EVALUATION OF ROTATIONAL CONSTANTS

The moment of inertia of a polyatomic molecule in any given vibrational energy state may be calculated from well-known formulas in terms of the equilibrium moment of inertia and of n rotational constants, where n is the number of normal vibrational frequencies of the molecule. For CO_2, the rotational constants have been evaluated by Dennison[6] from a discussion of four infra-red bands observed in the laboratory and of three bands observed in the Venus spectrum. New values of the constants were later obtained by Herzberg[10] from a re-discussion of the same observations. It is believed that the new data given in Table II are sufficiently accurate to warrant a re-determination of the rotational constants.

TABLE IV. Constants of least squares solutions.

Band	ν_0	a	b	c
		$C^{13}O_2^{16}$		
2.06μ	4853.48	0.77926	−0.00209	-6.2×10^{-7}
2.01μ	4977.78	0.77722	−0.00371	-7.5×10^{-7}
1.96μ	5099.64	0.77905	−0.00267	-7.8×10^{-7}
1.65μ	6075.98	0.78065	−0.00138	-2.2×10^{-6}
1.60μ	6227.90	0.77614	−0.00357	-1.8×10^{-7}
1.57μ	6349.56	0.77640	−0.00371	-4.1×10^{-7}
1.54μ	6503.08	0.77963	−0.00212	-3.6×10^{-7}
2.08μ (J even)	4807.62	0.77920	−0.00184	-4.0×10^{-7}
2.08μ (J odd)	4807.57	0.77737	−0.00262	-1.0×10^{-6}
2.01μ (J even)	4965.37	0.78000	−0.00338	-6.9×10^{-7}
2.01μ (J odd)	4965.35	0.77870	−0.00371	-3.2×10^{-7}
		$C^{13}O_2^{16}$		
2.10μ	4748.06	0.77980	−0.00142	-2.0×10^{-7}
2.05μ	4887.30	0.77716	−0.00344	-3.5×10^{-6}
		$C^{12}O^{16}O^{18}$		
2.09μ	4791.22	0.73140	−0.00249	-3.8×10^{-6}
2.04μ	4904.75	0.73128	−0.00324	-4.3×10^{-6}

[9] Mohler, McMath, and Goldberg, Phys. Rev. **75**, 520 (1949).
[10] See reference 8, p. 395.

Ground-State Bands

We shall discuss first the analysis of the seven bands that arise from the ground vibrational state of $C^{12}O_2^{16}$. These bands result from transitions of type $\Sigma_g^+-\Sigma_u^+$ and consequently only those lines occur that originate from lower rotational levels of even J. The wave numbers of the lines in a vibration-rotation band may be represented by the well-known formula:

$$\nu=\nu_0+am+bm^2+cm^3, \tag{7}$$

where, for the CO_2 bands under consideration, $m=1, 3, 5,\cdots$ for the lines of the positive branch, and $m=-2, -4, -6,\cdots$ for those of the negative branch. In Eq. (7), ν_0 is the band center in cm^{-1}, $a=B'+B''$, $b=B'-B''$, and $c=-2(D'+D'')$. The constant $B=h/8\pi^2Ic$, where I is the moment of inertia for the given vibrational state, the single and double primes referring to the upper and lower vibrational states, respectively. The quantity D measures the centrifugal stretching of the molecule.

The constants of Eq. (7) may be determined for each band from the observed wave numbers by the method of combination differences, or by least squares. The latter method was followed in the present investigation, the values of the constants being given in Table IV. The wave numbers calculated from Eq. (7) with these constants yielded the O−C residuals in column four of Table II. From the relations $a+b=2B'$ and $a-b=2B''$, the B-values appropriate to the various vibrational levels were calculated and appear in the third and fifth columns of Table V. For the seven bands originating from the ground state, the values of B'' should in theory be identical. The total spread found is 0.0009 cm^{-1}, which is not surprising in view of uncertainties in the wave-length scales and of the blending

TABLE V. Observed and calculated convergences of CO_2 bands.

Band	Transition	B''(obs)	B''(calc)	B'(obs)	B'(calc)
		$C^{12}O_2^{16}$			
2.06μ	$0\,0_0\,0-\begin{Bmatrix}0\,4_0\,1\\1\,2_0\,1\\2\,0_0\,1\end{Bmatrix}$	0.39068	0.39055	0.38858	0.38852
2.01μ		0.39046	0.39055	0.38676	0.38693
1.96μ		0.39086	0.39055	0.38819	0.38775
1.65μ	$0\,0_0\,0-\begin{Bmatrix}0\,6_0\,1\\1\,4_0\,1\\2\,2_0\,1\\3\,0_0\,1\end{Bmatrix}$	0.39102	0.39055	0.38964	0.38931
1.60μ		0.38986	0.39055	0.38628	0.38723
1.57μ		0.39006	0.39055	0.38634	0.38679
1.54μ		0.39088	0.39055	0.38876	0.38809
	(J'' even)	0.39052		0.38868	
2.08μ	$0\,1_1\,0-\begin{Bmatrix}0\,5_1\,1\\1\,3_1\,1\\2\,1_1\,1\end{Bmatrix}$		0.39118		
	(J'' odd)	0.39000		0.38738	
	(J'' even)	0.39169		0.38830	
2.01μ			0.39118		
	(J'' odd)	0.39120		0.38750	
—		—		—	
		$C^{13}O_2^{16}$			
2.10μ	$0\,0_0\,0-\begin{Bmatrix}0\,4_0\,1\\1\,2_0\,1\\2\,0_0\,1\end{Bmatrix}$	0.39061	—	0.38919	
2.05μ		0.39030	—	0.38686	
—		—		—	
		$C^{12}O^{16}O^{18}$			
2.09μ	$0\,0_0\,0-\begin{Bmatrix}0\,4_0\,1\\1\,2_0\,1\\2\,0_0\,1\end{Bmatrix}$	0.36694		0.36446	
2.04μ		0.36728		0.36400	
—		—		—	

TABLE VI. Squares of the coefficients of CO_2 zero-order wave functions.

i	a_i^2	b_i^2	c_i^2	d_i^2
1	0.4506	0.4399	0.1095	
2	0.3098	0.0260	0.6642	
3	0.2351	0.5352	0.2297	
4	0.3587	0.4394	0.1792	0.0227
5	0.2990	0.0002	0.3309	0.3699
6	0.2159	0.1361	0.1143	0.5337
7	0.1264	0.4243	0.3756	0.0737

of the 1.6μ bands with solar and telluric lines. It is to be noted that the agreement among the B''-values is considerably better for the 2μ bands, which were measured in the laboratory.

The data of Table V may now be employed for the evaluation of the rotational constants of CO_2 and of the equilibrium moment of inertia. Let n_1, n_2, and n_3 be the vibrational quantum numbers of a particular CO_2 state. Then the convergence of the rotational levels is given by[6]

$$B_{n_1n_2n_3}=B_e[1+\alpha_1(n_1+\tfrac{1}{2})+\alpha_2(n_2+1)+\alpha_3(n_3+\tfrac{1}{2})] \quad (8)$$

where B_e refers to the equilibrium position of the molecule and the constants α give the interaction between vibration and rotation. Equation (8) is valid only in the absence of Fermi resonance. For a group of n levels in resonance interaction, the following expressions may be written for the individual levels.[6] Let B_1^0, $B_2^0\cdots B_n^0$ be the appropriate values of B in the absence of resonance, as given by Eq. (8). Also, let B_1, $B_2\cdots B_n$ be the actual B values. Then

$$\begin{aligned} B_1&=a_1^2B_1^0+b_1^2B_2^0+\cdots \\ B_2&=a_2^2B_1^0+b_2^2B_2^0+\cdots \\ &\cdots \\ B_n&=a_n^2B_1^0+b_n^2B_2^0+\cdots, \end{aligned} \quad (9)$$

where each summation is carried out over all n levels. The coefficients a, b, $c,\cdots$ are defined as follows. If Ψ_1^0, $\Psi_2^0,\cdots$ are the wave functions of the respective unperturbed states, the true wave function for state i is

$$\Psi_i=a_i\Psi_1^0+b_i\Psi_2^0+\cdots, \quad (10)$$

wher the sum of the squares of the coefficients is unity. The coefficients may be determined from the minors of the secular energy determinant, which for the triad of resonating levels

$$\begin{Bmatrix} 2 & 0_0 & 1 \\ 1 & 2_0 & 1 \\ 0 & 4_0 & 1 \end{Bmatrix} \quad (11)$$

is given by Eq. (3). A similar determinant may be written for the four resonating levels,

$$\begin{Bmatrix} 0 & 6_0 & 1 \\ 1 & 4_0 & 1 \\ 2 & 2_0 & 1 \\ 3 & 0_0 & 1 \end{Bmatrix} \quad (12)$$

that are responsible for the 1.6μ bands. The squares of the coefficients for both sets of resonating levels are given in Table VI, where the index i is 1, 2, and 3 for the triad of levels (11) and 4, 5, 6 and 7 for the quartet of levels (12).

The observed convergences $B'-B''$ of the 1.6μ and 2μ bands are given in the fourth column of Table IV. The theoretical values of $B'-B''$ may be obtained in terms of B_e and the rotational constants from Eqs. (8) and (9). Equating the theoretical and observed convergences and inserting the numerical values of the coefficients of Eq. (9), we obtain an equation for each of the seven bands as follows:

2μ bands

$$B_e(0.6589\alpha_1+2.6822\alpha_2+\alpha_3)=-0.002093; \quad (13)$$
$$B_e(1.3544\alpha_1+1.2912\alpha_2+\alpha_3)=-0.003708; \quad (14)$$
$$B_e(0.9946\alpha_1+2.0108\alpha_2+\alpha_3)=-0.002649; \quad (15)$$

1.6μ bands

$$B_e(0.8659\alpha_1+4.2228\alpha_2+\alpha_3)=-0.001383; \quad (16)$$
$$B_e(1.7717\alpha_1+2.4566\alpha_2+\alpha_3)=-0.003573; \quad (17)$$
$$B_e(1.9658\alpha_1+2.0684\alpha_2+\alpha_3)=-0.003706; \quad (18)$$
$$B_e(1.3966\alpha_1+3.2068\alpha_2+\alpha_3)=-0.002116. \quad (19)$$

Solution of the foregoing equations by least squares gave $B_e\alpha_1=-0.00103$; $B_e\alpha_2=+0.00064$; $B_e\alpha_3=-0.00306$.

In similar fashion, Eqs. (8) and (9) may be employed in obtaining formulas for the average line spacing $B'+B''$, for which the observed values appear in the

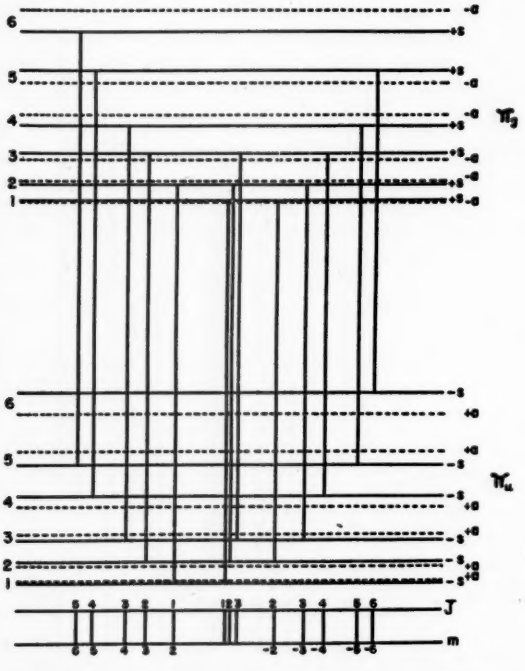

FIG. 7. Schematic energy level diagram and band pattern for Π_u–Π_g transition in CO_2.

third column of Table IV. Substitution of the previously calculated $B_e\alpha$ in these formulas yields seven independent determinations of B_e as follows:

Band	B_e	Band	B_e
1.54μ	0.3924	1.96μ	0.3924
1.57μ	0.3915	2.01μ	0.3918
1.60μ	0.3911	2.06μ	0.3921
1.64μ	0.3924	Mean=	0.3920

Finally, the derived values of B_e and α have been employed to obtain the calculated values of B'' and B' in the fourth and sixth columns of Table V. The value $B_e=0.3920$ yields for the equilibrium moment of inertia $I_e=71.35\times10^{-40}$ g cm^2, where we have taken $h=6.624\times10^{-27}$ erg sec.

The rotational constants obtained here differ somewhat from those appearing in the literature, as is shown in Table VII. We understand from a private communication, however, that Professor Herzberg has recently secured new results from a study of the photographic infra-red bands of CO_2 which agree more closely with those of this paper. In particular, he obtains $B_{000}=0.39037$.

Difference Bands

The difference bands originating from the lower level 01_10 are of the type $\Pi_u-\Pi_g$.[11] A schematic energy level diagram for this transition is shown in Fig. 7. Each J-level is split into two sub-levels, the separation $\Delta\nu$ increasing with J according to

$$\Delta\nu=qJ(J+1) \tag{20}$$

where q is a constant. The symmetric levels are represented by solid and the antisymmetric levels by dotted lines. In CO_2 only the symmetric levels are populated. It will be noted that in the Π_u state the lower sub-levels of odd J and the upper sub-levels of even J are symmetric, whereas the converse is true for Π_g. The resulting band will therefore consist of two series of lines, originating, respectively, from lower levels of even and odd J, and characterized by slightly different values of B' and B''. Thus

$$\nu(J_{\text{even}})=\nu_0+(B'+B'')_{\text{even}}m+(B'-B'')_{\text{even}}m^2 \tag{21}$$
$$m=+1,+3,+5,\cdots$$
$$-2,-4,-6,\cdots$$

$$\nu(J_{\text{odd}})=\nu_0+(B'+B'')_{\text{odd}}m+(B'-B'')_{\text{odd}}m^2 \tag{22}$$
$$m=+2,+4,+6,\cdots\quad -1,-3,-5.$$

Also,

$$B_{\text{even}}-B_{\text{odd}}=q. \tag{23}$$

The constants of Eqs. (21) and (22) were determined by least squares from the wave numbers of the bands observed at 2.01μ and 2.08μ, with the results given in Tables IV and V. Two independent values of q for the ground state may now be obtained by application of Eq. (23). From the 2.01μ band we find $q=0.00049$ cm^{-1} and from the 2.08μ band $q=0.00052$ cm^{-1}, which is to be compared with Herzberg's[10] determination, from other infra-red bands, of $q=0.00034$ cm^{-1}. Similarly, for the two upper sets of levels, we get $q=0.00080$ cm^{-1} and 0.00130 cm^{-1}.

[11] See reference 8, p. 389.

TABLE VII. Rotational constants of CO_2.

	Lake Angelus	Dennison	Herzberg
B_e	0.3920	0.3925	0.3906
B_{000}	0.3906	0.3911	0.3895
$B_e\alpha_1$	−0.00103	−0.00058	−0.00056
$B_e\alpha_2$	+0.000640	+0.00045	+0.00062
$B_e\alpha_3$	−0.00306	−0.00307	−0.0029

The accuracy of the foregoing results is perhaps questionable, in view of the fact that the values of B_{010} derived from the 2.01μ and 2.08μ bands should be identical, whereas actually they differ by about 0.0011 cm^{-1}. The discrepancy is not surprising because relatively few lines in each band are free from blending with other lines of CO_2 or of H_2O. We would nevertheless expect higher accuracy for the determination of q than for the individual values of B.

It is interesting to compare the observed values of B_{010} with the value calculated from Eq. (8). The computed value, $B_{010}=0.3913$, is to be compared with the mean of the two values determined from each band, *viz.*, 0.3914 for the 2.01μ band and 0.3903 for the 2.08μ band. Further analysis of the II–II bands in the laboratory would be highly desirable, especially if the measurements are carried out with a heated sample, and in the absence of water vapor.

Isotope Bands

Four bands arising from isotopes of CO_2 are suitable for analysis, the 2.05μ and 2.10μ bands of $C^{13}O_2^{16}$ and the 2.04μ and 2.09μ bands of $C^{12}O^{16}O^{18}$. All four bands suffer from overlapping by neighboring telluric bands. One result of the blending is to render uncertain the assignment of quantum numbers to the lines of the $C^{12}O^{16}O^{18}$ bands, for which the gap across the band center is twice the mean line spacing, rather than $\frac{3}{2}$ as in the case of symmetrical CO_2. The assignments for the 2.09μ band of $C^{12}O^{16}O^{18}$ are based on the relative line intensities near the apparent band origin. For the 2.04μ band of $C^{12}O^{16}O^{18}$, the center was located with the aid of the value of B_{000} determined from the 2.09μ band.

The B values corresponding to the four isotope bands are given in Table V. The close agreement between the values found for $C^{13}O_2^{16}$ and for $C^{12}O_2^{16}$ is to be expected, since the carbon atom is at the center of mass of the molecule. On the other hand, an elementary calculation indicates that the equilibrium moment of inertia for $C^{12}O^{16}O^{18}$ should be greater than that for $C^{12}O_2^{16}$ by a factor of 1.0605. Assuming that the same ratio holds for the zero vibrational state and adopting $B_{000}=0.3906$ for $C^{12}O_2^{16}$, we obtain a corresponding value of 0.3683

for $C^{12}O^{16}O^{18}$, in good agreement with the experimental value 0.3670.

ACKNOWLEDGMENTS

The authors wish to express their thanks to those who have contributed to the success of the above investigation. Dr. D. M. Dennison, of the University of Michigan, has given generously of his advice, while Dr. Frederick H. Seares, of the Mount Wilson Observatory has read the manuscript and made valuable editorial suggestions. Mr. John T. Brodie made many of the observations and Mr. Russel E. Donovan carried out the bulk of the measurement and reduction of the tracings. Finally, the investigation could not have been accomplished without the generous financial assistance of McGregor Fund of Detroit.

PHYSICAL REVIEW VOLUME 76, NUMBER 12 DECEMBER 15, 1949

A Comparison of the g Value of the Electron in Hydrogen with That in Deuterium

EDWARD B. NELSON* AND JOHN E. NAFE**
Columbia University, New York, New York
(Received August 24, 1949)

The g value of the electron in the $^2S_{\frac{1}{2}}$ state of H has been compared with the g value of the electron in the corresponding state of D by the atomic beam magnetic resonance method. The frequencies, f_H, of the transition $(1, 0 \leftrightarrow 1, -1)$ in H, and f_D, of the transition $(\frac{3}{2}, -\frac{1}{2} \leftrightarrow \frac{1}{2}, -\frac{3}{2})$ in D were observed in the same magnetic field and the ratio $(g_J)_H/(g_J)_D$ was computed from the Breit-Rabi formula. The principal uncertainty is caused by the drift of the magnetic field. The average of 36 observations in 4 runs in which f_H and f_D were measured alternately is $(g_J)_H/(g_J)_D = 1.000004 \pm 0.000025$. The average of 3 runs in which the two resonances were observed simultaneously is $(g_J)_H/(g_J)_D = 0.999991 \pm 0.000010$. The uncertainty indicated in each result is the mean deviation of the residuals. We conclude that the g value of the electron when bound to the proton differs from that when bound to the deuteron by less than 0.001 percent.

INTRODUCTION

THIS experiment has as its purpose a comparison of the moment of the electron in the ground state of hydrogen with its moment in the ground state of deuterium.[1] In view of the deviations from the straightforward Dirac theory which occur in the hyperfine structure of the ground state and shift of the $2S$ level in hydrogen, and of the difference of about one part in 4000 between the reduced masses of the electron in H and D, it was considered of interest to measure the ratio of the moments.[2-4] The experiment was performed by measuring the frequency of atomic transitions in a magnetic field large enough to insure a large measure of decoupling of the electron spin from the nuclear spin. The transitions chosen were those amounting essentially to a reorientation of the electron in the external field. The atomic beam magnetic resonance method was used to detect these transitions. Since the magnetic field has not been measured with sufficient accuracy this method suffices only to measure the ratio of the moments and could detect an effect only if it were not common to the two atoms. Absolute values of the moments are not measured in this experiment.

GENERAL DISCUSSION

The ground state of an atom is split into a number of magnetic levels by the combined influence of an external magnetic field and the magnetic interaction between the nuclear spin I and the total electronic angular momentum J. In this experiment the transitions $(1, 0 \leftrightarrow 1, -1)$ in H and $(\frac{3}{2}, -\frac{1}{2} \leftrightarrow \frac{3}{2}, -\frac{3}{2})$ in D have been studied. The quantum numbers (F, m) refer to the low field designation of the states. The field dependence of these transitions is found from the Breit-Rabi[5] formula. The frequencies of the transitions are

$$f_H = \frac{\nu_H}{2}\left[(1+X_H)^{\frac{1}{2}} - (1-X_H) + 2\left(\frac{g_I}{g_J - g_I}\right)X_H\right], \quad (1)$$

$$f_D = \frac{\nu_D}{2}\left[(1-\tfrac{2}{3}X_D+X_D^2)^{\frac{1}{2}} - (1-X_D) + 2\left(\frac{g_I}{g_J - g_I}\right)X_D\right], \quad (2)$$

where ν_H (or ν_D) is the h.f.s. separation for H (or D) in absolute frequency units. The parameter X, which is proportional to the magnetic field intensity, is given by

$$X = (g_J - g_I)\mu_0 H/\Delta W. \quad (3)$$

In Eqs. (1)–(3) g_J is the g value of the electron in the $^2S_{\frac{1}{2}}$ state, g_I is the g value of the nucleus, ΔW is the

* Now at the State University of Iowa, Iowa City, Iowa.
** Now at the University of Minnesota, Minneapolis, Minnesota.
[1] E. B. Nelson and J. E. Nafe, Phys. Rev. **74**, 1210 (1948).
[2] J. E. Nafe and E. B. Nelson, Phys. Rev. **73**, 718 (1948).
[3] W. E. Lamb, Jr. and R. C. Retherford, Phys. Rev. **72**, 241 (1947).
[4] P. Kusch and H. M. Foley, Phys. Rev. **74**, 250 (1948).
[5] G. Breit and I. I. Rabi, Phys. Rev. **38**, 2028 (1931).

h.f.s. splitting in energy units, μ_0 the Bohr magneton and H the magnetic field intensity.

If the transitions in H and D are observed in the same magnetic field the ratio of the parameters, X_H/X_D, will be proportional to the ratio $(g_J)_H/(g_J)_D$. The value of the parameter X, corresponding to a frequency f_H or f_D, may be computed from Eqs. (1) and (2) with a precision which is comparable with that of f_H or f_D. The ratio $(g_J)_H/(g_J)_D$ is calculated from X_H/X_D by

$$\frac{(g_J)_H}{(g_J)_D}=\frac{X_H}{X_D}\frac{\nu_H}{\nu_D}\left[1-\left(\frac{g_I}{g_J}\right)_D\right]\left[1-\left(\frac{g_I}{g_J}\right)_H\right]^{-1}. \quad (4)$$

The value of the ratio $(g_J)_H/(g_J)_D$ is thus obtainable from measured frequencies and is independent of any natural constants. The final result is not affected by the uncertainty in the values of the small correction terms involving the nuclear g factors.

It is essential that the transitions in H and D be induced in the same magnetic field or that correction be made for the drift of the field. The erratic nature of the drift of the field limits the precision obtainable in this experiment.

APPARATUS AND PROCEDURE

The atomic beam apparatus used in this experiment is the one employed in our measurement of the h.f.s. of H and D.[2] In this apparatus the atoms are deflected through a collimating slit by an inhomogeneous field and then focused on a Pirani detector by a second inhomogeneous field whose gradient is oppositely directed with respect to the first field. Between the deflecting and focusing fields the atom traverses a uniform magnetic field where a radiofrequency magnetic field may induce transitions between the magnetic components of the h.f.s. levels. If the magnetic moments of the atom in the initial and final h.f.s. levels differ by an amount of the order of one Bohr magneton the beam will not be focused by the second inhomogeneous field. The intensity of the beam is observed as a function of the frequency of the r-f field inducing the transitions. The frequency associated with the minimum intensity of the beam is assumed to be the center of the resonance line.

The r-f currents, at frequencies near 1000 and 1200 mc, were supplied by coaxial line oscillators which use Lighthouse tubes. The frequency was measured by heterodyning the signals with harmonics of a 240 mc crystal controlled frequency standard. The precision of the measurement of the ratio $(g_J)_H/(g_J)_D$ was not limited by the stability of the oscillators or the accuracy in the measurement of frequency.

In the first series of measurements correction was made for the drift in the magnetic field intensity by taking alternate observations of f_H and f_D. The time required for each observation was about 10 min. The drift in the magnetic field intensity between successive observations of f_H and f_D was about 1 part in 20,000. The drift was not associated with changes in the magnet current, which was held constant by manual adjustment to better than 1 part in 20,000. Each value of f_H was paired with a value of f_D obtained by linear interpolation and conversely.

A technique for observing the transitions in H and D simultaneously was developed to avoid the error introduced by the drift in the intensity of the magnetic field. In this method a beam containing approximately equal parts of H and D atoms was employed. Two oscillators were connected to the r-f loop in which the transition field is produced. On varying the magnetic field the H and D resonances were observed in general to occur at different magnet currents. Holding the frequency of one oscillator fixed, that of the other oscillator was changed stepwise in such a direction as to cause the resonances to coalesce. The depth of the composite line was then investigated by varying the magnet current for each pair of values of frequency to find the minimum beam intensity. The reduction in beam intensity was plotted as a function of the varied frequency. The resulting curve has a maximum when the transitions in H and D occur in the same field. The half-widths of the composite line is approximately the sum of the half-widths of the individual lines. Thus the increased precision due to the simultaneous measurement of f_H and f_D is offset, in part, by the increased width of the composite line.

RESULTS

(A) Alternate Measurement of f_H and f_D

A sample of the data from a run of alternate observations of f_H and f_D is given below,

$$\begin{aligned} f_H&=1000.371 \text{ mc},\\ f_D&=1216.924 \text{ mc},\\ X_H&=0.999292,\\ X_D&=4.329941,\\ H_0&=506.1 \text{ gauss},\\ (g_J)_H/(g_J)_D&=1.000020,\\ \delta&=20\times10^{-6}, \end{aligned}$$

where δ is given by $(g_J)_H/(g_J)_D=1+\delta$. The mean value of δ obtained from 36 observations (pairs of frequencies) made in 4 different runs is $\delta=(4\pm25)\times10^{-6}$. The average deviation ($\pm25\times10^{-6}$) of the individual values from the mean is to be compared with the fractional half-width of the lines, $\Delta f/f\sim100\times10^{-6}$, and the average drift of the magnetic field intensity between successive observations, $\Delta H/H\sim50\times10^{-6}$.

(B) Simultaneous Observations of f_H and f_D

A sample curve obtained in the simultaneous measurement of f_H and f_D is given in Fig. 1. The total reduction in beam intensity is plotted as a function of the frequency required to induce the H transition. The

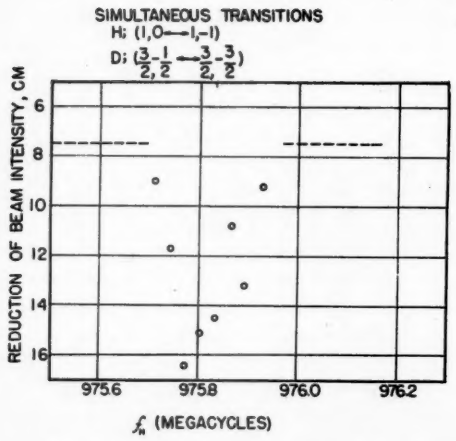

FIG. 1. The total reduction in the intensity of an atomic beam of H and D is plotted as a function of the frequency inducing the H transition when the frequency inducing the D transition was held fixed. The dashed lines indicate the reduction in beam intensity caused by the deuterium resonance. The frequency inducing the deuterium resonance was held constant at 1187.329 mc.

frequency of the r-f field inducing the D transition was set at 1187.329 mc. The reduction in beam intensity caused by the D transition was 7.5 cm, independent of the frequency inducing the H transition. When the frequency inducing the H transition is such that both the H and D transition occur at the same intensity of the magnetic field the two resonance lines coincide. The frequency inducing the H transition was 975.810 mc. The result obtained from three measurements of this type is $\delta=(-9\pm10)\times10^{-6}$. The mean deviation, $(\pm10\times10^{-6})$ is to be compared with the fractional half-width of the combined lines, $\Delta f/f\sim150\times10^{-6}$, which is the limiting factor in the precision of the measurement.

As a test of the accuracy of the method of superposition a measurement was made of the h.f.s. separation of the ground state of D. The transitions $(\frac{3}{2},\frac{3}{2}\leftrightarrow\frac{1}{2},\frac{1}{2})$ and $(\frac{3}{2},-\frac{1}{2}\leftrightarrow\frac{3}{2},-\frac{3}{2})$ were observed simultaneously. The frequencies were 1150.670 ± 0.020 mc and 720.000 mc respectively, in a field of about 325 gauss. From these observations the value of ν_D is 327.395 ± 0.020 mc which is to be compared with $\nu_D=327.384\pm0.003$ mc which was obtained previously by direct measurement. The precision to be expected in the value of the ratio $(g_J)_H/(g_J)_D$ is about four times that found in the measurement of ν_D for the ratio of the g factors depends almost directly on the ratio of the measured frequencies, while the value of the h.f.s., determined by the superposition method, depends on the difference between the frequencies of the two transitions.

DISCUSSION OF SYSTEMATIC ERRORS

The observed transitions in H and D are those which, in high field, would correspond to a reorientation of the electronic moment with respect to the external magnetic field; thus the frequencies f_H and f_D are approximately the Larmor precession frequency of the electron. The ratio, f_H/f_D, differs from the ratio, $(g_J)_H/(g_J)_D$, by about 20 percent. This difference is a consequence of the h.f.s. interaction of the electronic and nuclear moments. The validity of the Breit-Rabi formula to describe the field dependence of the magnetic components of the h.f.s. doublet has been demonstrated by Kusch, Millman and Rabi[6] to ±0.005 percent in K^{39} and Li^7 for magnetic fields ranging from a few gauss up to 4000 gauss. The uncertainty introduced in the ratio $(g_J)_H/(g_J)_D$ by the use of the Breit-Rabi formula is, at most, ±0.001 percent.

The calculation of X_H and X_D from observed transition frequencies and of $(g_J)_H/(g_J)_D$ from these values of x involve small correction terms containing the ratio of the nuclear to electronic g factors. The term $(g_I/(g_J-g_I))X$ in Eqs. (1) and (2) contributes only $+0.179$ percent to the calculated value of X_H and the similar term contributes $+0.024$ percent to X_D. The terms $(g_I/g_J)_H$ and $(g_I/g_J)_D$ in Eq. (4) contribute -0.152 percent and -0.023 percent, respectively, and the sign of their contribution is opposite to that of $(g_I/(g_J-g_I))X$ entering X. The final result is quite independent of $(g_I/g_J)_D$ and the total dependence on $(g_I/g_J)_H$ is $+0.027$ percent. It is concluded that the uncertainty in the ratio $(g_I/g_J)_H$ and $(g_I/g_J)_D$ has a negligible effect on the ratio of the electronic g factors.

In the fields of intermediate strength used in this experiment, the decoupling of the nuclear and electronic moments is such that a 1 percent error in ν_H or ν_D would change the calculated value of $(g_J)_H/(g_J)_D$ by 0.17 percent and 0.13 percent, respectively. As ν_H and ν_D are known to ±0.001 percent their uncertainty introduces no error into the ratio.

CONCLUSION

The g factors of the electron in the ground state of H and D have been found to be equal to within ±0.001 percent. The precision of measurement is limited by the half-width of the resonance lines and the uncertainty in the value of the magnetic field due to the erratic drift of the field intensity in time.

The authors wish to thank Professor I. I. Rabi, who suggested this problem, for his advice and encouragement.

[6] Kusch, Millman, and Rabi, Phys. Rev. **57**, 765 (1940).

PHYSICAL REVIEW VOLUME 76, NUMBER 12 DECEMBER 15, 1949

Theory of Critical Fluctuations

M. J. KLEIN* AND L. TISZA
*Department of Physics and Research Laboratory of Electronics, Massachusetts Institute of Technology, Cambridge, Massachusetts***

(Received August 24, 1949)

A macroscopic system is subdivided into cells of identical size and shape arranged in a regular spatial array. The method of canonical ensembles would consider one of the cells, schematizing the rest into a "reservoir." The present "cellular method" treats the cells on an equal footing and is appropriate to deal with the fluctuations near the critical point for which the standard theory yields infinite results. Earlier theories dealing with the same problem appear as special cases of the present treatment. In particular, the critical points are defined generally enough to include the so-called λ-points in solids. The macroscopic system is invariant under the group of translations which displaces one cell into another. The macroscopic quantities (e.g., the thermodynamic parameters) are invariants of this group.

I. INTRODUCTION

THE role of fluctuations in statistical thermodynamics is primarily a negative one. Indeed, the very existence of thermodynamics can be said to be based on the fact that the fluctuations in the macroscopic thermodynamic variables are negligible compared to the mean values of these variables. The proof of this fact is essential in the statistical foundation of thermodynamics. The agreement in the results obtained from different statistical representations of a physical system is also a consequence of the negligible character of the fluctuations. Thus, whether one uses a microcanonical ensemble which corresponds to a completely closed system, or a canonical ensemble which corresponds to a system in contact with a reservoir, the results are the same since fluctuations can be neglected.

It is therefore of fundamental interest that fluctuations are not negligible at the so-called critical points of physical systems, of which the gas-liquid critical point is the best known case. As a matter of fact, if the fluctuations are calculated according to standard procedures, infinite results are obtained. Experimental results indicate that critical-point fluctuations, although finite, are orders of magnitude larger than usual and give rise to macroscopic phenomena, e.g., critical opalescence.

Several theories[1–4] have been proposed for treating the problem of critical-point fluctuations, each based on a different analysis of the physical situation. There are several reasons for our reconsidering the question. In the first place, the relation between the above-mentioned theories is rather obscure and none of them can claim general acceptance. In the second place, all of them appear to be too specialized. (In fact, one of the authors has recently shown[5] that critical points are of rather common occurrence, since the well-known λ-point phenomena observed in solids and some liquids may be considered as critical points.) The above-mentioned theories refer only to the gas-liquid critical points and to the critical mixing points in liquids. Finally, these theories are often based, in part, on rather special molecular models and do not really treat the basic statistical problem.

In Section II we sum up the results of the conventional theory of fluctuations in a form general enough for our purposes. The difficulties arising at the critical point are discussed in detail.

In Section III we introduce the "cellular method" which can be considered a refinement of the ordinary treatment of generalized canonical ensembles. This method allows one to treat the correlation of fluctuations in different volume elements, an effect which is of great importance at critical points and which is ignored by the standard method. The importance of these correlations was first pointed out by Ornstein and Zernike,[2] and our method is a development of their idea. This development, on its formal side, leads to a general criterion for the definition of macroscopic variables, i.e., those variables which can be used in discussing macroscopic phenomena.

In Section IV we present a calculation of fluctuations and their correlations.

Section V is devoted to a discussion of the relationships between our theory and those previously mentioned, as well as to some clarification of the relationships of these theories to each other. In particular, the question of critical opalescence is discussed.

II. FLUCTUATIONS AND CRITICAL POINTS

The thermodynamic properties of a closed system can be adequately described in terms of a so-called

* Present address: Department of Physics, Case Institute of Technology, Cleveland, Ohio.

** This work has been supported in part by the Signal Corps, the Air Materiel Command, and the ONR.

[1] M. V. Smoluchowski, Ann. d. Physik. IV (Folge) **25**, 205 (1908).

[2] L. Ornstein and F. Zernike, Proc. Amst. Akad. Sci. **17**, 793 (1914); **18**, 1520 (1916); **19**, 1321 (1917); Physik. Zeits. **19**, 134 (1918); **27**, 761 (1926).

[3] Y. Rocard, J. de phys. et rad. **4**, 165 (1933).

[4] J. Yvon, Actualités Scientifiques et Industrielles, Nos. 542, 543 (Paris, 1937).

[5] L. Tisza, "General theory of phase transitions," National Research Council Conference on Phase Transformations in Solids, 1948 (to appear in book form).

fundamental equation

$$U=U(X_1, X_2, \cdots, X_{r+1}), \tag{1}$$

where U is the internal energy and $X_1, X_2, \cdots, X_{r+1}$ are the extensive variables characterizing the system. (The X_i include volume, entropy, mole numbers, etc.) We shall assume our system to be spatially homogeneous on a macroscopic scale so that U is a first-order homogeneous function of its arguments. It is then most convenient to let $X_{r+1}=V$, the volume, and to define the "densities":

$$x_i=\frac{X_i}{X_{r+1}}; \quad u=\frac{U}{X_{r+1}}. \tag{2}$$

The fundamental equation can then be written

$$u=u(x_1, x_2, \cdots, x_r). \tag{3}$$

The generalized forces conjugate to X_k or x_k are

$$P_k=\partial U/\partial X_k=\partial u/\partial x_k. \tag{4}$$

In order to obtain the fluctuations of the quantities x_k about their mean values, we shall consider our system as a part of a large closed system, e.g., one cm³ of a gas in a large container. We now have the possibility of processes in which the quantities X_k flow from the sub-system to the remainder of the system, called a "reservoir," and vice versa; these processes are subject only to the condition that there is no change in the value of X_k for the whole closed system. The assumed difference in size between the sub-system and the reservoir implies that these processes may lead to a noticeable change in the state of the sub-system while the quantities x_k and P_k are essentially unchanged in the reservoir.

It is well known[6] that the probability of finding the sub-system in a state $x_{1\alpha}, x_{2\alpha}, \cdots, x_{r\alpha}$, which may differ from the equilibrium state $x_1, \cdots, x_r$, is given by a generalized canonical distribution function:

$$p_\alpha=w_\alpha \exp 1/kT\left[\psi-E_\alpha+\sum_{k=2}^{r}P_k x_{k\alpha}\right]. \tag{5}$$

Here p_α is the probability of finding a state of the system described by the index α, w_α is the statistical weight (degeneracy) of this state, E_α its energy, and $x_{k\alpha}$ the value of the variable x_k in this state. The index k runs from 2 to r omitting x_1 which is the entropy density. The function ψ is the thermodynamic potential

$$\psi=U-\sum_{k=1}^{r}P_k x_k. \tag{6}$$

We can put the expression for p_α into a more symmetrical form as follows. Let us define:

$$S_\alpha=k \ln w_\alpha.^{a} \tag{7}$$

Then:

$$p_\alpha=\exp\frac{\left[U-E_\alpha-\sum_{k=1}^{r}P_k(x_k-x_{k\alpha})\right]}{kT}, \tag{8}$$

where the summation now goes from 1 to r (including the entropy term). We can also write:

$$p_\alpha=\exp\frac{[\psi-\psi_\alpha]}{kT} \tag{9}$$

where:

$$\psi_\alpha=E_\alpha-\sum_{k=1}^{r}P_k x_{k\alpha}. \tag{10}$$

This "microscopic free energy" ψ_α will be of interest to us subsequently.

The physical meaning of $\psi-\psi_\alpha$ is the minimum work required to bring about the state α. Hence Eq. (9) expresses the well-known principle of Boltzmann. Let us introduce the notation:

$$\delta x_k=x_{k\alpha}-x_k. \tag{11}$$

If we expand E_α as a function of the δx_k, we obtain

$$E_\alpha=\bar{E}_\alpha+\sum_{k=1}^{r}\left(\frac{\partial E_\alpha}{\partial x_k}\right)_0\delta x_k+\frac{1}{2}\sum_{k,\,l=1}^{r}\left(\frac{\partial^2 E_\alpha}{\partial x_k\partial x_l}\right)_0\delta x_k\delta x_l, \tag{12}$$

keeping second-order terms. Now $\bar{E}_\alpha=U$, $(\partial E_\alpha/\partial x_k)_0=P_k$; and we can define

$$\left(\frac{\partial^2 E_\alpha}{\partial x_k\partial x_l}\right)_0=u_{kl}=\frac{\partial^2 U}{\partial x_k\partial x_l}. \tag{13}$$

Then to this approximation we find

$$p_\alpha=c\exp\left\{\frac{-\frac{1}{2}\sum_{k,\,l=1}^{r}u_{kl}\delta x_k\delta x_l}{kT}\right\}, \tag{14}$$

where c is a normalization constant which is needed because Eq. (14) is only an approximation to Eq. (8).

In terms of this Gaussian distribution, one can immediately write down the fluctuations in which we are interested:

$$\langle\delta x_k\delta x_l\rangle_{Av}=\left\{\frac{\int(\delta x_k)(\delta x_l)p_\alpha d(\delta x_1)\cdots, d(\delta x_r)}{\int p_\alpha d(\delta x_1)\cdots, d(\delta x_r)}\right\}$$

$$=kTv_{kl}, \tag{15}$$

[6] E. A. Guggenheim, J. Chem. Phys. 7, 103 (1939).

[a] S_α is the entropy one assigns to a system known to be in a state α of statistical weight w_α.

where the matrix $\|v_{kl}\|$ is the inverse of the matrix $\|u_{kl}\|$. These matrices have been called stiffness $\|u_{kl}\|$ and compliance $\|v_{kl}\|$ matrices.[5]

The smallness of kT compared to the internal energy of macroscopic systems assures us that the relative fluctuations are small, hence the microcanonical and canonical methods are essentially equivalent. Speaking more physically, the behavior of the sub-system is the same whether it is isolated from the rest by a real wall or isolated only in imagination.

This situation is different, however, at the so-called critical point where $\|u_{ik}\|$ is positive semidefinite ($\mathrm{Det}\|u_{ik}\|=0$) and where the matrix elements v_{ik} and hence the fluctuations become infinite.[5] Actually, the experimentally observed fluctuations become extremely high at the critical point, as manifested in the phenomenon of critical opalescence, for example. The fluctuations are, however, finite and our formalism must be improved, so as to provide a finite result.

The weak point in the above discussion, which is essentially the same as the standard discussion of fluctuations, is in the use of the canonical ensemble to represent the behavior of a sub-system of our whole system while idealizing the remainder by treating it as a reservoir. When the fluctuations are large, as in the vicinity of a critical point, the microcanonical and canonical ensembles no longer give the same results, and it is essential to treat the system as a whole in a proper manner. This will involve a modification of the usual canonical ensemble which will be carried out in the next section. At this stage, we merely need to point out that such a modification is necessitated by the large critical-point fluctuations which indicate a breakdown of the usual approach discussed above.

Before going on to examine the statistical problem in more detail, it seems convenient to simplify the definition of the critical point. As presented above, it appears as a result of the "co-operation" of all extensive variables $x_1, x_2, \cdots, x_r$. Instead, we can choose $P_1, P_2, \cdots, P_{r-1}, x_r$ as independent variables, and introduce the corresponding free energy

$$A(x_r)=u-\sum_{k=1}^{r-1}P_k x_k. \tag{16}$$

(A is a function of $P_1, P_2, \cdots, P_{r-1}$ as well as x_r, but it is the latter dependence which will interest us.) It can be shown[5] that a critical point may also be defined as follows:

$$\frac{\partial^2 A}{\partial x_r^2}=0, \quad \frac{\partial^3 A}{\partial x_r^3}=0, \quad \frac{\partial^4 A}{\partial x_r^4}>0. \tag{17}$$

The advantage of this formulation is that it refers explicitly to a single independent variable. Of course, this can be chosen to be any of the $x_1, x_2, \cdots, x_r$. The various formalisms arising are not identical, but lead to the same conclusions.

III. THE CELLULAR METHOD

We generalize the concept of a canonical ensemble by introducing what we call the cellular method. Instead of concentrating our attention on a sub-system and schematizing the rest into a "reservoir," we divide the whole system into cells which we treat on an equal footing. We choose these cells as identical in size and shape and arranged in a regular spatial array. If we are dealing with a fluid system, we can choose a simple cubic array of cubical cells. If we deal with a crystalline system, it will be natural to let our array have the symmetry of the crystal; the individual cells can then consist either of single unit cells of the crystal or of groups of contiguous unit cells. To avoid the necessity of introducing the reciprocal lattice, we shall work with a cubic array, but our considerations can easily be transcribed so as to apply to the general case.

The position of any cell is then specified by a vector k:

$$k=k_1 j_1+k_2 j_2+k_3 j_3, \tag{18}$$

where k_1, k_2, k_3 are integers between 0 and $M-1$ if there are M^3 cells, and j_1, j_2, j_3 are the unit vectors defining the primitive translations of our array. (In the rest of the paper the symbols k, l, m, j_1, j_2, and j_3 designate vectors, whereas k_1, k_2, k_3, l_1, l_2, l_3, m_1, m_2, and m_3 are integers.)

In the previous section, we pointed out that if one works with the appropriate thermodynamic potential $A(x_r)$, the conditions for a critical point can be expressed in terms of the one variable x_r. We are now interested in considering states of our large system specified by the set of values x_{rk}, where k varies over all the M^3 cells; x_{rk} is the value of x_r in the cell k. (We take the variables $P_1, P_2, \cdots, P_{r-1}$ as fixed for our system.)

By applying an argument similar to that used in the preceding section, one can easily show that the probability of finding a state $\{x_{rk}\}$, is given by:

$$p=C\exp\left(-\frac{1}{2}\sum_{kl}a_{kl}z_k z_l\right), \tag{19}$$

where[b]

$$a_{kl}=\frac{1}{kT}\left(\frac{\partial^2 A}{\partial x_{rk}\partial x_{rl}}\right)_0=\frac{1}{kT}\left(\frac{\partial^2 A}{\partial z_k \partial z_l}\right)_0; \tag{20}$$

$$z_k=x_{rk}-\bar{x}_r. \tag{21}$$

In spite of the great formal similarity between Eq. (14) and Eq. (19), one must be very careful to distinguish between the two quadratic forms appearing in the exponential in these two equations. The first, Eq. (14), refers to a set of different thermodynamic variables $x_1 \cdots, x_r$; the second, Eq. (19), refers to the set of values x_{rk} of one thermodynamic variable x_r in the different cells k of the whole system. Both quadratic

[b] It is necessary to average over all of the "internal coordinates" of the system, e.g., thermal vibration coordinates; in other words, we preserve only the dependence on the set of variables z_k.

forms express the minimum work necessary to carry the system from its equilibrium state to one deviating from equilibrium.

We should point out an important restriction on the values of the z_k, the deviations of x_{rk} from its average value x_r; namely, we must have:

$$\sum_k z_k = 0. \tag{22}$$

This expresses the fact that our whole system is closed, so there can be no net fluctuation in x_r if we sum over all cells.

The eigenvalues and eigenvectors of this form are of considerable interest, so we shall now determine them. This is simple, if we notice that the set of coefficients a_{kl} for fixed k, l varying over all cells, is just a permutation of the set $a_{k'l}$ for any other fixed k'. This expresses the fact that the interactions (as measured by a_{kl}) of any cell with its neighbors of all orders are independent of the particular cell considered. (We impose periodic boundary conditions on our whole system, so that the cells near the boundary "surfaces" need not be considered separately.)

The eigenvalues λ_m and eigenvectors ξ_{lm} must satisfy

$$\sum_l a_{kl}\xi_{lm} = \lambda_m \xi_{km}; \tag{23}$$

(k, m varying over all cells, i.e., $m = m_1 j_1 + m_2 j_2 + m_3 j_3$, $m_i = 0, 1, \cdots, M-1$). The solutions to Eq. (23) are:

$$\lambda_m = \sum_l a_{kl} \exp\left[\frac{2\pi i}{M} m \cdot (l-k)\right], \tag{24}$$

$$\xi_{lm} = \frac{1}{M^{\frac{3}{2}}} \exp\left[\frac{2\pi i}{M} l \cdot m\right], \tag{25}$$

where

$$\sum_k \xi_{km}\xi_{km'}{}^* = \delta(m-m'). \tag{26}$$

Since a_{kl} depends only on $l-k$, λ_m is actually independent of k as it must be.

The eigenvalues can be written in a simpler form if we note that it is sufficient to take only two distinct values of the a_{kl}:

$$\begin{aligned} &a_{kk} = a_0; \quad a_0 > 0 \quad \text{(all } k\text{)}, \\ &a_{kl} = a_1 \qquad\quad \text{(}k, l \text{ nearest neighbors)}, \\ &a_{kl} = 0 \qquad\quad \text{(otherwise)}. \end{aligned} \tag{27}$$

The first of these conditions states that all cells are equivalent. The second condition, nearest-neighbor "interactions" only, is not necessary for most of the following work but simplifies the form of the equations to some extent.

The eigenvalues are now:

$$\lambda_m = a_0 + 2a_1 \sum_{i=1}^{3} \cos\frac{2\pi}{M} m_i; \quad (m = m_1 j_1 + m_2 j_2 + m_3 j_3). \tag{28}$$

The eigenvector corresponding to $\lambda_0 (\lambda_0 = \lambda_{M(j_1+j_2+j_3)} = a_0 + 6a_1)$ is of especial significance. It is

$$\xi_0 = \frac{1}{M^{\frac{3}{2}}}(1, 1, \cdots, 1).$$

This is the only eigenvector which does not involve phase differences between the different cells. Now, while the eigenvalues λ_m depend on the properties of the quadratic form of Eq. (19), the eigenvectors really furnish an appropriate and flexible coordinate system, as it were, for describing our physical system.

We may use the unique character of the eigenvector ξ_0 to suggest a characterization of those variables of our system which can be handled in a macroscopic discussion; namely, only variables which transform like ξ_0, i.e., which are the invariants of the translation group, can qualify as macrovariables, since all others involve unobservable phase differences as one goes from cell to cell.

The variables which satisfy this criterion are of two rather different kinds. In the first class, we have thermodynamic variables such as magnetic moment per unit volume, average particle density, etc. The additional characteristic feature of these variables is that their conjugate "forces" exist and, consequently, the values of these variables are subject to the control of the experimenter. In the second class are variables which might be called quasi-thermodynamic ones, such as the atomic coordinates in a crystal and the long-range order in alloys, etc. Here there are no conjugate forces, so the variables in question cannot be controlled freely. Nevertheless, they are of a macronature in the sense described above and, correspondingly, are subject to measurement—by their coherent x-ray scattering, for example.

The variables which do not behave like ξ_0 are perhaps typified by the thermal vibrations or phonons which essentially involve phase differences between cells and must always be averaged over in macroscopic treatments.

Let us finally apply our study of the eigenvalues to the case of the critical point. This is now redefined as the point where:

$$\frac{1}{2}\sum_{k,l} a_{kl} z_k z_l,$$

becomes positive semidefinite, i.e., one of its eigenvalues must vanish. It is not difficult to see that the eigenvalue which vanishes (the others remaining positive) is λ_0. Thus, at the critical point,

$$\lambda_0 = a_0 + 6a_1 = 0. \tag{29}$$

This result is, of course, to be expected in the light of the above discussion, but it can be proved directly and, therefore, is an example in support of the arguments advanced.

In fact, we notice that if $a_0+6a_1=0$, all other λ_m are positive; but if $\lambda_m=0$, $m\neq 0$, then some $\lambda_m<0$, contradicting our requirement that the quadratic form be positive semidefinite. In the absence of correlations $a_1=0$ and Eq. (29) reduces to the previous definition of critical points.

IV. FLUCTUATIONS WITH CORRELATIONS

We can now turn to the calculations of the mean-square fluctuation in the value of x_r in cell k and the correlations of the fluctuations in different cells. We shall use the approach of the preceding section.

We have already written in Eq. (19) the expression for the probability of finding a state of the system characterized by a given set of values of the x_{rk}. It has also been pointed out that there is a restriction, Eq. (22), on the values of the set of variables z_k, because our system is closed. We now want to calculate

$$\langle z_k z_l\rangle_{Av}=\frac{\int z_k z_l \exp\left[-\frac{1}{2}\sum_{k,l}a_{kl}z_k z_l\right]d\tau'}{\int \exp\left[-\frac{1}{2}\sum_{k,l}a_{kl}z_k z_l\right]d\tau'}, \tag{30}$$

where $d\tau'$ means that we integrate over the M^3-1 dimensional space of the z_k, subject to the restriction of Eq. (22).

In order to take into account this restriction in the simplest way, we go over to the coordinate system determined by the eigenvectors of the matrix $\|a_{kl}\|$. The calculation is given in the Appendix; we quote only the result here:

$$\langle z_k z_l\rangle_{Av}=\frac{1}{M^3}{\sum_p}'\frac{\cos(2\pi/M)p\cdot(k-l)}{\lambda_p}. \tag{31}$$

The primed summation means that we sum over all p except $p=0$, i.e., that the eigenvalue λ_0 does not appear in the sum. This follows immediately from the restriction of Eq. (22), as is shown in the Appendix.

Let us first analyze this result for the case $k=l$. Introducing the explicit expressions for the eigenvalues, we have

$$\langle z_k^2\rangle_{Av}=\frac{1}{M^3}{\sum_{p_1,p_2,p_3}}' \times\frac{1}{a_0+2a_1[\cos(2\pi/M)p_1+\cos(2\pi/M)p_2\cos(2\pi/M)p_3]}. \tag{32}$$

Now, far from the critical point, where the interactions between cells should not be important, this reduces to the conventional result. For, in this case, it follows from Eq. (29) that

$$a_0\gg -6a_1, \tag{33}$$

and, therefore,

$$\lambda_p\simeq a_0, \tag{34}$$

$$\langle z_k^2\rangle_{Av}\simeq\frac{1}{a_0}=\frac{kT}{(\partial^2 A/\partial x_r^2)_{P_1,\ldots,P_{r-1}}} \tag{35}$$

which is the result obtained by the method of Section II in this particular case (one variable).

Closer to the critical point, we can transform the sum in Eq. (32) into an integral, since M is as large as we please;

$$\langle z_k^2\rangle_{Av}=\frac{1}{a_0}\frac{1}{(2\pi)^3}\int_0^{2\pi}\int_0^{2\pi}\int_0^{2\pi} \times\frac{dq_1dq_2dq_3}{\{1+(2a_1/a_0)[\cos q_1+\cos q_2+\cos q_3]\}}. \tag{36a}$$

Equation (36a) shows that the fluctuations become larger as we approach the critical point. At the critical point, where $(2a_1/a_0)=-\frac{1}{3}$, the integral still converges[e] and can even be evaluated exactly. Thus

$$\langle z_k^2\rangle_{Av}=\frac{1}{a_0}\frac{3}{\pi^3}\int_0^{\pi}\int_0^{\pi}\int_0^{\pi}\frac{dq_1dq_2dq_3}{3-(\cos q_1+\cos q_2+\cos q_3)} =\frac{3}{a_0}(18+12\sqrt{2}-10\sqrt{3}-7(6)^{\frac{1}{2}})\left(\frac{2K_2}{\pi}\right)^2, \tag{36b}$$

where K_2 is the complete elliptic integral of modulus $(2-\sqrt{3})(\sqrt{3}-\sqrt{2})$. Numerically:

$$\langle z_k^2\rangle_{Av}=1.5164/a_0, \tag{36c}$$

at the critical point.

Let us now analyze the physical meaning of our results. In the first place we know that at the critical point $a_0=-6a_1\neq 0$. Since thermodynamics assures us that $a_0>0$, it follows that $a_1<0$ at and near the critical point. This means that a fluctuation in any cell increases the probability of a fluctuation of like sign in the neighboring cells. This is most readily seen from Eq. (40) below.

Secondly, we see that the fluctuations are kept finite by the physical requirement that the entire system be closed with respect to the thermodynamic variable x_r whose fluctuations we are considering. This entered our formalism in the restriction of Eq. (22) which automatically led to the omission of the term in λ_0 from the sum of Eq. (32). Thus the convergence of the integral in Eq. (36b) and the closure of our whole system lead to finite critical fluctuations.

Considering now the case $k\neq l$, i.e., the correlation of the fluctuations in different cells, we may make several remarks. In the first place, it is clear that, in the limit of vanishing interaction between cells, all $\langle z_k z_l\rangle_{Av}$ are

[e] The proof of convergence and the more difficult evaluation of the integral are due to G. N. Watson, Quart. J. Math. (Oxford) **10**, 266 (1939).

We should like to express our sincere thanks to Dr. Elliott Montroll for informing us of this reference.

zero ($k \neq l$). For, in this case, $\lambda_p = a_0$ and the phase factors cancel out.[d] Second, as $|k-l|$ increases the cancellation between successive terms increases and $\langle z_k z_l \rangle_{Av}$ becomes small.

This point can be brought out more clearly by another method which we now discuss. This method is of interest in itself and it establishes the connection between our work and that of Ornstein and Zernike[2] (see Section V). The essential point is to derive an equation relating the correlation coefficient of the fluctuations in different cells to the basic coefficients a_{kl} which are derivatives of the free energy and thus express the forces within our system.

The correlation coefficient g_{kl} is defined[7] by

$$g_{kl} = \frac{\langle z_k z_l \rangle_{Av}}{(\langle z_k^2 \rangle_{Av} \langle z_l^2 \rangle_{Av})^{\frac{1}{2}}} \tag{37}$$

Instead of using the expressions given above for these quantities, it is more convenient to evaluate them in terms of the minors of the determinant of $\|a_{kl}\|$. Let A be the determinant of $\|a_{kl}\|$ and A_{kl} be the co-factor (with its appropriate sign) of a_{kl} in A. Then[8]

$$\langle z_k z_l \rangle_{Av} = \frac{\int z_k z_l \exp\left[-\frac{1}{2}\sum_{k,l} a_{kl} z_k z_l\right] d\tau}{\int \exp\left[-\frac{1}{2}\sum_{k,l} a_{kl} z_k z_l\right] d\tau} = \frac{A_{kl}}{A}. \tag{38}$$

Since $A_{kk} = A_{ll}$ for all k, l as a result of the properties of $\|a_{kl}\|$, we have

$$g_{kl} = A_{kl}/A_{ll}. \tag{39}$$

Let us define

$$f_{kl} = -a_{kl}/a_{kk}. \tag{40}$$

The quantity f_{kl} is the average of z_k when $z_l = 1$ and all other variables are zero (linear regression coefficient).[7] We see that f_{kl} is a direct index of the "energetic" interaction between cells k and l, and vanishes under our assumptions unless k and l are nearest neighbors. Using Eqs. (39) and (40), one can easily show[e] that

$$g_{kl} = f_{kl} + \sum_{m \neq k,l} f_{km} g_{ml}. \quad (k \neq l) \tag{41}$$

Equation (41) has a simple interpretation: it states that the correlation coefficient g_{kl} (which measures the statistical effect of cell l on cell k) is equal to the sum of two terms. The first is the direct interaction f_{kl}, present only for nearest neighbors; the second is the sum giving the effect g_{ml} of cell l on all other cells m which have a non-vanishing interaction f_{km} with cell k.

We need consider the set of Eqs. (41) only for some definite value of l, since the set g_{kl} for this l value is the same, except for permutation, as any other set g_{km}. Hence we shall fix l and, with this understanding, drop it from our notation. We then have, as our final result,

$$g_k = f_k + \sum_{m \neq k} f_{km} g_m. \tag{42}$$

V. DISCUSSION

In this section, we shall point out the connections between the theory presented in this paper and the earlier work done on this problem, particularly with respect to the theory of critical opalescence.

It was shown in Section II that the customary statistical treatment of fluctuations leads to infinite critical-point fluctuations. The physical reason for this was that the minimum work necessary to produce such a fluctuation vanishes at the critical point in the usual approximation. It is clear from the nature of the problem that any additional contribution to the work, usually neglected, will limit the fluctuations to finite values at the critical point. A number of theories have been advanced which have this result, and it is our purpose to point out the nature of the additional term in each case and to discuss the interrelations of these theories in the light of our own.

In the first place, it should be said that virtually all previous work on the subject has been concerned with the ordinary gas-liquid critical point of a pure substance or with the critical mixing point of a binary mixture of liquids. Our theory has been set up in such a manner as to be applicable to λ-points as well as critical points in the ordinary sense. For this reason, we shall be interested in discussing only those other theories which are capable, in principle, of such generalization. Hence we have not considered the mechanism proposed by Yvon,[4] who has pointed out that infinite fluctuations are avoided if one considers the effect of gravity. Briefly, near the ordinary critical point the compressibility is large and the gravitational field of the earth gives rise to a non-uniformity of density, "thickening" the gas-liquid interface into a layer. Although this effect undoubtedly exists, it seems to be special, insofar as it cannot be of importance in λ-points in solids, for example.

The original suggestion for obtaining finite critical-point fluctuations is due to Smoluchowski.[1] His proposal was to continue the expansion of the free energy to the next non-vanishing term (quartic term), at the critical point (see Eq. (12)). This insures a non-zero

---

[d] The cancellation is not complete and $\langle z_k z_l \rangle_{Av} = (-1/a_0)(1/M^3)$ because we do not sum over the eigenvalue λ_0. This term is, of course, negligible for large M.

[7] H. Cramér, *Mathematical Methods of Statistics* (Princeton University Press, Princeton, 1946).

[8] The restriction of Eq. (22) has not been imposed here. It can be shown [M. J. Klein, Ph.D. thesis in physics, M.I.T. (1948)] that this restriction plays no important role in these considerations.

[e] For:

$$\sum_{m \neq k,l} f_{km} g_{ml} = -\sum_{m \neq k,l} \frac{a_{km} A_{ml}}{a_{kk} A_{ll}}$$

$$= -\frac{1}{a_{kk} A_{ll}} \left[\sum_m a_{km} A_{ml} - a_{kk} A_{kl} - a_{kl} A_{ll}\right]$$

$$= -\frac{A \delta_{kl}}{a_{kk} A_{ll}} + g_{kl} - f_{kl} = g_{kl} - f_{kl} \quad \text{as} \quad k \neq l.$$

minimum work and gives finite results. This method cannot be considered satisfactory because it is based on the consideration of one volume element with the remainder treated as a reservoir, and when the fluctuations are large (though finite) the difference of the states of neighboring volume elements and their correlations must be taken into account.

The first major attempt to give a more adequate treatment of critical-point fluctuations considering correlations is due to Ornstein and Zernike.[2] We have already mentioned that their papers served as a stimulus to the present work. Their chief contributions were the introduction of the idea of correlations and the development of an integral equation for determining the correlation coefficient in terms of the intermolecular forces. This integral equation, which they derived by other methods, follows from our Eq. (42) if one redefines f_k and g_k by dividing by the volume of one cell. Going over to the continuum, one then obtains

$$g(\mathbf{r})=f(\mathbf{r})+\int f(\mathbf{r}'-\mathbf{r})g(\mathbf{r}')d\mathbf{r}'. \tag{43}$$

They have shown that if $f(r)$ is a short-range isotropic function, one can transform Eq. (43) into a differential equation whose asymptotic solution is

$$g(r)\sim e^{-\kappa r}/r, \tag{44}$$

where

$$\kappa^2=\frac{2(1-F)}{E};\quad F=\int f(r)d\tau;\quad E=\frac{1}{3}\int r^2 f(r)d\tau. \tag{45}$$

This solution is instructive, since it shows that for $\kappa>0$ (above the critical point) $g(r)$, the correlation coefficient of the fluctuations, drops to zero exponentially as the distance increases. At the critical point where $\kappa=0$,[f] $g(r)\sim 1/r$, a long-range function, so that fluctuations make their influence felt over long distances.

Having indicated how the equations of Ornstein and Zernike follow from our work, under suitable approximations, we now turn to another important development, the theory of Rocard.[3] Rocard's starting point is the observation that the thermodynamic variable in question, our x_r (the density in his case), is actually a function of position in the system, due to the fact that fluctuations occur locally rather than over the system as a whole. Although this remark is in agreement with the theories given here and by Ornstein and Zernike, Rocard's method of working out its consequences is different. Since Rocard himself has stressed this difference, it is of interest that his equations also can be made to follow from our theory if certain approximations are made.

Rocard's method is to consider the modification in the effective "force," P_r (pressure in his case), due to the spatial variation of x_r. P_r is modified by an additive term proportional to the Laplacian of x_r, thus giving rise to a corresponding term in the minimum work. This latter term does not vanish at the critical point and, thus, finite fluctuations are obtained.

We shall now show how our theory can be made to give results of this form. The effective force P_{rk} (or simply P_k) in the cell k is given by

$$P_k=\frac{\partial}{\partial z_k}\left[\frac{1}{2}\sum_{k,l}a_{kl}z_k z_l\right]=\sum_l a_{kl}z_l, \tag{46}$$

since the quadratic form expresses the minimum work. Applying the nearest-neighbor approximation of Eq. (27) we obtain:

$$P_k=a_0 z_k+a_1(z_{k+j_1}+z_{k-j_1}+z_{k+j_2}+z_{k-j_2}+z_{k+j_3}+z_{k-j_3})\simeq(a_0+6a_1)z(k)+a_1\nabla^2 z(k), \tag{47}$$

where we have gone over to a continuous position vector k and we have approximated

$$z(k+j_1)+z(k-j_1)-2z(k)\ \text{by}\ \frac{\partial^2 z(k)}{\partial x^2},\ \text{etc.}$$

It is seen that Eq. (47) is essentially equivalent to Rocard's assumptions, since the first term gives rise to a vanishing work at the critical point where $a_0+6a_1=0$, and the second term is Rocard's additional term. It is worth pointing out that Rocard's approach does not take full account of the correlation effects since, after setting up an equivalent to Eq. (47), he considers only one cell and not its interactions with its neighbors.

The last theory to be considered is that of Yvon.[4] His fundamental approach is essentially similar to ours, but his method of treating the system as a whole is based on a rather different viewpoint. Our theory is based on treating the system as an assembly of interacting cells whose basic properties we do not compute but in terms of which we work. Yvon attempts a completely molecular description of the system (liquid in his case); he works in terms of an Ursell development but, due to the complexity of his method, he is able to handle only the terms corresponding to "binary clusters" of molecules when it comes to making explicit calculations. Since there is no reason to believe that this limitation is plausible in the neighborhood of the critical point, we do not think this method is fruitful in practice although it is probably correct in principle.

Let us conclude by comparing the predictions of the various theories discussed so far as critical opalescence[9–11] is concerned. We have not made here an explicit calculation of our own, but we have indicated that both the Ornstein-Zernike and the Rocard theories are, in a sense, special cases of ours.

[f] $F=\Sigma_l f_{kl}=-6a_1/a_0$; hence $F=1$ at the critical point and $\kappa=0$.

[9] H. A. Stuart and H. G. Trieschmann, "Lichtzerstreuung," Hand und Jahrbuch d. Chem. Phys. Bd. 8, Abschn. II (Leipzig, 1936).

[10] J. Cabannes and Y. Rocard, *La Diffusion Moléculaire de la Lumière* (Les Presses Universitaires de France, Paris, 1929).

[11] G. Oster, Chem. Rev. **43**, 319 (1948).

Our interest is only in the dependence on wave-length and the angular distribution.

The Smoluchowski theory predicts

$$I/I_0 \propto 1/\lambda^4(1+\cos^2\theta)\beta, \tag{48a}$$

$$I/I_0 \propto 1/\lambda^4(1+\cos^2\theta)(\gamma)^{\frac{1}{2}}. \tag{48b}$$

Here I/I_0 is the ratio of scattered to incident intensity of light of wave-length λ observed in the direction θ; β is the compressibility,

$$\beta=-1/V(\partial V/\partial P)_T,$$

and $\gamma=\partial^3 V/\partial P^3$. The expression (48a) is valid away from the critical point, and (48b) at the critical point, in this theory.

Ornstein and Zernike's theory predicts

$$\frac{I}{I_0}\propto\frac{1}{\lambda^4}(1+\cos^2\theta)\frac{1}{\{1/\beta+d^2[\sin(\theta/2)/\lambda]^2\}}. \tag{49}$$

The constant d^2 is a measure of the radius of the intermolecular forces and is proportional to E defined in Eq. (45). The additional term in the denominator arises from the correlation of fluctuations in different volume elements giving rise to a $1/\lambda^2$ dependence and an enhancement of the forward scattering at the critical point. The result is not quite complete as it stands, since it makes I/I_0 infinite for $\theta=0$ at the critical point. Placzek[12] has shown that taking the finite volume of the scattering medium into account introduces a factor preserving the finiteness without modifying the result for experimentally realizable situations.

Rocard's theory predicts

$$\frac{I}{I_0}\propto\frac{1}{\lambda^4}(1+\cos^2\theta)\frac{1}{[(1/\beta)+c]}, \tag{50}$$

where c is a constant arising from the additional term in the pressure ($\propto\nabla^2\rho$).

The predictions of the Ornstein-Zernike and Rocard theories differ in two ways: the wave-length dependence, which becomes $1/\lambda^2$ at the critical point in the former theory, and the angular distribution, which is preferentially forward at the critical point in this theory. The two effects must go together here, as can be seen from the derivation of Eq. (49). (The theory of Yvon gives a wave-length dependence $\sim A\lambda^{-4}-B\lambda^{-6}$ where A, B are positive. We discuss this no further for reasons given above.)

Experimental work on critical opalescence has not settled the question in any clear fashion. The results of Andant[13] and Battacharya[14] show a change in wave-length dependence in the immediate vicinity of the critical point. Both find a dependence on $1/\lambda^2$ at the critical point and Andant has studied the change in exponent in (λ^{-n}) quite carefully. On the other hand, Rousset,[15] working with fluid mixtures (for which the theoretical predictions are essentially the same), finds no such definite results. For several types of fluids, the λ^{-4}-law and the angular symmetry (forward and backward) are preserved up to the critical point. In other cases, the exponent n decreases to a value of about 3 and, at the same time, an asymmetry between forward and backward scattering appears.

Summing up, it seems safe to say that there are experimental indications that the correlation effects are real and observable, although not in all cases.

[12] G. Placzek, Physik Zeits. 31, 1052 (1930).
[13] A. Andant, J. de phys. et rad. 5, 193 (1924).
[14] D. K. Battacharya, Proc. Ind. Assoc. Cultiv. Sci. 8, 277 (1923).

APPENDIX

We wish to evaluate

$$\langle z_k z_l\rangle_{Av}=\frac{\int z_k z_l \exp\left[-\frac{1}{2}\sum_{k,l} a_{kl}z_k z_l\right]d\tau'}{\int \exp\left[-\frac{1}{2}\sum_{k,l} a_{kl}z_k z_l\right]d\tau'}. \tag{A1}$$

Let us introduce the (real) eigenvectors of $\|a_{kl}\|$:

$$\eta_{kl}=\left(\frac{2}{M^3}\right)^{\frac{1}{2}}\cos\left(\frac{2\pi}{M}k\cdot l+\frac{\pi}{2}\frac{l_1+l_2+l_3}{3M}\right);\quad l\neq 0. \tag{A2}$$

$$\eta_{k0}=\left(\frac{1}{M^3}\right)^{\frac{1}{2}}.$$

The eigenvalues are given in Eq. (24). We use real eigenvectors to avoid complex integration.

Let

$$z_k=\sum_l \eta_{kl}y_l;\quad y_l=\sum_k \eta_{lk}^{-1}z_k=\sum_k \eta_{kl}z_k; \tag{A3}$$

(since $\|\eta_{kl}\|$ is orthogonal).

The restriction of Eq. (22) is now simple:

$$\sum_k z_k=\sum_{k,l}\eta_{kl}y_l=\sum_l y_l\sum_k \eta_{kl}=M^{3/2}y_0=0. \tag{A4}$$

Hence, all we need to do to observe the restriction is to set $y_0=0$ and drop this variable.

$$\sum_{k,l} a_{kl}z_k z_l=\sum_k \lambda_k y_k^2. \tag{A5}$$

$$\langle z_k z_l\rangle_{Av}=\frac{\sum_{m,n}\eta_{km}\eta_{ln}\int y_m y_n \exp\left[-\frac{1}{2}\sum_k{}'\lambda_k y_k^2\right]d\tau'}{\int \exp\left[-\frac{1}{2}\sum_k{}'\lambda_k y_k^2\right]d\tau'}, \tag{A6}$$

$$\langle z_k z_l\rangle_{Av}=\frac{\sum_m \eta_{km}\eta_{lm}\int y_m^2 \exp\left[-\frac{1}{2}\sum_k{}'\lambda_k y_k^2\right]d\tau'}{\int \exp\left[-\frac{1}{2}\sum_k{}'\lambda_k y_k^2\right]d\tau'}. \tag{A7}$$

The integrals are now simple and we obtain:[7]

$$\langle z_k z_l\rangle=\sum_m{}'\frac{\eta_{km}\eta_{lm}}{\lambda_m}, \tag{A8}$$

Let us put this expression into a simple explicit form by introducing the values of the η_{km} from Eq. (A2).

$$\langle z_k z_l\rangle_{Av}=\frac{2}{M^3}\sum_m{}'\frac{\cos[(2\pi/M)k\cdot m+(\pi/2)(m_1+m_2+m_3/3M)]}{\lambda_m}$$
$$\times\cos[(2\pi/M)l\cdot m+(\pi/2)(m_1+m_2+m_3/3M)]. \tag{A9}$$

Expanding the cosines and making use of the fact that $\lambda_m=\lambda_{M(j_1+j_2+j_3)-m}$, we obtain

$$\langle z_k z_l\rangle_{Av}=\frac{1}{M^3}\sum_m{}'\frac{\cos(2\pi/M)(k-l)\cdot m}{\lambda_m}, \tag{A10}$$

which is the result given in the text, Eq. (31).

[15] A. Rousset, Ann. de physique 5, 5 (1936).

On the Conductivity Produced in CdS Crystals by Irradiation with Gamma-Rays*

RUDOLF FRERICHS
Department of Physics, Northwestern University, Evanston, Illinois
(Received August 1, 1949)

By combining the theory of secondary photo-currents developed by Hilsch, Pohl, Schottky, and others, with the model of a crystal phosphor by Johnson and Seitz and by Riehl and Schoen a theory of the photo-conductivity in CdS crystals is given. The theory agrees qualitatively with the results of previous and present experiments. A quantitative energy scheme, which is the basis for this theory, has been determined from measurements of the emission and absorption spectra of these crystals. According to the new determined sign of the thermal e.m.f.: CdS against Cu, the photo-current in CdS is predominantly carried by electrons. The dark current follows the usual law: $\log\sigma \sim 1/T$ with the constants $\epsilon = 0.67$ ev and $\sigma_0 = 1.7 \cdot 10^{-3}$ mho cm^{-1}. In accordance with the theory the final current reached after prolonged irradiation is proportional to the square root of the intensity of irradiation. The final current follows Ohms law. The initial slope of the decay curve is proportional to the intensity of irradiation. Under periodical irradiation with gamma-rays the amplitude of the resulting alternating current slowly increases to a final value. If the electric field is temporarily removed the original conductivity is slowly restored. When a CdS crystal is heated and then cooled to liquid air temperature irradiation produces a small primary current of less than 10^{-13} amp. at first. With continuous irradiation and after a slight delay this current suddenly increases until it reaches a constant value of 10^{-8} amp.

INTRODUCTION

SINCE the appearance of the first papers on the use of crystals for detecting nuclear radiation (diamond,[1] silver chloride[2] and cadmium sulfide[3]) there has been a growing interest in these so-called "counting crystals."[4] Further, a volume of literature on the photoelectric properties of CdS crystals has now accumulated.[3,4a,5–21] Inasmuch as CdS and the other counting crystals are phosphors, without exception,[22] and inasmuch as the mechanism of the photo-conductivity of a crystal phosphor was not yet explained, the author felt a detailed investigation of the relation between photo-conductivity and phosphorescence was warranted.

This paper attempts to give a model for this mechanism in CdS and describes several experiments which are the basis for the model.

A. The Mechanism of the Photo-Conductivity in CdS Crystals

Kallmann and Warminsky[11] were the first to point out that those CdS crystals which show large secondary currents are strongly phosphorescent. Thus the secondary currents in CdS as well as other crystal phosphors must be explained on the basis of the collective electron model for crystal phosphors. It will be shown, by combining the theory of secondary currents in photo-conductors, first proposed by Hilsch, Pohl, and Schottky,[23] with the generally accepted model for a crystal phosphor of Seitz, Johnson, Riehl, and Schoen, that the effects observed in CdS crystals can be explained.

Irradiation of a crystal phosphor by light or by fast particles produces a positive hole at an activating impurity.[24] The hole is produced either by a direct lifting up of the electron from the impurity state into the conduction band or it may first be produced in the filled valence band and then shift to an activating impurity by transfer of an electron. In each case the net result is a positive hole localized in the lattice at the position of the activating impurity. It is fundamental to the mechanism described in this paper that the positive charges remain stationary. This type of photo-

* This work was sponsored by the U. S. Navy, Bureau of Ships.
[1] G. Stetter, Berh. d. D. Phys. Ges. **22**, 13 (1941); see W. Jentschke, Phys. Rev. **73**, 77 (1948).
[2] P. J. Van Heerden, "The crystal counter," dissertation, Utrecht, 1945.
[3] R. Frerichs and R. Warminsky, Naturwiss **33**, 251 (1946).
[4] A review of this development is given by: R. Hofstadter, Nucleonics 4, No. 4, 1; No. 5, 29 (1949).
[4a] S. G. Sizzo and J. B. Platt, Phys. Rev. **76**, 704 (1949).
[5] R. Frerichs, Naturwiss **33**, 281 (1946).
[6] R. Frerichs, Phys. Rev. **72**, 594 (1947).
[7] R. Frerichs, Research **1**, 208 (1948).
[8] C. J. Humphreys, J. Opt. Soc. Am. **39**, 664A (1948).
[9] J. Fassbender, Naturwiss **34**, 212 (1947).
[10] K. Weiss, Zeits. f. Naturforsch. **2a**, 650 (1947).
[11] H. Kallmann and R. Warminsky, Ann. d. Physik **4**, 69 (1948).
[12] H. Kallmann, Research **2**, 62 (1949).
[13] H. Kallmann and R. Warminsky, Research **2**, 87 (1949).
[14] I. Broser and H. Kallmann, Ann. d. Physik (6) **3**, 317 (1948).
[15] H. Kallmann and R. Warminsky, Research **2**, 389 (1949).
[16] H. Kallmann, Ann. d. Physik **4**, 61 (1948).
[17] G. C. Goldsmith and K. Lark Horowitz, Phys. Rev. **75**, 526 (1949).
[18] R. Frerichs and A. F. J. Siegert, Phys. Rev. **74**, 1875 (1948).
[19] Rose, Weimer, and Forgue, Phys. Rev. **76**, 179 (1949).
[20] Fassbender, Moglich, Rompe, Ann. d. Physik (6) **3**, 327 (1948).
[21] G. Hohler, Ann. d. Physik (6) **4**, 371 (1948).
[22] ZnS and diamond have been used in the early investigations on subjective counting of scintillations. Type II diamonds, which are best suited as crystal counters are according to Pohl and to Robertson, photo-conductors as well as phosphors. AgCl is a phosphor at low temperatures.
[23] R. Hilsch and R. W. Pohl, Zeits. f. Physik **108**, 55 (1937); **112**, 252 (1939); R. Schottky, *Das freie Electron in Physik und Technik* (Verlag, Julius Springer, Berlin, 1940), p. 57; R. Pohl and F. Stockmann, Ann. d. Physik (6) **1**, 275 (1947).
[24] The nature of the impurity states has been discussed by N. F. Mott and R. W. Gurney, *Electronic Processes in Ionic Crystals* (Oxford University Press, New York, 1948), second edition, Chapter VI.

conductivity therefore has to be distinguished from other types[25] in which holes and electrons both move.

How does the excitation behave when a strong electric field is applied to the crystal? We first assume a good insulating crystal, as for instance CdS at low temperatures. In this case the electron lifted up into the conduction band follows the field without delay. If the field is high enough the electron will eventually reach the anode. When the liberation of the electron takes place near the cathode the maximum current is attained. One electron is moved across the crystal per one quantum of energy effective. Since no electrons can enter the crystal at the cathode, this process is complete as soon as the electron reaches the anode. At low fields the electron will be captured in trapping states or will recombine with the positive hole. But above a certain field, determined by the lifetime of the free electron, it reaches the anode before this trapping or recombination occurs. Further increase of the field strength does not increase the current; the current is saturated.

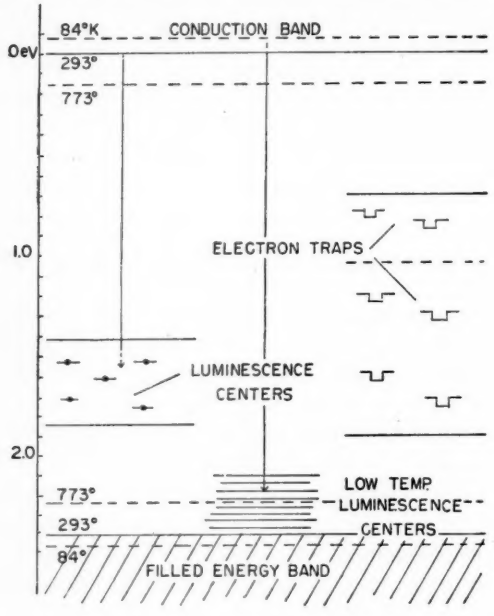

FIG. 1. Band scheme of CdS.

If we assume instead a crystal with a small electron conductivity, as for instance CdS crystals at room temperature, the process will be different. A small number of electrons will be continually lifted up by thermal impact into the conduction band from the highest intermediate filled states between the valence and the conduction band. These states may be due either to filled electron traps or to activating impurities which can give up electrons to the conduction band. There are many more of the latter, hence the transition from the activating impurities represents a more probable process. If one electron is lifted up by irradiation the positive charge of the hole as well as the negative charge of the electron become neutralized by a redistribution of the density of the conduction electrons within the crystal. The hole attracts electrons and the electron produced repels other electrons. The net effect is that an extra electron is now available in the conduction band. When the electron leaves the crystal at the anode another electron enters at the cathode. The current due to these electrons is given by

$$i=e\cdot v\cdot(P/l)\cdot\tau, \tag{1}$$

where v=mobility of the electron, P=potential applied, l=distance between the electrodes, τ=lifetime of the hole. If a large number of primary electrons is lifted up into the conduction band and if the lifetime of the holes is long then an electron chain results, giving a large secondary current.

We consider the processes which interrupt the chain and thus restore the crystal to its original state. Electrons can be prevented from reaching the anode in three ways. They can recombine with a positive hole at the activating impurity, emitting light in this process. They can return to the activating impurity with a simultaneous loss of their energy to the lattice as "phonons." Finally they can be captured by an electron trap. The electron traps may be cracks, interfaces between crystals or dislocations of the lattice.[26] Storage of electrons in traps and their subsequent release accounts for the phosphorescence. The return of the electrons, which transfer some of their energy as heat, causes energy losses observed in phosphorescence.

The recombination with the activating impurities follows the usual quadratic law: $dn/dt=-bn^2$ (b=coefficient of recombination), provided the number of holes is equal to the number of electrons n in the conduction band. The dark currents are of the order of 10^{-11} to 10^{-14} amp. but the photo-currents reach 10^{-8} amp. and more. Thus the number of the electrons in the conduction band is given approximately by the number of electrons lifted up from the activating impurities and it is proportional to the absorbed energy of irradiation, J. The equation for the lifting up and recombining the electrons is represented by:

$$dn/dt=aJ-bn^2. \tag{2}$$

This equation neglects the capturing of electrons in traps. The trapping of a single electron affects the current in two ways. Its removal from the conduction band reduces the number of electrons available by one and at the same time the corresponding electron chain is broken. Releasing of the electron from the traps affects the current also in two ways. First it may be released into the conduction band and initiate an electron chain. This corresponds to "stimulation" in the terminology of phosphorescence. When the electron returns from the conduction band to the activating

[25] The latter type has been thoroughly investigated by K. G. McKay, Phys. Rev. 74, 1606 (1948).

[26] In phosphors of the ZnS type, the traps are generally assumed to be separate from the luminescent centers.

impurity, the crystal looses the trapping energy by emission of light. Second, in the alternative process, the electron may be released from the trap and lose its energy stepwise to the lattice in "phonons." It does not reach the conduction band and therefore does not take part in electron chain building. It returns to the activating impurities without emission of light. This process is the "quenching" in the terminology of phosphorescence. While stimulation temporarily increases the secondary current, quenching reduces it.

B. Experimental Results

a. The Band Scheme of CdS

Since the proposed theory is derived from the optical data it must agree with the band scheme of the electrons. The energies of the valence band, the conduction band, the activating impurities and the traps are given in Fig. 1. The ev values are plotted downward from the lower edge of the conduction band. For a crystal at room temperature the upper edge of the valence or highest filled band is situated at 2.41 ev below the lower edge of the conduction band. This energy difference varies inversely with the temperature,[27] and the levels shift correspondingly, as represented in Fig. 1.

The activating impurities, i.e., the luminescent centers, extended from 1.42 to 1.85 ev in the crystals investigated.[28] These values were determined by measurements on the red and infra-red emission spectrum of the crystal under irradiation with ultraviolet light.[29] The luminescence corresponds to a transition from the lower edge of the conduction band into levels of the activating impurities and defines their position. At low temperatures a second set of equi-distant levels situated closely above the valence gives rise to a second system of emission bands in the green.[30] The energy of the traps is given by the range of the extinguishing infra-red radiation. This corresponds to a transition from these traps into the lower edge of the conduction band. The traps extend over a region with two maxima at about 0.9 and 1.5 ev.[6,31]

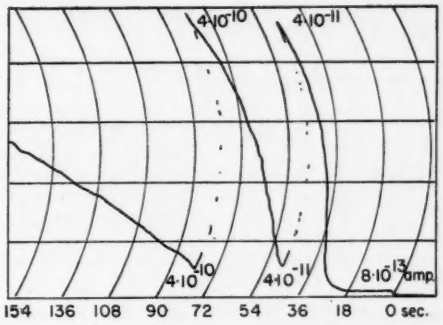

FIG. 3. Rise of the photo-current in CdS at liquid air temperature (curves taken with stepwise decrease of input resistances).

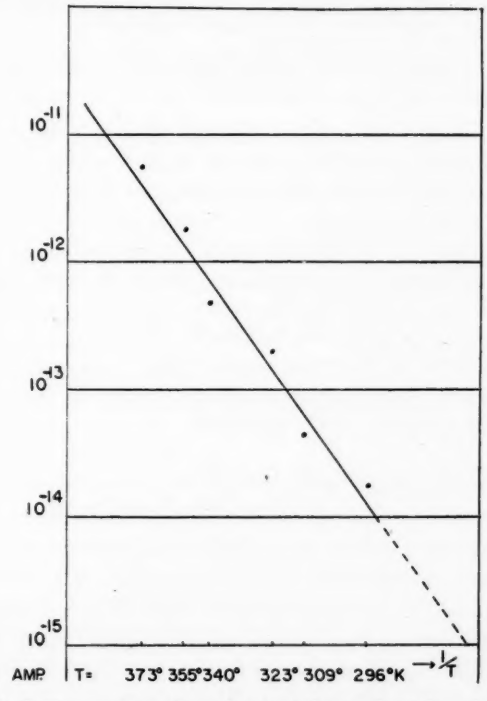

FIG. 2. Temperature dependence of the conductivity of CdS.

b. The Nature of the Current Carriers

In this model we assume that the current is carried solely by electrons and that the positive holes are immobile. The sign of the current carriers was determined by the sign of the thermal e.m.f. between CdS and Cu in the temperature range 23°C and 70°C. The average thermal e.m.f. of nine crystals investigated amounted to 7×10^{-4} volt per degree centigrade when the crystals were in the dark. At strong irradiation with light or with gamma-rays it was about 1.6×10^{-4} volts/°C. Measurement of the thermal e.m.f. determines only the predominance of the one or the other sign of conductivity. Each of the nine crystals investigated showed predominantly electron conductivity under irradiation. Eight showed predominantly electron conductivity in the dark. The conductivity of one crystal in the dark was predominantly due to holes. But under irradiation the crystal showed predominantly electron conductivity. This behavior is not yet explained. The measurements were made with an electron tube voltmeter of high

[27] F. A. Kroger, Physica **7**, 1 (1940); F. Moglich and R. Rompe, Zeits. f. Physik **119**, 473 (1942); A. Radkovsky, Phys. Rev. **73**, 749 (1948); G. Hohler, reference 21.

[28] The nature of the activating impurities in the crystal used is not known. By suitable activation for instance with silver, this emission can be shifted. The resultant shift of the activator levels will change the activation energy of the dark current accordingly.

[29] Photographs were taken with a Hilger wave-length spectrometer. The spectrum of the crystal investigated did not extend beyond 8700A.

[30] F. A. Kroger, Physica **7**, 1 (1940).

[31] It is however possible that additional traps are situated between 0 ev and 0.7 ev. These traps would be empty at room temperature and are only effective in capturing at low temperatures.

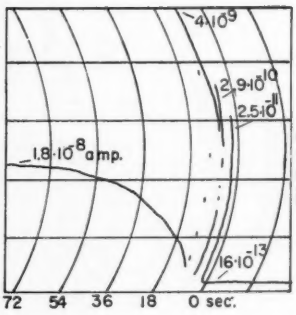

FIG. 4. Rise of the photocurrent in CdS at room temperature (curves taken with stepwise decrease of input resistances).

input resistance (up to 5×10^{11} ohms). Dember effects were balanced out by reversing the terminals of the crystals.

c. Low Temperature, No Irradiation

In a crystal which has been kept in the dark the highest occupied levels are at the activating impurities. Since the energy difference between the conduction band and the activating impurities is large, small conductivity is to be expected at low temperature. The dark current of some crystals investigated at liquid air temperature were less than 1×10^{-14} amp. This is the lower limit of the electronic voltmeter.

d. Higher Temperatures, No Irradiation

According to the energy scheme a few electrons should be lefted up from the activating impurities into the conduction band by thermal impact. The conductivity was observed to follow the usual law:

$$\sigma=\sigma_0 e^{-(\epsilon/kT)}. \tag{3}$$

Measurements in the range 25°C to 100°C gave $\epsilon=0.67$ and $\sigma_0=1.7\times10^{-3}$ mho cm^{-1}. Figure 2 shows the logarithm of the current plotted against $1/T$. The crystal was not heated above 100°C to prevent deterioration.

The optical value of the activating energy usually is about twice the electrical value.[32] This was confirmed by these measurements. The electron donators fall well into the region of the activating impurities, which contain loosely bound electrons. They can be lifted up into the conduction band and thus account for the dark current. In a crystal which is irradiated and then placed in the dark some electrons remain trapped. They may be released by thermal impact and thus temporarily augment the dark current. The measurements of the dark current are thus found to be in agreement with the optically derived energy scheme.

e. Low Temperatures, Irradiation, Initial Stage

According to the crystal phosphor model, electrons lifted up from the activating impurities into the conduction band are captured by the traps and remain there at low temperatures. The photo-conductivity connected with this process should be small since the trapping probability is high.

The experiments to check this process were performed with gamma-rays. The crystal was in a brass tube which could be lowered into baths of various temperatures. The tube was airtight and kept dry by "drierite." It was possible to insert a radium needle (platinum 0.5-mm walls, 5-mg radium equivalent) through a tube to within 4 mm of the crystal. The irradiation was about 70 mr/sec. The curves were drawn by a paper tape recorder fed by a sensitive d.c. amplifier. The crystal in the tube was heated to 100°C before each measurement to empty the electrons from the traps. Ionization in the air surrounding the crystal was avoided by applying a low potential of 2.9 volts at the crystal. At liquid air temperature the dark current ($\ll10^{-13}$ amp.) reached 8×10^{-13} amp. in about three seconds after the radium was brought close to the crystal (Fig. 3).

f. Low Temperature, Irradiation, Advanced Stage

In this part of the experiment the traps are filled slowly. The capture of electrons is reduced and they stay in the conduction band longer. It was found that the current was constant for 18 sec., then started to rise.[32a] After three hours the current reached 1.5×10^{-8} amp. but the final value had not yet been reached.

g. Low Temperature, Irradiation, Interruption of Irradiation

The lifetime of electrons in traps is very long at low temperatures. According to our model, electrons are lifted up from the activating impurities into the traps and a metastable state of the crystal results. If under these conditions the irradiation is interrupted the photocurrent immediately drops to values $<10^{-13}$ amp., because the electrons in the conduction band recombine with the activating impurities. If the crystal is irradiated for a second time, a new delay does not occur. The current rises immediately and comes to the same value of 1.5×10^{-9} amp. as before.

h. Low Temperature, Irradiation, Interruption of Irradiation, Warming up of the Crystal

The energy stored in a crystal phosphor at low temperatures can be released by warming it. If a crystal previously irradiated at liquid air temperature is heated to 70°C, there is a sudden surge of current. This current is several orders of magnitude larger than the dark current at this temperature. This agrees with the band scheme. Some filled traps are situated higher than the

[32] T. H. de Boer and Ch. van Geel, Physica **2**, 286 (1935); Mott and Gurney, reference 24, p. 160.

[32a] Analogous observations were made by W. Lehfeldt, Göttinger Nachrichten II, **1**, 171 (1935) with AgCl at low temperatures. AgCl is used as a crystal counter. This confirms our assumption (reference 22) that counting crystals are phosphors.

activating impurities (Fig. 1). In these experiments the additional charge carried across the crystal amounted to about 1.7×10^{-7} coulomb. Since this represents secondary currents no immediate conclusions concerning the number of traps and trapped electrons can be drawn.

If the experiment is repeated at 100°C there is a second and smaller surge of current of electrons coming from the deeper traps.

i. Room Temperature, Irradiation

At room temperature the traps continually discharge electrons and the metastable state cannot be sustained (Fig. 4). The dark current, 1.3×10^{-12} amp. starts to rise immediately upon irradiation, and reaches 1.8×10^{-8} amp. after 72 seconds. If the traps are empty at the beginning of the irradiation the current at first rises slowly. As the traps are filled the current increases at a faster rate. Finally the rate of increase tapers off and the current reaches a constant value. Then the rate of raising the electrons into the conduction band equals the rate of recombination with the activating impurities. At high intensities the number of electrons in the conduction band equals the rate of recombination with the activating impurities. At high intensities the number of electrons in the conduction band exceeds the number of trapped electrons.[33] The number of electrons in the conduction band at equilibrium is given by

$$dn/dt=aJ-bn^2=0, \quad aJ=bn^2. \tag{4}$$

To test this relation equilibrium currents under different irradiation intensities were measured. Measurements with four crystals gave averaged ratios of the photo-currents of 2.06:1 when the distance between radium needle and crystal was increased from 28 to 56 mm.

j. Room Temperature, Intermittent Irradiation

If the irradiation is interrupted, Eq. (4) changes to

$$dn/dt=-bn^2.$$

The crystal was irradiated for a period of hours until the current at the recorder became constant. Then the radium was withdrawn for two seconds and immediately replaced. At a chart speed of 19 mm=4.1 sec. a small dip in the curve was observed. The current returned to its former value within a few seconds after the radium was replaced. This indicates that during the interruption the occupancy of the traps is not seriously affected. Measurements were made at relative intensities of irradiation of 4 and 1. The corresponding ratio of the downward slope of the short decay curves was 4.3:1.

When the irradiation was kept constant and the potential applied at the crystal increased in steps from 1:2:3 the initial downward slope of the decay curve increased from 1 to 2.1 to 2.9. When the distance between radium and crystal was varied so that the current remained constant at different potentials V the initial downward slope of the decay curves was proportional to $1/V$. Both of the results agree with the theory. Equation (2) giving the initial slope of the decay curve cannot be expected to hold for the rise curve. This is because the initial state of the crystal depends strongly on the occupancy of the traps. If some electrons remain in the traps at the beginning of the experiment the current rises faster than in a crystal with empty traps.

k. Room Temperature, Non-Equilibrium Conditions

At equilibrium the photo-current is proportional to the square root of the intensity of irradiation. Also the number of electrons captured per second by the traps is equal to the number of electrons thermally released per second into the conduction band. From the proportionality of n with J it follows that the number of electrons captured per second is a constant fraction of the number in the conduction band. This relation can only hold if enough empty traps are available. The capturing is determined then by the number of electrons available and not by the number of empty traps. At room temperature the traps discharge rapidly and a large number of empty traps is always available.

Non-equilibrium conditions were observed as follows: The photo-current was kept at a chosen constant value by the rate at which the radium needle was withdrawn. When the photo-current was kept at a constant value and the exposure time varied, it was found that the initial slope of the decay curve decreased markedly with increasing exposure time. This experiment indicates traps extending over a wide region in the energy diagram in accordance with the optical observations of the

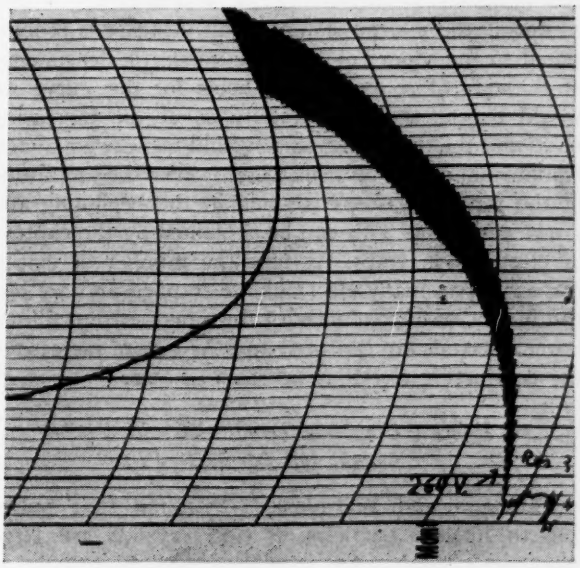

FIG. 5. Current produced in CdS by periodical irradiation with γ-rays.

[33] Preparation and characteristics of solid luminescent materials Cornell Symposium of the American Physical Society, p. 115, ff.

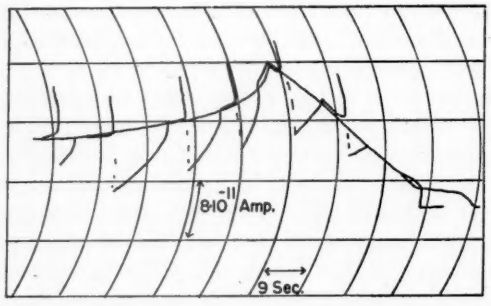

FIG. 6. Curves showing that the building up of stationary positive space charges is independent of the electric field to the first approximation. Continuous curve: Field applied at the CdS crystal during irradiation. Interrupted curve: Field periodically removed during irradiation.

extinguishing absorption. The electrons captured in the traps of different depths rearrange themselves with time until finally predominantly deeper traps are filled. This experiment further shows that the interpretation of these curves offers the same difficulties as the interpretation of the optical decay curves of phosphors with more than one trap level.

l. Room Temperature, Periodical Irradiation

To produce periodic gamma-ray pulses, the needle was attached to the end of a long lever and moved by a cam. A five seconds irradiation period at 1.0 cm was followed by a five second period at 35 cm. Travel time per cycle was less than a second. When the crystal is irradiated periodically the current builds up according to Fig. 5. This curve is explained qualitatively as follows. At each period of irradiation equal numbers of electrons are lifted up from the activating impurities into the conduction band. This number decreases by recombination during the period of irradiation as well as during the intermission and this decrease is proportional to the square of n. If the quadratic dependence of the rate of recombination holds for this curve we would expect that the amplitudes of the increasing steps and the decreasing steps would become equal and equilibrium would be reached. However the amplitude of the increasing steps is small in the beginning and grows with time. This can be explained by the capture of electrons in traps. At first the number of empty traps is large, many electrons are trapped and are lost to the process of conductivity. In time the traps fill up, fewer electrons are captured and the rate of increase of the conducting electrons becomes greater.

m. Effect of Combined Irradiation with Visible Light and Particles

Kallmann and Warminsky[11,33a] found that pulses due to nuclear particles in CdS crystals are large when the crystal is also irradiated with white light or with electrons. This irradiation fills the traps with electrons in agreement with our model. The capturing probability is smaller and the electrons remain in the conduction band for a longer time.

[33a] See also A. G. Chynoweth, Phys. Rev. **76**, 310 (1949).

n. Unipolar Conductivity in CdS Crystals

CdS crystals show unipolar conductivity when one end of the crystal is irradiated. The current is stronger when the cathode is irradiated.

These unipolar effects, first observed by Gudden and Pohl in ZnS, have been emphasized by Kallmann and Warminsky[11] as well as by Rose, Weimer, and Forgue.[19] According to the model assumed, positive stationary holes are formed close to the origin of the liberated electron. If a positive stationary space charge occurs close to the cathode the entrance of the electrons is made easier and longer electron chains will result.

o. Irradiation, Raising and Lowering the Temperature

The final current in a crystal irradiated with constant intensity depends upon the temperature of the crystal. At low temperatures the photo-current is large, at high temperatures it is small. According to measurements of Brentano and Davis[34] the photo-conductivity reaches a maximum at about $-120°C$ and decreases again at lower temperature. The decrease of photo-conductivity at high temperatures parallels the quenching of phosphorescence. At high temperature an increased number of direct recombinations between the electron and the activating impurities can take place. The energy difference is transformed in "phonons." This increased probability of recombination reduces the maximum current and decreases the inertia in accordance with the observations. The processes involved at very low temperatures, where the current again decreases, cannot be explained. It might be possible that the appearance of the green system of phosphorescence bands offers an additional way for the return of the electron to low states. Thus it would diminish the number of electrons in the conduction band.

p. Crystal Irradiated at Room Temperature, Electrical Fields Periodically Interrupted

The building up of stationary positive space charges in the body of the crystal is independent of the electric field to the first approximation. Figure 6 shows two curves which were taken, one on top of the other, with the same irradiation and field. In the continuous curve the irradiation on the crystal was interrupted after 27 seconds. In the discontinuous curve the conditions were unchanged but the field was interrupted periodically. If the initial deviations due to the capacitance of the crystal have disappeared this procedure gives the same results on both the rise curve and the decay curve. These experiments have to be performed with strong irradiation and weak fields. Then the formation and the

[34] J. M. C. Brentano and D. H. Davis, Phys. Rev. **74**, 711 (1948).

lifetime of the positive space charges is determined by the individual absorption processes of incident gamma-radiation and by the recombination rate of the electrons lifted up into the conduction band.

At strong fields and weak irradiation the shift of the electrons simultaneously shifts the location of the recombination processes towards the anode. Finally a uniform distribution of positive space charges in the crystal is achieved. The slow restoration of the conductivity can be accelerated by application of alternating fields. If the potential at the electrodes is reversed every 10 seconds the final current for each phase is reached immediately. This experiment is related to the important observations of McKay on diamonds irradiated with slow electrons.

C. Other Theories of Photo-Conductivity in CdS

Kallman and Warminsky[11] first clarified the amplification process when they pointed out that photo-conductivity and phosphorescence are closely related. They showed that strongly phosphorescent crystals yield the largest secondary current. They did not, however, take recombination into account and deduced an exponential dependence of the decreasing current on the number of electrons in the conduction bands. This dependence does not agree with the measurements given here.

Rose, Weimer, and Forgue[19] assumed that the large secondary currents are due to "opening up" of multiple thin barriers between conducting sections of the crystal. They pointed out that irradiation with narrow pencils of light in CdS produces currents the intensity of which depends on the irradiated spot.

CdS crystals produced by the usual method consist often of many small crystals grown together in the form of ribbed strips. The short crystal needles are lined up side by side to form a ribbed polycrystal. Inspection of the ribbed areas under polarized light reveals crystal boundaries coinciding with the edges of the ribs. The photoelectric properties are identical whether the current flows parallel to the long axis, or crosswise. This proves that barriers between individual crystals do not affect the photo-currents. According to earlier measurements of the author, photo-currents can be observed in CdS at field strengths of less than 0.1 volt/cm. This is hard to explain by the barrier layer model.

Fassbender, Moglich, and Rompe[20] give an interpretation of the ideas of Hilsch, Pohl, Stockmann, and others on secondary currents by means of the collective electron model of solids. The differences between their theory and the one presented here should be pointed out. These authors considered a photo-conductor containing a set of discrete energy levels between valence and conduction band. Electrons are brought up into the conduction band thermally as well as by irradiation. They return to the discrete levels by recombination only. Thus if the dark current resulting from the thermal activation is small, the photo-current i_{final} is proportional to the square root of irradiation. The theory in this form however does not explain the present observations on CdS. The presence of traps, capturing and releasing of electrons, stimulating and quenching are not considered. In CdS the dark currents are so small that in the tail of the decay curve the trapped electrons determine exclusively the dependence of the current on time.

CONCLUSION

The collective electron model of the crystal phosphor is adequate to give a qualitative picture of the secondary photo-currents induced by irradiation in CdS crystals. The quantitative relations between current and irradiation and initial declining slope, after the irradiation has been interrupted, can be explained by simple assumptions. None of the properties observed up to now are in contradiction with this theory.

To summarize the observations:

a. The photo-current in a crystal phosphor is directly proportional to n, the number of electrons in the conduction band.

b. The luminescence intensity is proportional to the recombination rate bn^2.

ACKNOWLEDGMENT

The author acknowledges the valuable discussions and the kind help of Dr. R. J. Cashman, Dr. A. W. Ewald, Mr. L. W. Gildart, Dr. E. W. Lothrop Jr., and Dr. A. J. F. Siegert.

Letters to the Editor

PUBLICATION of brief reports of important discoveries in physics may be secured by addressing them to this department. The closing date for this department is five weeks prior to the date of issue. No proof will be sent to the authors. The Board of Editors does not hold itself responsible for the opinions expressed by the correspondents. Communications should not exceed 600 words in length.

Experimental Beta-Gamma-Angular Correlation

RICHARD L. GARWIN*
Department of Physics and Institute for Nuclear Studies, University of Chicago, Chicago, Illinois
November 2, 1949

THE number of gamma-rays emitted by a nucleus into unit solid angle has been measured as a function of angle with the preceding coincident beta-ray. Scintillation counters were used, the gamma-sensitive counter consisting of a 1-cm thick clear anthracene crystal subtending 0.13 steradian at the source. The beta counter active element is a 50 mg/cm² sheet of anthracene cleavings mounted with collodion on the face of an RCA 5819 photo-multiplier. The beta-counter subtends an angle of 0.07 steradian at the source, having efficiency 100 percent for beta- and 1 percent for gamma-rays. The beta-counter is fixed with respect to the source, the surrounding tank being evacuated to avoid loss of correlation by scattering. The sources are sufficiently thin (0.01 to 0.1 mg/cm²) so that no appreciable beta-scattering arises in the source.[1] Detailed tests indicate that the correlation measured is that existing at the atom in question. A coincidence resolving time of 0.04 microsecond is available from a simple modified Rossi pair.

Measurements are taken at 20 positions, giving 10 points of the correlation curve between 45° and 180°. For the most part, 20,000 counts are taken for each activity, and a $1+b\cos^2\theta$ function fitted by least squares to the experimental points. The observed beta-gamma-coincidence rate at each point is divided by the gamma-single rate at that point to allow for the shadow of the source holder, etc.

The resulting values for b and their standard deviations (induced through the least squares process by the finite number of counts) are listed in Table I.

In no case was any anisotropic correlation observed, larger than the statistical error. According to the theory[2,3] the only general way of obtaining spherical correlation is either for the beta-ray to be permitted or for the spin of the residual nucleus (after the beta-decay) to be 0 or ½. Typical values of the coefficient b range from 0.10 to 0.80 when these selection rules are not fulfilled.

For the isotopes Na^{24}, Co^{60}, and Au^{198} the spin of the intermediate nucleus is known to be non-zero,[4] and the beta-ray is classified as forbidden by Konopinski.[5] This suggests an inconsistency in the beta-ray theory, since the resulting angular correlations should be readily observable.

It is not known to what cause to ascribe the lack of correlation. The probability that these results are due to the operation of the selection rules in all cases, i.e., allowed betas or zero intermediate spins, is very small—of the order of 1 percent.[6,7] A large class of possible causes are made improbable by the fact that many gamma-gamma-correlations have been observed,[4] substantiating a considerable part of the theory.

TABLE I. Coefficient b in the function $1+b\cos^2\theta$ fitted by least squares to the experimental points.

Isotope	b
Na^{24}	$-0.02\ \pm0.02$
Co^{60}	-0.003 ± 0.01
Ru^{103}	$+0.025\pm0.025$
Ru^{105}	-0.002 ± 0.009
Cd^{115}	$+0.02\ \pm0.02$
Ir^{193}	-0.004 ± 0.03
Au^{198}	$+0.006\pm0.01$

Further experiments are under way on more test cases of the theory; these are forbidden beta-transition followed by a single gamma-ray to an even-even ground state.

Grateful acknowledgment is made of helpful discussions with Professor E. Fermi and Dr. C. N. Yang.

A fuller account of these investigations will be published in this journal.

* The work reported here was performed under an AEC Predoctoral Fellowship.
[1] Pile irradiation of the sources, and some of the measurements were carried out at the Argonne National Laboratory. I should like to thank the staff of the Argonne Laboratory for their help and cooperation.
[2] D. L. Falkoff, Ph.D. Thesis, University of Mich. (1948).
[3] C. N. Yang, Phys. Rev. **74**, 764 (1948).
[4] L. Brady and M. Deutsch, Phys. Rev. **74**, 1541 (1948).
[5] E. J. Konopinski, Rev. Mod. Phys. **15**, 209 (1943).
[6] In addition to the work reported here on the beta-gamma-problem, M. L. Wiedenbeck and K. Y. Chu inform me (August 10, 1949) that they have found no anisotropic correlation to 4 percent in Na^{24}, K^{42}, Co^{60}, Au^{198}, Cs^{134}, and I^{131}.
[7] Also Na^{24} and Co^{60} at 90° and 180° by Grace, Allen, and Halban, Nature **164** (Sept. 24, 1949).

Hyperfine Structure and Nuclear Moment of Pb^{207}

A. L. SCHAWLOW,* J. N. P. HUME,** AND M. F. CRAWFORD
McLennan Laboratory, University of Toronto, Toronto, Canada
October 26, 1949

THE recent radiofrequency induction measurement[1] of the nuclear magnetic moment of Pb^{207} makes possible an additional confirmation of the effect of finite nuclear radius on the electron-nuclear magnetic interaction constant.[2,3] The theory is tested by comparing the nuclear moment calculated from the spectroscopically determined interaction constant of a single s electron with the directly measured moment. For the one-electron spectrum Pb IV there are no measurements of hyperfine structure splittings of s levels. However a_{6s}, the interaction constant for the $6s$ electron of Pb IV, has been deduced from the levels of Pb III using the measurements of Crooker[4] and Crawford, making allowance for interconfiguration perturbations.[5] It is found that all the hyperfine structure splittings of the $6s6d$, $6s7d$, $6s8s$, $5d^96s6p$, $6s7p$, $6s5f$ configurations are fitted by $a_{6s}=2.60$ cm^{-1}. It is believed that this interval factor is accurate within ±0.05 cm^{-1}.

The Goudsmit-Fermi-Segrè formula is

$$g(I)=\frac{a_{6s}\cdot 3n^{*3}\cdot 1837}{8R\alpha^2Z_iZ_0^2\kappa(\frac{1}{2},Z_i)(1-d\sigma/dn)}$$

where the symbols have the usual meanings.[6,7] For $5d^{10}6s$ of Pb IV, $n^*=2.268$ and the Fermi-Segrè correction factor $(1-d\sigma/dn)$ from a Rydberg-Ritz formula[3] is 1.16, and $\kappa=2.38$. Then $g(I)=0.99(4)$ and since $I=\frac{1}{2}$, μ for $Pb^{207}=0.49(7)$ nuclear magnetons.

The value obtained by the nuclear induction measurement,[1] $\mu=0.588\pm0.001$ nuclear magnetons, is 18 percent higher than the spectroscopic value. It has been shown for thallium[3] that the correction due to the finite volume occupied by the nuclear electric charge, with approximately uniform charge density, increases the spectroscopic value by about 15 percent. The same, or a slightly larger, correction is to be expected for lead. A further correction in the same direction of about 3 percent probably should be added because the magnetic moment is distributed through the nuclear volume. Thus for lead as well as thallium, lanthanum and caesium the correction for the finite volume of the nucleus brings the spectroscopic values of the magnetic moment into agreement with the induction measurement.

* Now at Columbia University, New York, New York.
** Now at Rutgers University, New Brunswick, New Jersey.
[1] W. G. Proctor, Phys. Rev. **76**, 684 (1949).
[2] J. E. Rosenthal and G. Breit, Phys. Rev. **41**, 459 (1932).
[3] M. F. Crawford and A. L. Schawlow, Phys. Rev. **76**, 1310 (1949).
[4] A. M. Crooker, Can. J. Research **A14**, 115 (1936).
[5] J. N. P. Hume, Ph.D. Thesis, Toronto (1949).
[6] S. Goudsmit, Phys. Rev. **43**, 636 (1933).
[7] E. Fermi and E. Segrè, Zeits. f. Physik **82**, 729 (1933).

Energy Levels of a Vector Meson in a Smeared Coulomb Field

ALBERT SIMON
University of Rochester, Rochester, New York
November 7, 1949

CORBEN and Schwinger[1] have derived the radial equations for a vector meson in a central field. They show that the states of a vector meson having a definite j (total angular momentum) and a definite parity fall into two groups. One is a group for which $l=j$ (l is the orbital angular momentum). These states give the ordinary scalar meson levels. The second group of states contains linear combinations of states for which $l=j-1$ and $l=j+1$. Corben and Schwinger have shown that solutions for the latter group of states, in a pure Coulomb field, exist only for the special case $j=0$.

Since, in reality, the Coulomb field is smeared out by the finite size of the nucleus, the states corresponding to $j\neq 0$ will also exist. The interesting point is that the position of the energy levels for a smeared Coulomb field will not depend on the character of the smearing to the first order of perturbation theory. Thus, if one takes the equations of Corben and Schwinger and eliminates their quantity $\bar{G}$ (related to the 4th component of the 4-vector-Eq. (35)) by use of the subsidiary condition, then the first two equations (Eq. (41)) may be put in the form of simultaneous eigenvalue equations for F_1 and F_2. Linear combinations of these give the coupled equations for F^1 and F^2 (Eq. (36)). These equations have the form of Klein-Gordon operators on the left, and small perturbing terms on the right. These equations may now be solved by a perturbation method expanding in powers of $(Z\alpha)$.[2] The zero order terms are chosen to be the non-relativistic Schroedinger equations. The first order correction then enables one to compute the corrections to the scalar meson levels. No cut-off for the Coulomb field is necessary in this order. This would not be the case in higher orders.

The corrections to the scalar meson level for $n=1$, $j=1$, "l"$=0$ (ground state) was found to be $+2/3(Z\alpha)^4\mu c^2$ (μ is the mass of the meson). The state $n=2$, $j=1$, "l"$=0$ was found to be shifted by the amount $+1/12(Z\alpha)^4\mu c^2$, which makes this state and the state $n=2$, $j=2$, "l"$=1$ (which is unshifted) coincide at the scalar level $2p$. For $n=3$, the $j=1$, "l"$=0$ level again coincides with the "l"$=1$ level after correction. The $j=2$, "l"$=1$, the $j=3$ "l"$=2$, and the $j=1$ "l"$=2$ levels are unchanged from the corresponding scalar levels.

If this same treatment is applied to the radial equations for a meson of arbitrary magnetic moment $(1+\gamma)$, it is found that a cut-off would be necessary in the first order for states of "l"$=0$.

It is interesting to note that if the π-meson were a vector meson, the shift of its lowest energy level (compared to the scalar level) would be of the same order of magnitude as its broadening due to the effect of nuclear absorption,[2] except for the case of hydrogen where it may be larger by an order of magnitude.[3]

I am greatly indebted to Dr. R. E. Marshak and Dr. A. S. Wightman for many valuable discussions.

[1] H. C. Corben and J. Schwinger, Phys. Rev. **58**, 953 (1940).
[2] J. A. Wheeler, Phys. Rev. **71**, 320 (1947).
[3] R. E. Marshak and A. S. Wightman, Phys. Rev. **76**, 114 (1949).

A Precise Method of Determining the Faraday by Magnetic Resonance

J. A. HIPPLE, H. SOMMER, AND H. A. THOMAS
National Bureau of Standards, Washington, D. C.
November 4, 1949

A METHOD of determining the Faraday has been developed in which the cyclotron resonance frequency of protons in a known magnetic field is measured. The ions are formed by electron impact as in the usual mass spectrometer. They are prevented from escaping axially by means of a d.c. electric field in the same way that electrons are trapped in the Phillips ion gauge. A uniform r-f electric field of variable frequency at right angles to the magnetic field accelerates ions of a selected charge-to-mass ratio at resonance until they attain a radius of 1.0 cm at which point they strike the collector and the current is measured with an electrometer tube amplifier. An ion having a different charge-to-mass ratio cannot attain a radius of this magnitude unless the frequency is tuned for ions of this type. The width of the resonance peak depends on the number of cycles in the time required for the ions to reach the collector. This width may be decreased by decreasing the amplitude of the r-f voltage supplying the field and therefore the limiting resolution depends on the length of time it is possible to trap the ion and still detect resonance. The peak width is also limited by the uniformity of the magnetic field as in nuclear resonance.

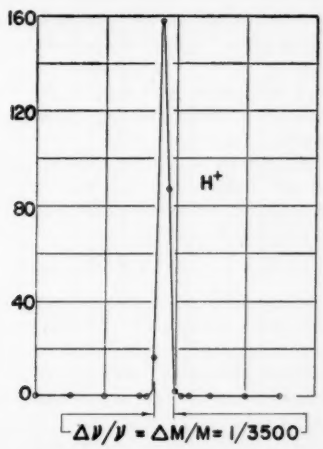

FIG. 1. Peak shape for protons as the frequency is varied and the magnetic field held constant at approximately 4700 gauss.

Figure 1 shows the peak shape for protons as the frequency is varied and the magnetic field held constant at approximately 4700 gauss (resonance frequency about 7 Mc). Higher resolution than this is attainable, but this was a convenient width for the initial experiments with the frequency control readily available. It was found that the instrument was so sensitive that the residual gas pressure could be used so no hydrogen was admitted to the tube. An ion gauge on the pumping arm near the tube indicated a pressure of 3×10^{-7} mm Hg. An electron current of 10 μa was used and the peak shown in Fig. 1 corresponds to an ion current of approximately 10^{-13} amp.

The magnet is the same one used in the measurement of the gyromagnetic ratio of the proton[1] and the resonance frequency was measured in relation to the nuclear resonance frequency of the proton. For this purpose the two resonance probes (cyclotron and nuclear) could be quickly interchanged while a third nuclear resonance probe held the field constant. We wish to emphasize the fact that the value reported in this note is a preliminary one until a more exhaustive study is made for possible systematic errors. This preliminary result is

$$\nu_c/\nu_n=0.358106\pm0.000010,$$

where ν_c=cyclotron frequency of the proton, and ν_n=nuclear resonance frequency of the proton. The Faraday is obtained from the relation

$$F=\gamma M_p[\nu_c/\nu_n],$$

where γ=gyromagnetic ratio for proton$=(2.67524\pm0.00020)\times10^4$ (no diamagnetic correction) sec.$^{-1}$ gauss^{-1},[2] and M_p=isotopic weight of $H^+=1.007580\pm0.000003$.[3,4]

The Faraday is then

$$F=9652.8\pm0.8 \text{ e.m.u./g (physical scale).}$$

This is to be compared[5] with the value 9650.5 from the silver voltameter and 9652.2 from the iodine voltameter. (This is discussed in reference 4.)

The accuracy will be limited principally by the uncertainty in the gyromagnetic ratio. Work is in progress here which should considerably decrease the uncertainty in the gyromagnetic ratio. The agreement of our result with that of the voltameter gives added support to the value of e/m for the electron[6,7] resulting from our value of γ.

If our value of the ratio ν_c/ν_n is combined with the measurement of Gardner and Purcell,[7] one obtains a value of the ratio of the mass of the proton to the mass of the electron of greatly improved accuracy. This new result is

$$M_p/m_e = 1835.979 \pm 0.056.$$

Several possible applications of this instrument suggest themselves. In the first place, it looks very promising for the measurement of packing fractions. Its simplicity, high sensitivity, and variable resolution should make it useful in many other research and analytical applications. Since this device measures ω, it is suggested that it be called the omegatron.

[1] Thomas, Driscoll, and Hipple, Phys. Rev. **75**, 902 (1949).
[2] Thomas, Driscoll, and Hipple, Phys. Rev. (to be published).
[3] K. T. Bainbridge, "Isotopic weights of the fundamental isotopes," Preliminary Report No. 1, National Research Council (June, 1948).
[4] J. W. M. DuMond and E. R. Cohen, Rev. Mod. Phys. **20**, 82 (1948).
[5] S. J. Bates and G. W. Vinal, J. Acous. Soc. Am. **36**, 916 (1914); G. W. Vinal and S. J. Bates, Bull. Bur. Stand. **10**, 425 (1914); G. W. Vinal, Comptes Rendus **3**, 95 (1932).
[6] Thomas, Driscoll, and Hipple, Phys. Rev. **75**, 992 (1949).
[7] J. H. Gardner and E. M. Purcell, Phys. Rev. **76**, 1262 (1949).
[8] F. G. Dunnington, Phys. Rev. **52**, 475 (1937).

Theory of the Electric Resistivity of Polycrystalline Graphite*

DWAIN BOWEN
North American Aviation, Inc., Los Angeles, California
October 24, 1949

IT is possible to explain the observed temperature dependence of electric resistivity in commercial polycrystalline graphite by an extension of the theory of single crystal graphite as developed by Wallace.[1] There are two mechanisms required. First, one assumes that the conduction in the polycrystalline sample takes place in the planes of cleavage of the individual crystals. The large anisotropy (of the order of 10^4) prevents any appreciable conduction across the planes. This confinement of the current to the direction of orientation of the crystals, which will not necessarily be in the direction of gross current flow, increases the resistivity of the polycrystalline material over that of a single crystal in the plane of cleavage by a geometrical factor, s, depending on the ratio of the principal dimensions of the crystals, and their orientation with respect to gross current flow. For completely random orientation and a common ratio of crystal dimensions of 10, this factor is about 7. Second, it is assumed that the electron waves are scattered off the crystallite boundaries. Since these boundaries are regions of disorder, there is almost a certainty of scattering at these regions. Thus the probability of scattering per unit time can be estimated from the size of the crystallites, and the velocity of the waves in the crystal. Using estimates of crystallite size based on the width of x-ray diffraction lines, one computes the scattering probability per second to be 10^{14}. Furthermore, this probability should be temperature independent since the percentage change in crystallite dimension with temperature will be small. Adding this scattering probability to the thermal lattice scattering probability in Wallace's formula and multiplying by the geometrical factor s, one has

$$\rho = \frac{h^3 cs}{16\pi e^2 kT 1n^2}\left(\frac{1}{\tau_T}+\frac{1}{\tau_b}\right),$$

where the τ's are the inverse scattering probabilities.

By computing τ_T from the original Wallace equation, and measurements on single crystals, a typical plot showing the variation of resistivity with temperature for polycrystalline graphite has been reproduced in Fig. 1.

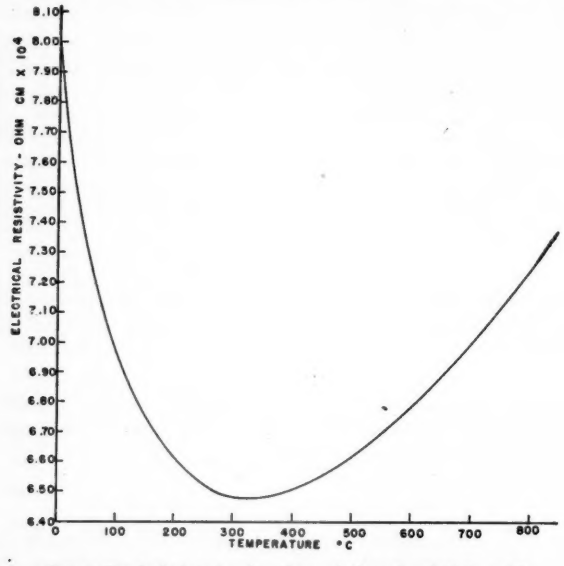

FIG. 1. Typical plot showing the variation of resistivity with temperature for polycrystalline graphite.

* This document is based on work performed under Contract No. AT-11-1-GEN-8 for the AEC at North American Aviation, Inc.
[1] P. R. Wallace, Phys. Rev. **71**, 622 (1947).

A Note on the Variational Method for the Scattering Problem

SU-SHU HUANG
Yerkes Observatory, University of Chicago, Williams Bay, Wisconsin
October 20, 1949

AS we have already pointed out,[1] Hulthén's formulation of the variational principle[2] has the advantage over other formulations[3] in that a more flexible trial wave function can be used. But in his practical applications he adopts a method which leads to a very inconvenient numerical procedure. Moreover, the manner of his application does not utilize the variational principle in its strict form: one of the equations he uses is not logically connected with the principle. In this note we shall indicate how we can improve Hulthén's method by making it more rigorous and at the same time much simpler for practical purposes. We shall illustrate the proposed method by considering S-scattering by a potential field of the Yukawa type.

Considering for the sake of simplicity only S-scattering, we define, following Hulthén

$$\mathfrak{L} = \int_0^\infty \psi(H-k^2)\psi dr, \tag{1}$$

where

$$H = -d^2/dr^2 + V(r). \tag{2}$$

It can then be shown that

$$\delta\mathfrak{L} = 2\int_0^\infty \delta\psi(H-k^2)\psi dr + k\delta\eta, \tag{3}$$

where η represents the phase shift. After obtaining this equation Hulthén suggested a variational method in which

$$\mathfrak{L} = 0 \tag{4}$$

is used to determine η while

$$\delta\mathfrak{L} = 0 \tag{5}$$

is used for obtaining a set of equations for the variational parameters. In this manner with a trial function of the form

$$\psi(r) = f(r)\cos\eta \sin kr + g(r)\sin\eta\cos kr, \tag{6}$$

Hulthén obtains a system of equations each of which is of the second degree in $\tan\eta$ and solves them by a method of successive approximations.

Now Eq. (4) is not essential in the formulation of variational principle for the *free state*, because it can be satisfied even if ψ is not an exact solution of the wave equation. Moreover in deriving Eq. (3) the condition $\mathfrak{L}=0$ is nowhere used. In fact, instead of using Eq. (4), we might with equal justification have used any integral involving $(H-k^2)\psi$ as the equation for $\tan\eta$. The use of $\mathfrak{L}=0$ would therefore seem to be arbitrary and not inherent for the variational principle derived from Eq. (3). The fact that Hulthén finds by his method two solutions for $\tan\eta$ is a consequence of this ambiguity resulting from the use of the condition $\mathfrak{L}=0$; he actually rejects one of the two solutions as not "good" though there is no way of deciding as to which of the two solutions is "good," except by comparison with results obtained by other methods. A rigorous method for computing the wave function for the continuous spectrum should, therefore, be based solely on Eq. (3) or its equivalent:

$$\delta\mathfrak{L}=k\delta\eta. \tag{7}$$

We now assume a trial wave function of the form

$$\psi(r)=f(r)\sin kr+g(r)\cos kr, \tag{8}$$

subject to the boundary conditions

$$\left.\begin{aligned} &f(0)=\text{finite}, \quad \lim_{r\to\infty} f(r)=1;\\ &g(0)=0, \quad \lim_{r\to\infty} g(r)=\lambda=\tan\eta. \end{aligned}\right\} \tag{9}$$

For ψ given by (8)–(9), the variational integral becomes

$$\mathfrak{L}\equiv\int_0^\infty [f_1^2\sin^2kr+g_1^2\cos^2kr+k(fg_1-gf_1) +V(f^2\sin^2kr+g^2\cos^2kr)+(g_1f_1+Vgf)\sin 2kr]dr, \tag{10}$$

where f_1 and g_1 denote the derivatives of f and g.

Equation (7) then becomes

$$\delta\mathfrak{L}=k\delta\lambda \tag{11}$$

when $\mathfrak{L}$ is computed with the wave function (9). Now we determine λ and all the parameters by the equations

$$\partial\mathfrak{L}/\partial c_i=0, \quad i=1, 2, \cdots, n \tag{12}$$

and

$$\partial\mathfrak{L}/\partial\lambda=k. \tag{13}$$

Equations (12) express the stationary property of the phase shift, while Eq. (13) follows from Eq. (11) directly. Now if we assume for $f(r)$ and $g(r)$ the forms

$$\begin{aligned} f(r)&=1+\sum_{n=1} P_n(r)e^{-nr},\\ g(r)&=(1-e^{-r})[\lambda+\sum_{n=1} Q_n(r)e^{-nr}], \end{aligned} \tag{14}$$

where $P_n(r)$ and $Q_n(r)$ may, for example, be polynomials in r, involving a set of coefficients $c_1, c_2, \cdots, c_n$ which we subject to the variation, Eqs. (12)–(14) will then give a set of $(n+1)$ linear equations for $\lambda, c_1, \cdots, c_n$. The coefficients of this set of equations form a symmetrical determinant, which can be readily solved.

The method derived in the foregoing paragraph differs from Hulthén's in that by using Eq. (13) instead of Eq. (4) we have made the method more rigorous by conforming to the variational principle, Eq. (11); also by introducing the λ-formulation (as we may call it) we have essentially facilitated the actual calculations.

As an illustration of the foregoing method we shall consider the scattering by the potential

$$V(r)=le^{-r}/r, \tag{15}$$

where l is a constant. In conformity with Eqs. (14) we write

$$\begin{aligned} f(r)&=1+(c_1+c_2r)e^{-r},\\ g(r)&=(1-e^{-r})[\lambda+(c_3+c_4r)e^{-r}]. \end{aligned} \tag{16}$$

After some elementary calculations, a set of linear equations in $\lambda, c_1, \cdots, c_4$ are finally obtained. The coefficients in these equations can best be expressed in terms of certain standard functions of k.[4]

In order to compare our results with Hulthén's, we have computed the phase shift for two values of l and k, namely $l=-1.5$, $k=0.8$ and $l=-2.1$, $k=0.8$ respectively. The results are tabulated below together with Hulthén's best values of the phase shift. In Table I in addition to the results for the 4-parameter (c_1, c_2, c_3, c_4) trial wave functions (Eqs. (16)) we have also included the results derived for 3-parameter (c_1, c_3, c_4) and (c_1, c_2, c_3) and 2-parameter (c_1, c_2) trial functions.

TABLE I. The phase shifts and the constants for the expansion of the wave function at $k=0.8$.

$-l$	Approx.	λ	c_1	c_2	c_3	c_4	η
1.5	(c_1, c_2, c_3, c_4)	1.11469	0.02278	0.01492	0.92077	−0.06414	0.83958
	(c_1, c_3, c_4)	1.11524	0.05205	.....	0.89689	−0.06512	0.83982
	(c_1, c_2, c_3)	1.11188	0.59566	−0.28842	0.44184	.....	0.83832
	(c_1, c_2)	1.10430	0.03493	.....	0.90190	.....	0.83492
	Hulthén						0.83708
2.1	(c_1, c_2, c_3, c_4)	3.31023	0.61034	0.02359	3.48932	−0.49419	1.27742
	(c_1, c_3, c_4)	3.31111	0.65660	.....	3.45157	−0.49574	1.27749
	(c_1, c_2, c_3)	3.28028	4.86017	−2.22788	−0.08688	.....	1.27489
	(c_1, c_2)	3.22313	0.52837	.....	3.47190	.....	1.26996
	Hulthén						1.27515

The present method can be extended to electron scattering by the hydrogen atom, and to allow also for exchange effects. The calculations relating to these extensions are now in progress.

Finally, I should like to express my sincere thanks to Professor S. Chandrasekhar for his interest in this problem and also for his valuable discussions.

[1] S. S. Huang, Phys. Rev. **76**, 866 (1949).
[2] L. Hulthén, K. Fysiogr. Sällsk. Lund Förhandl. **14**, No. 21 (1944); N. F. Mott and H. S. W. Massey, *The Theory of Atomic Collisions* (Oxford University Press, London, 1949), 2nd ed., pp. 128–9. W. Kohn, Phys. Rev. **74**, 1763 (1948).
[3] L. Hulthén, Arkiv. f. Mat. Ast. o. Fys. **35A**, No. 25 (1948); I. E. Tamm, J. Exper. Theor. Phys. U.S.S.R. **18**, 337 (1948).
[4] S. S. Huang, Phys. Rev. **75**, 980 (1949); **76**, 477 (1949).

Photo-Disintegration of the Deuteron at Intermediate Energies

J. F. MARSHALL* AND E. GUTH
Physics Department, University of Notre Dame, Notre Dame, Indiana
October 24, 1949

IN the photo-disintegration process, all but a small fraction of the γ-ray energy appears as relative energy of neutron and proton, while in N-P scattering half of the incident neutron energy appears as kinetic energy of the center of mass of the N-P system. Consequently, for energies well above the threshold, photo-disintegration experiments should yield as much information about the N-P interaction as N-P scattering experiments performed at twice the energy. Therefore, energies up to 20 Mev, which are of particular interest because of the large number of electrostatic generators and betatrons operating in this range, are of considerable theoretical importance. (A copy of a letter by Fuller[1] describing preliminary photo-disintegration experiments in this energy region arrived when this report was in preparation.)

In this energy range computations are relatively simple. Only a small number of multipoles are involved (electric dipole, magnetic dipole, and electric quadrupole). For well radii below 2.8×10^{-13} cm, range-corrected Bethe-Peierls formulas are essentially correct, and the total electric cross section is given by:

$$\sigma_e=\frac{8\pi}{3}\frac{e^2}{\hbar c}\frac{\hbar^2}{M}\frac{W_1^{\frac{1}{2}}(\hbar\omega-W_1)^{\frac{1}{2}}}{(\hbar\omega)^3}\frac{\sin^2(k_t r_t)\exp(2\alpha r_t)}{(1+\alpha r_t)}, \tag{1}$$

where W_1 is the binding energy of the deuteron. (The photomagnetic contribution can be neglected except for very low energies.) For a 50-50 mixture for which the outgoing nucleons may be treated as free, expression (1) is only slightly modified by the inclusion of tensor forces. The total cross section including tensor forces is given by (we use the approximation[2] in which contributions from inside the well are neglected. This approximation gives the right order of magnitude for our case, the

results being in agreement with the exact computations of Rarita and Schwinger[3]):

$$\frac{\sigma_{e,\text{ tensor}}}{\sigma_e}=\frac{1}{1+bq^2}\left\{1+\frac{5}{18}q^2\left(1+\frac{3}{5}\frac{\hbar\omega-W_1}{W_1}\right)^2\right\}, \quad (2)$$

where q is the ratio of the D component of the ground state wave function to the S component at $r=r_t$, and b is given by:

$$b=\frac{1}{9}+\frac{2}{3}\frac{(1+\alpha r_t)^2}{(\alpha r_t)^3}. \quad (3)$$

In the energy region considered, the total cross section is decreased slightly by the inclusion of tensor forces. For $r_t=2.8\times10^{-13}$ cm, the correction is less than two percent, and for $r_t=1.8\times10^{-13}$ cm, the correction is less than five percent.

The angular distribution for unpolarized γ-rays, in the center-of-mass system is given by:†

$$f(\theta)=a+\sin^2\theta(1+2\beta\cos\theta), \quad \beta=\frac{v}{c}=\left\{\frac{\hbar\omega-W_1}{Mc^2}\right\}^{\frac{1}{2}}. \quad (4)$$

The term $2\beta\cos\theta$, which is a correction of the first order in β, arises from interference between electric dipole and electric quadrupole terms and leads to a distinct asymmetry.‡ In the laboratory system the finite momentum of the incident photon will introduce a further asymmetry. The distribution corresponding to (4) can be obtained by replacing $\sin^2\theta$ by:

$$\sin^2\theta\left[1+2\beta\left(1+\frac{W_1}{\hbar\omega-W_1}\right)\cos\theta\right]. \quad (5)$$

The photoelectric part of the angular distribution (4) in the laboratory system is identical with that obtained by Sommerfeld for atomic hydrogen, because of the kinematic nature of the retardation effect which is independent of the particular atomic or nuclear system involved. It is of interest to point out that this asymmetry sets in at energies as low as 10 Mev, while qualitatively one would expect the quadrupole term to play a role around 70 Mev where $\lambda\!\!\!^{-}=r_t$.

The data obtained by Fuller[1] indicate that the total cross section decreases less rapidly with energy than that given by Eq. (1), but by fitting at 13 Mev rather than at 7 Mev as he has done, Eq. (1) is found to yield agreement within the experimental error. However, the large statistical errors in these data do not permit any definite conclusions in this respect. (The approximate expression (2) and the exact calculations of Hu and Massey[4] indicate that at energies greater than 20 Mev the cross section should fall off less rapidly than indicated by (1), because of the influence of tensor forces. In the energy range of Fuller's experiments, however, this effect should not be important.) In Fig. 1 the angular distribution (4) ($f(\theta)$), (computed for $\hbar\omega=17$ Mev) in the laboratory system, is compared with Fuller's data ($F(\theta)$) for the energy range 14.0 to 20.3 Mev. It is seen that the agreement is quite good but the experimental error is too large to justify any definite conclusions.

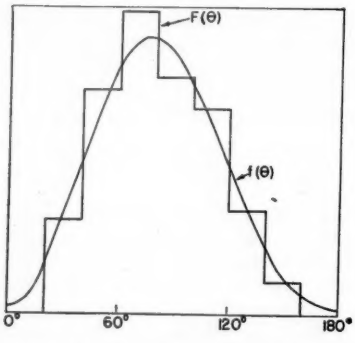

FIG. 1. Comparison of the angular distribution $f(\theta)$ with Fuller's data $F(\theta)$ in the energy range 14.0 to 20.3 Mev.

Further experiments in this energy region would certainly have considerable significance, since they would yield information on the following aspects of the N-P interaction.

(a) Percentage mixture. Rarita and Schwinger and Hu and Massey have shown that the magnitude of the isotropic term in Eq. (2) is very sensitive to the choice of mixture. (For zero percent charge exchange $a=0.4$ at 17.5 Mev, while for mixtures near 50-50, $a=0.02$ including magnetic dipole contributions.) Furthermore the asymmetry in the angular distribution will be greater for pure ordinary forces than that given by (4).

(b) Range of the N-P interaction. Since the magnitude of the total cross section (for intermediate energies) depends only on the triplet well radius and on the deuteron binding energy, measurements of total cross sections should give a good indication of the range of the N-P interaction.

A more complete treatment including the influence of the shape of the interaction potential and a more detailed analysis of the effect of tensor forces is in preparation.

* AEC Predoctoral Fellow.

† This expression is rigorously correct for zero-range N-P interaction, but for energies up to 20 Mev it is an excellent approximation for both square-well and Hulthen potentials.

‡ There is some confusion about this asymmetry in the literature. A. Pais [Kgl. Danske Vid. Sels. Math.-fys. Medd. Bind 20, No. 17 (1943)] and J. M. Jauch [Phys. Rev. **69**, 276 (1946)] conclude that there can be no interference between terms corresponding to final states of different parity because such states correspond to different isotopic spin functions. However, L. Rosenfeld [*Nuclear Forces* (Interscience Publishers, Inc., New York, 1949), Vol. I, p. 47] and others have shown that the inclusion of isotopic spin and the assumption that proton and neutron are simply different states of the same nucleon leads to the same results in any physical processes as the assumption that proton and neutron are distinct particles. We wish to thank Dr. L. L. Foldy for an illuminating discussion of this isotopic spin formalism.

[1] E. G. Fuller, Phys. Rev. **76**, 576 (1949).
[2] W. Hepner and R. Peierls, Proc. Roy. Soc. **A181**, 43 (1942).
[3] W. Rarita and J. Schwinger, Phys. Rev. **59**, 436, 556 (1941).
[4] Tsi-Ming Hu and H. S. W. Massey, Proc. Roy. Soc. **A196**, 135 (1949).

High Energy Photo-Disintegration of the Deuteron

J. F. MARSHALL* AND E. GUTH
Department of Physics, University of Notre Dame, Notre Dame, Indiana
October 24, 1949

COMPUTATIONS of total cross sections and angular distributions for the photo-disintegration process have been carried out for square-well radii of 1.8 and 2.8×10^{-13} cm in the energy range 20–100 Mev, and for zero radius in the range 20–300 Mev on the following assumptions.

(a) The electromagnetic interaction is represented by $\mathbf{E}\cdot\mathbf{r}$ (rather than $\mathbf{A}\cdot\mathbf{v}$) and $\boldsymbol{\mu}\cdot\mathbf{H}$ for electric and magnetic dipole

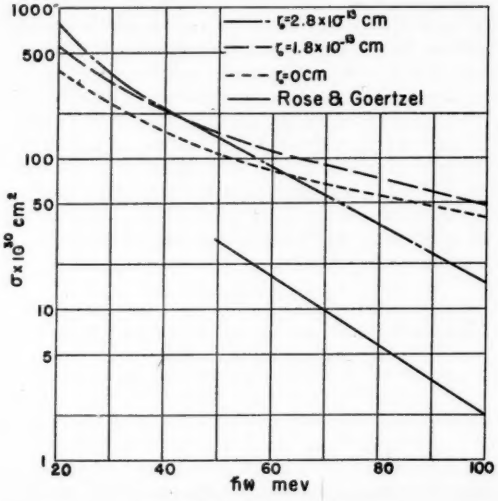

FIG. 1. Total cross section.

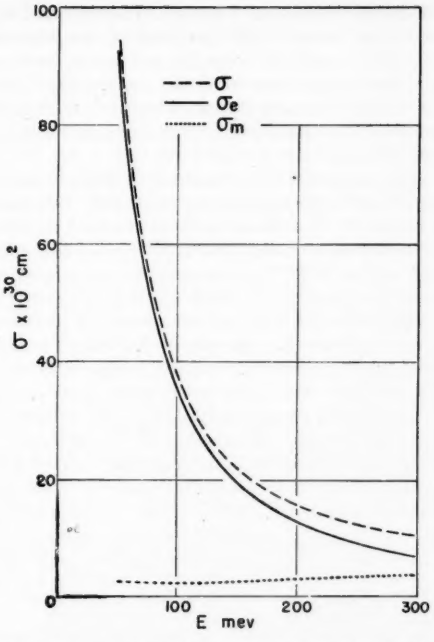

FIG. 2. Zero-range cross sections including all multipoles.

transitions, respectively, and by equivalent expressions for higher poles.†

(b) The wells for the triplet and singlet states are assumed to have the same radius ($r_0=r_t=r_s$). This assumption is probably a fair approximation for energies up to 100 Mev.

(c) A 50-50 mixture of ordinary and Majorana forces is assumed for both triplet and singlet states and the outgoing nucleon is consequently free, by hypothesis, for transitions to states of odd parity.‡ For final states of even parity the effect of binding is included. The results of these computations are as follows:

I. Total cross section.—Total cross sections for the three radii are shown in Fig. 1 in the energy range 20–100 Mev. (The total cross sections obtained by Rose and Goertzel are also shown in the energy range 50–100 Mev.) It is found that only a few multipoles (electric and magnetic dipole and quadrupole) need be considered, and even at 100 Mev the electric dipole contribution accounts for more than 90 percent of the total cross section for all radii considered. The values of the total cross section at this energy are $\sigma_{tot}=15.0$, 48.0, 40.0×10^{-30} cm² for $r_0=2.8$, 1.8, and zero, respectively. Interference between initial and final state wave functions is quite important, $\sigma(2.8)$ being smaller than $\sigma(0)$ because of *destructive* interference, while $\sigma(1.8)$ (1.8×10^{-13} cm is now considered the best value of r_t) is larger than $\sigma(0)$ because of constructive interference. Binding in the even states decreases the importance of magnetic dipole and electric quadrupole contributions considerably. For example, at 100 Mev electric quadrupole transitions ($^3S-^3D$) account for only two percent of the cross section for $r_0=2.8$ and for four percent for $r_0=1.8$. The value of $\sigma(2.8)$ at 100 Mev is eight times larger than that obtained by Rose and Goertzel for the same radius. Figure 2 shows the total cross section including all multipoles for $r_0=0$ and for energies from 50–300 Mev. Electric and magnetic contributions are shown separately, and it can be seen that while magnetic contributions are unimportant at 100 Mev they become increasingly significant at higher energies.

II. Angular distribution.—The angular distribution of the photo-protons ($f(\theta)$) at 100 Mev for $r_0=2.8\times10^{-13}$ cm (in the energy region considered, the angular distribution is not very sensitive to the choice of r_0) and a 50-50 mixture is shown in Fig. 3 along with Rose and Goertzel's result ($F(\theta)$) for a 100–0

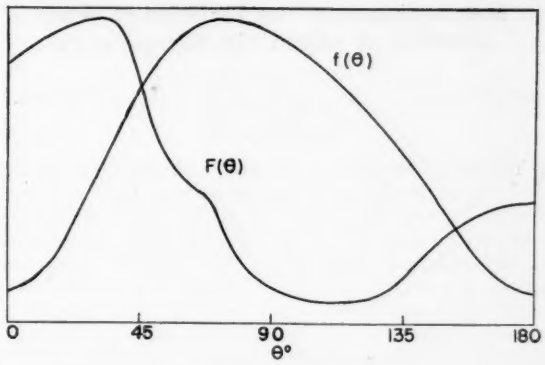

FIG. 3. Angular distribution.

mixture. As can be seen, there is a slight asymmetry in the forward direction because of interference between electric dipole and quadrupole terms. This asymmetry is not very great, however, because binding in the D state reduces the quadrupole cross section. The asymmetry would be very pronounced for a 100–0 mixture, as indicated by the Rose and Goertzel distribution which, however, is not exact because the effect of binding in final states is quite important.

The wide divergence between these results and those reported by Rose and Goertzel both in total cross section and in angular distribution (see Figs. 1 and 3) can be traced to the large difference between the $\mathbf{A}\cdot\mathbf{v}$ and $\mathbf{E}\cdot\mathbf{r}$ "types" of interaction which are equivalent for a 100–0 mixture but not for a 50-50 mixture.

The present results indicate that the following information about the N-P interaction might be obtained from experiments on the high energy photo-disintegration of the deuteron:

(a) Since the total cross section is sensitive to the choice of radius, the magnitude of the total cross section should provide some information about the range of the N-P interaction.

(b) Since the angular distribution is very sensitive to the mixture (see Fig. 3) and relatively insensitive to the choice of radius, information could be obtained about the ratio of ordinary to exchange forces.

Consequently, it would be quite interesting to check the theoretical trend indicated by Figs. 1–3 using the various betatrons and synchrotrons spanning the range from 10–300 Mev.¶

A detailed report of the photo-disintegration of the deuteron, including the energy range 2.2–10 Mev is in preparation. The effects of relativity corrections, tensor forces and the long-range tail of the N-P interaction will also be discussed.‖

* AEC Predoctoral Fellow.

† It has been found [A. F. Siegert, Phys. Rev. **52**, 787 (1937); R. G. Sachs, Phys. Rev. **74**, 433 (1948); C. Møller and I. Rosenfeld, Kgl. Danske, Vid. Sels. Math.-fys. Medd. Bind 20, No. 12 (1943)] that for low energies $\mathbf{E}\cdot\mathbf{r}$ is equivalent to $\mathbf{A}\cdot\mathbf{v}$ *plus* interaction with exchange currents. It has also been shown [L. Rosenfeld, *Nuclear Forces* (Interscience Publishers, Inc., New York, 1949), Vol. II, p. 449] that at low energies the electromagnetic interaction with the magnetic moments of the nucleons is correctly given by $\boldsymbol{\mu}\cdot\mathbf{H}$. The expressions $\mathbf{E}\cdot\mathbf{r}$ and $\boldsymbol{\mu}\cdot\mathbf{H}$ are consequently correct for electric and magnetic dipole and transitions which alone play a role at low energies. For higher energies, however, there is at present no unique expression for the electromagnetic interaction. Thus, for higher poles the interaction will depend upon the details of the meson field theory assumed, but at any rate, since one has to correct $\mathbf{A}\cdot\mathbf{v}$ for exchange currents, expressions of the $\mathbf{E}\cdot\mathbf{r}$ type are probably better approximations than $\mathbf{A}\cdot\mathbf{v}$.

‡ This problem has been treated by M. E. Rose and G. Goertzel [Phys. Rev. **72**, 749 (1947)] for ordinary N-P interaction and an electromagnetic interaction of the form $\mathbf{A}\cdot\mathbf{v}$ on the assumption that the outgoing nucleons can be treated as free for energies above 50 Mev. For ordinary forces, electromagnetic interactions of the form $\mathbf{E}\cdot\mathbf{r}$ and $\mathbf{A}\cdot\mathbf{v}$ are equivalent but for exchange forces they lead to radically different results. Rose and Goertzel's results are shown in Figs. 1 and 3, since they indicate the results to be expected for ordinary N-P interaction.

¶ The Compton effect on the proton will be of some importance at the higher energies. However, the Compton cross section has been found to be considerably smaller than the photo-cross section [J. L. Powell, Phys. Rev. **74**, 1258 (1948); L. L. Foldy and R. G. Sachs (private communication)]. Furthermore, if an energy-sensitive detector is used the Compton particles will be eliminated automatically.

‖ According to R. S. Christian and R. Serber the high energy N-P scattering results are best fitted by long-range potentials of the Yukawa and exponential type. These potentials can be simulated by two-step square well, used previously for low energy scattering by Bohm and Richman.

Measurements of the Variation of Work Function of Silicon with Temperature

B. J. ROTHLEIN AND P. H. MILLER, JR.
Randal Morgan Laboratory of Physics, University of Pennsylvania, Philadelphia, Pennsylvania
November 8, 1949

ATTEMPTS have been made to determine whether the change in electrochemical potential that is known to occur whenever a semi-conductor is heated from its extrinsic to its intrinsic temperature range causes a corresponding change in the work function. An apparatus capable of measuring a change in average work function with an accuracy of 0.05 volt is shown in Fig. 1. This apparatus measures the deflection of an electron beam after it has passed between a parallel plate condenser composed of the sample and a reference plate. The deflection of the beam is detected by observing the difference in the beam current to the two halves of the target plate. If the work function of the sample should change when the temperature is raised by Joule heating into its intrinsic range, the field between the two plates would change and this would cause a deflection of the electron beam. A battery in the external circuit which connects the two plates is used to return the beam to its original position and thereby make this method a null measurement.

The presence of surface states as described by Bardeen[1] would prevent any observable change in work function. Within the experimental limit of the apparatus no change in work function is detected as an outgassed N or P type silicon surface is cooled rapidly from its intrinsic range into its extrinsic range. In some of the experiments the pressure was sufficiently low so that the time for cooling was long in comparison with the time required for 10^{15} gas molecules to hit one cm^2 of the surface. The calculations of Markham and Miller[2] for materials having the observed room temperature donator or acceptor density as well as observations on the conductivity of the samples assures us of the fact that the intrinsic temperature range was approached.

Attempts have been made to determine whether the surface states assumed responsible for this phenomenon arise from the inherent nature of any real crystal, Tamm or Shockley levels, or from impurities on the surface. Because of the difficulty of removing the oxide layer from the surface of the silicon and the fact that the samples must themselves contain doping impurities, no definite conclusion could be drawn on this point.

When a previously outgassed silicon sample which has been allowed to remain at room temperature for several minutes is heated to approximately 800°C a decrease in work function of 2–3 volts occurs. About 30 seconds after the sample is allowed to cool the reverse increase in work function occurs. The sample cools from 800°C to 300°C in about 5 seconds. The time and magnitude of this change on cooling is independent of the vacuum within the range 1×10^{-3} to 2×10^{-7} mm Hg and is also independent of any surface treatment. Because of the magnitude of this change and the time delay it can be stated with certainty that this effect is not associated with the shift in electrochemical potential within the body of the sample.

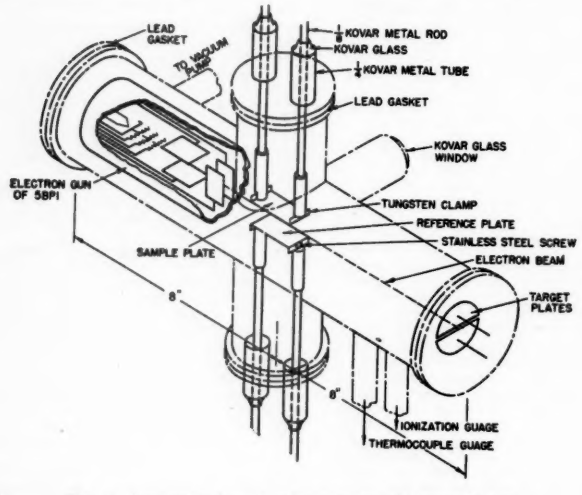

FIG. 1. Apparatus for the measurement of change in the average work function.

In an effort to study the properties of surface oxide several metals, including tungsten, have been studied. The results were similar in regard to time effects to these obtained for silicon. The observations on tungsten are typical. When the tungsten sample was heated above 1500°C a decrease in contact potential of approximately 1 volt was observed within a few seconds. If the sample is then maintained at this temperature a further decrease of approximately 3–4 volts was observed. When the sample was then allowed to cool the reverse 1 volt change occurred within 1 second. The reverse 3–4 volt change occurred in about 30 seconds. When the sample was heated to 1200°C it was possible to obtain the large change but not the small one. The one-volt change is attributed to the removal of the oxide layer. The 3–4-volt change is attributed to the motion of adsorbed gases or impurities.

We are indebted to the Bureau of Ships for financial support.

* A more extended account of this work will be found in the Ph.D. thesis of Mr. B. J. Rothlein which has been published as Technical Report No. 16 (September 27, 1949), BuShips Contract NObsr-42487. Copies may be obtained from P. H. Miller, Jr., Randal Morgan Laboratory of Physics, University of Pennsylvania.

[1] J. Bardeen, Phys. Rev. **71**, 717 (1947).

[2] J. J. Markham and P. H. Miller, Jr., Phys. Rev. **75**, 959 (1949).

The Influence of Piezo-Electrification on Tribo-Electrification*

JOHN W. PETERSON
Department of Physics, University of California, Berkeley, California
October 24, 1949

A POSSIBLE explanation of certain cases of tribo-electric charging is the transfer of charge to any surface making contact with a charged face of a strained piezo-electric crystal.[1,2] To investigate this possibility, studies have been made of the charge acquired by sized ground amorphous quartz particles in sliding over the face of an x-cut quartz crystal, compressed along the y-axis. Two crystals were used, so oriented that one presented a positive and the other a negative surface charge, together with a quartz funnel and receiving bucket system, which made it possible to direct the sliding quartz sand over a surface of either charge. The surface charge could be varied by changing the pressure on the crystals, and the atmosphere could be carefully controlled. By means of x-rays, the sand could be sufficiently discharged so that measurements could be taken at intervals of a few hours.

The sand was always negatively charged, regardless of the sign of the surface charge over which it had passed. On the average, with zero surface charge on the crystal, the sand acquired a negative charge of about 8×10^{-11} coulomb. There were 1.2×10^4 particles, averaging 400 microns in diameter, giving an average charge per particle of 4×10^4 electrons. Maximum stressing of either crystal produced a total surface charge of 2.5×10^{-10} coulomb, of which up to 1.5×10^{-11} coulomb was transferred to the sand. Since the sand made contact with only about half the surface area of a crystal, a maximum of about 12 percent of the available surface charge was transferred to the sand. The amount of charge transferred was the same for both signs of surface charge, under the same conditions.

The electric field perpendicular to the piezo-electric charged surface of the quartz crystal seems much too small for the observed transfer to be explained by the work of Gill and Alfrey,[3] who investigated the relation between charging and surface field strength.

The experiment was conducted in air dried by liquid nitrogen, since slight traces of moisture greatly decreased the charging.

Gases evolving from the brass walls of the container resulted in gradually decreasing charging, which could be returned to the original value by pumping for several hours at 1×10^{-5} mm of mercury. These results indicate that this type of tribo-electric charging strongly depends on the gas layers adhering to the surfaces involved. The amorphous quartz particles might be expected, because of the differences in structure, to acquire charge in friction with crystalline quartz. Actually, however, there was greater charging when the amorphous quartz particles struck the amorphous quartz receiving bucket, which further substantiates the belief that so-called "tribo-electric" series have little meaning.

Since the piezo-electric contribution to the charging of the sand amounted to less than 20 percent of its total charge, when the crystal was strained by a force of nearly 5×10^{6} dynes, it seems evident that the piezo-electric effect is not an important factor in tribo-electrification.

* This work was supported by ONR funds.
[1] L. B. Loeb, Science **102** (No. 2658), 573 (1945).
[2] Ernst Burkhardt, Zeits. f. Wirts. Zuckerindustrie **89**, 244–79 (1939).
[3] E. W. B. Gill and G. F. Alfrey, Nature **163**, 172 (1949).

The *K*-Shell Internal Conversion Coefficients*

M. E. Rose, G. H. Goertzel,† B. I. Spinrad‡
Oak Ridge National Laboratory, Oak Ridge, Tennessee
AND
J. Harr and P. Strong
The Computation Laboratory of Harvard University, Cambridge, Massachusetts
November 7, 1949

THE purpose of this letter is to report the fact that numerical calculation of the K-shell internal conversion coefficients has been carried out and to describe the results briefly. These calculations were carried out using relativistic (Dirac) wave functions for the Coulomb field, for the following parameters: $10\leq Z\leq96$ (comprising 23 values of Z); $0.3\leq k\leq5.0$ (for $Z\leq78$, 16 values of k) and $0.5\leq k\leq5.0$ (for $Z>78$, 14 values of k), where $k\,mc^2$ is the gamma-ray energy, and for both electric and magnetic multipoles of order 2^l with $1\leq l\leq5$. The domain of computation in the $Z-k$ plane is indicated in Fig. 1. A total of 680 values of the conversion coefficient have been obtained on the automatic sequence relay calculator (Mark I) at Harvard University (for 12 values of Z and 5 to 6 values of k) and 2560 additional values were obtained by interpolation. The values obtained on the Mark I are given to four significant figures and the interpolated values are given to three. While extensive tables have been prepared, space limitations prevent their inclusion here.[1] It is planned to present these results in a subsequent publication in which they would appear in the form of families of curves to be given for essentially all values of Z throughout the periodic table. In addition, internal conversion coefficients for all three sub-shells of the L-shell will then be presented for $10k$ values, 10 multipoles and all Z values. These results which include the effect of screening will be supplemented by low energy K-shell coefficients computed in the same manner, i.e., with screening.

In Fig. 1 the contour lines for the electric dipole and 2^5 pole (α_1 and α_5)[2] give an indication of the numerical results. Comparison with the approximate calculations of Hebb and Uhlenbeck[3] (non-relativistic, electric multipoles), of Drell[4] ("non-relativistic," magnetic multipoles) and of Dancoff and Morrison[5] (Born approximation) shows that these approximations give reliable results in a much more restricted range of Z and k than had been previously thought to be applicable. Their application, even in the range $Z<50$, can lead to an error of a factor 3 or more (especially in the case of higher order multipoles and magnetic conversion) and in many cases the error is such as to lead to an incorrect assignment of multipole order.[6]

Comparison was also made with the relativistic calculations of Hulme[7] (α_1; $Z=84$), Taylor and Mott[8] (α_2; $Z=84$), Fisk and Taylor[9] (β_1, β_2, β_3; $Z=84$) and Griffith and Stanley[10] (α_1; $Z=69$

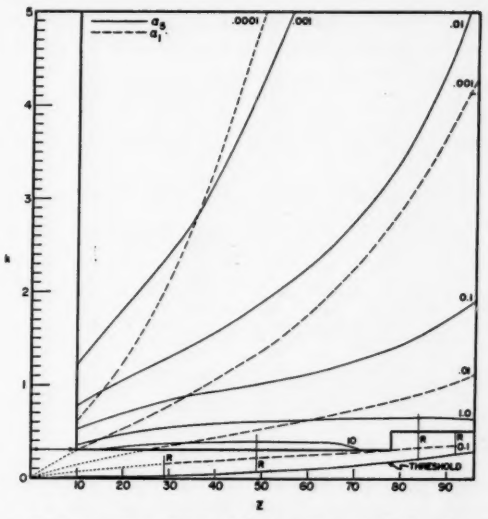

FIG. 1. The heavy lines ($Z\geq10$, $k\geq0.3$, 0.5) show the domain of calculation. Contour lines for electric dipole (α_1) and electric 2^5 pole (α_5) are also shown with values of the internal conversion coefficients affixed to the curves and α_1 has been extrapolated to low k. The lines marked R show where Reitz's calculations were made.

(5) 89). In all cases, except for α_2 where the results of Taylor and Mott differ slightly, there was agreement within the mutual precision of the calculations (of order 3 percent). The neglect of screening, which is the only significant effect omitted in these calculations, is *a posteriori* justified by comparison with the results of Reitz[11] who has computed the low energy K-shell coefficients, taking screening into account with a Thomas-Fermi-Dirac field, in the cases α_1, α_2, and β_1 for $Z=29$, 49, 84, and 92. In the region of k for which our calculations overlap those of Reitz the screened results exceed our unscreened values by at most 10 percent (where screening would be expected to be most serious) and in the large majority of cases by an amount which is less than 3 percent. The $Z-k$ values for which Reitz's calculations were made are shown in Fig. 1 by the vertical lines marked R. The dashed curves for $k<0.3$ are rough extrapolations for α_1 using Reitz's results and the approximation values for $Z<10$.

This work was performed under contract No. W-7405, eng. 26 for the AEC at the Oak Ridge National Laboratory.

* A preliminary report of the work was given at the 1949 Washington meeting of the American Physical Society, Phys. Rev. **76**, 184 (1949).
† Now at New York University, Washington Square College, New York, New York.
‡ Now at Argonne National Laboratory, Chicago, Illinois.
[1] Some copies of these tables have been circulated prior to publication. Requests should be addressed to the first-named author.
[2] The electric and magnetic conversion coefficients for the 2^l pole are denoted by α_l and β_l respectively.
[3] M. H. Hebb and G. E. Uhlenbeck, Physica **5**, 605 (1938).
[4] S. D. Drell, Phys. Rev. **75**, 132 (1949).
[5] S. M. Dancoff and P. Morrison, Phys. Rev. **55**, 122 (1939).
[6] See also P. Axel and S. M. Dancoff, Phys. Rev. **76**, 892 (1949).
[7] H. R. Hulme, Proc. Roy. Soc. **A138**, 643 (1932).
[8] H. M. Taylor and N. F. Mott, Proc. Roy. Soc. **A138**, 665 (1932).
[9] J. B. Fisk and H. M. Taylor, Proc. Roy. Soc. **A143**, 674 (1934); **A146**, 178 (1934).
[10] B. A. Griffith and J. P. Stanley, Phys. Rev. **75**, 534, 1110 (1949).
[11] J. R. Reitz, unpublished. We are indebted to Dr. Reitz for an opportunity to see his results before publication.

The Disintegration of In^{114}

J. Y. Mei, Allan C. G. Mitchell, and Daniel J. Zaffarano*
Department of Physics, Indiana University, Bloomington, Indiana
November 2, 1949

THE 50-day activity of In^{114} was investigated some years ago by Lawson and Cork[1] who found that the 50-day isomer decays to a 72-second isomeric state, under the emission of a highly internally converted gamma-ray of energy 0.192 Mev. The state of In^{114} of 72-sec. half-life then decays to the ground state of Sn^{114} with the emission of a beta-ray whose end point

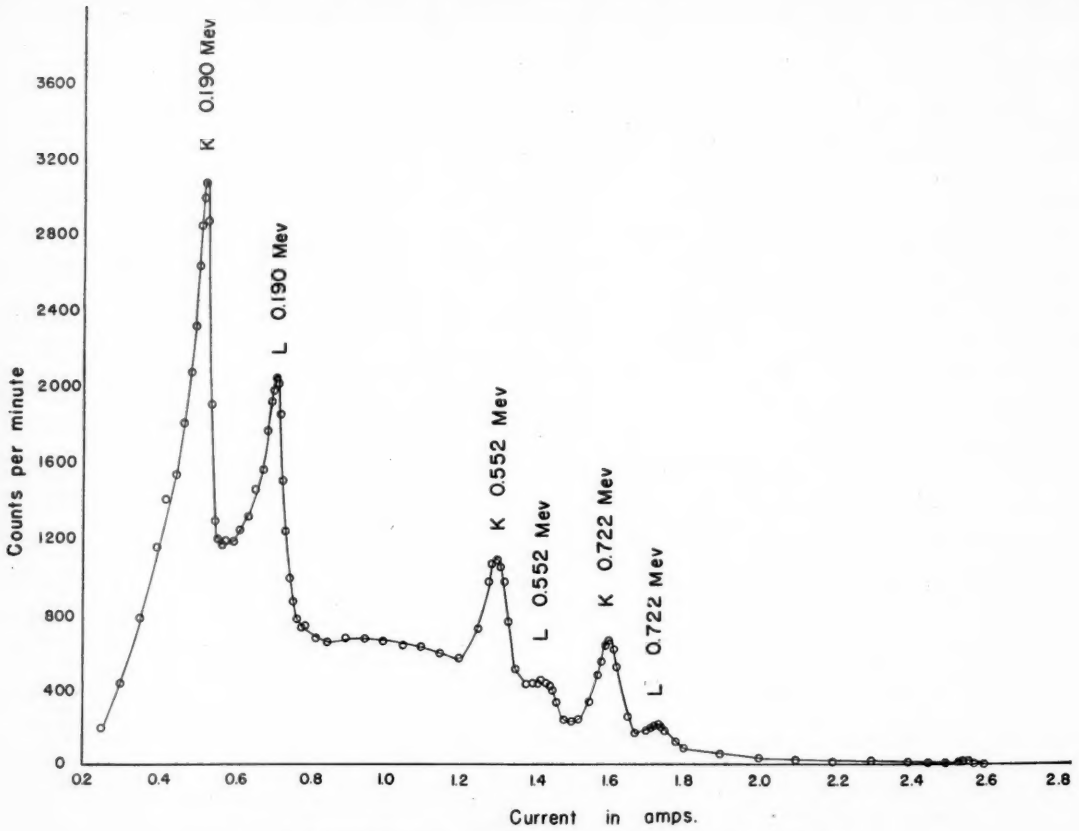

FIG. 1. Gamma-rays from indium 114. Photoelectrons from lead radiator.

energy is 1.98 Mev. Recently Cork, Shreffler, and Fowler[2] reported that In^{114} also emits a gamma-ray of energy approximately 0.8 Mev. This result was found by lead absorption. In view of the fact that the beta-ray spectrum of the 72-second In^{114} has been usually considered to be simple and allowed, it was decided to investigate the gamma-rays both by coincidence counting and spectroscopic techniques. The results of the coincidence studies have been published by Maienschein and Meem.[3] While the spectroscopic work was in progress, experiments of a similar nature were reported by Boehm and Preiswerk[4] with results substantially in agreement with ours. We have, however, found an additional gamma-ray not reported by them.

Metallic indium was irradiated by neutrons in the Oak Ridge Pile. Both unpurified and chemically purified sources were measured in a magnetic lens spectrograph. It was established by chemical experiments that all the gamma-rays belong to indium.

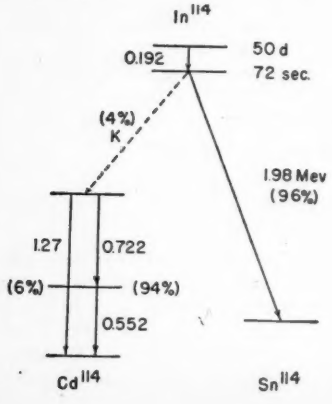

FIG. 2. Disintegration scheme of indium 114.

The energies of the several gamma-rays were determined from the energies of photoelectrons ejected from a lead or uranium radiator. Figure 1 shows the distribution of the photoelectrons from a lead radiator. K and L lines from gamma-rays at 0.190 $\pm$0.004; 0.552$\pm$0.005; and 0.722$\pm$0.005 Mev are shown on the figure. In addition, a very weak gamma-ray of energy 1.27$\pm$0.01 Mev was found with both lead and uranium radiators. The relative intensities of the several gamma-rays were obtained with the help of Gray's[5] formula for the photoelectric efficiency as a function of the energy of the gamma-ray. The results are shown in Table I.

TABLE I. Relative intensity of gamma-rays.

Energy (Mev)	Relative intensity arbitrary units
0.190	257
0.552	47.9
0.722	47.7
1.27	3.2

The energy of the gamma-ray at 1.27 Mev is the sum of the energies of those at 0.552 and 0.722 Mev. Since the two lines at 0.552 and 0.722 Mev are of equal intensity, it is assumed that they are in cascade. This assumption is borne out by the fact that gamma-gamma-coincidences are found.[3] The line at 1.27 Mev connects the higher excited state of the cascade process with the ground state and occurs in about 6 percent of the transitions. This line was also found in the coincidence experiments. Since there are no beta-ray groups in the beta-ray spectrum of the 72-sec. In^{114} which correspond to these gamma-rays and since characteristic x-rays of Cd have been found,[3,4] it is assumed that the three higher energy gamma-rays arise as a result of K-electron capture. In order to calculate the percentage of transitions which go by K-electron capture, it is necessary to know the ratio

$N_e^-/(N_e+N_\gamma)$ for the internally converted 0.190-Mev line. This has been given by Lawson and Cork as 1.00±0.30, by Boehm and Preiswerk as 0.80±0.05, and Langer and Price[6] as 0.80±0.10. Taking the value of 0.80 as correct the percentage K-capture is found to be 4.0 percent in good agreement with Boehm and Preiswerk. The disintegration scheme is shown in Fig. 2.

This research was assisted by the Joint Program of the ONR and AEC.

* Present address, Physics Department, Iowa State College.

[1] J. L. Lawson and J. M. Cork, Phys. Rev. **57**, 982 (1940).
[2] Cork, Shreffler, and Fowler, Phys. Rev. **74**, 1657 (1948).
[3] F. Maienschein and J. L. Meem, Jr., Phys. Rev. **76**, 899 (1949).
[4] F. Boehm and P. Preiswerk, Helv. Phys. Acta **22**, 331 (1949).
[5] L. H. Gray, Proc. Camb. Phil. Soc. **27**, 103 (1931).
[6] L. M. Langer and H. C. Price, Jr., private communication.

Penetration and Diffusion of Hard X-Rays through Thick Barriers. IV. Multiply Scattered γ-Rays: Angular Distribution*

L. V. Spencer and Fannie Jenkins
National Bureau of Standards, Washington, D. C.
August 22, 1949

In order to gain some insight into the angular distribution of γ-rays which are scattered many times within a barrier, the following quite schematic problem has been studied theoretically: A source of monochromatic γ-rays of energy E_0 is distributed uniformly throughout an isotropic medium. Each γ-ray is emitted in exactly the same direction. What will be the distribution in angle, $N(E,\theta)$, of those photons which are degraded by Compton scattering to the energy E? (θ is measured from the initial direction.)

This might be said to be a study of the manner in which photons "forget" their original direction as they lose their energy through Compton scattering.

Under the conditions of this problem, $N(E,\theta)$ obeys the following integral equation:

$$\mu(E)N(E,\theta)=\int_E^{E_0}k(E',E)dE'\int_{4\pi}(1/2\pi)\delta\times(\omega\cdot\omega'-1+mc^2/E-mc^2/E')\times N(E',\theta')d\omega'+k(E_0,E)\delta\times(\cos\theta-1+mc^2/E-mc^2/E_0) \quad (1)$$

where $\mu(E)$ is the probability, per unit path length, that a photon of energy E will undergo scattering, photoelectric absorption, or pair formation; $k(E',E)$ is the probability, per unit path length, that a photon of energy E' will attain the energy E through a scattering process; δ is the Dirac function and ω represents a unit vector with direction coordinates (θ,ϕ). The first term in (1) gives the rate of disappearance of photons having energy E and inclination θ. This must be balanced (under steady state conditions) by contributions coming from the source in a single scattering, represented by the third term, plus those contributions coming from the source in two or more scatterings, represented by the second term.

Using an expansion in Legendre polynomials,[1] that is,

$$N(E,\theta)=\sum_{l=0}^{\infty}[(2l+1)/4\pi]N_l(E)P_l(\cos\theta) \quad (2)$$

$$\delta(\omega\cdot\omega'-1+mc^2/E-mc^2/E')=\sum_{l=0}^{\infty}[(2l+1)/2]P_l(1-mc^2/E+mc^2/E')P_l(\omega\cdot\omega') \quad (3)$$

we can carry out the integral over ω'. Introducing (2) and (3) into (1) we find that the coefficients $N_l(E)$ must fulfill the integral equation

$$\mu(E)N_l(E)=\int_E^{E_0}k(E',E)P_l(1-mc^2/E+mc^2/E')N_l(E')dE'+k(E_0,E)P_l(1-mc^2/E+mc^2/E_0). \quad (4)$$

For $l=0$, this equation coincides with Eq. (1) in the accompanying paper.[2]

We solve Eq. (1) in the following manner: We obtain the contributions to $N(E,\theta)$ which are scattered only one time or only two times through iteration of (1). We subtract these same contributions from Eqs. (4), likewise through iteration. Orders of scattering higher than the second can contain at most a discontinuity in the derivative $dN/d\theta$; consequently the part of the sum (2) representing these higher orders of scattering will converge reasonably well. Actually, we found that using values of l up to four we obtain sufficiently good convergence at all except the highest energies.

We did some numerical work for purposes of orientation choosing $E_0=10$ mc²; and for materials we used aluminum and lead as representative light and heavy elements. Figures 1 and 2 show the results of our calculations for various values of E in the case of aluminum. In Fig. 1, the vertical straight lines indicate the portion of the radiation of each energy which arises from single scattering and whose angular distribution is peaked like a δ-function. The dotted rectangles give a measure of the intensity of this component. The other discontinuity in each curve is at the maximum angle obtainable by a photon going from E_0 to E in two scatterings. These last appear also in Fig. 2.

The high orders of scattering become increasingly effective as the energy decreases, as evidenced by the increase in the number of photons at larger angles than the "two-scattering" cut-off. It will be noticed that at $E=0.476$ mc², which corresponds to a single scattering through 180°, this multiply scattered beam tends to ∞ at the backward pole. This is because those photons attaining 0.476 mc² in two scatterings can reach this direction no matter what the intermediate energy is. At still lower energies than

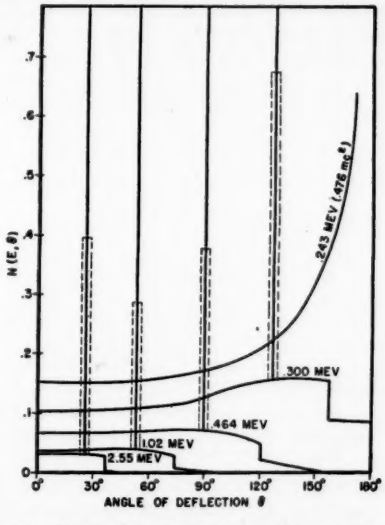

FIG. 1. Angular distribution of secondary photons for various energies of degradation. Initial energy $E_0=5.1$ Mev (10 mc²). The dotted rectangles represent the strength of the corresponding sharp lines.

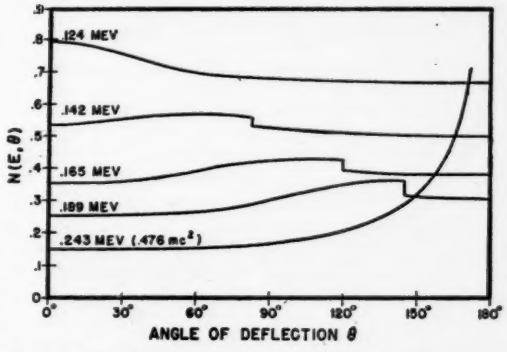

FIG. 2. Angular distribution of secondary photons for various energies of degradation. Initial energy $E_0=5.1$ Mev (10 mc²).

$E=0.476$ mc² there is no longer a singly scattered beam; the solution has the appearance of a wave running across as the energy decreases. Not all the departure from isotropy at these lower energies is due to the beam which is scattered twice—there is still a slight "wave" in existence when the second scattered beam is eliminated. This is largely due to photons which are scattered every time except once through angles close to 0° or to 180° and thus have some remembrance of their original direction.

The solution in the case of lead has the same general features, except that the low orders of scattering are much more important, due to the increased competition which pair production and photoelectric effect give to Compton scattering. Also, instead of a build-up in the total density of photons at lower energies, there is a sharp decrease, due to photoelectric effect.

A more detailed account of this work will appear in the Journal of Research of the National Bureau of Standards.

We should like to thank Dr. U. Fano for suggesting this problem and for many valuable discussions during the course of the work.

* Work supported by an ONR grant.

[1] See e.g. M. Verde and G. C. Wick, Phys. Rev. **71**, 852 (1947).

[2] P. R. Karr and J. C. Lamkin, Phys. Rev. **76**, 1843 (1949). This is paper III of the series; papers I and II are quoted there.

Radioactive Lanthanum 140

J. M. Cork, H. B. Keller, W. C. Rutledge, and A. E. Stoddard
Department of Physics, University of Michigan, Ann Arbor, Michigan

November 4, 1949

THE single natural isotope of lanthanum of mass 139 should, on neutron capture in the pile, yield the radioactive isotope of mass 140. This emitter has been previously studied by many investigators.[1] Because of the difficulty of chemical purification, impurities are likely to be present. A highly purified sample separated by Dr. G. E. Boyd was kindly made available and irradiated in the Oak Ridge pile.

This specimen shows a remarkably pure decay through eight octaves with a half-life of 41.4 hours. In photographic beta-spectrometers, many electron conversion lines are observed, about 16 in all, with energies less than 500 kev. These are shown in Table I, together with their proposed interpretation and the values of the resultant probable 12 gamma-rays. The $K-L$ differences where observed are characteristic of cerium, indicating that gamma-emission follows the loss of a beta-particle from the lanthanum nucleus.

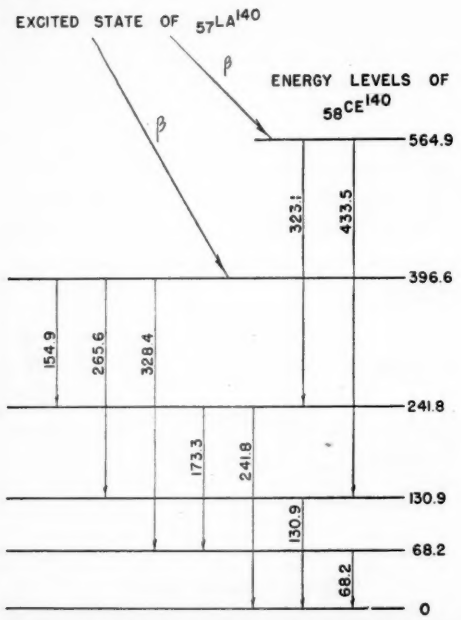

FIG. 1. A possible level scheme associated with $_{57}La^{140}$.

The observed gamma-rays may be fitted into a level scheme as shown in Fig. 1. The sums of all possible combinations agree as expected to within about 0.2 kev. The gamma-rays observed at 109.1 and 487.1 kev do not, however, fit into the level diagram. The only positions they could occupy and remain consistent with the scheme would be either above or below the group of levels shown in Fig. 1. The electron line at 483.2 kev may also be interpreted as a K line, in which case the gamma-energy is 523.5 kev. This value happens to be almost exactly the sum of three observed gamma-rays of 109.1, 173.3, and 241.8 kev. The presence of these two anomalies indicates that some ultimate revision of the proposed level scheme may be necessary, to include also the higher energy gamma-rays.

TABLE I. Conversion electron and probable gamma-ray energies.

Electron energy	Probable identification	Energy total	Gamma-energy
27.9 kev	K_1	68.2 kev	68.2 kev
68.7	K_2	109.0	109.1
90.7	K_3	131.0	130.9
103.0	L_2	109.2	
107.9	M_2	109.3	
114.6	K_4	154.9	154.9
124.5	L_3	130.7	
133.0	K_5	173.3	173.3
201.5	K_6	241.8	241.8
225.3	K_7	265.6	265.6
282.8	K_8	323.1	323.1
288.2	K_9	328.5	328.4
322.0	L_9	328.2	
393.2	K_{10}	433.5	433.5
446.8	K_{11}	487.1	487.1
483.2	K_{12} or L_{11}	523.5 489.4	523.5

The beta-emission had been previously shown to be complex. Higher energy gamma-radiation is present which by absorption in lead had an energy of 1.88 Mev. The long-lived 140-day activity previously reported does not appear to be present in this specimen.

This investigation was made possible by the joint support of the ONR and the AEC.

[1] Weimar, Pool, and Kurbatov, Phys. Rev. **63**, 67 (1943); R. Osborne and M. Peacock, Phys. Rev. **69**, 679 (1946); C. Mandeville and M. Scherb, Phys. Rev. **73**, 1434 (1948); Mitchell, Langer, and Brown, Phys. Rev. **71**, 140 (1947); Cork, Shreffler, and Fowler, Phys. Rev. **74**, 240 (1948).

Ferroelectricity in the Ilmenite Structure

B. T. Matthias and J. P. Remeika
Bell Telephone Laboratories, Murray Hill, New Jersey

November 7, 1949

SINGLE crystals of $LiTaO_3$ and $LiCbO_3$ have been found to be strongly ferroelectric as is indicated by the existence of a saturation polarization in their dielectric hysteresis loop. The saturation value increases rapidly with temperature as shown in Fig. 1. $LiCbO_3$ exhibits a similar behavior at higher temperatures.

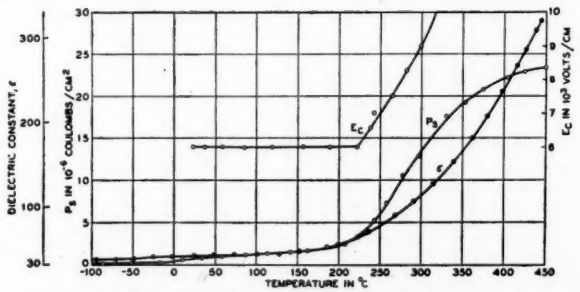

FIG. 1. Saturation values in a single crystal of $LiTaO_3$ as a function of temperature.

$LiCbO_3$, with which $LiTaO_3$ is isomorphous, was described by Zachariasen[1] as belonging to the ilmenite structure, which is centro-symmetric. The existence of a spontaneous polarization, however, indicates the absence of a center of symmetry. A further

proof hereof is that the crystals are piezoelectric, which effect cannot occur if there is a center of symmetry.

In the perovskite system and in WO_3 it appeared that ferroelectricity occurred when the metal oxygen octahedra fulfilled certain conditions for size and electronic configuration.[2,3] A comparison between metatitanates, columbates and tantalates showed that the ferroelectric behavior was much more sensitive to a change of lattice constant in the case of Ti than in that of Cb or Ta, because all metacolumbates or tantalates of the perovskite system were ferroelectric. This fact now seems to extend even to a quite different crystal system such as the ilmenite structure. There the octahedra do not share corners with each other as in perovskite, but edges and faces, and the crystal symmetry is lower. It might be added that none of the ferroelectric crystals mentioned fits into the scheme of adding over-all polarizabilities, which was first suggested by Jonkers and van Santen[4] and then extended to non-ferroelectric crystals by Roberts.[5]

Any investigation of $LiTaO_3$ and $LiCbO_3$ has to be carried out with single crystals because ceramics show hardly any effect. The reason for this is the rather low crystal symmetry, compared to the perovskite system; another consequence of the low symmetry is the absence of domains.

We are very grateful to Dr. E. A. Wood for doing all the x-ray work.

[1] W. H. Zachariasen, Skr. Norske Vid.-Akad., Oslo, Mat. Naturv. No. 4 (1928).
[2] Matthias, Wood, and Holden, Phys. Rev. **75**, 1771 (1949).
[3] B. T. Matthias, Phys. Rev. **76**, 430 (1949).
[4] G. H. Jonkers and J. H. van Santen, Chem. Weekbl. **43**, 672 (1947).
[5] S. Roberts, Phys. Rev. **76**, 1215 (1949).

Optical Absorption in Barium Oxide Films

WINFIELD W. TYLER*
Department of Physics, Cornell University, Ithaca, New York
November 3, 1949

MEASUREMENTS of the optical absorption of small single crystals of barium oxide[1] indicated that any information concerning structure in the absorption band could only be obtained from the study of thin films. Absorption in such films has recently been measured as part of the study of photo-conductivity and optical properties of BaO.

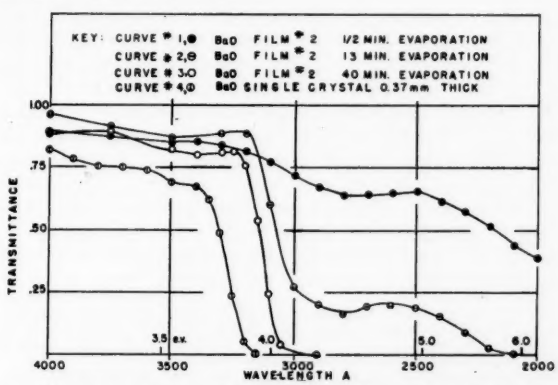

FIG. 1. Transmittance as a function of wave-length for a BaO film at different thicknesses and for a BaO single crystal.

BaO films from 2×10^{-5} cm to 4×10^{-5} cm thick were evaporated from a coated platinum filament onto a quartz plate. Evaporation and subsequent measurements were carried out in the same vacuum system. The filament was initially coated with c.p. $BaCO_3$ in nitrocellulose and amyl acetate. This was converted to BaO and outgassed before the quartz plate was moved into position to receive the film. After the absorption measurements were completed, the quartz plate was removed from the vacuum and the film was weighed as $Ba(OH)_2$. The thickness of the original film was then obtained by assuming a density of 5.7 for BaO. Film thicknesses for intermediate evaporation times

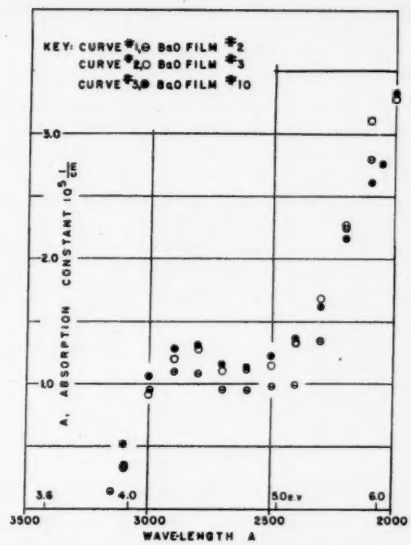

FIG. 2. Absorption constant as a function of wave-length for three different BaO films.

were obtained by using the absorption data to interpolate between zero thickness and final thickness. Film thickness was nearly proportional to evaporation time for all films studied. The transmission of the film was measured by moving the quartz plate so that the light beam passed through the quartz alone and then

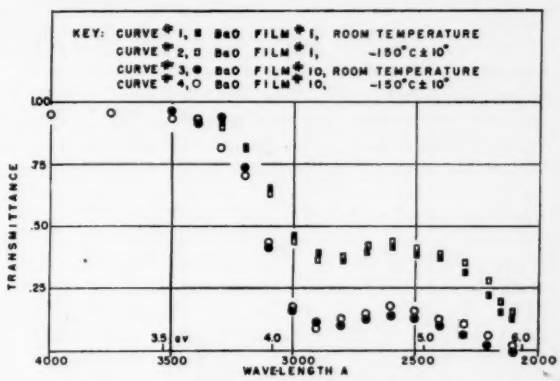

FIG. 3. Transmittance as a function of wave-length for two BaO films showing temperature dependence.

through quartz plus the BaO film. A Hanovia hydrogen discharge tube and a Bausch & Lomb quartz ultraviolet monochromator provided fairly continuous monochromatic radiation in the spectral region from 4000A to 2000A. At several wave-lengths, a high pressure Hg arc was used to study the effect of changing light intensity on the absorption constant. The detector used was an RCA 1P28 photo-multiplier tube.

Curves 1, 2, and 3 of Fig. 1 show the transmittance of a BaO film as a function of wave-length for three different thicknesses. The crossing over of transmission curves in the region from 3200A to 4000A as the film is built up has been observed in all of the films studied and is probably due to interference effects. Curve 4 of Fig. 1 shows the transmittance of a 0.37-mm single crystal of BaO. The agreement between transmission data for evaporated films and single crystals indicates that the BaO film is deposited in the form of small crystals of the same form as the larger single crystals studied. Figure 2 shows the absorption constant A as a function of wave-length for three different films. A is defined by the expression $T=\exp(-Ax)$ where T is the transmittance and x the thickness of the film. A has been calculated from the transmission curves without correcting for reflection and interference

effects. Figure 3 shows the effect of film temperature on absorption for two different films.

These studies of BaO films confirm the fact that the optical absorption threshold coincides with the threshold for photoconductivity[1] at about 3.8 ev. The magnitude of the absorption constant is so large that the absorption process cannot be attributed to impurity centers in the crystal lattice. Temperature variation of the absorption constant from room temperature down to about −150°C is small but appears to indicate a slight accenting of the structure in the absorption constant curve near 2900A. The absorption constant does not change appreciably for variation of light intensity by a factor of 20.

The author is indebted to Professor Robert L. Sproull, who directed the research, and to Dr. Arnold R. Moore for valuable discussions. The work has been assisted by the ONR and the Research Corporation.

* Charles A. Coffin Fellow, 1948–49.
[1] W. W. Tyler, Phys. Rev. **76**, 179 (1949).

Beta-Spectrum of Praeseodymium 143

L. Feldman, L. Lidofsky, P. Macklin, and C. S. Wu
Pupin Physics Laboratories, Columbia University, New York, New York
November 7, 1949

PRAESEODYMIUM 143, a radioactive daughter substance of Ce^{143} which has a half-life of 33 hr., can be produced either by ordinary nuclear reactions,[1] such as $Ce^{142}(d, p)Ce^{143}$ and $Ce^{142}(n, \gamma)Ce^{143}$, or by nuclear fission process. Pr^{143} emits beta-particles with half-life determinations varying from 12.7 to 14.2 days,[1] and it does not emit gamma-rays. The beta-spectrum end point, investigated by means of aluminum absorption methods and estimated by Feather's empirical method, has been reported in the range between 0.83 and 1.0 Mev.[1] Recent spectrometer measurements[2] with sources containing a mixture of Ce^{141} and Pr^{143} yield straight line Fermi plots of the beta-spectrum from 565 kev, the end point of the Ce^{141} spectrum, to the end point of the Pr^{143} spectrum. The upper limit to the energy of the Pr^{143} spectrum is reported as 920±10 kev by Ter-Pogossian *et al.* and as 930±20 kev by Shepherd.[2]

Recently, a strong source of Pr^{143} of very high specific activity was obtained from the Isotopes Branch of the AEC at Oak Ridge in the form of a PrCl solution. This high specific activity material is suitable for beta-spectrum investigation in a beta-ray spectrometer. The Pr^{143} source was prepared by depositing, on a collodion film of 10 $\mu g/cm^2$ thickness, a drop of PrCl solution to which an extremely small quantity of detergent (Anotrox X) had been added. The total amount of solid contained in the source is around 20 μg and is spread over a circular area of 0.5 cm^2.

The Columbia solenoid magnetic spectrometer was used in this investigation. The resolution used was three percent defined as the full width at half-intensity. Both Nylon and collodion window counters were used to cover the upper and lower energy range of the spectrum. In plotting the Fermi plot, the explicit form[3] of the relativistic Coulomb factor

$$F(Z, \epsilon) \approx \frac{2\pi\delta}{1-\rho^{-2\pi\delta}} [\epsilon^2(1+4\gamma^2)-1]^S,$$

where $S=(1-\gamma^2)^{\frac{1}{2}}-1$, $\gamma=Z\alpha=Z/137$, $\delta=\gamma(\epsilon/\eta)$ was used.

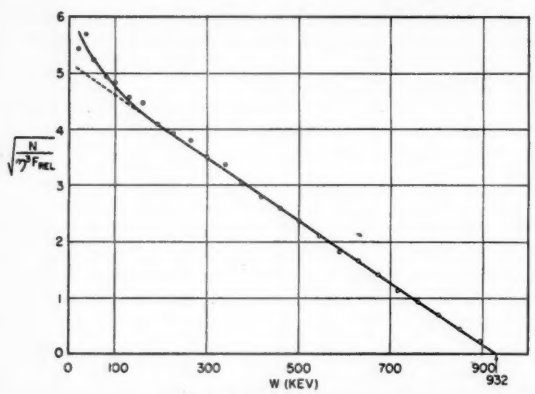

FIG. 1. Fermi plot of Pr^{143} beta-spectrum.

This approximation is accurate to about 0.5 percent in this case. The Fermi plot thus obtained gives a straight line from the upper energy limit down to 170 kev (Fig. 1). Below 170 kev, the Fermi plot starts to deviate upward very gradually, which could be attributed to local variations in source thickness due to non-uniformity. The upper energy limit given by the intercept of the straight line in the Fermi plot is 932±2 kev. This spectrum was investigated in the spectrometer many times, using sources from two different shipments. The results were reproducible and consistent.

Other Pr^{143} sources were made from the same solutions, and the half-life was continuously followed in a G-M counter over a period of ten weeks. The decay curve (Fig. 2) is definitely a straight line on a semilogarithmic plot and gives a value of 13.7±0.1 days for the half-life.

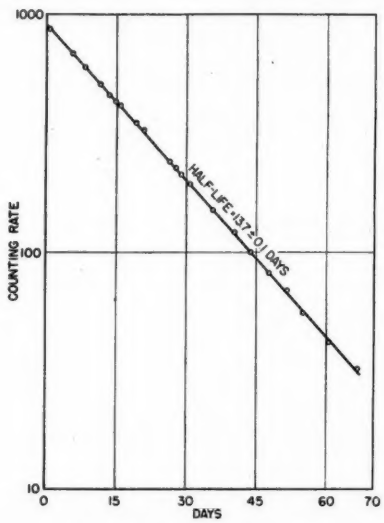

FIG. 2. Decay curve of Pr^{143}.

The *ft* value calculated is 1.3×10^7. For such a high atomic number ($Z=59$), the beta-radiation from Pr^{143} should be classified empirically into the group of first- or second-forbidden transitions. Nevertheless, the shape of the spectrum follows the allowed shape as in the many other cases where the *ft* value indicates a highly forbidden transition.

We should like to thank the United States AEC which aided materially in the performance of this research.

[1] G. T. Seaborg and I. Perlman, Rev. Mod. Phys. **20**, 622 (1948); C. E. Mandeville and E. Shapiro, Phys. Rev. **75**, 1834 (1949).
[2] L. R. Shepherd, Research **1**, 67 (1948); Ter-Pogossian, Cook, Goddard, and Robinson, Phys. Rev. **76**, 909 (1949).
[3] H. Bethe and R. F. Bacher, Rev. Mod. Phys. **8**, 194 (1936).

The Beta-Spectrum of $_{61}Pm^{147}$

L. Lidofsky, P. Macklin, and C. S. Wu
Pupin Physics Laboratories, Columbia University, New York, New York
November 7, 1949

HIGH specific activity Pm^{147} has recently become available from the Isotopes Division of the AEC at Oak Ridge where it is made as a fission product. This high specific activity material, when used in the high transmission solenoidal focusing β-ray spectrometer, makes it possible to investigate its beta-spectrum using sources less than 30 $\mu g/cm^2$ thick.

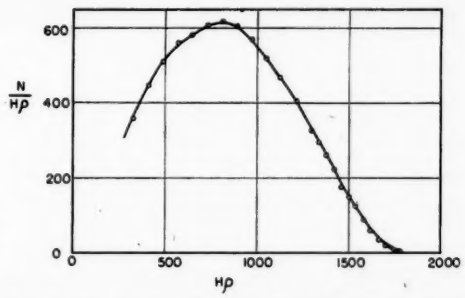

FIG. 1. $_{61}Pm^{147}$ spectrum corrected to constant sensitivity.

The Pm^{147}, received as Pm^{147} Cl_3 in 0.1 N HCl was evaporated to dryness and then redissolved in distilled water to which a small amount of wetting agent (Antorox) was added. A 0.01-ml drop placed on a collodion backing ($\sim$10 μg/cm^2) formed a uniform source spread over a circular area of about 0.5 cm^2.

Several runs were made with the resolution set at 3 percent yielding results of which Figs. 1 and 2 are typical. Bethe's explicit

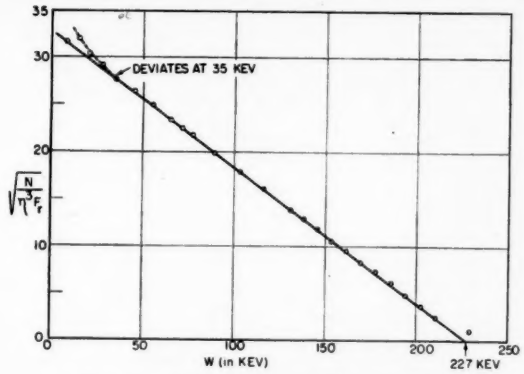

FIG. 2. Fermi plot of the beta-spectrum of $_{61}Pm^{147}$.

form of the relativistic Coulomb factor[1] was used in making the Fermi plot. The end point obtained was 227$\pm$1 kev. The plot was straight from the end point down to at least 35 kev. Below this energy, the curve deviated slightly upward and then again downward in a manner which could be attributed to finite source thickness and window absorption (40–50 μg/cm^2 collodion).

The above end point in conjunction with the reported value of the half-life (3.7 years)[2] yielded an ft value for the transition of 1.2×10^7 which for an element with a Z of 61 indicates a first- or second-forbidden spectrum. Although the curve has an allowed shape this is not a contradiction since, for certain interactions, a forbidden transition may exhibit an allowed shape.

We should like to thank the United States AEC which aided materially in the performance of this research.

[1] H. A. Bethe and R. F. Bacher, Rev. Mod. Phys. **8**, 194 (1936).
[2] G. T. Seaborg and I. Perlman, Rev. Mod. Phys. **20**, 623 (1948).

On the Low Energy Spectrum of Primary Cosmic Radiation and the Sun's Magnetic Dipole Moment*

M. A. POMERANTZ
Bartol Research Foundation of The Franklin Institute, Swarthmore, Pennsylvania
AND
M. S. VALLARTA**
Instituto de Física, Universidad de México, México, D. F.

November 7, 1949

FOR various reasons which will be discussed in detail later,[1] it was deemed important to compare directly the vertical primary cosmic-ray intensity at Swarthmore, Pennsylvania (52° N geomagnetic latitude) with that at Fort Churchill, Manitoba (69° N geomagnetic latitude), both with and without a lead absorber.

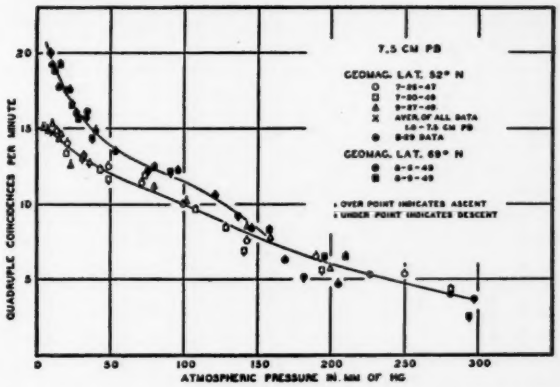

FIG. 1. Intensity *vs.* altitude curves for cosmic rays arriving vertically and capable of penetrating 7.5 cm of Pb at $\lambda=52°$ N and at 69° N. The increase in the primary intensity at high latitudes is clearly evident. The reproducibility of the data should be noted.

The measurements were obtained with standard quadruple-coincidence counter trains identical with those used earlier.[2] Typical results are shown in Figs. 1 and 2. The records of other balloon flights have not yet been analyzed, although spot checks have shown good agreement with the points plotted here. A total of 13 flights was conducted at Fort Churchill, most of them in the morning.

The ratio of the vertical intensities with no lead absorber extrapolated to the top of the atmosphere is found to be $I(69°)/I(52°)=1.46$.

From this figure, and assuming that the change of intensity is a pure geomagnetic effect, one may easily calculate, using the same method of analysis outlined in a previous paper,[3] that this ratio

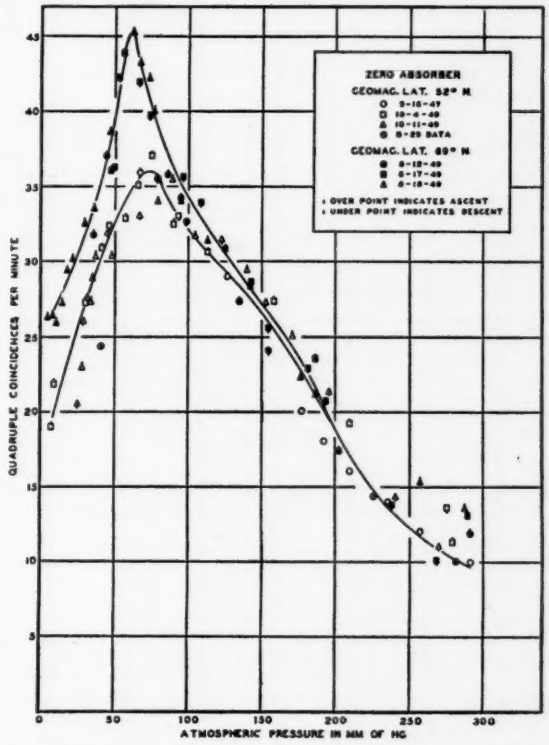

FIG. 2. Intensity *vs.* altitude curves with no lead absorber for cosmic rays arriving vertically at $\lambda=52°$ N and at 69° N. Similar data were obtained with lead absorbers of intermediate thicknesses.

is consistent with a differential energy spectrum in the energy range from 0.1 to 1.6 Bev for protons of the form $(K/E^{1.14})dE$.

According to the calculations of Dwight,[4] one should expect an increase of at least five percent from 6 to 12 hr. local solar time at 69° N geomagnetic latitude and a decrease of about three percent in the same interval at 52°, on the assumption of a sun's permanent magnetic dipole moment[5] of 10^{34} gauss-cm^3, which is inconsistent with the observations reported here. Nor does it seem possible to account for these results by a shift in the latitude of the knee due to the diurnal variation of the vertical intensity. In point of fact, according to Dwight's calculations, one would expect a difference of vertical intensity between 52° and 69° of about seven percent with maximum in the early morning and decreasing towards noon local solar time. In particular, at 6 hr. the intensity at 52° should be seven percent greater than at 69°, contrary to observation.

This in turn means that the sun's magnetic dipole moment in August, 1949, was not 10^{34} gauss-cm^3 but at most 0.6×10^{33} gauss-cm^3, assuming that the knee on that date was at least at 75° N geomagnetic latitude. This raises the interesting possibility that the sun, like certain stars the magnetic fields of which have been measured by Babcock,[6] has a variable magnetic field and hence a magnetic dipole moment which varies as a function of time.[7] This possibility has far-reaching consequences as regards the mechanism for the acceleration of charged particles of all kinds up to cosmic-ray energies in the neighborhood of the sun. It would thus appear that systematic observations of the vertical intensity at high geomagnetic latitudes and at high altitude, over extended intervals of time, would be highly desirable as a means of studying the variation of the solar magnetic field with time.

One of us (M.A.P.) expresses his grateful appreciation to all those without whose cooperation these experiments could never have been performed, to the National Geographic Society, and to the Defense Research Board of Canada. It is a pleasure for the other author (M.S.V.) to thank Professor J. R. Oppenheimer and Dr. M. A. Tuve for their generous hospitality.

* Supported in part by the Joint Program of the ONR and the AEC.
** Present address: Institute for Advanced Study, Princeton, New Jersey, or Department of Terrestrial Magnetism, Carnegie Institution of Washington, Washington, D. C.
[1] M. A. Pomerantz, Phys. Rev. **77**, 1950.
[2] M. A. Pomerantz, Phys. Rev. **75**, 69 (1949); **75**, 1721 (1949); **75**, 1335 (1949).
[3] Vallarta, Perusquía, and de Oyarzábal, Phys. Rev. **71**, 393 (1947).
[4] Kirby Dwight, Jr., Princeton University thesis, 1949 (unpublished).
[5] M. S. Vallarta, Nature **139**, 839 (1937).
[6] H. W. Babcock, Publ. Astr. Soc. Pacific **59**, 260 (1947); Phys. Rev. **74**, 489 (1948).
[7] This suggestion arose from a conversation with Dr. S. E. Forbush.

PHYSICAL REVIEW VOLUME 76, NUMBER 12 DECEMBER 15, 1949

Proceedings of the American Physical Society

Minutes of the Meeting of the Ohio Section at Cleveland, November 5, 1949

THE Ohio Section of the American Physical Society held its fall meeting in Cleveland at The Case Institute of Technology, on November 5, 1949. There was no business other than the programme of ten contributed papers (the abstracts of nine of which follow) and the invited talk by E. C. Gregg on the Case Institute betatron and plans for its use. Abstracts of these papers follow.

Leon E. Smith, *Secretary*
Denison University,
Granville, Ohio

Apparatus for Acoustical Measurements with Pulse-Modulated Ultrasonic Waves. Ernest Yeager, Hyman Chessin, John Bugosh, and Frank Hovorka, *Western Reserve University*.—A thousand-watt, pulse-modulated ultrasonic generator has been constructed for operation in the range 200 to 1200 kc at pulse repetition rates from 15 to 2500 sec.$^{-1}$ with pulse durations from 25 μsec. to one-half the repetition period. Acoustical output is stable within 0.4 db after an initial warm-up period of one hour. The ultrasonic generator consists of a pulse generator, r-f oscillator, pulse modulator, and four stages of Class C amplification using tetrodes with a final thousand-watt, push-pull stage. The transducer mounting, which accommodates 3-in., circular, x-cut, quartz crystals from 200 to 1200 kc, permits propagation directly into water in a glass thermostatic bath, 6 ft. in length. Investigations of electrochemical effects are normally carried on in an acoustical cell which is placed within the tank in such a fashion that the acoustical waves enter and leave the cell through rho-c rubber windows. Oscillograms are presented which indicate the ease with which this equipment can be used for investigations of electroacoustical effects.

[1] This research has been supported by the ONR.

A High Frequency Barium Titanate Hydrophone.* John Bugosh, Ernest Yeager, and Frank Hovorka, *Western Reserve University*.—A microphone has been constructed with a pressure-sensitive cylinder of radially polarized barium titanate, 0.125 in. long, 0.125 in. diameter, and a 0.012-in. wall.[1] Pyseal has been used to cap one end of the cylinder while the other end is fitted into a Monel tube, 20 in. long. The underwater calibration[2] of this unit indicates that the response is flat within ±3 db from 50 to 100 kc and from 200 to 500 kc at a level of −130 db re one volt/dyne/cm^2. It is non-directional within ±2 db through 300 kc and ±4 db through 750 kc. Several microphones of this type have performed very well with constant use for six months. A $\frac{1}{16}$-in. microphone of similar design has also been constructed and is under investigation.

* This research has been supported by the ONR.
[1] This type of ceramic cylinder was suggested by Mr. J. P. Arndt of the Brush Development Company of Cleveland.
[2] U.S.N. Underwater Sound Reference Laboratory, Orlando, Florida.

A High Frequency Electroacoustic Effect and Its Utilization in the Construction of Hydrophones.* JOHN BUGOSH, ERNEST YEAGER, AND FRANK HOVORKA, *Western Reserve University.*—A stable microphonic effect has been obtained by immersing a double cotton covered wire in distilled water or an aqueous solution of low conductivity. This effect has been distinguished from direct electrical coupling effects by means of pulsed ultrasonic waves and an aqueous delay line. At 200 kc the sensitivity is, approximately, 0.1 μv/dyne/cm^2. Considerable increase in sensitivity seems entirely possible. Using this effect, one can easily and cheaply construct a microphone which is non-directional and virtually a point probe. Present indications are that the effect arises because of electrokinetic phenomena on the cotton covering.[2] The expected inverse relation between the magnitude of the effect and the conductivity of the solution has been found experimentally in a semiquantitative fashion. Other porous, adherent substances in addition to cotton give a similar effect, although usually diminished in magnitude. The copper base metal can also be replaced by other metals.

* Research supported by the ONR.
[1] L. V. Nikitin [J. Phys. Chem. U.S.S.R. 22, 1090 (1948)] has extensively investigated in the audio region numerous electroacoustic effects which seemed to be of a similar nature.

The Condensation of Evaporated Metals on Surfaces.* LEONARD O. OLSEN, E. C. CRITTENDEN, JR., AND R. W. HOFFMAN, *Case Institute of Technology.*—The condensation of metals such as cadmium, zinc, tin, etc. on clean glass is greatly affected by the temperature of the glass surface.[1] It is possible to speak of a "critical temperature" for each of these substances above which a good metallic deposit does not form. This critical temperature turns out to be a function of the rate of arrival of the metal atoms at the surface. These results are in agreement with the point of view that adsorbed atoms form a very mobile two-dimensional gas on the surface until sufficient nuclei are formed and a bulk metallic film develops.

* Supported by the ONR.
[1] See, for example, Cockroft, Proc. Roy. Soc. 119, 295 (1928).

Use of WWV Signals to Time Pendulums. J. T. MCCARTHY, *Western Reserve University.*—An experiment has been devised in which the half-period of a pendulum is determined with the method of coincidences by comparison with the pulses transmitted on 5 Mc by the National Bureau of Standards. The pulses, after reception by an inexpensive crystal-controlled receiver, pass through a filter and actuate a mechanical relay by means of a thyratron circuit. Reception of the pulses is very seldom poor enough to hinder the experiment. Measurements made on one edge of a Kater's pendulum have yielded results which appear to be more accurate and consistent than the results obtained by means of a standard pendulum clock. When measurements are made on coincidences for about a half-hour, the error in the calculated value of the half-period is usually about two or three parts per million. This error is of the same order as the error due to a fluctuation of a fraction of a degree in the temperature of the Kater's pendulum. The accuracy of the results was sufficiently high to show that the variation of the half-period with the amplitude does not quite agree with the prediction of simple theory.

A Novel Magnetostriction Effect. R. F. JANOFSKY, M. MELAMED, AND R. A. BETH, *Western Reserve University.*—It has been known that a ferromagnetic rod can be made to twist by imposing simultaneous longitudinal and circular magnetic fields (Wiedemann, 1883).[1] A simpler method of setting up the helical flux required for this magnetostrictive effect is to cut a helical groove in the specimen and to impress only a longitudinal magnetizing field by means of a solenoid. A groove 1.3 mm deep and 2.0 mm wide was cut in a nickel rod 6.35 mm in diameter and 71.3 cm long. The helical groove made an angle of 38° at the surface with the axial direction. A maximum twist of 2.7×10^{-3} radian was observed with an axial magnetizing field of 175 oersted. This compares favorably with the twist obtained by the classical methods of superimposed fields,[1] and avoids the heating effects associated with heavy axial currents. By calculation, torsional resonance should occur for this rod at 1 kc. The only observed resonance up to 20 kc occurs at this frequency when the surrounding solenoid is driven by a General Radio oscillator. This suggests the possibility of using such rods to control low frequency magnetostriction oscillators.

[1] S. R. Williams, *Magnetic Phenomena* (McGraw-Hill Book Company, Inc., New York, 1931), p. 114 ff., gives literature references.

An Adjustable Mounting For Large Mirrors.* WILLIAM H. HAYNIE, *The Ohio State University.*— This paper describes a gimbal type suspension for large mirrors. The outstanding feature of this type of mounting is the ease and simplicity with which the mirror may be aligned. Rotational and translational adjustments are completely independent. This type of mounting, already being used in a spectrophotometer, should be of value in other applications such as schlieren equipment, etc.

* The work described in this paper was carried out, in part, under contract between The Wright-Patterson Air Force Base, Air Material Command, and The Ohio State University Research Foundation.

Monochromatic Electron Groups in Long-Life Manganese. W. S. EMMERICH, L. H. BALLWEG, AND J. D. KURBATOV, *Ohio State University.*—Manganese of 310-day half-life was produced by bombardment of iron with 12-Mev deuterons. The Mn was chemically separated and purified. This species has been identified previously as Mn 54 disintegrating by orbital electron capture followed by emission of 0.835-Mev gamma-rays.[1,2] The present study of this species was made mainly by cloud chamber. Two groups of monochromatic electrons ranging from 0.38 to 0.43 Mev and from 0.49 to 0.55 Mev were observed. The intensity of these radiations does not exceed by 1×10^{-3} the number of disintegrations by 0.835-Mev photons. The results obtained may indicate: (1) an additional excited state of Cr 54; (2) excited states of Cr 53 since the radioactive species Mn 53 is not known. Beta-decay spectrum of Mn 54 was not established conclusively, even though the presence of electrons in the range from 0.850 Mev to 1 Mev was observed.

[1] J. J. Livingood and G. T. Seaborg, Phys. Rev. **54**, 391–397 (1938).
[2] M. Deutsch and L. G. Elliott, Phys. Rev. **65**, 211–215 (1944).

Radiations Emitted by Long-Life Species of Nickel. D. G. THOMAS AND J. D. KURBATOV, *Ohio State University.*—The present study was made with nickel activated in Oak Ridge National Laboratories U.S.A.E.C. Due to low specific activity and to very long life of radioactive isotopes of nickel, a specially constructed large window G-M tube was used. The following groups of photons were observed: (1) $\sim7\pm1$ kev; (2) 15 ± 1 kev; (3) 45 ± 5 kev with ratio in intensity 3:1:1, respectively. In addition, photon of (4) 75 ± 5 kev and 0.3 relative intensity was identified. Cloud-chamber studies showed the presence of monochromatic electron group corresponding to photon (3) and (4) energies. If 7 ± 1 kev photon is assumed to be x-rays due to orbital electron capture in Ni 59 and due to internal conversions, the emitted photons may be identified with excited states of Co 59.[1]

[1] Barschall, Bockelman, and Seagondollar, Phys. Rev. **73**, 659 (1948).

Author Index to Volume 76

References with (A) are to abstracts of papers presented at meetings of the American Physical Society, and those with (T) designate title only. References with (L) are to Letters to the Editor.

Aamodt, L. C. (see Townes, C. H.)—691(L)
Abraham, B. M., B. Weinstock, and D. W. Osborne. Lambda-temperatures of He^3-He^4 mixtures—864(L)
Achter, M. R. and R. Smoluchowski. Grain boundary diffusion 470(A)
Adair, R. K. (see Barschall, H. H.)—1146
—— (see Bockelman, C. K.)—277
——, **H. H. Barschall, C. K. Bockelman, R. L. Henkel, and R. E. Peterson.** Evidence for broad nuclear energy levels in lead—463(A)
——, **C. K. Bockelman, and R. E. Peterson.** Experimental corroboration of the theory of neutron resonance scattering —308(L)
Adams, Mac C. Shock waves in inhomogeneous flow—877(A)
Adams, Norman I., Jr. (see Page, Leigh)—381
Addario, Margherita and Sara Tamburino. Frequency of stars of different sizes produced by the cosmic radiation in photographic plates exposed at 29,000 meters—983(L)
Adel, Arthur. Observation of non-Rayleigh scattering of the infra-red solar spectrum by the earth's atmosphere—446(L)
Aiken, Howard. Uses of computing machines—452(T)
Alburger, David E. Gamma-radiation from Na^{22} and Co^{60}—435(L)
Alers, P. B. (see Love, W. F.)—305(L)
Alger, R. S. (see von Hippel, A.)—127
Allen, A. J., J. F. Nechaj, K. H. Sun, and B. Jennings. Fast neutrons from bombardment with the cyclotron particles —463(A)
——, **J. F. Nechaj, K. H. Sun, and B. Jennings.** Neutron yield from 15-Mev deuterons—188(A)
Allen, K. W. (see Dewan, J. T.)—181(A)
Allis, William P. Error in a paper by Landau on Coulomb interactions in a plasma—146(L)
Allred, J. C. (see Stovall, E. J., Jr.)—589(A)
——, **K. W. Erickson, J. L. Fowler, and E. J. Stovall, Jr.** Angular distribution of 10.8-Mev deuterons scattered by deuterons—1430
Alpert, D. (see Holstein, T.)—1259(L)
—— (see Krasik, S.)—722
——, **A. O. McCoubrey, and T. Holstein.** Imprisonment of resonance radiation in mercury vapor—1257(L)
——, **A. O. McCoubrey, and T. Holstein.** Measurements on the imprisonment of resonance radiation in mercury vapor —457(A)
Altar, W. and M. Garbuny. Absolute speed gauge for high voltage particles—496
Alvarez, Luis W. Nitrogen 12—183(A)
—— Recent experimental work at the Berkeley Radiation Laboratory—161(T)
Ammiraju, P. Angular distribution of neutrons from targets bombarded by 18-Mev deuterons—1421(L)
Anderson, Carl D. (see Leighton, Robert B.)—159(L)
Anderson, Donald A. Magnetic moment of B^{11}—434(L)
Anderson, Herbert L. Precise measurement of the gyromagnetic ratio of He^3—1460
Anderson, P. W. On the limits of validity of the Van Vleck-Weisskopf line shape formula—471(A)
—— Pressure broadening in the microwave and infra-red regions—647
Anderson, Paul A. Work function of copper—388
Anderson, W. E. and E. F. Barker. Infra-red absorption spectrum of diborane—177(A)
Andrews, D. H., R. D. Fowler, and M. C. Williams. Effect of alpha-particles on a superconductor—154(L)
Angus, J. (see Curran, S. C.)—853(L)
Apker, L., E. Taft, and J. Dickey. Photoelectric studies on the energy structure of barium oxide—453(T)
——, **E. Taft, and J. Dickey.** Some semimetallic characteristics of the photoelectric emission from As, Sb, and Bi—270
Araki, Gentaro. Erratum: on the difficulty of the meson theory of nuclear forces—437(L)
Arfken, G. B. (see Breit, G.)—1299
—— (see Brown, G. E.)—1305
Argo, H. V. (see Jarvis, G. A.)—168(A)
—— (see Taschek, R. F.)—325
——, **H. T. Gittings, A. Hemmendinger, G. A. Jarvis, H. Mayer, and R. F. Taschek.** Observation of 20-Mev gamma-rays from the $T^3(p,\gamma)He^4$ reaction—182(A)
Armistead, F. C., J. C. Pennock, and L. W. Mead. Conductivity changes in dielectrics during 2.5-Mev x-radiation—860(L)
Arons, A. B. and D. R. Yennie. Oblique reflection of low amplitude, exponential shock waves from the sea bed—172(A)
Arroe, O. H. (see Mack, J. E.)—173(A), 1002(L)
—— **and J. E. Mack.** Hollow cathode-tube design for spectroscopic hyperfine structure studies with small samples—173(A)
—— **and J. E. Mack.** Nuclear spin 5/2 for $_{40}Zr^{91}$—873(L)
Ashkin, J. and R. E. Marshak. Bremsstrahlung in high energy nucleon-nucleon collisions—58——Erratum—989(L)
Auluck, F. C. (see Kothari, D. S.)—433(L)
Axel, P. and S. M. Dancoff. Classification of nuclear isomers —892

Badger, Richard M. (see Wilson, M. Kent)—472(A)
Baker, C. P. (see Corson, D. R.)—162(A)
Baldwin, G. C. X-ray yield curves for $(\gamma,2n)$ and (γ,p) reactions—182(A)
Baldwin, H. W. (see Simpson, J. A., Jr.)—165(A)
Ballweg, L. H. (see Emmerich, W. S.)—1891(A)
Band, William. Anomalous adsorption of helium at liquid helium temperatures—441(L)
—— Non-equilibrium phenomena in a Bose-Einstein gas. I. Transmission of second sound—558
—— **and Lothar Meyer.** Non-equilibrium state in helium II —417
Barbour, Ian. Magnetic deflection of cosmic-ray mesons using nuclear plates—320(L)
—— Magnetic deflection of mesons in photographic plates—170(A)
Bardeen, J. Diffusion in binary alloys—1403
Barkas, W. H. (see Bradner, H.)—587(A)
Barker, E. F. (see Anderson, W. E.)—177(A)
Barker, P. H. Variation of meson intensity with height—141(L)
Barnett, S. J. and Louis A. Giamboni. New gyromagnetic effect—1542(L)
Barnothy, J. Comment on the nuclear capture of negative mesons—303(L)
Barschall, H. H. (see Adair, R. K.)—463(A)
—— (see Bockelman, C. K.)—277
——, **C. K. Bockelman, R. E. Peterson, and R. K. Adair.** Investigation of nuclear energy levels in lead—1146
Bartholomew, G. A. (see Clarke, R. L.)—146(L)
Bartlett, James H. Helium wave equation—460(A)
Bass, Arnold M. and H. Sponer. Fluorescence studies on some mono-substituted benzenes in the near ultraviolet—177(A)
Bassi, P., E. Clementel, I. Filosofo, and G. Puppi. On positive excess of meson component near sea level—854(L)

Batchelor, G. K. Nature of turbulent motion at large wave numbers—875(T)
Beach, Louis A., Charles L. Peacock, and Roger G. Wilkinson. Radiation spectra of barium^{140} and lanthanum^{140}—1624
——, **Charles L. Peacock, and Roger G. Wilkinson.** Radiations of Re^{186} and Re^{188}—187(A)
——, **Charles L. Peacock, and Roger G. Wilkinson.** Radiations of tantalum^{182}, rhenium$^{186, 188}$, and gold^{199}—1585
Beams, J. W. High speed rotors—195(T)
Becker, G. E. and D. A. Caswell. Operation of a linear electron accelerator—587(A)
Becker, M. and H. Y. Fan. Optical properties of semiconductors. II. Infra-red transmission of germanium—1530(L)
—— **and H. Y. Fan.** Optical properties of semiconductors. III. Infra-red transmission of silicon—1531(L)
Becker, R. A. and F. S. Kirn. Radioactive sources of high specific activity produced with a betatron—182(A)
——, **F. S. Kirn, and W. L. Buck.** Betatron-produced sources of high specific activity: copper 62—1406(L)
Beeman, W. W. (see Dexter, David L.)—1782
—— (see Hanson, Harold)—118
Belinfante, Frederik J. Brownian motion in liquids—473(A)
—— Interaction representation for mesons—191(A)
—— Interaction representation of the Proca field—66
—— On the part played by scalar and longitudinal photons in ordinary electromagnetic fields—226
—— Positon theory—461(A)
Bell, E. E. (see Rhodes, K. B.)—1273(L)
Bell, P. R. and J. M. Cassidy. Beta-spectrum of Be^{10}—183(A)
——, **B. H. Ketelle, and J. M. Cassidy.** Beta-decay of In^{115*}—574(L)
Bell, R. E. (see Elliott, L. G.)—168(A)
—— **and H. E. Petch.** Upper limit for the lifetime of the 411-kev excited state of Hg^{198}—1409(L)
Benade, A. H. and R. D. Sard. Time distribution of decay electrons from mesons stopped in magnesium at 3500 meter altitude—488
Bender, R. S., F. C. Shoemaker, S. G. Kaufmann, and G. M. B. Bouricius. Resonance scattering of protons by aluminum —273
Bendt, P. J. and I. W. Ruderman. Determination of the phase of scattering of neutrons and of incoherent residual scattering cross sections—463(A)
Bene, G. J., P. M. Denis, and R. C. Extermann. Electric quadrupole moments of nuclei—1255(L)
Benesch, William M. Atmospheric ozone temperatures as determined by spectroscopic observations from below—863(L)
Benfield, A. E. Temperature distribution in an accreting medium containing a source of heat—456(A)
Bennett, F. D. and W. C. Carter. Interferometric analysis of flow around small caliber projectiles—880(A)
Benoist, P., R. Bouchez, P. Daudel, R. Daudel, and A. Rogozinski. Decay probability of Be^7 as a function of the ionization of the atom—1000(L)
Benson, James M. (see Williams, Thomas W.)—456(A)
Benzer, S. Hall effect in metal-semiconductor point contacts —150(L)
Bergdolt, V. E., A. J. Greenwald, and D. B. Sleator. Pressurized range for small caliber projectiles in free flight—879(A)
Bergman, Stefan. On flows of a compressible fluid—876(A)
Bergmann, Peter G. and Johanna H. M. Brunings. Covariant field theories—191(A)
Bergström, Ingmar (see Thulin, Sigvard)—871(L)
—— **and Sigvard Thulin.** Internal conversion coefficient and mass assignment of the 57-min. Se isomer—1718(L)
—— **and Sigvard Thulin.** Mass assignment of the 43-minute Hg isomer—313(L)
Beringer, Robert and J. G. Castle, Jr. Microwave magnetic resonance absorption in nitric oxide—868(L)
Berman, R. Thermal conductivity of glasses at low temperatures—315(L)
Bernardini, G., G. Cortini, and A. Manfredini. On the nuclear evaporation in cosmic rays and the absorption of the nucleonic component. I—1792
Bershader, D. Momentum thickness development in a turbulent boundary layer at $M=1.7$—171(A)
—— **and G. P. Wachtell.** Boundary layer optics in two-dimensional gas flow interferometry—880(A)
Best, George. Emittances of copper and aluminum spheres—166(A)
Betchov, R. Non-linear cooling of the hot-wire anemometer—879(A)
Beth, R. A. (see Janofsky, R. F.)—1891(A)
Bethe, H. A. Fourth-order interaction between nucleosn in the pseudoscalar meson theory—191(A)
—— Scattering of neutrons and protons and the range of nuclear forces—161(T)
—— Theory of the effective range in nuclear scattering—38
——, **U. Fano, and P. R. Karr.** Penetration and diffusion of hard x-rays through thick barriers. I. The approach to spectral equilibrium—538
Beyer, Robert T. and Ming-Yi Wei. Extension of a theory of magnetic amplifiers—455(A)
Bianco, D., G. Matlack, and A. Roberts. Isotopic frequencies in the microwave spectra of OCS and CH_3Cl—473(A)
Bickford, L. R., Jr. Ferromagnetic resonance absorption magnetite—137(L)
Biehl, A. T., H. V. Neher, and W. C. Roesch. Cosmic-ray experiments at high altitudes over a wide range of latitudes —914
Binder, Daniel. Analysis of delayed coincidence counting experiments—856(L)
Biondi, Manfred A. and Sanborn C. Brown. Measurement of electron-ion recombination—169?
—— **and Sanborn C. Brown.** Measurements of electron-ion recombination in diatomic gases—457(A)
—— **and Sanborn C. Brown.** Measurements of positive ion-electron recombination—190(A)
—— **and Sanborn C. Brown.** Note on measurements of ambipolar diffusion in helium—302(L)
Birnbaum, George. Dispersion in NH_3 in the microwave region—178(A)
Bishop, A. S. (see Bradner, H.)—587(A)
——, **H. Bradner, and F. M. Smith.** Improved mass values of π^--, π^+-, and μ^+-mesons—588(A)
Bishop, G. R., C. H. Collie, H. Halban, and R. Wilson. Lower limit for the binding energy of the deuteron—683(L)
Bitondo, D. (see Patterson, G. N.)—881(A)
Bitter, F. Nuclear magnetic moments and hyperfine structure of the rubidium isotopes—150(L)
—— Optical detection of radiofrequency resonance—465(A), 833
Bjorklund, Russell (see York, Herbert F.)—187(A)
Black, Robert F. (see Duckworth, Henry E.)—462(A)
Blatt, John M. and J. David Jackson. On the interpretation of neutron-proton scattering data by the Schwinger variational method—18
Blau, M., M. M. Block, and J. E. Nafe. Heavy particles in cosmic-ray stars—860(L)
Bleakney, W. Experimental study of the interaction of shock waves—875(T)
—— (see Fletcher, C. H.)—881(A)
——, **C. H. Fletcher, and D. K. Weimer.** Density field in Mach reflection of shock waves—323(L)
Bleaney, B. and D. J. E. Ingram. Hyperfine structure of the paramagnetic resonance spectrum of cobalt—466(A)
Bless, A. A. (see Ellioff, R.)—200(A)
Bleuler, E. (see Seidlitz, L.)—453(A), 861(L)
Blevin, W. R. (see Somerville, J. M.)—982(L)

Blewitt, T. H. and J. S. Koehler. Increase in the resistivity of ordered $AuCu_3$ produced by single slip—470(A)
Bloch, F. and David H. Garber. Nuclear induction proton signals below noise level from gases at one atmosphere—585(A)
Block, M. M. (see Blau, M.)—860(L)
Blosser, D. R. (see Weidner, R. T.)—1727(L)
Blunt, R. F. (see Love, W. F.)—305(L)
—— **and W. F. Love.** Dielectric properties of barium titanate at low temperatures—1202
Bockelman, C. K. (see Adair, R. K.)—308(L), 463(A)
—— (see Barschall, H. H.)—1146
——, **R. E. Peterson, R. K. Adair, and H. H. Barschall.** Total cross-section measurements for fast neutrons—277
Bockstahler, Lester I. and Harmon Plumb. Large diameter "Hilsch tubes"—166(A)
Bode, Donald and Henry Levinstein. Photo-conductivity of indium selenide—179(A)
Bogdonoff, S. M. (see Lees, L.)—875(T)
Bøggild, J. K., L. Minnhagen, and O. B. Nielsen. Cloud-chamber study of fission fragment ranges in air—988(L)
Bohlman, P. G. (see Bondelid, R. O.)—865(L)
Bohm, D., M. Weinstein, and H. Kouts. Finite relativistic charge-current distributions—867(L)
Bondelid, R. O., P. G. Bohlman, and K. B. Mather. Proton-proton scattering at 5.11 Mev—865(L)
Bonner, Norman A. and William C. Orr. Yields of manganese in spallation reactions—140(L)
Bonner, T. W. (see Phillips, G. C.)—169(A)
Borowitz, Sidney and Walter Kohn. On the electromagnetic properties of nucleons—818
Bortner, E. E. Portable vacuum tube electrometer of wide utility—197(A)
Bouchez, R. (see Benoist, P.)—1000(L)
Bouricius, G. M. B. (see Bender, R. S.)—273
Bousser, F. (see Leprince-Ringuet, L.)—1273(L)
Bowe, J. C. and Gertrude Scharff-Goldhaber. Decay scheme of Te^{125m}—437(L)
Bowen, Dwain. Theory of the electric resistivity of polycrystalline graphite—1878(L)
Bowers, W. A. On the rate of energy loss of protons and deuterons—196(A)
—— On the vibrational spectrum of crystals—467(A)
Boyd, J. E. and Catherine Yoe. Effects of meteorological conditions on microwave propagation at 3, 10, and 25 cm—203(A)
Bozorth, R. M. (see Mason, W. P.)—470(A)
Braden, C. H. (see Shull, F. B.)—453(A)
Bradner, H. (see Bishop, A. S.)—588(A)
——, **A. S. Bishop, and W. H. Barkas.** Range-energy relations for high energy protons in photographic emulsions—587(A)
Bradt, H. L. (see Kaplon, M. F.)—1735(L)
—— **and B. Peters.** Flux of heavy nuclei of the primary cosmic radiation at geomagnetic latitudes $\lambda=55°$ and $\lambda=30°$—156(L)
Bragg, J. K. (see Sharbaugh, A. H.)—1419(L), 1529(L)
Braithwaite, J. W. and J. L. Frame. Some aspects of air flow at Mach No. 7 as observed in the University of Minnesota Aeronautical Laboratory—883(A)
Brattain, W. H. (see Shockley, W.)—459(A)
Bray, Ralph. Dependence of resistivity of germanium on electric field—152(L)
—— Electron injection in *P*-type germanium—458(A)
—— (see Fan, H. Y.)—458(A)
Breit, G. and G. E. Brown. Perturbation methods for Dirac radial equations—1307
——, **G. E. Brown, and G. B. Arfken.** Effect of nuclear motion on the hyperfine structure of hydrogen—1299
Britten, Roy. Highly excited states of the magnesium nucleus created by proton bombardment—169(A)
Brode, Robert B. Positive excess in the mesotron spectrum—468(A)
Brolley, John E., Jr., M. B. Sampson, and Allan C. G. Mitchell. Energy levels of Si^{30}—624
Brossel, Jean. Hyperfine structure of Fe^{57}—858(L)
Brown, C. Bradner. Magnetically biased transistors—1736(L)
Brown, G. E. (see Breit, G.)—1299, 1307
—— **and G. B. Arfken.** Effects of the proton radius on nuclear motion correction for the hyperfine structure of hydrogen—1305
Brown, H. (see Perez-Mendez, V.)—689(L)
Brown, Harrison and Edward Goldberg. New determination of the relative abundance of rhenium in nature—1260(L)
Brown, J. R. (see Lind, David A.)—591(A), 1838
Brown, J. S., G. M. Farrior, and Arthur Waltner. Photomultiplier detector for x-ray spectrometer—196(A)
Brown, R. H. Study of ions formed in a Hg resonance cell containing N_2—591(A)
Brown, Sanborn C. Studies of electrons in gases by high frequency techniques—453(T)
—— (see Biondi, Manfred A.)—190(A), 302(L), 457(A), 1697
—— (see Everhart, Edgar)—839
—— (see Lax, Benjamin)—457(A)
—— (see MacDonald, A. D.)—1634
—— (see Varnerin, Lawrence J., Jr.)—457(A)
—— **and A. D. MacDonald.** Limits for the diffusion theory of high frequency gas discharge breakdown—1629
Brown, Vinton A. and F. L. Yost. Universal low frequency modulation technique—201(A)
Brown, W. W. (see Palmatier, E. D.)—196(A)
—— **and A. S. McKay.** Cloud-chamber study of extensive air showers at 3260 meters elevation—1034
——, **A. S. McKay, and E. D. Palmatier.** On the knock-on secondaries of penetrating particles—506
Brubaker, Wilson M. Potential and gradient distributions in parallel plane diodes at currents below space charge limited values—592(A)
Brueckner, K. A. and M. L. Goldberger. Excess of negative over positive mesons produced by high energy photons—1725(L)
Brunauer, Stephen (see Maxwell, Louis R.)—175(A), 459(A)
Brunings, Johanna H. M. (see Bergmann, Peter G.)—191(A)
Brunton, D. C. Division of nuclear charge in fission—1798
—— **and W. B. Thompson.** Energy distribution of fission fragments from Pu^{239}—848(L)
Buchanan, J. O. (see Davison, P. W.)—890
Buchdahl, H. A. Temperature equilibrium in a stationary gravitational field—427(L)
Buck, W. L. (see Becker, R. A.)—1406(L)
Buechner, W. W. (see Strait, E. N.)—1766
—— **and E. N. Strait.** Excited state in Be^{10}—168(A)
—— **and E. N. Strait.** Magnetic analysis of $Be^9(d,\alpha)Li^7$ and $Be^9(d,p)Be^{10}$ reactions—1547
——, **E. N. Strait, A. Sperduto, and R. Malm.** Magnetic analysis of the $C^{12}(d,p)C^{13}$ and $O^{16}(d,p)O^{17}$ reactions—1543
Bugosh, John (see Yeager, Ernest)—1890(A)
——, **Ernest Yeager, and Frank Hovorka.** High frequency barium titanate hydrophone—1890(A)
——, **Ernest Yeager, and Frank Hovorka.** High frequency electroacoustic effect and its utilization in the construction of hydrophones—1891(A)
Bulloch, W. D. On the attenuation of sunlight in natural bodies of water—201(A)
Bundy, F. P. (see Strong, H. M.)—458(A)
—— **and H. M. Strong.** Measurement of temperatures in complex flame structures by high resolution spectroscopy of the sodium *D*-lines, I.—457(A)
Burgess, H. (see Smoluchowski, R.)—309(L)
Burgess, John S. Frequency ν_2 in the infra-red spectrum of CH_4—302(L)

—— Note on the infra-red spectra of the deutero-ammonias —1267(L)
Burgy, M. T. (see Hughes, D. J.)—463(A), 1413(L)
——, **D. J. Hughes, and W. E. Woolf.** Neutron transmission and polarization measurements with an iron single crystal —188(A)
Burkhart, L. E. (see Peed, W. F.)—143(L)
Burkheimer, G. E. Flow characteristics during the starting and stopping of a supersonic wind tunnel—880(A)
Burkig, J. W. and J. Reginald Richardson. Proton induced activities in tantalum—586(A)
Burnight, T. R. Soft x-radiation in the upper atmosphere—165(A)
Burns, G. Preston. Equation of the magnetic threshold curve of a superconductor—999(L)
Burstein, Elias (see Schulman, J. H.)—178(A)
—— **and J. J. Oberly.** Infra-red color center bands in the alkali halides—1254(L)
—— **and Paul L. Smith.** Thermo-optic properties of cubic crystals—175(A)
Burwell, J. T. and C. D. Strang. Influence of molecular structure of lubricant on the variation of incremental friction coefficient with speed—455(A)
Byatt, W. J., F. T. Rogers, and A. W. Waltner. On the beta-spectrum of tritium—199(A)

Caldwell, R. L., E. der Mateosian, and M. Goldhaber. Transition energies of some nuclear isomers—187(A)
Calkin, J. W. Elaboration of the Schrödinger formalism with applications to nuclear physics—846(L)
Callen, Herbert B. Electric breakdown in ionic crystals—1394
Campbell, Edward C. and Wilfred M. Good. Neutron-induced short life activities—195(A)
Cannon, C. V. and G. H. Jenks. Micro-calorimeter suitable for study of easily absorbed nuclear radiations—455(A)
Cardwell, Alvin B. Photoelectric and thermionic properties of nickel—125
Carmichael, G. (see Linz, A., Jr.)—202(A)
—— (see Scherrer, V. E.)—202(A)
—— (see Varwig, R. L.)—201(A)
Carpenter, R. O'B. Dynamic measurement of electro-optic coefficients in ADP crystals—467(A)
Carson, A. (see Curtiss, L. F.)—1412(L)
Carter, R. E. (see Koch, H. W.)—172(A)
Carter, W. C. Supersonic flow with vorticity about a slightly yawing body of revolution—878(A)
—— (see Bennett, F. D.)—880(A)
Carter, W. W. Measurement of f values in the iron spectrum with applications to solar and stellar atmospheres—962
Case, K. M. Equivalence theorems for meson-nucleon couplings—14
—— On nucleon moments and the neutron-electron interaction—1
Cassidy, J. M. (see Bell, P. R.)—183(A), 574(L)
Castillejo, L. and H. T. Richardson. Neutron-proton and proton-proton cross sections at 83 Mev—1732(L)
Castle, J. G., Jr. (see Beringer, Robert)—868(L)
Caswell, D. A. (see Becker, G. E.)—587(A)
Chambers, William H. and Dudley Williams. Nuclear gyromagnetic ratios—461(A)
—— **and Dudley Williams.** Nuclear gyromagnetic ratios II —638
Chandrasekhar, S. Development of Heisenberg's theory of the decay of isotropic turbulence—875(T)
—— On the decay of isotropic turbulence—158(L)
Chang, C. S. Wang and D. L. Falkoff. On the continuous gamma-radiation accompanying the beta-decay of nuclei —365
Chang, H. P. (see Chao, K. T.)—970
Chang, W. Y. Further experiments on sea-level mesons stopped at thin Pb foils—170(A)
Chao, C. Y., C. C. Lauritsen, and A. V. Tollestrup. Q value for $B^{10}(p\alpha)Be^{7}$—586(A)
——, **T. Lauritsen, and V. K. Rasmussen.** High energy gamma-radiation from $Be^{9}+D^{2}$—582(L)
Chao, K. T. and H. P. Chang. Process of ionization in active nitrogen—970
Charpie, R. A., Kuan-Han Sun, B. Jennings, and J. F. Nechaj. On the delayed neutron emitter $_{7}N^{17}$—1255(L)
Chastel, R. and L. Vigneron. On the tripartition and quadripartition of uranium nuclei—870(L)
Chatterjee, G. P. and S. S. Sidhu. X-ray diffraction study of the gold-beryllium alloy system—175(A)
Chessin, Hyman (see Yeager, Ernest)—1890(A)
Christy, R. F. Interpretation of recent experiments with protons on lithium—161(T)
Chubb, Talbot. Apparatus for the study of the Philips gauge discharge—198(A)
Chynoweth, A. G. Removal of space charge in diamond crystal counters—310(L)
Clapp, R. E. Binding energy of the triton—873(L)
Clark, J. S., W. W. Drake, and C. Y. Tsao. Magnetic measurements on the M. I. T. 300-Mev electron synchrotron—162(A)
Clarke, R. L. and G. A. Bartholomew. Proton range-energy relation—146(L)
Clemence, G. H. Primary time standards in astronomy—161(T)
Clementel, E. (see Bassi, P.)—854(L)
Clifford, J. (see Tochilin, E.)—590(A)
Clippinger, R. F. and J. H. Giese. Numerical computation of three-dimensional supersonic flows with vorticity—878(A)
Cocconi, Giuseppe. Meson background in penetrating shower experiments—984(L)
—— **and V. Cocconi Tongiorgi.** Angular distribution and multiplicity of neutrons associated with local cosmic-ray showers—318(L)
——, **V. Cocconi Tongiorgi, and K. Greisen.** Lateral structure of cosmic-ray air showers—1020
——, **V. Cocconi Tongiorgi, and K. Greisen.** Structure of the extensive cosmic-ray showers—192(A)
Cockroft, A. L. (see Curran, S. C.)—853(L)
Coggeshall, Norman D. Hydrogen bonding and isomeric forms in bis-phenols—174(A)
Cohen, B. (see Thomas, J. E., Jr.)—162(A)
Cohen, Marvin S. (see Kinnamon, R. C.)—198(A)
—— **and Clyde B. Crawley.** Critical damping and time of return of a galvanometer coil—198(A)
Cohen, Victor W. (see Knight, W. D.)—1421(L)
——, **W. S. Koski, and T. Wentink, Jr.** Nuclear spin and quadrupole coupling of S^{35}—703(L)
Coles, D. K. and R. H. Hughes. Microwave spectra of nitrous oxide—178(A)
—— **and R. H. Hughes.** Microwave spectrum of CF_3Cl—858(L)
Collie, C. H. (see Bishop, G. R.)—683(L)
Compaan, K. (see van Kranendonk, J.)—998(L), 1728(L)
Condon, E. U. Development of American physics—452(T)
—— **and E. Maxwell.** Investigation of the attractive forces between the persistent currents in a superconductor and the lattice—578(L)
Conforto, A. M. (see Sard, R. D.)—1134
Conner, C. H. (see Yagoda, Herman)—171(A)
Conversi, Marcello. Altitude dependence of mesons of energy between 224 and 255 Mev—849(L)
—— Altitude dependence of penetrating particles slowed down after traversing 15 cm of lead—851(L)——Erratum—1541(L)
—— Latitude dependence at 30,000 feet of penetrating particles slowed down after traversing 15 cm of lead—444(L)
—— Positive excess of mesons at 30,000 feet—311(L)

Cook, C. Sharp (see Goddard, C. Harold)—1419(L)
—— (see Owen, George E.)—1536(L), 1726(L)
—— (see Ter-Pogossian, Michel)—909
—— **and George E. Owen.** Instrumental errors in the shape of beta-spectra—183(A)
Cool, R. L. (see Fowler, E. C.)—171(A)
——, **E. C. Fowler, and J. C. Street.** Examples of meson production and absorption—468(A)
Coon, J. H. and R. F. Taschek. Interaction of 14-Mev neutrons with deuterons—710
Cooper, D. (see Wagner, Norbert)—449(L)
Cooper, Eugene P. On the theory of the establishment of flow in water entry—592(A)
Corak, W. S. (see Wexler, A.)—432(L)
Corben, H. C. Internal coordinates of a particle—460(A)
—— Transformation theory of thermodynamics—166(A)
Cork, J. M., H. B. Keller, W. C. Rutledge, and A. E. Stoddard. Radioactive lanthanum 140—1886(L)
——, **H. B. Keller, and A. E. Stoddard.** Neutron induced radioactivities in V^{52}, Mo^{99}, and W^{135}—575(L)
——, **H. B. Keller, and A. E. Stoddard.** Radioactivity in holmium 166, thulium 170, and lutecium 177—986(L)
Corrsin, Stanley (see Kovasznay, Leslie S. G.)—1263(L)
Corson, Dale R. (see McDaniel, Boyce D.)—162(A)
——, **C. P. Baker, J. W. DeWire, B. D. McDaniel, C. D. Swartz, R. L. Walker, R. R. Wilson, and W. M. Woodward.** Initial performance of the Cornell synchrotron—162(A)
Cortini, G. (see Bernardini, G.)—1792
Cowan, C. E. (see DeBenedetti, S.)—440(L)
Cranberg, L. and J. Halpern. Conversion electrons of RaD—187(A)
Crawford, B. L. Vibrational spectrum of the ethylene molecule—161(T)
Crawford, F. H. Jacobian thermodynamics—456(A)
Crawford, G. W. and F. T. Rogers, Jr. Generalized theory for the string galvanometer—199(A)
Crawford, M. F. (see Schawlow, A. L.)—174(A), 1876(L)
—— (see Welsh, H. L.)—580(L)
——, **F. M. Kelly, A. L. Schawlow, and W. M. Gray.** Nuclear moments of Mg^{25}—1527(L)
—— **and N. Olson.** Nuclear moments of $_{39}Y^{89}$—1528(L)
—— **and A. L. Schawlow.** Electron-nuclear potential fields from hyperfine structure—1310
Crawley, Clyde B. (see Cohen, Marvin S.)—198(A)
—— (see Kinnamon, R. C.)—198(A)
—— (see Ritchie, R. H.)—197(A)
Creagan, Robert J. Particle groups from the alpha-particle bombardment of boron—1769
Creutz, E. Shielding material for high energy accelerators—162(A)
—— (see Falk, C. E.)—322(L)
Creveling, L. G., J. R. Hood, and M. L. Pool. Delayed neutrons from thorium—946
Critchfield, C. L. Scattering of protons by helium 4—161(T)
—— **and D. C. Dodder.** Phase shifts in proton-alpha-scattering—602
Crittenden, E. C., Jr. (see Olsen, Leonard O.)—1891(A)
Crooker, A. M. Infra-red studies with the Perkin-Elmer spectrometer—592(A)
Crouch, M. F. (see Sard, R. D.)—1134
Crown, J. C. Flow of a gas characterized by the Beattie-Bridgman equation of state and variable specific heats: Part I. Isentropic flows—882(A)
Curran, S. C., J. Angus, and A. L. Cockroft. Beta-spectrum of tritium—853(L)
Curtiss, Charles F. and Joseph O. Hirschfelder. Thermodynamics of flow systems—883(A)
Curtiss, L. F. and A. Carson. Reproducibility of photoneutron standards—1412(L)
Dailey, B. P. (see Townes, C. H.)—472(A), 700(L)
——, **J. M. Mays, and C. H. Townes.** Microwave rotational spectra and structures of GeH_3Cl, SiH_3Cl, and CH_3Cl—136(L)
——, **J. M. Mays, and C. H. Townes.** Molecular structure and dipole moment of chlorosilane—472(A)
Dancoff, S. M. (see Axel, P.)—892
—— (see Kubitschek, H. E.)—182(A), 531
—— **and S. D. Drell.** Electrostatic scattering of neutrons—205
Darden, Edgar B. (see Stuhlman, Otto, Jr.)—197(A)
—— **and Otto Stuhlman, Jr.** Precision method for measuring bioelectric potentials—197(A)
Darling, B. T. (see Garvey, J. E.)—184(A)
Darrow, K. K. Recent years of the American Physical Society—452(T)
Daudel, P. (see Benoist, P.)—1000(L)
Daudel, R. (see Benoist, P.)—1000(L)
Daunt, J. G. (see Heer, C. V.)—854(L)
—— **and C. V. Heer.** Addendum: heat flow in metals below 1°K and a new method for magnetic cooling—985(L)
—— **and C. V. Heer.** Some properties of superconductors below 1°K. I. Titanium—715
—— **and C. V. Heer.** Some properties of superconductors below 1°K. II. Aluminum and zinc—1324
Davis, Luther, Jr. Nuclear spin and magnetic moment of Cs^{137}—435(L)
——, **Bernard T. Feld, Carrol W. Zabel, and Jerrold R. Zacharias.** Hyperfine structure and nuclear moments of the stable chlorine isotopes—1076
——, **Darragh E. Nagle, and Jerrold R. Zacharias.** Atomic beam magnetic resonance experiments with radioactive elements Na^{22}, K^{40}, Cs^{135}, and Cs^{137}—1068
Davis, R. H. (see Tochilin, E.)—590(A)
—— **and J. D. Graves.** Energy dependence of several organic and inorganic counters—590(A)
Davison, P. W., J. O. Buchanan, and Ernest Pollard. Proton groups from the bombardment of argon by deuterons—890
Daykin, P. N. (see Mann, K. C.)—1719(L)
DeBenedetti, S., C. E. Cowan, and W. R. Konneker. Angular distribution of annihilation radiation—440(L)
de Boer, J. Statistical mechanics of mixtures of He^3 and He^4—852(L)
—— (see van Kranendonk, J.)—998(L), 1728(L)
de Broglie, Louis. On a new conception of the interaction between charges and electromagnetic field—862(L)
de Carvalho, Hervasio G. Stopping power of nuclear emulsions for ionizing particles—1729(L)
de Fériet, J. Kampé. Spectral tensor of a homogeneous turbulence—875(T)
DeJuren, J., N. Knable, and B. Moyer. Nuclear cross sections for 95- and 270-Mev neutrons (measured with bismuth fission chambers)—589(A)
Delaney, C. F. G. (see Poole, J. H. J.)—1253(L)
de Launay, Jules (see Dolecek, R. L.)—445(L)
Deloume, Fernand E. and John R. Holmes. Source of highly forbidden lines in CdI—174(A)
Denis, P. M. (see Bene, G. J.)—1255(L)
der Mateosian, E. (see Caldwell, R. L.)—187(A)
—— **and M. Goldhaber.** Nuclear isomers produced by slow neutron capture—187(A)
Deutsch, Martin (see Fluharty, R. G.)—182(A)
—— (see Metzger, Franz)—187(A)
—— (see Shearer, James W.)—462(A)
—— (see Siegbahn, Kai)—1263(L)
—— **and Donald T. Stevenson.** Nuclear lifetime for quadrupole transition in Cd^{111}—184(A)
Dewan, J. T. and K. W. Allen. Ternary fission in uranium—181(A)
DeWire, John W. (see Corson, D. R.)—162(A)
—— (see McDaniel, Boyce D.)—162(A)

Dexter, David L. and W. W. Beeman. Multiple diffuse small angle scattering of x-rays—1782
Dickey, Fred P. (see Lagemann, Robert T.)—159(L)
Dickey, J. (see Apker, L.)—270, 453(T)
Dickinson, W. C. Magnetic moment of La^{139}—1414(L)
Dieke, G. H. Bands from doubly excited levels of the hydrogen molecule—50
—— **and F. S. Tomkins.** Molecular spectrum of hydrogen. The Fulcher bands of TH and T_2—283
Diven, B. C. (see Hanson, A. O.)—578(L)
Dodder, D. C. Double scattering of protons in helium—683(L)
—— (see Critchfield, C. L.)—602
Dolecek, R. L. and Jules de Launay. Superconducting torus—445(L)
Domenicali, C. A. Magnetic and electric properties of magnetite single crystals—460(A)
Douglas, A. E. and G. Herzberg. Nuclear spin of He^3—1529(L)
Dow, W. G. Ionospheric measurements employing a voltage-scanning probe—453(T)
—— (see Reifman, A.)—987(L)
Drake, W. W. (see Clark, J. S.)—162(A)
Drell, S. D. Anomalous magnetic moments of nucleons—427(L)
—— (see Dancoff, S. M.)—205
Drosd, Ralph D. (see Liddiard, Thomas P.)—879(A)
Drost-Hansen, W. (see Koch, J.)—279
Drukey, D. L. Radiation from a uniformly accelerated charge—543
Duckworth, Henry E. New measurement of the Pt^{195}-Cu^{65} packing fraction difference—690(L)
——, **Robert F. Black, and Richard F. Woodcock.** Search for some rare stable isotopes—462(A)
Duffendack, O. S. (see Fowler, R. G.)—81
Duffield, R. B. (see Hanson, A. O.)—578(L)
—— **and J. D. Knight.** Radioactivity of Mo^{91} and Mo^{93}—573(L)
—— **and L. M. Langer.** Disintegrations of Sn^{121} and Sn^{123}—1272(L)
DuMond, Jesse W. M. (see Lind, David A.)—591(A), 1838
Duncan, D. B. Magnetic analyzer for electrostatic generators—587(A)
Dunipace, Donald W. Solar position calculator—464(A)
du Pré, F. K. (see Rittner, E. S.)—996(L)
Dyer, R. M. (see Finston, H. L.)—465(A)
Dyson, F. J. Recent developments in the quantum theory of fields—162(T)

Eber, G. R. Measurement of temperature recovery factors and heat transfer coefficients on cones at supersonic speeds in the 40 by 40 cm^2 White Oak wind tunnel—879(A)
Eckart, G. (see Kahan, T.)—406
Edgell, W. F. (see Roberts, A.)—178(A)
Edwards, H. D. (see Gilliam, O. R.)—195(A)
——, **O. R. Gilliam, and W. Gordy.** Microwave spectrum of methyl alcohol and of methyl amine—196(A)
Eichholz, G. G. and N. J. Harrick. Absorption of alpha-particles in gases—589(A)
Einbinder, Harvey. Further deductions from the $\mathfrak{N}$-theorem—410
Eisenbud, L. Distributions from resonance reactions and angular correlation experiments—185(A)
Ekstein, H. Magnetic interaction between neutrons and electrons—1328
Elder, F. R. (see Westendorp, W. F.)—445(L)
Ellioff, R. and A. A. Bless. Electrical energy of seeds at various stages of growth—200(A)
Elliott, L. G. and R. E. Bell. Lifetime of the 479-kev excited state of Li^7—168(A)
Elliott, Norman. Magnetic susceptibilities of some tetravalent uranium fluorides—431(L)
Elsasser, W. M. and I. Isenberg. Electronic phase transition in iron at extreme pressures—469(A)
Emmerich, Werner S., L. H. Ballweg, and J. D. Kurbatov. Monochromatic electron groups in long-life manganese—1891(A)
—— **and J. D. Kurbatov.** Beta-spectrum of silver-110—454(A)
Epstein, P. S. Aerothermodynamics of sound waves—875(T)
Erdman, K. L., G. T. Kokotailo, and D. B. Scott. Positive particles associated with beta-ray emitters—1262(L)
Erickson, K. W. (see Allred, J. C.)—1430
—— (see Stovall, E. J., Jr.)—589(A)
——, **J. L. Fowler, and E. J. Stovall, Jr.** Cross section as a function of angle for the $D(d,n)He^3$ reaction for 10-Mev bombarding deuterons—1141
Errett, D., J. MacKay, R. Pepper, F. Rieke, D. Roller, and L. Silber. Microwave linear accelerator for electrons—180(A)
Evans, Lyle W. (see Schulman, James H.)—178(A), 459(A)
Everhart, Edgar and Sanborn C. Brown. Admittance of high frequency gas discharges—839
Extermann, R. C. (see Bene, G. J.)—1255(L)
Eyges, L. Straggling of electrons near the critical energy—264

Fagin, S. (see Rogers, M.)—884(A)
Fahy, Edward F. and Marcel Schein. "Off-scale" bursts under 26.7-cm lead at an altitude of 3500 meters—170(A)
Fairbank, Henry A. (see Reynolds, Charles A.)—64, 167(A)
—— (see Webber, Robert T.)—609
—— **and C. T. Lane.** Rollin film rates in liquid helium—1209
Fairbank, William M. High frequency surface resistivity of tin in the normal and superconducting states—1106
—— Surface resistance of superconducting tin at 9400 mc/sec.—167(A)
Falk, C. E., E. Creutz, and F. Seitz. Angular distribution of neutrons from (d,n) reactions—322(L)
Falkoff, David L. (see Chang, C. S. Wang)—365
—— (see Ling, Daniel S., Jr.)—431(L), 1639
Fan, H. Y. (see Becker, M.)—1530(L), 1531(L)
—— **and R. Bray.** Barrier layer on *P*-type germanium—458(A)
Fano, U. Penetration and diffusion of x-rays through thick barriers. II. Asymptotic behavior when pair production is important—739
—— (see Bethe, H. A.)—538
Farmer, E. C., H. B. Moore, and Clark Goodman. Studies on synthetic LiF as a scintillation detector of heavy particles and quanta—454(A)
Farrior, G. M. (see Brown, J. S.)—196(A)
Faul, Henry and Clark Goodman. Neutron distributions in cylindrical geometry—463(A)
Feenberg, Eugene. Notes on the *j-j* coupling shell model—1275
Feer, Daniel B. Polarization of mesons produced at threshold in gamma-nucleon collisions—306(L)
Feld, Bernard T. Angular correlations in successive $\alpha-\gamma$ emission and the excited state of Li^7—168(A)
—— (see Davis, Luther, Jr.)—1076
—— (see Osborne, L. S.)—468(A)
Feldman, David. On realistic field theories and the polarization of the vacuum—1369
Feldman, L. (see Wu, C. S.)—692(L), 693(L), 696(L), 698(L)
——, **L. Lidofsky, P. Macklin, and C. S. Wu.** Beta-spectrum of praeseodymium 143—1888(L)
—— **and C. S. Wu.** Improved baffle system for helical focusing β-ray spectrometer—180(A)
—— **and C. S. Wu.** Interpretation of beta-spectra from thick sources—697(L)
Feldmeier, J. R. (see Serin, B.)—167(A)
Fermi, E. and C. N. Yang. Are mesons elementary particles?—1739
Feshbach, Herman. Phenomenological theory of nuclear forces—185(A)

—— (see Lax, Melvin)—190(A)
—— **and Melvin Lax.** Production of mesons by photons and electrons—134——Erratum—689(L)
—— **and V. F. Weisskopf.** Schematic theory of nuclear cross sections—1550
Feynman, R. P. Recent advances in quantum electrodynamics—584(T)
—— Space-time approach to quantum electrodynamics—769
—— Theory of positrons—749
Filosofo, I. (see Bassi, P.)—854(L)
Finck, J. L. Thermodynamics: the meaning of the first law, and its relation to the behavior of material systems—166(A)
Finkelnburg, Wolfgang. Electron screening, electron quantum numbers, and ionization potentials of atoms and ions—173(A)
Finkelstein, R. (see Ruderman, M.)—1458
Finston, H. L. and R. M. Dyer. Ion exchange and chromatography—465(A)
Fleeman, J., D. B. Nicodemus, and H. H. Staub. Neutron polarization—1774
—— **and H. H. Staub.** Neutron polarization—586(A)
Fletcher, C. H. (see Bleakney, W.)—323(L)
—— **and W. Bleakney.** Reflection of a weak plane shock at nearly glancing incidence—881(A)
Fletcher, R. C. Impulse breakdown in the 10^{-9}-sec. range of air at atmospheric pressure—1501
Fluharty, R. G. and Martin Deutsch. Low emission probability gamma-rays—182(A)
Foldy, Leslie L. Single production of mesons by gamma-rays near threshold—372
—— (see Milford, F. J.)—468(A)
Foley, H. M. (see Townes, C. H.)—1415(L)
Forbes, Stephen H. (see Swann, W. F. G.)—467(A)
Forbush, S. E. and I. Lange. Search for systematic variations in cosmic-ray intensity predicted on the basis of a permanent solar magnetic moment—164(A)
Forgue, S, V. (see Rose, A.)—179(A)
Forman, Guy. Color produced in quartz by x-rays—196(A)
Forsbergh, P. W., Jr. Domain structures and phase transition in barium titanate—1187
Fowler, E. C. (see Cool, R. L.)—468(A)
——, **R. L. Cool, and J. C. Street.** Delayed proton-electron activity induced in aluminum by non-ionizing cosmic rays—171(A)
Fowler, J. L. (see Allred, J. C.)—1430
—— (see Erickson, K. W.)—1141
—— (see Stovall, E. J., Jr.)—589(A)
—— **and J. M. Slye.** $Cu^{63}(n,2n)Cu^{62}$ cross section as a function of neutron energy near the threshold—169(A)
Fowler, R. D. (see Andrews, D. H.)—154(L)
Fowler, R. G. and O. S. Duffendack. Radiative processes in thermionically controlled discharges in helium—81
Fowler, W. A. Nuclear spectroscopy—584(T)
—— (see Schardt, A. W.)—587(A)
—— (see Tollestrup, A. V.)—181(A), 428(L)
—— **and C. C. Lauritsen.** Gamma-radiation from light nuclei under proton bombardment—314(L)
——, **C. C. Lauritsen, and A. V. Tollestrup.** Investigations of the capture of protons and deuterons by deuterons—1767
Fowles, G. R. Hyperfine structure of Te^{125}—571(L)
Fox, R., C. Leith, K. McKenzie, and L. Wouters. Total cross sections of nuclei for 280-Mev neutrons—590(A)
Frame, J. L. (see Braithwaite, J. W.)—883(A)
Franzen, W., J. Halpern, and W. E. Stephens. Ionization measurement of $He^3(np)$ and $N^{14}(np)$ and the neutron hydrogen mass difference—317(L)
——, **J. Halpern, and W. E. Stephens.** Reactions $N^{14}(n,p)C^{14}$ and $He^3(n,p)H^3$ and the neutron-hydrogen mass difference—462(A)
Fraser, J. S. Disintegration scheme of Tm^{170}—1540(L)
Freier, G. (see Lampi, E. E.)—188(A)
Freistadt, Hans and Nathan Rosen. Field of a gravitational dipole—201(A)
Frenkiel, F. N. Erratum: influence of the length of a hot wire on the measurements of turbulence—686(L)
—— On a method of measurement of some characteristics of turbulence using non-compensated hot-wires—171(A)
—— On the hot-wire length correction—999(L)
—— Some remarks on turbulent diffusion—875(T)
Frerichs, Rudolf. On the conductivity produced in CdS crystals by irradiation with gamma-rays—1869
Fretter, W. B. Penetrating showers—511
—— (see Ise, John, Jr.)—933
Fritz, J. J., O. D. Gonzales, and H. L. Johnston. Magnetic moment and eddy current damping in spherical superconductors—580(L)
Frye, Royal M. (see Merritt, Thomas P.)—470(A)
Fulbright, H. W. and J. C. D. Milton. Beta-spectrum of Be^{10}—1271(L)
Fuller, Everett G. Photo-disintegration of deuterium by seven- to twenty-Mev x-rays—576(L)
Furry, W. H. (see Neuman, M.)—1677
—— (see Snyder, James N.)—359
—— **and M. Neuman.** Interaction of mesons with the electromagnetic field—432(L)
Fye, Paul M. and Robert S. Price. High speed photography of explosion bubbles at depths of one and two miles—881(A)

Gaerttner, E. R. and M. L. Yeater. Note on the resonance scattering of high energy γ-rays by nuclei of carbon and copper—363
Gamow, George. Astronomical, radioactive, and atomic time—161(T)
Garber, David H. (see Bloch, F.)—585(A)
Garbuny, M. (see Altar, W.)—496
Gardner, Clifford. Method for solving certain time-dependent problems for wings in supersonic flow, with an application to the calculation of stability derivatives—882(A)
Gardner, J. H. and E. M. Purcell. Precise determination of the proton magnetic moment in Bohr magnetons—1262(L)
Garfunkel, M. (see Serin, B.)—167(A)
Garvey, J. E. and B. T. Darling. ThC-C″ alpha-transition according to the water drop model of alpha-decay—184(A)
Garwin, Richard L. Experimental beta-gamma-angular correlation—1876(L)
Gebbie, H. A., W. R. Harding, C. Hilsum, and V. Roberts. Atmospheric HDO—1534(L)
Geiger, F. W. Shock tube as a tool for the investigation of flow phenomena—881(A)
Geiger, Felix E., Jr. Effect of finite aperture on the fringe intensity distribution of Fabry Perot interferometers—173(A)
Geiringer, Hilda. Two-dimensional problems of the ideal plastic body—875(A)
Genevese, Frank. Angular distribution of neutrons from the photo-disintegration of the deuteron—1288
George, Waller (see Kauffmann, John)—467(A)
—— (see LaTorre, Richard)—470(A)
Gerjuoy, Edward (see Halpern, Otto)—1117
Ghiorso, A. (see Thompson, S. G.)—1406(L)
——, **W. W. Meinke, and G. T. Seaborg.** New low mass isotopes of emanation (element 86)—1414(L)
Ghosh, Amal (see Siegbahn, Kai)—307(L)
Giamboni, Louis A. (see Barnett, S. J.)—1542(L)
Gião, Antonio. Equations of Codazzi and the relations between electromagnetism and gravitation—764
Gideon, D. (see Waldman, B.)—181(A)
Giese, J. H. (see Clippinger, R. F.)—878(A)
Gilbert, D. A., A. Roberts, and P. A. Griswold. Nuclear and molecular information from the microwave spectrum of FCl—1723(L)

Gilliam, O. R. (see Edwards, H. D.)—196(A)
—— (see Gordy, Walter)—443(L)
——, **H. D. Edwards, and W. Gordy.** Microwave spectrum of methyl fluoride, fluoroform, and phosphorus tri-fluoride—195(A)
Ginther, Robert J. (see Schulman, James H.)—178(A), 459(A)
Gittings, H. T. (see Argo, H. V.)—182(A)
Glass, I. I. (see Patterson, G. N.)—881(A)
Glauberman, M. H. (see Stoner, R. G.)—882(A)
Glendenin, L. E. and A. K. Solomon. Self-absorption and backscattering of soft beta-radiations—462(A)
Goddard, C. Harold (see Ter-Pogossian, Michel)—453(A), 909, 1407(L)
—— **and C. Sharp Cook.** On the photo-electron spectrum of Ta^{182}—1419(L)
Goeckermann, R. H. and I. Perlman. High energy induced fission of bismuth and lead—628
Goertzel, G. H. (see Rose, M. E.)—184(A), 1883(L)
Goldberg, Edward (see Brown, Harrison)—1260(L)
Goldberg, Leo (see McMath, Robert R.)—1533(L)
——, **Orren C. Mohler, Robert R. McMath, and A. Keith Pierce.** Carbon dioxide in the infra-red solar spectrum—1848
Goldberger, M. L. Recent theoretical work at the Radiation Laboratory—548(T)
—— (see Brueckner, K. A.)—1725(L)
Goldhaber, M. (see Caldwell, R. L.)—187(A)
—— (see der Mateosian, E.)—187(A)
—— (see Lowry, L. L.)—189(A)
—— (see Sunyar, A. W.)—189(A)
Goldin, A. S., G. B. Knight, P. A. Macklin, and R. L. Macklin. U-234 specific alpha-activity—336
Goldman, J. E. Magnetostriction and order in $FeNi_3$—471(A)
Goldstein, J. H. (see Westenberg, A. A.)—472(A)
Goldstein, Louis and Max Goldstein. On exchange energy in He_3 assemblies—464(A)
Goldstein, Max (see Goldstein, Louis)—464(A)
Gonzales, O. D. (see Fritz, J. J.)—580(L)
Good, W. B. (see Melchor, J. L.)—202(A)
Good, Wilfred M. (see Campbell, Edward C.)—195(A)
Goodman, Clark (see Farmer, E. C.)—454(A)
—— (see Faul, Henry)—463(A)
Gordy, Walter. Relation of nuclear quadrupole moment to nuclear shell structure—139(L)
—— (see Edwards, H. D.)—196(A)
—— (see Gilliam, O. R.)—195(A)
—— **and O. R. Gilliam.** Nuclear magnetic moments from microwave spectra: I^{127} and I^{129}—443(L)
Goudsmit, S. A. (see Richards, Paul I.)—180(A)
Goward, F. K. (see Titterton, E. W.)—142(L)
Grabner, Ludwig (see Hughes, Vernon)—471(A)
——, **Vernon Hughes, and I. I. Rabi.** Radiofrequency spectrum of $K^{39}F$—472(A)
Grad, Harold. On the kinetic theory of rarefied gases—882(A)
Graham, John W. Permanency of magnetism in sedimentary rocks—176(A)
Graves, E. R. and D. I. Meyer. End point of the tritium beta-ray spectrum—183(A)
Graves, J. D. (see Davis, R. H.)—590(A)
—— (see Koch, G. E.)—590(A)
—— **and G. E. Koch.** RCA 1P21 photo-multiplier tube as a gamma-ray detector—590(A)
Gray, W. M. (see Crawford, M. F.)—1527(L)
Green, Alex E. S. Future nuclear interaction—870(L)
—— Spin dependence of nuclear forces—460(A)
Green, L. L. and D. L. Livesey. Alpha-particles emitted in fission—580(L)
Greenwald, A. J. (see Bergdolt, V. E.)—879(A)
Gregory, Bernard (see Tinlot, John)—170(A)
Greisen, K. Interpretation of underground cosmic-ray data—1718(L)
—— (see Cocconi, G.)—192(A), 1020
Griffel, Maurice (see Stout, J. W.)—144(L)
Griswold, P. A. (see Gilbert, D. A.)—1723(L)
Grosskreutz, J. C. Neutrons from $C(d,n)N$ and $Cu(d,n)Zn$ 482
Grunlund, Jean M. (see Yaffe, L.)—617
Gugelot, P. C. and M. G. White. Neutron spectra from (p,n) reactions with 16-Mev protons—463(A)
Gum, Jane R., Lowell E. Thompson, and M. L. Pool. Silver and cadmium activities—184(A)
Gundlach, J. C. (see Jordan, W. H.)—196(A)
Gunlock, H. F. Radioactive materials as x-ray sources—453(A)
Gurevitch, M. and J. G. Teasdale. Nuclear spin of Fe^{57}—151(L)
Guth, Eugene (see Marshall, J. F.)—1879(L), 1880(L)
—— (see Mullin, C. J.)—682(L)
—— **and Charles J. Mullin.** Theory of the photo- and electro-disintegration of Be^9—234

Hahn, Erwin L. Accurate nuclear magnetic resonance method for measuring spin-lattice relaxation times—145(L)
—— Nutation of the nuclear magnetic moment—461(A)
Hainer, R. M. and Gilbert W. King. Infra-red spectrum of benzene at liquid-helium temperature—473(A)
Haisley, W. E. and Joseph W. Straley. High-speed spectrometer for Raman studies—200(A)
Halban, H. (see Bishop, G. R.)—683(L)
Hall, Newman A. Performance of multiple shock diffusers—884(A)
Halpern, I. (α,n) cross sections of beryllium, magnesium, and aluminum—248
—— (see Woodward, W. M.)—107
Halpern, J. (see Cranberg, L.)—187(A)
—— (see Franzen, W.)—317(L), 462(A)
Halpern, Otto. On magneto optics of neutrons and some related phenomena—1130
—— **and Edward Gerjuoy.** Small angle diffraction of neutrons and similar wave phenomena—1117
—— **and R. K. Luneberg.** Multiple scattering of neutrons. II. Diffusion in a plate of finite thickness—1811
Hamermesh, Bernard. Capture γ-ray spectrum of cadmium—182(A)
——, **M. Hamermesh, and A. Wattenberg.** Angular distribution of the photo-neutrons from beryllium—611
—— **and Albert Wattenberg.** Angular distribution of the photo-neutrons from deuterium at 2.76 Mev—1408(L)
—— **and Albert Wattenberg.** Photo-neutrons from neutron capture gamma-rays—1420(L)
Hamermesh, M. (see Hamermesh, B.)—611
Hanau, Richard. Cathode sputtering in the abnormal glow discharge—153(L)
Hanna, S. S. Excited state of Li^7 and the angular yield in $Li^6(d,p)Li^{7*}(\gamma)Li^7$—686(L)
—— (see Resnick, I.)—168(A)
Hansen, John L. and John E. Willard. Thermal neutron absorption cross section of K^{39}—577(L)
Hanson, A. O., R. B. Duffield, J. D. Knight, B. C. Diven, and H. Palevsky. Thresholds for photo-neutron reactions in Mn, Zn, Zr, Mo, Cd, Pr, Nd, Au, Hg, Tl, and Pb—578(L)
Hanson, Harold and W. W. Beeman. MnK absorption edge in manganese metal and manganese compounds—118
Hansson, Ingvar F. E. and Lamek Hulthén. Photo-disintegration of the deuteron—1163
Harding, W. R. (see Gebbie, H. A.)—1534(L)
Harkins, William D. Effect of nuclear shells upon the pattern of the atomic species—1538(L)
—— **and Martin Popelka, Jr.** Existence of stable nuclei as related to the principle of regularity and continuity of series and the ends of nuclear shells—989(L)
Harr, J. (see Rose, M. E.)—184(A), 1883(L)

Harrick, N. J. (see Eichholz, G. G.)—589(A)
Harris, G. G. (see White, L. D.)—468(A)
Harris, Louis and Lloyd H. Shaffer. Conduction processes in thin deposits of antimony—943
Harris, S. and C. O. Muehlhause. Neutron resonance scattering by W^{186}—189(A)
Harrison, F. B. (see Reynolds, George T.)—169(A)
—— **and George T. Reynolds.** Uniformity of response of a scintillation counter—169(A)
Harrison, S. W. (see Hutter, R. G. E.)—453(T)
Haslam, R. N. H., L. Katz, H. E. Johns, and H. J. Moody. Confirmation of Cl^{39} activity—704(L)
Havens, W. W., Jr. (see Ruderman, I. W.)—434(L)
Haynie, William H. Adjustable mounting for large mirrors—1891(A)
Hays, Earl E. (see Richards, Paul I.)—180(A)
Head, R. Wind tunnel investigation of condensation phenomena—882(A)
Hedgran, Arne (see Siegbahn, Kai)—1263(L)
—— (see Thulin, Sigvard)—871(L)
Heer, C. V. (see Daunt, J. G.)—715, 985(L), 1324
—— **and J. G. Daunt.** Heat flow in metals below 1°K and a new method for magnetic cooling—854(L)
Hemmendinger, A. (see Argo, H. V.)—182(A)
—— (see Jarvis, G. A.)—168(A)
—— (see Taschek, R. F.)—325
——, **G. A. Jarvis, and R. F. Taschek.** Scattering of protons by tritons—1137
Henderson, Joseph E. (see Miller, Charles E.)—165(A), 591(A)
—— (see Potter, D. S.)—590(A)
—— (see Todd, Jay, Jr.)—591(A)
Henkel, R. L. (see Adair, R. K.)—463(A)
Henkels, Herbert W. Properties of single crystal selenium prepared from a melt—1737(L)
Henri, V. P. (see Thomas, J. E., Jr.)—162(A)
Henry, Hugh F. (see Pryor, W. A.)—199(A)
—— (see Young, R. L.)—198(A)
Herb, R. G. Proton-proton scattering—161(T)
Hereford, Frank L. Nature of the penetrating particles in extensive showers—171(A)
—— On the penetrating component of cosmic-ray air showers—142(L)
—— (see Pomerantz, Martin A.)—997(L)
—— **and C. P. Swann.** Penetration of high energy electrons in aluminum—570(L)
Herlin, Melvin A. (see Maurer, R. D.)—948
Hernqvist, K. G. (see Linder, E. G.)—453(T)
Herzberg, G. Where we stand in repsect to spectra of diatomic molecules—161(T)
—— (see Douglas, A. E.)—1529(L)
Herzfeld, K. F. Effect of relaxation on shock waves in gases—875(T)
Herzog, R. F. K. and F. P. Viehböck. Ion source for mass spectrography—855(L)
Hess, David C., Jr. (see Inghram, Mark G.)—1717(L)
—— **and Mark G. Inghram.** Slow neutron cross sections of the neodymium isotopes—300(L)
—— **and Mark G. Inghram.** On the occurrence of vanadium 50 in nature—1717(L)
Hess, Victor F. and Roger P. Vancour. New methods of determining the absolute intensity of cosmic rays in the atmosphere and the residual ionization in ionization chambers—1205
Hibdon, C. T. and C. O. Muehlhause. Neutron cross section at 115 ev and 300 ev—188(A)
—— **and C. O. Muehlhause.** Neutron cross sections at 115 ev and 300 ev—I—100
Hicks, Bruce L. Non-linear problem in transient heat flow—166(A)
Hildebrand, R. H. and C. E. Leith. Total cross sections of nuclei for 40-Mev neutrons—587(A)
Hill, R. D. Internal conversion electrons from long-lived tellurium isomers—186(A)
—— Long-lived tellurium isomers—333
—— Nuclear quadrupole moments and shell structure—998(L)
Hilsum, C. (see Gebbie, H. A.)—1534(L)
Hinshaw, R. A. Radioactive tin 111—454(A)
—— **and M. L. Pool.** Radioactive tin 111—358
Hipple, J. A., H. Sommer, and H. A. Thomas. Precise method of determining the Faraday by magnetic resonance—1877(L)
Hirschfelder, Joseph O. Transport properties of gases—875(T)
—— (see Curtiss, Charles F.)—883(A)
Hoang-Tchang-Fong (see Leprince-Ringuet, L.)—1273(L)
Hoffman, R. W. (see Olsen, Leonard O.)—1891(A)
Hofstadter, Robert and John A. McIntyre. Experimental study of the Compton effect at 1.2 Mev—1269(L)
—— **and John A. McIntyre.** Simultaneity in the Compton effect—172(A)
Holden, A. N. (see Matthias, B. T.)—175(A)
Holmes, D. K. Calculations of the energy levels in elemental silicon—178(A)
Holmes, John R. (see Deloume, Fernand E.)—174(A)
Holstein, T. Self-broadening of monatomic resonance lines—457(A)
—— (see Alpert, D.)—457(A), 1257(L)
——, **D. Alpert, and A. O. McCoubrey.** Persistence of band fluorescence in mercury vapor—1259(L)
Holt, R. B., J. M. Richardson, B. Howland, and B. T. McClure. Recombination spectrum and electron density measurements in neon afterglows—456(A)
Hood, J. R. (see Creveling, L. G.)—946
Hopfield, Helen S. (see Hornbeck, George A.)—174(A)
Hornbeck, George A. and Helen S. Hopfield. Spectroscopic investigation of the carbon monoxide-oxygen reaction—174(A)
Hornbeck, J. A. Townsend discharge on a microsecond time-scale—453(T)
Hornbostel, J. and E. O. Salant. Energetic events in emulsions at high altitude—859(L)
—— **and E. O. Salant.** High energy events at high altitude—468(A)
Hornig, D. F. Selection rules for infra-red and Raman spectra of molecular crystals—161(T)
Hornyak, W. F. (see Rasmussen, V. K.)—581(L)
——, **T. Lauritsen, and V. K. Rasmussen.** Gamma-ray measurements with a magnetic lens spectrometer—731
Hough, P. V. C. Automatic grain counting of tracks in nuclear emulsions—163(A)
Houston, W. V. and C. F. Squire. Electromagnetic induction in a superconductor—685(L)
Hovorka, Frank (see Bugosh, John)—1890(A), 1891(A)
—— (see Yeager, Ernest)—1890(A)
Howard, Raydeen (see Smith, William V.)—473(A)
Howland, B. (see Holt, R. B.)—456(A)
Hsieh, Yu-Chang (see Slack, F. G.)—197(A)
Hu, Ning. On the treatment of quantum electrodynamics without eliminating the longitudinal field—391
Huang, Su-Shu. Elastic scattering of electrons by neutral hydrogen atoms by the variational method—477
—— New formulation of the variational principle for scattering problems—866(L)
—— Note on the variational method for the scattering problem—1878(L)
Hudson, Alvin M. (see Rosen, Louis)—181(A)
Hudspeth, Emmett L. (see Swann, Charles P.)—168(A)
—— **and Charles P. Swann.** Deuteron bombardment of boron isotopes—1150

—— **and Charles P. Swann.** Neutron spectrum from $N^{15}(d,n)$—464(A)
Huff, L. D. On the freezing of fresh water lakes—200(A)
Hughes, D. J. (see Burgy, Merle)—188(A)
—— (see Sherman, D. F.)—188(A)
—— **and M. T. Burgy.** Reflection and polarization of neutrons by magnetized mirrors—1413(L)
—— **and M. T. Burgy.** Reflection of neutrons from magnetized mirrors—463(A)
Hughes, Harold Kenneth. Rotational Stark spectrum of linear molecules—1675
Hughes, R. H. (see Coles, D. K.)—178(A), 858(L)
Hughes, Vernon. Experimental limit for the inequality of the electron and proton charges—474(A)
—— (see Grabner, Ludwig)—472(A)
——, **Ludwig Grabner, and I. I. Rabi.** Radiofrequency spectrum of $Rb^{85}F$ and $Rb^{87}F$—471(A)
Hulburt, E. O. Light of the night sky—453(T)
Hull, G. F., Sr. Early meetings of the American Physical Society—452(T)
Hulsizer, Robert I. Further results in the search for electrons in the primary cosmic radiation—164(A)
Hulthén, Lamek (see Hansson, Ingvar F. E.)—1163
Hume, J. N. P. (see Schawlow, A. L.)—1876(L)
Hunter, G. T. and H. T. Richards. Yield and angular distribution of the *D-D* neutrons—1445
Huntington, H. B. and Frederick Seitz. Energy for diffusion by direct interchange—1728(L)
Huntoon, R. D. and H. A. Thomas. Amplitude bridge for nuclear resonance detection—163(A)
Hurwitz, H., Jr. Note on the variational method for finding extrapolated endpoints—867(L)
Hutner, R. A. (see Rittner, E. S.)—996(L)
Hutter, R. G. E., L. H. McKee, and S. W. Harrison. Deflection defocusing in cathode-ray tubes and methods for correction—453(T)
Huus, Torben and C. B. Madsen. Proton stopping power of gold—323(L)

Inghram, Mark G. (see Hess, David C., Jr.)—300(L), 1717(L)
——, **David C. Hess, Jr. and John H. Reynolds.** On the relative yields of fission cesium isotopes—1717(L)
—— **and John H. Reynolds.** On the double beta-process—1265(L)
Inglis, D. R. (see Resnick, Robert)—1318
Ingram, D. J. E. (see Bleaney, B.)—466(A)
Ise, John, Jr. and W. B. Fretter. Extensive penetrating cosmic-ray showers—933
Isenberg, I. (see Elsasser, W. M.)—469(A)
Iskenderian, Haig P. Magnetic properties of ferromagnetic ferrite—175(A)
Ivey, Henry F. Cathode field in diodes under partial space-charge conditions—554
—— Thermionic electron emission from carbon—567(L)

Jackson, J. David (see Blatt, John M.)—18
Jackson, J. L. On the continuity of the first derivative in the Wigner-Eisenbud formalism—185(A)
—— (see Rose, M. E.)—1540(L)
Jacobs, S. J. and A. A. Klebra. New high speed frame camera—881(A)
Jacobsohn, B. A. Propagation rate of streamers in high pressure sparks—585(A)
James, Hubert M. Electronic states in perturbed periodic systems—1611
—— Energy bands and wave functions in periodic potentials—1602
Janofsky, R. F., M. Melamed, and R. A. Beth. Novel magnetostriction effect—1891(A)
Jarrell, Herman and Joseph W. Straley. Infra-red absorption spectrum of hydrogen telluride vapor from 3.8μ–5.5μ—199(A)
Jarvis, G. A. (see Argo, H. V.)—182(A)
—— (see Hemmendinger, A.)—1137
—— (see Taschek, R. F.)—325
——, **A. Hemmendinger, H. V. Argo, and R. F. Taschek.** Differential cross sections for the reaction $T^3(p,n)He^3$ from 1- to 2.5-Mev proton energies—168(A)
Jashemski, Stanley A. and W. C. Wineland. Magnetic effect of eddy currents induced in a conducting plane by the approach of a bar magnet—198(A)
Jastram, P. S. Measurement of probability-amplitude distributions—190(A)
Jauneau, L. (see Leprince-Ringuet, L.)—1273(L)
Jech, Č. Detection of radioactive atoms in the air with nuclear emulsions—1731(L)
Jen, C. K. Paschen-Back effect in NH_3 and N_2O microwave spectra—1494
—— Rotational magnetic moments of H_2O and HDO—471(A)
Jenkins, F. A. (see Tollestrup, A. V.)—181(A)
Jenkins, Fannie (see Spencer, L. V.)—462(A), 1885(L)
Jenkins, J. F., Jr. Zenith angle dependence of flux of the hard cosmic-ray component up to 36,000 feet—992(L)
Jenks, G. H. (see Cannon, C. V.)—455(A)
Jennings, B. (see Allen, A. J.)—188(A), 463(A)
—— (see Charpie, R. A.)—1255(L)
—— (see Shoupp, W. E.)—502
Jensen, Erling N. Radiations from Hf^{181}—958
——, **L. Jackson Laslett, and William W. Pratt.** Revaluation of the gamma-radiations from Co^{60} and Zn^{65}—430(L)
Jesse, William P. and John Sadauskis. Corrections to the range-energy curves for alpha-particles and protons—163(A)
Johns, H. E. (see Haslam, R. N. H.)—704(L)
Johnson, E. O. and L. Malter. Double-probe method for determination of electron temperatures in steady and time-varying gas discharges—1411(L)
Johnson, Gerald W. Temperature dependence of structure of thin silver films—588(A)
—— **and T. Watanabe.** Surface self-diffusion of silver on thin single crystals—588(A)
Johnson, M. H. and B. A. Lippmann. Motion in a constant magnetic field—828
—— **and B. A. Lippmann.** Note on wave functions in a magnetic field—184(A)
Johnson, W. E. and K. Lark-Horovitz. Neutron irradiated semiconductors—442(L)
Johnston, H, L. (see Fritz, J. J.)—580(L)
Jones, Ernest A. (see Kirby-Smith, J. S.)—200(A)
—— (see Parkinson, T. F.)—199(A)
—— (see Woltz, P. J. H.)—200(A)
——, **T. F. Parkinson, R. B. Murray, and J. S. Kirby-Smith.** Infra-red and Raman spectra of chlorine tri-fluoride—200(A)
Jones, J. G. (see Jones, M. W.)—581(L)
Jones, M. W. and J. G. Jones. Tidal effects in the *F* layer—581(L)
Jones, Stanley B. and R. Stephan White. Yield of negative π-mesons produced by high energy protons as a function of proton energy—588(A)
Jones, W. (see Shoupp, W. E.)—502
Jones, W. M. Determination of the half-life of carbon 14—885
Jordan, W. H. and J. C. Gundlach. Threefold coincidence counter—196(A)
Jungerman, J. and S. C. Wright. Kinetic energy release in fission of U^{238}, U^{235}, Th^{232}, and Bi^{209} by high energy neutrons—1112
Jurney, E. T. Coincidence and absorption investigation of the disintegration of Rh^{106}, Sb^{125}, and Pr^{142}—290

Kahan T. and G. Eckart. On the electromagnetic surface wave of Sommerfeld—406
Kamei, T. (see Murakawa, K.)—1721(L)
Kammer, E. W. and T. E. Pardue. Instrumentation for studying electric resistance changes of fine wires during elastic and plastic strains—202(A)
—— **and T. E. Pardue.** Results of electric resistance changes of fine wires during elastic and plastic strains—202(A)
Kaplan, J. (see Kash, S.)—584(A)
Kaplan, Nathan (see Yagoda, Herman)—171(A), 702(L)
Kaplon, M. F., B. Peters, and H. L. Bradt. Evidence for multiple meson and γ-ray production in cosmic-ray stars—1735(L)
Karplus, Robert and Norman M. Kroll. Fourth-order corrections in quantum electrodynamics and the magnetic moment of the electrons—846(L)
Karr, P. R. (see Bethe, H. A.)—538
—— **and J. C. Lamkin.** Penetration and diffusion of hard x-rays through thick barriers. III. Studies of spectral distributions—1843
Kash, S. and J. Kaplan. Forbidden oxygen lines in afterglows—584(A)
Kasha, Michael. Fluorescence and phosphorescence spectra of organic molecules—161(T)
Katz, L. (see Haslam, R. N. H.)—704(L)
Kauffman, John and Waller George. Model for the plastic flow of oriented Nylon fibers—467(A)
Kaufman, Bruria. Crystal statistics. II. Partition function evaluated by spinor analysis—1232
—— **and Lars Onsager.** Crystal statistics. III. Short-range order in a binary ising lattice—1244
Kaufmann, S. G. (see Bender, R. S.)—273
Kaylor, Hoyt M. (see Talley, R. M.)—201(A)
—— **and Alvin H. Nielsen.** Infra-red spectrum and molecular constants of deuterium fluoride—200(A)
Kê, T'ing-Sui. Analysis of the temperature coefficient of shear modulus of aluminum—579(L)
—— Anomalous internal friction associated with the precipitation of Cu in plastically deformed Al-Cu alloys—470(A)
Keepin, George R. and James H. Roberts. On the measurement of the energy of fast neutrons by photographic emulsions loaded with enriched Li^6—154(L)
Keim, C. P. Electromagnetic separation of the isotopes of mercury—1270(L)
Keller, H. B. (see Cork, J. M.)—575(L), 986(L), 1886(L)
Keller, Joseph M., Ernest Koenigsberg, and Arthur Paskin. Ring focus in a thin magnetic lens beta-ray spectrometer—454(A)
Kelly, E., C. Leith, and C. Wiegand. *N-P* scattering experiments at 280 Mev—589(A)
Kelly, F. M. (see Crawford, M. F.)—1527(L)
Kendall, J. M. Electrical analog for heat flow with varying parameters—879(A)
Kern, Bernard D., Allan C. G. Mitchell, and Daniel J. Zaffarano. Nuclear spectra of Sb^{125}, Te^{125*}, Cr^{51}, and I^{131}—94
Kerst, D. W. (see Price, G. A.)—182(A)
Ketelle, B. H. New radioactive isotopes of dysprosium—1256(L)
—— (see Bell, P. R.)—574(L)
—— **and G. W. Parker.** Sm^{151} beta-ray spectrum—1416(L)
Kienberger, C. A. Uranium 234 content of natural uranium and the specific alpha-activities of the isotopes—1561
Kilmister, C. W. Two-component wave equations—568(L)
Kimball, G. E. (see Weingarten, I. R.)—177(A)
King, Gilbert W. Empirical formula for the refractive indices of infra-red dispersing materials—473(A)
—— (see Hainer, R. M.)—473(A)
King, Ronold (see Tomiyasu, K.)—456(A)
Kingdon, K. H. Distribution in mass and charge of fission products—136(L)
Kinnamon, R. C., M. S. Cohen, and C. B. Crawley. Equivalent electrical circuit for a galvanometer—198(A)
Kirby-Smith, J. S. (see Jones, Ernest A.)—200(A)
—— **and E. A. Jones.** Raman spectrum of hydrogen fluoride—200(A)
Kirn, F. S. (see Becker, R. A.)—182(A), 1406(L)
Kirsch, M. (see Yaffe, L.)—617
Kissinger, C. W. (see Perlow, G. J.)—164(A)
——, **C. A. Schroeder, and G. J. Perlow.** Gamma-rays in the primary cosmic-radiation—164(A)
Kittel, Charles. Gyromagnetic ratios and splitting factors of ferromagnetic substances—176(A)
—— On the gyromagnetic ratio and spectroscopic splitting factor of ferromagnetic substances—743
—— Theory of the formation of powder patterns on ferromagnetic crystals—1527(L)
Klebra, A. A. (see Jacobs, S. J.)—881(A)
Klein, M. J. and L. Tisza. Theory of critical fluctuations—1861
Klick, Clifford C. (see Schulman, James H.)—459(A)
—— **and R. J. Maurer.** Mobility of electrons in diamond—179(A)
Knable, N. (see DeJuren, J.)—589(A)
Knight, G. B. (see Goldin, A. S.)—336
Knight, J. D. (see Duffield, R. B.)—573(L)
—— (see Hanson, A. O.)—578(L)
Knight, W. D. Nuclear magnetic resonance shift in metals—1259(L)
—— **and V. W. Cohen.** Nuclear gyromagnetic ratio of V^{51}—1421(L)
Koch, G. E. (see Graves, J. D.)—590(A)
—— **and J. D. Graves.** Temperature dependence of a scintillation counter using several organic and inorganic phosphors—590(A)
Koch, H. W., R. E. Carter, and C. S. Robinson. Determination of the energy distribution of bremsstrahlung from 19.5-Mev electrons—172(A)
Koch, Jørgen, O. Kofoed-Hansen, P. Kristensen, and W. Drost-Hansen. Measurements on radioactive krypton isotopes from fission after mass-spectrographic separation—279
—— **and Ebbe Rasmussen.** Hyperfine structure and nuclear spin of Kr^{83} and Ne^{21} investigated with separated isotopes—1417(L)
Koehler, J. S. (see Blewitt, T. H.)—470(A)
Koenigsberg, Ernest (see Keller, Joseph M.)—454(A)
Kofoed-Hansen, O. (see Koch, J.)—279
Kohman, Truman P. Binding energies of alpha-particles in medium-heavy nuclides—448(L)
Kohn, Walter (see Borowitz, Sidney)—818
Kokotailo, G. T. (see Erdman, K. L.)—1262(L)
Konneker, W. R. (see DeBenedetti, S.)—440(L)
Kopal, Z. Shock wave phenomena in astronomy—875(T)
Koppe, H. On the production of mesons—688(L)
Korff, S. A. and A. D. Krumbein. Tests of self-regenerating fillings for Geiger counters—1412(L)
Koski, W. S. (see Cohen, Victor W.)—703(L)
—— **and Carl O. Thomas.** Scintillations produced by α-particles in a series of structurally related organic crystals—308(L)
Kothari, D. S. and F. C. Auluck. Thompson scattering and the hole theory—433(L)
Kothari, L. S. (see Singwi, K. S.)—305(L)
Kouts, H. (see Bohm, D.)—867(L)
Kovasznay, Leslie S. G., Mahinder S. Uberoi, and Stanley Corrsin. Transformation between one- and three-dimensional power spectra for an isotropic scalar fluctuation field—1263(L)
Kraft, Hans. Calculation and use of logarithmic singularities in the hodograph representation of isentropic subsonic compressible flow—877(A)
Kramer, R. L. (see McMillen, J. Howard)—875(T)

Krasik, S., D. Alpert, and A. O. McCoubrey. Breakdown and maintenance of microwave discharges in argon—722
Kratz, H. R. and J. E. Mack. Forbidden absorption lines from extraordinarily large orbits in alkali metal atoms—173(A)
Kraushaar, William L. Cosmic-ray mesons near sea level—1045
Kraybill, Henry L. Extensive air showers at high altitudes—1092
Kristensen, P. (see Koch, J.)—279
Kroll, Norman M. (see Karplus, Robert)—846(L)
Kruger, P. Gerald (see Leiter, H. A.)—167(A)
—— (see Phillips, J. A.)—1471
Krumbein, A. D. (see Korff, S. A.)—1412(L)
Kruschwitz, W. H. (see Rudnick, P.)—201(A)
Krzywoblocki, M. Z. On the non-existence of limiting lines and their relation to shock in viscous gases—877(A)
Kubitschek, H. E. and S. M. Dancoff. Capture gamma-ray studies—182(A), 531
Kundu, D. N. and M. L. Pool. Columbium 90, 96 and molybdenum 91, 93—183(A)
Kurbatov, J. D. (see Emmerich, Werner S.)—454(A), 1891(A)
—— (see Thomas, D. G.)—1891(A)
Kusch, Polycarp. On the sign of the electric quadrupole moment of Li^7—138(L)
—— Some design considerations of an atomic clock using atomic beam techniques—161(T)
—— (see Mann, A. K.)—163(A)
—— **and A. K. Mann.** Precision measurement of the ratio of the nuclear g values of Li^7 and Li^6—707
Kyhl, R. L. (see Lawrance, R. B.)—472(A)

Lachenbruch, S. H. (see Marton, L.)—460(A)
Ladenburg, R., C. C. Van Voorhis, and J. Winckler. Interferometric studies of faster than sound phenomena. Part II. Analysis of supersonic air jets—662
Lagemann, Robert T. Overtones in the absorption spectra of color centers in alkali halide crystals—199(A)
——, **Alvin H. Nielsen, and Fred P. Dickey.** Erratum: the infra-red spectrum and molecular constants of $C^{12}O^{16}$ and $C^{13}O^{16}$—159(L)
La Mer, Victor K. (see Reiss, Howard)—192(A)
Lamkin, J. C. (see Kaar, P. R.)—1843
Lampi, E. E., G. Freier, and J. H. Williams. Total cross section of carbon and hydrogen for fast neutrons—188(A)
Lanczos, Cornelius. Logical extension of the field equations of general relativity—592(A)
Land, E. H. and W. A. Shurcliff. Rotating illumination method of locating stars in nuclear track plates—469(A)
Landé, Alfred. Interaction between elementary particles. Part I—1176
—— On the classical theory of the electron—191(A)
Landshoff, Rolf. Transport phenomena in a completely ionized gas in presence of a magnetic field—904
Lane, C. T. Note on the resistivity of gold at low temperatures—304(L)
—— (see Fairbank, Henry A.)—1209
—— (see Reynolds, Charles A.)—64, 167(A)
—— (see Webber, Robert T.)—609
Lang, R. J. and A. R. J. Stephenson. Extinction coefficients for oxygen in the Schumann region—464(A)
Lange, I. (see Forbush, S. E.)—164(A)
Langer, Lawrence M. (see Duffield, R. B.)—1272(L)
—— (see Price, H. Clay., Jr.)—454(A)
——, **R. D. Moffat, and H. C. Price, Jr.** Beta-spectra of Cu^{64}—1725(L)
—— **and H. Clay Price, Jr.** Beta-spectra of forbidden transitions—641
—— **and H. Clay Price, Jr.** Shapes of forbidden beta-spectra—186(A)
Laporte, Otto. Theory and applications of the shock tube—584(T)
Lark-Horovitz, K. (see Johnson, W. E.)—442(L)
—— **and K. W. Meissner.** Optical properties of semiconductors. I. The reflectivity of germanium semiconductors—1530(L)
Laslett, L. Jackson. On the half-life of Na^{22}—858(L)
—— (see Jensen, Erling N.)—430(L)
LaTorre, Richard and Waller George. Strain rate effects in polycrystalline cadmium wire—470(A)
Lauritsen, C. C. (see Chao, C. Y.)—586(A)
—— (see Fowler, W. A.)—314(L), 1767
—— (see Tollestrup, A. V.)—181(A), 428(L)
Lauritsen, Thomas. Gamma-ray spectroscopy—161(T)
—— (see Chao, C. Y.)—582(L)
—— (see Hornyak, W. F.)—731
—— (see Rasmussen, V. K.)—581(L)
Lawrance, R. B., R. L. Kyhl, and M. W. P. Strandberg. Microwave spectrum of formaldehyde—472(A)
Lawson, A. W. and Ting-Yuan Tang. Concerning the high pressure allotropic modification of cerium—301(L)
Lax, Benjamin and Sanborn C. Brown. High frequency breakdown in magnetic field—457(A)
Lax, Melvin (see Feshbach, Herman)—134, 689(L)
—— **and H. Feshbach.** Meson production in a photonuclear collison—190(A)
Lazarus, David. Variation of the adiabatic elastic constants of KCl, NaCl, CuZn, and Al with pressure to 10,000 bars—545
Lee, J. C. and M. L. Pool. Radioactive tin 121, 123, and 125—192(A), 606
Lees, L. and S. M. Bogdonoff. Study of condensation of components of air at high Mach numbers—875(T)
Lehovec, K. On the structure of the barrier layer in dry disk rectifiers—178(A)
Leighton, Robert B., Carl D. Anderson, and Aaron J. Seriff. Addendum: energy spectrum of the decay particles and the mass and spin of the mesotron—159(L)
Leininger, R. F., E. Segrè, and C. Wiegand. Experiments on the effect of atomic electrons on the decay constant of Be^7. II—897
Leiter, H. A., R. E. Meagher, F. A. Rodgers, and P. Gerald Kruger. Angular distribution of protons from the *D-D* reaction for 10-Mev deuterons—167(A)
Leith, C. E. (see Fox, R.)—590(A)
—— (see Hildebrand, R. H.)—587(A)
—— (see Kelly, B.)—589(A)
Leland, Wallace T. Naturally occurring odd-odd isotope of vanadium—1722(L)
—— On the abundance of I^{129}, Te^{118}, and Pt^{190}—992(L)
Lepore, J. V. (see Watson, K. M.)—193(A), 1157
Leprince-Ringuet, L., F. Bousser, Hoang-Tchang-Fong, L. Jauneau, and D. Morellet. Two kinds of very high energy cosmic-ray stars—1273(L)
Lessen, Martin. On the stability of the laminar boundary layer between parallel streams—879(A)
Levinger, J. S. Photoelectric disintegration of the deuteron—699(L)
Levinstein, Henry (see Bode, Donald)—179(A)
Lew, Hin. Hyperfine structure of the $^2P_{3/2}$ state of Al^{27}. The nuclear electric quadrupole moment—1086
Lewis, H. W. Note on meson production—566(L)
Li, Yin-Yuan. Quasi-chemical method in the statistical theory of regular mixtures—972
Liddiard, Thomas P. and Ralph D. Drosd. Electrically exploded wires as a light source for hydrodynamical studies—879(A)
Lidofsky, L. (see Feldman, L.)—1888(L)
——, **P. Macklin, and C. S. Wu.** Beta-spectrum of $_{61}Pm^{147}$—1888(L)
Lieber, Paul. Some studies in gas dynamics, conducted at the Polytechnic Institute of Brooklyn—882(A)

Liebermann, Leonard N. Erratum: second viscosity of liquids —440(L)
—— Sound propagation in chemically active media—1520
Lin, C. C. Flow behind stationary shocks of varying strength —875(T)
Lind, David A. Direct crystal spectroscopy of gamma-radiation —584(T)
——, **J. R. Brown, and J. W. M. DuMond.** Precision determination of the energy of the 1.1- and 1.3-Mev gamma-radiations from Co^{60} by direct crystal diffraction—591(A)
——, **J. R. Brown, and Jesse W. M. DuMond.** Precision wavelength measurements of the 1.1- and 1.3-Mev lines of Co^{60} with the 2-meter focusing curved-crystal spectrometer—1838
Lind, S. C. (see Watson, John H. L.)—466(A)
Linder, E. G. and K. G. Hernqvist. Space-charge effects in electron beams and their reduction by positive-ion trapping —453(T)
Ling, Daniel S., Jr. and David L. Falkoff. Interference effects in gamma-gamma-angular correlations—1639
—— **and David L. Falkoff.** On the γ-γ-angular correlation in Pd^{106}—431(L)
Linker, Mary Jane A. Apparent straggling of $_{16}S^{35}$ beta-particles in glass—428(L)
—— Electrostatic analyzer—198(A)
Linz, A., Jr. (see Scherrer, V. E.)—202(A)
—— (see Varwig, R. L.)—201(A)
——, **V. E. Scherrer, and G. Carmichael.** Inductive method of detection of speed of brittle fractures in steel plates—202(A)
Lipkin, H. J. Beta-ray spectra—567(L)
Lippmann, B. A. (see Johnson, M. H.)—184(A), 828
Livesey, D. L. (see Green, L. L.)—580(L)
Livingston, Ralph. Nuclear spin and quadrupole moment of I^{129}—149(L)
Locke, J. L. (see Welsh, H. L.)—580(L)
Loeb, Leonard B. Role of the cathode in discharge instability —255
Lofgren, E. J. High intensity cyclotron—587(A)
Long, Earl A. and Lothar Meyer. Anomalous adsorption of helium at liquid helium temperatures—440(L)
Longmire, C., C. S. Wu, and C. H. Townes. On the spin and beta-spectrum of Cl^{36}—695(L)
Longuet-Higgins, H. C. Spectra and structure of borohydrides and related compounds—161(T)
Loomis, F. W. Future of physics—452(T)
Lord, J. J. (see Schein, Marcel)—170(A)
——, **Marcel Schein, and M. Vidale.** Altitude and latitude dependence of nuclear disintegrations measured in photographic emulsions in the stratosphere—171(A)
——, **Marcel Schein, and M. Vidale.** Large nuclear disintegration produced by a very high energy alpha-particle of the cosmic radiation—321(L)
Loubser, J. H. N. and C. H. Townes. Spectroscopy between 1.5- and 2-mm wave-length using magnetron harmonics—178(A)
Louw, J. D. and S. M. Naudé. Spurious counts in Geiger counters and the pretreatment of the electrodes—571(L)
Love, W. F. (see Blunt, R. F.)—1202
——, **R. F. Blunt, and P. B. Alers.** Magnetic effects of a rotating superconductor—305(L)
Low, W. (see Townes, C. H.)—1415(L)
—— **and C. H. Townes.** Molecular dipole moments and Stark effects. I. Stark effects on symmetric top molecules with nuclear quadrupole coupling—1295
Lowance, F. E. and R. A. Martin. Method for microwave propagation study in the lower troposphere—202(A)
Lowen, I. S. (see Tralli, N.)—1541(L)
Lowry, L. L. and M. Goldhaber. Widths of neutron resonances —189(A)
Lundby, Arne. Angular correlation of delayed radiations—993(L)
—— Decay scheme of Hf^{181}—1809
Lundquist, S. Experimental investigations of magneto-hydrodynamic waves—1805
Luneberg, R. K. (see Halpern, Otto)—1811
Lyons, Harold. Atomic clock of the National Bureau of Standards—161(T)

MacDonald, A. D. (see Brown, Sanborn C.)—1629
—— **and Sanborn C. Brown.** High frequency gas discharge breakdown in hydrogen—1634
MacIntyre, W. J. Measurement of a 2.3×10^{-8}-second metastable state in Hg^{198}—312(L)
Mack, J. E. (see Arroe, O. H.)—173(A), 873(L)
—— (see Kratz, H. R.)—173(A)
—— **and O. H. Arroe.** Hyperfine structure and isotope shift studies, especially of the nuclear spin of Se^{77}—173(A)
—— **and O. H. Arroe.** Nuclear spin $\frac{1}{2}$ for Te^{123} and isotope shift in the tellurium spectrum—1002(L)
MacKay, J. (see Errett, D.)—180(A)
Macklin, P. A. (see Feldman, L.)—1888(L)
—— (see Goldin, A. S.)—336
—— (see Lidofsky, L.)—1888(L)
Macklin, R. L. U-235 gamma-radiation—595
—— (see Goldin, A. S.)—336
MacLeod, David W., Jr. (see Mingins, Charles R.)—467(A)
Madison, T. C. (see Sharbaugh, A. H.)—1419(L), 1529(L)
Madsen, C. B. (see Huus, Torben)—323(L)
Maienschein, Fred C. (see Meem, J. Lawrence, Jr.)—328
—— (see Mitchell, Allan, C. G.)—1450
—— **and J. Lawrence Meem, Jr.** Coincidence experiments in Ni^{65}, Ni^{67}, Ag^{110}, and In^{114}—899
Mallary, E. C. and M. L. Pool. Radioactive In and Sn—186(A)
—— **and M. L. Pool.** Radioactive In^{107}, In^{108}, In^{109}, and Sn^{108} —1454
Malm, R. (see Buechner, W. W.)—1543
Malter, L. (see Johnson, E. O.)—1411(L)
Mandeville, C. E. Neutrons from the disintegration of sodium by deuterons—436(L)
—— **and M. V. Scherb.** Radiations from the 11-day neodymium and the 47-hour element 61—186(A)
—— **and E. Shapiro.** Radiations from indium (114) and barium (140)—454(A), 718
——, **C. P. Swann, and S. C. Snowdon.** Neutrons from deuterons on lithium (6)—980(L)
Manfredini, A. (see Bernardini, G.)—1792
Mann, A. K. (see Kusch, P.)—707
—— **and P. Kusch.** Further data on the spin gyromagnetic ratio of the electron—163(A)
Mann, K. C., D. Rankin, and P. N. Daykin. Radiations from Zn^{65}—1719(L)
Manning, Thurston E. Isotope shift in the HeI spectrum—173(A)
—— Isotopic spectra of lead—464(A)
Marcus, Jules A. Magnetic susceptibility of zinc at liquid hydrogen temperatures—413
—— Temperature dependence of susceptibility of zinc, cadmium, and gamma-brass—621
Marcus, P. M. (see Maxwell, E.)—1332
Margenau, Henry. Inversion frequency of ammonia and molecular interaction—1423
—— Pressure broadening in the inversion spectrum of ammonia—121
—— Pressure dependence of the inversion frequency of NH_3 —585(A)
—— (see Van Vleck, J. H.)—585(A), 1211
Marshak, R. E. Remarks on multiple meson and gamma-ray production—1736(L)
—— (see Ashkin, J.)—58, 989(L)

—— **and A. S. Wightman.** Absorption of negative π-mesons by protons—114
Marshall, J. F. and E. Guth. High energy photo-disintegration of the deuteron—1880(L)
—— **and E. Guth.** Photo-disintegration of the deuteron at intermediate energies—1879(L)
Martin, John H. Ionization of neon by atomic projectiles of neon—190(A)
Martin, L. Recent developments in electron microscopy—584(T)
Martin, M. H. Plane, rotational, Prandtl-Meyer flows—877(A)
Martin, R. A. (see Lowance, F. E.)—202(A)
Martinelli, E. A. Half-life of the positive π-meson—589(A)
Marton, L. Field mapping by electron-optical methods—162(T)
—— **and S. H. Lachenbruch.** Fringe fields of ferromagnetic domains—460(A)
Mason, W. P., R. M. Bozorth, H. J. McSkimin, and J. G. Walker. Elastic constants of single crystals of nickel—470(A)
Mather, K. B. Fading of proton tracks in vacuum—486
—— (see Bondelid, R. O.)—865(L)
Matlack, G. (see Bianco, D.)—473(A)
Matossi, Frank, Pressure dependence of line width in infra-red spectra—1845
——, **Robert Mayer, and Emma Rauscher.** On total absorption in spectra with overlapping lines—760
Matthews, P. T. Application of Dyson's methods to meson interactions—684(L)——Erratum—1419(L)
—— Application of the Tomonaga-Schwinger theory to the interaction of nucleons with neutral scalar and vector mesons—1657
—— *S*-matrix for meson-nucleon interactions—1254(L)
Matthias, B. T. Ferroelectric properties of WO_3—430(L)
—— **and J. P. Remeika.** Ferroelectricity in the ilmenite structure—1886(L)
——, **Elizabeth A. Wood, and A. N. Holden.** New ferroelectric crystals—175(A)
Maurer, R. D. and Melvin A. Herlin. Second sound velocity in helium II—948
Maurer, R. J. (see Klick, C. C.)—179(A)
Mautz, C. W. Factors affecting the production of steady flow past models in the shock tube—172(A)
Maxwell, E. (see Condon, E. U.)—578(L)
——, **P. M. Marcus and J. C. Slater.** Surface impedance of normal and superconductors at 24,000 megacycles per second—1332
Maxwell, Louis R. and Stephen Brunauer. Thermomagnetic investigations of promoted iron oxide and iron catalysts—175(A)
——, **J. Samuel Smart, and Stephen Brunauer.** Dependence of the intensity of magnetization and the Curie point of certain iron oxides upon the ratio of Fe^{++}/Fe^{+++}—459(A)
Mayer, H. (see Argo, H. V.)—182(A)
Mayer, Maria G. Closed shells in nuclei—185(A)
—— **and Edward Teller.** On the origin of elements—1226
Mayer, Robert (see Matossi, Frank)—760
Mays, J. M. (see Dailey, B. P.)—136(L), 472(A)
—— (see Townes, C. H.)—700(L)
McCarthy, J. T. Use of WWV signals to time pendulums—1891(A)
McClure, B. T. (see Holt, R. B.)—456(A)
McCormick, R. C. (see Poole, J. H. J.)—1253(L)
McCoubrey, A. O. (see Alpert, D.)—457(A), 1257(L)
—— (see Holstein, T.)—1259(L)
—— (see Krasik, S.)—722
McCray, P. R. (see Schroeder, C. A.)—163(A)
McCaniel, Boyce D. (see Corson, D. R.)—162(A)
——, **John W. DeWire, Dale R. Corson, and Robert R. Wilson.** Design and construction of the Cornell synchrotron—162(A)
McGowan, F. K. Metastable state of half-life 13×10^{-8} sec. in $_{71}Lu^{177}$—1730(L)
McGuire, T. R. Magnetic susceptibility measurements at liquid helium temperatures—167(A)
—— (see Webber, Robert T.)—293
McInteer, B. B. (see Reynolds, Charles A.)—64, 167(A)
McIntyre, John A. (see Hofstadter, Robert)—172(A), 1269(L)
McKay, A. S. (see Brown, W. W.)—506, 1034
—— (see Palmatier, E. D.)—196(A)
McKay, Kenneth G. Germanium counter—1537(L)
McKee, L. H. (see Hutter, R. G. E.)—453(T)
McKellar, Andrew. Isotopes in stellar atmospheres—584(T)
McKenzie, K. (see Fox, R.)—590(A)
McLachlan, Dan, Jr. Electrodynamic examination of the hydrogen atom—592(A)
McMath, Robert R. (see Goldberg, Leo)—1848
——, **Orren C. Mohler, A. Keith Pierce, and Leo Goldberg.** Note on methane in the infra-red solar spectrum—1533(L)
McMillen, J. Howard and R. L. Kramer. Impact shock waves in water—875(T)
McReynolds, Andrew W. Martensitic transformations in iron-nickel—469(A)
McSkimin, H. J. (see Mason, W. P.)—470(A)
Mead, L. W. (see Armistead, F. C.)—860(L)
Meagher, R. E. (see Leiter, H. A.)—167(A)
Meem, J. Lawrence, Jr. (see Maienschein, Fred)—899
—— **and Fred Maienschein.** Coincidence and absorption measurements on Cs^{134}, I^{124}, Au^{199}, and Ca^{45}—328
Meggers, W. F. Where we stand with respect to atomic spectra—161(T)
Mei, J. Y. (see Mitchell, Allan C. G.)—1450
——, **Allan C. G. Mitchell, and Daniel J. Zaffarano.** Disintegration of In^{114}—1883(L)
Meiners, Edwin P., Jr. Angular distribution of photo-neutrons from deuterium—259
Meinke, W. W. (see Ghiorso, A.)—1414(L)
Meissner, K. W. (see Lark-Horovitz, K.)—1530(L)
Melamed, M. (see Janofsky, R. F.)—1891(A)
Melchor, J. L., W. B. Good, and T. E. Pardue. Energy losses and fracture of some metals subjected to high repeated strains—202(A)
Melkonian, Edward. Precise determination of the slow neutron cross section of the free proton—1744
—— Slow neutron velocity spectrometer studies of O_2, N_2, A, H_2, H_2O, and seven hydrocarbons—1750
Melvin, M. Avramy. Handedness in space-time and the nature of magnetic poles—592(A)
Mendenhall, H. E. Secondary emission from silicon and germanium oxides—458(A)
Meneghetti, D. Small angle scattering of neutrons—188(A)
Menius, A. C., Jr. (see Watkins, J. M., Jr.)—196(A)
Merritt, Thomas P. and Royal M. Frye. Lattice energy, lattice constant and compressibility of metallic copper and silver—470(A)
Merz, Walter J. Electric and optical behavior of $BaTiO_3$ single-domain crystals—1221
—— Spontaneous polarization of $BaTiO_3$ single-domain crystals—459(A)
Metzger, Franz and Martin Deutsch. Correlation between direction and polarization of successive gamma-ray quanta—187(A)
Meyer, D. I. (see Graves, E. R.)—183(A)
Meyer, H. A. and G. Schwachheim. Exchange phenomena of the nucleons that generate penetrating showers—149(L)
——, **G. Schwachheim, A. Wataghin, and G. Wataghin.** On penetrating showers in cosmic radiation—598
Meyer, Lothar (see Band, William)—417

—— (see Long, Earl A.)—440(L)
Michels, A. M. J. F. High pressure experiments and molecular physics—162(T)
Michels, Walter C. and Sally E. Wilford. Spectral emissivity and conductivity of titanium—174(A)
Milford, F. J. and L. L. Foldy. Energy degeneration of cosmic-ray primaries—468(A)
Miller, A. R. Phenomenological theory of superconductors—1001(L)
Miller, Charles E. (see Potter, D. S.)—590(A)
—— (see Todd, Jay, Jr.)—591(A)
——, **J. E. Henderson, D. S. Potter, and Jay Todd, Jr.** Penetrating component of cosmic-rays at 3.4 km—591(A)
——, **Joseph E. Henderson, D. S. Potter, Jay Todd, Jr., and A. W. Wotring.** Momentum spectra and positive excess of cosmic-ray particles at 11,000 feet—165(A)
Miller, P. H., Jr. (see Rothlein, B. J.)—1882(L)
—— (see Russell, B. R.)—190(A)
—— **and Julius Taylor.** Pressure coefficient of resistance in intrinsic semiconductors—179(A)
Miller, W. C. (see Waldman, B.)—181(A)
Millikan, R. A. Recollections of the American Physical Society—453(T)
Milton, J. C. D. (see Fulbright, H. W.)—1271(L)
Mingins, Charles R., Carl A. Stevens, and David W. McLeod, Jr. Studies of the vibrational characteristics of a piezoid—467(A)
Minnhagen, L. (see Bøggild, J. K.)—988(L)
Mitchell, Allan C. G. Survey of the energy-levels of radioactive nuclei—161(T)
—— (see Brolley, John E., Jr.)—624
—— (see Kern, Bernard D.)—94
—— (see Mei, J. Y.)—1883(L)
——, **J. Y. Mei, Fred C. Maienschein, and Charles L. Peacock.** Disintegration of I^{124} and I^{126}—1450
Miyazaki, Y. Cosmic rays at a great depth—1733(L)
Mizushima, Masataka. Theory of pressure absorption—1268(L)
Moeckel, W. E. Approximate method for predicting the form and location of detached shock waves—877(A)
Moffat, R. D. (see Langer, L. M.)—1725(L)
Mohler, Orren C. (see Goldberg, Leo)—1848
—— (see McMath, Robert R.)—1533(L)
Montgomery, C. G. (see Wei, John)—1488
—— **and D. D. Montgomery.** Analysis of bursts of cosmic-ray-ionization—1482
—— **and A. R. Tobey.** Neutron production at mountain altitudes—1478
Montgomery, D. D. (see Montgomery, C. G.)—1482
Moody, H. J. (see Haslam, R. N. H.)—704(L)
Moore, Benjamin L. Pentode counting or control ring—465(A)
Moore, George E. Thermionic emission of (BaSr)O without metallic support—458(A)
Moore, H. B. (see Farmer, E. C.)—454(A)
Moore, John W. Electric current transients through human tissue and skin—190(A)
Moorhouse, R. G. Bosons in an electromagnetic field—1691
Morellet, D. (see Leprince-Ringuet, L.)—1273(L)
Morette, Cecile. On the production of π-mesons by nucleon-nucleon collisions—1432
Morganstern, Kennard H. and Karl P. W. Wolf. Cloud-chamber study of high energy positrons from Na^{22}—1261(L)
Morrish, A. H. Absolute voltage determination of two nuclear resonances below 0.4 Mev—1651
Morrison, H. L. and F. T. Rogers, Jr. Dependence of convective process on thickness of porous medium—203(A)
Moseley, H. M. Composite particles—197(A)
Mostow, Wolfe. Plastic behavior of stiffened panels subjected to underwater explosive load—876(A)
Moulton, J. F., Jr. (see Shafer, P. E.)—881(A)
Moyer, Burton J. High energy gamma-rays from the cyclotron target—584(T)
—— (see DeJuren, J.)—589(A)
—— (see York, Herbert F.)—187(A)
Mrozowski, S. Hyperfine structure in the band spectrum of the mercury hydride HgH—1820
—— Structure of the mercury bands λ2540 and λ2476—1714
Muehlhause, C. O. (see Harris S.)—189(A)
—— (see Hibdon, C. T.)—100, 188(A)
Muether, Herbert (see White, M. G.)—161(T)
Mulliken, R. S. Where we stand in respect to the electronic structure of molecules—161(T)
—— (see Shull, Harrison)—176(A)
Mullin, Charles J. (see Guth, Eugene)—234
—— **and Eugene Guth.** Theory of the angular distribution of photo-neutrons from Be^9—682(L)
Murakawa, K. and S. Suwa. Quadrupole moment of Sb^{121} and Sb^{123}—433(L)
——, **S. Suwa, and T. Kamei.** Structure of the line λ4686 of He II—1721(L)
Murray, R. B. (see Jones, Ernest A.)—200(A)
Myers, Vernon. Forces between ammonia molecules—177(A)

Nafe, John E. (see Blau, M.)—860(L)
—— (see Nelson, Edward B.)—1858
Nagle, Darragh E. Nuclear spin and magnetic moment of Cs^{135} and Cs^{137}—847(L)
—— (see Davis, Luther, Jr.)—1068
Nakamura, Seitaro (see Sakai, Mitsuo)—967
—— (see Taketani, Mituo)—60
Nakano, Yashihiro. On the angular distribution of *D-D* reaction products—981(L)
Narlikar, V. V. and Ramji Tiwari. Particular case in Einstein's generalized theory of gravitation—868(L)
Naudé, S. M. (see Louw, J. D.)—571(L)
Nechaj, J. F. (see Allen, A. J.)—188(A), 463(A)
—— (see Charpie, R. A.)—1255(L)
Neher, H. V. Correlation of cosmic-ray geomagnetic effects—164(A)
—— (see Biehl, A. T.)—914
Nelson, Edward B. and John E. Nafe. Comparison of the *g* value of the electron in hydrogen with that in deuterium—1858
Neuman, M. (see Furry, W. H.)—432(L)
—— **and W. H. Furry.** On the interactions of mesons with the electromagnetic field—1677
Newkirk, J. B. and R. Smoluchowski. Mechanism of ordering in Co-Pt—471(A)
Newton, T. D. and E. P. Wigner. Invariant theoretical determination of position operators—191(A)
Ney, E. P. (see Oppenheimer F.)—1418(L)
Nicodemus, D. B. (see Fleeman, J.)—1774
Nielsen, Alvin H. (see Kaylor, Hoyt M.)—200(A)
—— (see Lagemann, Robert T.)—159(L)
—— (see Parkinson, T. F.)—199(A)
—— (see Woltz, P. J. H.)—200(A)
Nielsen, O. B. (see Bøggild, J. K.)—988(L)
Nier, Alfred O. C. (see Reynolds, Charles A.)—64, 167(A)
Nordheim, Gertrud P. and H. Sponer. Remarks on the low lying singlet electronic levels in naphthalene—177(A)
Nottingham, W. B. Studies of thermionic emission, photoelectric emission and conductivity of oxide-coated cathodes—453(T)
Nowak, W. B. and J. C. Slater. Surface impedance of metals at 24,000 Mc/sec.—469(A)

Oberly, J. J. (see Burstein, E.)—1254(L)
O'Day, Marcus. Rocketborne upper atmospheric experiments of the Air Materiel Command—195(T)
Oguchi, Takehiko. Statistics of the three-dimensional ferromagnet—1001(L)

Olsen, Leonard O., E. C. Crittenden, Jr., and R. W. Hoffman. Condensation of evaporated metals on surfaces—1891(A)
Olson, N. (see Crawford, M. F.)—1528(L)
Ono, Kenichi (see Taketani, Mituo)—60
Onsager, Lars (see Kaufman, Bruria)—1244
Oppenheimer, F. and E. P. Ney. Wide angle sprays of minimum ionization particles—1418(L)
Orr, J. B. Uranium^{235} in thucholite—155(L)
Orr, William C. (see Bonner, Norman A.)—140(L)
Osborne, D. W. (see Abraham, B. M.)—864(L)
Osborne, L. S. and B. T. Feld. Measurements and interpretation on the "showers" associated with stars in nuclear emulsions—468(A)
Osborne, M. F. M. Bose-Einstein condensation for charged particles in a magnetic field—400
—— Bose-Einstein condensation for thin films—396
Osoba, J. S. Forbidden transition of yttrium^{91} and cesium^{137}—345
Ott, D. G. (see Wyly, L. D.)—1532(L)
Otto, William H. Use of the density-gradient tube in the study of finely divided materials—465(A)
Overhauser, Albert W. Clustering of ions and the mobilities in gaseous mixtures—250
Owen, George E. (see Cook, C. Sharp)—183(A)
—— **and C. Sharp Cook.** On the shape of the positron spectrum of Cu^{61}—1536(L)
—— **and C. Sharp Cook.** Positron and negatron spectra of Cu^{64}—1726(L)
Oxholm, Mary Louise and Dudley Williams. Infra-red absorption by homonuclear diatomic molecules—151(L)
Oxley, Charles L. Proton-proton scattering experiment at 250 Mev—461(A)

Page, Leigh and Norman I. Adams, Jr. Diode space charge for any initial velocity and current—381
Palevsky, H. (see Hanson, A. O.)—578(L)
Palmatier, E. D. (see Brown, W. W.)—506
——, **W. W. Brown, and A. S. McKay.** On the knock-on secondaries of penetrating particles—196(A)
Panofsky, Wolfgang K. H. Proton-proton scattering—584(T)
Paraghamian, Berg (see Sanderson, H. C., Jr.)—878(A)
Pardue, T. E. (see Kammer, E. W.)—202(A), 202(A)
—— (see Melchor, J. L.)—202(A)
—— (see Parker, J. P.)—202(A)
Parkash, Om. On the temperature dependence of counter characteristics in self-quenching G-M counters—568(L)
Parker, G. W. (see Ketelle, B. H.)—1416(L)
Parker, J. P. and T. E. Pardue. Instrumentation for studying energy losses and fracture of some metals subjected to large repeated strains—202(A)
Parkinson, T. F. (see Jones, Ernest A.)—200(A)
——, **E. A. Jones, and A. H. Nielsen.** Infra-red spectrum of chlorine monofluoride—199(A)
Parkinson, W. C. Absorption of gamma-rays in aluminum—1348
Parzen, G. Some results in the scattering theory of the Dirac equation—592(A)
Paskin, Arthur (see Keller, Joseph M.)—454(A)
Patten, R. B. (see Thomas, J. E., Jr.)—162(A)
Patterson, G. M., I. I. Glass, and D. Bitondo. Interaction of a plane shock wave with a contact surface of general type—881(A)
Peacock, Charles L. Disintegration of Cs^{137}—186(A)
—— (see Beach, Louis A.)—187(A), 1585, 1624
—— (see Mitchell, Allan C. G.)—1450
Pearson, G. L. Electrical properties of crystal grain boundaries in germanium—459(A)
—— Electron and hole mobilities in germanium single crystals—179(A)
—— (see Shockley, W.)—180(A), 459(A)
Peck, Edson. Infra-red recording spectrograph of high resolution and high precision—584(T)
Peck, R. A., Jr. Photographic study of neutrons from Al+H^2—1279
Peed, W. F., E. J. Spitzer, and L. E. Burkhart. *L* spectrum of element 61—143(L)
Pegram, G. B. Early years of the American Physical Society—452(T)
Pell, E. M. (see Tomboulian, D. H.)—172(A)
—— **and D. H. Tomboulian.** Absorption by aluminum between 100A and 300A—172(A)
Pellam, John R. Correlations in measurements on the superfluidity in liquid helium II—158(L)
—— Second sound and classical heat flow—872(L)
—— **and Russell B. Scott.** Second sound velocity in paramagnetically cooled liquid helium II—869(L)
Pennock, J. C. (see Armistead, F. C.)—860(L)
Pepper, R. (see Errett, D.)—180(A)
Perez-Mendez, V. and H. Brown. Beta-spectrum of O^{15}—689(L)
Perlman, I. (see Goeckermann, R. H.)—628
Perlow, G. J. (see Kissinger, C. W.)—164(A)
——, **C. W. Kissinger, and C. A. Schroeder.** Search for cosmic-ray diurnal effects at rocket altitudes—164(A)
Perry, J. E. New California Institute electrostatic generator—584(T)
Petch, H. E. (see Bell, R. E.)—1409(L)
Peters, B. (see Bradt, H. L.)—156(L)
—— (see Kaplon, M. F.)—1735(L)
Peterson, John W. Influence of piezo-electrification on triboelectrification—1882(L)
Peterson, R. E. (see Adair, R. K.)—308(L), 463(A)
—— (see Barschall, H. H.)—1146
—— (see Bockelman, C. K.)—277
Pfann, W. G. and J. H. Scaff. *P*-type germanium transistor—459(A)
Phillips, G. C., T. W. Bonner, and J. E. Richardson. Study of the long range protons from the bombardment of carbon by deuterons—169(A)
Phillips, J. A. and P. Gerald Kruger. On the production of electron pairs in the field of an electron—1471
Phillips, M. Effect of nuclear motion on atomic magnetic moments—1803
Pickup, E. and L. Voyvodic. Disintegration electrons from Li_3^8 nuclei ejected cosmic stars—1534(L)
—— **and L. Voyvodic.** Large cosmic stars in electron sensitive emulsions—447(L)
Pierce, A. Keith (see Goldberg, Leo)—1848
—— (see McMath, Robert R.)—1533(L)
Pierce, J. R. Note on plasma oscillation—565(L)
Pietenpol, William J. and John D. Rogers. Microwave absorption spectrum of methylene bromide—690(L)
Pine, J. and R. Sherr. Constant sensitivity gamma-ray detector—455(A)
Platt, Joseph B. (see Zizzo, Samuel G.)—704(L)
Plumb, Harmon (see Bockstahler, Lester I.)—166(A)
Plyler, Earle K. Infra-red absorption spectra of seven freons—177(A)
—— New developments in infra-red spectrometry—195(T)
Podgor, S. Preliminary note on nuclear periodic scheme in three dimensions—1271(L)
Polachek, H. (see Seeger, R. J.)—875(T)
Pollard, Ernest C. Deep energy levels in nuclei from neon to calcium—161(T)
—— (see Davison, P. W.)—890
Pomerance, H. S. Some isotopic neutron absorption cross sections—195(A)

Pomeranchuk, I. On a generalization of the lambda-limiting process and the non-uniqueness in the removal of divergence difficulties in the quantum theory of elementary particles —298
Pomerantz, Martin A. Properties of cosmic radiation in the lower atmosphere—165(A)
—— **and Frank L. Hereford.** Detection of heavy particles in the primary cosmic radiation—997(L)
—— **and M. S. Vallarta.** On the low energy spectrum of primary cosmic radiation, and the sun's magnetic dipole moment—1889(L)
Pool, M. L. (see Creveling, L. G.)—946
—— (see Gum, Jane R.)—184(A)
—— (see Hinshaw, R. A.)—358
—— (see Kundu, D. N.)—183(A)
—— (see Lee, J. C.)—192(A), 606
—— (see Mallary, E. C.)—186(A), 1454
—— (see Robertson, B. E.)—1408(L), 1649
—— (see Scott, W. E.)—183(A)
Poole, J. H. J., C. F. G. Delaney, and R. C. McCormick. Possible existence of the $4n+1$ radioactive series in chloritized ytterby mica—1253(L)
Pooler, L. G. Free flight aerodynamics—880(A)
Popelka, Martin, Jr. (see Harkins, William D.)—989(L)
Potter, D. S. (see Miller, Charles E.)—165(A), 591(A)
—— (see Todd, Jay, Jr.)—591(A)
——, **J. E. Henderson, C. E. Miller, and Jay Todd, Jr.** Portable high intensity magnet and cloud chamber for use in cosmic-ray research—590(A)
Potter, J. G. (see Simons, L. H.)—467(A)
Pound, R. V. On the spatial alignment of nuclei—1410(L)
Power, S. Decay of a heavy τ-meson into three lighter mesons —865(L)
Pratt, William W. (see Jensen, Erling N.)—430(L)
Price, G. A. and D. W. Kerst. Angular distribution and relative yields of gamma-n processes with bremsstrahlung—182(A)
Price, H. Clay, Jr. (see Langer, Lawrence M.)—186(A), 641, 1725(L)
—— **and Lawrence M. Langer.** Forbidden beta-spectra of Sr^{89} and Y^{90}—454(A)
Price, Robert S. (see Fye, Paul M.)—881(A)
Proctor, W. G. Magnetic moments of Sn^{117}, Sn^{119}, and Pb^{207}—684(L)
—— **and F. C. Yu.** On the magnetic moments of Sn^{115}, Cd^{111}, Cd^{113}, Pt^{195}, and Hg^{199}—1728(L)
Pryor, W. A. and Hugh F. Henry. Spectral color determination by the human eye—199(A)
Pugh, Emerson M. Hall effect in ferromagnetics. I—176(A)
—— (see Schindler, Albert I.)—176(A)
Puppi, G. (see Bassi, P.)—854(L)
Purcell, E. M. Progress in the study of nuclear magnetic resonance since the 1949 symposium at Washington—162(T)
—— (see Gardner, J. H.)—1262(L)
—— (see Sachs, A. M.)—466(A)
—— (see Slichter, C. P.)—466(A)
—— (see Turner, E. H.)—465(A)
Purcell, J. D., R. Tousey, and K. Watanabe. Observations at high altitudes of extreme ultraviolet and x-rays from the sun—165(A)

Rabi, I. I. (see Grabner, Ludwig)—472(A)
—— (see Hughes, Vernon)—471(A)
Racah, Giulio. Theory of complex spectra. IV—1352
Rainwater, L. J. Recent results with the slow-neutron spectrometer at Columbia University—161(T)
—— (see Ruderman, I. W.)—434(L)
Ramsey, Norman F. New molecular beam resonance method —996(L)
Rank, D. H. Some recent results on molecular structure obtained by means of the Raman effect—161(T)
Rankin, D. (see Mann, K. C.)—1719(L)
Rasmussen, Ebbe (see Koch, Jørgen)—1417(L)
Rasmussen, J. O. (see Thompson, S. G.)—1406(L)
Rasmussen, V. K. (see Chao, C. Y.)—582(L)
—— (see Hornyak, W. F.)—731
——, **W. F. Hornyak, and T. Lauritsen.** Gamma-radiation from deuteron bombardment of Be^9—581(L)
Rauscher, Emma (see Matossi, Frank)—760
Reed, Charles Albert and William Schriever. Macroscopic space charge in electrolytes during electrolysis—197(A)
Reifman, A. and W. G. Dow. Dynamic probe measurements in the ionosphere—987(L)
Reiss, Howard and Victor K. La Mer. Approximate solution of certain boundary value problems involving moving boundaries—192(A)
Reissner, H. J. Results of a theory of the blade shapes of compressors—878(A)
Remeika, J. P. (see Matthias, B. T.)—1886(L)
Resnick, I. and S. S. Hanna. Angular yield of protons, tritons, and alphas from the bombardment of Be^9 by deuterons—168(A)
Resnick, Robert and D. R. Inglis. Theory of the lithium two-alpha-reactions. II. Angular distribution of $Li^6(d,\alpha)\alpha$—1318
Reynolds, Charles A., Henry A. Fairbank, C. T. Lane, B. B. McInteer, and Alfred O. Nier. "Heat flush" method of He^3 separation—64
——, **H. A. Fairbank, C. T. Lane, B. B. McInteer, and A. O. C. Nier.** Heat flux separation of He^3 in liquid helium II—167(A)
Reynolds, George T. (see Harrison, F. B.)—169(A)
—— (see White, L. D.)—468(A)
—— **and F. B. Harrison.** Measurements of meson decay by scintillation counters—169(A)
Reynolds, J. M. (see Webber, Robert T.)—293
Reynolds, John H. (see Inghram, Mark G.)—1265(L), 1717(L)
Rhodes, J. Elmer, Jr. Statistical consideration of collisions—202(A)
Rhodes, K. B. and E. E. Bell. ν_3-fundamental of nitrous oxide —1273(L)
Rice, O. K. Thermodynamics of liquid helium on the basis of the two-fluid theory—1701
Richards, H. T. (see Hunter, G. T.)—1445
—— (see Williamson, R. M.)—453(A), 614
Richards, J. (see Saxon, D.)—186(A), 982(L)
Richards, Paul I., Earl E. Hays, and S. A. Goudsmit. Magnetic time-of-flight mass spectrometer—180(A)
Richardson, H. T. (see Castillejo, L.)—1732(L)
Richardson, J. E. (see Phillips, G. C.)—169(A)
Richardson, J. M. (see Holt, R. B.)—456(A)
Richardson, J. Reginald (see Burkig, J. W.)—586(A)
Rieke, F. (see Errett, D.)—180(A)
Ritchie, R. H. and C. B. Crawley. Conduction of heat from a long circular cylinder—197(A)
Rittner, E. S., F. K. du Pré, and R. A. Hutner. Suggestion regarding emission phenomena in (Ba-Sr)O cathodes—996(L)
Roberts, A. (see Bianco, D.)—473(A)
—— (see Gilbert, D. A.)—1723(L)
—— **and W. F. Edgell.** Microwave rotational spectrum of $CH_2=CF_2$—178(A)
Roberts, J. A. Wave amplification by interaction with a stream of electrons—340
Roberts, James H. (see Keepin, George R.)—154(L)
Roberts, Shepard. Dielectric constants and polarizabilities of ions in simple crystals and barium titanate—1215
Roberts, V. (see Gebbie, H. A.)—1534(L)
Roberts, Walter O. Solar activity variations and their apparent consequences—584(T)

Robertson, B. E. (see Scott, W. E.)—183(A)
—— **and M. L. Pool.** 28.7-hour Ba^{135}—1408(L)
——, **W. E. Scott, and M. L. Pool.** Radioactive Y^{84}, Y^{88}, and Zr^{87}—1649
Robertson, J. M. (see Ross, Donald)—879(A)
Robinson, C. S. (see Koch, H. W.)—172(A)
Robinson, C. V. Design of small, self-quenching, G-M counter —455(A)
Robinson, J. Eugene (see Ter-Pogossian, Michel)—453(A), 909, 1407(L)
Rodgers, Eric. Experiment in x-ray scattering—196(A)
Rodgers, F. A. (see Leiter, H. A.)—167(A)
Roesch, W. C. (see Biehl, A. T.)—914
Rogers, E. H. and H. H. Staub. Nuclear resonances in rotating magnetic fields—585(A)
—— **and H. H. Staub.** Signs of the magnetic moments of neutron and proton—980(L)
Rogers, F. T., Jr. Relations in quasi-isothermal slow fracture. I. General considerations—203(A)
—— (see Byatt, W. J.)—199(A)
—— (see Crawford, G. W.)—199(A)
—— (see Morrison, H. L.)—203(A)
—— (see Rogers, Marguerite M.)—203(A)
Rogers, John D. (see Pietenpol, William J.)—690(L)
Rogers, M. and S. Fagin. Effects of heat addition on the aerodynamic design of ramjet diffusers—884(A)
Rogers, Marguerite M. and F. T. Rogers, Jr. Relations in quasi isothermal slow fracture. II. The problem of brittleness—203(A)
Rogozinski, A. (see Benoist, P.)—1000(L)
Rojansky, V. and Frank Stern. Relativity corrections for energy levels—184(A)
Roller, D. (see Errett, D.)—180(A)
Rose, A., P. K. Weimer, and S. V. Forgue. Some observations on the photo-effect in cadmium sulphide—179(A)
Rose, M. E. Electron neutrino correlation in heavy elements —195(A)
—— Internal pair formation—461(A), 678
——, **G. H. Goertzel, B. I. Spinrad, J. Harr, and P. Strong.** K-shell internal conversion coefficients—184(A), 1883(L)
—— **and J. L. Jackson.** Ratio of L_I to K capture—1540(L)
Rosen, Louis (see Williams, J. H.)—168(A)
—— **and Alvin M. Hudson.** On the tripartition of U^{235} nuclei by thermal neutrons—181(A)
——, **Francis K. Tallmadge, and John H. Williams.** Range distribution of the charged particles from the D-D reactions for 10-Mev deuterons: differential elastic scattering cross section at 40 degrees, 60 degrees and 80 degrees in the center-of-mass system—1283
Rosen, Nathan. Quantum mechanics of a particle on a string —202(A)
—— (see Freistadt, Hans)—201(A)
Rosenbaum, Alma (see Rusk, Rogers D.)—1166
Rosenbluth, Marshall N. Electromagnetic interactions of a vector meson with a scalar excited state—951
Rosenthal, Jenny E. Deflection of electrons in an inhomogeneous electrostatic field—180(A)
Ross, Donald and J. M. Robertson. Shear stress in a turbulent boundary layer—879(A)
Rothlein, B. J. and P. H. Miller, Jr. Measurements of the variation of work function of silicon with temperature—1882(L)
Ruderman, I. W. Scattering of slow neutrons by paramagnetic crystals—1572
—— (see Bendt, P. J.)—463(A)
——, **W. W. Havens, Jr., T. I. Taylor, and L. J. Rainwater.** Erratum: scattering of slow neutrons by paramagnetic crystals—434(L)
Ruderman, M. and R. Finkelstein. Note on the decay of the π-meson—1458
Rudnick, P. and W. H. Kruschwitz. Measurement of the velocity of a flow of a combustible gas mixture just prior to ignition—201(A)
Rueger, L. J. (see Todd, F. C.)—189(A)
—— **and F. C. Todd.** Dynamic system for secondary electron emission measurements at high temperatures—189(A)
Rusk, Rogers D. and Alma Rosenbaum. Effects of scattering and absorption of mesons on coincidence-anticoincidence measurements—1166
Russell, B. R. and P. H. Miller, Jr. Noise characteristics of dry cells—190(A)
Rutledge, W. C. (see Cork, J. M.)—1886(L)

Sachs, A. M. (see Turner, E. H.)—465(A)
——, **E. H. Turner, and E. M. Purcell.** Study of internal motion in ammonium salts by nuclear spin-lattice relaxation time measurements—466(A)
Sadauskis, John (see Jesse, William P.)—163(A)
Sailor, Vance L. Q values for $Ca^{40}(d,p)Ca^{41}$ and the mass difference (Ca^{40}-A^{40})—169(A)
—— (see Wyly, L. D.)—1532(L)
Sakai, Mitsuo and Seitaro Nakamura. New method of analysis of the beta-ray spectrum—967
Salant, E. O. (see Hornbostel, J.)—468(A), 859(L)
Sampson, M. B. (see Brolley, John E., Jr.)—624
Sanderson, H. C., Jr. and Berg Paraghamian. Supersonic aerodynamic characteristics of triangular planform wings—878(A)
Sard, R. D. (see Benade, A. H.)—488
——, **A. M. Conforto, and M. F. Crouch.** Further results on neutron production by cosmic-ray particles at sea level—1134
Sargent, B. W. (see Yaffe, L.)—617
Sartain, C. C. Measurement of the Thompson coefficient for tungsten at high temperatures—197(A)
Sasaki, Muneo (see Taketani, Mituo)—60, 852(L)
Sawyer, G. A. and M. L. Wiedenbeck. Gamma-ray of K^{40}—1535(L)
Saxon, D. Neutrinos from the sun and the source of the earth's heat—986(L)
—— **and J. Richards.** Beta-spectrum of Tl^{204}, magic numbers, and neutron pairing—982(L)
—— **and J. Richards.** Beta-spectrum of Tm^{170}—186(A)
Scaff, J. H. (see Pfann, W. G.)—459(A)
Schardt, A. W., E. J. Woodbury, and W. A. Fowler. Application of proportional counter to p-α-reactions at 100 kev—587(A)
Scharff-Goldhaber, Gertrude (see Bowe, J. C.)—437(L)
Schawlow, A. L. (see Crawford, M. F.)—1310, 1527(L)
—— **and M. F. Crawford.** Electron-nuclear potential fields from hyperfine structure—174(A)
——, **J. N. P. Hume, and M. F. Crawford.** Hyperfine structure and nuclear moment of Pb^{207}—1876(L)
Schedling, J. A. Movement of small metal particles having six degrees of freedom in air around a wire carrying a constant electric current—843
Scheibner, E. J. Mathematical method for determining points of maximum and minimum intensity in the Fresnel diffraction pattern of a single slit—201(A)
Schein, Marcel (see Fahy, Edward F.)—170(A)
—— (see Lord, J. J.)—171(A), 321(L)
—— **and J. J. Lord.** Production of mesons in the stratosphere —170(A)
Schenck, J. (see Stroud, W. G.)—1005
Scherb, M. V. (see Mandeville, C. E.)—186(A)
Scherrer, V. E. (see Linz, A., Jr.)—202(A)
—— (see Varwig, R. L.)—201(A)
——, **G. Carmichael, R. Varwig, and A. Linz.** Photographic method of detection of the speed of fracture in steel plates —202(A)

Schiff, L. I. Radiation accompanying meson creation—89
—— Spontaneous decay rate of heavy mesons—303(L), 468(A)
—— (see Stein, Irving)—461(A)
—— **and D. L. Weisman.** Spontaneous decay rate of heavy mesons. II—1266(L)
Schindler, Albert I. and Emerson M. Pugh. Hall effect in nickel. II—176(A)
Schlegel, Richard. Operator matrices for relations of space and time intervals—191(A)
Schmidt, F. H. Solenoidal beta-ray spectrometer with uniform magnetic field—586(A)
Schriever, William (see Reed, Charles Albert)—197(A)
Schroeder, C. A. (see Kissinger, C. W.)—164(A)
—— (see Perlow, G. J.)—164(A)
——, **J. D. Shipman, Jr., and P. R. McCray.** Laboratory coincidence, anticoincidence unit—163(A)
Schubaer, G. B. Some features of boundary-layer turbulence—878(A)
Schulman, James H., E. Burstein, R. J. Ginther, M. White, and L. W. Evans. Sensitized luminescence of alkali-halide phosphors—178(A)
——, **Robert J. Ginther, Clifford C. Klick, and Lyle W. Evans.** Effect of x-rays on the absorption and luminescence of alkali halide phosphors—459(A)
Schwachheim, G. (see Meyer, H. A.)—149(L), 598
Schwartz, Herman M. Basic electromagnetic theory and the correspondence principle—192(A)
Schwarzmann, Gertrude. On the uncertainty principle—192(A)
Schwinger, Julian. Quantum electrodynamics—453(T)
—— Quantum electrodynamics. III. Electromagnetic properties of the electron-radiative corrections to scattering—790
Scott, D. B. (see Erdman, K. L.)—1262(L)
Scott, Russell B. (see Pellam, John R.)—869(L)
Scott, W. E. (see Robertson, B. E.)—1649
——, **B. E. Robertson, and M. L. Pool.** New radioactive isotopes of yttrium and zirconium—183(A)
Scott, W. T. Correlated probabilities in multiple scattering—212
—— (see Snyder, H. S.)—220
Seaborg, G. T. (see Ghiorso, A.)—1414(L)
—— (see Thompson, S. G.)—1406(L)
Seeger, R. J. and H. Polachek. Shock wave phenomena: water-like substances—875(T)
Segrè, E. (see Leininger, R. F.)—897
Seidlitz, L., E. Bleuler, and D. J. Tendam. Disintegration energy of Al^{29}—453(A), 861(L)
Seitz, Frederick. On the theory of electron multiplication in crystals—1376
—— (see Falk, C. E.)—322(L)
—— (see Huntington, H. B.)—1728(L)
Selove, W. Rotating-shutter time-of-flight neutron spectrometer for the resonance region—187(A)
Serber, Robert. Interpretation of high-energy experiments at the Berkeley Radiation Laboratory—162(T)
Seriff, Aaron J. (see Leighton, Robert B.)—159(L)
Serin, B., J. R. Feldmeier, and M. Garfunkel. Experiment with alternating currents on tin superconductors—167(A)
Serpe, J. Two-component wave equations—1538(L)
Shafer, P. E. and J. F. Moulton, Jr. Ratio delay device for simplifying the photography of shocks in a tube—881(A)
Shaffer, Lloyd H. (see Harris, Louis)—943
Shakespeare, W. M., Jr. (see Thomas, J. E., Jr.)—162(A)
Shanks, Daniel. Non-linear transformations of divergent and slowly convergent sequences and an example from hydrodynamics—876(A)
Shanley, T. J. B. (see Winckler, J. R.)—1012
Shapiro, E. (see Mandeville, C. E.)—454(A), 718
Sharbaugh, A. H., J. K. Bragg, T. C. Madison, and V. G. Thomas. Determination of the molecular structure of bromosilane by microwave measurements—1419(L)
——, **T. C. Madison, and J. K. Bragg.** Inversion spectrum of ammonia—1529(L)
Shaw, T. M. and J. J. Windle. Measurement of electrical anisotropy of high polymers at microwave frequencies—586(A)
Shearer, James W. and Martin Deutsch. Lifetime of positrons in matter—462(A)
Sherman, D. F., D. J. Hughes, and J. R. Wallace. Fast neutron cross sections and nuclear shell structure—188(A)
Sherr, Rubby (see Pine, J.)—455(A)
—— (see White, M. G.)—161(T)
Sherwin, C. W. Recoils from the beta-decay of Y^{90}—183(A)
Shipman, J. D., Jr. (see Schroeder, C. A.)—163(A)
Shive, J. N. New germanium photo-resistance cell—575(L)
Shockley, W. (see Suhl, H.)—180(A)
——, **G. L. Pearson, and M. Sparks.** Current flow across n-p junctions—180(A)
——, **G. L. Pearson, M. Sparks, and W. H. Brattain.** Modulation of the resistance of a germanium filament by hole injection—459(A)
Shoemaker, F. C. (see Bender, R. S.)—273
Shor, S. W. W. Theoretical treatment of neutron attenuation in thick shields—474(A)
Shoupp, W. E., B. Jennings, and W. Jones. Absolute calibration of the $Li^7(p,n)$ threshold voltage—502
Shue, G. L. Method for calculating the drag coefficient from data obtained in a precision aeroballistics range—879(A)
Shull, C. G. (see Strauser, W. A.)—195(A)
—— **and J. Samuel Smart.** Detection of antiferromagnetism by neutron diffraction—1256(L)
Shull, F. B., C. H. Braden, and L. Slack. Forbidden beta-spectra of Sr^{89}, Sr^{90}, and Y^{90}—453(A)
Shull, Harrison and R. S. Mulliken. Theoretical computation of transition probabilities for electronic spectra of C_2 and N_2^+—176(A)
Shulman, R. G. (see Townes, C. H.)—472(A)
Shultz, W. S. (see Slifko, John P.)—881(A)
Shurcliff, W. A. (see Land, E. H.)—469(A)
Sibert, H. W. Inconsistencies in the Prandtl-Glauert transformation—877(A)
Sidhu, S. S. (see Chatterjee, G. P.)—175(A)
Siegbahn, Kai and Amal Ghosh. Decay scheme of Ni^{65}—307(L)
——, **Arne Hedgran, and Martin Deutsch.** Gamma-radiation from Br^{82}—1263(L)
Siegel, Armand. Relativistic generalization of phenomenological n-p interactions—185(A)
Siegert, Arnold J. F. On the approach to statistical equilibrium—1708
Silber, L. (see Errett, D.)—180(A)
Silver, Lorna M. Precision measurement of half-lives—589(A)
Simon, Albert. Energy levels of a vector meson in a smeared Coulomb field—1877(L)
Simmons, James W. Microwave spectra of CD_3Cl and CD_3I—686(L)
Simons, L. H., D. F. Weekes, and J. G. Potter. X-ray analysis of clays for quantity of montmorillonite—467(A)
Simpson, J. A., Jr., H. W. Baldwin, and R. B. Uretz. On the neutrons in the atmosphere—165(A)
—— **and R. B. Uretz.** On the latitude dependence of nuclear disintegrations and neutrons at 30,000 feet—569(L)
Singer, S. F. Specific ionization of the cosmic radiation above the atmosphere—701(L)
Singwi, K. S. and L. S. Kothari. Viscosity and thermal conductivity of mixtures of He^3 and He^4—305(L)
Sitte, K. Test set for measurement of dead time and recovery time of counters—164(A)

Slack, F. G. and Hsieh Yu-Chang. Electric field and discharge photographs—197(A)
Slack, L. (see Shull, F. B.)—453(A)
Slater, J. C. Electrons in perturbed periodic lattices—1592
—— (see Maxwell, E.)—1332
—— (see Nowak, W. B.)—469(A)
Slawsky, Z. I. Investigation of the excitation of molecular vibrations by high speed missiles—882(A)
Sleator, D. B. (see Bergdolt, V. E.)—879(A)
Slichter, C. P. and E. M. Purcell. Measurements of spin-lattice relaxation times in paramagnetic solids by the saturation method—466(A)
Slifko, John P., E. Swift, Jr., and W. S. Shultz. Explosion bubble period at great depths—881(A)
Slye, J. M. (see Fowler, J. L.)—169(A)
Smart, J. Samuel. Computed binding energies of some light nuclei—439(L)
—— (see Maxwell, Louis R.)—459(A)
—— (see Shull, C. G.)—1256(L)
Smith, F. M. (see Bishop, A. S.)—588(A)
Smith, P. D. P. Difficulty in using mk^3 as a residual charge to explain stellar magnetism—690(L)
Smith, Paul L. (see Burstein, Elias)—175(A)
Smith, William V. and Raydeen Howard. Quadrupole interactions in pressure broadening of ammonia inversion spectrum by non-polar gases—473(A)
Smoluchowski, R. (see Achter, M. R.)—470(A)
—— (see Newkirk, J. B.)—471(A)
—— **and H. Burgess.** Vacancies and diffusion in NiAl—309(L)
Snay, H. G. and E. Swift, Jr. Determination of adiabatic parameters of explosion bubbles from charges fired at great depths—881(A)
Snell, A. H. Search for beta-proton coincidences associated with neutron decay—195(T)
Snowdon, S. C. (see Mandeville, C. E.)—980(L)
Snyder, Hartland S. Comparison of calculations on cascade theory—1563
—— **and W. T. Scott.** Multiple scattering of fast charged particles—220
Snyder, James N. and W. H. Furry. Note on perturbation theory as applied to collision stimulated processes—359
Sollenberger, Paul. Present status of astronomical time standards—161(T)
Sollfrey, William. Propagation modes of a helix—455(A)
Solomon, A. K. (see Glendenin, L. E.)—462(A)
—— (see Steinberg, Daniel)—453(A)
Somerville, J. M. and W. R. Blevin. Current densities in the cathode spots of transient arcs—982(L)
Sommer, H. (see Hipple, J. A.)—1877(L)
Sparks, M. (see Shockley, W.)—180(A), 459(A)
Spencer, L. V. and Fannie Jenkins. Multiply scattered γ-rays: angular distribution—462(A)
—— **and Fannie Jenkins.** Penetration and diffusion of hard x-rays through thick barriers. IV. Multiply scattered γ-rays: angular distribution—1885(L)
Sperduto, A. (see Buechner, W. W.)—1543
Spinrad, B. I. (see Rose, M. E.)—184(A), 1883(L)
Spitzer, E. J. (see Peed, W. F.)—143(L)
Spitzer, Lyman, Jr. On the origin of heavy cosmic-ray particles—583(L)
Sponer, H. (see Bass, Arnold M.)—177(A)
—— (see Nordheim, Gertrud P.)—177(A)
Springer, George. On conformal mapping of multiply connected domains—876(A)
Squire, C. F. (see Houston, W. V.)—685(L)
Squire, H. B. Investigation of the turbulence characteristics of an experimental low turbulence wind tunnel—875(T)
Standil, S. (see Yaffe, L.)—617
Stanton, John S. Study of transient stresses in photo-elastic media—174(A)
Staub, H. H. (see Fleeman, J.)—586(A), 1774
—— (see Rogers, E. H.)—585(A), 980(L)
Stearns, Martin. Mean square angles of bremsstrahlung and pair production—836
Steele, M. C. Proximity effects in the measurement of magnetic susceptibility—566(L)
Stein, Irving and L. I. Schiff. Capture of μ-mesons by deuterons—461(A)
Steinberg, Daniel and A. K. Solomon. Effect of C^{14}, Ca^{45}, P^{32}, I^{131}, and Zn^{65} on photographic emulsions—453(A)
Steinberger, J. On the use of subtraction fields and the lifetimes of some types of meson decay—1180
—— **and G. C. Wick.** On the polarization of slow neutrons—994(L)
Stephens, William E. Neutron-hydrogen mass difference—181(A)
—— (see Franzen, W.)—317(L), 462(A)
Stephenson, A. R. J. (see Lang, R. J.)—464(A)
Stephenson, Harold P. Ultraviolet absorption spectra of some pyridine derivatives in liquid solution—199(A)
Stern, Frank (see Rojansky, V.)—184(A)
Sternglass, E. J. Interpretation of secondary electron emission data for homogeneous solids—189(A)
Stevens, Carl A. (see Mingins, Charles R.)—467(A)
Stevenson, Donald T. (see Deutsch, Martin)—184(A)
Stewart, Ellen S. (see Stewart, James L.)—464(A)
Stewart, H. J. Note on non-stationary supersonic wing theory—882(A)
Stewart, James L. and Ellen S. Stewart. Rotational dispersion of ultrasonics in deuterium and hydrogen—464(A)
Stoddard, A. E. (see Cork, J. M.)—575(L), 986(L), 1886(L)
Stoner, R. G. and M. H. Glauberman. Refraction of shock waves at a gas interface—882(A)
Stout, J. W. Solutions of He^3 in He^4—864(L)
—— **and Maurice Griffel.** Paramagnetic anisotropy of manganous fluoride—144(L)
Stovall, E. J., Jr. (see Allred, J. C.)—1430
—— (see Erickson, K. W.)—1141
——, **J. C. Allred, K. W. Erickson, and J. L. Fowler.** Angular distribution of 10.8-Mev deuterons scattered by deuterons—589(A)
Strait, E. N. (see Buechner, W. W.)—168(A), 1543, 1547
—— **and W. W. Buechner.** Magnetic analysis of the $Li^6(d,p)Li^7$ and $Li^7(d,p)Li^8$ reactions—1766
Straley, Joseph W. (see Haisley, W. E.)—200(A)
—— (see Jarrell, Herman)—199(A)
Strandberg, M. W. P. (see Lawrance, R. B.)—472(A)
Strang, C. D. (see Burwell, J. T.)—455(A)
Strauser, W. A., C. G. Shull, and E. O. Wollan. Neutron diffraction studies of AgCl, $Ag^{107}Cl$, and $Ag^{109}Cl$—195(A)
Street, J. C. (see Cool, R. L.)—468(A)
—— (see Fowler, E. C.)—171(A)
—— (see Voorhies, H. G.)—1100
—— (see Whittemore, W. L.)—170(A), 1786
Stresau, Richard H. F. Vacuum thermocouple microsecond timer—880(A)
Strick, E. Creation of mesons by high energy nucleons—190(A)
—— **and D. ter Haar.** Production of π-mesons by high energy nucleons—304(L)
Strong, H. M. (see Bundy, F. P.)—457(A)
—— **and F. P. Bundy.** Measurement of temperatures in complex flame structures by high resolution spectroscopy of the sodium *D*-lines, II—458(A)
Strong, P. (see Rose, M. E.)—184(A), 1883(L)
Stroud, W. G. (see Winckler, J. R.)—1012
——, **J. Schenck, and J. R. Winckler.** Preliminary directional study of cosmic rays at high altitude. I. Apparatus and procedure—1005

Stuhlman, Otto, Jr. Bioelectric potential transients accompanying closing movement of the lobes of Venus' Fly-Trap —464(A)
—— (see Darden, Edgar B.)—197(A)
—— **and Edgar B. Darden.** Bioelectric transients accompanying the closing movement of the lobes of Venus' Fly-Trap—197(A)
Suhl, H. and W. Shockley. Concentration of holes and electrons by magnetic fields—180(A)
Suits, C. G. Physics in industry—452(T)
Sun, Kuan-Han. On the negative proton—1266(L)
—— (see Allen, A. J.)—188(A), 463(A)
—— (see Charpie, R. A.)—1255(L)
Sunyar, A. W. and M. Goldhaber. Resonance neutron activation of "even-even" nuclei—189(A)
Suwa, S. Hyperfine structure of 4^3P-4^3D of the spectrum of Al II—847(L)
—— (see Murakawa, K.)—433(L), 1721(L)
Swann, Charles P. (see Hereford, F. L.)—570(L)
—— (see Hudspeth, Emmett L.)—464(A), 1150
—— (see Mandeville, C. E.)—980(L)
—— **and Emmett L. Hudspeth.** Bombardment of B^{10} with deuterons—168(A)
Swann, W. F. G. Mean life considerations in relation to curvature of cosmic-ray paths in a magnetic field—157(L)
—— **and Stephen H. Forbes.** Cosmic-ray variations at high altitudes resulting from meteorological variations—467(A)
Swartz, C. D. (see Corson, D. R.)—162(A)
Swartz, Gwynne B. Temperature variation of the thermal diffusion constant of HCl—166(A)
Swift, E., Jr. (see Slifko, John P.)—881(A)
—— (see Snay, H. G.)—881(A)
Szabó, Zoltán. Actinide series and the periodic table—147(L)

Taft, E. (see Apker, L.)—270, 453(T)
Tai, C. T. Application of a variational principle to biconical atennas—456(A)
Taketani, Mituo, Seitaro Nakamura, Kenichi Ono, and Muneo Sasaki. On the two-meson theory—60
—— **and M. Sasaki.** On the μ-meson capture—852(L)
Talley, R. M. and H. M. Kaylor. Calibration of an engraved circle by a constant angle method—201(A)
Tallmadge, Francis K. (see Rosen, Louis)—1283
—— (see Williams, J. H.)—168(A)
Tamburino, Sara (see Addario, Margherita)—983(L)
Tang, Ting-Yuan (see Lawson, A. W.)—301(L)
Taschek, R. F. Scattering and reactions of protons on tritons —584(T)
—— (see Argo, H. V.)—182(A)
—— (see Coon, J. H.)—710
—— (see Hemmendinger, A.)—1137
—— (see Jarvis, G. A.)—168(A)
——, **H. V. Argo, A. Hemmendinger, and G. A. Jarvis.** Neutron-hydrogen mass difference from the $T^3(p,n)He^3$ reaction threshold—325
Taylor, Julius (see Miller, P. H., Jr.)—179(A)
Taylor, T. I. (see Ruderman, I. W.)—434(L)
Taylor, William J. Radial density function for crystals from x-ray intensity data—175(A)
Tchen, Chan-Mou. Heat delivery in a two-dimensional compressible flow at subsonic and supersonic speeds—883(A)
Teasdale, John G. Experimental method for determining relative stopping power—588(A)
—— (see Gurevitch, M.)—151(L)
Teeter, Charles E., Jr. Thermal conductivity and heat capacity of beryllium carbide—466(A)
Teichmann, T. and E. P. Wigner. Applications of the dispersion formula for nuclear reactions—185(A)
Teller, Edward (see Mayer, Maria G.)—1226
Temmer, Georges M. Excitation functions for (α,n), $(\alpha,2n)$, and $(\alpha,3n)$ reactions on indium—424; Erratum—1002(L)
Tendam, D. J. (see Seidlitz, L.)—453(A), 861(L)
ter Haar, D. Energy level density and partition function of nuclei—1525
—— Series expansion at high temperatures for the partition function of the three-dimensional ferromagnet—176(A)
—— (see Strick, E.)—304(L)
Ter-Pogossian, Michel, C. Sharp Cook, C. Harold Goddard, and J. Eugene Robinson. Disintegration of Ce^{141}—909
——, **J. Eugene Robinson, and C. Harold Goddard.** Energy of an excited state of Li^7—1407(L)
——, **J. Eugene Robinson,and C. Harold Goddard.** On the excited states of Li^7—453(A)
Thackeray, E. R. Absorption spectrum of atomic sodium—173(A)
Thomas, Carl O. (see Koski, W. S.)—308(L)
Thomas, D. G. and J. D. Kurbatov. Radiations emitted by long-life species of nickel—1891(A)
Thomas, H. A. (see Hipple, J. A.)—1877(L)
—— (see Huntoon, R. D.)—163(A)
Thomas, J. E., Jr., W. M. Shakespeare, Jr., B. Cohen, R. B. Patten, and V. P. Henri. Ceramic materials for synchrotron vacuum tubes—162(A)
Thomas, Roy. Three-body scattering with central and tensor forces—1002(L)
Thomas, V. G. (see Sharbaugh, A. H.)—1409(L)
Thompson, Lowell E. (see Gum, Jane R.)—184(A)
Thompson, Stanley G. Relation between half-life and disintegration energy in orbital electron capture by heavy nuclei—319(L)
——, **A. Ghiorso, J. O. Rasmussen, and G. T. Seaborg.** Alpha-decay in isotopes of atomic number less than 83—1406(L)
Thompson, W. B. (see Brunton, D. C.)—848(L)
Thulin, Sigvard (see Bergström, Ingmar)—313(L), 1718(L)
———, **Ingmar Bergström, and Arne Hedgran.** Mass assignment of xenon activities produced in fission—871(L)
Tinlot, John and Bernard Gregory. Interactions of ionizing cosmic-ray particles at 10,600 ft. altitude—170(A)
Tiomno, J. On the spin of μ-mesons—856(L)
Tisza, L. (see Klein, M. J.)—1861
Titterton, E. W. and F. K. Goward. Evidence for the photofission of uranium into three charged fragments—142(L)
Tiwari, Ramji (see Narlikar, V. V.)—868(L)
Tobey, A. R. (see Montgomery, C. G.)—1478
Tochilin, E., R. H. Davis, and J. Clifford. Calibrated x-ray film badge dosimeter—590(A)
Todd, F. C. (see Rueger, L. J.)—189(A)
—— **and L. J. Rueger.** Secondary electron emission from oxides at high temperatures—189(A)
Todd, Jay, Jr. (see Miller, Charles E.)—165(A), 591(A)
—— (see Potter, D. S.)—590(A)
——, **J. E. Henderson, C. E. Miller, and D. S. Potter.** Cosmic-ray protons at 3.4 km—591(A)
Tollestrup, A. V. (see Chao, C. Y.)—586(A)
—— (see Fowler, W. A.)—1767
——, **W. A. Fowler, and C. C. Lauritsen.** Energy release in beryllium and lithium reactions with protons—428(L)
——, **F. A. Jenkins, W. A. Fowler, and C. C. Lauritsen.** Neutron-proton mass difference from the *D-D* reactions—181(A)
Tomboulian, D. H. (see Pell, E. M.)—172(A)
—— **and E. M. Pell.** On the position of L_1 absorption edge in aluminum—172(A)
Tomiyasu, K. and Ronold King. Terminal impedance and generalized two-wire line theory—456(A)
Tomkins, F. S. (see Dieke, G. H.)—283
Tongiorgi, Vanna Cocconi. Neutrons in the cosmic radiation —192(A)

—— On the mechanism of production of the neutron component of the cosmic radiation—517
—— (see Cocconi, G.)—192(A), 318(L), 1020
Torrey, H. C. Transient nutations in nuclear magnetic resonance—1059
Tousey, R. (see Purcell, J. D.)—165(A)
Townes, C. H. Ultimate accuracy of an atomic clock using absorption lines—161(T)
—— Where we stand in respect to radiofrequency studies of molecular structure—161(T)
—— (see Dailey, B. P.)—136(L), 472(A)
—— (see Longmire, C.)—695(L)
—— (see Loubser, J. H. N.)—178(A)
—— (see Low, W.)—1295
—— (see Wu, C. S.)—692(L)
—— **and L. C. Aamodt.** Nuclear spin and quadrupole moment of Cl^{36}—691(L)
——, **H. M. Foley, and W. Low.** Nuclear quadrupole moments and nuclear shell structure—1415(L)
——, **J, M. Mays, and B. P. Dailey.** Evidence on nuclear moments of stable Ge and Si isotopes from microwave spectra—700(L)
——, **R. G. Shulman, and B. P. Dailey.** Dipole moments from microwave spectra—472(A)
Townsend, J. W., Jr. Presentation of mass spectra with a cathode-ray oscillograph—465(A)
Tralli, N. and I. S. Lowen. Magnetic multipole internal conversion—1541(L)
Trischka, J. W. Moment of inertia and electric dipole moment of CsF from radiofrequency spectra—1365
Truesdell, C. Effect of viscosity on circulation—192(A)
Tsao, C. Y. (see Clark, J. S.)—162(A)
Turnbull, D. Rate of self-diffusion in single and polycrystals of silver—471(A)
Turner, C. M. Branching ratio in Be^{7} decay—148(L), 588(A)
Turner, E. H. (see Sachs, A. M.)—466(A)
——, **A. M. Sachs, and E. M. Purcell.** Some measurements of nuclear spin-lattice relaxation times in solids—465(A)
Tyler, Winfield W. Optical absorption in barium oxide films —1887(L)
—— Photo-conductivity and optical absorption in BaO crystals—179(A)

Uberoi, Mahinder S. (see Kovasznay, Leslie S. G.)—1263(L)
Uehling, E. A. Transients in the phenomena of nuclear induction—585(A)
Uhlenbeck, G. E. Transport phenomena in dilute gases—875(T)
Uretz, R. B. (see Simpson, J. A., Jr.)—165(A), 569(L)

Vallarta, M. S. Sun and cosmic rays—453(T)
—— (see Pomerantz, M. A.)—1889(L)
Vancour, Roger P. (see Hess, Victor F.)—1205
Van der Grinten, W. Fast electron tracks in nuclear emulsions —163(A)
Van der Ziel, A. Thermal noise at very high frequencies—591(A)
van Kranendonk, J., K. Compaan, and J. de Boer. Equation of state of gaseous He^{3}—998(L); Erratum—1728(L)
Van Name, F. W., Jr. Note on analysis of delayed coincidence counting experiments—1734(L)
Van Patter, D. M. New gamma-ray resonance in the reaction $C^{12}(p,\gamma)N^{13}$—1264(L)
Vanpee, Marcel (see Watson, John H. L.)—466(A)
Van Vleck, J. H. and Henry Margenau. Collision theories of pressure broadening of spectral lines—585(A), 1211
Van Voorhis, C. C. (see Ladenburg, R.)—662
Varnerin, Lawrence J., Jr. and Sanborn C. Brown. Method for determining the average energy of electrons in a gas discharge—457(A)
Varwig, R. L. (see Scherrer, V. E.)—202(A)
——, **V. E. Scherrer, G. Carmichael, and A. Linz.** Photomultiplier trigger for flash photography—201(A)
Vidale, M. (see Lord, J. J.)—171(A), 321(L)
Viehböck, F. P. (see Herzog, R. F. K.)—855(L)
Vigneron, L. (see Chastel, R.)—870(L)
Volkoff, G. M. On the theory of neutron reflectors for chain-reacting spheres—589(A)
von Hippel, A. and R. S. Alger. Breakdown of ionic crystals by electron avalanches—127
Voorhies, H. G. and J. C. Street. Star production by negative μ-mesons in a silver chloride crystal—1100
Voyvodic, L. (see Pickup, E.)—447(L), 1534(L)

Wachtell, G. P. (see Bershader, D.)—880(A)
Wagner, Norbert and D. Cooper. τ-meson—449(L)
Waldman, B., W. C. Miller, and D. Gideon. Electron excitation of In^{115*}—181(A)
Walker, J. G. (see Mason, W. P.)—470(A)
Walker, L. R. Note on wave amplification by interaction with a stream of electrons—1721(L)
Walker, R. L. Absorption of 17.6-Mev gamma-rays in C, Al, Cu, Sn, and Pb—527
—— (α,n) cross section of boron—244
—— Relative cross sections for pair production at 17.6 Mev—1440
—— (see Corson, D. R.)—162(A)
Wallace, J. R. (see Sherman, D. F.)—188(A)
Waltner, Arthur W. Improved scintillation counter—196(A)
—— (see Brown, J. S.)—196(A)
—— (see Byatt, W. J.)—199(A)
Wang, An (see Woo, W. D.)—465(A)
Wang, P. K. S. and M. Wiener. Spectral analysis of 10-Mev betatron radiation by nuclear emulsion—1724(L)
Wannier, G. H. On the energy band structure of insulators—438(L)
Warshaw, S. D. Stopping power of protons in several metals —1759
Watanabe, K. (see Purcell, J. D.)—165(A)
Watanabe, Satosi. Wave equations in the de Sitter space—296
Watanabe, T. (see Johnson, Gerald W.)—588(A)
Wataghin, A. (see Meyer, H. A.)—598
Wataghin, G. (see Meyer, H. A.)—598
Watkins, J. M., Jr. and A. C. Menius, Jr. Optimum thickness for alpha-particles of phosphor surface in scintillation counters—196(A)
Watson, John H. L., Marcel Vanpee, and S. C. Lind. Solids condensed from carbon monoxide by alpha-particles—466(A)
Watson, K. M. and J. V. Lepore. Neutron-proton scattering —193(A)
—— **and J. V. Lepore.** Radiative corrections to nuclear forces in the pseudoscalar meson theory—1157
Wattenberg, Albert (see Hamermesh, Bernard)—611, 1408(L), 1420(L)
Webb, J. H. Fogging of photographic film by radioactive contaminants in cardboard packaging materials—375
Webber, Robert T. Time effects in superconducting cylinders —167(A)
——, **Henry A. Fairbank, and C. T. Lane.** On the film transfer rate in helium II—609
——, **J. M. Reynolds, and T. R. McGuire.** Superconductors in alternating magnetic fields—293
Weekes, D. F. (see Simons, L. H.)—467(A)
Wegener, P. P. Experiments on the influence of temperature gradient and humidity on condensation shocks in supersonic wind tunnels—883(A)
Wehausen, J. V. Ship forms of least wave resistance—878(A)
Wei, John and C. G. Montgomery. Narrow air showers of cosmic rays—1488

Wei, Ming-Yi (see Beyer, Robert T.)—455(A)
Weidner, R. T., P. R. Weiss, C. A. Whitmer, and D. R. Blosser. Magnetic resonance absorption of diluted iron ammonium alum—1727(L)
Weimer, D. K. (see Bleakney, W.)—323(L)
Weimer, P. K. (see Rose, A.)—179(A)
Weinberg, A. M. Oak Ridge National Laboratory—195(T)
Weingarten, I. R. and G. E. Kimball. Characteristics of the untuned cavity microwave spectroscope—177(A)
Weinstein, M. (see Bohm, D.)—867(L)
Weinstock, B. (see Abraham, B. M.)—864(L)
Weisman, D. L. (see Schiff, L. I.)—1266(L)
Weiss, P. R. (see Weidner, R. T.)—1727(L)
Weisskopf, V. F. (see Feshbach, H.)—1550
Weissler, G. L. and T. N. Wilson. Work functions of gas-coated silver surfaces—591(A)
Wellard, H. J. Extension of the theory of Mason and Matthias to the low temperature transitions in $BaTiO_3$—565(L)
Welsh, H. L., M. F. Crawford, and J. L. Locke. Infra-red absorption of hydrogen and carbon dioxide induced by intermolecular forces—580(L)
Welton, T. A. Field formalism without self-action—460(A)
Wentink, T., Jr. (see Cohen, Victor W.)—703(L)
Wergeland, H. Bremsstrahlung in heavy elements—184(A)
Werner, F. D. Investigation of the possible utilization of an electrical glow discharge as a means for measuring air flow characteristics—883(A)
Wert, C. and C. Zener. Interstitial atomic diffusion coefficients—1169
Wessel, Walter. On infinite relativistic particle matrices—1512
Westenberg, A. A., J. H. Goldstein, and E. B. Wilson, Jr. Microwave spectrum of chloroacetylene and deuterochloroacetylene—472(A)
Westendorp, W. F. and F. R. Elder. Electron gun emission and x-ray output for three betatrons—445(L)
Wexler, A. and W. S. Corak. Electromagnetic induction in a superconductor—432(L)
White, L. D., G. G. Harris, and George T. Reynolds. Penetrating power of extensive shower particles—468(A)
White, M. (see Schulman, J. H.)—178(A)
White, M. G. (see Gugelot, P. C.)—463(A)
——, **Rubby Sherr, and Herbert Muether.** Radioactivity of carbon 10 and oxygen 14—161(T)
White, R. Stephan (see Jones, Stanley B.)—588(A)
Whitmer, C. A. (see Weidner, R. T.)—1727(L)
Whittemore, W. L. and J. C. Street. Density effect for cosmic-ray mesons—170(A), 1786
Wick, G. C. On fission-asymmetry—181(A)
—— (see Steinberger, J.)—994(L)
Wiedenbeck, M. L. (see Sawyer, G. A.)—1535(L)
Wiegand, C. (see Kelly, E.)—589(A)
—— (see Leininger, R. F.)—897
Wiener, M. (see Wang, P. K. S.)—1724(L)
—— **and H. Yagoda.** Background eradication of thick-layered nuclear emulsions 469(A)
Wigner, E. P. Recent progress in the understanding of beta-ray disintegration—161(T)
—— (see Newton, T. D.)—191(A)
—— (see Teichmann, T.)—185(A)
Wightman, A. S. (see Marshak, R. E.)—114
Wilford, Sally E. (see Michels, Walter C.)—174(A)
Wilkinson, Roger G. (see Beach, Louis A.)—187(A), 1585, 1624
Willard, John E. (see Hansen, John L.)—577(L)
Williams, Dudley (see Chambers, William H.)—461(A), 538
—— (see Oxholm, Mary Louise)—151(L)
—— (see Zimmerman, John R.)—163(A), 350, 1264(L)
Williams, F. E. Recent experimental results and theoretical interpretations on ionic phosphors—453(T)
Williams, John H. (see Lampi, E. E.)—188(A)
—— (see Rosen, Louis)—1283
——, **F. K. Tallmadge, and L. Rosen.** Use of photographic plate detectors in experiments with 10-Mev deuterons—168(A)
Williams, M. C. (see Andrews, D. H.)—154(L)
Williams, Thomas W. and James M. Benson. Afterglow of nitrogen and argon in low density supersonic streams—456(A)
Williamson, R. M. and H. T. Richards. *K* capture of Be^7 and the excited state of Li^7—453(A), 614
Willoughby, A. B. Erratum: the chi-square test as a criterion for testing halogen-filled Geiger tubes—1266
Wilson, E. Bright, Jr. Molecular spectroscopy and molecular structure—453(T)
—— (see Westenberg, A. A.)—472(A)
Wilson, H. A. Energy levels of the N^{14} nucleus—687(L)
—— Rotation levels of the Na^{24} and Ca^{41} nuclei—687(L)
Wilson, M. Kent and Richard M. Badger. Reinvestigation of the vibration spectrum of nitrogen dioxide—472(A)
Wilson, R. (see Bishop, G. R.)—683(L)
Wilson, Robert R. (see Corson, D. R.)—162(A)
—— (see McDaniel, Boyce D.)—162(A)
Wilson, T. N. (see Weissler, G. L.)—591(A)
Winckler, J. R. (see Ladenburg, R.)—662
—— (see Stroud, W. G.)—1005
——, **W. G. Stroud, and T. J. B. Shanley.** Preliminary directional study of cosmic rays at high altitude. II. Experimental results and interpretation—1012
Windle, J. J. (see Shaw, T. M.)—586(A)
Wineland, W. C. Detection pattern of a magnetic gradiometer—198(A)
—— (see Jashemski, Stanley A.)—198(A)
Winkler, E. H. Light-intensity distribution in the Mach-Zehnder interferometer—880(A)
Witmer, Enos E. Integral ratios between nuclear masses and binding energies—181(A)
Wolf, Karl P. W. (see Morganstern, Kennard H.)—1261(L)
Wolfenstein, Lincoln. Polarization effects in *n-p* and *p-p* scattering—541
Wollan, E. O. (see Strauser, W. A.)—195(A)
Woltz, P. J. H., Ernest A. Jones, and A. H. Nielsen. Infra-red and Raman spectra of carbonyl fluoride—200(A)
Woo, W. D. and An Wang. Static storage system utilizing magnetic retentivity—465(A)
Wood, Elizabeth A. (see Matthias, B. T.)—175(A)
Woodbury, E. J. (see Schardt, A. W.)—587(A)
Woodcock, Richard F. (see Duckworth, Henry E.)—462(A)
Woodward, W. M. (see Corson, D. R.)—162(A)
—— **and I. Halpern.** Angular distribution of the photodisintegration of the deuteron—107
Woolf, W. E. (see Burgy, Merle)—188(A)
Wotring, A. W. (see Miller, Charles E.)—165(A)
Wouters, L. (see Fox, R.)—590(A)
Wright, Arianna. Some aspects of paramagnetic relaxation—1826
Wright, S. C. (see Jungerman, J.)—1112
Wright, W. Whittier and W. B. Wrigley. Pulse degradation in the transient response of stable linear systems—198(A)
Wrigley, W. B. (see Wright, W. Whittier)—198(A)
Wu, C. S. (see Feldman, L.)—180(A), 697(L), 1888(L)
—— (see Lidofsky, L.)—1888(L)
—— (see Longmire, C.)—695(L)
—— **and L. Feldman.** Beta-ray spectrum of chlorine^{36}—693(L)
—— **and L. Feldman.** Beta-spectrum of Be^{10}—698(L)
—— **and L. Feldman.** Beta-spectrum of Y^{91}—696(L)
——, **C. H. Townes, and L. Feldman.** Radioactivity of chlorine^{36}—692(L)
Wyly, L. D. Angular distribution of protons in the $N^{14}(dp)N^{15}$ reaction—104

—— Energy levels in N^{15} and N^{16}—316(L)
—— Nuclear energy levels in N^{15} and N^{16}—462(A)
——, **V. L. Sailor, and D. G. Ott.** Protons from the bombardment of He^3 by deuterons—1532(L)

Yadav, H. N. Neutron-proton scattering—1720(L)
Yaffe, L., B. W. Sargent, M. Kirsch, S. Standil, and Jean M. Grunlund. Neutron-capture cross section of 85-minute Ba^{139}—617
Yagoda, Herman (see Wiener, M.)—469(A)
—— **and Nathan Kaplan.** Spontaneous neutron emission from uranium and samarium—702(L)
——, **Nathan Kaplan, and C. H. Conner.** Variation of cosmic star production with altitude—171(A)
Yang, C. N. (see Fermi, E.)—1739
Yeager, Ernest (see Bugosh, John)—1890(A), 1891(A)
——, **Hyman Chessin, John Bugosh, and Frank Hovorka.** Apparatus for acoustical measurements with pulse-modulated ultrasonic waves—1890(A)
Yeater, M. L. (see Gaerttner, E. R.)—363
Yennie, D. R. (see Arons, A. B.)—172(A)
Yevick, George J. On the vector meson-photon interaction—461(A)
Yoe, Catherine (see Boyd, J. E.)—203(A)
York, Herbert F., Burton J. Moyer, and Russell Bjorklund. Production of very high energy photons by 350-Mev protons—187(A)
Yost, F. L. (see Brown, Vinton A.)—201(A)
Young, D. R. Electric breakdown in CO_2 from low pressures to the liquid state—457(A)
Young, R. L. and Hugh F. Henry. Anode spark breakdown on distilled water surfaces—198(A)
Yu, F. C. (see Proctor, W. G.)—1728(L)
Yuan, Luke C. L. Distribution of slow neutrons in free atmosphere up to 102,000 feet—165(A)
—— On the latitude dependence of the absolute neutron intensities in cosmic radiation—1267(L)
—— On the measurement of slow neutrons in the cosmic radiation on a B-29 plane—1268(L)
Yudowitch, K. L. Collimation error in small angle x-ray scattering—455(A)
Yukawa, Hideki. On the radius of the elementary particle—300(L)
—— Remarks on non-local spinor field—1731(L)

Zabel, Carrol W. (see Davis, Luther, Jr.)—1076
Zacharias, Jerrold R. (see Davis, Luther, Jr.)—1068, 1076
Zaffarano, Daniel J. (see Kern, Bernard D.)—94
—— (see Mei, J. Y.)—1883(L)
Zeichner, Arthur. Representation of transonic flow patterns around a closed body—876(A)
Zener, C. (see Wert, C.)—1169
Zettler-Seidel, P. Differential relations of rotationally symmetric and plane supersonic flows—877(A)
Zimmerman, John R. and Dudley Williams. Détermination of nuclear gyromagnetic ratios I—350; Erratum—1264(L)
—— **and Dudley Williams.** Nuclear gyromagnetic ratios—163(A)
Zizzo, Samuel G. and Joseph B. Platt. Detection of x-ray quanta by a cadmium sulphide crystal counter—704(L)
Zucker, F. J. Waves guided by a single surface—586(A)

PHYSICAL REVIEW VOLUME 76, NUMBER 12 DECEMBER 15, 1949

Analytic Subject Index to Volume 76

References with (A) are to abstracts of papers presented at meetings of the American Physical Society. References with (L) are to Letters to the Editor.

Absorption of radiation
Attenuation of sunlight in natural bodies of water, W. D. Bulloch—201(A)
In BaO films, Winfield W. Tyler—1887(L)
Of γ-rays in C, Al, Cu, Sn, and Pb, R. L. Walker—527
By oxygen in Schumann region, R. J. Lang and A. R. J. Stephenson—464(A)
Acoustics (see also **Ultrasonics**)
High frequency barium titanate hydrophone, John Bugosh, Ernest Yeager, and Frank Hovorka—1890(A)
High frequency electroacoustic effect, construction of hydrophones, John Bugosh, Ernest Yeager, and Frank Hovorka—1891(A)
Propagation in chemically active media, Leonard Liebermann—1520
Pulse-modulated ultrasonic generator, Ernest Yeager, Hyman Chessin, John Bugosh, and Frank Hovorka—1890(A)
Second sound, non-equilibrium phenomena in Bose-Einstein gas, William Band—558
Second sound velocity in He II, John R. Pellam and Russell B. Scott—869(L); R. D. Maurer and Melvin A. Herlin—948
Adsorption
Of helium at liquid helium temperatures, Earl A. Long and Lothar Meyer—440(L); William Band—441(L)
Aerodynamics (see also **Hydrodynamics; Supersonic phenomena**)
Boundary-layer turbulence, G. B. Schubaer—878(A)
Calculating drag coefficient, G. L. Shue—879(A)
Condensation phenomena in wind tunnel, R. Head—882(A)
Flow of a gas, Beattie-Bridgman equation of state, J. C. Crown—882(A)
Free flight aerodynamics, L. G. Pooler—880(A)
Glow discharge, measuring air flow characteristics, F. D. Werner—833(A)
Heat delivery in two-dimensional flow, Chan-Mou Tchen—883(A)
Interferometric analysis of flow around projectiles, F. D. Bennett and W. C. Carter—880(A)

Aerodynamics (continued)
Multiple shock diffusers, Newman A. Hall—884(A)
Non-stationary supersonic wing theory, H. J. Stewart—882(A)
Ramjet diffusers, effects of heat addition, M. Rogers and S. Fagin—884(A)
Stability of laminar boundary layer, Martin Lessen—879(A)
Stress in turbulent boundary layer, Donald Ross and J. M. Robertson—879(A)
Supersonic air jets, R. Ladenburg, C. C. Van Voorhis, and J. Winckler—662
Triangular planform wings, H. C. Sanderson, Jr. and Berg Paraghamian—878(A)
Wings in supersonic flow, stability, Clifford Gardner—882(A)

Afterglow
Forbidden oxygen lines, S. Kash and J. Kaplan—584(A)
In low density supersonic streams, Thomas W. Williams and James M. Benson—456(A)
Ionization in active nitrogen, K. T. Chao and H. P. Chang—970
Recombination in neon afterglows, R. B. Holt, J. M. Richardson, B. Howland, and B. T. McClure—456(A)

Astrophysics
Atmospheric HDO, H. A. Gebbie, W. R. Harding, C. Hilsum, and V. Roberts—1534(L)
CO_2, infra-red solar spectrum, Leo Goldberg, Orren C. Mohler, Robert R. McMath, and A. Keith Pierce—1848
Methane in the solar spectrum, Robert R. McMath, Orren C. Mohler, A. Keith Pierce, and Leo Goldberg—1533(L)
Residual charge, stellar magnetism, P. D. P. Smith—690(L)
Soft x-radiation in upper atmosphere, T. R. Burnight—165(A)
Solar and stellar atmospheres, f values in iron spectrum, W. W. Carter—962
Sun's magnetic dipole, M. A. Pomerantz and M. S. Vallarta—1889(L)
Ultraviolet and x-rays from sun, J. D. Purcell, R. Tousey, and K. Watanabe—165(A)

Atmosphere (see **Meteorology**)

Atomic mass (see **Isotopes**)

Atomic structure (see also **Spectra**)
Helium wave equation, James H. Bartlett—460(A)
Of hydrogen atom, electrodynamic examination, Dan McLachlan, Jr.—592(A)
Relativity corrections for energy levels, V. Rojansky and Frank Stern—184(A)

Biophysics
Bioelectric potentials, Edgar B. Darden and Otto Stuhlman, Jr.—197(A)
Bioelectric transients, movements of lobes of Venus' Fly-Trap, Otto Stuhlman, Jr. and Edgar B. Darden—197(A); Otto Stuhlman, Jr.—464(A)
Color determination by human eye, W. A. Pryor and Hugh F. Henry—199(A)
Current transients through human tissue and skin, John W. Moore—190(A)
Electrical energy of seeds, R. Ellioff and A. A. Bless—200(A)

Bremsstrahlung (see **Radiation**)

Broadening of spectral lines
Of ammonia inversion spectrum by non-polar gases, William V. Smith and Raydeen Howard—473(A)
Collision theories, J. H. Van Vleck and Henry Margenau—585(A), 1211
Inversion spectrum of ammonia, Henry Margenau—121; William and Raydeen Howard—473(A)
Microwave and infra-red regions, P. W. Anderson—647
Monatomic resonance lines, T. Holstein—457(A)

Brownian movement
Einstein equation, Frederik J. Belinfante—473(A)

Chemical reactions
Actinide series and the periodic table, Zoltán Szabó—147(L)
Ion exchange and chromatography, H. L. Finston and R. M. Dyer—465(A)

Compton effect (see **X-rays, absorption, diffraction, scattering,** etc.)

Conductivity, thermal (see **Thermal conductivity**)

Constants, physical standards
Proton magnetic moment in Bohr magnetons, J. H. Gardner and E. M. Purcell—1262(L)

Cosmic radiation
Absolute intensity, Victor F. Hess and Roger P. Vancour—1205
Absolute neutron intensities, latitude dependence, Luke C. L. Yuan—1267(L)
Air showers at high altitudes, Henry L. Kraybill—1092
Altitude and latitude dependence, disintegrations in stratosphere, J. J. Lord, Marcel Schein, and M. Vidale—171(A)
Altitude dependence of penetrating particles, Marcello Conversi—849(L), 851(L), 1541(L)
Analysis of bursts, C. G. Montgomery and D. D. Montgomery—1482
Background eradication, M. Wiener and H. Yagoda—469(A)
Capture of negative mesons, J. Barnothy—303(L)
Cascade theory, comparison of calculations, Hartland S. Snyder—1563
Coincidence, anticoincidence unit, C. A. Schroeder, J. D. Shipman, Jr., and P. R. McCray—163(A)
Decay electrons from mesons, A. H. Benade and R. D. Sard—488
Delayed proton-electron activity induced in Al by non-ionizing rays, E. C. Fowler, R. L. Cool, and J. C. Street—171(A)
Density effect for mesons, W. L. Whittemore and J. C. Street—170(A), 1786
Detection of heavy particles, method, Martin A. Pomerantz and Frank L. Hereford—997(L)
Direction study at high altitude, apparatus and procedure, W. G. Stroud, J. Schenck, and J. R. Winckler—1005
Directional study at high altitude, results and interpretation, J. R. Winckler, W. G. Stroud, and T. J. B. Shanley—1012
Disintegration electrons from Li_3^8, E. Pickup and L. Voyvodic—1534(L)
Disintegration produced by very high energy alpha-particle, J. J. Lord, Marcel Schein, and M. Vidale—321(L)
Disintegrations and neutrons at 30,000 ft., latitude dependence, J. A. Simpson, Jr. and R. B. Uretz—569(L)
Distribution and multiplicity of neutrons, local showers, G. Cocconi and V. Cocconi Tongiorgi—318(L)
Diurnal effects at rocket altitudes, G. J. Perlow, C. W. Kissinger, and C. A. Schroeder—164(A)
Electrons in primary radiation, Robert I. Hulsizer—164(A)
Energetic events in emulsions at high altitude, J. Hornbostel and E. O. Salant—859(L)
Energy degeneration, F. J. Milford and L. L. Foldy—468(A)
Exchange phenomena, penetrating showers, H. A. Meyer and G. Schwachheim—149(L)
Extensive penetrating showers, John Ise, Jr. and W. B. Fretter—933; W. W. Brown and A. S. McKay—1034
Frequency of stars of different sizes, Margherita Addario and Sara Tamburino—983(L)
Gamma-rays in primary radiation, C. W. Kissinger, C. A. Schroeder, and G. J. Perlow—164(A)
Geomagnetic effects at 30,000 ft., H. V. Neher—164(A)
At great depth, Y. Miyazaki—1733(L)

Heavy nuclei, H. L. Bradt and B. Peters—156(L)
Heavy particles in stars, M. Blau, M. M. Block, and J. E. Nafe—860(L)
High altitude experiments over wide range of latitudes, A. T. Biehl, H. V. Neher, and W. C. Roesch—914
High energy events at high altitude, J. Hornbostel and E. O. Salant—468(A)
High energy stars, L. Leprince-Ringuet, F. Bousser, Hoang-Tchang-Fong, L. Jauneau, and D. Morellet—1273(L)
Intensity of particles, absorption in lower atmosphere, Martin A. Pomerantz—165(A)
Interactions of ionizing particles at 10,600 ft., John Tinlot and Bernard Gregory—170(A)
Knock-on secondaries of penetrating particles, E. D. Palmatier, W. W. Brown, and A. S. McKay—196(A)
Lateral structure showers, G. Cocconi, V. Cocconi Tongiorgi, and K. Greisen—1020
Latitude dependence at 30,000 ft. of penetrating particles, Marcello Conversi—444(L)
Locating stars in nuclear track plates, E. H. Land and W. A. Shurcliff—469(A)
Low energy spectrum of primary radiation, sun's magnetic dipole, M. A. Pomerantz and M. S. Vallarta—1889(L)
Magnetic deflection of mesons in nuclear plates, Ian Barbour—320(L)
Mean life and curvature of paths, W. F. G. Swann—157(L)
Mechanism of production of neutrons, Vanna Cocconi Tongiorgi—517
Meson background in showers, Giuseppe Cocconi—984(L)
Meson intensity with height, P. H. Barker—141(L)
Meson production and absorption, R. L. Cool, E. C. Fowler, and J. C. Street—468(A)
Mesons near sea level, William L. Kraushaar—1045
Momentum spectra at 11,000 ft., Charles E. Miller, Joseph E. Henderson, D. S. Potter, Jay Todd, Jr., and A. W. Wotring—165(A)
Multiple meson and gamma-ray production, R. E. Marshak —1736(L)
Multiple meson and γ-ray production in stars, M. F. Kaplon, B. Peters, and H. L. Bradt—1735(L)
Narrow air showers, John Wei and C. G. Montgomery—1488
Nature of penetrating particles in showers, Frank L. Hereford—171(A)
Neutron production at mountain altitudes, C. G. Montgomery and A. R. Tobey—1478
Neutron production at sea level, R. D. Sard, A. M. Conforto, and M. F. Crouch—1134
Neutrons in atmosphere, J. A. Simpson, Jr., H. W. Baldwin, and R. B. Uretz—165(A); Luke C. L. Yuan—165(A); Vanna Cocconi Tongiorgi—192(A)
Origin of heavy particles, Lyman Spitzer, Jr.—583(L)
Penetrating showers, Frank L. Hereford—142(L); L. D. White, G. G. Harris, and George T. Reynolds—468; W. B. Fretter—511; C. E. Miller, J. E. Henderson, D. S. Potter, and Jay Todd, Jr.—591(A); H. A. Meyer, G. Schwachheim, A. Wataghin, and G. Wataghin—598
Portable magnet and cloud chamber, D. S. Potter, J. E. Henderson, C. E. Miller, and Jay Todd, Jr.—590(A)
Positive excess of meson component, Robert B. Brode—468(A); P. Bassi, E. Clementel, I. Filosofo, and G. Puppi —854(L)
Positive mesons at 30,000 ft., Marcello Conversi—311(L)
Protons at 3.4 km, Jay Todd, Jr., J. E. Henderson, C. E. Miller, and D. S. Potter—591(A)
Sea-level mesons stopped at Pb foils, W. Y. Chang—170(A)
Scattering and absorption of mesons, effect on coincidence-anticoincidence measurements, Rogers D. Rusk and Alma Rosenbaum—1166
Secondaries of penetrating particles, W. W. Brown, A. S. McKay, and E. D. Palmatier—506
Showers associated with stars, L. S. Osborne and B. T. Feld —468(A)
Slow neutrons at high altitudes, Luke C. L. Yuan—1268(L)
Soft x-radiation in upper atmosphere, T. R. Burnight—165(A)
Specific ionization of radiation above atmosphere, S. F. Singer—701(L)
Spontaneous decay of heavy mesons, L. I. Schiff—303(L)
Star producing radiation, G. Bernardini, G. Cortini, and A. Manfredini—1792
Star production by negative μ-mesons in AgCl, H. G. Voorhies and J. C. Street—1100
Stars in electron sensitive emulsions, E. Pickup and L. Voyvodic—447(L)
Structure of extensive showers, G. Cocconi, V. Cocconi Tongiorgi, and K. Greisen—192(A)
τ-meson, Norbert Wagner and D. Cooper—449(L)
Underground cosmic-ray data, K. Greisen—1718(L)
Variation of star production with altitude, Herman Yagoda, Nathan Kaplan, and C. H. Conner—171(A)
Variations at high altitudes, W. F. G. Swann and Stephen H. Forbes—467(A)
Variations in intensity, permanent solar magnetic moment, S. E. Forbush and I. Lange—164(A)
Very large bursts under 26.7 cm Pb, Edward F. Fahy and Marcel Schein—170(A)
Wide angle sprays of minimum ionization particles, F. Oppenheimer and E. P. Ney—1418(L)
Zenith angle dependence of hard component, J. F. Jenkins, Jr.—992(L)

Cross section, measurements, theory (see also **Scattering of electrons, neutrons, and ions**)
Absorption of γ-rays in C, Al, Cu, Sn, and Pb, R. L. Walker —527
For (α,n) of Be, Mg, and Al, I. Halpern—248
Of Ba^{139}, neutron-capture, L. Yaffe, B. W. Sargent, M. Kirsch, S. Standil, and Jean M. Grunlund—617
For $B^{10,11}(\alpha,n)N^{13,14}$, R. L. Walker—244
Of C and H for fast neutrons, E. E. Lampi, G. Freier, and J. H. Williams—188(A)
$Cu^{63}(n,2n)Cu^{62}$ cross section, neutron energy near threshold, J. L. Fowler and J. M. Slye—169(A)
D-D reactions, Louis Rosen, Francis K. Tallmadge, and John H. Williams—1283
D-D neutrons, G. T. Hunter and H. T. Richards—1445
Of $D(d,\gamma)$ and $D(p,\nu)$ reactions, W. A. Fowler, C. C. Lauritsen, and A. V. Tollestrup—1767
$D(d,n)He^3$ reaction, function of angle, K. W. Erickson, J. L. Fowler, and E. J. Stovall, Jr.—1141
For fast neutrons, nuclear shell structure, D. F. Sherman, D. J. Hughes, and J. R. Wallace—188(A)
Isotopic neutron absorption cross section, H. S. Pomerance —195(A)
Of K^{39}, thermal neutrons, John L. Hansen and John E. Willard—577(L)
Of Nd isotopes, slow neutrons, David C. Hess, Jr. and Mark G. Inghram—300(L)
Neutron cross sections at 115 and 300 ev, C. T. Hibdon and C. O. Muehlhause—100
n-p and *p-p* at 83 Mev, L. Castillejo and H. T. Richardson —1732(L)
N-P scattering, E. Kelly, C. Leith, and C. Wiegand—589(A)
For 95- and 270-Mev neutrons, J. DeJuren, N. Knable, and B. Moyer—589(A)
Of nuclei for 40-Mev neutrons, R. H. Hildebrand and C. E. Leith—587(A)
Nucleon-nucleon collisions, bremsstrahlung, J. Ashkin and R. E. Marshak—58

Cross section, measurements, theory (continued)
At 115 ev and 300 ev, neutrons, C. T. Hibdon and C. O. Muehlhause—188(A)
Pair production at 17.6 Mev, R. L. Walker—1440
For $T^3(p,n)He^3$ from 1- to 2.5-Mev proton energies, G. A. Jarvis, A. Hemmendinger, H. V. Argo, and R. F. Taschek —168(A)
Schematic theory, H. Feshbach and V. F. Weisskopf—1550
Slow neutron cross section of free proton, Edward Melkonian—1744
Slow neutron studies of O_2, N_2, A, H_2, H_2O and hydrocarbons, Edward Melkonian—1750
Total for fast neutrons, C. K. Bockelman, R. E. Peterson, R. K. Adair, and H. H. Barschall—277
Total for 280-Mev neutrons, R. Fox, C. Leith, K. McKenzie, and L. Wouters—590(A)
Crystal structure
Allotropic modification of Ce, A. W. Lawson and Ting-Yuan Tang—301(L)
Analysis of clays for montmorillonite, L. H. Simons, D. F. Weekes, and J. G. Potter—467(A)
Ilmenite structure and ferroelectricity, B. T. Matthias and J. P. Remeika—1886(L)
Partition function by spinor analysis, Bruria Kaufman—1232
Short-range order in binary ising lattice, Bruria Kaufman and Lars Onsager—1244
Vacancies and diffusion in NiAl, R. Smoluchowski and H. Burgess—309(L)
Crystalline state
Anomalous internal friction, Al-Cu alloys, T'ing-Sui Kê—470(A)
Barrier layer in rectifiers, K. Lehovec—178(A)
Breakdown of ionic crystals, A. von Hippel and R. S. Alger —127
Color center bands in alkali halides, E. Burstein and J. J. Oberly—1254(L)
Color produced in quartz by x-rays, Guy Forman—196(A)
Conduction processes in thin deposits of Sb, Louis Harris and Lloyd H. Shaffer—943
Diffusion in binary alloys, J. Bardeen—1403
Electric breakdown in ionic crystals, Herbert B. Callen—1394
Electron multiplication in crystals, Frederick Seitz—1376
Electronic phase transition in iron, W. M. Elsasser and I. Isenberg—469(A)
Electronic states in perturbed periodic systems, Hubert M. James—1611
Electrons in perturbed periodic lattices, J. C. Slater—1592
Energy band structure of insulators, G. H. Wannier—438(L)
Energy bands and wave functions in periodic potentials, Hubert M. James—1602
Energy for diffusion by direct interchange, H. B. Huntington and Frederick Seitz—1728(L)
Energy levels in elemental Si, D. K. Holmes—178(A)
Ferroelectric crystals, B. T. Matthias, Elizabeth A. Wood, and A. N. Holden—175(A)
Ferroelectric properties of WO_3, B. T. Matthias—430(L)
Ferromagnetic ferrite, Haig P. Iskenderian—175(A)
Ferromagnetic resonance absorption in magnetite, L. R. Bickford, Jr.—137(L)
Fringe fields of domains, L. Marton and S. H. Lachenbruch —460(A)
Grain boundary diffusion, M. R. Achter and R. Smoluchowski—470(A)
Interstitial atomic diffusion coefficients, C. Wert and C. Zener—1169
Lattice energy of metallic Cu and Ag, Thomas P. Merritt and Royal M. Frye—470(A)
Low temperature transitions in $BaTiO_3$, H. J. Wellard—565(L)
Magnetostriction and order in $FeNi_3$, J. E. Goldman—471(A)
Martensitic transformations in iron-nickel, Andrew W. McReynolds—469(A)
Mobility of electrons in diamond, C. C. Klick and R. J. Maurer—179(A)
Nuclear magnetic resonance shift in metals, W. D. Knight —1259(L)
Nuclear spin-lattice relaxation time, internal motion, A. M. Sachs, E. H. Turner, and E. M. Purcell—466(A)
Nuclear spin-lattice relaxation times in solids, E. H. Turner, A. M. Sachs, and E. M. Purcell—465(A)
Ordering in Co-Pt, J. B. Newkirk and R. Smoluchowski—471(A)
Paramagnetic anisotropy of MnF_2, J. W. Stout and Maurice Griffel—144(L)
Partition function of the three-dimensional ferromagnet, D. ter Haar—176(A)
Polarizability of ions in simple crystals, Shepard Roberts—1215
Powder patterns on ferromagnetic crystals, Charles Kittel —1527(L)
Radial density function for crystals from x-ray intensity data, William J. Taylor—175(A)
Removal of space charge in diamond counters, A. G. Chynoweth—310(L)
Self-diffusion in silver, D. Turnbull—471(A); Gerald W. Johnson and T. Watanabe—588(A)
Single crystal selenium, properties, Herbert W. Henkels—1737(L)
Solids condensed from CO by alpha-particles, John H. L. Watson, Marcel Vanpee, and S. C. Lind—466(A)
Spin-lattice relaxation times in paramagnetic solids, C. P. Slichter and E. M. Purcell—466(A)
Statistical theory of regular mixtures, Yin-Yuan Li—972
Structures and phase transitions in barium titanate, P. W. Forsbergh, Jr.—1187
Thermo-optic properties of cubic crystals, Elias Burstein and Paul L. Smith—175(A)

Dielectric constants (see **Dielectrics and dielectric properties**)
Dielectrics and dielectric properties
Barium titanate at low temperatures, R. F. Blunt and W. F. Love—1202
Barium titanate, polarizabilities of ions in simple crystals, Shepard Roberts—1215
$BaTiO_3$ single-domain crystals, Walter J. Merz—1221
Diffraction of neutrons (see **Neutron diffraction**)
Diffusion (see also **Thermal diffusion**)
In binary alloys, J. Bardeen—1403
Interstitial atomic diffusion, C. Wert and C. Zener—1169
Self-diffusion of silver, D. Turnbull—471(A); Gerald W. Johnson and T. Watanabe—588(A)
Temperature variation for HCl, Gwynne B. Swartz—166(A)
Discharge of electricity in gases
Admittance of high frequency gas discharges, Edgar Everhart and Sanborn C. Brown—839
Amplification by interaction with stream of electrons, J. A. Roberts—340; L. R. Walker—1721(L)
Average energy of electrons in discharge, Lawrence J. Varnerin, Jr. and Sanborn C. Brown—457(A)
Coulomb interactions in a plasma, error, William P. Allis —146(L)
Clustering of ions and mobilities, Albert W. Overhauser—250
Densities in cathode spots, J. M. Somerville and W. R. Blevin—982(L)

Diffusion in helium, erratum, Manfred A. Biondi and Sanborn C. Brown—302(L)
Discharge instability, role of cathode, Leonard B. Loeb—255
Double-probe method, electron temperatures in gas discharges, E. O. Johnson and L. Malter—1411(L)
Electric breakdown in CO_2, D. R. Young—457(A)
Electric field and discharge photographs, F. G. Slack and Hsieh Yu-Chang—197(A)
Electron-ion recombination in diatomic gases, Manfred A. Biondi and Sanborn C. Brown—457(A)
High frequency breakdown in magnetic field, Benjamin Lax and Sanborn C. Brown—457(A)
High frequency discharge breakdown in H_2, A. D. MacDonald and Sanborn C. Brown—1634
High frequency gas discharge breakdown, diffusion theory, Sanborn C. Brown and A. D. MacDonald—1629
Imprisonment of resonance radiation, D. Alpert, A. O. McCoubrey, and T. Holstein—457(A)
Impulse breakdown in air, R. C. Fletcher—1501
Ionization measurement of $He^3(np)$ and $N^{14}(np)$, W. Franzen, J. Halpern, and W. E. Stephens—317(L)
Ions in Hg resonance cell containing N_2, R. H. Brown—591(A)
Microwave discharges in A, S. Krasik, D. Alpert, and A. O. McCoubrey—722
Plasma oscillation, J. R. Pierce—565(L)
Positive ion-electron recombination, Manfred A. Biondi and Sanborn C. Brown—190(A)
Potential and gradient distributions in parallel plane diodes, Wilson M. Brubaker—592(A)
Probe measurements in ionosphere, A. Reifman and W. G. Dow—987(L)
Propagation of streamers in sparks, B. A. Jacobsohn—585(A)
Radiative processes in discharges in He, R. G. Fowler and O. S. Duffendack—81
Sputtering in abnormal glow discharge, Richard Hanau—153(L)
Transport phenomena in presence of magnetic field, Rolf Landshoff—904

Discharge of electricity in high vacuum (see also **Thermionic emission**)
Cathode field in diodes, Henry F. Ivey—554
Diode space charge, Leigh Page and Norman I. Adams, Jr.—381

Disintegration and excitation of nucleus (see also **Nuclear spectra; Radioactivity**)
Of Al^{29}, L. Seidlitz, E. Bleuler, and D. J. Tendam—453(A)
Angular distribution from (d,n) reactions, C. E. Falk, E. Creutz, and F. Seitz—322(L)
Angular distribution of $Li^6(d,\alpha)\alpha$, Robert Resnick and D. R. Inglis—1318
Angular distribution, photo-disintegration of deuteron, W. M. Woodward and I. Halpern—107
Branching ratio in Be^7 decay, C. M. Turner—148(L)
Of Be^9, theory, Eugene Guth and Charles J. Mullin—234
Capture γ-ray spectrum of Cd, Bernard Hamermesh—182(A)
Capture gamma-ray studies, H. E. Kubitschek and S. M. Dancoff—182(A), 531
D-D reaction products, angular distribution, Yashihiro Nakano—981(L)
Deuteron bombardment of boron, Charles P. Swann and Emmett L. Hudspeth—168(A); Emmett L. Hudspeth and Charles P. Swann—1150
Disintegration electrons from Li_3^8, E. Pickup and L. Voyvodic—1534(L)
Disintegration energy of Al^{29}, L. Seidlitz, E. Bleuler, and D. J. Tendam—861(L)
Dispersion formula, applications, T. Teichmann and E. P. Wigner—185(A)
Distribution of photo-neutrons from deuterium, Edwin P. Meiners, Jr.—259
Distribution of protons from *D-D* reaction, H. A. Leiter, R. E. Meagher, F. A. Rodgers, and P. Gerald Kruger—167(A)
Distribution of protons in $N^{14}(dp)N^{15}$, L. D. Wyly—104
Electron excitation of In^{115*}, B. Waldman, W. C. Miller, and D. Gideon—181(A)
Electron-neutrino correlation in heavy elements, M. E. Rose—195(A)
Energy release in Be and Li reactions, A. V. Tollestrup, W. A. Fowler, and C. C. Lauritsen—428(L)
Excited state in Be^{10}, W. W. Buechner and E. N. Strait—168(A)
Excited states of Mg, proton bombardment, Roy Britten—169(A)
Gamma-n processes with bremsstrahlung, G. A. Price and D. W. Kerst—182(A)
Gamma-radiation from light nuclei, W. A. Fowler and C. C. Lauritsen—314(L)
Gamma-ray measurements, magnetic lens spectrometer, levels in Li^{7*}, B^{10*}, and Ni^{60*}, W. F. Hornyak, T. Lauritsen, and V. K. Rasmussen—731
Gamma-ray resonance in $C^{12}(p,\gamma)N^{13}$, D. M. Van Patter—1264(L)
γ-rays, deuteron bombardment of Be^9, V. K. Rasmussen, W. F. Hornyak, and T. Lauritsen—581(L); C. Y. Chao, T. Lauritsen, and V. K. Rasmussen—582(L)
Gamma-rays, direction and polarization, Franz Metzger and Martin Deutsch—187(A)
Gamma-rays from $T^3(p,\gamma)He^4$, H V. Argo, H. T. Gittings, A. Hemmendinger, G. A. Jarvis, H. Mayer, and R. F. Taschek—182(A)
Gamma-rays, interference effects, angular correlation, Daniel S. Ling and David L. Falkoff—1639
High energy photons by 350-Mev protons, Herbert F. York, Burton J. Moyer, and Russell Bjorklund—187(A)
K capture of Be^7, R. M. Williamson and H. T. Richards—453(A)
Lifetime of 479-kev state of Li^7, L. G. Elliott and R. E. Bell—168(A)
$Li^7(p,n)$ threshold voltage, absolute calibration, W. E. Shoupp, B. Jennings, and W. Jones—502
Long-range protons from bombardment of C by deuterons, G. C. Phillips, T. W. Bonner, and J. E. Richardson—169(A)
Low emission probability gamma-rays, R. G. Fluharty and Martin Deutsch—182(A)
Magnetic analysis of $Be^9(d,\alpha)Li^7$ and $Be^9(d,p)Be^{10}$, W. W. Buechner and E. N. Strait—1547
Magnetic analysis of $C^{13}(d,p)C^{13}$ and $O^{16}(d,p)O^{17}$, W. W. Buechner, E. N. Strait, A. Sperduto, and R. Malm—1543
Magnetic analysis of Li, *d* reactions, E. N. Strait and W. W. Buechner—1766
Neutrons from deuterons on Li^6, C. E. Mandeville, C. P. Swann, and S. C. Snowdon—980(L)
Neutrons from disintegration of Na by deuterons, C. E. Mandeville—436(L)
Particle groups from alpha-bombardment of boron isotopes, Robert J. Creagan—1769
Proton groups from bombardment of argon by deuterons, P. W. Davison, J. O. Buchanan, and Ernest Pollard—890
Protons from $He^3(d,p)He^4$, L. D. Wyly, V. L. Sailor, and D. G. Ott—1532(L)
Q value for $B^{10}(p\alpha)Be^7$, C. Y. Chao, C. C. Lauritsen, and A. V. Tollestrup—586(A)
Q values for $Ca^{40}(d,p)Ca^{41}$, mass difference (Ca^{40}-A^{40}), Vance L. Sailor—169(A)

Disintegration and excitation of nucleus (continued)
Range of charged particles from *D-D* reactions, Louis Rosen, Francis K. Tallmadge, and John H. Williams—1283
Relativistic generalization of *n-p* interactions, Armand Siegel—185(A)
Resonance reactions and angular correlation, L. Eisenbud—185(A)
Of Rh^{106}, Sb^{125}, and Pr^{143}, E. J. Jurney—290
Successive α-γ-emission and excited state of Li^7, Bernard T. Feld—168(A)
Thresholds for photo-neutron reactions, A. O. Hanson, R. B. Duffield, J. D. Knight, B. C. Diven, and H. Palevsky—578(L)
Voltage determination of resonances $F^{19}(p\alpha',\gamma)$, $B^{11}(p,\alpha)$ and $B^{11}(p,\gamma)$, A. H. Morrish—1651
X-ray yield curves for $(\gamma,2n)$ and (γ,p) reactions, G. C. Baldwin—182(A)
Yield of protons, tritons, and alphas from bombardment of Be^9, I. Resnick and S. S. Hanna—168(A)
Yields of Mn in spallation reactions, Norman A. Bonner and William C. Orr—140(L)

Elasticity
Constants of single crystals of Ni, W. P. Mason, R. M. Bozorth, H. J. McSkimin, and J. G. Walker—470(A)
Energy losses and fracture, J. L. Melchor, W. B. Good, and T. E. Pardue—202(A)
Ideal plastic body, Hilda Geiringer—875(A)
Large repeated strains of metals, instrumentation, J. P. Parker and T. E. Pardue—202(A)
Lattice energy of metallic Cu and Ag, Thomas P. Merritt and Royal M. Frye—470(A)
Plastic behavior of stiffened panels, Wolfe Mostow—876(A)
Quasi-isothermal slow fracture, F. T. Rogers, Jr.—203(A)
Shear modulus of Al, temperature coefficient, T'ing-Sui Kê—579(L)
Slow fracture, brittleness, Marguerite M. Rogers and F. T. Rogers, Jr.—203(A)
Statistical consideration of collisions, J. Elmer Rhodes, Jr.—202(A)
Strain rate effects, Richard LaTorre and Waller George—470(A)
Variation of constants of KCl, NaCl, CuZn, Cu, and Al with pressure, David Lazarus—545
Vibrational characteristics of piezoid, Charles R. Mingins, Carl A. Stevens, and David W. MacLeod, Jr.—467(A)
Vibrational spectrum of crystals, W. A. Bowers—467(A)

Electrical conductivity and resistance
Alpha-particles on superconductor, D. H. Andrews, R. D. Fowler, and M. C. Williams—154(L)
Al and Zn as superconductors below 1°K, J. G. Daunt and C. V. Heer—1324
Anode spark breakdown on distilled water surfaces, R. L. Young and Hugh F. Henry—198(A)
Barrier layer in rectifiers, K. Lehovec—178(A)
Barrier layer on *P*-type germanium, H. Y. Fan and R. Bray—458(A)
Bose-Einstein condensation for particles in magnetic field, superconductivity, M. F. M. Osborne—400
Breakdown of ionic crystals, A. von Hippel and R. S. Alger—127; Herbert B. Callen—1394
Concentration of holes and electrons by magnetic fields, H. Suhl and W. Shockley—180(A)
Crystal grain boundaries in Ge, G. L. Pearson—459(A)
In dielectrics during 2.5-Mev x-radiation, F. C. Armistead, J. C. Pennock, and L. W. Mead—860(L)
Electron injection in *P*-type germanium, Ralph Bray—458(A)
Electron multiplication in crystals, Frederick Seitz—1376
Energy band structure of insulators, G. H. Wannier—438(L)
Flow across *n-p* junctions, W. Shockley, G. L. Pearson, and M. Sparks—180(A)
Forces between currents in a superconductor and the lattice, E. U. Condon and E. Maxwell—578(L)
Of Au at low temperatures, C. T. Lane—304(L)
Induction in a superconductor, A. Wexler and W. S. Corak—432(L); W. V. Houston and C. F. Squire—685(L)
Infra-red transmission of germanium, M. Becker and H. Y. Fan—1530(L); of silicon, M. Becker and H. Y. Fan—1531(L)
Magnetic effects of rotating superconductor, W. F. Love, R. F. Blunt, and P. B. Alers—305(L)
Magnetic moments, spherical superconductors, J. J. Fritz, O. D. Gonzales, and H. L. Johnston—580(L)
Magnetic threshold of a superconductor, G. Preston Burns—999(L)
Magnetically biased transistors, C. Bradner Brown—1736(L)
Mobilities in Ge single crystals, G. L. Pearson—179(A)
Modulation of resistance of Ge filament, W. Shockley, G. L. Pearson, M. Sparks, and W. H. Brattain—459(A)
Neutron irradiated semiconductors, W. E. Johnson and K. Lark-Horovitz—442(L)
Of ordered $AuCu_3$ produced by single slip, T. H. Blewitt and J. S. Koehler—470(A)
P-type germanium transistor, W. F. Pfann and J. H. Scaff—459(A)
Of polycrystalline graphite, theory, Dwain Bowen—1878(L)
Pressure coefficient of resistance in semiconductors, P. H. Miller, Jr. and Julius Taylor—179(A)
Reflectivity of germanium semiconductors, K. Lark-Horovitz and K. W. Meissner—1530(L)
Resistance changes during strains, E. W. Kammer and T. E. Pardue—202(A); instrumentation, E. W. Kammer and T. E. Pardue—202(A)
Resistivity of Ge, electric field, Ralph Bray—152(L)
Single crystal selenium, properties, Herbert W. Henkels—1737(L)
Superconducting torus, R. L. Dolecek and Jules de Launay—445(L)
Superconductors at 24,000 megacycles per second, E. Maxwell, P. M. Marcus, and J. C. Slater—1332
Superconductors below 1°K, Ti, J. G. Daunt and C. V. Heer—715
Superconductors in alternating fields, Robert T. Webber, J. M. Reynolds, and T. R. McGuire—293
Surface impedance of metals at 24,000 Mc/sec., W. B. Nowak and J. C. Slater—469(A)
Theory of superconductors, A. R. Miller—1001(L)
Thin deposits of Sb, Louis Harris and Lloyd H. Shaffer—943
Time effects in superconducting cylinders, Robert T. Webber—167(A)
Of Sn in normal and superconducting states, surface resistiviy, William M. Fairbank—167(A), 1106
Of tin superconductors, B. Serin, J. R. Feldmeier, and M. Garfunkel—167(A)
Of Ti, Walter C. Michels and Sally E. Wilford—174(A)

Electrodynamics (see **Electromagnetic theory; Quantum electrodynamics**)

Electrolysis
Space charge in electrolytes, Charles Albert Reed and William Schriever—197(A)

Electromagnetic theory
Amplification by interaction with stream of electrons, J. A. Roberts—340; L. R. Walker—1721(L)
Basic theory and correspondence principle, Herman M. Schwartz—192(A)
Biconical antennas, C. T. Tai—456(A)
Deflection of electrons in inhomogeneous electrostatic field, Jenny E. Rosenthal—180(A)

Eddy currents induced in conducting plane, Stanley A. Jashemski and W. C. Wineland—198(A)
Finite relativistic charge-current distributions, D. Bohm, M. Weinstein, and H. Kouts—867(L)
Impedance and generalized two-wire line theory, K. Tomiyasu and Ronold King—456(A)
Induction in a superconductor, A. Wexler and W. S. Corak —432(L); W. V. Houston and C. F. Squire—685(L)
Magneto-hydrodynamic waves, S. Lundquist—1805
Motion in constant magnetic field, M. H. Johnson and B. A. Lippmann—828
Propagation modes of a helix, William Sollfrey—455(A)
Radiation from uniformly accelerated charge, D. L. Drukey —543
Scalar and longitudinal photons in electromagnetic fields, Frederik J. Belinfante—226
Superconducting torus, R. L. Dolecek and Jules de Launay —445(L)
Surface wave of Sommerfeld, T. Kahan and G. Eckart—406
Waves guided by single surface, F. J. Zucker—586(A)

Electrons (see also **Positrons**)
Classical theory, Alfred Landé—191(A)
Inequality of electron and proton charges, experimental limit, Vernon Hughes—474(A)

Electrons, scattering of (see **Scattering of electrons, neutrons, and ions**)

Electrons, secondary
At high temperatures, F. C. Todd and L. J. Rueger—189(A)
From homogeneous solids, interpretation, E. J. Sternglass —189(A)
From silicon and germanium oxides, H. E. Mendenhall— 458(A)

Elements
Abundance of Re in nature, Harrison Brown and Edward Goldberg—1260(L)
Actinide series and the periodic table, Zoltán Szabó—147(L)
Origin, Maria G. Mayer and Edward Teller—1226
Regularity and continuity of nuclear series, William D. Harkins and Martin Popelka, Jr.—989(L)
V^{50} in nature, David C. Hess, Jr. and Mark G. Inghram— 1717(L)

Equations of state
For gaseous He^3, J. van Kranendonk, K. Compaan, and J. de Boer—998(L); 1728(L)

Errata
Altitude dependence of penetrating particles slowed down after traversing 15 cm of lead, Marcello Conversi— 1541(L)
Application of Dyson's method to meson interactions, P. T. Matthews—1419(L)
Bremsstrahlung in high energy nucleon-nucleon collisions, J. Ashkin and R. E. Marshak—989(L)
Chi-square test as a criterion for testing halogen-filled Geiger tubes, A. B. Willoughby—1266(L)
Determination of nuclear gyromagnetic ratios, John R. Zimmerman and Dudley Williams—1264(L)
On the difficulty of the meson theory of nuclear forces, Gentaro Araki—437(L)
Equation of state of gaseous He^3, J. van Kranendonk, K. Compaan, and J. de Boer—1728(L)
Excitation functions for (α,n), $(\alpha,2n)$, and $(\alpha,3n)$ reactions on indium, Georges M. Temmer—1002(L)
Influence of the length of a hot wire on the measurements of turbulence, F. N. Frenkiel—686(L)
Infra-red spectrum and molecular constants of $C^{12}O^{16}$ and $C^{13}O^{16}$, Robert T. Lagemann, Alvin H. Nielsen, and Fred P. Dickey—159(L)
Measurements of ambipolar diffusion in helium, Manfred A. Biondi and Sanborn C. Brown—302(L)
Paper by Landau on Coulomb interactions in a plasma, William P. Allis—146(L)
Production of mesons by photons and electrons, Herman Feshbach and Melvin Lax—689(L)
Scattering of slow neutrons by paramagnetic crystals, I. W. Ruderman, W. W. Havens, Jr., T. I. Taylor, and L. J. Rainwater—434(L)
Second viscosity of liquids, L. N. Liebermann—440(L)

Excitation of nuclei (see **Disintegration and excitation of nucleus; Nuclear structure**)

Explosion phenomena (see also **Shock waves**)
Adiabatic parameters of explosion bubbles, H. G. Snay and E. Swift, Jr.—881(A)
Bubble period at great depths, John P. Slifko, E. Swift, Jr., and W. S. Shultz—881(A)
Photography of explosion bubbles, Paul M. Fye and Robert S. Price—881(A)

Ferroelectric properties (see also **Crystalline state**)
Barium titanate at low temperatures, R. F. Blunt and W. F. Love—1202
Barium titanate, polarizabilities of ions in simple crystals, Shepard Roberts—1215
$BaTiO_3$ single-domain crystals, Walter J. Merz—1221
Ferroelectric crystals, B. T. Matthias, Elizabeth A. Wood, and A. N. Holden—175(A)
Of ferromagnetic ferrite, Haig P. Iskenderian—175(A)
In ilmenite structure, B. T. Matthias and J. P. Remeika —1886(L)
Spontaneous polarization of $BaTiO_3$, W. J. Merz—459(A)
Structures and phase transitions in barium titanate, P. W. Forsbergh, Jr.—1187
Of WO_3, B. T. Matthias—430(L)

Ferromagnetism (see **Magnetic properties**)

Field theory (see also **Quantum electrodynamics**)
Covariant field theories, Peter G. Bergmann and Johanna H. M. Brunings—191(A)
Relations between electromagnetism and gravitation, Antonio Gião—764

Films, properties of
Condensation of metals on surfaces, effect of temperature, Leonard O. Olsen, E. C. Crittenden, Jr., and R. W. Hoffman—1891(A)
Temperature dependence of structure, Ag films, Gerald W. Johnson—588(A)

Fission of nucleus
Alpha-particles emitted, L. L. Green and D. L. Livesey— 580(L)
Of Bi and Pb, R. H. Goeckermann and I. Perlman—628
Cloud-chamber study of fragments, J. K. Bøggild, L. Minnhagen, and O. B. Nielsen—988(L)
Delayed neutrons from thorium, L. G. Creveling, J. R. Hood, and M. L. Pool—946
Division of nuclear charge, D. C. Brunton—1798
Energy distribution of fragments, D. C. Brunton and W. B. Thompson—848(L)
Fission-asymmetry, G. C. Wick—181(A)
Kinetic energy release in fission of U^{238}, U^{235}, Th^{232}, and Bi^{209}, J. Jungerman and S. C. Wright—1112
Mass and charge of fission products, K. H. Kingdon—136(L)
Mass of xenon activities, Sigvard Thulin, Ingmar Bergström, and Arne Hedgran—871(L)
Radioactive krypton isotopes, J. Koch, O. Kofoed-Hansen, P. Kristensen, and W. Drost-Hansen—279
Ternary fission in U, J. T. Dewan and K. W. Allen—181(A); Louis Rosen and Alvin M. Hudson—181(A)
Tripartition and quadripartition of uranium, R. Chastel and L. Vigneron—870(L)
Uranium^{235} in thucholite, J. B. Orr—155(L)
Widespread detection of fission products, J. H. Webb—375

Fission of nucleus (continued)
Yields of Cs isotopes, Mark G. Inghram, David C. Hess, Jr., and John H. Reynolds—1717(L)
Fluid dynamics (see also **Aerodynamics; Hydrodynamics**)
Flow past models in shock tube, C. W. Mautz—172(A)
Momentum thickness in turbulent layer, D. Bershader—171(A)
Turbulence by using non-compensated hot-wires, F. N. Frenkiel—171(A)
Fluorescence
Of mono-substituted benzenes in near ultraviolet, Arnold M. Bass and H. Sponer—177(A)
Persistence in Hg vapor, T. Holstein, D. Alpert, and A. O. McCoubrey—1259(L)
Friction
Anomalous internal friction, Al-Cu alloys, T'ing-Sui Kê—470(A)
Molecular structure of lubricant, J. T. Burwell and C. D. Strang—455(A)

Gamma-rays (see **Disintegration and excitation of nucleus; Radioactivity**)
Gases (see **Aerodynamics; Kinetic theory**)
Geophysics
Convective process and thickness of porous medium, H. L. Morrison and F. T. Rogers, Jr.—203(A)
Magnetism in sedimentary rocks, John W. Graham—176(A)
Neutrinos from the sun, source of earth's heat, D. Saxon—986(L)
Gravitation
Einstein's generalized theory, V. V. Narlikar and Ramji Tiwari—868(L)
Relations between electromagnetism and gravitation, Antonio Gião—764
Gyromagnetic effect
New effect, S. J. Barnett and Louis A. Giamboni—1542(L)
Gyromagnetic ratio (see **Magnetic properties; Nuclear moments and spin**)

Hall effect
In ferromagnetics, Emerson M. Pugh—176(A)
Metal-semiconductor point contacts, S. Benzer—150(L)
In Ni, Albert I. Schindler and Emerson M. Pugh—176(A)
Heat conduction (see **Thermal conductivity**)
Hydrodynamics
Conformal mapping of multiply-connected domains, George Springer—876(A)
Convective process and thickness of porous medium, H. L. Morrison and F. T. Rogers, Jr.—203(A)
Effect of viscosity on circulation, C. Truesdell—192(A)
Establishment of flow in water entry, Eugene P. Cooper—592(A)
Flows of compressible fluid, Stefan Bergman—876(A)
Isotropic turbulence, S. Chandrasekhar—158(L)
Magneto-hydrodynamic waves, S. Lundquist—1805
Non-linear transformations, Daniel Shanks—876(A)
Plane, rotational, Prandtl-Meyer flows, M. H. Martin—877(A)
Prandtl-Glauert transformation, inconsistencies, H. W. Sibert—877(A)
Representation of isentropic subsonic compressible flow, Hans Kraft—877(A)
Ship forms of least resistance, J. V. Wehausen—878(A)
Symmetric and plane supersonic flows, P. Zettler-Seidel—877(A)
Transformation between one- and three-dimensional power spectra, fluctuation field, Leslie S. G. Kovasznay, Mahinder S. Uberoi, and Stanley Corrsin—1263(L)
Transonic flow around a closed body, Arthur Zeichner—876(A)

Hyperfine structure (see also **Nuclear moments and spin**)
Band spectrum of HgH, S. Mrozowski—1714
Of Co, B. Bleaney and D. J. E. Ingram—466(A)
Electron-nuclear potential fields, M. F. Crawford and A. L. Schawlow—1310
Of 4^3P-4^3D of Al II, S. Suwa—847(L)
Of hydrogen, effect of nuclear motion, G. Breit, G. E. Brown, and G. B. Arfken—1299
Of hydrogen, effects of proton radius, G. E. Brown and G. B. Arfken—1305
Of Fe 57, Jean Brossel—858(L)
Of Kr^{83} and Ne^{21}, Jørgen Koch and Ebbe Rasmussen—1417(L)
Potential fields from hyperfine structure, A. L. Schawlow and M. F. Crawford—174(A)
Resonance experiments with Na^{22}, K^{40}, Cs^{135}, and Cs^{137}, Luther Davis, Jr., Darragh E. Nagle, and Jerrold R. Zacharias—1068
Of Se^{77}, J. E. Mack and O. H. Arroe—173(A)
Of stable chlorine isotopes, Luther Davis, Jr., Bernard T. Feld, Carrol W. Zabel, and Jerrold R. Zacharias—1076
Of Te^{125}, G. R. Fowles—571(L)
Of $^2P_{3/2}$ state of Al^{27}, Hin Lew—1086

Ionization potentials
Electron quantum numbers of atoms and ions, Wolfgang Finkelnburg—173(A)
Of neon by atomic projectiles, John H. Martin—190(A)
Ionosphere
Probe measurements, A. Reifman and W. G. Dow—987(L)
Tidal effects in *F* layer, M. W. Jones and J. G. Jones—581(L)
Isomers, nuclear (see **Nuclear structure; Radioactivity**)
Isotopes
Abundance of I^{129}, Te^{118}, and Pt^{190}, Wallace T. Leland—992(L)
Abundance of Re in nature, Harrison Brown and Edward Goldberg—1260(L)
Neutron-hydrogen mass difference, William E. Stephens—181(A)
Nuclear periodic scheme in three dimensions, S. Podgor—1271(L)
Odd-odd isotope of V, Wallace T. Leland—1722(L)
Pt^{195}-Cu^{65} packing fraction difference, Henry E. Duckworth—690(L)
Rare stable isotopes, Henry E. Duckworth, Robert F. Black, and Richard F. Woodcock—462(A)
Regularity and continuity of nuclear series, William D. Harkins and Martin Popelka, Jr.—989(L)
Separation of He^3, Charles A. Reynolds, Henry A. Fairbank, C. T. Lane, B. B. McInteer, and Alfred O. Nier—64, 167(A)
Separation of isotopes of Hg, C. P. Keim—1270(L)
V^{50} in nature, David C. Hess, Jr. and Mark G. Inghram—1717(L)
Xe isotopes produced in fission, Sigvard Thulin, Ingmar Bergström, and Arne Hedgran—871(L)

Kinetic theory
Gas dynamics, Paul Lieber—882(A)
Of rarefied gases, Harold Grad—882(A)
Transport phenomena in ionized gas, Rolf Landshoff—904

Liquids (see also **Hydrodynamics**)
Absorption and dispersion of sound, Leonard Liebermann—1520
Adsorption of helium at liquid helium temperatures, Earl A. Long and Lothar Meyer—440(L); William Band—441(L)
Bose-Einstein condensation for particles in magnetic field, M. F. M. Osborne—400

Film transfer rate in He II, Robert T. Webber, Henry A. Fairbank, and C. T. Lane—609
He^3 assemblies, Louis Goldstein and Max Goldstein—464(A)
He^3 in He^4, J. W. Stout—864(L)
Lambda-temperatures of He^3-He^4 mixtures, B. M. Abraham, B. Weinstock, and D. W. Osborne—864(L)
Non-equilibrium states in He II, William Band and Lothar Meyer—417
Rollin film in liquid helium, Henry A. Fairbank and C. T. Lane—1209
Second sound and classical heat flow, John R. Pellam—872(L)
Second sound velocity in He II, John R. Pellam and Russell B. Scott—869(L); R. D. Maurer and Melvin A. Herlin—948
Separation of He^3, Charles A. Reynolds, Henry A. Fairbank, C. T. Lane, B. B. McInteer, and Alfred O. Nier—64, 167(A)
Superfluidity in He II, correlations in measurements, John R. Pellam—158(L)
Thermodynamics of liquid He, O. K. Rice—1701

Magnetic properties (see also **Nuclear moments and spin**)
Antiferromagnetism, detection of, C. G. Shull and J. Samuel Smart—1256(L)
Ferromagnetic ferrite, Haig P. Iskenderian—175(A)
Ferromagnetic resonance absorption in magnetite, L. R. Bickford, Jr.—137(L)
Fringe fields of domains, L. Marton and S. H. Lachenbruch—460(A)
Gyromagnetic ratios and splitting factors of ferromagnetic substances, Charles Kittel—176(A)
Magnetic threshold of a superconductor, G. Preston Burns—999(L)
Of magnetite single crystals, C. A. Domenicali—460(A)
Magnetization and Curie point of iron oxides, Louis R. Maxwell, J. Samuel Smart, and Stephen Brunauer—459(A)
Magnetostriction and order in $FeNi_3$, J. E. Goldman—471(A)
Magnetostriction, twisting of rod, R. F. Janofsky, M. Melamed, and R. A. Beth—1891(A)
Movement of small metal particles about an electric current, J. A. Schedling—843
Nature of magnetic poles, M. Avramy Melvin—592(A)
Paramagnetic anisotropy of MnF_2, J. W. Stout and Maurice Griffel—144(L)
Paramagnetic relaxation, absorption line width, Arianna Wright—1826
Powder patterns on ferromagnetic crystals, Charles Kittel—1527(L)
Proximity effects, magnetic susceptibility, M. C. Steele—566(L)
Of rotating superconductor, W. F. Love, R. F. Blunt, and P. B. Alers—305(L)
Of sedimentary rocks, John W. Graham—176(A)
Susceptibilities of tetravalent uranium fluorides, Norman Elliott—431(L)
Susceptibility at liquid He temperatures, T. R. McGuire—167(A)
Susceptibility of zinc, cadmium, and gamma-brass, temperature dependence, Jules A. Marcus—621
Susceptibility of Zn at low temperatures, Jules A. Marcus—413

Magnetic resonance absorption (see also **Nuclear moments and spin**)
Of diluted iron ammonium alum, R. T. Weidner, P. R. Weiss, C. A. Whitmer, and D. R. Blosser—1727(L)
Gyromagnetic ratios for 6 nuclei, William H. Chambers and Dudley Williams—638
In magnetite, L. R. Bickford, Jr.—137(L)
In NO, Robert Beringer and J. G. Castle, Jr.—868(L)
Nuclear magnetic resonance shift in metals, W. D. Knight—1259(L)

Magnetostriction (see **Magnetic properties**)

Mass ratios (see **Isotopes**)

Mass spectroscopy (see also **Isotopes**)
Magnetic time-of-flight mass spectrometer, Paul I. Richards, Earl E. Hays, and S. A. Goudsmit—180(A)

Mechanics, quantum—atomic structure and spectra
Complex spectra, theory, Giulio Racah—1352
Helium wave equation, James H. Bartlett—460(A)
Relativity corrections for energy levels, V. Rojansky and Frank Stern—184(A)

Mechanics, quantum—general
Internal coordinates of a particle, H. C. Corben—460(A)
Invariant determination of position operators, T. D. Newton and E. P. Wigner—191(A)
Lambda-limiting process; theory of elementary particles, I. Pomeranchuk—298
Operator matrices for space and time intervals, Richard Schlegel—191(A)
Particle on a string, Nathan Rosen—202(A)
Radius of elementary particle, Hideki Yukawa—300(L)
Two-component wave equations, C. W. Kilmister—568(L); J. Serpe—1538(L)
Wave equations in de Sitter Space, Satosi Watanabe—296
Wave functions in magnetic field, M. H. Johnson and B. A. Lippmann—184(A)

Mechanics, quantum—nuclear
Continuity of first derivative in Wigner-Eisenbud formalism, J. L. Jackson—185(A)
Elaboration of Schrödinger formalism, J. W. Calkin—846(L)
Future nuclear interaction, Alex E. S. Green—870(L)
Interaction between neutrons and electrons, H. Ekstein—1328
Meson energy levels in a Coulomb field, Albert Simon—1877(L)
Nuclear forces in pseudoscalar meson theory, K. M. Watson and J. V. Lepore—1157
Perturbation methods for Dirac radial equations, G. Breit and G. E. Brown—1307
Phase shifts in proton-alpha-scattering, C. L. Critchfield and D. C. Dodder—602
Scalar and longitudinal photons in electromagnetic fields, Frederik J. Belinfante—226

Mechanics, quantum—of solid state
Electronic states in perturbed periodic systems, Hubert M. James—1611
Electrons in perturbed periodic lattices, J. C. Slater—1592
Energy bands and wave functions in periodic potentials, Hubert M. James—1602

Mechanics, statistical
H-theorem, deductions, Harvey Einbinder—410
Approach to statistical equilibrium, Arnold J. F. Siegert—1708
Bose-Einstein condensation for particles in magnetic field, M. F. M. Osborne—400
Bose-Einstein condensation for thin films, M. F. M. Osborne—396
Of mixtures of He^3 and He^4, J. de Boer—852(L)
Statistical theory of regular mixtures, Yin-Yuan Li—972
Theory of critical fluctuations, M. J. Klein and L. Tisza—1861
Three-dimensional ferromagnet, Takehiko Oguchi—1001(L)

Mesons (see also **Cosmic radiation**)
Are mesons elementary particles? E. Fermi and C. N. Yang—1739

Mesons (continued)
Capture of μ-mesons by deuterons, Irving Stein and L. I. Schiff—461(A)
Capture of negative mesons, J. Barnothy—303(L)
Creation by high energy nucleons, E. Strick—190(A)
Decay electrons from mesons, A. H. Benade and R. D. Sard—488
Decay of heavy τ-meson, S. Power—865(L)
Decay of π-meson, M. Ruderman and R. Finkelstein—1458
Density effect, W. L. Whittemore and J. C. Street—170(A)
Dyson's methods, meson interactions, P. T. Matthews—684(L); erratum—1419(L)
Energy levels in a Coulomb field, Albert Simon—1877(L)
Energy spectrum of decay particles, Robert B. Leighton, Carl D. Anderson, and Aaron J. Seriff—159(L)
Excess of negative over positive, K. A. Brueckner and M. L. Goldberger—1725(L)
Half-life of positive π-meson, E. A. Martinelli—589(A)
Interaction between nucleons in pseudoscalar meson theory, H. A. Bethe—191(A)
Interaction representation, Frederik J. Belinfante—191(A)
Interaction with electromagnetic field, W. H. Furry and M. Neuman—432(L); M. Neuman and W. H. Furry—1677
Interactions of vector meson with scalar excited state, Marshall N. Rosenbluth—951
Magnetic deflection in photographic plates, I. Barbour—170(A)
Mass values of π^--, π^+-, and μ^+-mesons, A. S. Bishop, H. Bradner, and F. M. Smith—588(A)
Meson decay by scintillation counters, George T. Reynolds and F. B. Harrison—169(A)
Meson-nucleon couplings, K. M. Case—14
Mesons near sea level, William L. Kraushaar—1045
μ-meson capture, M. Taketani and M. Sasaki—852(L)
Negative π-mesons produced by protons, Stanley B. Jones and R. Stephan White—588(A)
Nuclear forces in pseudoscalar meson theory, K. M. Watson and J. V. Lepore—1157
π-mesons by high energy nucleons, E. Strick and D. ter Haar—304(L)
π-mesons by nucleon-nucleon collisions, Cecile Morette—1432
Polarization of mesons in gamma-nucleon collisions, Daniel B. Feer—306(L)
Positive excess, Robert B. Brode—468(A)
Positive excess at 30,000 ft., Marcello Conversi—311(L)
Production, H. W. Lewis—566(L)
Production and absorption, R. L. Cool, E. C. Fowler, and J. C. Street—468(A)
Production by gamma-rays, Leslie L. Foldy—372
Production by photons and electrons, Herman Feshbach and Melvin Lax—134
Production in photo-nuclear collision, Melvin Lax and H. Feshbach—190(A)
Production in stratosphere, Marcel Schein and J. J. Lord—170(A)
Production of; interaction of light nuclei, H. Koppe—688(L)
Production of positive mesons, erratum, Herman Feshbach and Melvin Lax—689(L)
Radiation accompanying meson creation, L. I. Schiff—89
Spin of μ-mesons, J. Tiomno—856(L)
Spontaneous decay of heavy mesons, L. I. Schiff—303(L), 468(A); L. I. Schiff and D. L. Weisman—1266(L)
Star production by negative μ-mesons, H. G. Voorhies and J. C. Street—1100
Subtraction fields and lifetimes of meson, J. Steinberger—1180
τ-meson, Norbert Wagner and D. Cooper—449(L)
Theory of nuclear forces, erratum, Gentaro Araki—437(L)
Tomonaga-Schwinger theory, interaction of nucleons with mesons, P. T. Matthews—1657
Two-meson theory, Mituo Taketani, Seitaro Nakamura, Kenichi Ono, and Muneo Sasaki—60; M. Taketani and M. Sasaki—582(L)
Underground cosmic-ray data, K. Greisen—1718(L)
Variation of intensity with height, P. H. Barker—141(L)
Vector meson-photon interaction, George J. Yevick—461(A)

Metals (see **Crystalline state**)

Metastable atoms and molecules
Of $_{71}Lu^{177}$, F. K. McGowan—1730(L)

Meteorology
Atmospheric ozone temperatures, William M. Benesch—863(L)
Effects of meteorological conditions on microwave propagation, J. E. Boyd and Catherine Yoe—203(A)
Microwave propagation study in lower troposphere, F. E. Lowance and R. A. Martin—202(A)

Methods and instruments
Afterglow in low density supersonic streams, Thomas W. Williams and James M. Benson—456(A)
Alpha-particles on a superconductor, counter, D. H. Andrews, R. D. Fowler, and M. C. Williams—154(L)
Amplification by interaction with stream of electrons, J. A. Roberts—340; L. R. Walker—1721(L)
Amplitude bridge for nuclear resonance detection, R. D. Huntoon and H. A. Thomas—163(A)
Analysis of betatron radiation, nuclear emulsion, P. K. S. Wang and M. Wiener—1724(L)
Analysis of delayed coincidence counting, Daniel Binder—856(L); F. W. Van Name, Jr.—1734(L)
Antiferromagnetism, detection of, C. G. Shull and J. Samuel Smart—1256(L)
Automatic grain counting of tracks, P. V. C. Hough—163(A)
Background eradication in emulsions, M. Wiener and H. Yagoda—469(A)
Beta-ray spectrometer, ring focus, Joseph M. Keller, Ernest Koenigsberg, and Arthur Paskin—454(A)
Beta-ray spectrometer with uniform magnetic field, F. H. Schmidt—586(A)
Beta-ray spectrum, analysis, Mitsuo Sakai and Seitaro Nakamura—967
Bioelectric potentials, precision method, Edgar B. Darden and Otto Stuhlman, Jr.—197(A)
Blade shapes of compressors, H. J. Reissner—878(A)
Boundary layer optics in two-dimensional flow, D. Bershader and G. P. Wachtell—880(A)
Boundary value problems involving moving boundaries, Howard Reiss and Victor K. La Mer—192(A)
Cadmium sulfide crystal counter, detection of x-ray, Samuel G. Zizzo and Joseph B. Platt—704(L)
Calculating drag coefficient, G. L. Shue—879(A)
Cathode field in diodes, Henry F. Ivey—554
Cavity microwave spectroscopy, I. R. Weingarten and G. E. Kimball—177(A)
Ceramic materials for synchrotron vacuum tubes, J. E. Thomas, Jr., W. M. Shakespeare, Jr., B. Cohen, R. B. Patten, and V. P. Henri—162(A)
Coincidence, anticoincidence unit, C. A. Schroeder, J. D. Shipman, Jr., and P. R. McCray—163(A)
Condensation of metals on surfaces, effect of temperature, Leonard O. Olsen, E. C. Crittenden, Jr., and R. W. Hoffman—1891(A)
Conduction of heat, long circular cylinder, R. H. Ritchie and C. B. Crawley—197(A)
Construction of hydrophones, high frequency electroacoustic effect, John Bugosh, Ernest Yeager, and Frank Hovorka—1891(A)

Cornell synchrotron, design, Boyce D. McDaniel, John W. DeWire, Dale R. Corson, and Robert R. Wilson—162(A)
Cornell synchrotron, initial performance, D. R. Corson, C. P. Baker, J. W. DeWire, B. D. McDaniel, C. D. Swartz, R. L. Walker, R. R. Wilson, and W. M. Woodward—162(A)
Criterion for testing halogen-filled Geiger tubes, A. B. Willoughby—1266(L)
Damping and time of return of galvanometer coil, Marvin S. Cohen and Clyde B. Crawley—198(A)
Dead time and recovery time, counters, K. Sitte—164(A)
Deflection of electrons in inhomogeneous electrostatic field, Jenny E. Rosenthal—180(A)
Density-gradient tube, finely divided materials, William H. Otto—465(A)
Detection of radioactive atoms in air, Č. Jech—1731(L)
Double-probe method, electron temperatures in gas discharges, E. O. Johnson and L. Malter—1411(L)
Effect of C^{14}, Ca^{45}, P^{32}, I^{131}, and Zn^{65} on emulsions, Daniel Steinberg and A. K. Solomon—453(A)
Electrical analog for heat flow, J. M. Kendall—879(A)
Electro-optic coefficients in ADP crystals, R. O'B. Carpenter—467(A)
Electrostatic analyzer, Mary Jane A. Linker—198(A)
Emulsions for ionizing particles, stopping power, Hervasio G. de Carvalho—1721(L)
Energy dependence of counters, R. H. Davis and J. D. Graves—590(A)
Energy of fast neutrons by photographic emulsions, George R. Keepin and James H. Roberts—154(L)
Engraved circle by constant angle method, R. M. Talley and H. M. Kaylor—201(A)
Equivalence theorems for meson-nucleon couplings, K. M. Case—14
Equivalent electrical circuit for galvanometer, R. C. Kinnamon, M. S. Cohen, and C. B. Crawley—198(A)
Fading of proton tracks, K. B. Mather—486
Faraday by magnetic resonance, J. A. Hipple, H. Sommer, and H. A. Thomas—1877(L)
Finite aperture fringe intensity, Fabry Perot interferometers, Felix E. Geiger, Jr.—173(A)
Focusing curved-crystal spectrometer, improved, David A. Lind, J. R. Brown, and Jesse W. M. DuMond—1838
Gamma-ray detector, constant sensitivity, J. Pine and R. Sherr—455(A)
Germanium counter, Kenneth G. McKay—1537(L)
Germanium photo-resistance cell, J. N. Shive—575(L)
Glow discharge, measuring air flow characteristics, F. D. Werner—883(A)
Heat flow below 1°K, J. G. Daunt and C. V. Heer—985(L)
High frequency barium titanate hydrophone, John Bugosh, Ernest Yeager, and Frank Hovorka—1890(A)
High intensity cyclotron, E. J. Lofgren—587(A)
High speed frame camera, S. J. Jacobs and A. A. Klebra—881(A)
Hollow cathode for hyperfine structure, O. H. Arroe and J. E. Mack—173(A)
Hot wire anomometer, R. Betchov—879(A)
Hot wire length correction, F. N. Frenkiel—999(L)
Hot wire measurements of turbulence, erratum, F. N. Frenkiel—686(L)
Intensity of cosmic rays, residual ionization, Victor F. Hess and Roger P. Vancour—1205
Ion source for mass spectrography, R. F. K. Herzog and F. P. Viehböck—855(L)
Large diameter "Hilsch tubes," Lester I. Bockstahler and Harmon Plumb—166(A)
Light intensity in Mach-Zehnder interferometer, E. H. Winkler—880(A)
Light source for hydrodynamical studies, exploded wires, Thomas P. Liddiard and Ralph D. Drosd—879(A)
Linear electron accelerator, G. E. Becker and D. A. Caswell—587(A)
LiF as a scintillation detector, E. C. Farmer, H. B. Moore, and Clark Goodman—454(A)
$Li^7(p,n)$ threshold voltage, absolute calibration, W. E. Shoupp, B. Jennings, and W. Jones—502
Locating stars in nuclear track plates, E. H. Land and W. A. Shurcliff—469(A)
Low frequency modulation technique, Vinton A. Brown and F. L. Yost—201(A)
Magnetic amplifiers, theory, Robert T. Beyer and Ming-Yi Wei—455(A)
Magnetic analyzer for electrostatic generators, D. B. Duncan—587(A)
Magnetic cooling, C. V. Heer and J. G. Daunt—854(L); J. G. Daunt and C. V. Heer—985(L)
Magnetic deflection mesons in nuclear plates, Ian Barbour—320(L)
Magnetic time-of-flight mass spectrometer, Paul I. Richards, Earl E. Hays, and S. A. Goudsmit—180(A)
Magnetically biased transistors, C. Bradner Brown—1838(L)
Magnetostriction, control of oscillators, R. F. Janofsky, M. Melamed, and R. A. Beth—1891(A)
Mass spectra with a cathode-ray oscillograph, J. W. Townsend, Jr.—465(A)
M.I.T. 300-Mev electron synchrotron, J. S. Clark, W. W. Drake, and C. Y. Tsao—162(A)
Maximum and minimum intensity in the Fresnel diffraction pattern, E. J. Scheibner—201(A)
Micro-calorimeter, C. V. Cannon and G. H. Jenks—455(A)
Microwave linear accelerator, D. Errett, J. MacKay, R. Pepper, F. Rieke, D. Roller, and L. Silber—180(A)
Molecular beam resonance method, Norman F. Ramsey—996(L)
Mounting for large mirrors, William H. Haynie—1891(A)
Neutron-proton scattering data, interpretation, John M. Blatt and J. David Jackson—18
Noise characteristics of dry cells, B. R. Russell and P. H. Miller, Jr.—190(A)
Nuclear periodic scheme in three dimensions, S. Podgor—1271(L)
Nuclear resonances in rotating magnetic fields, E. H. Rogers and H. H. Staub—585(A)
Optical detection of radiofrequency resonance, F. Bitter—465(A)
Pattern of magnetic gradiometer, W. C. Wineland—198(A)
Pentode counting ring, Benjamin L. Moore—465(A)
Perkin-Elmer spectrometer, A. M. Crooker—592(A)
Perturbation theory and collision processes, James N. Snyder and W. H. Furry—359
Philips gauge discharge, Talbot Chubb—198(A)
Phosphor surface in scintillation counters, J. M. Watkins, Jr. and A. C. Menius, Jr.—196(A)
P-type germanium transistor, W. G. Pfann and J. H. Scaff—459(A)
Photographic plate detectors, experiments with 10-Mev deuterons, J. H. Williams, F. K. Tallmadge, and L. Rosen—168(A)
Photography of shocks, P. E. Shafer and J. F. Moulton, Jr.—881(A)
Photo-multiplier for x-ray spectrometer, J. S. Brown, G. M. Farrior, and Arthur Waltner—196(A)
Photo-multiplier tube as gamma-ray detector, J. D. Graves and G. E. Koch—590(A)
Photo-neutron standards, L. F. Curtiss and A. Carson—1412(L)

Methods and instruments (continued)
Portable magnet and cloud chamber, D. S. Potter, J. E. Henderson, C. E. Miller, and Jay Todd, Jr.—590(A)
Precision measurement of half-lives, Lorna M. Silver—589(A)
Pressurized range for small caliber projectiles, V. E. Bergdolt, A. J. Greenwald, and D. B. Sleator—879(A)
Proportional counter and p-α-reactions, A. W. Schardt, E. J. Woodbury, and W. A. Fowler—587(A)
Probability-amplitude distributions, P. S. Jastram—190(A)
Pulse-modulated ultrasonic generator, Ernest Yeager, Hyman Chessin, John Bugosh, and Frank Hovorka—1890(A)
Removal of space-charge in diamond counters, A. G. Chynoweth—310(L)
Resistance changes of fine wires during strains, E. W. Kammer and T. E. Pardue—202(A)
Response of scintillation counter, F. B. Harrison and George T. Reynolds—169(A)
Scattering and absorption of mesons, effect on coincidence-anticoincidence measurements, Rogers D. Rusk and Alma Rosenbaum—1166
Scintillation counter, Arthur Waltner—196(A)
Scintillations produced by α-particles in organic crystals, W. S. Koski and Carl O. Thomas—308(L)
Self-quenching G-M counter, C. V. Robinson—455(A)
Self-quenching G-M counters, temperature dependence, Om Parkash—568(L)
Self-regenerating fillings for Geiger counters, S. A. Korff and A. D. Krumbein—1412(L)
Separation of He^3, Charles A. Reynolds, Henry A. Fairbank, C. T. Lane, B. B. McInteer, and Alfred O. Nier—64, 167(A); B. M. Abraham, B. Weinstock, and D. W. Osborne—864(L)
Separation of isotopes of Hg, C. P. Keim—1270(L)
Shielding material for accelerators, E. Creutz—162(A)
Shock tube, flow phenomena, F. W. Geiger—881(A)
Short half-lives, measurement of, W. J. MacIntyre—312(L)
Size of particle, x-ray scattering, David L. Dexter and W. W. Beeman—1782
Solar position calculator, Donald W. Dunipace—464(A)
Spatial alignment of nuclei, R. V. Pound—1410(L)
Spectrometer for Raman studies, W. E. Haisley and Joseph W. Straley—200(A)
Speed gauge for high voltage particles, W. Altar and M. Garbuny—496
Speed of fracture, photographic method, V. E. Scherrer, G. Carmichael, R. Varwig, and A. Linz—202(A)
Speed of fractures, inductive method, A. Linz, Jr., V. E. Scherrer, and G. Carmichael—202(A)
Spin-lattice relaxation times, Erwin L. Hahn—145(L)
Spurious counts in counters, J. D. Louw and S. M. Naudé—571(L)
Storage system utilizing magnetic retentivity, computers, W. D. Woo and An Wang—465(A)
String galvanometer, generalized theory, G. W. Crawford and F. T. Rogers, Jr.—199(A)
System for secondary electron emission measurements, L. J. Rueger and F. C. Todd—189(A)
Temperature dependence of counter, G. E. Koch and J. D. Graves—590(A)
Temperatures in complex flame, F. P. Bundy and H. M. Strong—457(A); H. M. Strong and F. P. Bundy—458(A)
Thermal noise, A. van der Ziel—591(A)
Thermocouple microsecond timer, Richard H. F. Stresau—880(A)
Threefold coincidence counter, W. H. Jordan and J. C. Gundlach—196(A)
Time-of-flight neutron spectrometer, W. Selove—187(A)
Transient response of stable linear systems, W. Whittier Wright and W. B. Wrigley—198(A)
Transient stresses in photo-elastic media, John S. Stanton—174(A)
Trigger for flash photography, R. L. Varwig, V. E. Scherrer, G. Carmichael, and A. Linz—201(A)
Turbulence by using non-compensated hot-wires, F. N. Frenkiel—171(A)
Vacuum tube electrometer, portable, E. E. Bortner—197(A)
Variational method for finding extrapolated endpoints, H. Hurwitz, Jr.—867(L)
Variational principle for scattering problems, Su-Shu Huang—866(L)
Velocity of flow of gas mixture, P. Rudnick and W. H. Kurschwitz—201(A)
WWV signals to time pendulums, J. T. McCarthy—1891(A)
X-ray film badge dosimeter, E. Tochilin, R. H. Davis, and J. Clifford—590(A)
X-ray output for betatrons, W. F. Westendorp and F. R. Elder—445(L)

Molecular structure and constants (see also **Spectra, molecular, etc.; Raman spectra**)
Of bromosilane by microwave measurements, A. H. Sharbaugh, J. K. Bragg, T. C. Madison, and V. G. Thomas—1419(L)
Of CsF from radiofrequency spectra, J. W. Trischka—1365
Of chlorosilane, B. P. Dailey, J. M. Mays, and C. H. Townes—472(A)
Of deuterium fluoride, Hoyt M. Kavlor and Alvin H. Nielsen—200(A)
Of FCl, microwave spectrum, D. A. Gilbert, A. Roberts, and P. A. Griswold—1723(L)
Forces between NH_3 molecules, Vernon Myers—177(A)
Hydrogen bonding and isomeric forms, Norman D. Coggeshall—174(A)
Linear molecules, rotational Stark spectrum, Harold Kenneth Hughes—1675
Singlet electronic levels in naphthalene, Gertrud P. Nordheim and H. Sponer—177(A)
Stark effects on symmetric top molecules, W. Low and C. H. Townes—1295

Moments of particles (see also **Nuclear moments and spin**)
Moment of electron in hydrogen and deuterium, Edward B. Nelson and John E. Nafe—1858
Nuclear motion and atomic magnetic moments, M. Phillips—1803
Nucleon moments and neutron-electron interaction, K. M. Case—1

Neutrino (see also **Radioactivity; Scattering of electrons, neutrons, and ions**)
From the sun, source of earth's heat, D. Saxon—986(L)

Neutrons
From $Al+H^2$, R. A. Peck, Jr.—1279
Angular distribution from (d, n) reactions, C. E. Falk, E. Creutz, and F. Seitz—322(L)
Angular distribution from various targets, P. Ammiraju—1421(L)
Angular distribution, photo-neutrons from deuterium, Bernard Hamermesh and Albert Wattenberg—1408(L)
In atmosphere, J. A. Simpson, Jr., H. W. Baldwin, and R. B. Uretz—165(A)
Attenuation in thick shields, S. W. W. Shor—474(A)
Binding energy of triton, R. E. Clapp—873(L)
From $C(d,n)N$ and $Cu(d,n)Zn$, energy distribution, J. C. Grosskreutz—482
Cross section at 115 ev and 300 ev, C. T. Hibdon and C. O. Muehlhause—188(A)
Delayed neutron emitter, R. A. Charpie, Kuan-Han Sun, B. Jennings, and J. F. Nechaj—1255(L)

Delayed neutrons from thorium fission, L. G. Creveling, J. R. Hood, and M. L. Pool—946
From deuterons on Li^6, C. E. Mandeville, C. P. Swann, and S. C. Snowdon—980(L)
Diffraction studies of AgCl, $Ag^{107}Cl$, and $Ag^{109}Cl$, W. A. Strauser, C. G. Shull, and E. O. Wollan—195(A)
Diffusion, plate of finite thickness, Otto Halpern and R. K. Luneberg—1811
From disintegration of Na by deuterons, C. E. Mandeville —436(L)
Distribution and multiplicity of neutrons, local showers, G. Cocconi and V. Cocconi Tongiorgi—318(L)
Distributions in cylindrical geometry, Henry Faul and Clark Goodman—463(A)
Electrostatic scattering of neutrons, S. M. Dancoff and S. D. Drell—205
Fast neutrons from cyclotron particles, A. J. Allen, J. F. Nechaj, K. H. Sun, and B. Jennings—463(A)
In free atmosphere up to 102,000 ft., Luke C. L. Yuan—165(A)
Interaction between neutrons and electrons, H. Ekstein—1328
Magneto optics of neutrons, Otto Halpern—1130
Mechanism of production in cosmic radiation, Vanna Cocconi Tongiorgi—517
Neutron-electron interaction, K. M. Case—1
From $N^{16}(d,n)$, Emmett L. Hudspeth and Charles P. Swann —464(A)
Phase of scattering, residual cross sections, P. J. Bendt and I. W. Ruderman—463(A)
Photo-disintegration of deuteron, angular distribution of neutrons, Frank Genevese—1288
Photo-neutrons from gamma-rays produced by neutron capture, Bernard Hamermesh and Albert Wattenberg—1420(L)
Polarization, J. Fleeman and H. H. Staub—586(A); J. Steinberger and G. C. Wick—994(L); J. Fleeman, D. B. Nicodemus, and H. H. Staub—1774
Polarization by magnetized mirrors, D. J. Hughes and M. T. Burgy—463(A), 1413(L)
Production at mountain altitudes, C. G. Montgomery and A. R. Tobey—1478
Production at sea level, R. D. Sard, A. M. Conforto, and M. F. Crouch—1134
Resonance activation of "even-even" nuclei, A. W. Sunyar and M. Goldhaber—189(A)
Resonance scattering by W^{180}, S. Harris and C. O. Muehlhause—189(A)
Resonance scattering, corroboration, R. K. Adair, C. K. Bockelman, and R. E. Peterson—308(L)
Small angle scattering, D. Meneghetti—188(A)
Spectra from (p,n) reactions, P. C. Gugelot and M. G. White—463(A)
Spontaneous emission from U and Sm, Herman Yagoda and Nathan Kaplan—702(L)
Theory of reflectors, G. M. Volkoff—589(A)
Transmission and polarization, iron single crystal, Merle Burgy, D. J. Hughes, and W. E. Woolf—188(A)
Widths of neutron resonances, L. L. Lowry and M. Goldhaber—189(A)
Yield and angular distribution, *D-D*, G. T. Hunter and H. T. Richards—1445
Yield from 15-Mev deuterons, A. J. Allen, J. F. Nechaj, K. H. Sun, and B. Jennings—188(A)

Neutron diffraction
Small angle diffraction, Otto Halpern and Edward Gerjuoy —1117

Nuclear masses (see also **Isotopes**)
Integral ratios between nuclear masses and binding energies, Enos E. Witmer—181(A)
Neutron-hydrogen mass difference, William E. Stephens—181(A); W. Franzen, J. Halpern, and W. E. Stephens—317(L), 462(A); R. F. Taschek, H. V. Argo, A. Hemmendinger, and G. A. Jarvis—325
Neutron-proton mass difference, A. V. Tollestrup, F. A. Jenkins, W. A. Fowler, and C. C. Lauritsen—181(A)

Nuclear moments and spin (see also **Hyperfine structure; Moments of particles**)
Anomalous moments of nucleons, S. D. Drell—427(L)
Of Sb^{121}, K. Murakawa and S. Suwa—433(L)
Of B^{11}, Donald A. Anderson—434(L)
Of Cs^{135} and Cs^{137}, Darragh E. Nagle—847(L)
Of Cs^{137}, Luther Davis, Jr.—435(L)
Electric quadrupole moments, G. J. Bene, P. M. Denis, and R. C. Extermann—1255(L)
Electromagnetic properties of nucleons, Sidney Borowitz and Walter Kohn—818
Of Fe^{57}, M. Gurevitch and J. G. Teasdale—151(L)
Of Ge and Si from microwave spectra, C. H. Townes, J. M. Mays, and B. P. Dailey—700(L)
Gyromagnetic ratio, ferromagnetic substances, Charles Kittel—743
Gyromagnetic ratio of electron, A. K. Mann and P. Kusch —163(A)
Gyromagnetic ratios, various nuclei, John R. Zimmerman and Dudley Williams—163(A), 350, 1264(L); William H. Chambers and Dudley Williams—638
Of He^3, Herbert L. Anderson—1460
Hyperfine structure, Rb isotopes, F. Bitter—150(L)
Of Kr^{83} and Ne^{21}, Jørgen Koch and Ebbe Rasmussen—1417(L)
Of Mg^{25}, M. F. Crawford, F. M. Kelly, A. L. Schawlow, and W. M. Gray—1527(L)
Magnetic moment of La^{139}, W. C. Dickinson—1414(L)
Magnetic moments of Sn^{115}, Cd^{111}, Cd^{113}, Pt^{195}, and Hg^{199}, W. G. Proctor and F. C. Yu—1728(L)
From microwave spectra; I^{127} and I^{129}, Walter Gordy and O. R. Gilliam—443(L)
Nuclear induction proton signals, F. Bloch and David H. Garber—585(A)
Nuclear resonances in rotating magnetic fields, E. H. Rogers and H. H. Staub—585(A)
Nutation of nuclear magnetic moment, Erwin L. Hahn—461(A)
Nutations in magnetic resonance, H. C. Torrey—1059
Proton magnetic moment in Bohr magnetons, J. H. Gardner and E. M. Purcell—1262(L)
Quadrupole moments and shell structure, C. H. Townes, H. M. Foley, and W. Low—1415(L)
Quadrupole moment of Cl, Hin Lew—1086
Ratio of g values of Li^7 and Li^6, P. Kusch and A. K. Mann —707
Resonance experiments with Na^{22}, K^{40}, Cs^{135}, and Cs^{137}, Luther Davis, Jr., Darragh E. Nagle, and Jerrold R. Zacharias—1068
Rotational magnetic moments in H_2O and HDO, C. K. Jen—471(A)
Sign of electric quadrupole moment of Li^7, P. Kusch—138(L)
Signs of magnetic moments of neutron and proton, E. H. Rogers and H. H. Staub—980(L)
Of slow neutrons by paramagnetic crystals, I. W. Ruderman —1572
Spin and quadrupole coupling of S^{35}, Victor W. Cohen, W. S. Koski, and T. Wentink, Jr.—703(L)
Spin and quadrupole moment of Cl^{36}, C. H. Townes and L. C. Aamodt—691(L)
Spin and quadrupole moment of I^{129}, Ralph Livingston—149(L)

Nuclear moments and spin (continued)
Spin-lattice relaxation times in solids, E. H. Turner, A. M. Sachs, and E. M. Purcell—465(A)
Spin of He^3, A. E. Douglas and G. Herzberg—1529(L)
Of stable chlorine isotopes, Luther Davis, Jr., Bernard T. Feld, Carrol W. Zabel, and Jerrold R. Zacharias—1076
Of Te^{123}, J. E. Mack and O. H. Arroe—1002(L)
Of Sn^{117}, Sn^{119}, and Pb^{207}, W. G. Proctor—684(L)
Transients in nuclear induction, E. A. Uehling—585(A)
Of V^{51}, W. D. Knight and V. W. Cohen—1421(L)
Of $_{39}Y^{89}$, M. F. Crawford and N. Olson—1528(L)
Of $_{40}Zr^{91}$, O. H. Arroe and J. E. Mack—873(L)

Nuclear spectra (see also **Disintegration and excitation of nucleus**)
Of Sb^{125}, Te^{125*}, Cr^{51}, and I^{131}, Bernard D. Kern, Allan C. G. Mitchell, and Daniel J. Zaffarano—94
γ-γ-angular correlation in Pd^{106}, Daniel S. Ling, Jr. and David L. Falkoff—431(L)
Of Pb^{207}, A. L. Schawlow, J. N. P. Hume, and M. F. Crawford—1876(L)
Positron spectrum of Cu^{61}, George E. Owen and C. Sharp Cook—1536(L)

Nuclear structure (see also **Disintegration and excitation of nucleus; Isotopes; Nuclear spectra; Radioactivity**)
Are mesons elementary particles? E. Fermi and C. N. Yang—1739
Of argon, P. W. Davison, J. O. Buchanan, and Ernest Pollard—890
Binding energies of alpha-particles, Truman P. Kohman—448(L)
Binding energies of light nuclei, J. Samuel Smart—439(L)
Binding energy of deuteron, lower limit, G. R. Bishop, C. H. Collie, H. Halban, and R. Wilson—683(L)
Broad levels in lead, R. K. Adair, H. H. Barschall, C. K. Bockelman, R. L. Henkel, and R. E. Peterson—463(A)
Of Ce^{141}, Michel Ter-Pogossian, C. Sharp Cook, C. Harold Goddard, and J. Eugene Robinson—909
Closed shells, Maria G. Mayer—185(A)
Composite particles, H. M. Moseley—197(A)
Energy level density and partition function, D. ter Haar—1525
Excited state of Li^7, Michel Ter-Pogossian, J. Eugene Robinson, and C. Harold Goddard—453(A), 1407(L); R. M. Williamson and H. T. Richards—453(A)
Of Hf^{181}, Erling N. Jensen—958
Of I^{124} and I^{126}, Allan C. G. Mitchell, J. Y. Mei, Fred C. Maienschein, and Charles L. Peacock—1450
Isomers, classification of, P. Axel and S. M. Dancoff—892
Isomers produced by neutron capture, E. der Mateosian and M. Goldhaber—187(A)
j-j coupling shell model, Eugene Feenberg—1275
Levels in lead, H. H. Barschall, C. K. Bockelman, R. E. Peterson, and R. K. Adair—1146
Of Li^7, excited state, angular yield in $Li^6(d,p)Li^{7*}(\gamma)Li^7$, S. S. Hanna—686(L)
Long-lived Te isomers, R. D. Hill—333
Of Ni^{65}, Kai Siegbahn and Amal Ghosh—307(L)
Of Ni^{65}, Ni^{57}, Ag^{110}, and In^{114}, coincidence experiments, Fred Maienschein and J. Lawrence Meem, Jr.—899
Of N^{14}, H. A. Wilson—687(L)
Of N^{15} and N^{16}, L. D. Wyly—316(L), 462(A)
Nuclear shells, pattern of atomic species, William D. Harkins—1538(L)
Origin of elements, Maria G. Mayer and Edward Teller—1226
Phenomenological theory of forces, Herman Feshbach—185(A)
Quadrupole moment and nuclear shell structure, Walter Gordy—139(L)
Quadrupole moments and shell structure, R. D. Hill—998(L)
Of Rh^{106}, Sb^{125}, and Pr^{142}, E. T. Jurney—290
Of Se isomer, I. Bergström and S. Thulin—1718(L)
Of Si^{30}, John E. Brolley, Jr., M. B. Sampson, and Allan C. G. Mitchell—624
Of Na^{24} and Ca^{41}, rotation levels, H. A. Wilson—687(L)
Spin dependence of nuclear forces, Alex E. S. Green—460(A)
Of Ta^{182}, $Re^{186,188}$, and Au^{199}, Louis A. Beach, Charles L. Peacock, and Roger G. Wilkinson—1585
Of Tm^{170}, J. S. Fraser—1540(L)
Transition energies of isomers, R. L. Caldwell, E. der Mateosian, and M. Goldhaber—187(A)
Widths of neutron resonances, L. L. Lowry and M. Goldhaber—189(A)

Optical constants and properties
Of BaO films, Winfield W. Tyler—1887(L)
Of $BaTiO_3$ single-domain crystals, Walter J. Merz—1221
Electro-optic coefficients in ADP crystals, R. O'B. Carpenter—467(A)
Empirical formula for refractive indices of dispersing materials, Gilbert W. King—473(A)
Infra-red transmission of germanium, M. Becker and H. Y. Fan—1530(L); of silicon, M. Becker and H. Y. Fan—1531(L)
Reflectivity of germanium semiconductors, K. Lark-Horovitz and K. W. Meissner—1530(L)
Thermo-optic properties of cubic crystals, Elias Burstein and Paul L. Smith—175(A)

Optical instruments (see **Methods and instruments**)

Optical theory
Maximum and minimum intensity in the Fresnel diffraction pattern, E. J. Scheibner—201(A)

Pair production
Bremsstrahlung and pair production, Martin Stearns—836
In field of an electron, J. A. Phillips and P. Gerald Kruger—1471
Internal formation, M. E. Rose—461(A), 678
Relative cross sections at 17.6 Mev, R. L. Walker—1440

Packing fraction (see also **Isotopes**)
Pt^{195}-Cu^{65} packing fraction difference, Henry E. Duckworth—690(L)

Paschen-Back effect (see also **Zeeman effect**)
In NH_3 and N_2O microwave spectra, C. K. Jen—1494

Phosphorescence
Effect of x-rays on alkali halide phosphors, James H. Schulman, Robert J. Ginther, Clifford C. Klick, and Lyle W. Evans—459(A)
Luminescence of alkali-halide phosphors, J. H. Schulman, E. Burstein, R. J. Ginther, M. White, and L. W. Evans—178(A)

Photo-conductivity
In BaO, Winfield W. Tyler—179(A)
In cadmium sulfide, A. Rose, P. K. Weimer, and S. V. Forgue—179(A)
In CdS, irradiation with gamma-rays, Rudolf Frerichs—1869
In indium selenide, Donald Bode and Henry Levinstein—179(A)
Mobility of electrons in diamond, C. C. Klick and R. J. Maurer—179(A)

Photo-disintegration
Angular distribution, photo-disintegration of deuteron, W. M. Woodward and I. Halpern—107
Of Be, distribution of photo-neutrons, B. Hamermesh, M. Hamermesh, and A. Wattenberg—611; C. J. Mullin and E. Guth—682(L)

Of deuteron, Everett G. Fuller—576(L); J. S. Levinger—699(L); Ingvar F. E. Hansson and Lamek Hulthén—1163
Of deuteron, high energy, J. F. Marshall and E. Guth—1880(L)
Of deuteron, low energy, J. F. Marshall and E. Guth—1879(L)
Distribution of photo-neutrons from deuterium, Edwin P. Meiners, Jr.—259
Theory of Be^9, Eugene Guth and Charles J. Mullin—234
Thresholds for photo-neutron reactions, A. O. Hanson, R. B. Duffield, J. D. Knight, B. C. Diven, and H. Palevsky—578(L)
Of U, E. W. Titterton and F. K. Goward—142(L)

Photo-elasticity
Transient stresses, John S. Stanton—174(A)

Photoelectric effect and properties; cells
Of Ni, Alvin B. Cardwell—125
Semimetallic characteristics of As, Sb, and Bi, L. Apker, E. Taft, and J. Dickey—270

Photography (see also **Methods and instruments**)
Automatic grain counting of tracks, P. V. C. Hough—163(A)
Effect of C^{14}, Ca^{45}, P^{32}, I^{131}, and Zn^{65} on emulsions, Daniel Steinberg and A. K. Solomon—453(A)
Electric field and discharge photographs, F. G. Slack and Hsieh Yu-Chang—197(A)
Electron tracks in nuclear emulsions, W. Van der Grinten—163(A)
Emulsions for ionizing particles, stopping power, Hervasio G. de Carvalho—1729(L)
Fading of proton tracks, K. B. Mather—486
Fogging of film by radioactive contaminants, J. H. Webb—375
High speed frame camera, S. J. Jacobs and A. A. Klebra—881(A)
Trigger for flash photography, R. L. Varwig, V. E. Scherrer, G. Carmichael, and A. Linz—201(A)

Piezoelectric effect
Influence on tribo-electrification, John W. Peterson—1882(L)

Plasticity
Behavior of stiffened panels, Wolfe Mostow—876(A)
Ideal plastic body, Hilda Geiringer—875(A)
Model for flow of oriented nylon fibers, John Kauffman and Waller George—467(A)

Polymerization, properties of polymers
Anisotropy of high polymers at microwave frequencies, T. M. Shaw and J. J. Windle—586(A)

Positrons
Lifetime in matter, James W. Shearer and Martin Deutsch—462(A)
Theory, Frederik J. Belinfante—461(A); R. P. Feynman—749

Proceedings of the American Physical Society
Southeastern Section, Clemson College, Clemson, South Carolina, April 15–16, 1949—195
Washington, D. C., Meeting, April 28–30, 1949—160
Semi-Centennial Meeting, Cambridge, Massachusetts, June 16–18, 1949—451
University of Washington Meeting, Seattle, Washington, June 27–29, 1949—584
Division of Fluid Dynamics Meeting, White Oak, Maryland, June 30–July 1, 1949—875
Ohio Section, Cleveland, Ohio, November 5, 1949—1890

Quantum electrodynamics (see also **Field theory**)
Action between charges and field, Louis de Broglie—862(L)
Bosons in electromagnetic field, R. G. Moorhouse—1691
Electromagnetic properties of nucleons, Sidney Borowitz and Walter Kohn—818
Electromagnetic theory and correspondence principle, Herman M. Schwartz—192(A)
Electron-radiative corrections to scattering, Julian Schwinger—790
Field formalism without self-action, T. A. Welton—460(A)
Field theories and polarization of vacuum, David Feldman—1369
Fourth-order corrections, magnetic moment of electrons, Robert Karplus and Norman M. Kroll—846(L)
Interaction between elementary particles, Alfred Landé—1176
Interaction representation of Proca field, Frederik J. Belinfante—66
Interactions of mesons with electromagnetic field, M. Neuman and W. H. Furry—1677
Interactions of vector meson with scalar excited state, Marshall N. Rosenbluth—951
Meson interactions, Dyson's methods, P. T. Matthews—684(L)
Motion in constant magnetic field, M. H. Johnson and B. A. Lippmann—828
Nucleon-nucleon collisions, bremsstrahlung, J. Ashkin and R. E. Marshak—58
Radiation accompanying meson creation, L. I. Schiff—89
Radius of elementary particle, Hideki Yukawa—300(L)
S matrix for meson-nucleon interactions, P. T. Matthews—1254(L)
Space-time approach, R. P. Feynman—769
Subtraction fields and lifetimes of meson, J. Steinberger—1180
Tomonaga-Schwinger theory, interaction of nucleons with mesons, P. T. Matthews—1657
Treatment without eliminating longitudinal field, Ning Hu—391
Two-meson theory, Mituo Taketani, Seitaro Nakamura, Kenichi Ono, and Muneo Sasaki—60

Quantum mechanics (see **Mechanics, quantum,** etc.)

Radiation (see also **Thermal radiation**)
Annihilation radiation, angular distribution, S. DeBenedetti, C. E. Cowan, and W. R. Konneker—440(L)
Bremsstrahlung in heavy elements, H. Wergeland—184(A)
Bremsstrahlung, nucleon-nucleon collisions, J. Ashkin and R. E. Marshak—58, 989(L)
High energy photons by 350-Mev protons, Herbert F. York, Burton J. Moyer, and Russell Bjorklund—187(A)

Radio (see also **Ionosphere; Electromagnetic theory**)
Impedance and generalized two-wire line theory, K. Tomiyasu and Ronold King—456(A)

Radioactivity (see also **Disintegration of nucleus**)
Alpha-decay, atomic number less than 83, S. G. Thompson, A. Ghiorso, J. O. Rasmussen, and G. T. Seaborg—1406(L)
Analysis of delayed coincidence counting, Daniel Binder—856(L)
Angular correlation of delayed radiations, Arne Lundby—993(L)
Of Ba^{135}, B. E. Robertson and M. L. Pool—1408(L)
Of Ba^{140} and La^{140}, Louis A. Beach, Charles L. Peacock, and Roger G. Wilkinson—1624
Of Be^7, *K* capture, R. M. Williamson and H. T. Richards—614
Of Be^{10}, C. S. Wu and L. Feldman—698(L); H. W. Fulbright and J. C. D. Milton—1271(L)
Beta-decay of Y^{90}, recoils, C. W. Sherwin—183(A)
Beta-gamma-angular correlation, Richard L. Garwin—1876(L)
Beta-ray spectra, H. J. Lipkin—567(L)
Beta-ray spectrum, analysis, Mitsuo Sakai and Seitaro Nakamura—967

Radioactivity (continued)
Beta-spectra from thick sources, L. Feldman and C. S. Wu —697(L)
Beta-spectra of Cu^{64}, L. M. Langer, R. D. Moffat, and H. C. Price, Jr.—1725(L); George E. Owen and C. Sharp Cook —1726(L)
Beta-spectrum of Be^{10}, P. R. Bell and J. M. Cassidy—183(A)
Beta-spectrum of $_{61}Pm^{147}$, L. Lidofsky, P. Macklin, and C. S. Wu—1888(L)
Beta-spectrum of Tm^{170}, D. Saxon and J. Richards—186(A)
Beta-spectrum of tritium, W. J. Byatt, F. T. Rogers, and A. W. Waltner—199(A)
Branching ratio in Be^{7}, C. M. Turner—588(A)
Of Br^{82}, Kai Siegbahn, Arne Hedgran, and Martin Deutsch —1263(L)
Of C^{14}, half-life, W. M. Jones—885
Of Ce^{141}, Michel Ter-Pogossian, C. Sharp Cook, C. Harold Goddard, and J. Eugene Robinson—909
Of Cs isotopes, Mark G. Inghram, David C. Hess, Jr., and John H. Reynolds—1717(L)
Of Cs^{134}, I^{134}, Au^{199}, and Ca^{45}, coincidence and absorption measurements, J. Lawrence Meem, Jr. and Fred Maienschein—328
Of Cs^{137}, Charles L. Peacock—186(A)
Of Cl^{36}, C. S. Wu, C. H. Townes, and L. Feldman—692(L); C. S. Wu and L. Feldman—693(L); C. Longmire, C. S. Wu, and C. H. Townes—695(L)
Of Cl^{39}, R. N. H. Haslam, L. Katz, H. E. Johns, and H. J. Moody—704(L)
Of Co^{60} and Zn^{65}, gamma-radiations, Erling N. Jensen, L. Jackson Laslett, and William W. Pratt—430(L)
Of Cb and Mo, D. N. Kundu and M. L. Pool—183(A)
Conversion electrons of Ra D, L. Cranberg and J. Halpern —187(A)
Continuous gamma-radiation, theory, C. S. Wang Chang and D. L. Falkoff—365
Of Cu^{61}, George E. Owen and C. Sharp Cook—1536(L)
Of Cu^{62}, R. A. Becker, F. S. Kirn, and W. L. Buck—1406(L)
Decay constant of Be^{7}, effect of atomic electrons, R. F. Leininger, E. Segrè, and C. Wiegand—897
Decay probability of Be^{7} as function of ionization of atom, P. Benoist, R. Bouchez, P. Daudel, R. Daudel, and A. Rogozinski—1000(L)
Double beta-process, $_{52}Te \rightarrow _{54}Xe$, Mark G. Inghram and John H. Reynolds—1265(L)
Of Dy, isomers, B. H. Ketelle—1256(L)
Of element 86, new isotopes, A. Ghiorso, W. W. Meinke, and G. T. Seaborg—1414(L)
Existence of $4n+1$ radioactive series, J. H. J. Poole, C. F. G. Delaney, and R. C. McCormick—1253(L)
Forbidden beta-spectra, Lawrence M. Langer and H. Clay Price, Jr.—186(A), 641
Gamma-radiations from Co^{60}, precision determination, D. A. Lind, J. R. Brown, and J. W. M. DuMond—591(A), 1838
Of Hf^{181}, Erling N. Jensen—958; Arne Lundby—1809
Half-life and orbital electron capture, Stanley G. Thompson —319(L)
Half-life of Na^{22}, L. Jackson Laslett—858(L)
High energy positrons from Na^{22}, Kennard H. Morganstern and Karl P. W. Wolf—1261(L)
High specific activity produced with betatron, R. A. Becker and F. S. Kirn—182(A)
Of Ho^{166}, Tm^{170}, and Lu^{177}, J. M. Cork, H. B. Keller, and A. E. Stoddard—986(L)
Of In, α-bombardment, Georges M. Temmer—424, 1002(L)
Of In and Sn, E. C. Mallary and M. L. Pool—186(A)
Of In^{107}, In^{108}, In^{109}, and Sn^{108}, E. C. Mallary and M. L. Pool —1454
Of In^{114}, J. Y. Mei, Allan C. G. Mitchell, and Daniel J. Zaffarano—1833(L)
Of In^{114} and Ba^{140}, C. E. Mandeville and E. Shapiro—454(A), 718
Of In^{116*}, P. R. Bell, B. H. Ketelle, and J. M. Cassidy—574(L)
Of I^{124} and I^{126}, Allan C. G. Mitchell, J. Y. Mei, Fred C. Maienschein, and Charles L. Peacock—1450
Isotopes of Y and Zr, W. E. Scott, B. E. Robertson, and M. L. Pool—183(A)
K-shell internal conversion coefficients, M. E. Rose, G. H. Goertzel, B. I. Spinrad, J. Harr, and P. Strong—184(A); 1883(L)
Krypton isotopes from fission, J. Koch, O. Kofoed-Hansen, P. Kristensen, and W. Drost-Hansen—279
Of La^{140}, J. M. Cork, H. B. Keller, W. C. Rutledge, and A. E. Stoddard—1886(L)
Lifetime of positrons, James W. Shearer and Martin Deutsch—462(A)
LiF as scintillation detector, E. C. Farmer, H. B. Moore, and Clark Goodman—454(A)
Of $_{71}Lu^{177}$, metastable state, F. K. McGowan—1730(L)
Magnetic multipole internal conversion, N. Tralli and I. S. Lowen—1541(L)
Of Mn, monochromatic electron groups, W. S. Emmerich, L. H. Ballweg, and J. D. Kurbatov—1891(A)
Of Hg^{198}, lifetime of 411-kev excited state, R. E. Bell and H. E. Petch—1409(L)
Of Hg^{198}, measurement of short half-lives, W. J. MacIntyre —312(L)
Of Hg^{199}, 43 m activity, Ingmar Bergström and Sigvard Thulin—313(L)
Of Mo^{91} and Mo^{93}, R. B. Duffield and J. D. Knight—573(L)
Negative proton, delayed neutron emitters, Kuan-Han Sun —1266(L)
Neutron-induced short-life activities, Edward C. Campbell and Wilfred M. Good—195(A)
Of Nd and element 61, C. E. Mandeville and M. V. Scherb —186(A)
Of Ni, long-life species, D. G. Thomas and J. D. Kurbatov —1891(A)
Of Ni^{65}, Kai Siegbahn and Amal Ghosh—307(L)
Of N^{12}, Luis W. Alvarez—183(A)
Of $_{7}N^{17}$, delayed neutron emitter, R. A. Charpie, Kuan-Han Sun, B. Jennings, and J. F. Nechaj—1255(L)
Of O^{15}, V. Perez-Mendez and H. Brown—689(L)
Perturbation theory and collision processes, lifetime changes, James N. Snyder and W. H. Furry—359
Photo-electron spectrum of Ta^{182}, C. Harold Goddard and C. Sharp Cook—1419(L)
Photo-neutron standards, L. F. Curtiss and A. Carson—1412(L)
Of K^{40}, G. A. Sawyer and M. L. Wiedenbeck—1535(L)
Positive particles associated with beta-ray emitters, K. L. Erdman, G. T. Kokotailo, and D. B. Scott—1262(L)
Of Pr^{143}, L. Feldman, L. Lidofsky, P. Macklin, and C. S. Wu —1888(L)
Precision measurement of half-lives, Lorna M. Silver—589(A)
Quadrupole transition in Cd^{111}, Martin Deutsch and Donald T. Stevenson—184(A)
Ratio of L_I to K, M. E. Rose and J. L. Jackson—1540(L)
Of Re^{186} and Re^{188}, Louis A. Beach, Charles L. Peacock, and Roger G. Wilkinson—187(A)
Sm^{151} beta-ray spectrum, B. H. Ketelle and K. W. Parker—1416(L)
Of Se isomer, I. Bergström and S. Thulin—178(L)
Self-absorption and backscattering of beta-radiations, L. E. Glendenin and A. K. Solomon—462(A)

Shape of beta-spectra, instrumental errors, C. Sharp Cook and George E. Owen—183(A)
Of Ag and Cd, Jane R. Gum, Lowell E. Thompson, and M. L. Pool—184(A)
Of Ag^{110}, Werner S. Emmerich and J. D. Kurbatov—454(A)
Of Na^{22} and Co^{60}, gamma-radiation, David E. Alburger—435(L)
Straggling of S^{35} beta-particles in glass, Mary Jane A. Linker—428(L)
Of Sr and Y, beta-spectra, F. B. Shull, C. H. Braden, and L. Slack—453(A); H. Clay Price, Jr.—454(A); H. Clay Price, Jr. and Lawrence M. Langer—454(A)
Of Ta, J. W. Burkig and J. Reginald Richardson—586(A)
Of Ta^{182}, $Re^{186, 188}$, and Au^{199}, Louis A. Beach, Charles L. Peacock, and Roger G. Wilkinson—1585
Tellurium isomers, R. D. Hill—186(A)
Of Te^{125m}, J. C. Bowe and Gertrude Scharff-Goldhaber—437(L)
Of Tl^{204}, neutron pairing, D. Saxon and J. Richards—982(L)
Of Tm^{170}, J. S. Fraser—1540(L)
Of Sn, J. C. Lee and M. L. Pool—192(A), 606; R. A. Hinshaw and M. L. Pool—358; R. A. Hinshaw—454(A); R. B. Duffield and L. M. Langer—1272(L)
Of tritium, E. R. Graves and D. I. Meyer—183(A); S. C. Curran, J. Angus, and A. L. Cockroft—853(L)
U^{234} in natural uranium, C. A. Kienberger—1561
U-234 specific alpha-activity, A. S. Goldin, G. B. Knight, P. A. Macklin, and R. L. Macklin—336
U-234 gamma-radiation, R. L. Macklin—595
Of V^{52}, Mo^{99}, and W^{185}, J. M. Cork, H. B. Keller, and A. E. Stoddard—575(L)
Water drop model of alpha-decay, J. E. Garvey and B. T. Darling—184(A)
Of Y^{84}, Y^{88}, and Zr^{87}, B. E. Robertson, W. E. Scott, and M. L. Pool—1649
Of Y^{91}, C. S. Wu and L. Feldman—696(L)
Of Y^{91} and Cs^{137}, forbidden transition, J. S. Osoba—345
Of Zn^{65}, K. C. Mann, D. Rankin, and P. N. Daykin—1719(L)

Raman spectra
Of carbonyl fluoride, P. J. H. Woltz, Ernest A. Jones, and A. H. Nielsen—200(A)
Of chlorine trifluoride, Ernest A. Jones, T. F. Parkinson, R. B. Murray, and J. S. Kirby-Smith—200(A)
Of HF, J. S. Kirby-Smith and E. A. Jones—200(A)

Range of particles
Alpha-particles in gases, G. G. Eichholz and N. J. Harrick—589(A)
Of charged particles from *D-D* reactions, Louis Rosen, Francis K. Tallmadge, and John H. Williams—1283
Of high energy electrons in Al, F. L. Hereford and C. P. Swann—570(L)
Proton range-energy relation, R. L. Clarke and G. A. Bartholomew—146(L)
Protons in photographic emulsions, H. Bradner, A. S. Bishop, and W. H. Barkas—587(A)
Range-energy curves for alpha-particles and protons, William P. Jesse and John Sadauskis—163(A)
Relative stopping power, experimental method, John G. Teasdale—588(A)

Recombination
Of electron-ion by microwave methods, Manfred A. Biondi and Sanborn C. Brown—1697

Relativity
Extension of field equations, Cornelius Lanczos—592(A)
Field of gravitational dipole, Hans Freistadt and Nathan Rosen—201(A)
Finite relativistic charge-current distributions, D. Bohm, M. Weinstein, and H. Kouts—867(L)
Generalized theory of gravitation, V. V. Narlikar and Ramji Tiwari—868(L)
Infinite relativistic particle matrices, Walter Wessel—1512
Interaction between elementary particles, Alfred Landé—1176
Wave equations in de Sitter space, Satosi Watanabe—296

Resonance radiation
Imprisonment in Hg vapor, D. Alpert, A. O. McCoubrey, and T. Holstein—457(A), 1257(A)

Scattering of electrons, neutrons, and ions (see also **Cross section, measurements, theory**)
D-D reaction products, angular distribution, Yashihiro Nakano—981(L)
Deuterons scattered by deuterons, angular distribution, E. J. Stovall, Jr., J. C. Allred, K. W. Erickson, and J. L. Fowler—589(A); J. C. Allred, K. W. Erickson, J. L. Fowler, and E. J. Stovall, Jr.—1430
Diffusion of neutrons in plate of finite thickness, Otto Halpern and R. K. Luneberg—1811
Double scattering of protons in helium, D. C. Dodder—683(L)
Effective range in nuclear scattering, theory, H. A. Bethe—38
Elastic scattering of electrons by neutral hydrogen atoms, Su-Shu Huang—477, 866(L)
Electrostatic scattering of neutrons, S. M. Dancoff and S. D. Drell—205
Energy loss of protons and deuterons, W. A. Bowers—196(A)
Of fast neutrons, C. K. Bockelman, R. E. Peterson, R. K. Adair, and H. H. Barschall—277
Interaction of 14-Mev neutrons with deuterons, J. H. Coon and R. F. Taschek—710
Magneto optics of neutrons, Otto Halpern—1130
Multiple scattering of fast particles, H. S. Snyder and W. T. Scott—220
Neutron-proton scattering, John M. Blatt and J. David Jackson—18; K. M. Watson and J. V. Lepore—193(A); H. N. Yadav—1720(L)
Neutron resonance scattering, corroboration, R. K. Adair, C. K. Bockelman, and R. E. Peterson—308(L)
Polarization effects in *n-p* and *p-p* scattering, Lincoln Wolfenstein—541
Phase shifts in proton-alpha-scattering, C. L. Critchfield and D. C. Dodder—602
Probabilities in multiple scattering, W. T. Scott—212
Of protons by Al, R. S. Bender, F. C. Shoemaker, S. G. Kaufmann, and G. M. B. Bouricius—273
Of protons by tritons, A. Hemmendinger, G. A. Jarvis, and R. F. Taschek—1137
Proton-proton at 5.11 Mev, R. O. Bondelid, P. G. Bohlman, and K. B. Mather—865(L)
Proton-proton scattering at 250 Mev, Charles L. Oxley—461(A)
Proton stopping power of gold, Torben Huus and C. B. Madsen—323(L)
Resonance scattering by W^{186}, S. Harris and C. O. Muehlhause—189(A)
Of slow neutrons by paramagnetic crystals, erratum, I. W. Ruderman, W. W. Havens, Jr., T. I. Taylor, and L. J. Rainwater—434(L)
Stopping power for protons in metals, S. D. Warshaw—1759
Straggling of electrons near critical energy, L. Eyges—264
Theory of Dirac equation, G. Parzen—592(A)
Three-body scattering, central and tensor forces, Roy Thomas—1002(L)
Variational method, Su-Shu Huang—1878(L)
Variational principle for scattering problems, Su-Shu Huang—866(L)

Scattering of radiation (see also **Raman spectra**)
In C, Al, Cu, Sn, and Pb, R. L. Walker—527
Of gamma-rays in aluminum, W. C. Parkinson—1348
Multiply scattered γ-rays, L. V. Spencer and Fannie Jenkins—462(A)
Non-Rayleigh scattering of infra-red solar spectrum, Arthur Adel—446(L)
Penetration and diffusion of x-rays, pair production, U. Fano—739
Resonance scattering of high energy γ-rays by C and Cu, E. R. Gaerttner and M. L. Yeater—363
Thompson scattering and hole theory, D. S. Kothari and F. C. Auluck—433(L)
Secondary electrons (see **Electrons, secondary**)
Semiconductors (see **Electrical conductivity and resistance**)
Shock waves (see also **Explosion phenomena; Fluid dynamics**)
Form and location of detached shock waves, W. E. Moeckel—877(A)
In inhomogeneous flow, Mac C. Adams—877(A)
Interaction of wave with contact surface, G. N. Patterson, I. I. Glass, and D. Bitondo—881(A)
Limiting lines, relation to shock in viscous gases, M. Z. Krzywoblocki—877(A)
Mach reflection of shock waves, W. Bleakney, C. H. Fletcher, and D. K. Weimer—323(L)
Photography of shocks, P. E. Shafer and J. F. Moulton, Jr.—881(A)
Reflection of plane shock at glancing incidence, C. H. Fletcher and W. Bleakney—881(A)
Reflection of shock waves from sea bed, A. B. Arons and D. R. Yennie—172(A)
Refraction at gas interface, R. G. Stoner and M. H. Glaubermann—882(A)
Shock tube, flow phenomena, F. W. Geiger—881(A)
Solid state (see **Crystalline state**)
Solutions
Of He^3 in He^4, J. W. Stout—864(L)
Sound (see **Acoustics**)
Spectra, absorption
Atmospheric HDO, H. A. Gebbie, W. R. Harding, C. Hilsum, and V. Roberts—1534(L)
Of atomic Na, E. R. Thackeray—173(A)
Of benzene at liquid-helium temperature, R. M. Hainer and Gilbert W. King—473(A)
Of chlorine monofluoride, T. F. Parkinson, E. A. Jones, and A. H. Nielsen—199(A)
Color centers in alkali halide crystals, Robert Lagemann—199(A)
Of diborane, W. E. Anderson and E. F. Barker—177(A)
Of H_2 and CO_2 at high densities, H. L. Welsh, M. F. Crawford, and J. L. Locke—580(L)
Of hydrogen telluride vapor, Herman Jarrell and Joseph W. Straley—199(A)
Infra-red absorption by homonuclear diatomic molecules, Mary Louise Oxholm and Dudley Williams—151(L)
Large orbits in alkali metal atoms, H. R. Kratz and J. E. Mack—173(A)
Line width in infra-red, pressure dependence, Frank Matossi—1845
ν_3-fundamental of N_2O, K. B. Rhodes and E. E. Bell—1273(L)
Of seven freons, Earle K. Plyler—177(A)
Source of highly forbidden lines in CdI, Fernand E. Deloume and John R. Holmes—174(A)
Theory of pressure absorption, Masataka Mizushima—1268(L)
Total absorption, overlapping lines, Frank Matossi, Robert Mayer, and Emma Rauscher—760
Ultraviolet of pyridine derivatives in solution, Harold P. Stephenson—199(A)
Spectra, atomic
Complex spectra, theory, Giulio Racah—1352
Electron-nuclear potential fields from hyperfine structure, M. F. Crawford and A. L. Schawlow—1310
Isotope shift in HeI, Thurston E. Manning—173(A)
Isotopic spectra of Pb, Thurston E. Manning—464(A)
Solar and stellar atmospheres, *f* values in iron spectrum, W. W. Carter—962
Structure of λ4686 of HeII, K. Murakawa, S. Suwa, and T. Kamei—1721(L)
Spectra, general
CO_2, infra-red solar spectrum, Leo Goldberg, Orren C. Mohler, Robert R. McMath, and A. Keith Pierce—1848
Collision theories of pressure broadening, J. H. Van Vleck and HenryMargenau—585(A), 1211
Color determination by human eye, W. A. Pryor and Hugh F. Henry—199(A)
Inversion spectrum of ammonia, pressure broadening, Henry Margenau—121; William V. Smith and Raydeen Howard—473(A)
Methane in solar spectrum, Robert R. McMath, Orren C. Mohler, A. Keith Pierce, and Leo Goldberg—1533(L)
Ultraviolet and x-rays from sun, J. D. Purcell, R. Tousey, and K. Watanabe—165(A)
Spectra, microwave
Of CD_3Cl and CD_3I, James W. Simmons—686(L)
Of CF_3Cl, D. K. Coles and R. H. Hughes—858(L)
Of $CH_2=CF_2$, A. Roberts and W. F. Edgell—178(A)
Of CH_2Br_2, William J. Pietenpol and John D. Rogers—690(L)
Of chloroacetylene and deuterochloroacetylene, A. A. Westenberg, J. H. Goldstein, and E. B. Wilson, Jr.—472(A)
Dipole moments from microwave spectra, C. H. Townes, R. G. Shulman, and B. P. Dailey—472(A)
Dispersion in NH_3, George Birnbaum—178(A)
Of FCl, D. A. Gilbert, A. Roberts, and P. A. Griswold—1723(L)
Of formaldehyde, R. B. Lawrance, R. L. Kyhl, and M. W. P. Strandberg—472(A)
Of $K^{39}F$, Ludwig Grabner, Vernon Hughes, and I. I. Rabi—472(A)
Of methyl alcohol and of methyl amine, H. D. Edwards, O. R. Gilliam, and W. Gordy—196(A)
Of methyl fluoride, fluoroform, and phosphorus tri-fluoride, O. R. Gilliam, H. D. Edwards, and W. Gordy—195(A)
Moment of CsF, J. W. Trischka—1365
Of nitrous oxide, D. K. Coles and R. H. Hughes—178(A)
Of OCS and CH_3Cl, isotopic frequencies, D. Bianco, G. Matlack, and A. Roberts—473(A)
Optical detection of radiofrequency resonance, F. Bitter—833
Paschen-Back effect in NH_3 and N_2O, C. K. Jen—1494
Pressure broadening, P. W. Anderson—647
Rotational magnetic moments of H_2O and HDO, C. K. Jen—471(A)
Rotational spectra and structures of GeH_3Cl, SiH_3Cl, and CH_3Cl, B. P. Dailey, J. M. Mays, and C. H. Townes—136(L)
Of $Rb^{85}F$ and $Rb^{87}F$, Vernon Hughes, Ludwig Grabner, and I. I. Rabi—471(A)
Van Vleck-Weisskopf line shape formula, P. W. Anderson—471(A)
Spectra, molecular (see also **Molecular structure and constants**)
CO-O_2 reaction, George A. Hornbeck and Helen S. Hopfield—174(A)
Of the deutero-ammonias, John S. Burgess—1267(L)
Doubly excited levels of H_2, G. H. Dieke—50

Excitation of molecular vibrations by high speed missiles, Z. I. Slawsky—882(A)
Fulcher bands of TH and T_2, G. H. Dieke and F. S. Tomkins—283
Hyperfine structure, HgH, S. Mrozowski—1820
Infra-red of CH_4, John S. Burgess—302(L)
Inversion spectrum of NH_3, H. Margenau—585(A), 1423; A. H. Sharbaugh, T. C. Madison, and J. K. Bragg—1529(L)
Linear molecules, rotational Stark spectrum, Harold. Kenneth Hughes—1675
Hg_2 and Hg_2^+ bands λ2540 and λ2476, S. Mrozowski—1714
Molecular constants of $C^{12}O^{16}$ and $C^{13}O^{16}$, errata, Robert T. Lagemann, Alvin H. Nielsen, and Fred P. Dickey—159(L)
Of nitrogen dioxide, M. Kent Wilson and Richard M. Badger—472(A)
Transition probabilities for electronic spectra of C_2 and N_2^+, Harrison Shull and R. S. Mulliken—176(A)

Spectroscopy, technique
Magnetron harmonics, 1.5- and 2-mm wave-length, J. H. N. Loubser and C. H. Townes—178(A)

Spinor analysis
Crystal statistics, partition function by spinor analysis, Bruria Kaufman—1232
Non-local spinor field, Hideki Yukawa—1731(L)

Stark effect
On symmetric top molecules with nuclear quadrupole coupling, W. Low and C. H. Townes—1295

Statistical mechanics (see **Mechanics, statistical**)

Stopping power (see **Scattering of electrons, neutrons, and ions**)

Superconductivity (see **Electrical conductivity and resistance**)

Supersonic phenomena
Analysis of air jets, R. Ladenburg, C. C. Van Voorhis, and J. Winckler—662
Boundary layer optics in two-dimensional flow, D. Bershader and G. P. Wachtell—880(A)
Characteristics of triangular planform wings, H. C. Sanderson, Jr. and Berg Paraghamian—878(A)
Condensation phenomena, wind tunnel, R. Head—882(A)
Excitation of molecular vibrations by high speed missiles, Z. I. Slawsky—882(A)
Flow of air at Mach No. 7, J. W. Braithwaite and J. L. Frame—883(A)
Heat delivery in two-dimensional flow, Chan-Mou Tchen—883(A)
Heat transfer coefficients on cones, G. R. Eber—879(A)
Multiple shock diffusers, Newman A. Hall—884(A)
Starting and stopping of wind tunnel, flow characteristics, G. E. Burkheimer—880(A)
Symmetric and plane supersonic flows, P. Zettler-Seidel—877(A)
Temperature gradient and humidity on condensation, P. P. Wegener—883(A)
Three-dimensional flows with vorticity, R. F. Clippinger and J. H. Giese—878(A)
Vorticity about a yawing body, W. C. Carter—878(A)

Thermal conductivity
Of beryllium carbide, Charles E. Teeter, Jr.—466(A)
Freezing of fresh water lakes, L. D. Huff—200(A)
Of glasses at low temperatures, R. Berman—315(L)
Of metals below 1°K, superconductors, C. V. Heer and J. G. Daunt—854(L)
Mixtures of He^3 and He^4, K. S. Singwi and L. S. Kothari—305(L)
Non-linear problem in transient flow, Bruce L. Hicks—166(A)
Second sound and classical heat flow, John R. Pellam—872(L)
Temperature distribution in an accreting medium, A. E. Benfield—456(A)

Thermal diffusion (see also **Diffusion**)
Of HCl, temperature variation, Gwynne B. Swartz—166(A)

Thermal radiation (see also **Radiation**)
Emittances of Cu and Al spheres, George Best—166(A)
Of Ti, Walter C. Michels and Sally E. Wilford—174(A)

Thermionic emission; emitting surfaces
Of (BaSr)O without metallic support, George E. Moore—458(A)
From carbon, Henry F. Ivey—567(L)
Emission phenomena in (Ba-Sr)O, E. S. Rittner, F. K. du Pré, and R. A. Hutner—996(L)
Of Ni, Alvin B. Cardwell—125
Work function of copper, Paul A. Anderson—388
Work function of silicon, change with temperature, B. J. Rothlein and P. H. Miller, Jr.—1882(L)
Work functions of gas-coated silver, G. L. Weissler and T. N. Wilson—591(A)

Thermodynamics
Chemical thermodynamics in Jacobian form, F. H. Crawford—456(A)
Of flow systems, Charles F. Curtiss and Joseph O. Hirschfelder—883(A)
Of liquid He, two-fluid theory, O. K. Rice—1701
Meaning of first law, J. C. Finck—166(A)
Non-equilibrium phenomena in Bose-Einstein gas, second sound, William Band—558
Temperature equilibrium in stationary gravitational field, H. A. Buchdahl—427(L)
Theory of critical fluctuations, M. J. Klein and L. Tisza—1861
Transformation theory, H. C. Corben—166(A)

Thermoelectric effects
Thompson coefficient for W at high temperatures, C. C. Sartain—197(A)

Thermomagnetic effects
In iron oxide and iron catalysts, Louis R. Maxwell and Stephen Brunauer—175(A)

Ultrasonics (see also **Acoustics**)
Rotational dispersion in deuterium and hydrogen, James L. Stewart and Ellen S. Stewart—464(A)

Uncertainty principle (see also **Mechanics, quantum—general**)
Test of principle, Gertrude Schwarzmann—192(A)

Viscosity
Mixtures of He^3 and He^4, K. S. Singwi and L. S. Kothari—305(L)
Second viscosity of liquids, erratum, L. N. Liebermann—440(L)

Wave mechanics (see **Mechanics, quantum**, etc.)

Work function (see **Thermionic emission; Photoelectric effect**)

X-rays, absorption, diffraction, scattering, reflection, refraction, and polarization
By Al between 100A and 300A, E. M. Pell and D. H. Tomboulian—172(A)
Angular scattering in Compton effect, Robert Hofstadter and John A. McIntyre—1269(L)
Collimation error in small angle scattering, K. L. Yudowitch—455(A)
Diffraction by Au-Be system, G. P. Chatterjee and S. S. Sidhu—175(A)
Diffusion through thick barriers, H. A. Bethe, U. Fano, and P. R. Karr—538; L. V. Spencer and Fannie Jenkins—1885(L)

X-rays, absorption, diffraction, scattering, reflection, refraction, and polarization (continued)
L_1 absorption edge in Al, D. H. Tomboulian and E. M. Pell —172(A)
Mn K absorption in Mn metal and compounds, Harold Hanson and W. W. Beeman—118
Scattering from large particles, David L. Dexter and W. W. Beeman—1782
Scattering of polarized x-rays, Eric Rodgers—196(A)
Simultaneity in Compton effect, R. Hofstadter and J. A. McIntyre—172(A)
Spectral distributions of hard x-rays in medium, P. R. Karr and J. C. Lamkin—1843

X-rays, emission
Energy distribution of bremsstrahlung, H. W. Koch, R. E. Carter, and C. S. Robinson—172(A)
K-shell internal conversion coefficients, M. E. Rose, G. H. Goertzel, B. I. Spinrad, J. Harr, and P. Strong—184(A)
L spectrum of element 61, W. F. Peed, E. J. Spitzer, and L. E. Burkhart—143(L)
Output for betatrons, W. F. Westendorp and F. R. Elder—445(L)
Radioactive materials as sources, H. F. Gunlock—453(A)
Spectral analysis of betatron radiation, P. K. S. Wang and M. Wiener—1724(L)

X-rays, tubes, apparatus
Helical focusing β-ray spectrometer, L. Feldman and C. S. Wu—180(A)
Photo-multiplier for x-ray spectrometer, J. S. Brown, G. M. Farrior, and Arthur Waltner—196(A)

Zeeman effect
Effect of nuclear motion, M. Phillips—1803

VOLUME 76 SECOND SERIES

CONTENTS

JULY 1, 1949

On Nucleon Moments and the Neutron-Electron Interaction . . . . . K. M. CASE 1
Equivalence Theorems for Meson-Nucleon Couplings . . . . . K. M. CASE 14
On the Interpretation of Neutron-Proton Scattering Data by the Schwinger Variational Method . . . . . JOHN M. BLATT AND J. DAVID JACKSON 18
Theory of the Effective Range in Nuclear Scattering . . . . . H. A. BETHE 38
Bands from Doubly Excited Levels of the Hydrogen Molecule . . . . . G. H. DIEKE 50
Bremsstrahlung in High Energy Nucleon-Nucleon Collisions . J. ASHKIN AND R. E. MARSHAK 58
On the Two-Meson Theory . . . . . MITUO TAKETANI, SEITARO NAKAMURA, KENICHI ONO, AND MUNEO SASAKI 60
"Heat Flush" Method of He^3 Separation . . . . . CHARLES A. REYNOLDS, HENRY A. FAIRBANK, C. T. LANE, B. B. MCINTEER, AND ALFRED O. NIER 64
Interaction Representation of the Proca Field . . . . . FREDERIK J. BELINFANTE 66
Radiative Processes in Thermionically Controlled Discharges in Helium . . . . . R. G. FOWLER AND O. S. DUFFENDACK 81
Radiation Accompanying Meson Creation . . . . . L. I. SCHIFF 89
Nuclear Spectra of Sb^{125}, Te^{125}, Cr^{51}, and I^{131} . . . . . BERNARD D. KERN, ALLAN C. G. MITCHELL, AND DANIEL J. ZAFFARANO 94
Neutron Cross Sections at 115 ev and 300 ev—I . . . C. T. HIBDON AND C. O. MUEHLHAUSE 100
Angular Distribution of Protons in the $N^{14}(d,p)N^{15}$ Reactions . . . . . L. D. WYLY 104
Angular Distribution of the Photo-Disintegration of the Deuteron . . . . . W. M. WOODWARD AND I. HALPERN 107
Absorption of Negative π-Mesons by Protons . . . . . R. E. MARSHAK AND A. S. WIGHTMAN 114
Mn K Absorption Edge in Manganese Metal and Manganese Compounds . . . . . HAROLD HANSON AND W. W. BEEMAN 118
Pressure Broadening in the Inversion Spectrum of Ammonia . . . . . HENRY MARGENAU 121
Photoelectric and Thermionic Properties of Nickel . . . . . ALVIN B. CARDWELL 125
Breakdown of Ionic Crystals by Electron Avalanches . . . . A. VON HIPPEL AND R. S. ALGER 127
Production of Mesons by Photons and Electrons . . . HERMAN FESHBACH AND MELVIN LAX 134

Letters to the Editor:

Distribution in Mass and Charge of Fission Products . . . . . K. H. KINGDON 136
Microwave Rotational Spectra and Structures of GeH_3Cl, SiH_3Cl, and CH_3Cl . . . . . B. P. DAILEY, J. M. MAYS, AND C. H. TOWNES 136
Ferromagnetite Resonance Absorption in Magnetite . . . . . L. R. BICKFORD, JR. 137
On the Sign of the Electric Quadrupole Moment of Li^7 . . . . . P. KUSCH 138
Relation of Nuclear Quadrupole Moment to Nuclear Shell Structure . . . . . WALTER GORDY 139
Yields of Manganese in Spallation Reactions . . . . . NORMAN A. BONNER AND WILLIAM C. ORR 140
Variation of Meson Intensity with Height . . . . . P. H. BARKER 141
Evidence for the Photo-Fission of Uranium into Three Charged Fragments . . . . . E. W. TITTERTON AND F. K. GOWARD 142
On the Penetrating Component of Cosmic-Ray Air Showers . . . . . FRANK L. HEREFORD 142
L Spectrum of Element 61 . . . . . W. F. PEED, E. J. SPITZER, AND L. E. BURKHART 143
Paramagnetic Anisotropy of Manganous Fluoride . . . . . J. W. STOUT AND MAURICE GRIFFEL 144
Accurate Nuclear Magnetic Resonance Method for Measuring Spin-Lattice Relaxation Times . . . . . ERWIN L. HAHN 145
Error in a Paper by Landau on Coulomb Interactions in a Plasma . . . . . WILLIAM P. ALLIS 146
Proton-Range-Energy Relation . . . . . R. L. CLARKE AND G. A. BARTHOLOMEW 146
Actinide Series and the Periodic Table . . . . . ZOLTÁN SZABÓ 147
Branching Ratio in Be^7 Decay . . . . . C. M. TURNER 148
Exchange Phenomena of the Nucleons that Generate Penetrating Showers . . . . . H. A. MEYER AND G. SCHWACHHEIM 149
Nuclear Spin and Quadrupole Moment of I^{129} . . . . . RALPH LIVINGSTON, O. R. GILLIAM, AND WALTER GORDY 149
Nuclear Magnetic Moments and Hyperfine Structure of the Rubidium Isotopes . . . . F. BITTER 150
Hall Effect of Metal-Semiconductor Point Contacts . . . . . S. BENZER 150
Nuclear Spin of Fe^{57} . . . . . M. GUREVITCH AND J. G. TEASDALE 151
Infra-Red Absorption by Homonuclear Diatomic Molecules . . . . . MARY LOUISE OXHOLM AND DUDLEY WILLIAMS 151
Dependence of Resistivity of Germanium on Electric Field . . . . . RALPH BRAY 152
Cathode Sputtering in the Abnormal Glow Discharge . . . . . RICHARD HANAU 153
On the Measurement of the Energy of Fast Neutrons by Photographic Emulsions Loaded with Enriched Li^6 . . . . . GEORGE R. KEEPIN AND JAMES H. ROBERTS 154
Effect of Alpha-Particles on a Superconductor . . . . . D. H. ANDREWS, R. D. FOWLER, AND M. C. WILLIAMS 154

Uranium^{235} in Thucholite . . . . . J. B. ORR 155
Flux of Heavy Nuclei of the Primary Cosmic Radiation at Geomagnetic Latitudes $\lambda = 55°$ and $\lambda = 30°$ . . . . . H. L. BRADT AND B. PETERS 156
Mean Life Considerations in Relation to Curvature of Cosmic-Ray Paths in a Magnetic Field . . . . . W. F. G. SWANN 157
On the Decay of Isotropic Turbulence . . . . . S. CHANDRASEKHAR 158
Correlations in Measurements on Superfluidity in Liquid Helium II . . . . . JOHN R. PELLAM 158
Erratum: The Infra-Red Spectrum and Molecular Constants of $C^{12}O^{16}$ and $C^{13}O^{16}$ . . . . . ROBERT T. LAGEMANN, ALVIN H. NIELSEN, AND FRED P. DICKEY 159
Addendum: Energy Spectrum of the Decay Particles and the Mass and Spin of the Mesotron . . . . . ROBERT B. LEIGHTON, CARL D. ANDERSON, AND AARON, J. SERIFF 159

Proceedings of the American Physical Society:

Minutes of the Meeting at Washington, D. C., April 28–30, 1949 160
Minutes of the Meeting of the Southeastern Section at Clemson College, April 15–16, 1949 195

JULY 15, 1949

Electrostatic Scattering of Neutrons . . . . . S. M. DANCOFF AND S. D. DRELL 205
Correlated Probabilities in Multiple Scattering . . . . . W. T. SCOTT 212
Multiple Scattering of Fast Charged Particles . . . . . H. S. SNYDER AND W. T. SCOTT 220
On the Part Played by Scalar and Longitudinal Photons in Ordinary Electromagnetic Fields . . . . . FREDERIK J. BELINFANTE 226
Theory of the Photo- and Electrodisintegration of Be^9 . EUGENE GUTH AND CHARLES J. MULLIN 234
(α, n) Cross Section of Boron . . . . . R. L. WALKER 244
(α, n) Cross Sections of Beryllium, Magnesium, and Aluminum . . . . . I. HALPERN 248
Clustering of Ions and the Mobilities in Gaseous Mixtures . . . . ALBERT W. OVERHAUSER 250
Role of the Cathode in Discharge Instability . . . . . LEONARD B. LOEB 255
Angular Distribution of Photo-Neutrons from Deuterium . . . . . EDWIN P. MEINERS, JR. 259
Straggling of Electrons near the Critical Energy . . . . . L. EYGES 264
Some Semimetallic Characteristics of the Photoelectric Emission from As, Sb, and Bi . . . . . L. APKER, E. TAFT, AND J. DICKEY 270
Resonance Scattering of Protons by Aluminum . . . . . R. S. BENDER, E. C. SHOEMAKER, S. G. KAUFMANN, AND G. M. B. BOURICIUS 273
Total Cross Section Measurements for Fast Neutrons . . . . . C. K. BOCKELMAN, R. E. PETERSON, R. K. ADAIR, AND H. H. BARSCHALL 277
Measurements on Radioactive Krypton Isotopes from Fission after Mass-Spectrographic Separation . . J. KOCH, O. KOFOED-HANSEN, P. KRISTENSEN, AND W. DROST-HANSEN 279
Molecular Spectrum of Hydrogen. The Fulcher Bands of Th and T_2 . . . . . G. H. DIEKE AND F. S. TOMKINS 283
Coincidence and Absorption Investigation of the Disintegration of Rh^{106}, Sb^{125}, and Pr^{142} . . . . . E. T. JURNEY 290
Superconductors in Alternating Magnetic Fields . . . . . ROBERT T. WEBBER, J. M. REYNOLDS, AND T. R. MCGUIRE 293
Wave Equations in the de Sitter Space . . . . . SATOSI WATANABE 296
On a Generalization of the Lambda-Limiting Process and the Non-Uniqueness in the Removal of Divergence Difficulties in the Quantum Theory of Elementary Particles . . . . . I. POMERANCHUK 298

Letters to the Editor:

Slow Neutron Cross Sections of the Neodymium Isotopes . . . . . DAVID C. HESS, JR. AND MARK G. INGHRAM 300
On the Radius of the Elementary Particle . . . . . HIDEKI YUKAWA 300
Concerning the High Pressure Allotropic Modification of Cerium . . . . . A. W. LAWSON AND TING-YUAN TANG 301
Frequency of ν_2 in the Infra-Red Spectrum of CH_4 . . . . . JOHN S. BURGESS 302
Note on Measurements of Ambipolar Diffusion in Helium . . . . . MANFRED A. BIONDI AND SANBORN C. BROWN 302
Comment on the Nuclear Capture of Negative Mesons . . . . . J. BARNOTHY 303
Spontaneous Decay Rate of Heavy Mesons . . . . . L. I. SCHIFF 303
Production of π-Mesons by High Energy Nucleons . . . . . E. STRICK AND D. TER HAAR 304
Note on the Resistivity of Gold at Low Temperatures . . . . . C. T. LANE 304
Magnetic Effects of a Rotating Superconductor . . W. F. LOVE, R. F. BLUNT, AND P. B. ALERS 305
Viscosity and Thermal Conductivity of Mixtures of He^3 and He^4 . K. S. SINGWI AND L. S. KOTHARI 305
Polarization of Mesons Produced at Threshold in Gamma-Nucleon Collisions . . DANIEL B. FEER 306
Decay Scheme of Ni^{65} . . . . . KAI SIEGBAHN AND AMAL GHOSH 307
Experimental Corroboration of the Theory of Neutron Resonance Scattering . . . . . R. K. ADAIR, C. K. BOCKELMAN, AND R. E. PETERSON 308
Scintillations Produced by α-Particles in a Series of Structurally Related Organic Crystals . . . . . W. S. KOSKI AND CARL O. THOMAS 308

Vacancies and Diffusion in NiAl . . . . . R. SMOLUCHOWSKI AND H. BURGESS 309
Removal of Space-Charge in Diamond Crystal Counters . . . . . A. G. CHYNOWETH 310
Positive Excess of Mesons at 30,000 Feet . . . . . MARCELLO CONVERSI 311
Measurement of a 2.3×10^{-6} Second Metastable State in Hg^{198} . . . . . W. J. MACINTYRE 312
Mass Assignment of the 43-Minute Hg Isomer . . . . INGMAR BERGSTRÖM AND SIGVARD THULIN 313
Gamma-Radiation from Light Nuclei under Proton Bombardment . . . . . W. A. FOWLER AND C. C. LAURITSEN 314
Thermal Conductivity of Glasses at Low Temperatures . . . . . R. BERMAN 315
Energy Levels in N^{15} and N^{16} . . . . . L. D. WYLY 316
Ionization Measurement of $He^3(np)$ and $N^{14}(np)$ and the Neutron-Hydrogen Mass Difference . . . . . W. FRANZEN, J. HALPERN, AND W. E. STEPHENS 317
Angular Distribution and Multiplicity of Neutrons Associated with Local Cosmic-Ray Showers . . . . . G. COCCONI AND V. COCCONI TONGIORGI 318
Relation between Half-Life and Disintegration Energy in Orbital Electron Capture by Heavy Nuclei . . . . . STANLEY G. THOMPSON 319
Magnetic Deflection of Cosmic-Ray Mesons Using Nuclear Plates . . . . . IAN BARBOUR 320
Large Nuclear Disintegration Produced by a Very High Energy Alpha-Particle of the Cosmic Radiation . . . . . J. J. LORD, MARCEL SCHEIN, AND M. VIDALE 321
Angular Distribution of Neutrons from (d,n) Reactions . C. E. FALK, E. CREUTZ, AND F. SEITZ 322
Proton Stopping Power of Gold . . . . . TORBEN HUUS AND C. B. MADSEN 323
Density Field in Mach Reflection of Shock Waves . . . . . W. BLEAKNEY, C. H. FLETCHER, AND D. K. WEIMER 323

AUGUST 1, 1949

Neutron-Hydrogen Mass Difference from the $T^3(p, n)He^3$ Reaction Threshold . . . . . R. F. TASCHEK, H. V. ARGO, A. HEMMENDINGER, AND G. A. JARVIS 325
Coincidence and Absorption Measurements on Cs^{134}, I^{124}, Au^{199}, and Ca^{45} . . . . . J. LAWRENCE MEEM, JR. AND FRED MAIENSCHEN 328
Long-Lived Tellurium Isomers . . . . . R. D. HILL 333
U-234 Specific Alpha-Activity . . . . . A. S. GOLDIN, G. B. KNIGHT, P. A. MACKLIN, AND R. L. MACKLIN 336
Wave Amplification by Interaction with a Stream of Electrons . . . . . J. A. ROBERTS 340
Forbidden Transition of Yttrium^{91} and Cesium^{137} . . . . . J. S. OSOBA 345
Determination of Nuclear Gyromagenetic Ratios I . . . . . JOHN R. ZIMMERMAN AND DUDLEY WILLIAMS 350
Radioactive Tin 111 . . . . . R. A. HINSHAW AND M. L. POOL 358
Note on Perturbation Theory as Applied to Collision Stimulated Processes . . . . . JAMES N. SNYDER AND W. H. FURRY 359
Note on the Resonance Scattering of High Energy γ-Rays by Nuclei of Carbon and Copper . . . . . E. R. GAERTTNER AND M. L. YEATER 363
On the Continuous Gamma-Radiation Accompanying the Beta-Decay of Nuclei . . . . . C. S. WANG CHANG AND D. L. FALKOFF 365
Single Production of Mesons by Gamma-Rays Near Threshold . . . . . LESLIE L. FOLDY 372
Fogging of Photographic Film by Radioactive Contaminants in Cardboard Packaging Materials . . . . . J. H. WEBB 375
Diode Space Charge for Any Initial Velocity and Current . . . . . LEIGH PAGE AND NORMAN I. ADAMS, JR. 381
Work Function of Copper . . . . . PAUL A. ANDERSON 388
On the Treatment of Quantum Electrodynamics without Eliminating the Longitudinal Field . . . . . NING HU 391
Bose-Einstein Condensation for Thin Films . . . . . M. F. M. OSBORNE 396
Bose-Einstein Condensation for Charged Particles in a Magnetic Field . . M. F. M. OSBORNE 400
On the Electromagnetic Surface Wave of Sommerfeld . . . . . T. KAHAN AND G. ECKART 406
Further Deductions from the $\mathcal{H}$-Theorem . . . . . HARVEY EINBINDER 410
Magnetic Susceptibility of Zinc at Liquid Hydrogen Temperatures . . . . JULES A. MARCUS 413
Non-Equilibrium States in Helium II . . . . . WILLIAM BAND AND LOTHAR MEYER 417
Excitation Functions for (α,n), $(\alpha,2n)$, $(\alpha,3n)$ Reactions on Indium . . . GEORGES M. TEMMER 424

Letters to the Editor:

Anomalous Magnetic Moments of Nucleons . . . . . S. D. DRELL 427
Temperature Equilibrium in a Stationary Gravitational Field . . . . . H. A. BUCHDAHL 427
Apparent Straggling of $_{16}S^{35}$ Beta-Particles in Glass . MARY JANE A. LINKER AND F. T. ROGERS, JR. 428
Energy Release in Beryllium and Lithium Reactions with Protons . . . . . A. V. TOLLESTRUP, W. A. FOWLER, AND C. C. LAURITSEN 428
Revaluation of the Gamma-Radiations from Co^{60} and Zn^{65} . . . . . ERLING N. JENSEN, L. JACKSON LESLETT, AND WILLIAM W. PRATT 430
Ferro-Electric Properties of WO_3 . . . . . B. T. MATTHIAS 430
On the γ-γ-Angular Correlation in Pd^{106} . . . . . DANIEL S. LING, JR. AND DAVID L. FALKOFF 431

Magnetic Susceptibilities of Some Tetravalent Uranium Fluorides . . . . . NORMAN ELLIOTT 431
Interaction of Mesons with the Electromagnetic Field . . . . . W. H. FURRY AND M. NEUMAN 432
Electromagnetic Induction in a Superconductor . . . . . A. WEXLER AND W. S. CORAK 432
Thompson Scattering and the Hole Theory . . . . . D. S. KOTHARI AND F. C. AULUCK 433
Quadrupole Moment of Sb^{121} and Sb^{123} . . . . . K. MURAKAWA AND S. SUWA 433
Magnetic Moment of B^{11} . . . . . DONALD A. ANDERSON 434
Erratum: The Scattering of Slow Neutrons by Paramagnetic Crystals . . . . . I. W. RUDERMAN, W. W. HAVENS, JR., T. I. TAYLOR, AND L. J. RAINWATER 434
Gamma-Radiation from Na^{22} and Co^{60} . . . . . DAVID E. ALBURGER 435
Nuclear Spin and Magnetic Moment of Cs^{137} . . . . . LUTHER DAVIS, JR. 435
Neutrons from the Disintegration of Sodium by Deuterons . . . . . C. E. MANDEVILLE 436
Erratum: On the Difficulty of the Meson Theory of Nuclear Forces . . . . . GENTARO ARAKI 437
Decay Scheme of Te^{125m} . . . . . J. C. BOWE AND GERTRUDE SCHARFF-GOLDHABER 437
On the Energy Band Structure of Insulators . . . . . G. H. WANNIER 438
Computed Binding Energies of Some Light Nuclei . . . . . J. SAMUEL SMART 439
Angular Distribution of Annihilation Radiation . . . . . S. DEBENEDETTI, C. E. COWAN, AND W. R. KONNEKER 440
Erratum: The Second Viscosity of Liquid . . . . . L. N. LIEBERMANN 440
Anomalous Adsorption of Helium at Liquid Helium Temperatures . . . . . EARL A. LONG AND LOTHAR MEYER 440
Anomalous Adsorption of Helium at Liquid Helium Temperatures . . . . . WILLIAM BAND 441
Neutron Irradiated Semiconductors . . . . . W. E. JOHNSON AND K. LARK-HOROVITZ 442
Nuclear Magnetic Moments from Microwave Spectra: I^{127} and I^{129} . . . . . WALTER GORDY, O. R. GILLIAM, AND RALPH LIVINGSTON 443
Latitude Dependence at 30,000 Feet of Penetrating Particles Slowed Down After Traversing 15 cm of Lead . . . . . MARCELLO CONVERSI 444
Electron Gun Emission and X-Ray Output for Three Betatrons . . . . . W. F. WESTENDORP AND F. R. ELDER 445
Superconducting Torus . . . . . R. L. DOLECEK AND JULES DE LAUNAY 445
Observation of Non-Rayleigh Scattering of the Infra-Red Solar Spectrum by the Earth's Atmosphere . . . . . ARTHUR ADEL 446
Large Cosmic Stars in Electron Sensitive Emulsions . . . . . E. PICKUP AND L. VOYVODIC 447
Binding Energies of Alpha-Particles in Medium-Heavy Nuclides . . . . . TRUMAN P. KOHMAN 448
τ-Meson . . . . . NORBERT WAGNER AND D. COOPER 449

Proceedings of the American Physical Society:

Minutes of the Semi-Centennial Meeting at Cambridge, Massachusetts, June 16–18, 1949 451

AUGUST 15, 1949

Elastic Scattering of Electrons by Neutral Hydrogen Atoms by the Variational Method . . . . . SU-SHU HUANG 477
Neutrons from C(d, n)N and Cu(d, n)Zn . . . . . J. C. GROSSKREUTZ 482
Fading of Proton Tracks in Vacuum . . . . . K. B. MATHER 486
Time Distribution of Decay Electrons from Mesons Stopped in Magnesium at 3500 Meter Altitude . . . . . A. H. BENADE AND R. D. SARD 488
Absolute Speed Gauge for High Voltage Particles . . . . . W. ALTAR AND M. GARBUNY 496
Absolute Calibration of the $Li^7(p, n)$ Threshold Voltage . . . . . W. E. SHOUPP, B. JENNINGS, AND W. JONES 502
On the Knock-On Secondaries of Penetrating Particles . . . . . W. W. BROWN, A. S. MCKAY, AND E. D. PALMATIER 506
Penetrating Showers . . . . . W. B. FRETTER 511
On the Mechanism of Production of the Neutron Component of the Cosmic Radiation . . . . . VANNA COCCONI TONGIORGI 517
Absorption of 17.6 Mev Gamma-Rays in C, Al, Cu, Sn, and Pb . . . . . R. L. WALKER 527
Capture Gamma-Ray Studies . . . . . H. KUBITSCHEK AND S. M. DANCOFF 531
Penetration and Diffusion of Hard X-Rays through Thick Barriers. I. The Approach to Spectral Equilibrium . . . . . H. A. BETHE, U. FANO, AND P. R. KARR 538
Polarization Effects in n-p and p-p Scattering . . . . . LINCOLN WOLFENSTEIN 541
Radiation from a Uniformly Accelerated Charge . . . . . D. L. DRUKEY 543
Variation of the Adiabatic Elastic Constants of KCl, NaCl, CuZn, Cu, and Al with Pressure to 10,000 Bars . . . . . DAVID LAZARUS 545
Cathode Field in Diodes under Partial Space-Charge Conditions . . . . . HENRY F. IVEY 554
Non-Equilibrium Phenomena in a Bose-Einstein Gas. I. Transmission of Second Sound . . . . . WILLIAM BAND 558

Letters to the Editor:

Extension of the Theory of Mason and Matthias to the Low Temperature Transitions in $BaTiO_3$ . . . . . H. J. WELLARD 565
Note on Plasma Oscillations . . . . . J. R. PIERCE 565
Note on Meson Production . . . . . H. W. LEWIS 566

Proximity Effects in the Measurement of Magnetic Susceptibility . . . . . M. C. Steele 566
Thermionic Electron Emission from Carbon . . . . . Henry F. Ivey 567
Beta-Ray Spectra . . . . . H. J. Lipkin 567
Two-Component Wave Equations . . . . . C. W. Kilmister 568
On Temperature Dependence of Counter Characteristics in Self-Quenching G-M Counters . . . . . Om Parkash 568
On the Latitude Dependence of Nuclear Disintegration and Neutrons at 30,000 Feet . . . . . J. A. Simpson, Jr. and R. B. Uretz 569
Penetration of High Energy Electrons in Aluminum . . . . . F. L. Hereford and C. P. Swann 570
Hyperfine Structure of Te^{125} . . . . . G. R. Fowles 571
Spurious Counts in Geiger Counters and the Pre-Treatment of the Electrodes . . . . . J. D. Louw and S. M. Naudé 571
Radioactivity of Mo^{91} and Mo^{93} . . . . . R. B. Duffield and J. D. Knight 573
Beta-Decay of In^{115} . . . . . P. R. Bell, B. H. Ketelle, and J. M. Cassidy 574
New Germanium Photo-Resistance Cell . . . . . J. N. Shive 575
Neutron Induced Radioactivities in V^{52}, Mo^{99}, and W^{185} . . . . . J. M. Cork, H. B. Keller, and A. E. Stoddard 575
Photo-Disintegration of Deuterium by Seven- to Twenty-Mev X-Rays . . . . Everett G. Fuller 576
Thermal Neutron Absorption Cross Section of K^{39} . . . . John L. Hansen and John E. Willard 577
Investigation of the Attractive Forces between the Persistent Currents in a Superconductor and the Lattice . . . . . E. U. Condon and E. Maxwell 578
Thresholds for Photo-Neutron Reactions in Mn, Zn, Zr, Mo, Cd, Pr, Nd, Au, Hg, Tl, and Pb . . . . A. O. Hanson, R. B. Duffield, J. D. Knight, B. C. Diven, and H. Palevsky 578
Analysis of the Temperature Coefficient of Shear Modulus of Aluminum . . . . . T'ing-Sui Kê 579
Infra-Red Absorption of Hydrogen and Carbon Dioxide Induced by Intermolecular Forces . . . . . H. L. Welsh, M. F. Crawford, and J. L. Locke 580
Alpha-Particles Emitted in Fission . . . . . L. L. Green and D. L. Livesey 580
Magnetic Moments and Eddy Current Damping in Spherical Superconductors . . . . . J. J. Fritz, O. D. Gonzales, and H. L. Johnston 580
Tidal Effects in the F Layer . . . . . M. W. Jones and J. G. Jones 581
Gamma-Radiation from Deuteron Bombardment of Be^9 . . . . . V. K. Rasmussen, W. F. Hornyak, and T. Lauritsen 581
High Energy Gamma-Radiation from Be^9+D^2 . C. Y. Chao, T. Lauritsen, and V. K. Rasmussen 582
On the Origin of Heavy Cosmic-Ray Particles . . . . . Lyman Spitzer, Jr. 583

Proceedings of the American Physical Society:

Minutes of the Meeting of the University of Washington 584

September 1, 1949

U-235 Gamma-Radiation . . . . . R. L. Macklin 595
On Penetrating Showers in Cosmic Radiation . . . . . H. A. Meyer, G. Schwachheim, A. Wataghin, and G. Wataghin 598
Phase Shifts in Proton-Alpha-Scattering . . . . . C. L. Critchfield and D. C. Dodder 602
Radioactive Tin 121, 123, 125 . . . . . J. C. Lee and M. L. Pool 606
On the Film Transfer Rate in Helium *II* . . . . . Robert T. Webber, Henry A. Fairbank, and C. T. Lane 609
Angular Distribution of the Photo-Neutrons from Beryllium . . . . . B. Hammermesh, M. Hammermesh, and A. Wattenberg 611
K-Capture of Be^7 and the Excited State of Li^7 . . R. M. Williamson and H. T. Richards 614
Neutron-Capture Cross Section of 85-Minute Ba^{139} . . . . . L. Yaffe, B. W. Sargent, M. Kirsch, S. Standil, and Jean M. Grunlund 617
Temperature Dependence of Susceptibility of Zinc, Cadmium, and Gamma-Brass . . . . . Jules A. Marcus 621
Energy Levels of Si^{30} . John E. Brolley, Jr., M. B. Sampson, and Allan C. G. Mitchell 624
High Energy Induced Fission of Bismuth and Lead . R. H. Goeckermann and I. Perlman 628
Nuclear Gyromagnetic Ratios II . . . . . William H. Chambers and Dudley Williams 638
Beta-Spectra of Forbidden Transitions . . Lawrence M. Langer and H. Clay Price, Jr. 641
Pressure Broadening in the Microwave and Infra-Red Regions . . . . . P. W. Anderson 647
Interferrometric Studies of Faster than Sound Phenomena. Part II. Analysis of Supersonic Air Jets . . . . . R. Ladenbuerg, C. C. Van Voorhis, and J. Winckler 662
Internal Pair Formation . . . . . M. E. Rose 678

Letters to the Editor:

Theory of the Angular Distribution of Photo-Neutrons from Be^9 . . . . C. J. Mullin and E. Guth 682
Double Scattering of Protons in Helium . . . . . D. C. Dodder 683
Lower Limit for the Binding Energy of the Deuteron . . . . . G. R. Bishop, C. H. Collie, H. Halban, and R. Wilson 683
Magnetic Moments of Sn^{117}, Sn^{119}, and Pb^{207} . . . . . W. G. Proctor 684
Application of Dysons's Methods to Meson Interactions . . . . . P. T. Matthews 684
Electromagnetic Induction in a Superconductor . . . . . W. V. Houston and C. F. Squire 685
Microwave Spectra of Cd_2Cl and Cd_2I . . . . . James W. Simmons 686

Erratum: The Influence of the Length of a Hot Wire on the Measurements of Turbulence . . . . F. N. FRENKIEL 686
Excited State of Li^7 and the Angular Yield in $Li^6(d, p)Li^{7*}(\gamma)Li^7$ . . . . . S. S. HANNA 686
Energy Levels of the N^{14} Nucleus . . . . . H. A. WILSON 687
Rotation Levels of the Na^{24} and Ca^{41} Nuclei . . . . . H. A. WILSON 687
On the Production of Mesons . . . . . H. KOPPE 688
Beta-Spectrum of O^{15} . . . . . B. PEREZ-MENDEZ AND H. BROWN 689
Erratum: The Production of Mesons by Photons and Electrons . . . . HERMAN FESHBACH AND MELVIN LAX 689
Difficulty in Using $mk^{1/2}$ as a Residual Charge to Explain Stellar Magnetism . . . P. D. P. SMITH 690
New Measurement of the Pt^{195}—Cu^{65} Packing Fraction Difference . . . . HENRY E. DUCKWORTH 690
Microwave Absorption Spectrum of Methylene Bromide . . . . WILLIAM J. PIETENPOL AND JOHN D. ROGERS 690
Nuclear Spin and Quadrupole Moment of Cl^{35} . . . . . C. H. TOWNES AND L. G. AAMODT 691
Radioactivity of Chlorine^{36} . . . . . C. S. WU, C. H. TOWNES, AND L. FELDMAN 692
Beta-Ray Spectrum of Chlorine^{36} . . . . . C. S. WU AND L. FELDMAN 693
On the Spin and Beta-Spectrum of Cl^{36} . . . . . C. LONGMIRE, C. S. WU, AND C. H. TOWNES 695
Beta-Spectrum of Y^{91} . . . . . C. S. WU AND L. FELDMAN 696
Interpretation of Beta-Spectra from Thick Sources . . . . . L. FELDMAN AND C. S. WU 697
Beta-Spectrum of Be^{10} . . . . . C. S. WU AND L. FELDMAN 698
Photoelectric Disintegration of the Deuteron . . . . . J. S. LEVINGER 699
Evidence on Nuclear Moments of Stable Ge and Si Isotopes from Microwave Spectra . . . . . C. H. TOWNES, J. M. MAYS, AND B. P. DAILEY 700
Specific Ionization of the Cosmic Radiation above the Atmosphere . . . . . S. F. SINGER 701
Spontaneous Neutron Emission from Uranium and Samarium . . . . . HERMAN YAGODA AND NATHAN KAPLAN 702
Nuclear Spin and Quadrupole Coupling of S^{35} . . . . . VICTOR W. COHEN, W. S. KOSKI, AND T. WENTINK, JR. 703
Confirmation of Cl^{39} Activity . . R. N. H. HASLAM, L. KATZ, H. E. JOHNS, AND H. J. MOODY 704
Detection of X-Ray Quanta by a Cadmium Sulphide Crystal Counter . . . . SAMUEL G. ZIZZO AND JOSEPH B. PLATT 704

SEPTEMBER 15, 1949

Precision Measurement of the Ratio of the Nuclear g Values of Li^7 and Li^6 . . . . P. KUSCH AND A. K. MANN 707
Interaction of 14-Mev Neutrons with Deuterons . . . . . J. H. COON AND R. F. TASCHEK 710
Some Properties of Superconductors below 1°K. I. Titanium . . J. G. DAUNT AND C. V. HEER 715
Radiations from Indium (114) and Barium (140) . . . . C. E. MANDEVILLE AND E. SHAPIRO 718
Breakdown and Maintenance of Microwave Discharges in Argon . . . . S. KRASIK, D. ALPERT, AND A. O. MCCOUBREY 722
Gamma-Ray Measurements with a Magnetic Lens Spectrometer . . . . W. F. HORNYAK, T. LAURITSEN, AND V. K. RASMUSSEN 731
Penetration and Diffusion of X-Rays through Thick Barriers. II. The Asymptotic Behavior when Pair Production Is Important . . . . . U. FANO 739
On the Gyromagnetic Ratio and Spectroscopic Splitting Factor of Ferromagnetic Substances . . . . CHARLES KITTEL 743
Theory of Positrons . . . . . R. P. FEYNMAN 749
On Total Absorption in Spectra with Overlapping Lines . . . . FRANK MATOSSI, ROBERT MAYER, AND EMMA RAUSCHER 760
Equations of Codazzi and the Relations between Electromagnetism and Gravitation . . . . ANTONIO GIÃO 764
Space-Time Approach to Quantum Electrodynamics . . . . . R. P. FEYNMAN 769
Quantum Electrodynamics. III. The Electromagnetic Properties of the Electron—Radiative Corrections to Scattering . . . . . JULIAN SCHWINGER 790
On the Electromagnetic Properties of Nucleons . . . SIDNEY BOROWITZ AND WALTER KOHN 818
Motion in a Constant Magnetic Field . . . . . M. H. JOHNSON AND B. A. LIPPMANN 828
Optical Detection of Radiofrequency Resonance . . . . . F. BITTER 833
Mean Square Angles of Bremsstrahlung and Pair Production . . . . . MARTIN STEARNS 836
Admittance of High Frequency Gas Discharges . EDGAR EVERHART AND SANBORN C. BROWN 839
Movement of Small Metal Particles Having Six Degrees of Freedom in Air around a Wire Carrying a Constant Electric Current . . . . . J. A. SCHEDLING 843

Letters to the Editor:

Elaboration of the Schrödinger Formalism with Applications to Nuclear Physics . . . J. W. CALKIN 846
Fourth-Order Corrections in Quantum Electrodynamics and the Magnetic Moment of the Electron . . . . ROBERT KARPLUS AND NORMAN M. KROLL 846
Hyperfine Structure of 4^3P—4^3D of the Spectrum of Al II . . . . . S. SUWA 847
Nuclear Spin and Magnetic Moment of Cs^{133} and Cs^{137} . . . . . DARRAGH E. NAGLE 847
Energy Distribution of Fission Fragments from Pu^{239} . . . D. C. BRUNTON AND W. B. THOMPSON 848
Altitude Dependence of Mesons of Energy between 224 and 255 Mev . . . MARCELLO CONVERSI 849

Altitude Dependence of Penetrating Particles Slowed Down After Traversing 15 Cm of Lead . . . MARCELLO CONVERSI 851
On the μ-Meson Capture . . . M. TAKETANI, S. NAKAMURA, AND M. SASAKI 852
Statistical Mechanics of Mixtures of He^3 and He^4 . . . J. DE BOER 852
Beta-Spectrum of Tritium . . . S. C. CURRAN, J. ANGUS, AND A. L. COCKCROFT 853
On Positive Excess of Meson Component near Sea Level . . . P. BASSI, E. CLEMENTEL, I. FILOSOFO, AND G. PUPPI 854
Heat Flow in Metals below 1°K and a New Method for Magnetic Cooling . . . C. V. HEER AND J. G. DAUNT 854
Ion-Source for Mass-Spectrography . . . R. F. K. HERZOG AND F. P. VIEHBÖCK 855
On the Spin of μ-Mesons . . . J. TIOMNO 856
Analysis of Delayed Coincidence Counting Experiments . . . DANIEL BINDER 856
On the Half-Life of Na^{22} . . . L. JACKSON LASLETT 858
Microwave Spectrum of CF_3Cl . . . D. K. COLES AND R. H. HUGHES 858
Hyperfine Structure of Fe 57 . . . JEAN BROSSEL 858
Energetic Events in Emulsions at High Altitude . . . J. HORNBOSTEL AND E. O. SALANT 859
Conductivity Changes in Dielectrics during 2.5-Mev X-Radiation . . . F. C. ARMISTEAD, J. C. PENNOCK, AND L. W. MEAD 860
Heavy Particles in Cosmic-Ray Stars . . . M. BLAU, M. M. BLOCK, AND J. E. NAFE 860
Disintegration Energy of Al^{29} . . . L. SEIDLITZ, E. BLEULER, AND D. J. TENDAM 861
On a New Conception of the Interaction between Charges and Electromagnetic Field . . . LOUIS DE BROGLIE 862
Atmospheric Ozone Temperatures as Determined by Spectroscopic Observations from Below . . . WILLIAM M. BENESCH 863
Lambda-Temperatures of He^3—He^4 Mixtures . . . B. M. ABRAHAM, B. WEINSTOCK, AND D. W. OSBORNE 864
Solutions of He^3 in He^4 . . . J. W. STOUT 864
Proton-Proton Scattering at 5.11 Mev . . . R. O. BONDELID, P. G. BOHLMAN, AND K. B. MATHER 865
Decay of a Heavy τ-Meson into Three Lighter Mesons . . . S. POWER 865
New Formulation of the Variational Principle for Scattering Problems . . . SU-SHU HUANG 866
Finite Relativistic Charge-Current Distributions . . . D. BOHM, M. WEINSTEIN, AND H. KOUTS 867
Note on the Variational Method for Finding Extrapolated Endpoints . . . H. HURWITZ, JR. 867
Microwave Magnetic Resonance Absorption in Nitric Oxide . . . ROBERT BERINGER AND J. G. CASTLE, JR. 868
Particular Case in Einstein's Generalized Theory of Gravitation . V. V. NARLIKER AND RAMJI TIWARI 868
Second Sound Velocity in Paramagnetically Cooled Liquid Helium II . . . JOHN R. PELLAM AND RUSSELL B. SCOTT 869
On the Tri-Partition and Quadri-Partition of Uranium Nuclei . . . R. CHASTEL AND L. VIGNERON 870
Future Nuclear Interaction . . . ALEX E. S. GREEN 870
Mass Assignment of Xenon Activities Produced in Fission . . . SIGVARD THULIN, INGMAR BERGSTRÖM, AND ARNE HEDGRAN 871
Second Sound and Classical Heat Flow . . . JOHN R. PELLAM 872
Nuclear Spin 5/2 for $_{40}Zr^{91}$ . . . O. H. ARROE AND J. E. MACK 873
Binding Energy of the Triton . . . R. E. CLAPP 873

Proceedings of the American Physical Society:

Minutes of the Meeting of the Division of Fluid Dynamics at White Oak, Maryland, June 30–July 1, 1949 . . . 874

OCTOBER 1, 1949

Determination of the Half-Life of Carbon 14 . . . W. M. JONES 885
Proton Groups from the Bombardment of Argon by Deuterons . . . P. W. DAVISON, J. O. BUCHANAN, AND ERNEST POLLARD 890
Classification of Nuclear Isomers . . . P. AXEL AND S. M. DANCOFF 892
Experiments on the Effect of Atomic Electrons on the Decay Constant of Be^7. II . . . R. F. LEININGER, E. SEGRÈ, AND C. WIEGAND 897
Coincidence Experiments in Ni^{65}, Ni^{67}, Ag^{110}, and In^{114} . . . FRED MAIENSCHEIN AND J. LAWRENCE MEEM, JR. 899
Transport Phenomena in a Completely Ionized Gas in Presence of a Magnetic Field . . . ROLF LANDSHOFF 904
Disintegration of Ce^{141} . . . MICHEL TER-POGOSSIAN, C. SHARP COOK, C. HAROLD GODDARD, AND J. EUGENE ROBINSON 909
Cosmic-Ray Experiments at High Altitudes over a Wide Range of Latitudes . . . A. T. BIEHL, H. V. NEHER, AND W. C. ROESCH 914
Extensive Penetrating Cosmic-Ray Showers . . . JOHN ISE, JR. AND W. B. FRETTER 933
Conduction Processes in Thin Deposits of Antimony . LOUIS HARRIS AND LLOYD H. SHAFFER 943
Delayed Neutrons from Thorium . . . L. G. CREVELING, J. R. HOOD, AND M. L. POOL 946
Second Sound Velocity in Helium II . . . R. D. MAURER AND MELVIN A. HERLIN 948
Electromagnetic Interactions of a Vector Meson with a Scalar Excited State . . . MARSHALL N. ROSENBLUTH 951
Radiations from Hf^{181} . . . ERLING N. JENSEN 958

Measurement of f-Values in the Iron Spectrum with Applications to Solar and Stellar Atmospheres . . . . . W. W. CARTER 962
New Method of Analysis of the Beta-Ray Spectrum . MITSUO SAKAI AND SEITARO NAKAMURA 967
Process of Ionization in Active Nitrogen . . . . . K. T. CHAO AND H. P. CHANG 970
Quasi-Chemical Method in the Statistical Theory of Regular Mixtures . . . . YIN-YUAN LI 972

Letters to the Editor:

Neutrons from Deuterons on Lithium (6) . C. E. MANDEVILLE, C. P. SWANN, AND S. C. SNOWDON 980
Signs of the Magnetic Moments of Neutron and Proton . . . . E. H. ROGERS AND H. K. STAUB 980
On the Angular Distribution of D-D Reaction Products . . . . . YOSHIHIRO NAKANO 981
Current Densities in the Cathode Spots of Transient Arcs . J. M. SOMERVILLE AND W. R. BLEVIN 982
Beta-Spectrum of Tl^{204}, Magic Numbers, and Neutron Pairing . . . . D. SAXON AND J. RICHARDS 982
Frequency of Stars of Different Sizes Produced by the Cosmic Radiation in Photographic Plates Exposed at 29,000 Meters . . . . . MARGHERITA ADDARIO AND SARA TAMBURINO 983
Meson Background in Penetrating Shower Experiments . . . . . GIUSEPPE COCCONI 984
Addendum: Heat Flow in Metals below 1°K and a New Method for Magnetic Cooling . . . . . J. G. DAUNT AND C. V. HEER 985
Neutrinos from the Sun and the Source of the Earth's Heat . . . . . D. SAXON 986
Radioactivity in Holmium 166, Thulium 170, and Lutecium 177 . . . . . J. M. CORK, H. B. KELLER, AND A. E. STODDARD 986
Dynamic Probe Measurements in the Ionosphere . . . . . A. REIFMAN AND W. G. DOW 987
Cloud-Chamber Study of Fission Fragment Ranges in Air . . . . . J. N. BØGGILD, L. MINNHAGEN, AND O. B. NIELSEN 988
Erratum: Bremsstrahlung in High Energy Nucleon-Nucleon Collisions . . . . . J. ASHKIN AND R. E. MARSHAK 989
Existence of Stable Nuclei as Related to the Principle of Regularity and Continuity of Series and the Ends of Nuclear Shells . . . . . WILLIAM D. HARKINS AND MARTIN POPELKA, JR. 989
On the Abundance of I^{129}, Te^{118}, and Pt^{190} . . . . . WALLACE T. LELAND 992
Zenith Angle Dependence of Flux of the Hard Cosmic-Ray Component up to 36,000 Feet . . . . . J. F. JENKINS, JR. 992
Angular Correlation of Delayed Radiations . . . . . ARNE LUNDBY 993
On the Polarization of Slow Neutrons . . . . . J. STEINBERGER AND G. C. WICK 994
New Molecular Beam Resonance Method . . . . . NORMAN F. RAMSEY 996
Suggestion Regarding Emission Phenomena in (Ba−Sr)O Cathodes . . . . . E. S. RITTNER, F. K. DU PRÈ, AND R. A. HUTNER 996
Detection of Heavy Particles in the Primary Cosmic Radiation . . . . . MARTIN A. POMERANTZ AND FRANK L. HEREFORD 997
Nuclear Quadrupole Moments and Shell Structure . . . . . R. D. HILL 998
Equation of State of Gaseous He^3 . . . . . J. VAN KRANENDONK, K. COMPAAN, AND J. DE BOER 998
On the Hot-Wire Length Correction . . . . . F. N. FRENKIEL 999
Equation of the Magnetic Threshold Curve of a Superconductor . . . . . G. PRESTON BURNS 999
Decay Probability of Be^7 as a Function of the Ionization of the Atom . . . . . P. BENOIST, R. BOUCHEZ, P. DAUDEL, AND R. DAUDEL, AND A. ROGOZINSKI 1000
Statistics of the Three-Dimensional Ferromagnet . . . . . TAKEHIKO OGUCHI 1001
Phenomenological Theory of Superconductors . . . . . A. R. MILLER 1001
Erratum: Excitation Functions for (α,n), $(\alpha,2n)$, and $(\alpha,3n)$ Reactions on Indium . . . . . GEORGES M. TEMMER 1002
Nuclear Spin ½ for Te^{123}, and Isotope Shift in the Tellurium Spectrum . . . . . J. E. MACK AND O. H. ARROE 1002
Three-Body Scattering with Central and Tensor Forces . . . . . ROY THOMAS 1002

OCTOBER 15, 1949

Preliminary Directional Study of Cosmic Rays at High Altitude. I. Apparatus and Procedure . . . . . W. G. STROUD, J. SCHENCK, AND J. R. WINCKLER 1005
Preliminary Directional Study of Cosmic Rays at High Altitude. II. Experimental Results and Interpretation . . . . . J. R. WINCKLER, W. G. STROUD, AND T. J. B. STANLEY 1012
Lateral Structure of Cosmic-Ray Air Showers . . . . . G. COCCONI, V. COCCONI TONGIORGI, AND K. GREISEN 1020
Cloud-Chamber Study of Extensive Air Showers at 3260 Meters Elevation . . . . . W. W. BROWN AND A. S. MCKAY 1034
Cosmic-Ray Mesons Near Sea Level . . . . . WILLIAM L. KRAUSHAAR 1045
Transient Nutations in Nuclear Magnetic Resonance . . . . . H. C. TORREY 1059
Atomic Beam Magnetic Resonance Experiments with Radioactive Elements Na^{22}, K^{40}, Cs^{135}, and Cs^{137} . . . LUTHER DAVIS, JR., DARRAGH E. NAGLE, AND JERROLD R. ZACHARIAS 1068
Hyperfine Structure and Nuclear Moments of the Stable Chlorine Isotopes . . . . . LUTHER DAVIS, JR., BERNARD T. FELD, CARROL W. ZABEL, AND JERROLD R. ZACHARIAS 1076
Hyperfine Structure of the $^2P_{3/2}$ State of Al^{27}. The Nuclear Electric Quadrupole Moment . . . . . HIN LEW 1086
Extensive Air Showers at High Altitudes . . . . . HENRY L. KRAYBILL 1092
Star Production by Negative μ-Mesons in a Silver Chloride Crystal . . . . . H. G. VOORHIES AND J. C. STREET 1100

High Frequency Surface Resistivity of Tin in the Normal and Superconducting States . . . . . WILLIAM M. FAIRBANK 1106
Kinetic Energy Release of U^{238}, U^{235}, Th^{232}, and Bi^{209} by High Energy Neutrons . . . . . J. JUNGERMAN AND S. C. WRIGHT 1112
Small Angle Diffraction of Neutrons and Similar Wave Phenomena . . . . . OTTO HALPERN AND EDWARD GERJUOY 1117
On Magneto Optics of Neutrons and Some Related Phenomena . . . . . OTTO HALPERN 1130
Further Results on Neutron Production by Cosmic-Ray Particles at Sea Level . . . . . R. D. SARD, A. M. CONFORTO, AND M. F. CROUCH 1134
Scattering of Protons by Tritons . . A. HEMMENDINGER, G. A. JARVIS, AND R. F. TASCHEK 1137
Cross Section as a Function of Angle for the $D(d,n)He^3$ Reaction for 10-Mev Bombarding Deuterons . . . . . K. W. ERICKSON, J. L. FOWLER, AND E. J. STOVALL, JR. 1141
Investigation of Nuclear Energy Levels in Lead . . . . . H. H. BARSCHALL, C. K. BOCKELMAN, R. E. PETERSON, AND R. K. ADAIR 1146
Deuteron Bombardment of Boron Isotopes . EMMETT L. HUDSPETH AND CHARLES P. SWANN 1150
Radiative Corrections to Nuclear Forces in the Pseudoscalar Meson Theory . . . . . K. M. WATSON AND J. V. LEPORE 1157
Photo-Disintegration of the Deuteron . . . . INGVAR F. E. HANSSON AND LAMEK HULTHÉN 1163
Effects of Scattering and Absorption of Mesons on Coincidence-Anticoincidence Measurements . . . . . ROGERS D. RUSK AND ALMA ROSENBAUM 1166
Interstitial Atomic Diffusion Coefficients . . . . . C. WERT AND C. ZENER 1169
Interaction between Elementary Particles. Part I. . . . . ALFRED LANDÉ 1176
On the Use of Subtraction Fields and the Lifetimes of Some Types of Meson Decay . . . . . J. STEINBERGER 1180
Domain Structures and Phase Transitions in Barium Titanate . . . . P. W. FORSBERGH, JR. 1187
Dielectric Properties of Barium Titanate at Low Temperatures . R. F. BLUNT AND W. F. LOVE 1202
New Methods of Determining the Absolute Intensity of Cosmic Rays in the Atmosphere and the Residual Ionization Chambers . . . . . VICTOR F. HESS AND ROGER P. VANCOUR 1205
Rollin Film Rates in Liquid Helium . . . . . HENRY A. FAIRBANK AND C. T. LANE 1209
Collision Theories of Pressure Broadening of Spectral Lines . . . . . J. H. VAN VLECK AND HENRY MARGENAU 1211
Dielectric Constants and Polarizabilities of Ions in Simple Crystals and Barium Titanate . . . . . SHEPARD ROBERTS 1215
Electric and Optical Behavior of $BaTiO_3$ Single-Domain Crystals . . . . . WALTER J. MERZ 1221
On the Origin of Elements . . . . . MARIA G. MAYER AND EDWARD TELLER 1226
Crystal Statistics. II. Partition Function Evaluated by Spinor Analysis . . BRURIA KAUFMAN 1232
Crystal Statistics. III. Short-Range Order in a Binary Ising Lattice . . . . . BRURIA KAUFMAN AND LARS ONSAGER 1244

Letters to the Editor:

Possible Existence of the $4n+1$ Radioactive Series in Chloritized Ytterby Mica . . . . . J. H. J. POOLE, C. F. G. DELANEY, AND R. C. MCCORMICK 1253
Infra-Red Color Center Band in the Alkali Halides . . . . . E. BURSTEIN AND J. J. OBERLY 1254
S-Matrix for Meson-Nucleon Interactions . . . . . P. T. MATTHEWS 1254
Electric Quadrupole Moments of Nuclei . . . G. J. BENE, P. M. DENIS, AND R. C. EXTERMANN 1255
On the Delayed Neutron Emitter $_7N^{17}$ . . . . . R. A. CHARPIE, KUAN-HAN SUN, B. JENNINGS, AND J. F. NECHAJ 1255
New Radioactive Isotopes of Dysprosium . . . . . B. H. KETELLE 1256
Detection of Antiferromagnetism by Neutron Diffraction . . C. G. SHULL AND J. SAMUEL SMART 1256
Imprisonment of Resonance Radiation in Mercury Vapor . . . . . D. ALPERT, A. O. MCCOUBREY, AND T. HOLSTEIN 1257
Persistence of Band Fluorescence in Mercury Vapor . . . . . T. HOLSTEIN, D. ALBERT, AND A. O. MCCOUBREY 1259
Nuclear Magnetic Resonance Shift in Metals . . . . . W. D. KNIGHT 1259
New Determination of the Relative Abundance of Rhenium in Nature . . . . . HARRISON BROWN AND EDWARD GOLDBERG 1260
Cloud-Chamber Study of High Energy Positrons from Na^{22} . . . . . KENNARD H. MORGANSTERN AND KARL P. W. WOLF 1261
Positive Particles Associated with Beta-Ray Emitters . . . . . K. L. ERDMAN, F. T. KOKOTAILO, AND D. B. SCOTT 1262
Precise Determination of the Proton Magnetic Moment in Bohr Magnetons . . . . . J. H. GARDNER AND E. M. PURCELL 1262
Gamma-Radiation from Br^{82} . . . . . KAI SIEGBAHN, ARNE HEDGRAN, AND MARTIN DEUTSCH 1263
Transformation between One- and Three-Dimensional Power Spectra for an Isotropic Scalar Fluctuation Field . . . . . LESLIE S. G. KOVASNAY, MAHINDER S. UBEROI, AND STANLEY CORRSIN 1263
Erratum: Determination of Nuclear Gyromagnetic Ratios I . . . . . JOHN R. ZIMMERMAN AND DUDLEY WILLIAMS 1264
New Gamma-Ray Resonance in the Reaction $C^{12}(p,\gamma)N^{13}$ . . . . . D. M. VAN PATTER 1264

On the Double Beta-Process . . . . . Mark G. Inghram and John H. Reynolds 1265
On the Negative Proton . . . . . Kuan-Han Sun 1266
Erratum: The Chi-Square Test as a Criterion for Testing Halogen-Filled Geiger Tubes . . . . A. B. Willoughby 1266
Spontaneous Decay Rate of Heavy Mesons. II . . . . . L. I. Schiff and D. L. Weisman 1266
Note on the Infra-Red Spectra of the Deutero-Ammonias . . . . . John S. Burgess 1267
On the Latitude Dependence of the Absolute Neutron Intensities in Cosmic Radiation . . . . . Luke C. L. Yuan 1267
On the Measurement of Slow Neutrons in the Cosmic Radiation on a B-29 Plane . . . . . Luke C. L. Yuan 1268
Theory of Pressure Absorption . . . . . Masataka Mizushima 1268
Experimental Study of the Compton Effect at 1.2 Mev . . . . . Robert Hofstadter and John A. McIntyre 1269
Electromagnetic Separation of the Isotopes of Mercury . . . . . C. P. Keim 1270
Preliminary Note on Nuclear Periodic Scheme in Three Dimensions . . . . . S. Podgor 1271
Beta-Spectrum of Be^{10} . . . . . H. W. Fulbright and J. C. D. Milton 1271
Disintegrations of Sn^{121} and Sn^{123} . . . . . R. B. Duffield and L. M. Langer 1272
σ_3-Fundamental of Nitrous Oxide . . . . . K. B. Rhodes and E. E. Bell 1273
Two Kinds of Very High Energy Cosmic-Ray Stars . . . . . L. Leprince-Ringuet, F. Bousser, Hoang-Tchang-Fong, L. Jauneau, and D. Morellet 1273

November 1, 1949

Notes on the *j-j* Coupling Shell Model . . . . . Eugene Feenberg 1275
Photographic Study of Neutrons from Al+H^2 . . . . . R. A. Peck, Jr. 1279
Range Distribution of the Charged Particles from the D-D Reactions for 10-Mev Deuterons: Differential Elastic Scattering Cross Section at 40 Degrees, 60 Degrees, and 80 Degrees in the Center-of-Mass System . . . . . Louis Rosen, Francis K. Tallmadge, and John H. Williams 1283
Angular Distribution of Neutrons from the Photo-Disintegration of the Deuteron . . . . . Frank Genevese 1288
Molecular Dipole Moments and Stark Effects. I. Stark Effects on Symmetric Top Molecules with Nuclear Quadrupole Coupling . . . . . W. Low and C. H. Townes 1295
Effect of Nuclear Motion on the Hyperfine Structure of Hydrogen . . . . . G. Breit, G. E. Brown, and G. B. Arfken 1299
Effects of the Proton Radius on Nuclear Motion Correction for the Hyperfine Structure of Hydrogen . . . . . G. E. Brown and G. B. Arfken 1305
Perturbation Methods for Dirac Radial Equations . . . . . G. Breit and G. E. Brown 1307
Electron-Nuclear Potential Fields from Hyperfine Structure . . . . . M. F. Crawford and A. L. Schawlow 1310
Theory of the Lithium Two-Alpha-Reactions. II. Angular Distribution of $Li^6(d,\alpha)\alpha$ . . . . . Robert Resnick and D. R. Inglis 1318
Some Properties of Superconductors below 1°K. II. Aluminum and Zinc . . . . . J. G. Daunt and C. V. Heer 1324
Magnetic Interaction between Neutrons and Electrons . . . . . H. Ekstein 1328
Surface Impedance of Normal and Superconductors at 24,000 Megacycles per Second . . . . . E. Maxwell, P. M. Marcus, and J. C. Slater 1332
Absorption of Gamma-Rays in Aluminum . . . . . W. C. Parkinson 1348
Theory of Complex Spectra. IV . . . . . Giulio Racah 1352
Moment of Inertia and Electric Dipole Moment of CsF from Radiofrequency Spectra . . . . . J. W. Trischka 1365
On Realistic Field Theories and the Polarization of the Vacuum . . . . . David Feldman 1369
On the Theory of Electron Multiplication in Crystals . . . . . Frederick Seitz 1376
Electric Breakdown in Ionic Crystals . . . . . Herbert B. Callen 1394
Diffusion in Binary Alloys . . . . . J. Bardeen 1403

Letters to the Editor:

Alpha-Decay in Isotopes of Atomic Number Less Than 83 . . . . . S. G. Thompson, A. Ghiorso, J. O. Rasmussen, and G. T. Seaborg 1406
Betatron-Produced Sources of High Specific Activity: Copper 62 . . . . . R. A. Becker, F. S. Kirn, and W. L. Buck 1406
Energy of an Excited State of Li^7 . . . . . Michel Ter-Pogossian, J. Eugene Robinson, and C. Harold Goddard 1407
Angular Distribution of the Photo-Neutrons from Deuterium at 2.76 Mev . . . . . Bernard Hamermesh and Albert Wattenberg 1408
28.7-Hour Ba^{135} . . . . . B. E. Robertson and M. L. Pool 1408
Upper Limit for the Lifetime of the 411-Kev Excited State of Hg^{198} . R. E. Bell and H. E. Petch 1409
On the Spatial Alignment of Nuclei . . . . . R. V. Pound 1410
Double-Probe Method for Determination of Electron Temperatures in Steady and Time-Varying Gas Discharges . . . . . E. O. Johnson and L. Malter 1411
Tests of Self-Regenerating Fillings for Geiger Counters . . S. A. Korff and A. D. Krumbein 1412

Reproducibility of Photo-Neutron Standards . . . . . L. F. CURTISS AND A. CARSON 1412
Reflection and Polarization of Neutrons by Magnetized Mirrors . . . . . D. J. HUGHES AND M. T. BURGY 1413
New Low Mass Isotopes of Emanation (Element 86) . . . . . A. GHIORSO, W. W. MEINKE, AND G. T. SEABORG 1414
Magnetic Moment of La^{139} . . . . . W. C. DICKINSON 1414
Nuclear Quadrupole Moments and Nuclear Shell Structure . . . . . C. H. TOWNES, H. M. FOLEY, AND W. LOW 1415
Sm^{151} Beta-Ray Spectrum . . . . . B. H. KETELLE AND G. W. PARKER 1416
Hyperfine Structure and Nuclear Spin of Kr^{83} and Ne^{21} Investigated with Separated Isotopes. . . . . JØRGEN KOCH AND EBBE RASMUSSEN 1417
Wide Angle Sprays of Minimum Ionization Particles . . . . F. OPPENHEIMER AND E. P. NEY 1418
Determination of the Molecular Structure of Bromosilane by Microwave Measurements . . . . . A. H. SHARBAUGH, J. K. BRAGG, T. C. MADISON, AND V. G. THOMAS 1419
Erratum: The Application of Dyson's Methods to Meson Interactions . . . . P. T. MATTHEWS 1419
On the Photo-electron Spectrum of Ta^{182} . . . . . C. HAROLD GODDARD AND C. SHARP COOK 1419
Photo-Neutrons from Neutron-Capture Gamma-Rays . . . . . BERNARD HAMERMESH AND ALBERT WATTENBERG 1420
Nuclear Gyromagnetic Ratio of V^{51} . . . . . W. D. KNIGHT AND V. W. COHEN 1421
Angular Distribution of Neutrons from Targets Bombarded by 18-Mev Deuterons . P. AMMIRAJU 1421

NOVEMBER 15, 1949

Inversion Frequency of Ammonia and Molecular Interaction . . . . . H. MARGENAU 1423
Angular Distribution of 10.8-Mev Deuterons Scattered by Deuterons . . . . . J. C. ALLRED, K. W. ERICKSON, J. L. FOWLER, AND E. J. STOVALL, JR. 1430
On the Production of π-Mesons by Nucleon-Nucleon Collisions . . . . . CECILE MORETTE 1432
Relative Cross Sections for Pair Production at 17.6 Mev . . . . . R. L. WALKER 1440
Yield and Angular Distribution of the D−D Neutrons . G. T. HUNTER AND H. T. RICHARDS 1445
Disintegration of I^{124} and I^{126} . . . . . ALLAN C. G. MITCHELL, J. Y. MEI, FRED C. MAIENSCHEIN, AND CHARLES L. PEACOCK 1450
Radioactive In^{107}, In^{108}, In^{109}, and Sn^{108} . . . . . E. C. MALLARY AND M. L. POOL 1454
Note on the Decay of the π-Meson . . . . . M. RUDERMAN AND R. FINKELSTEIN 1458
Precise Measurement of the Gyromagnetic Ratio of He^3 . . . . . HERBERT L. ANDERSON 1460
On the Production of Electron Pairs in the Field of an Electron . . . . . J. A. PHILLIPS AND P. GERALD KRUGER 1471
Neutron Production at Mountain Altitudes . . . . . C. G. MONTGOMERY AND A. R. TOBEY 1478
Analysis of Bursts of Cosmic-Ray Ionization . C. G. MONTGOMERY AND D. D. MONTGOMERY 1482
Narrow Air Showers of Cosmic Rays . . . . . JOHN WEI AND C. G. MONTGOMERY 1488
Paschen-Back Effect in NH_3 and N_2O Microwave Spectra . . . . . C. K. JEN 1494
Impulse Breakdown in the 10^{-9}-Sec. Range of Air at Atmospheric Pressure . R. C. FLETCHER 1501
On Infinite Relativistic Particle Matrices . . . . . WALTER WESSEL 1512
Sound Propagation in Chemically Active Media . . . . . LEONARD LIEBERMANN 1520
Energy Level Density and Partition Function of Nuclei . . . . . D. TER HAAR 1525

Letters to the Editor:

Theory of the Formation of Powder Patterns on Ferromagnetic Crystals . . . CHARLES KITTEL 1527
Nuclear Moments of Mg^{25} . M. F. CRAWFORD, F. M. KELLY, A. L. SCHAWLOW, AND W. M. GRAY 1527
Nuclear Moments of $_{39}Y^{89}$ . . . . . M. F. CRAWFORD AND N. OLSEN 1528
Nuclear Spin of He^3 . . . . . A. E. DOUGLAS AND G. HERZBERG 1529
Inversion Spectrum of Ammonia . . . . A. H. SHARBAUGH, T. C. MADISON, AND J. K. BRAGG 1529
Optical Properties of Semiconductors. I. The Reflectivity of Germanium Semiconductors . . . . K. LARK-HOROVITZ AND K. W. MEISSNER 1530
Optical Properties of Semiconductors. II. Infra-Red Transmission of Germanium . . . . . M. BECKER AND H. Y. FAN 1530
Optical Properties of Semiconductors. III. Infra-Red Transmission of Silicon . . . . . M. BECKER AND H. Y. FAN 1531
Protons from the Bombardment of He^3 by Deuterons . L. D. WYLY, V. L. SAILOR, AND D. G. OTT 1532
Note on Methane in the Infra-Red Solar Spectrum . . . . . ROBERT R. MCMATH, ORREN C. MOHLER, A. KEITH PIERCE, AND LEO GOLDBERG 1533
Atmospheric HDO . . . . . H. A. GEBBIE, W. R. HARDING, C. HILSUM, AND V. ROBERTS 1534
Disintegration Electrons for Li_3^8 Nuclei Ejected in Cosmic Stars . . E. PICKUP AND L. VOYVIDIC 1534
Gamma-Ray of K^{40} . . . . . G. A. SAWYER AND M. L. WIEDENBECK 1535
On the Shape of the Positron Spectrum of Cu^{61} . . . . . GEORGE E. OWEN AND C. SHARP COOK 1536
Germanium Counter . . . . . KENNETH G. MCKAY 1537
Two-Component Wave Equations . . . . . J. SERPE 1538
Effect of Nuclear Shells upon the Pattern of the Atomic Species . . . . . WILLIAM D. HARKINS 1538
Ratio of *LI* to *K*-Capture . . . . . M. E. ROSE AND J. L. JACKSON 1540
Disintegration Scheme of Tm^{170} . . . . . J. S. FRASER 1540
Erratum: Altitude Dependence of Penetrating Particles Slowed Down after Traversing 15 Cm of Lead . . . . . MARCELLO CONVERSI 1541
Magnetic Multipole Internal Conversion . . . . . N. TRALLI AND I. S. LOWEN 1541
New Gyromagnetic Effect . . . . . S. J. BARNETT AND LOUIS A. GIAMBONI 1542

DECEMBER 1, 1949

Magnetic Analysis of the $C^{12}(d,p)C^{13}$ and $O^{16}(d,p)O^{17}$ Reactions . . . . . W. W. BUECHNER, E. N. STRAIT, S. SPERDUTO, AND R. MALM 1543

Magnetic Analysis of $Be^{9}(d,\alpha)Li^{7}$ and $Be^{9}(d,p)Be^{10}$ Reactions . . . . . W. W. BUECHNER AND E. N. STRAIT 1547

Schematic Theory of Nuclear Cross Sections . . . . . H. FESHBACH AND V. F. WEISSKOPF 1550

Uranium 234 Content of Natural Uranium and the Specific Alpha-Activities of the Isotopes . . . . . C. A. KIENBERGER 1561

Comparison of Calculations on Cascade Theory . . . . . HARTLAND S. SNYDER 1563

Scattering of Slow Neutrons by Paramagnetic Crystals . . . . . I. W. RUDERMAN 1572

Radiations of Tantalum^{182}, Rhenium^{186,188}, and Gold^{199} . . . . . LOUIS A. BEACH, CHARLES L. PEACOCK, AND ROGER G. WILKINSON 1585

Electrons in Perturbed Periodic Lattices . . . . . J. C. SLATER 1592

Energy Bands and Wave Functions in Periodic Potentials . . . . . HUBERT M. JAMES 1602

Electronic States in Perturbed Periodic Systems . . . . . HUBERT M. JAMES 1611

Radiation Spectra of Barium^{140} and Lanthanum^{140} . . . . . LOUIS A. BEACH, CHARLES L. PEACOCK, AND ROGER G. WILKINSON 1624

Limits for the Diffusion Theory of High Frequency Gas Discharge Breakdown . . . . . SANBORN C. BROWN AND A. D. MACDONALD 1629

High Frequency Gas Discharge Breakdown in Hydrogen . . . . . A. D. MACDONALD AND SANBORN C. BROWN 1634

Interference Effects in Gamma-Gamma Angular Correlations . . . . . DANIEL S. LING, JR. AND DAVID L. FALKOFF 1639

Radioactive Y^{84}, Y^{88}, and Zr^{87} . . . . . B. E. ROBERTSON, W. E. SCOTT, AND M. L. POOL 1649

Absolute Voltage Determination of Two Nuclear Resonances below 0.4 Mev . . . . . A. H. MORRISH 1651

Application of the Tomonaga-Schwinger Theory to the Interaction of Nucleons with Neutral Scalar and Vector Mesons . . . . . P. T. MATTHEWS 1657

Rotational Stark Spectrum of Linear Molecules . . . . . HAROLD KENNETH HUGHES 1675

On the Interactions of Mesons with the Electromagnetic Field . M. NEUMAN AND W. H. FURRY 1677

Bosons in an Electromagnetic Field . . . . . R. G. MOORHOUSE 1691

Measurement of Electron-Ion Recombination . MANFRED A. BIONDI AND SANBORN C. BROWN 1697

Thermodynamics of Liquid Helium on the Basis of the Two-Fluid Theory . . . . O. K. RICE 1701

On the Approach to Statistical Equilibrium . . . . . ARNOLD J. F. SIEGERT 1708

Structure of the Mercury Bands λ2540 and λ2476 . . . . . S. MROZOWSKI 1714

Letters to the Editor:

On the Occurrence of Vanadium 50 in Nature . . . DAVID C. HESS, JR. AND MARK G. INGHRAM 1717

On the Relative Yields of Fission Cesium Isotopes . . . . . MARK G. INGHRAM, DAVID C. HESS, JR., AND JOHN H. REYNOLDS 1717

Internal Conversion Coefficient and Mass Assignment of the 57-Min. Se Isomer . . . . . I. BERGSTRÖM AND S. THULIN 1718

Interpretation of Underground Cosmic-Ray Data . . . . . K. GREISEN 1718

Radiations from Zn^{65} . . . . . K. C. MANN, D. RANKIN, AND P. N. DAYKIN 1719

Neutron-Proton Scattering . . . . . H. N. YADAV 1720

Structure of the Line λ4686 of He II . . . . . K. MURAKAWA, S. SUWA, AND T. KAMEI 1721

Note on Wave Amplification by Interaction with a Stream of Electrons . . . . . L. R. WALKER 1721

Naturally Occurring Odd-Odd Isotope of Vanadium . . . . . WALLACE T. LELAND 1722

Nuclear and molecular Information from the Microwave Spectrum of FCl . . . . . D. A. GILBERT, A. ROBERTS, AND P. A. GRISWOLD 1723

Spectral Analysis of 10-Mev Betatron Radiation by Nuclear Emulsion . . . . . P. K. S. WANG AND W. WIENER 1724

Excess of Negative over Positive Mesons Produced by High Energy Photons . . . . . K. A. BRUECKNER AND M. L. GOLDBERGER 1725

The Beta-Spectra of Cu^{64} . . . . . L. M. LANGER, R. D. MOFFAT, AND H. C. PRICE, JR. 1725

Positron and Negatron Spectra of Cu^{64} . . . . . GEORGE E. OWEN AND C. SHARP COOK 1726

Magnetic Resonance Absorption of Diluted Iron Ammonium Alum . . . . . R. T. WEIDNER, P. R. WEISS, C. A. WHITMER, AND D. R. BLOSSER 1727

Energy for Diffusion by Direct Interchange . . . . . H. B. HUNTINGTON AND FREDERICK SEITZ 1728

Erratum: The Equation of State of Gaseous He^{3} . . . . . J. VAN KRANENDONK, K. COMPAAN, AND J. DE BOER 1728

On the Magnetic Moments of Sn^{115}, Cd^{111}, Cd^{113}, Pt^{195}, and Hg^{199} . . W. G. PROCTOR AND F. C. YU 1728

Stopping Power of Nuclear Emulsions for Ionizing Particles . . . . . HERVASIO G. DE CARVALHO 1729

Metastable State of Half-Life 13×10^{-9} Sec. in $_{71}Lu^{177}$ . . . . . F. K. MCGOWAN 1730

Remarks on Non-Local Spinor Field . . . . . HIDEKI YUKAWA 1731

Detection of Radioactive Atoms in the Air with Nuclear Emulsions . . . . . Č. JECH 1731

Neutron-Proton and Proton-Proton Cross Sections at 83 Mev . . . . . L. CASTILLEJO AND H. T. RICHARDSON 1732

Cosmic Rays at a Great Depth . . . . . Y. MIYAZAKI 1733

Note on Analysis of Delayed Coincidence Counting Experiments . . . . . F. W. VAN NAME, JR. 1734

Evidence for Multiple Meson and γ-Ray Production in Cosmic-Ray Stars . . . . . M. F. KAPLON, B. PETERS, AND H. L. BRADT 1735

Remarks on Multiple Meson and Gamma-Ray Production . . . . . R. E. MARSHAK 1736

Magnetically Biased Transistors . . . . . C. BRADNER BROWN 1736

Properties of Single Crystal Selenium Prepared from a Melt . . . . . HERBERT W. HENKELS 1737

DECEMBER 15, 1949

Are Mesons Elementary Particles? . . . . . E. FERMI AND C. N. YANG 1739

Precise Determination of the Slow Neutron Cross Section of the Free Proton . . . . . EDWARD MELKONIAN 1744

Slow Neutron Velocity Spectrometer Studies of O_2, N_2, A, H_2, H_2O and Seven Hydrocarbons . . . . . EDWARD MELKONIAN 1750

Stopping Power for Protons in Several Metals . . . . . S. D. WARSHAW 1759

Magnetic Analysis of the $Li^6(d,p)Li^7$, and $Li^7(d,p)Li^8$ Reactions . . . . . E. N. STRAIT AND W. W. BUECHNER 1766

Investigations of the Capture of Protons and Deuterons by Deuterons . . . . . W. A. FOWLER, C. C. LAURITSEN, AND A. V. TOLLESTRUP 1767

Particle Groups from the Alpha-Particle Bombardment of Boron . . . . ROBERT J. CREAGAN 1769

Neutron Polarization . . . . . J. FLEEMAN, D. B. NICODEMUS, AND H. H. STAUB 1774

Multiple Diffuse Small Angle Scattering of X-Rays . . DAVID L. DEXTER AND W. W. BEEMAN 1782

Density Effect for Cosmic-Ray Mesons . . . . . W. L. WHITTEMORE AND J. C. STREET 1786

On the Nuclear Evaporation in Cosmic Rays and the Absorption of the Nucleonic Component. I . . . . . G. BERNARDINI, G. CORTINI, AND A. MANFREDINI 1792

Division of Nuclear Charge in Fission . . . . . D. C. BRUNTON 1798

Effect of Nuclear Motion on Atomic Magnetic Moments . . . . . M. PHILLIPS 1803

Experimental Investigations of Magneto-Hydrodynamic Waves . . . . . S. LUNDQUIST 1805

Decay Scheme of Hf^{181} . . . . . ARNE LUNDBY 1809

Multiple Scattering of Neutrons. II. Diffusion in a Plate of Finite Thickness . . . . . OTTO HALPERN AND R. K. LUNEBURG 1811

Hyperfine Structure in the Band Spectrum of the Mercury Hydride HgH . . S. MROZOWSKI 1820

Some Aspects of Paramagnetic Relaxation . . . . . ARIANNA WRIGHT 1826

Precision Wave-Length Measurements of the 1.1- and 1.3-Mev Lines of CO^{60} with the Two-Meter Focusing Curved-Crystal Spectrometer . . . . . DAVID A. LIND, J. R. BROWN, AND JESSE W. M. DUMOND 1838

Penetration and Diffusion of Hard X-Rays through Thick Barriers. III. Studies of Spectral Distributions . . . . . P. R. KARR AND J. C. LAMKIN 1843

Pressure Dependence of Line Width in Infra-Red Spectra . . . . . FRANK MATOSSI 1845

Carbon Dioxide in the Infra-Red Solar Spectrum . . . . . LEO GOLDBERG, ORREN C. MOHLER, ROBERT R. MCMATH, AND A. KEITH PIERCE 1848

Comparison of the g Value of the Electron in Hydrogen with That in Deuterium . . . . . EDWARD B. NELSON AND JOHN E. NAFE 1858

Theory of Critical Fluctuations . . . . . M. J. KLEIN AND L. TISZA 1861

On the Conductivity Produced in CdS Crystals by Irradiation with Gamma-Rays . . . . . RUDOLF FRERICHS 1869

Letters to the Editor:

Experimental Beta-Gamma-Angular Correlation . . . . . RICHARD L. GARWIN 1876

Hyperfine Structure and Nuclear Moment of Pb^{207} . . . . . A. L. SCHAWLOW, J. N. P. HUME, AND M. F. CRAWFORD 1876

Energy Levels of a Vector Meson in a Smeared Coulomb Field . . . . . ALBERT SIMON 1877

Precise Method of Determining the Faraday by Magnetic Resonance . . . . . J. A. HIPPLE, H. SOMMER, AND H. A. THOMAS 1877

Theory of the Electric Resistivity of Polycrystalline Graphite . . . . . DWAIN BOWEN 1878

Note on the Variational Method for the Scattering Problem . . . . . SU-SHU HUANG 1878

Photo-Disintegration of the Deuteron at Intermediate Energies . . J. F. MARSHALL AND E. GUTH 1879

High Energy Photo-Disintegration of the Deuteron . . . . . J. F. MARSHALL AND E. GUTH 1880

Measurements of the Variation of Work Function of Silicon with Temperature . . . . . B. J. ROTHLEIN AND P. H. MILLER, JR. 1882

Influence of Piezo-Electrification on Tribo-Electrification . . . . . JOHN W. PETERSON 1882

K-Shell Internal Conversion Coefficients . . . . . M. E. ROSE, G. H. GOERTZEL, B. I. SPINRAD, J. HARR, AND P. STRONG 1883

Disintegration of In^{114} . . . . . J. Y. MEI, ALLAN C. G. MITCHELL, AND DANIEL J. ZAFFARANO 1883

Penetration and Diffusion of Hard X-Rays through Thick Barriers. IV. Multiply Scattered γ-Rays: Angular Distribution . . . . . L. V. SPENCER AND FANNIE JENKINS 1885

Radioactive Lanthanum 140 . J. M. CORK, H. B. KELLER, W. C. RUTLEDGE, AND A. E. STODDARD 1886

Ferroelectricity in the Ilmenite Structure . . . . . B. T. MATTHIAS AND J. P. REMEIKA 1886

Optical Absorption in Barium Oxide Films . . . . . WINFIELD W. TYLER 1887

Beta-Spectrum of Praeseodymium 143 . . L. FELDMAN, L. LIDOFSKY, P. MACKLIN, AND C. S. WU 1888

Beta-Spectrum of $_{61}Pm^{147}$ . . . . . L. LIDOFSKY, P. MACKLIN, AND C. S. WU 1888

On the Low Energy Spectrum of Primary Cosmic Radiation and the Sun's Magnetic Dipole Moment . . . . . M. A. POMERANTZ, AND M. S. VALLARTA 1889

Proceedings of the American Physical Society:

Minutes of the Meeting of the Ohio Section at Cleveland, November 5, 1949 1890

Author Index to Volume 76 1892

Analytic Subject Index to Volume 76 1915

Volume Table of Contents iii

THE AMERICAN INSTITUTE OF PHYSICS

INCORPORATED

57 East 55 Street New York 22, N.Y.

MEMBER SOCIETIES:

American Physical Society
KARL K. DARROW, *Secretary*, Columbia University, New York 27, New York

Optical Society of America
ARTHUR C. HARDY, *Secretary*, Massachusetts Institute of Technology, Cambridge 39, Massachusetts

Acoustical Society of America
WALLACE WATENPAUGH, *Secretary*, 57 East 55th Street, New York 22, New York

Society of Rheology
G. J. DIENES, *Secretary*, North American Aviation, Inc., P. O. Box 309, Downey, California

American Association of Physics Teachers
R. F. PAUL, *Secretary*, University of Illinois, Urbana, Illinois

AFFILIATED SOCIETIES:

American Society for X-Ray and Electron Diffraction
Electron Microscopy Society of America
Physical Society of Pittsburgh
Physics Club of Chicago
Physics Club of Philadelphia
Cleveland Physics Society
Physics Club of the Lehigh Valley

ASSOCIATES:

Over seventy-five leading industrial corporations and other institutions which contribute to the support of the Institute

JOURNALS:

The Physical Review
JOHN T. TATE, *Editor*, University of Minnesota, Minneapolis, Minnesota

Reviews of Modern Physics
J. W. BUCHTA, *Editor*, University of Minnesota, Minneapolis, Minnesota

Journal of the Optical Society of America
GEORGE R. HARRISON, *Editor*, Massachusetts Institute of Technology, Cambridge, Massachusetts

The Journal of the Acoustical Society of America
FLOYD R. WATSON, *Editor*, 2323 Fourteenth Street, N.W., Washington, D. C.

American Journal of Physics
THOMAS H. OSGOOD, *Editor*, Michigan State College, East Lansing, Michigan

The Review of Scientific Instruments
GAYLORD P. HARNWELL, *Editor*, Randal Morgan Laboratory of Physics, University of Pennsylvania, Philadelphia, Pennsylvania

The Journal of Chemical Physics
JOSEPH E. MAYER, *Editor*, Kent Chemical Laboratory, University of Chicago, Chicago 37, Illinois

Journal of Applied Physics
ERNEST [illegible], *Editor*, Case Institute of Technology, Cleveland [illegible]

Physics Today
DAVID [illegible], *Editor*, American Institute of Physics, 57 East 55 Street, New York 22, New York

OFFICERS
GEORGE R. HARRISON, *Chairman*
Massachusetts Institute of Technology
GEORGE B. PEGRAM, *Treasurer*
Columbia University
JOHN T. TATE
Adviser on Publications
University of Minnesota

GOVERNING BOARD
LUIS W. ALVAREZ
I. W. BUMS
WALLACE R. BRODE
E. U. CONDON
W. F. FAIR, JR.
HARVEY FLETCHER
GEORGE R. HARRISON
W. V. HOUSTON
PAUL KIRKPATRICK
PAUL E. KLOPSTEG
F. W. LOOMIS
PHILIP M. MORSE
J. R. OPPENHEIMER
GEORGE B. PEGRAM
HAROLD K. SCHILLING
JOHN T. TATE
WALLACE WATENPAUGH
M. W. WHITE
Consultant on Printing
MELVIN LOOS

ADMINISTRATIVE STAFF
HENRY A. BARTON, *Director*
WALLACE WATENPAUGH, *Executive Secretary*
THEODORE VOORHEES, *Assistant Treasurer and Comptroller*
RUTH F. BRYANS, *Publication Manager*
BETTY HORSTAPEN, *Assistant Secretary*
EILEEN B. NEUMANN, *Circulation Manager*

THE American Institute of Physics was founded in 1931 as a federation of leading societies in the field of Physics. It combines into one operating agency those functions on behalf of physics which can best be done by the Societies jointly. Its purpose is the advancement and diffusion of physics and its applications to human welfare. To this end it publishes for itself or the Societies the nine journals listed on this page; promotes unity and effectiveness of effort among all who are interested in physics; renders numerous other services to physicists and to the public; and cooperates with government agencies, national associations, educational institutions, physical industries, and others in such manner as to realize the opportunities and fulfill the responsibilities of physics as an important and constructive human activity.